

**NASA Technical Memorandum 102642  
AVSCOM Technical Memorandum 90-B-007**

**INFLOW MEASUREMENTS MADE WITH A LASER VELOCIMETER ON A  
HELICOPTER MODEL IN FORWARD FLIGHT**

**Volume VIII: RECTANGULAR PLANFORM BLADES AT AN ADVANCE RATIO  
OF 0.23, 0.50 CHORD ABOVE THE TIP PATH PLANE**

Susan L. Althoff, Joe W. Elliott, and Danny R. Hoad  
Aerostructures Directorate  
USAARTA - AVSCOM  
Langley Research Center  
Hampton, Virginia

Richard H. Sailey  
Lockheed Engineering & Sciences Company  
Hampton, Virginia

May 1990

(NASA-TM-102642) INFLOW  
MEASUREMENTS MADE WITH A LASER  
VELOCIMETER ON A HELICOPTER MODEL  
IN FORWARD FLIGHT. VOLUME 8:  
RECTANGULAR PLANFORM BLADES AT AN  
ADVANCE RATIO OF 0.23, 0.50 CHORD  
ABOVE THE TIP PATH PLANE (Diskette G3/02 0159787  
Supplement) (NASA) 389 p

N93-24524

Unclass

**COLOR ILLUSTRATIONS**



National Aeronautics and  
Space Administration

Langley Research Center  
Hampton, Virginia 23665-5225



US ARMY  
AVIATION  
SYSTEMS COMMAND  
AVIATION R&T ACTIVITY



Inflow Measurements Made With a Laser Velocimeter  
on a Helicopter Model in Forward Flight  
Volume VIII: Rectangular Planform Blades  
at an Advance Ratio of 0.23, 0.50 Chord  
Above the Tip Path Plane

Susan L. Althoff, Joe W. Elliott, and Danny R. Hoad  
Aerostructures Directorate  
USAARTA - AVSCOM  
Langley Research Center  
Hampton, Virginia

Richard H. Sailey  
Lockheed Engineering & Sciences Company  
Hampton, Virginia

## SUMMARY

An experimental investigation was conducted in the 14- by 22-Foot Subsonic Tunnel at the NASA Langley Research Center to measure the inflow into a scale model helicopter rotor in forward flight ( $\mu = 0.23$ ). The measurements were made with a two-component Laser Velocimeter (LV) 0.50 chord above the plane formed by the path of the rotor tips (tip-path-plane). A conditional sampling technique was employed to determine the position of the rotor at the time that each velocity measurement was made so that the azimuthal fluctuations in velocity could be determined. Measurements were made at a total of 178 separate locations in order to clearly define the inflow character. The mean and standard deviation of the induced inflow ratios and the azimuthally dependent induced inflow ratios are included on 5.25 flexible disk in the pocket on the inside of the rear cover of this report. These data are presented herein without analysis.

## INTRODUCTION

One of the problems confronting the helicopter industry is the lack of detailed information about the velocity fluctuations around and through rotating blades. This information is needed for two reasons: to ensure a more complete understanding of the flow field environment associated with a thrusting rotor and to provide data for the validation of rapidly emerging computational codes. One explanation for the lack of available data is the absence, until recent years, of a suitable device for making

such measurements. Making measurements of the velocity around a system of rotating blades requires an accurate, nonintrusive measurement capability that presents a minimum risk to the systems involved. The Laser Velocimeter (LV), which uses high energy light beams to measure velocities, is ideally suited to this task.

The Laser Velocimeter has been successfully used to measure specific areas and localized phenomena within the rotor disk (references 1 thru 3). In addition, the hotwire anemometer and pressure probe, both having directional measuring limitations, have been employed in similar programs (references 4 and 5). This comprehensive investigation has been conducted to measure the flow into a representative rotor system as a function of azimuth using a two-component (streamwise and vertical direction) LV system.

## NOTATION

A	rotor disc area, ( $\pi R^2$ ), ft <sup>2</sup>
$A_0$	Constant term in Fourier series of blade feathering (collective) at $r/R = 0.75$ , deg
$A_1$	Coefficient of cosine term in Fourier series of blade feathering, deg
b	Number of blades
$B_1$	Coefficient of sine term in Fourier series of blade feathering, deg
$C_Q$	Rotor torque coefficient, $Q/(\rho A(12R)V_{tip}^2)$ , nondimensional
$C_D$	Rotor drag coefficient, $D/(\rho A V_{tip}^2)$ , nondimensional
$C_T$	Rotor thrust coefficient, $T/(\rho A V_{tip}^2)$ , nondimensional
D	Rotor drag, lbf (positive to the rear)
q	Dynamic pressure, lb/ft <sup>2</sup>
Q	Rotor torque, in-lbf
r	Local radius of the rotor system, ft
R	Rotor radius, ft
T	Thrust produced by the rotor, lbf
U	Freestream component of velocity, ft/sec, (positive downstream)

$u_i$	Induced component of velocity parallel to the tip path plane, ft/sec, (positive downstream)
$v$	Vertical component of velocity, ft/sec, (positive up)
$v_i$	Induced component of velocity normal to the tip path plane, ft/sec, (positive up)
$V_{tip}$	Rotor blade hover-tip velocity, ft/sec, ( $\Omega R$ )
$V_\infty$	Tunnel freestream velocity, ft/sec, (positive downstream)

## SYMBOLS

$\alpha$	Angle between rotor disk and freestream velocity (positive nose up), deg
$\lambda$	Inflow Ratio normal to tip path plane (positive up), $(V_\infty \sin \alpha + v_i)/V_{tip}$
$\lambda_i$	Induced Inflow Ratio normal to tip path plane (positive up), $v_i/V_{tip}$
$\mu_\infty$	Rotor advance ratio, $V_\infty \cos \alpha/V_{tip}$
$\mu$	Inflow Ratio parallel to tip path plane (positive downstream), $(V_\infty \cos \alpha + u_i)/V_{tip}$
$\mu_i$	Induced Inflow Ratio parallel to tip path plane (positive downstream), $u_i/V_{tip}$
$\Omega$	Rotor rotational speed, radians/sec
$\psi$	Rotor azimuth measured from downstream position, positive counterclockwise, as viewed from above, deg
$\rho$	Air density, slug/ft <sup>3</sup>
$\theta$	Blade pitch angle at a specific azimuth (positive nose up), deg, $\theta = A_0 - A_1 \cos \psi - B_1 \sin \psi$
$\overline{x}$	Mean value

## EXPERIMENTAL APPARATUS

The experimental apparatus used in this investigation included the NASA Langley Research Center 14- by 22-Foot Subsonic Tunnel, the 2-Meter Rotor Test System (2MRTS), and a two-component laser velocimeter system.

The 14- by 22-Foot Subsonic Tunnel is an atmospheric, closed-circuit wind tunnel of conventional design with enhancements for the testing of powered and high-lift configurations (reference 6). The tunnel is pictured in figure 1 and shown schematically in figure 2. When the tunnel is operated in the open configuration, the walls and ceiling of the test section are lifted out of the flow, leaving only a solid floor and a flow collector. In this configuration, the tunnel can be driven to about 170 knots. This investigation was conducted with the tunnel in the open configuration to allow complete optical access to the rotor flow field.

The 2MRTS is a general purpose rotorcraft model testing system which was mounted on a strut in the forward part of the test section (see figure 3). The system consists of a 29-horsepower electric drive motor and 90 degree speed-reducing transmission, a blade pitch remote control system, and two six-component strain gage balances used for measuring forces and moments on the rotor system and the generic fuselage shell (ROBIN). The four-bladed rotor hub is fully articulated with viscous dampers for lead-lag motion and coincident flap and lag hinges. A more detailed description of the 2MRTS and the ROBIN fuselage can be found in reference 7. The characteristics of the rotor blades used during this investigation can be found in table 1. No attempt was made to dynamically scale the rotor blades; rather, they were very rigid to minimize blade aeroelastic response uncertainties.

The LV system used in this investigation was designed to measure the instantaneous components of velocity in the longitudinal (freestream) and vertical directions. The LV system is described in reference 8. The system is comprised of four subsystems: optics, traverse, data acquisition, and seeding. The optics subsystem, which is shown in figure 4, operates in backscatter mode and at high power (3 watts in all lines) in order to accommodate the long focal lengths needed to scan the wide test section. The transmitting and receiving optics packages are augmented by a zoom lens system consisting of a 3-inch clear aperture negative lens and a 12-inch clear aperture positive lens. Bragg cells in each of the optical paths provide a directional measurement capability. The velocity measurements are made at a point in space where the four beams cross, called the sample volume. The length of the sample volume (transverse to the flow direction) increases as the sample volume is moved away from the optics assembly. The sample volume length, over the 10- to 20 foot focal length of the system, is less than 1 cm and has a nearly constant diameter of 0.2 mm.

The traverse subsystem provides five degrees of freedom in positioning the sample volume and is controlled by the same computer that is used for data acquisition. Translation of the sample volume in the horizontal and vertical direction is accomplished by displacing the entire optics platform. Translation along the lateral axes is accomplished by displacing the negative lens located in the zoom lens assembly, thus refocusing the sample volume along the axis of optical transmission. The other two degrees of freedom, pan and tilt, are implemented by rotating the final mirror about its vertical and horizontal axes in order to change the direction of optical transmission. The total range of the traversing system is 7 feet vertically, 6 feet streamwise, 16.5 feet laterally, and 10° in both pan and tilt. Measurements can be made outside of this envelope by re-positioning the optics platform, which is mounted on wheels to facilitate such relocations. For this study the traversing system was positioned to the left of the test section when looking downstream as shown in figure 3.

The data acquisition subsystem is shown schematically in figure 5 and interfaces with the optical signal processing equipment to receive two channels of raw LV data and up to five channels of auxiliary data. In this investigation, two of the auxiliary channels were used for the acquisition of data relative to blade position (one each for the U and V components). The system converts the raw LV data to engineering units and determines the statistical characteristics of the acquired data so that the test results can be evaluated during the acquisition process. The raw data and 64 parameters from the tunnel static data acquisition system are written to magnetic tape for later analysis. The final function performed by the data system is to control the five degree-of-freedom scan system.

The seeding subsystem, shown schematically in figure 6 and in the photo in figure 7, is a solid particle, liquid dispensing system (reference 9). Polystyrene latex microspheres are suspended in a mixture containing, by volume, 50 percent distilled water and 50 percent ethyl alcohol. The advantages of the polystyrene particles are their low density, high reflectivity, and precise particle size. The particles used in this investigation were 1.7 microns in diameter with a standard deviation of 0.0239 microns. The particle mixture is pumped to an array of nozzles where compressed air is used to atomize the mixture. These nozzles are mounted on a frame in the settling chamber of the tunnel; the position of the frame is remotely controlled by the laser operator during the data acquisition process. The low vapor pressure of water/alcohol mixture allows it to evaporate as it travels the 85 feet from the settling

chamber to the test section. This process provides isolated single particles in the flow field whose velocities are measured as they pass through the sample volume. The local fluid velocity is inferred from the seed particle velocity.

## ERROR ANALYSIS

The overall LV system error is obtained by summing the the error of all of the components that contribute to an error in the velocity measurement. The error sources are summarized the table below, and are defined in references 10 and 11. The resulting total bias error of 0.81 to 1.82 percent is obtained by adding the percents contributed by each error source. The total random error of 1.12 percent is obtained by taking the square root of the sum of the squared percents of the random sources. Taking the square root of the sum of the squares of the random and bias errors gives a total system error of 1.38 to 2.14 percent.

Error Source	Bias Error (percent)	Random Error (percent)
Cross beam angle measurement	$\pm 0.81$	N/A
Diverging fringes	A	A
Time jitter	N/A	N/A
Clock synchronization	0.51	$\pm 0.51$
Quantization	A	$\pm .99$
Velocity bias	B	B
Bragg Bias	B	B
Velocity Gradient	B	B
Particle Lag	<u><math>\pm 0.50</math></u>	<u>B</u>
Total error	-0.81 to 1.82	1.12
Total system error	1.38 to 2.14 percent velocity	
A	Not measured	
B	Negligible	
N/A	Not Applicable	

## TEST PROCEDURES

In all cases measurements were made at azimuthal increments of  $30^\circ$  from  $\psi = 0$ , at 1.30 inches (approximately 0.50 chord) above the plane formed by the tips of the blades. Measurements were made from a radial location of  $r/R = 0.2$  to  $r/R = 1.10$ , with the majority of the measurement locations concentrated toward the outboard portion of the disk. Figure 8 shows the measurement locations superimposed on the rotor disk. During the test, the rotor tip path plane was maintained at  $-3^\circ$  relative to the freestream by zeroing the blade flapping relative to the shaft and setting the shaft angle to  $-3^\circ$ . The operating tip speed for the test was held at 624 feet/sec (2113 rpm), the nominal tunnel speed was 144 ft/sec ( $\mu = 0.23$ ), and the nominal rotor thrust coefficient was 0.0065. Table 2 lists the nominal test conditions and selected test parameters. The LV data acquisition process consisted of placing the sample volume at the measurement location and acquiring data for a period of one minute or until 4096 velocity measurements were made in either the longitudinal or the vertical component. During this process, conditional sampling techniques were employed to permanently associate each measured velocity with the location of the rotor blades at the time when the measurement was made. At the conclusion of the process, the measurement location was changed and the acquisition process was repeated.

## DATA REDUCTION

Independent velocity measurements in the freestream and vertical direction were made at each measurement location. At the same instant in time that a velocity measurement was made, the location of the blades was recorded for that velocity component. The maximum time required to acquire this data was one minute (2113 rotor revolutions for this test) and the minimum approximately 10 seconds. These data, collected over many revolutions, were sorted into 128 equally spaced azimuth segments ( $2.81^\circ$  wide) that are representative of blade position. Careful measurements indicated that the lead-lag motion was well within this azimuth resolution ( $2.81^\circ$ ); therefore, no corrections to blade position were made due to lead-lag. The velocity value assigned to each interval at a measurement location is the arithmetic mean of all the measurements that were taken in the respective  $2.81$  degree wide azimuthal range. The results of this sorting process provide the azimuthally dependent velocity data. The "mean velocity" value refers to the velocity calculated from the arithmetic mean of all the measurements made at a single measurement location.

## EXPERIMENTAL RESULTS

Table 3 lists the measurement locations, the mean and standard deviation of the two components of induced inflow ratio, and the number of measurements in each of the measured components ( $U$  and  $V$ ). In figure 9 the mean longitudinal induced component of velocity,  $\mu_i$ , with a band of  $\pm$  one standard deviation is plotted vs. blade radius for each radial scan. The standard deviation represents the fluctuation in velocity at a given measurement location; it is not an indication of the error in the mean measurements. The size of the symbols used for plotting the mean velocity values is an approximation of the calculated error in the measurements. Figure 10 presents in the same format the mean normal induced component of velocity,  $\lambda_i$ . The same data without the  $\pm$  one standard deviation is presented in a contour plot format in figures 11 and 12 in order to show more clearly the interactions over the whole disk (viewed from above). Azimuth dependent data are presented in figures 13-190. The format of each of these figures shows the induced velocity vs azimuth at the top of the figure, the number of measurements that were used to determine the induced inflow velocity ratio for each azimuth segment in the center, and an order ratio analysis of the azimuthal variation at the bottom of the figure. The figure numbers for the azimuthal and radial measurement locations follow:

Azimuth	0	30	60	90	120	150	180	210	240	270	300	330
r/R												
0.20	--	27	42	57*	72	87	102	117	132	147	---	176
0.40	13	28	43	58	73	88	103	118	133	148	162	177
0.50	14	29	44	59	74	89	104	119	134	149	163	178
0.60	15	30	45	60	75	90	105	120	135	150	164	179
0.70	16	31	46	61	76	91	106	121	136	151	165	180
0.74	17	32	47	62	77	92	107	122	137	152	166	181
0.78	18	33	48	63	78	93	108	123	138	153	167	182
0.82	19	34	49	64	79	94	109	124	139	154	168	183
0.86	20	35	50	65	80	95	110	125	140	155	169	184
0.90	21	36	51	66	81	96	111	126	141	156	170	185
0.94	22	37	52	67	82	97	112	127	142	157	171	186
0.98	23	38	53	68	83	98	113	128	143	158	172	187
1.02	24	49	54	69	84	99	114	129	144	159	173	198
1.04	25	40	55	70	85	100	115	130	145	160	174	189
1.10	26	41	56	71	86	101	116	131	146	161	175	190

\* V-component measurement only

The mean and standard deviation of the induced inflow velocities (table 3) and the azimuthally dependent induced inflow velocities (figures 13 through 190) are included on a 5.25 flexible disk in the pocket on the inside of the rear cover of this report. The details of the data format and the file structure are located in the file "README.DOC". The disk format is 360 kbyte double-sided, written using the Microsoft Corporation MS-DOS operating system.

#### CONCLUDING REMARKS

The laser velocimeter provides an effective system for making measurements in the dynamic environment associated with rotor blades. It has been used on numerous occasions to measure the localized flow phenomena encountered in such flows. This investigation demonstrates the use of a matured LV system to map the flow into a representative rotor in forward flight by making velocity measurements at 178 locations above the rotor disk. These measurements provide both the mean and azimuthally-dependent velocity values, and they provide a detailed look at the nature

of this flow. The mean and standard deviation of the induced inflow velocities and the azimuthally dependent induced inflow velocities are included on a 5.25 flexible disk in the pocket on the inside of the rear cover of this report.

## REFERENCES

1. Landgrebe, A. J.; and Johnson, B. V.: Measurement of Model Helicopter Rotor Flow Velocities with a Laser Doppler Velocimeter. American Helicopter Society Journal, Vol 19, July 1974, p. 39-43.
2. Biggers, J. C.; and Orloff, K. L.: Laser Velocimeter Measurements of the Helicopter Rotor-Induced Flowfield. American Helicopter Society, Annual National V/STOL Forum, 30th, Washington, D.C. May 7-9, 1974.
3. Owen F. K.; and Taubert M. E.: Measurement and Prediction of Model-Rotor Flowfields. AIAA, 18th Fluid Dynamics, Plasmadynamics and Laser Conference, Cincinnati, Ohio, July 16-18, 1985.
4. Tangler, J. L.; Wohlfeld, R. M.; and Miley, S. J.: An Experimental Investigation of Vortex Stability, Tip Shapes, Compressibility and Noise for Hovering Models. NASA CR-2305, September 1973.
5. Junker, B.: Investigations of Blade-vortices in the Rotor Downwash. Twelfth European Rotorcraft Forum, Garmish-Partenkirchen, Federal Republic of Germany, September 22-25, 1986.
6. Applin, Z. T.: Flow Improvements in the Circuit of the Langley 4- by 7-Meter Tunnel. NASA TM 85662, December 1983.
7. Phelps, A. E. III; and Berry, J. D.: Description of the U.S. Army 2-Meter Rotor Test System. NASA TM 87762, AVSCOM TM 86-B-4, January 1987.
8. Sellers, W. L.; and Elliott, J. W.: Applications of a Laser Velocimeter in the Langley 4- by 7-Meter Tunnel. Proceedings of the Workshop on Flow Visualization and Laser Velocimetry for Wind Tunnels, NASA CP 2243, March 1982, pp. 283-293.
9. Elliott, J. W.; and Nichols, C. E.: Seeding Systems for Use with a Laser Velocimeter in Large Scale Wind Tunnels. Proceedings of the Workshop on Wind Tunnel Seeding Systems for Laser Velocimeters, NASA CP 2393, March 1985, pp. 93-103.
10. Young, W. H.; Meyers, J. F.; and Hepner, T. E.: Laser Velocimeter Systems Analysis to a Flow Survey above a Stalled Wing. NASA TN D-8408, August 1977.
11. Dring, R. P.: Sizing Criteria for Laser Anemometry Particles. Journal of Fluids Engineering, Vol. 104, March 1982, p. 15-17.

**TABLE 1 - 2MRTS ROTOR AND BLADE CHARACTERSTICS**

<b>Hub Type</b>	<b>Fully Articulated</b>
Number of blades	4
Airfoil section	NACA 0012
Hinge offset, in, r/R	2.00, .06
Root cutout, in, r/R	8.25, .24
Pitch-flap coupling angle, deg	0.0
Twist linear, deg	-8.0
Radius, R, in	33.88
Airfoil chord, C, in	2.6
Rotor solidity, bc/ $\pi$ R	0.0977
Blade stiffness	
Flapwise lb-in <sup>2</sup>	11500
Torsional lb-in <sup>2</sup>	25500
Blade weight, grams	259.3
Lead/lag damping in-lb/deg/sec	182.4

**TABLE 2 - NOMINAL ROTOR CONTROL AND PERFORMANCE PARAMETERS**

$C_T$	0.0065
$C_Q$	0.00035
$C_D$	0.00005
$\alpha$ , deg	-2.96
Coning, deg	0.50
$A_0$ , deg	6.8
$A_1$ , deg	-1.9
$B_1$ , deg	3.3
$\mu_\infty$	0.230
$V_\infty$ , ft/sec	143.7
$V_{tip}$ , ft/sec	624.8
Lag angle (mean), degrees	0.90

**TABLE 3 - INFLOW VELOCITY SUMMARY**

$\Psi$	r/R	$\mu_i$			$\lambda_i$		
		Mean	Standard deviation	# of Measurements	Mean	Standard deviation	# of Measurements
0	0.40	0.0117	0.0162	2274	-0.0261	0.0172	2898
0	0.50	0.0161	0.0154	2421	-0.0311	0.0145	2884
0	0.60	0.0174	0.0112	2307	-0.0323	0.0123	2905
0	0.70	0.0158	0.0102	2525	-0.0357	0.0125	2983
0	0.74	0.0166	0.0105	2573	-0.0366	0.0122	2898
0	0.78	0.0158	0.0101	2544	-0.0384	0.0112	2923
0	0.82	0.0141	0.0086	2408	-0.0386	0.0113	2931
0	0.86	0.0123	0.0087	2381	-0.0399	0.0101	2883
0	0.90	0.0082	0.0074	2705	-0.0412	0.0098	2984
0	0.94	0.0047	0.0082	2706	-0.0430	0.0095	3023
0	0.98	0.0024	0.0099	2783	-0.0431	0.0089	2983
0	1.02	-0.0014	0.0115	2798	-0.0428	0.0075	3031
0	1.04	-0.0029	0.0114	2778	-0.0417	0.0074	2957
0	1.10	-0.0048	0.0103	2794	-0.0395	0.0072	2939
30	0.20	0.0124	0.0162	2547	0.0038	0.0158	2716
30	0.40	0.0202	0.0094	2710	-0.0193	0.0124	2928
30	0.50	0.0181	0.0073	2728	-0.0287	0.0090	3058
30	0.60	0.0154	0.0067	2665	-0.0331	0.0080	2960
30	0.70	0.0132	0.0067	2694	-0.0360	0.0099	3026
30	0.74	0.0128	0.0066	2763	-0.0361	0.0089	2976
30	0.78	0.0115	0.0064	2720	-0.0370	0.0082	2928
30	0.82	0.0096	0.0065	2717	-0.0375	0.0078	2959
30	0.86	0.0073	0.0074	2645	-0.0384	0.0106	3115
30	0.90	0.0048	0.0070	2690	-0.0385	0.0107	3119
30	0.94	0.0023	0.0078	2696	-0.0380	0.0082	3042
30	0.98	0.0006	0.0078	2696	-0.0378	0.0066	3023
30	1.02	-0.0018	0.0081	2685	-0.0356	0.0048	2911
30	1.04	-0.0020	0.0075	2696	-0.0345	0.0045	2988
30	1.10	-0.0037	0.0067	2675	-0.0318	0.0050	2823
60	0.20	0.0176	0.0123	1979	-0.0003	0.0106	2902
60	0.40	0.0189	0.0090	1841	-0.0252	0.0093	2545
60	0.50	0.0150	0.0077	2684	-0.0260	0.0078	3136
60	0.60	0.0135	0.0080	2745	-0.0258	0.0095	3180
60	0.70	-0.0021	0.0058	2814	0.0228	0.0043	2855
60	0.74	-0.0013	0.0058	2730	0.0223	0.0042	2814
60	0.78	-0.0014	0.0055	2768	0.0219	0.0040	2953
60	0.82	-0.0022	0.0054	2797	0.0217	0.0037	3030
60	0.86	-0.0019	0.0052	2821	0.0213	0.0036	3034
60	0.90	-0.0018	0.0052	2877	0.0210	0.0037	2980
60	0.94	-0.0017	0.0049	2850	0.0205	0.0035	2988
60	0.98	-0.0007	0.0046	2826	0.0203	0.0034	3053
60	1.02	-0.0010	0.0047	2807	0.0197	0.0035	2982
60	1.04	-0.0016	0.0047	2857	0.0196	0.0033	3007
60	1.10	-0.0017	0.0047	2808	0.0194	0.0033	2996

**TABLE 3 - CONTINUED**

$\Psi$	r/R	$\mu_i$		$\lambda_i$			
		Mean	Standard deviation	# of Measurements	Mean	Standard deviation	# of Measurements
90	0.20	-----	-----	---	-0.0074	0.0048	2481
90	0.40	0.0193	0.0121	1378	-0.0196	0.0074	2979
90	0.50	0.0155	0.0098	1619	-0.0158	0.0095	2867
90	0.60	0.0154	0.0103	1996	-0.0137	0.0124	3131
90	0.70	-0.0022	0.0066	2758	0.0160	0.0033	3089
90	0.74	-0.0024	0.0070	2750	0.0156	0.0033	3022
90	0.78	-0.0019	0.0072	2801	0.0154	0.0033	3046
90	0.82	-0.0020	0.0074	2714	0.0149	0.0032	3060
90	0.86	-0.0029	0.0066	2728	0.0146	0.0031	3030
90	0.90	-0.0024	0.0070	2754	0.0144	0.0031	3065
90	0.94	-0.0027	0.0064	2657	0.0140	0.0032	3047
90	0.98	-0.0025	0.0065	2677	0.0138	0.0030	3010
90	1.02	-0.0029	0.0066	2661	0.0132	0.0030	3039
90	1.04	-0.0029	0.0065	2670	0.0130	0.0028	3001
90	1.10	-0.0024	0.0064	2812	0.0131	0.0030	3048
120	0.20	0.0082	0.0077	2368	-0.0039	0.0092	2788
120	0.40	0.0124	0.0083	2591	-0.0105	0.0122	2943
120	0.50	0.0123	0.0110	2622	-0.0070	0.0097	2824
120	0.60	0.0121	0.0093	2643	0.0005	0.0193	3045
120	0.70	-0.0043	0.0048	2776	0.0091	0.0024	3048
120	0.74	-0.0039	0.0049	2801	0.0088	0.0026	3084
120	0.78	-0.0040	0.0048	2838	0.0085	0.0025	3043
120	0.82	-0.0040	0.0050	2832	0.0082	0.0025	3083
120	0.86	-0.0044	0.0049	2836	0.0078	0.0024	3127
120	0.90	-0.0048	0.0048	2849	0.0074	0.0023	3103
120	0.94	-0.0053	0.0048	2837	0.0071	0.0023	3084
120	0.98	-0.0044	0.0048	2860	0.0068	0.0022	3088
120	1.02	-0.0046	0.0047	2810	0.0065	0.0021	3123
120	1.04	-0.0053	0.0049	2845	0.0065	0.0021	3081
120	1.10	-0.0040	0.0049	2884	0.0060	0.0022	3090
150	0.20	-0.0003	0.0085	2315	-0.0010	0.0111	2688
150	0.40	0.0107	0.0087	2643	-0.0033	0.0162	2980
150	0.50	0.0102	0.0082	2645	0.0012	0.0167	2948
150	0.60	0.0096	0.0087	2720	0.0048	0.0161	2968
150	0.70	0.0071	0.064	2637	0.0052	0.0081	2819
150	0.74	0.0063	0.0070	2522	0.0121	0.0180	2817
150	0.78	0.0047	0.0086	2531	0.0111	0.0143	2746
150	0.82	0.0037	0.0097	2632	0.0151	0.0181	2891
150	0.86	0.0016	0.0095	2635	0.0138	0.0117	2745
150	0.90	-0.0011	0.0090	2560	0.0141	0.0099	2728
150	0.94	-0.0024	0.0093	2651	0.0141	0.0071	2732
150	0.98	-0.0054	0.0059	2664	0.0130	0.0048	2827
150	1.02	-0.0058	0.0051	2631	0.0112	0.0040	2925
150	1.04	-0.0061	0.0050	2632	0.0098	0.0037	2958
150	1.10	-0.0065	0.0049	2667	0.0080	0.0032	2947

**TABLE 3 - CONTINUED**

$\Psi$	r/R	$\mu_i$	# of Measurements	Mean	Standard deviation	$\lambda_i$	# of Measurements
180	0.20	-0.0032	0.0074	2557	0.0014	0.0085	2656
180	0.40	0.0073	0.0087	2541	0.0036	0.0178	2902
180	0.50	0.0089	0.0083	2559	0.0053	0.0177	2837
180	0.60	0.0076	0.0087	2567	0.0092	0.0101	2720
180	0.70	0.0036	0.0100	2570	0.0161	0.0273	2771
180	0.74	0.0028	0.0106	2562	0.0172	0.0246	2782
180	0.78	0.0018	0.0115	2561	0.0191	0.0201	2712
180	0.82	0.0011	0.0114	2558	0.0205	0.0192	2745
180	0.86	-0.0001	0.0114	2467	0.0207	0.0174	2750
180	0.90	-0.0018	0.0110	2568	0.0197	0.0147	2777
180	0.94	-0.0033	0.0079	2538	0.0196	0.0124	2816
180	0.98	-0.0057	0.0055	2502	0.0164	0.0070	2773
180	1.02	-0.0073	0.0049	2571	0.0133	0.0051	2861
180	1.04	-0.0072	0.0048	2584	0.0122	0.0047	2845
180	1.10	-0.0071	0.0049	2626	0.0087	0.0037	2850
210	0.20	-0.0046	0.0075	2721	0.0040	0.0088	2690
210	0.40	0.0024	0.0081	2436	-0.0029	0.0142	2673
210	0.50	0.0063	0.0079	2435	-0.0022	0.0149	2664
210	0.60	0.0083	0.0075	2401	0.0002	0.0086	2628
210	0.70	0.0040	0.0126	2471	0.0064	0.0201	2581
210	0.74	0.0066	0.0129	2547	0.0054	0.0190	2612
210	0.78	0.0052	0.0143	2544	0.0089	0.0202	2631
210	0.82	0.0034	0.0139	2516	0.0115	0.0187	2631
210	0.86	0.0026	0.0136	2545	0.0116	0.0155	2521
210	0.90	-0.0019	0.0096	2418	0.0115	0.0125	2507
210	0.94	-0.0015	0.0094	2446	0.0117	0.0095	2497
210	0.98	-0.0034	0.0068	2421	0.0120	0.0063	2503
210	1.02	-0.0060	0.0050	2477	0.0105	0.0045	2556
210	1.04	-0.0057	0.0053	2488	0.0099	0.0041	2507
210	1.10	-0.0065	0.0048	2533	0.0083	0.0036	2737
240	0.20	-0.0018	0.0088	2660	0.0036	0.0105	2700
240	0.40	0.0031	0.0104	2690	-0.0046	0.0113	2702
240	0.50	0.0041	0.0100	2689	-0.0066	0.0119	2703
240	0.60	0.0059	0.0103	2705	-0.0076	0.0123	2791
240	0.70	0.0096	0.0134	2710	-0.0058	0.0127	2857
240	0.74	0.0066	0.0188	2645	0.0013	0.0244	2815
240	0.78	0.0092	0.0185	2634	0.0050	0.0269	2761
240	0.82	0.0096	0.0173	2613	0.0029	0.0262	2716
240	0.86	0.0096	0.0171	2646	0.0055	0.0242	2705
240	0.90	0.0102	0.0168	2572	0.0114	0.0248	2693
240	0.94	0.0104	0.0162	2560	0.0171	0.0215	2587
240	0.98	0.0073	0.0126	2494	0.0179	0.0143	2390
240	1.02	0.0033	0.0069	2179	0.0180	0.0082	2339
240	1.04	0.0006	0.0064	2436	0.0164	0.0068	2533
240	1.10	0.0008	0.0058	2455	0.0111	0.0044	2522

**TABLE 3 - CONCLUDED**

$\Psi$	r/R	$\mu_i$			$\lambda_i$		
		Mean	Standard deviation	# of Measurements	Mean	Standard deviation	# of Measurements
270	0.20	0.0046	0.0078	2599	-0.0110	0.0091	2715
270	0.40	0.0064	0.0108	2573	-0.0132	0.0083	2860
270	0.50	0.0059	0.0095	2649	-0.0177	0.0080	2799
270	0.60	0.0052	0.0100	2435	-0.0214	0.0095	1895
270	0.70	0.0062	0.0110	2828	-0.0245	0.0102	2662
270	0.74	0.0070	0.0106	2834	-0.0245	0.0115	2962
270	0.78	0.0101	0.0086	2703	-0.0248	0.0105	3004
270	0.82	0.0108	0.0100	2786	-0.0259	0.0106	2972
270	0.86	0.0108	0.0113	2813	-0.0234	0.0094	2790
270	0.90	0.0137	0.0121	2685	-0.0210	0.0136	2735
270	0.94	0.0142	0.0116	2499	-0.0148	0.0202	2114
270	0.98	0.0133	0.0083	2176	0.0065	0.0187	2417
270	1.02	0.0094	0.0068	1990	0.0139	0.0094	2224
270	1.04	0.0064	0.0071	1973	0.0150	0.0065	2137
270	1.10	0.0012	0.0074	2117	0.0117	0.0048	2231
300	0.40	0.0082	0.0067	2909	-0.0007	0.0051	3005
300	0.50	0.0082	0.0074	2838	-0.0054	0.0055	3068
300	0.60	0.0102	0.0091	2454	-0.0108	0.0066	3036
300	0.70	0.0112	0.0099	2428	-0.0175	0.0080	2987
300	0.74	0.0111	0.0101	2334	-0.0200	0.0086	2959
300	0.78	0.0110	0.0099	2373	-0.0227	0.0091	2948
300	0.82	0.0117	0.0096	2404	-0.0262	0.0097	2923
300	0.86	0.0113	0.0093	2298	-0.0275	0.0094	2926
300	0.90	0.0113	0.0098	2244	-0.0292	0.0094	2916
300	0.94	0.0106	0.0098	2252	-0.0319	0.0097	2886
300	0.98	0.0086	0.0097	2143	-0.0332	0.0090	2878
300	1.02	0.0066	0.0092	1930	-0.0321	0.0075	2819
300	1.04	0.0074	0.0089	1950	-0.0300	0.0069	2812
300	1.10	0.0044	0.0068	1920	-0.0165	0.0065	2930
330	0.20	0.0172	0.0086	2349	-0.0009	0.0101	2711
330	0.40	0.0144	0.0085	2380	-0.0018	0.0059	2617
330	0.50	0.0143	0.0081	2332	-0.0045	0.0086	2637
330	0.60	0.0146	0.0091	2422	-0.0056	0.0093	2655
330	0.70	0.0157	0.0085	2408	-0.0104	0.0103	2678
330	0.74	0.0143	0.0084	2465	-0.0127	0.0100	2634
330	0.78	0.0147	0.0088	2398	-0.0158	0.0107	2639
330	0.82	0.0131	0.0088	2335	-0.0190	0.0105	2601
330	0.86	0.0133	0.0089	2322	-0.0216	0.0105	2566
330	0.90	0.0112	0.0089	2347	-0.0254	0.0117	2608
330	0.94	0.0097	0.0092	2334	-0.0281	0.0106	2631
330	0.98	0.0075	0.0104	2353	-0.0301	0.0105	2619
330	1.02	0.0072	0.0113	2014	-0.0309	0.0089	2092
330	1.04	0.0060	0.0122	2022	-0.0303	0.0085	2101
330	1.10	0.0047	0.0122	2029	-0.0289	0.0086	2151

ORIGINAL PAGE  
BLACK AND WHITE PHOTOGRAPH

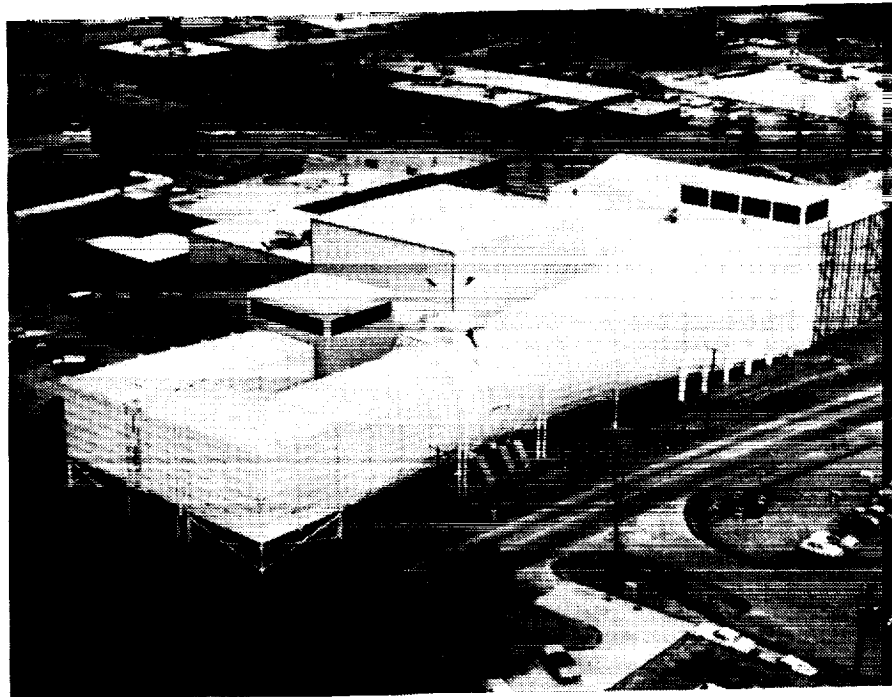


Figure 1. Aerial view of 14- by 22-Foot Subsonic Tunnel.

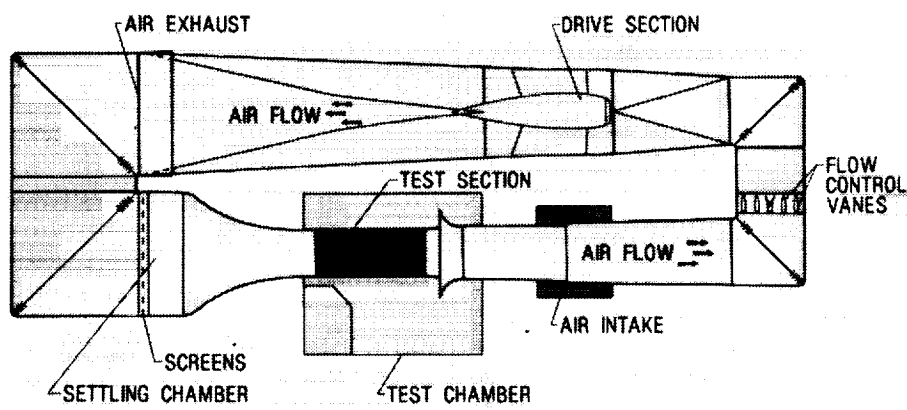


Figure 2. Schematic of 14- by 22-Foot Subsonic Tunnel.

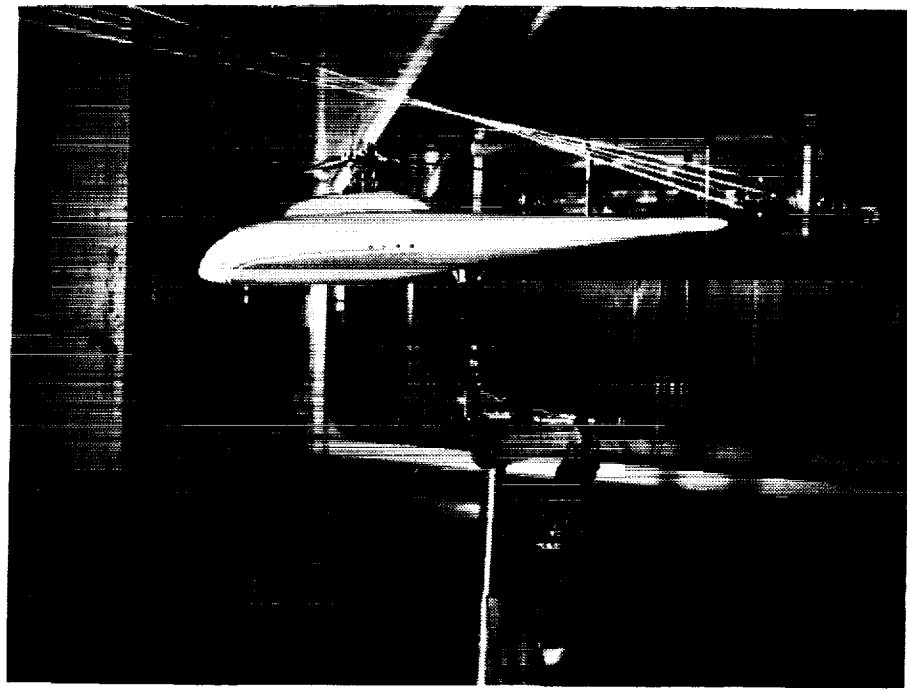


Figure 3. 2MRTS mounted in forward bay of the test section.

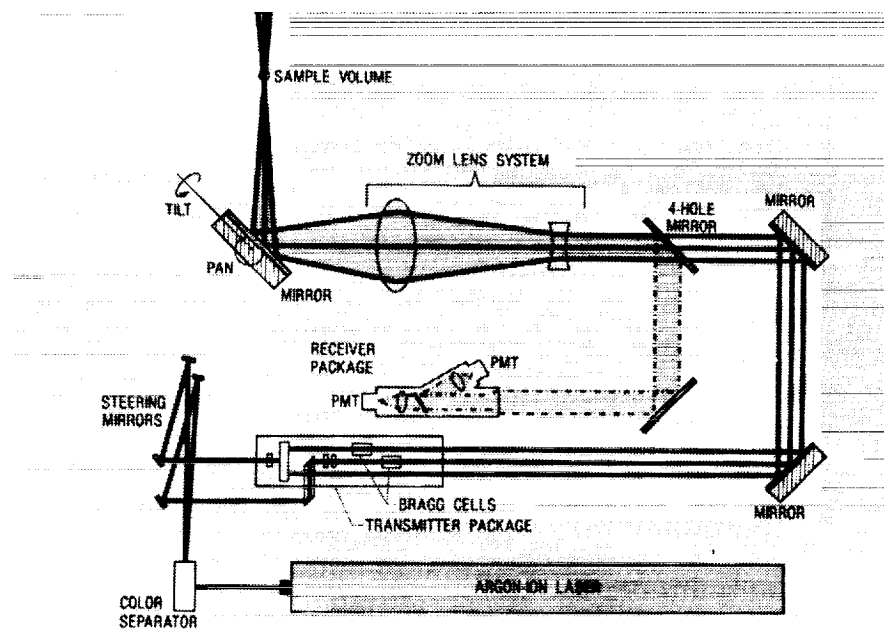


Figure 4. Schematic of laser velocimeter optics subsystem.

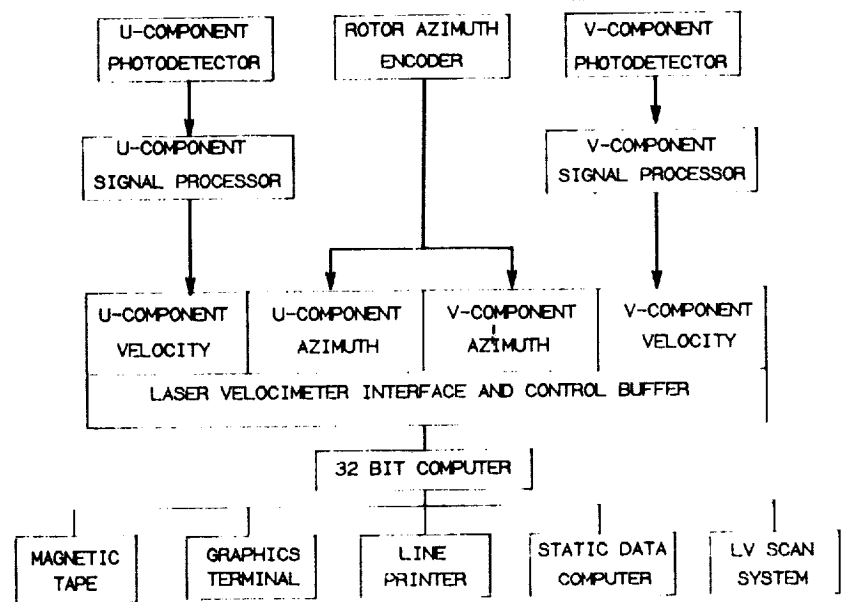


Figure 5. Schematic of data acquisition subsystem.

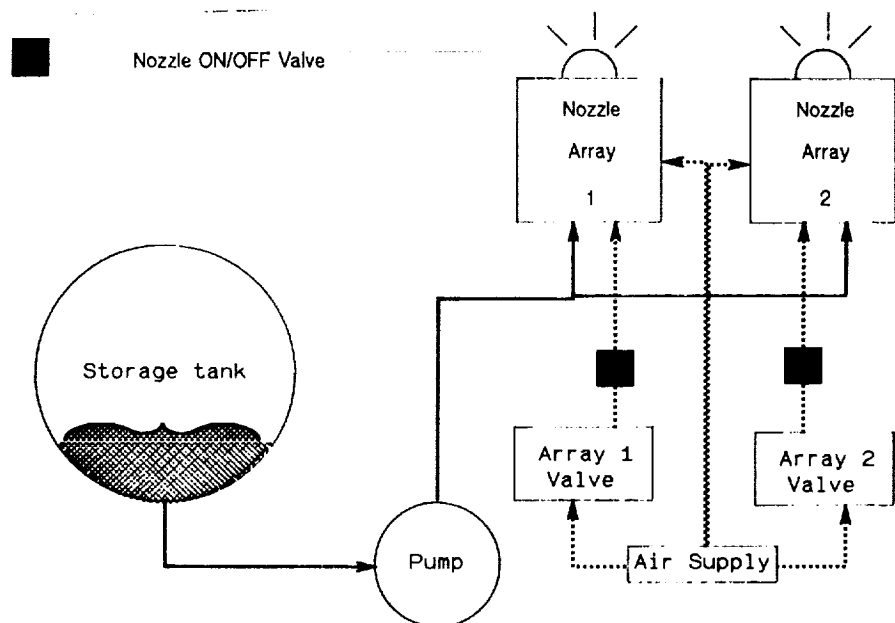


Figure 6. Schematic of seeding subsystem.

ORIGINAL PAGE  
BLACK AND WHITE PHOTOGRAPH

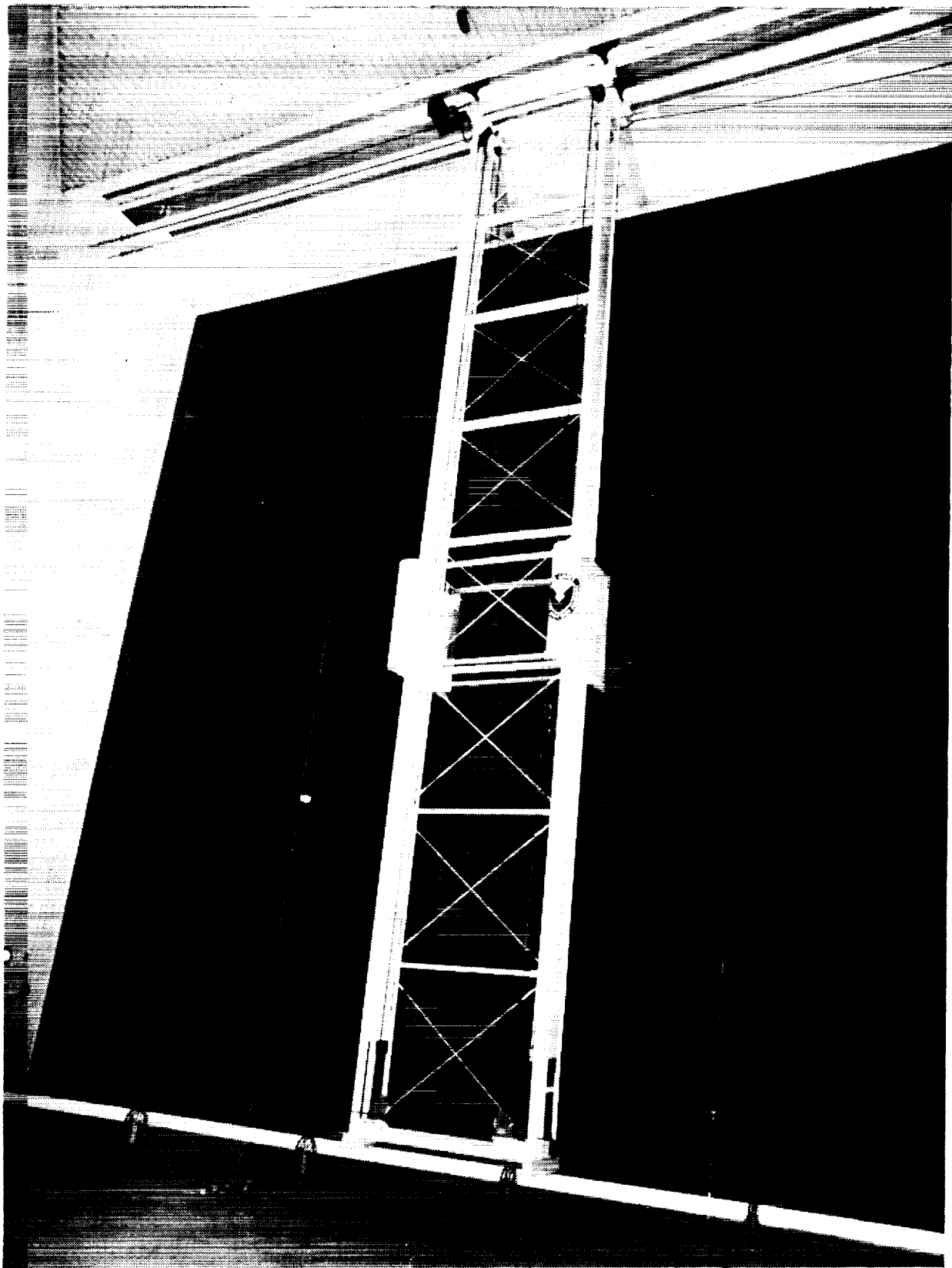


Figure 7. Photograph of remote control positioner for seeding system.

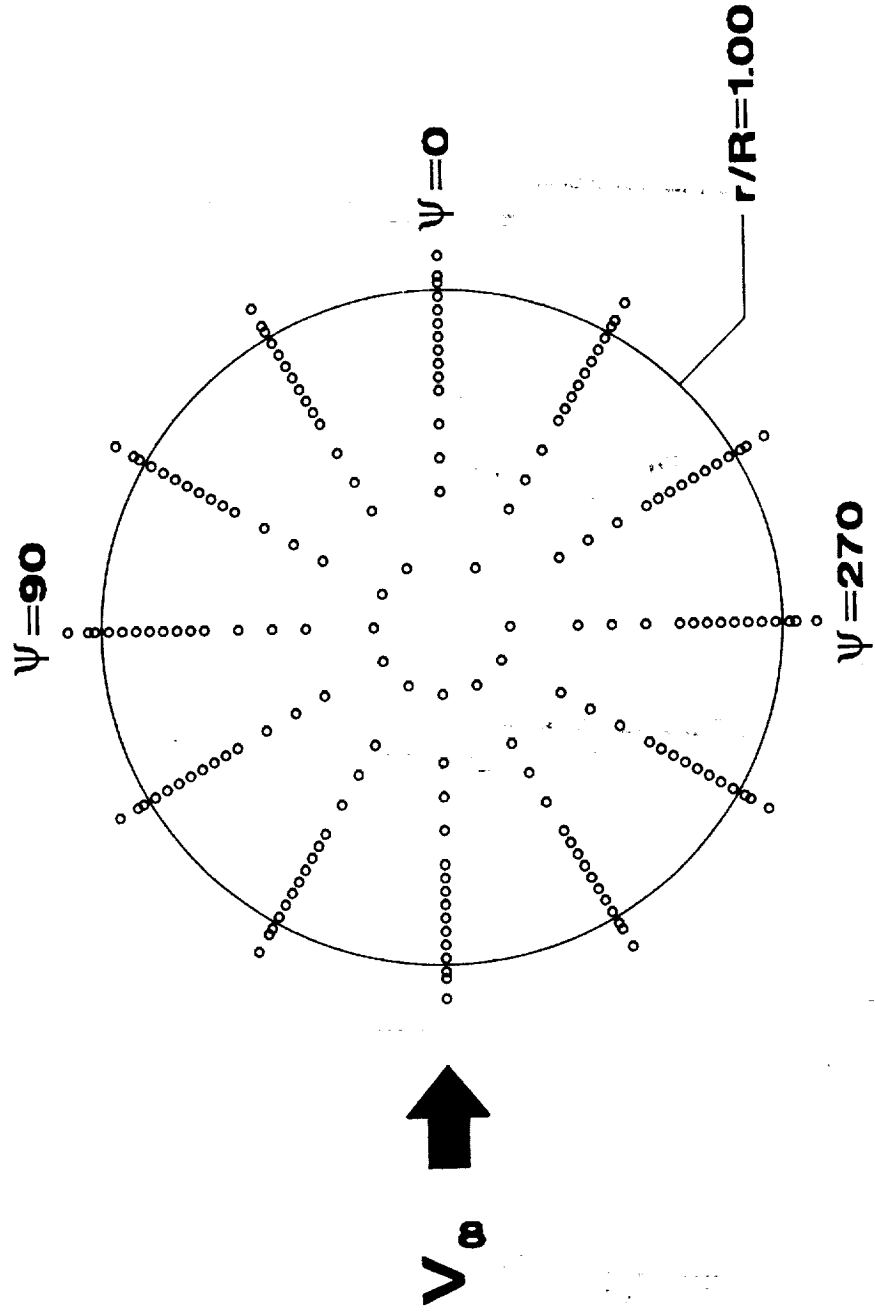


Figure 8. Locations of velocity measurements, 1.30 inches above rotor tip path plane.

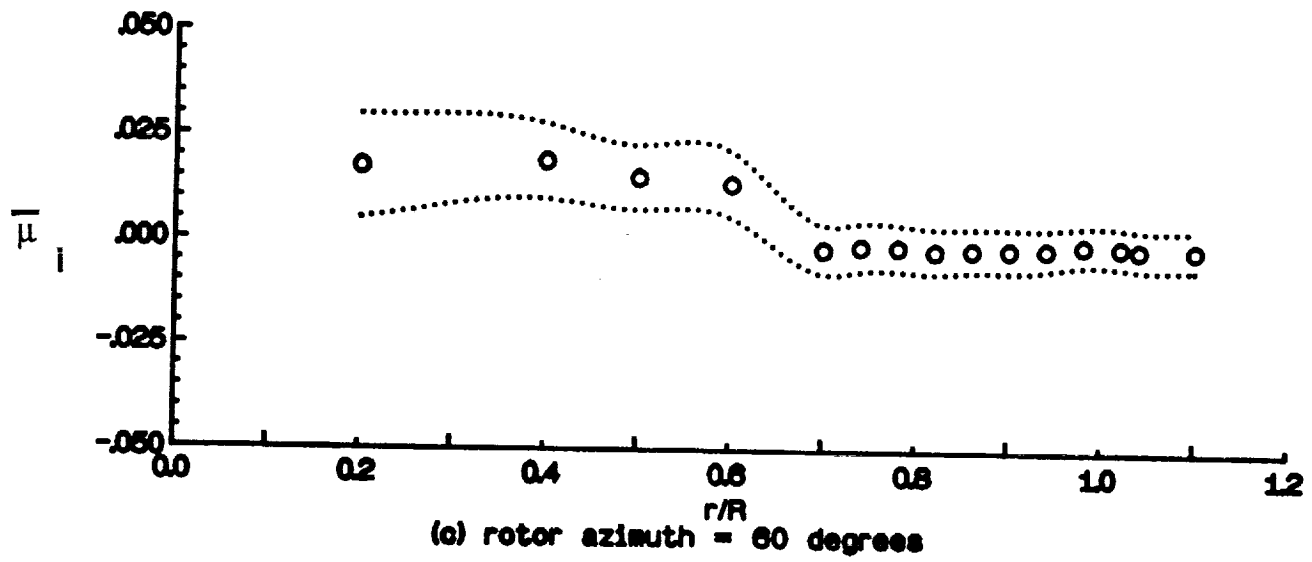
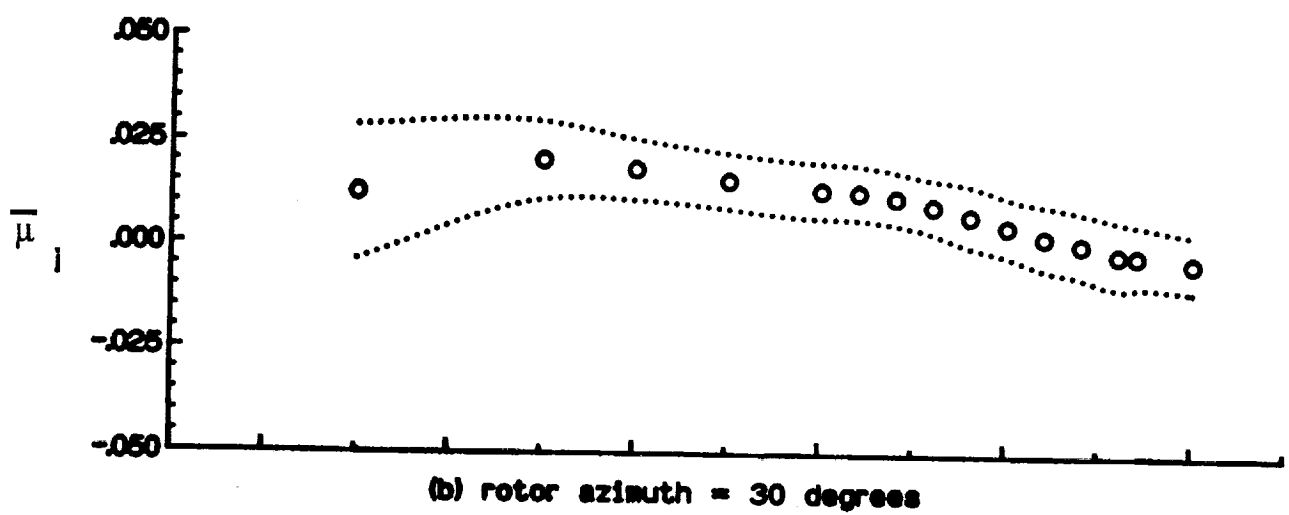
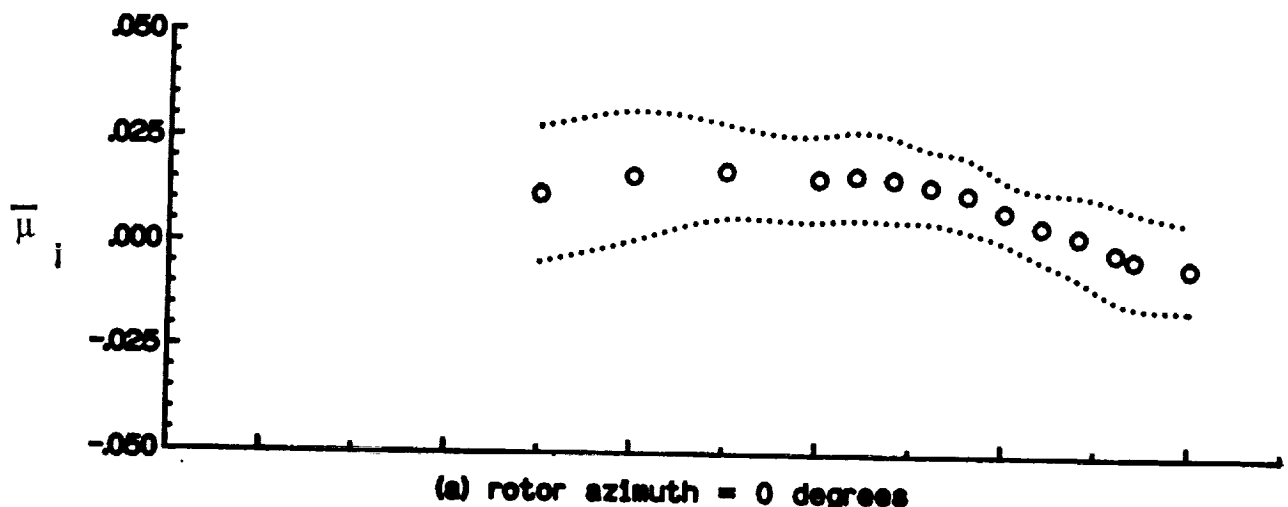


Figure 9.- Radial distribution of mean induced inflow ratio ( $\bar{\mu}$ ).

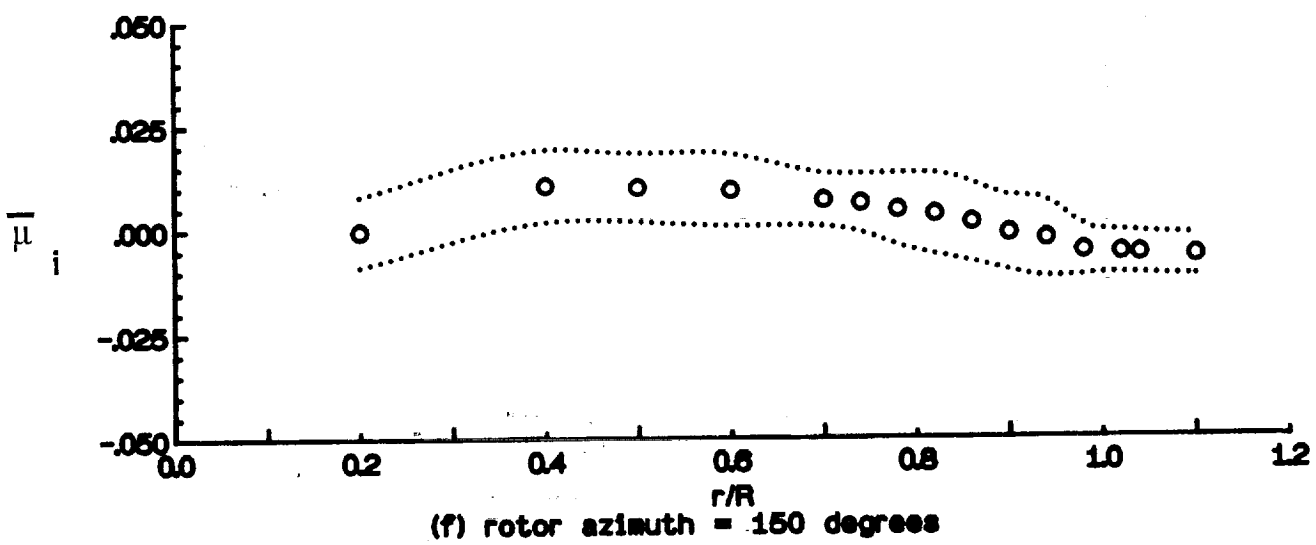
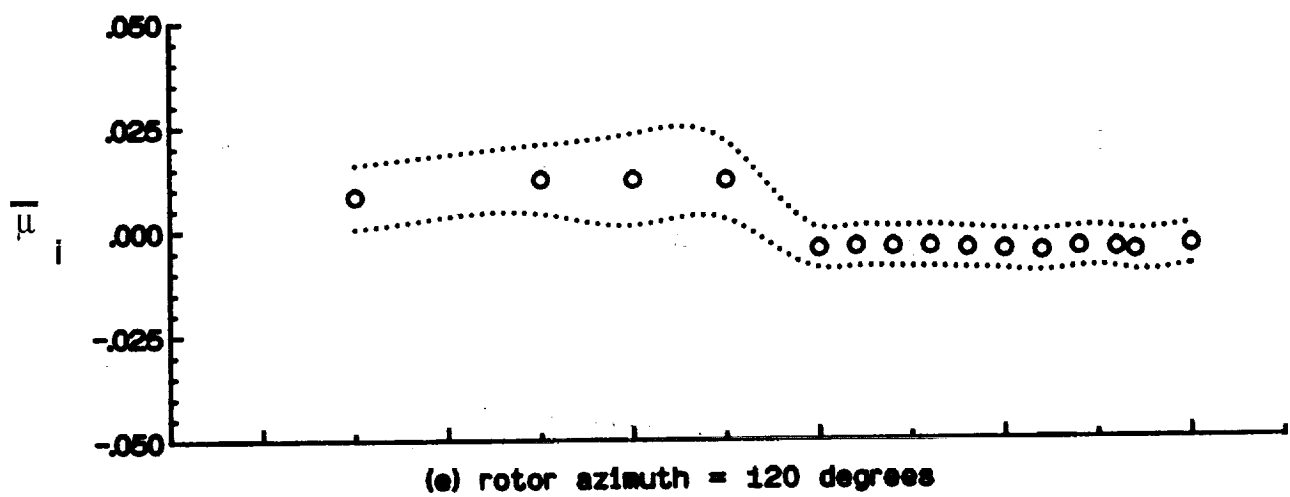
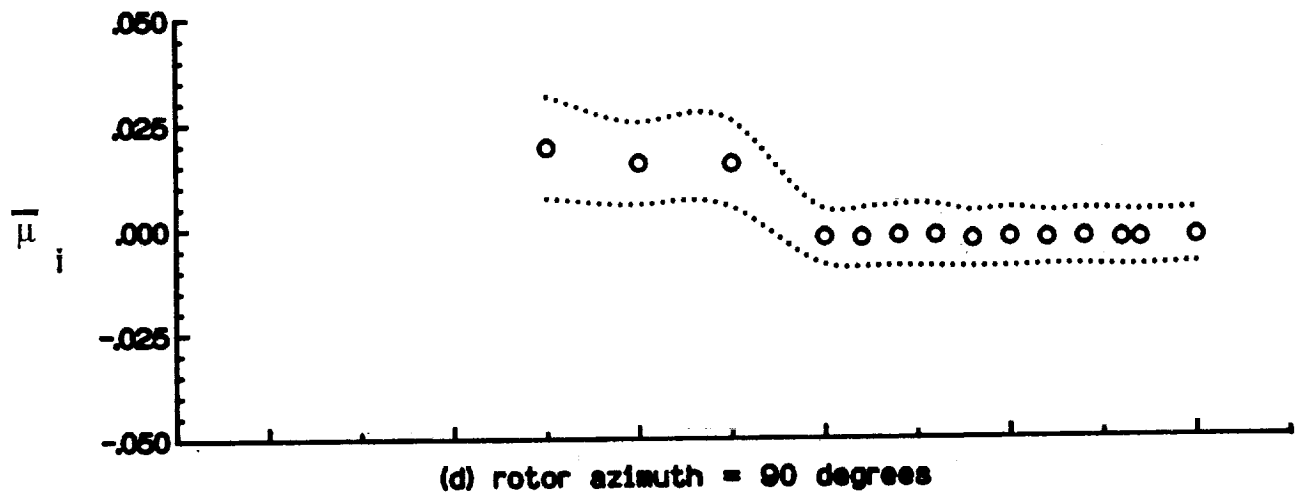
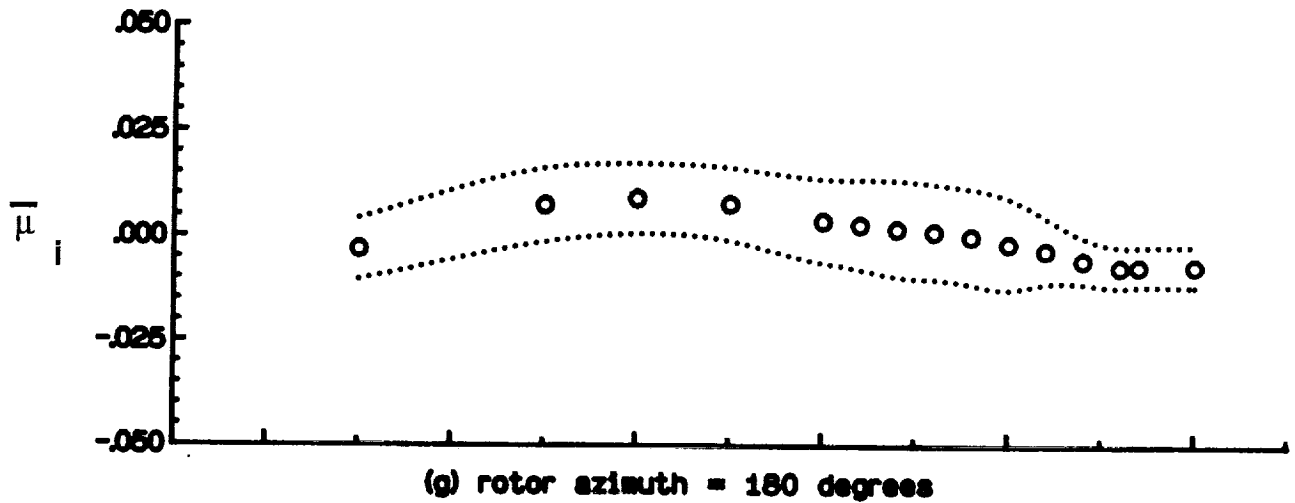
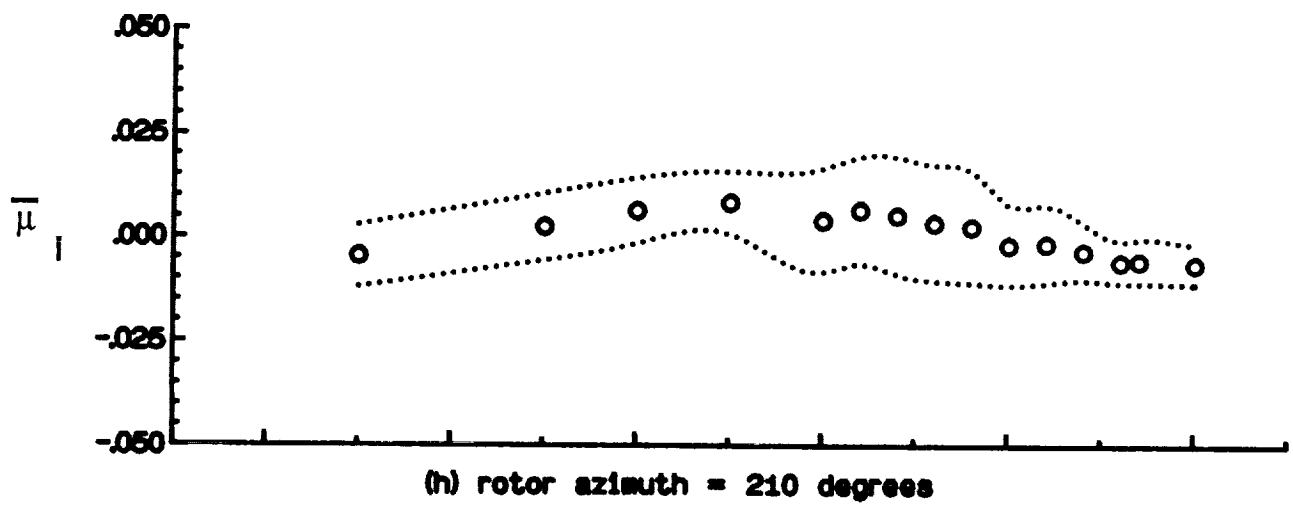


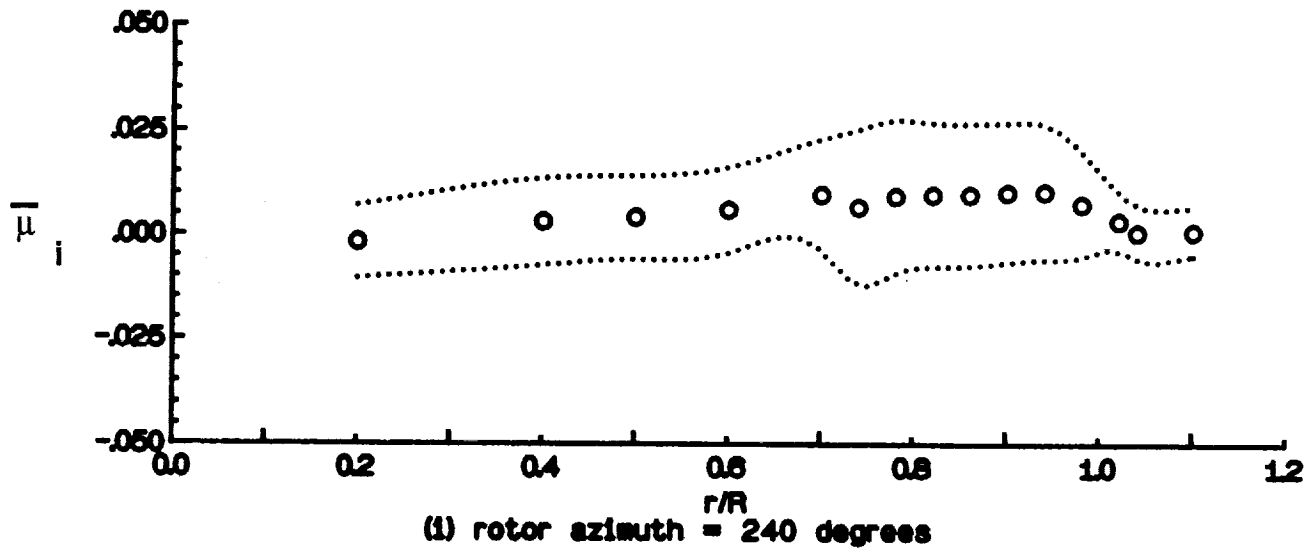
Figure 9.- Continued.



(g) rotor azimuth = 180 degrees

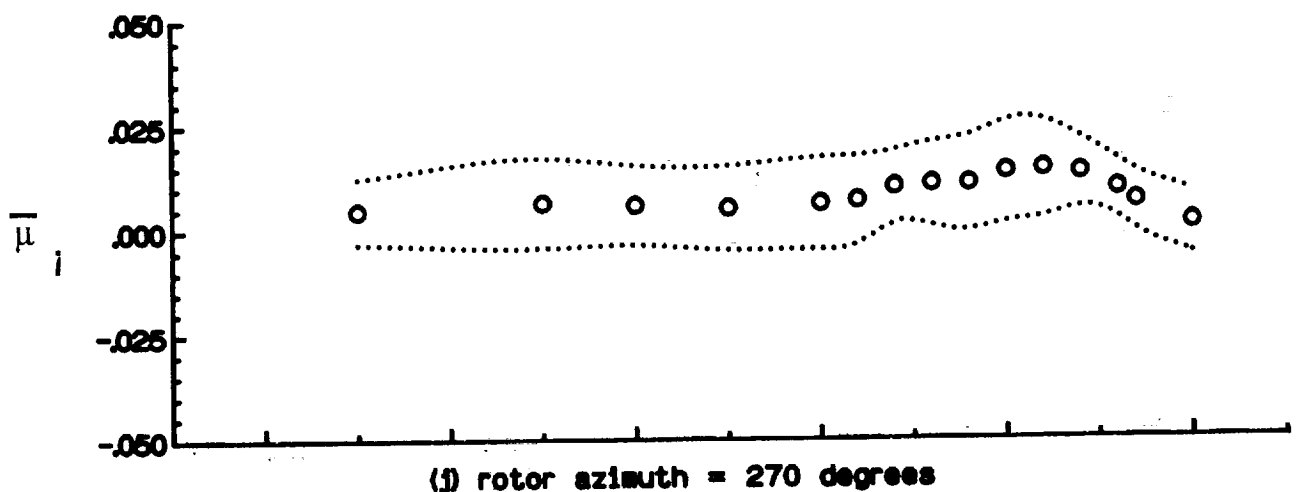


(h) rotor azimuth = 210 degrees

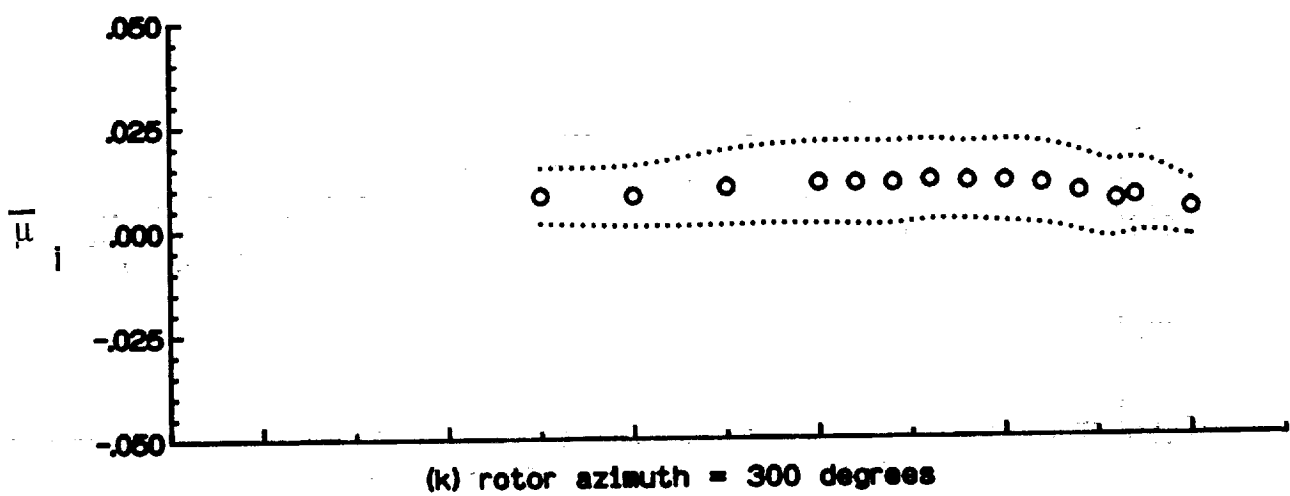


(l) rotor azimuth = 240 degrees

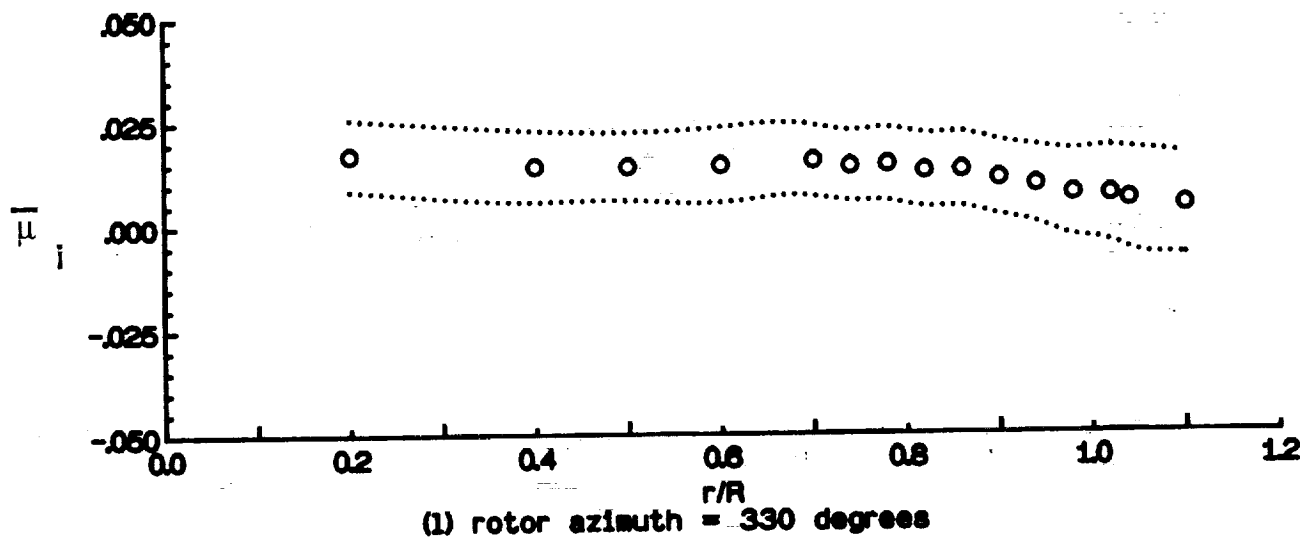
Figure 9.- Continued.



(j) rotor azimuth = 270 degrees



(k) rotor azimuth = 300 degrees



(l) rotor azimuth = 330 degrees

Figure 9.- Concluded.

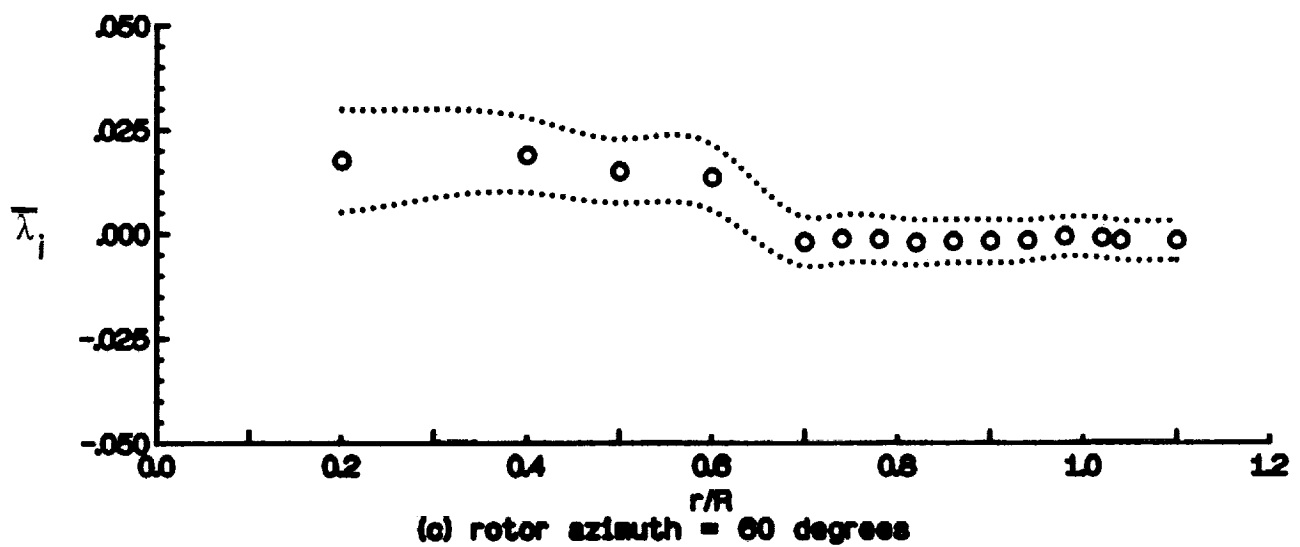
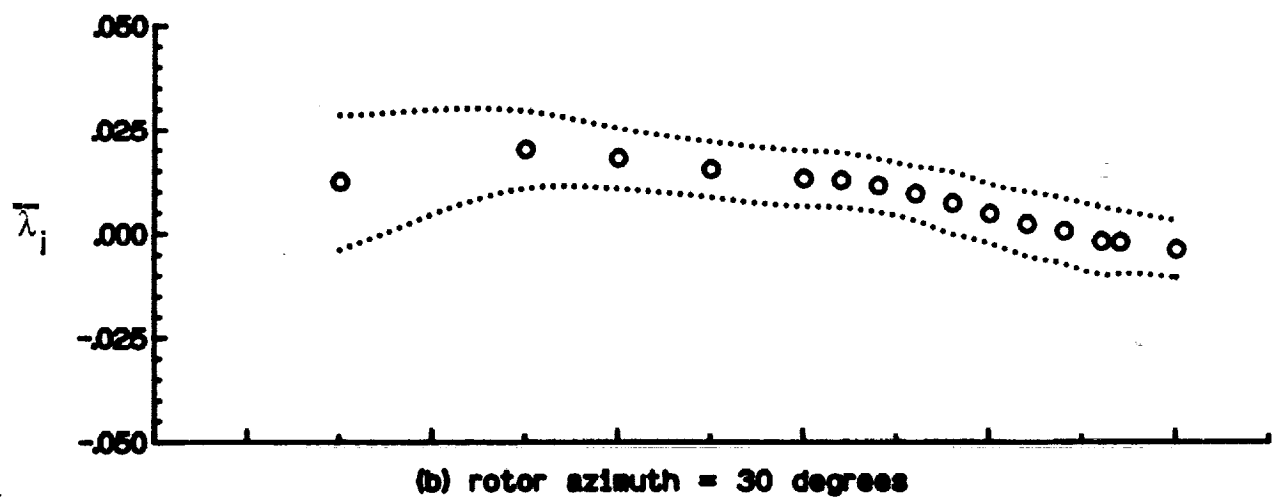
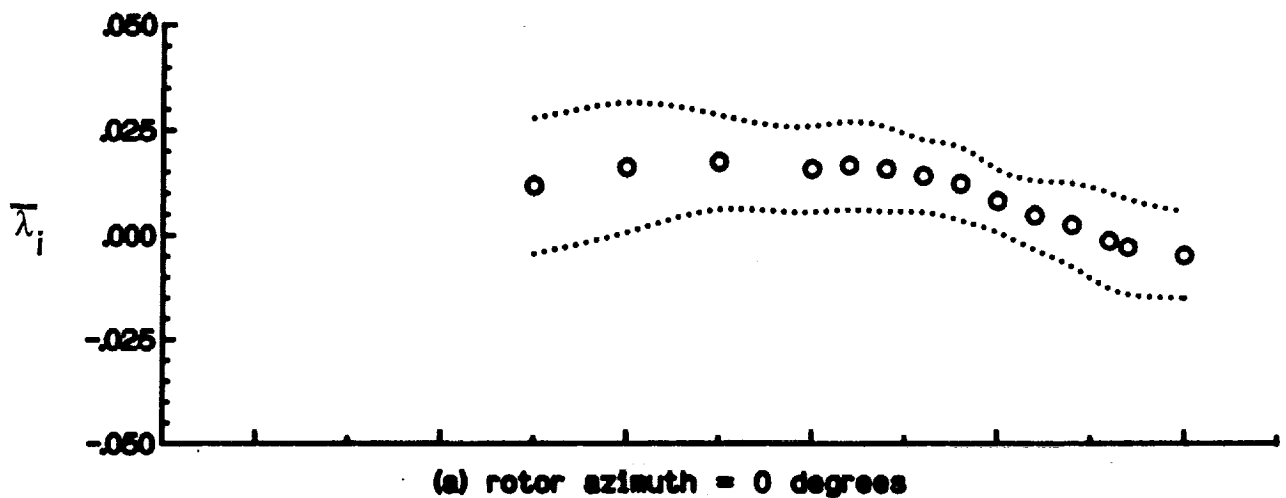


Figure 10.- Radial distribution of mean induced inflow ratio ( $\bar{\lambda}_i$ ).

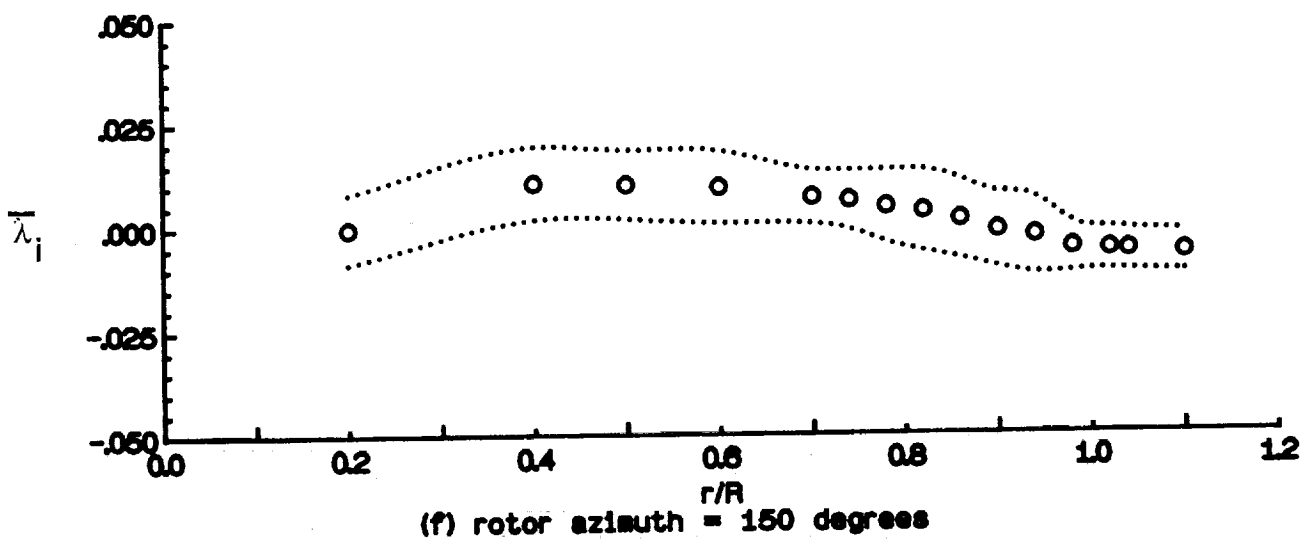
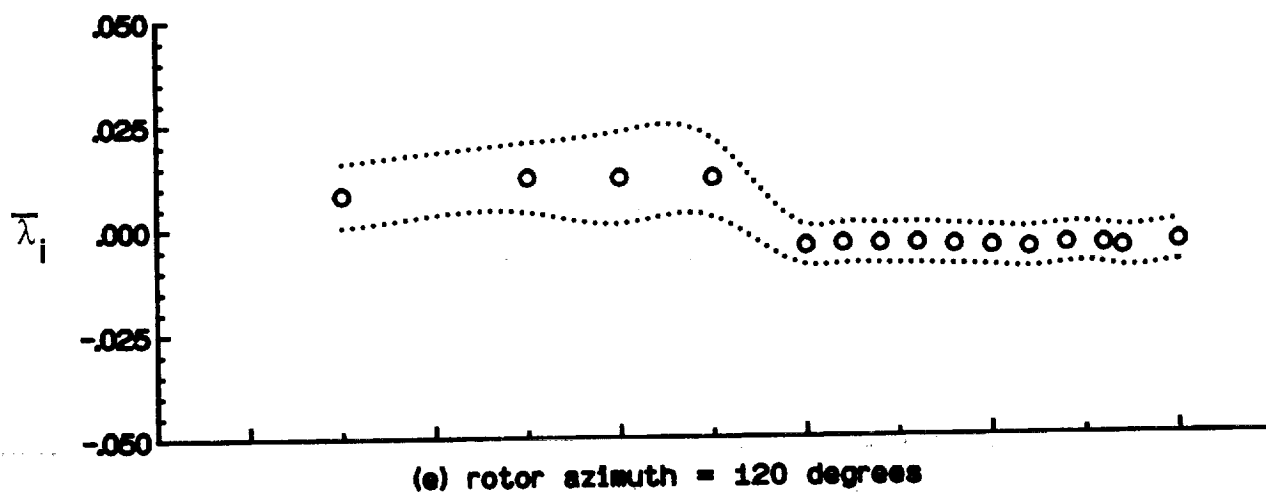
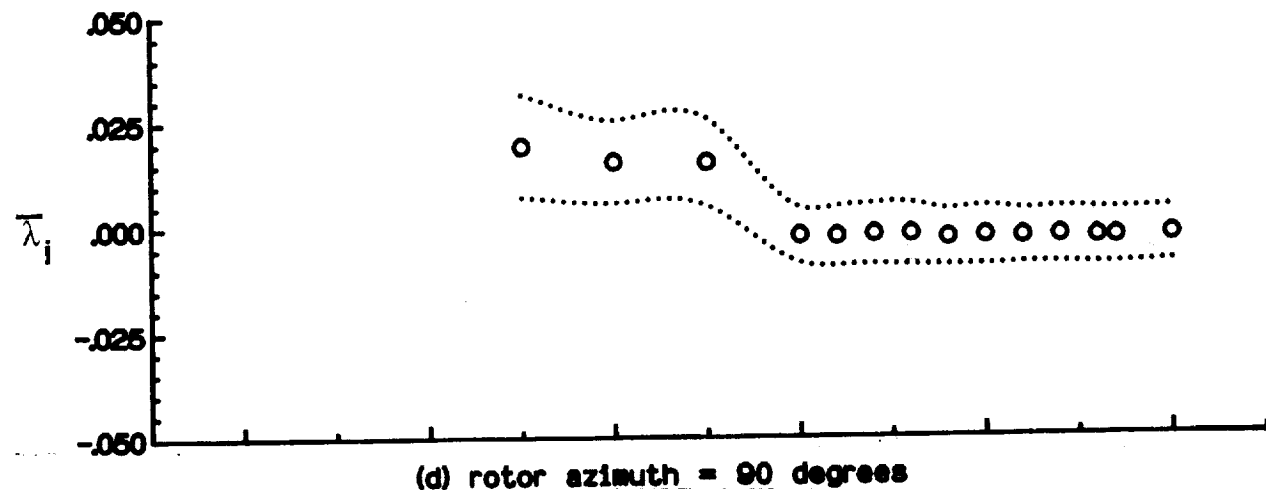


Figure 10.- Continued.

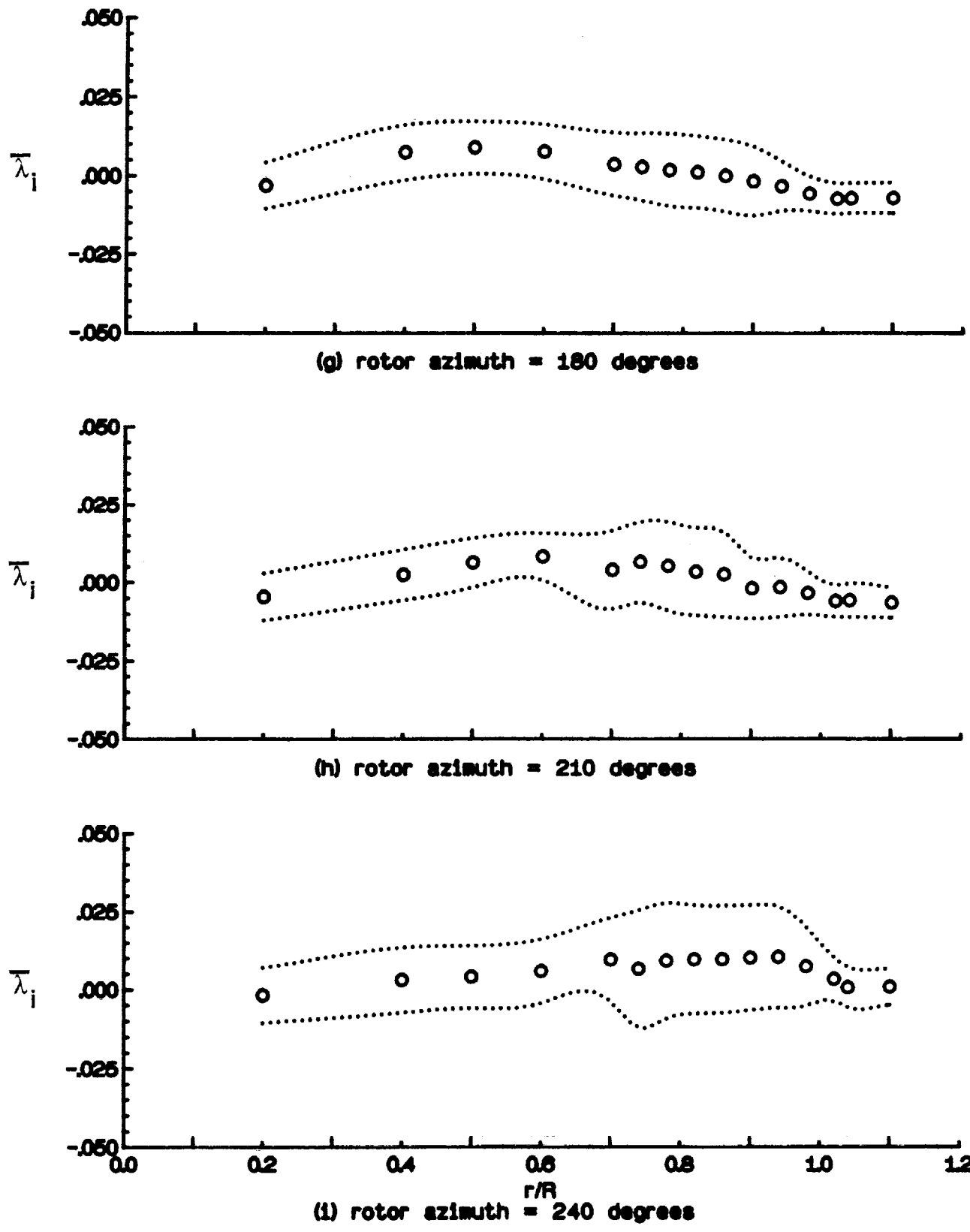


Figure 10.- Continued.

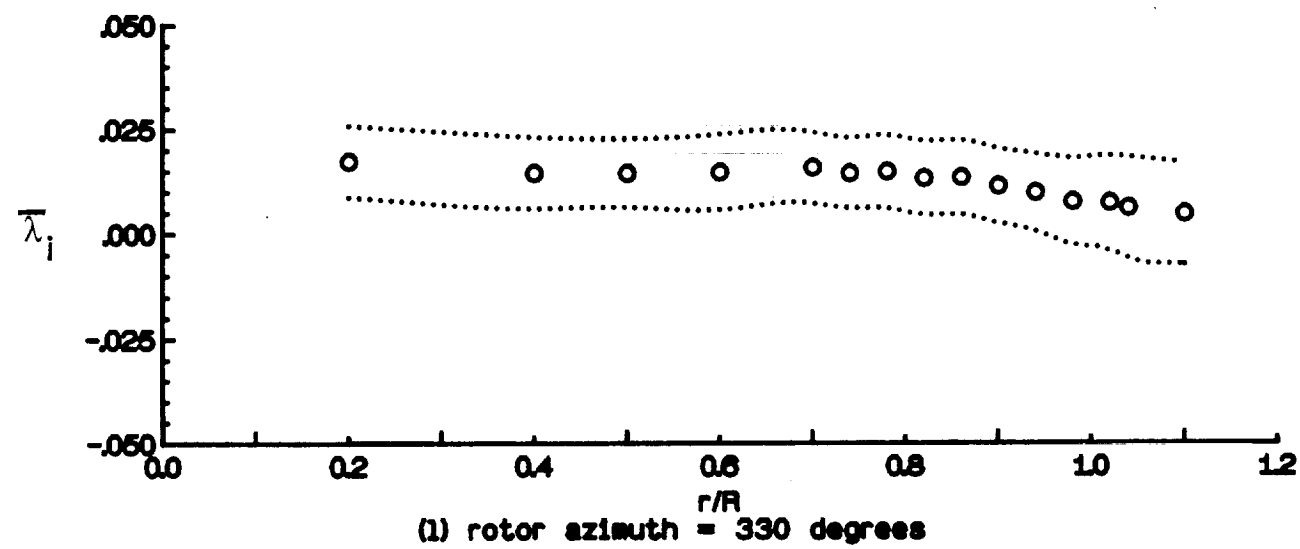
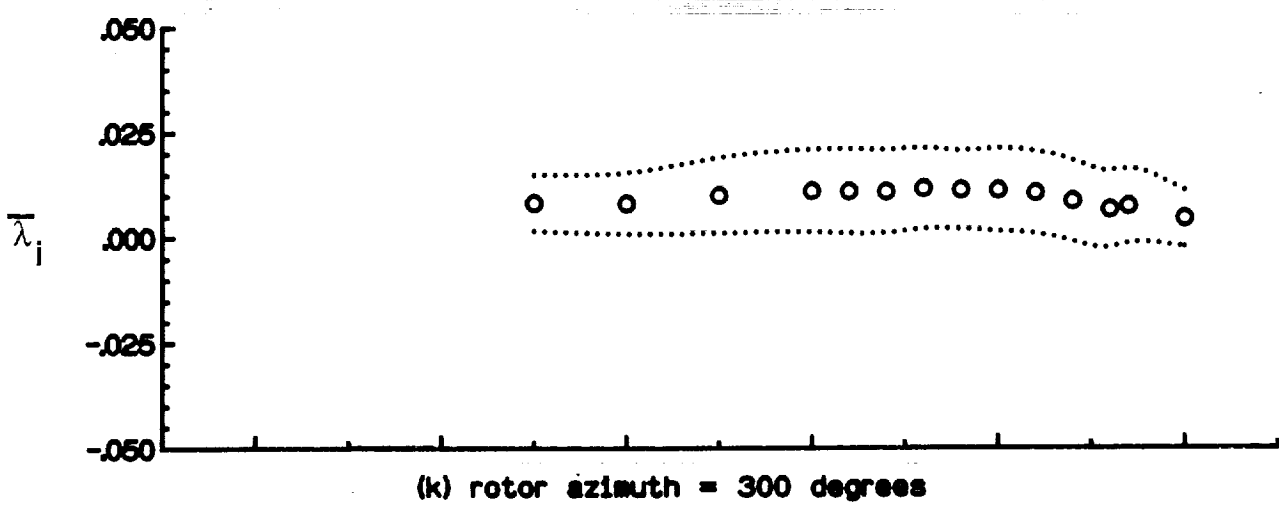
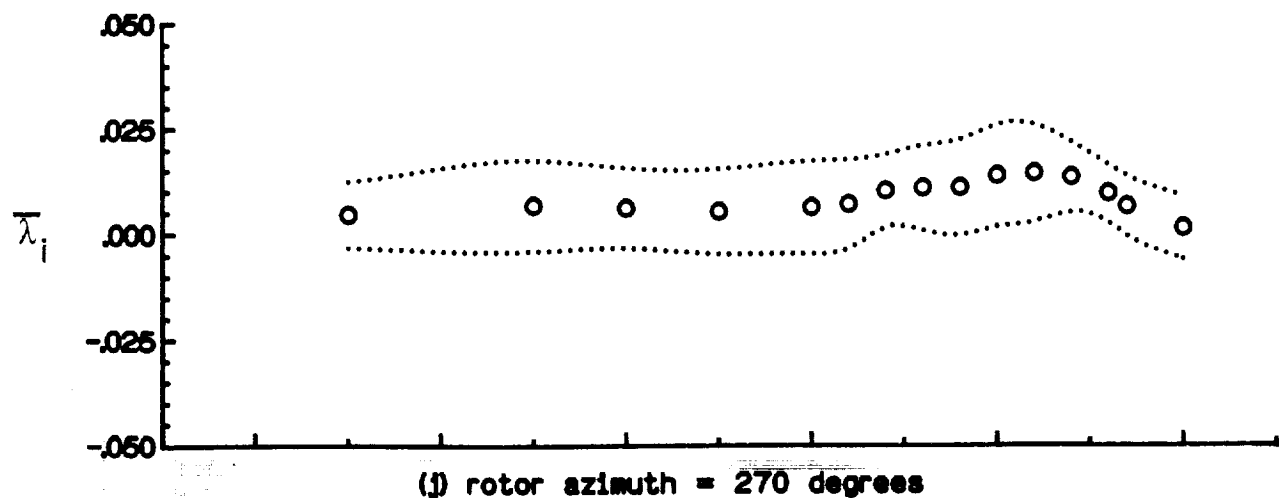


Figure 10.- Concluded.

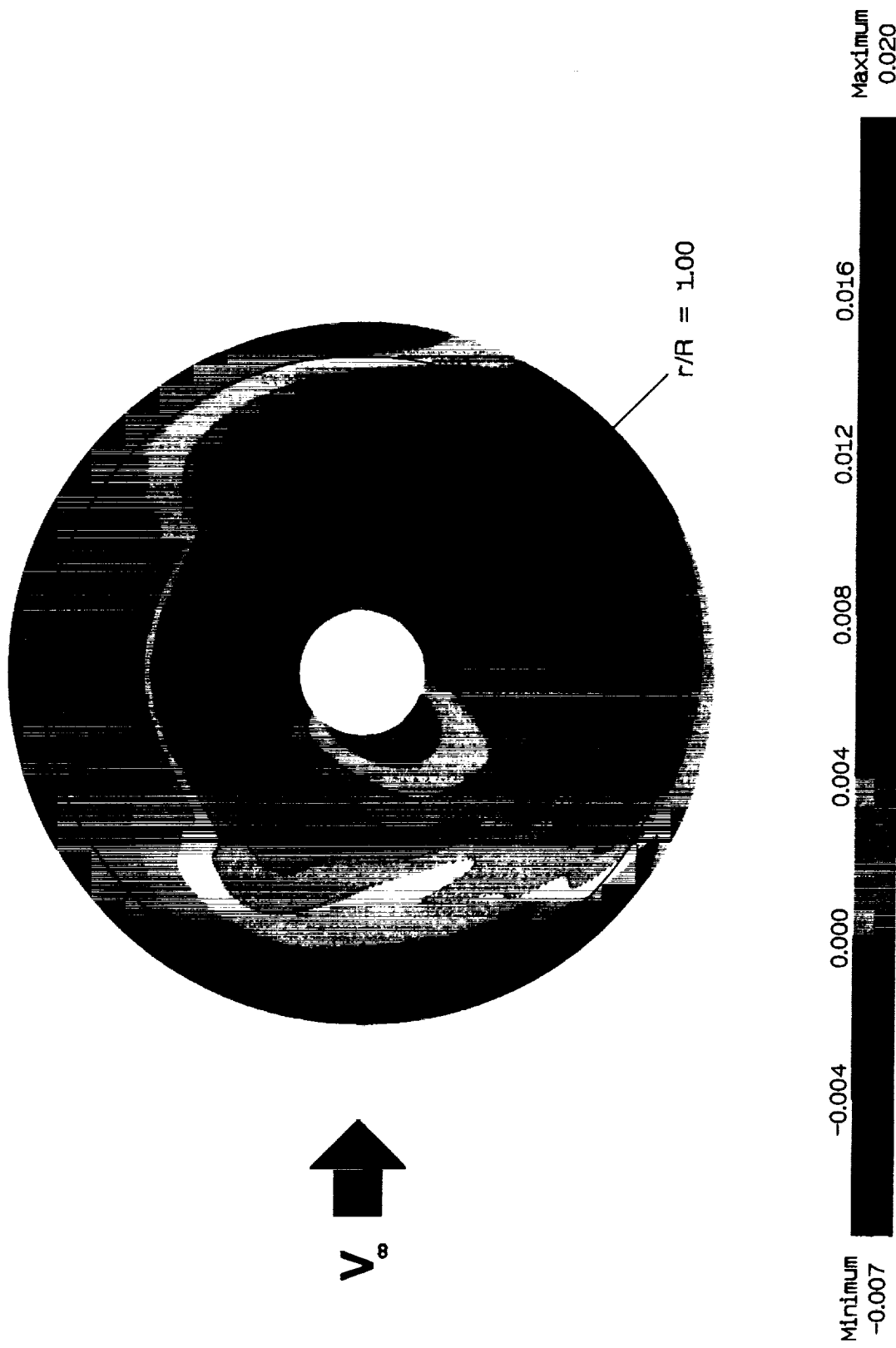


Figure 11. Contour plot of mean induced inflow ratio



Figure 12. Contour plot of mean induced inflow ratio

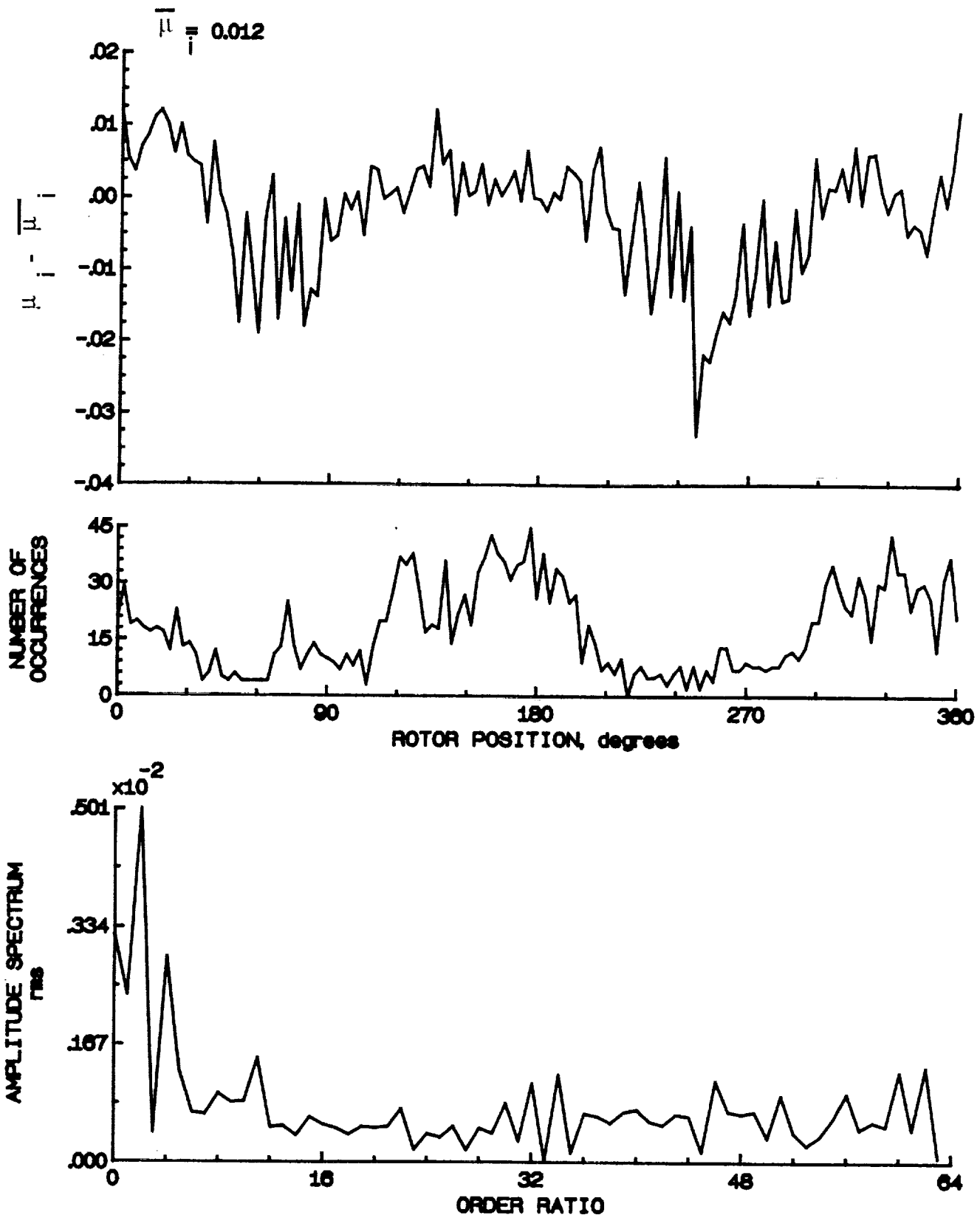


Figure 13.- Induced inflow velocity measured at 0 degrees and r/R of 0.40.

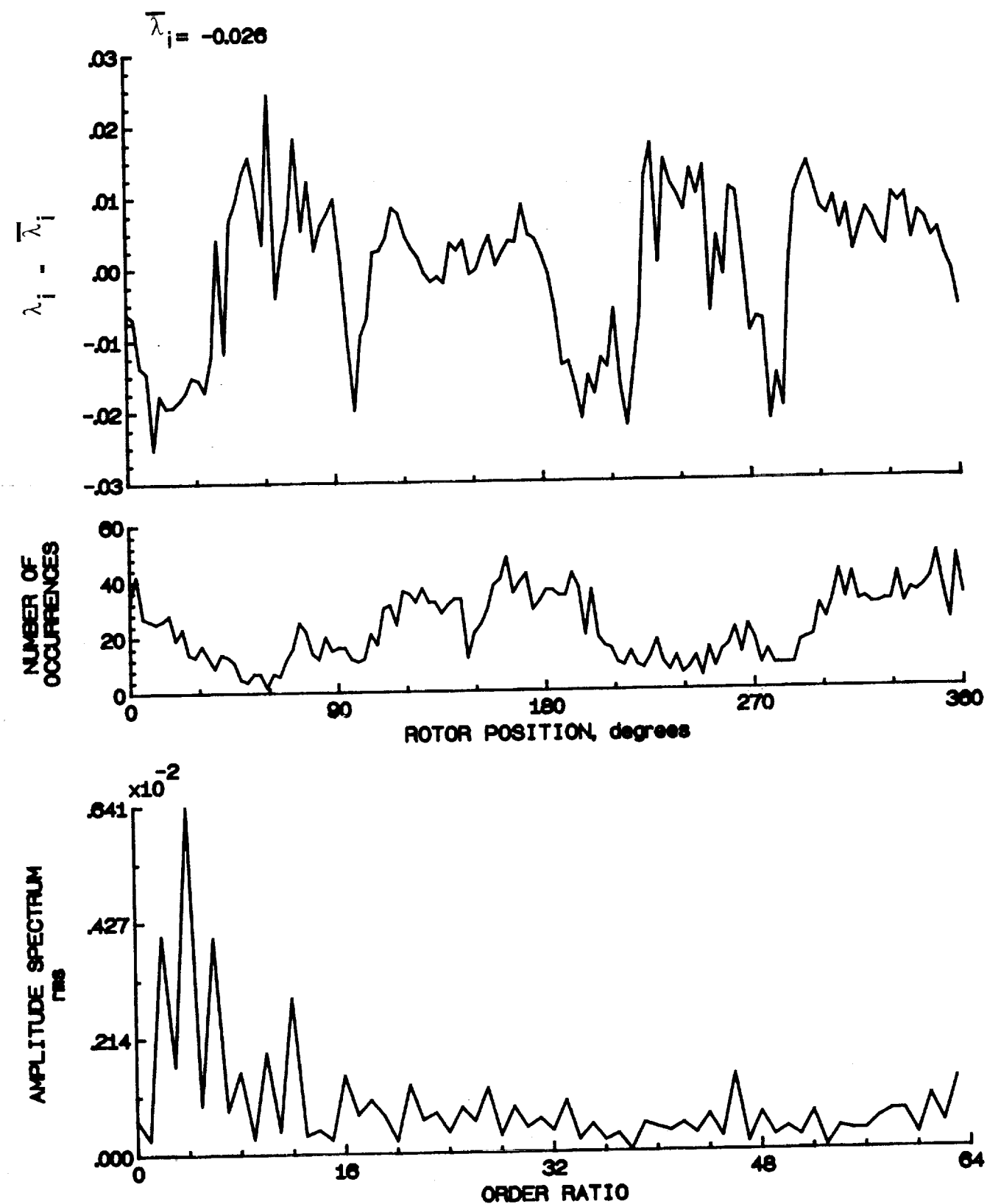


Figure 13.- Concluded.

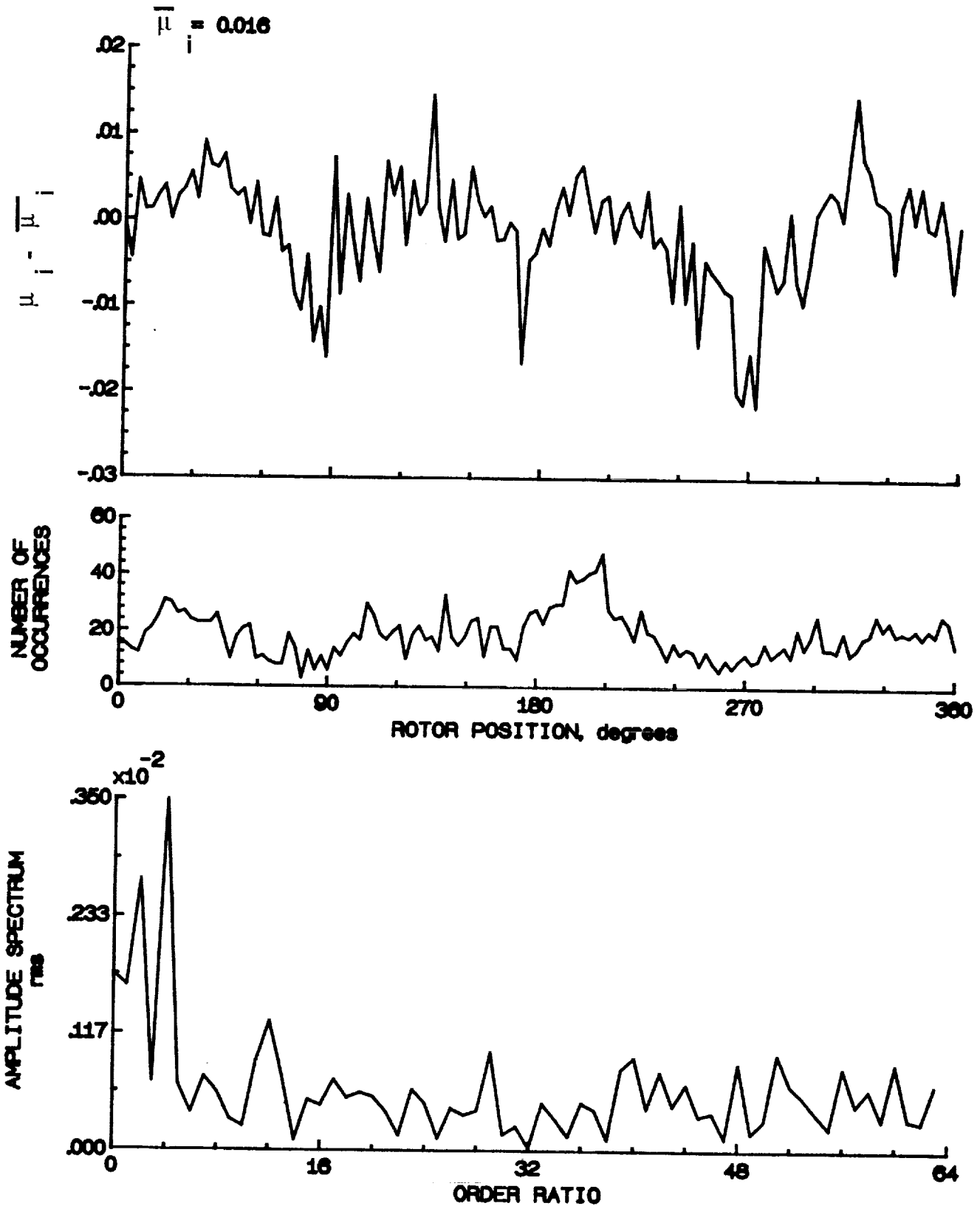


Figure 14.- Induced inflow velocity measured at 0 degrees and  $r/R$  of 0.50.

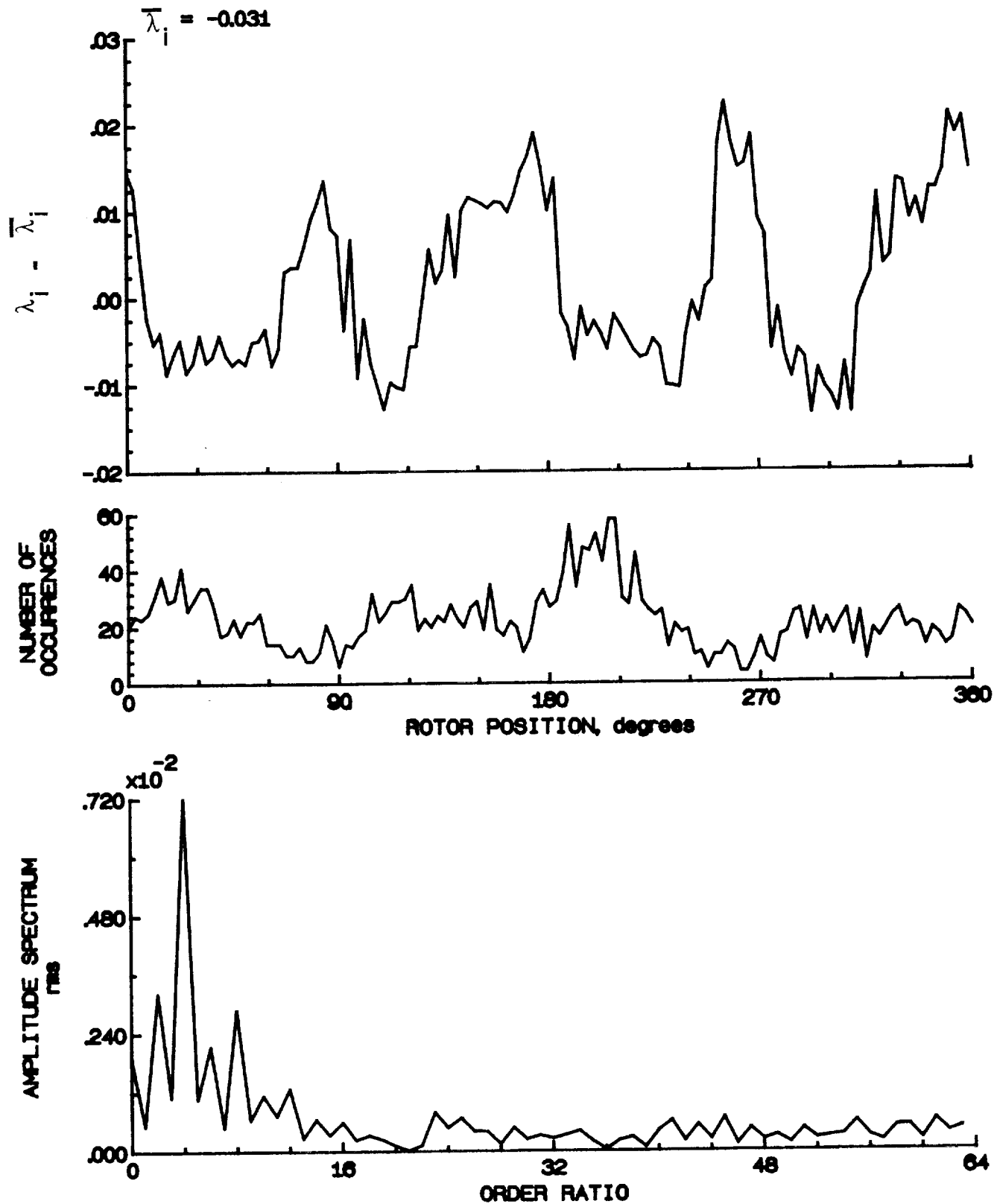


Figure 14.- Concluded.

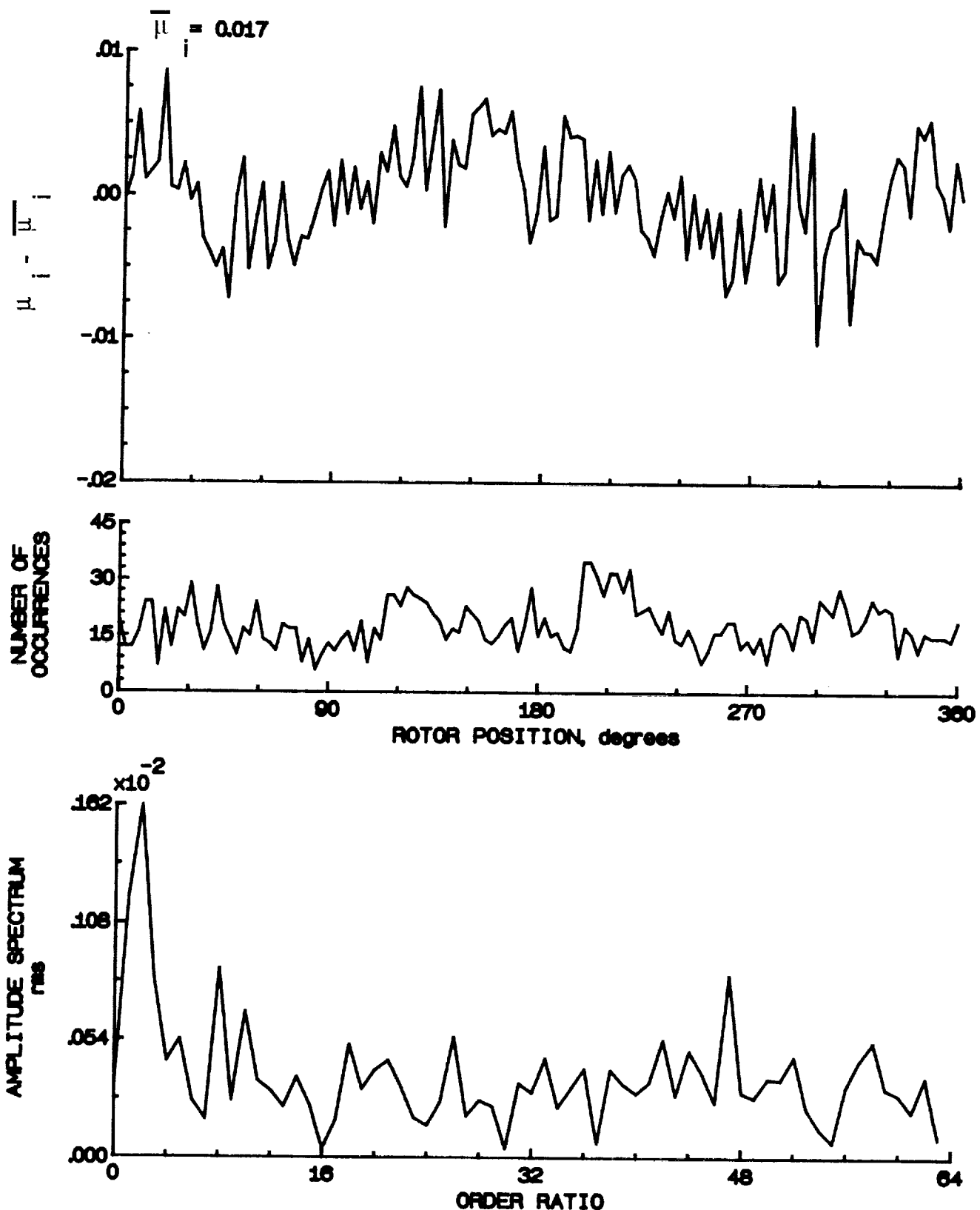


Figure 15.- Induced inflow velocity measured at 0 degrees and r/R of 0.60.

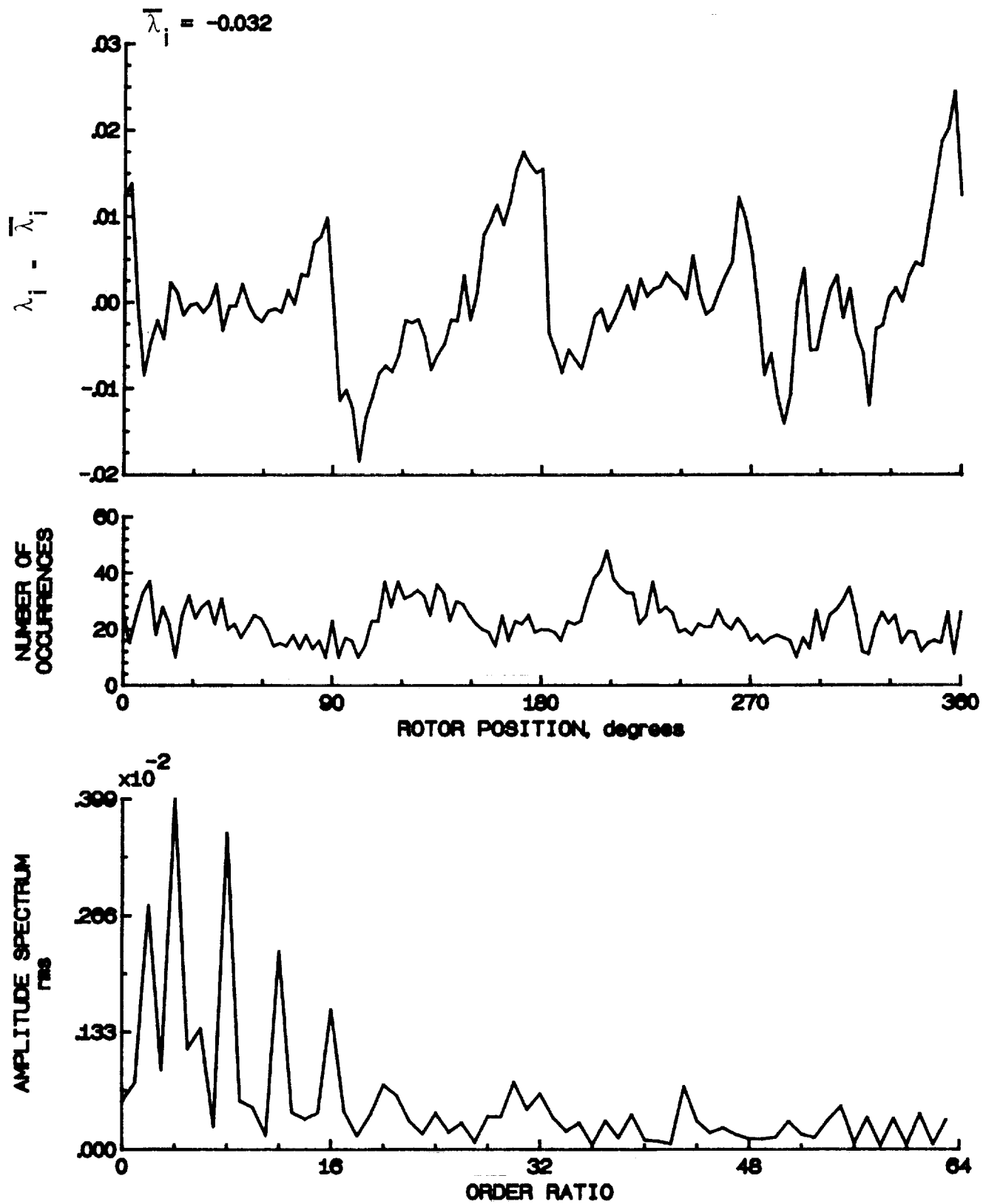


Figure 15.- Concluded.

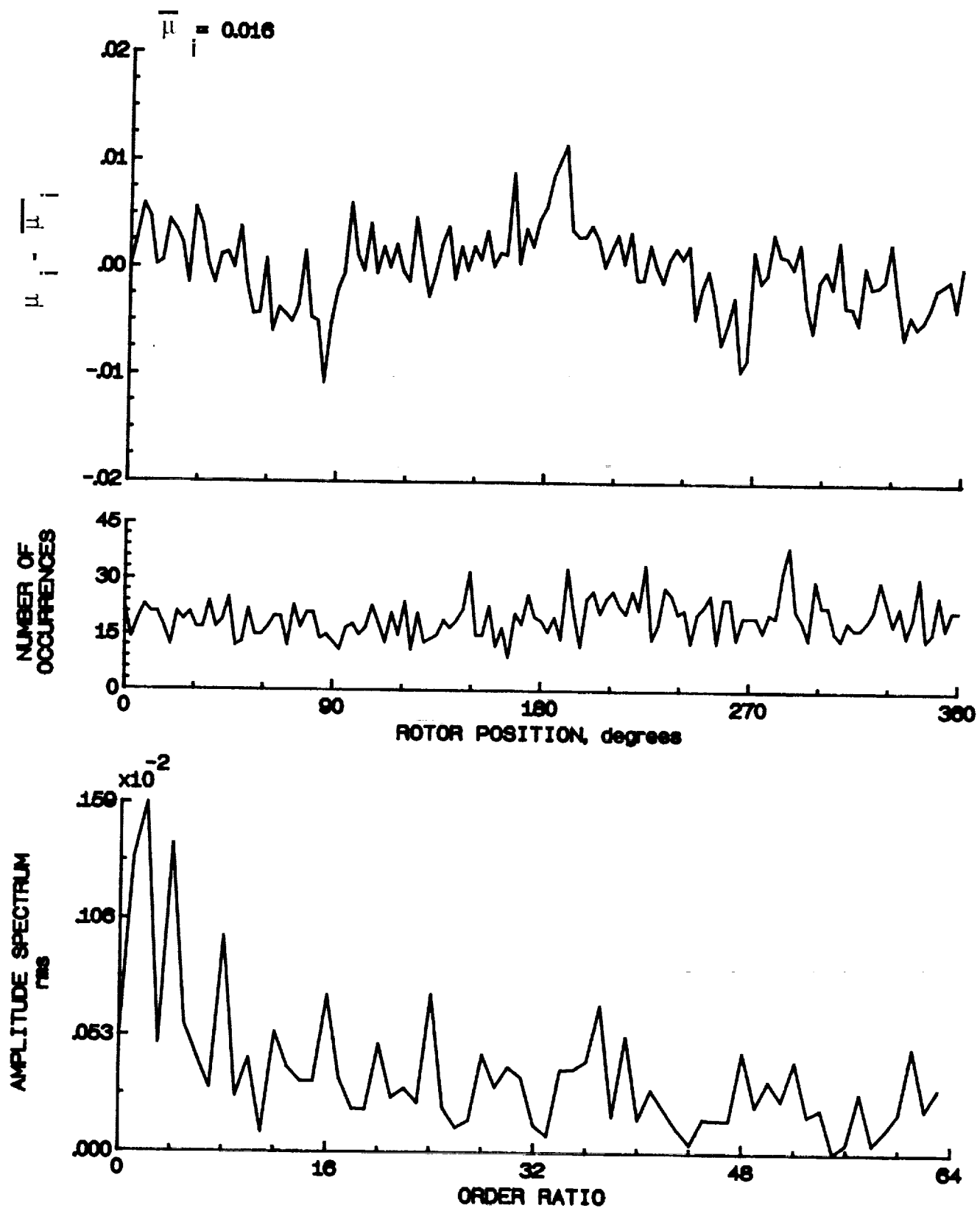


Figure 16.- Induced inflow velocity measured at 0 degrees and r/R of 0.70.

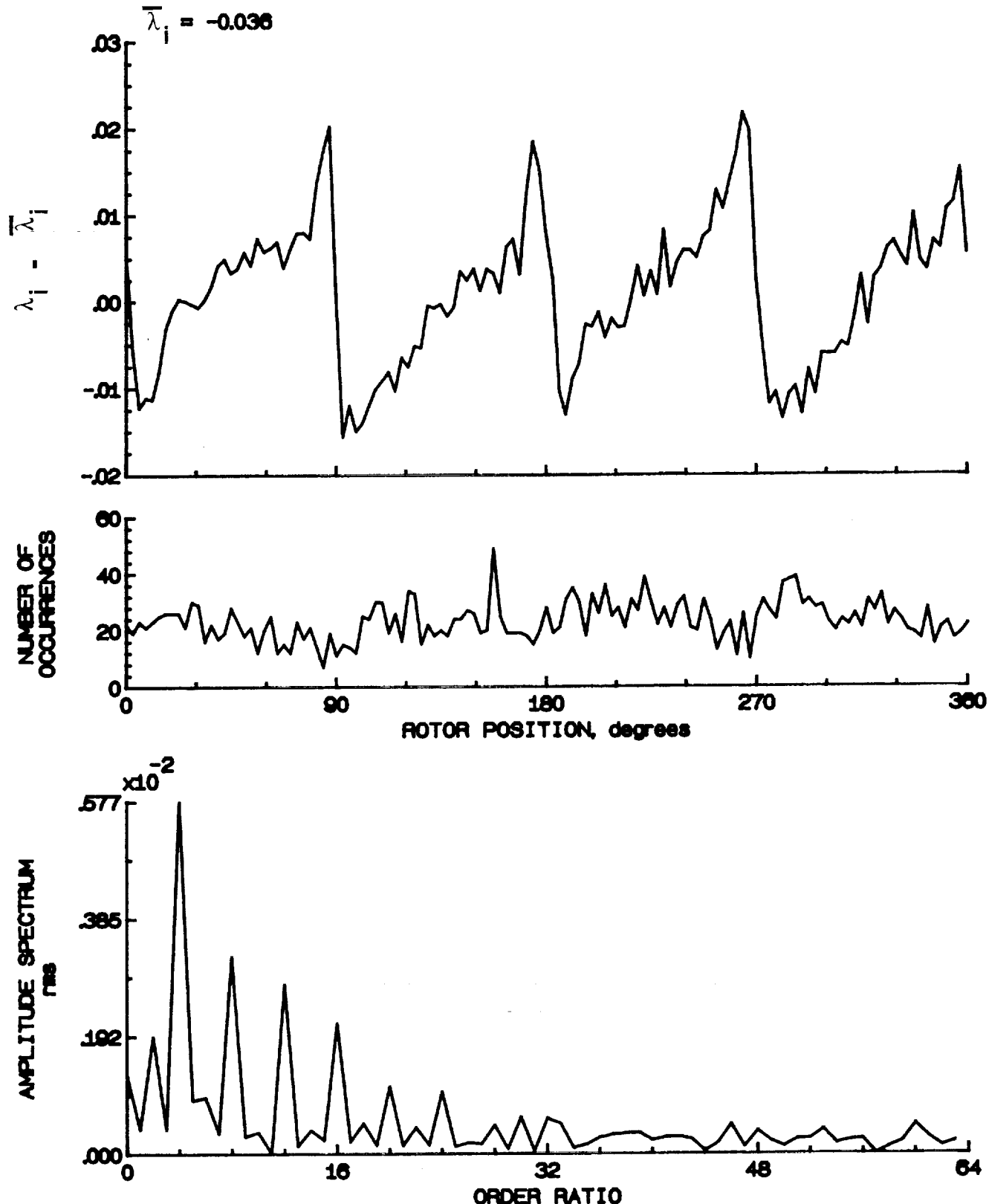


Figure 16.- Concluded.

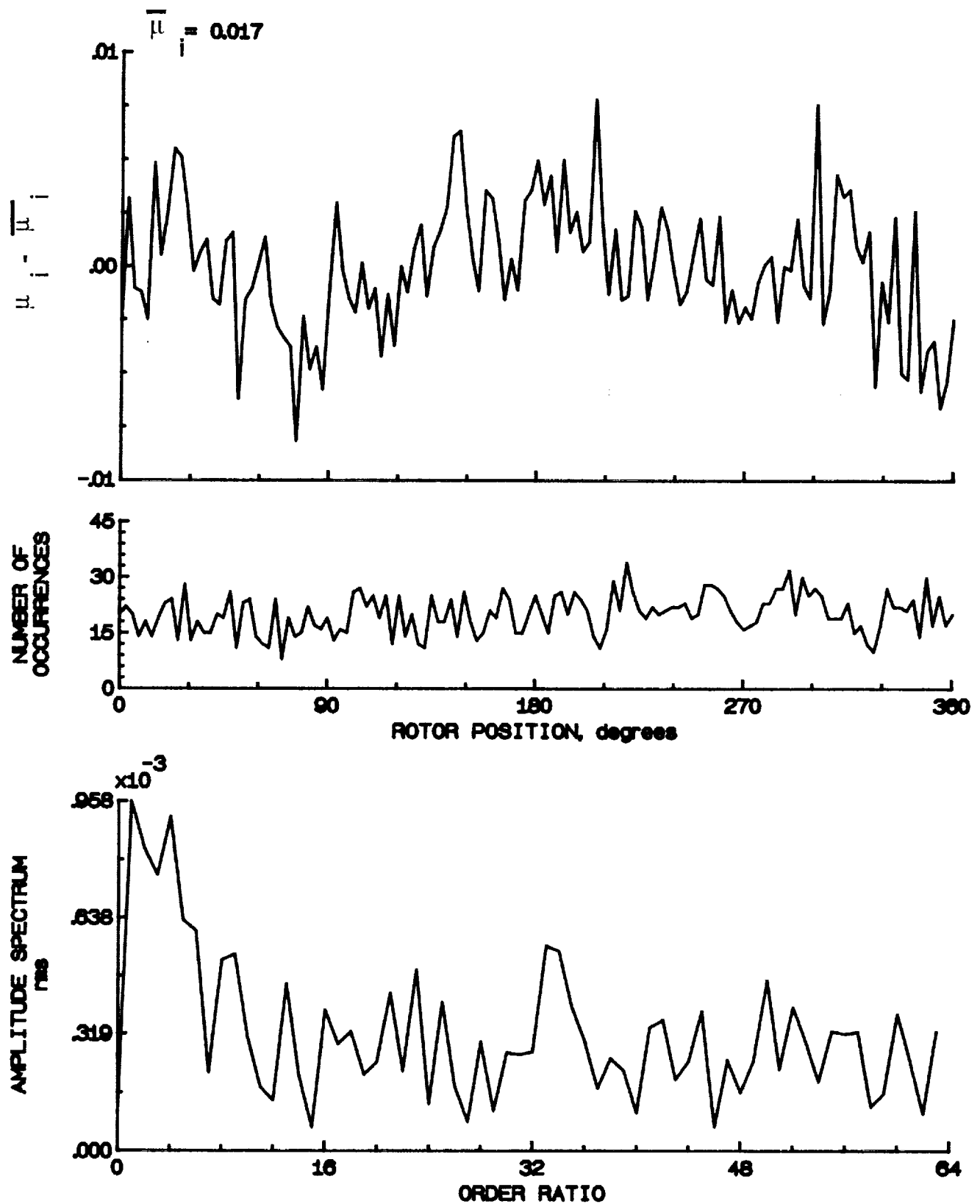


Figure 17.- Induced inflow velocity measured at 0 degrees and r/R of 0.74.

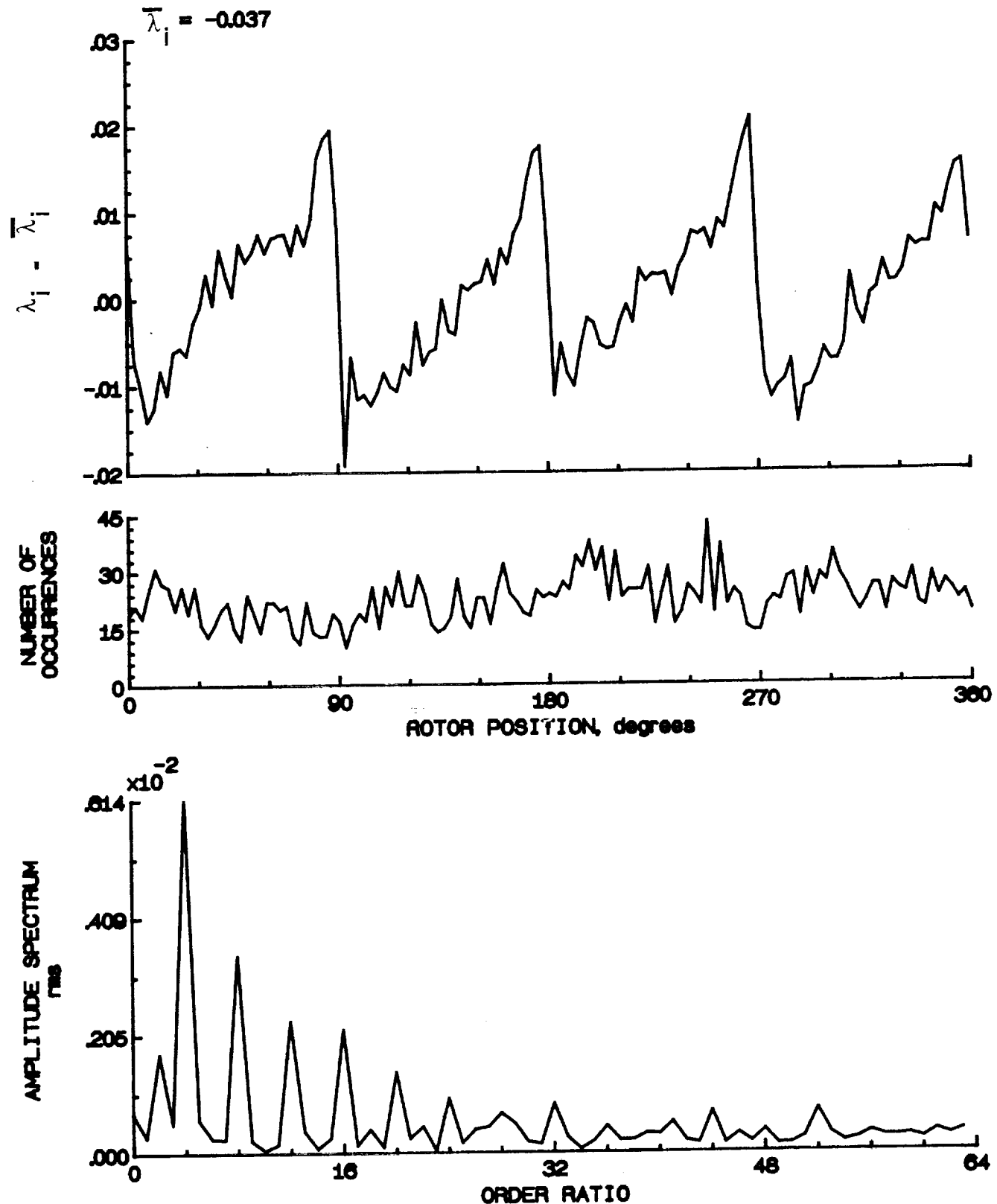


Figure 17.- Concluded.

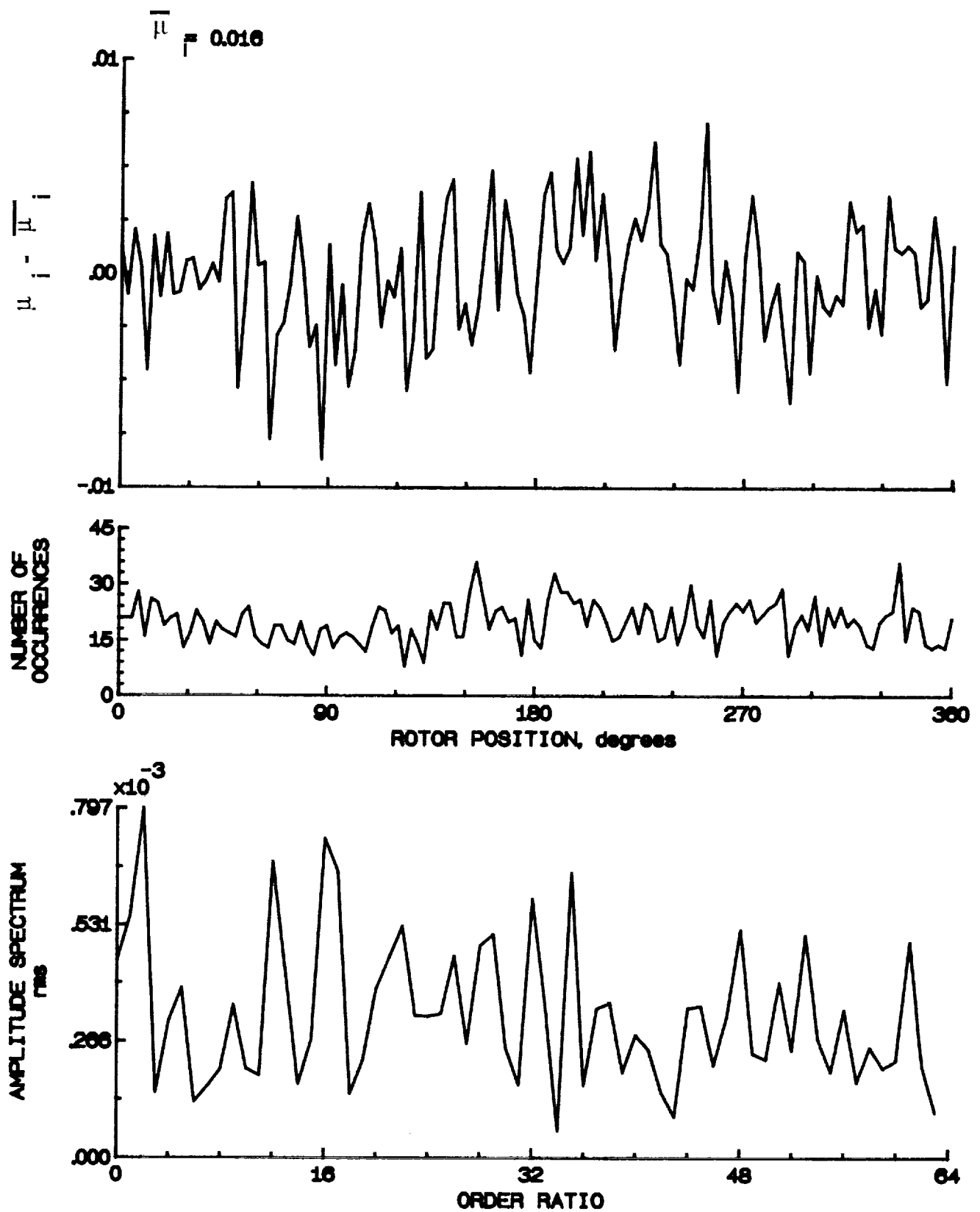


Figure 18.- Induced inflow velocity measured at 0 degrees and r/R of 0.78.

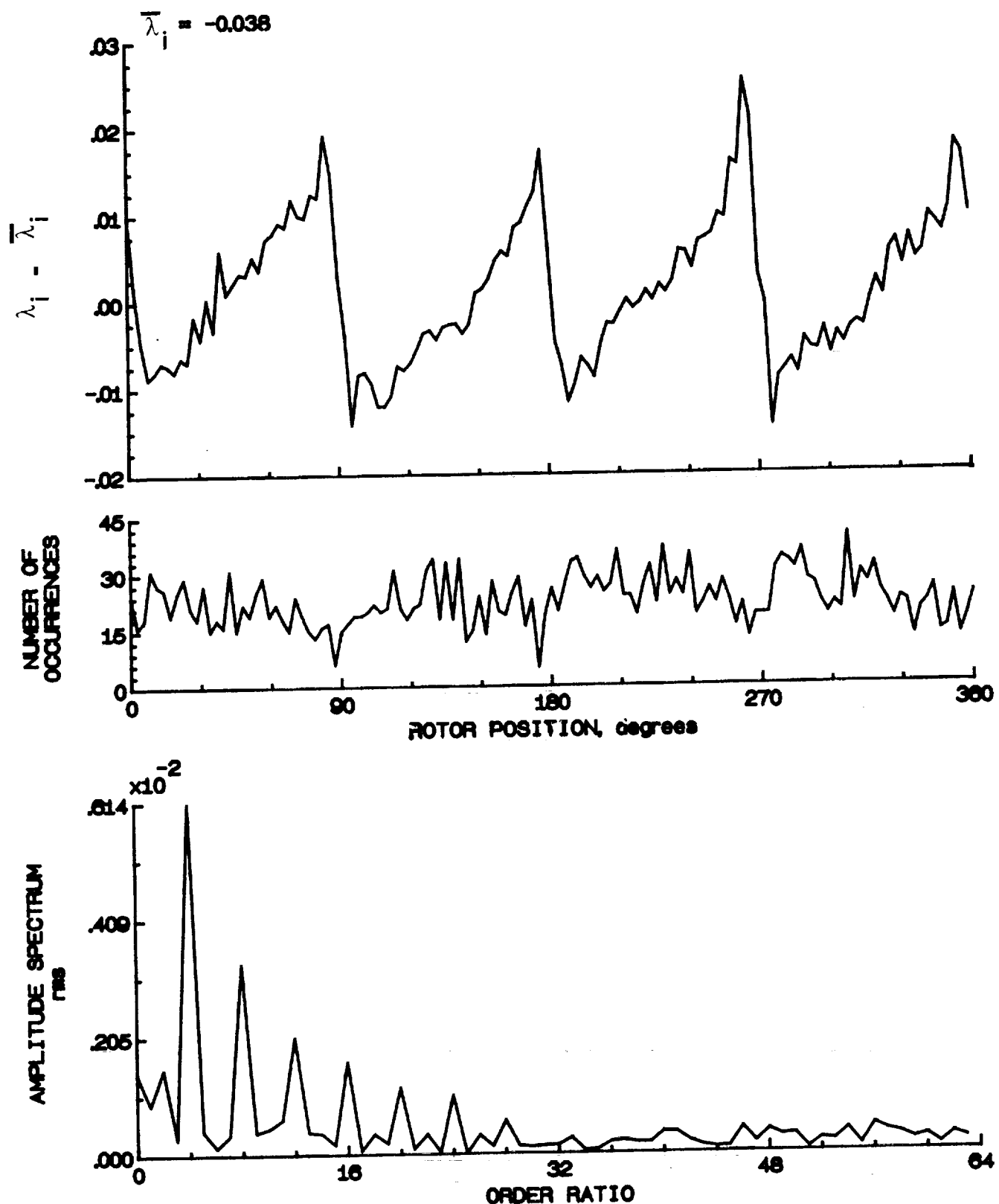


Figure 18.- Concluded.

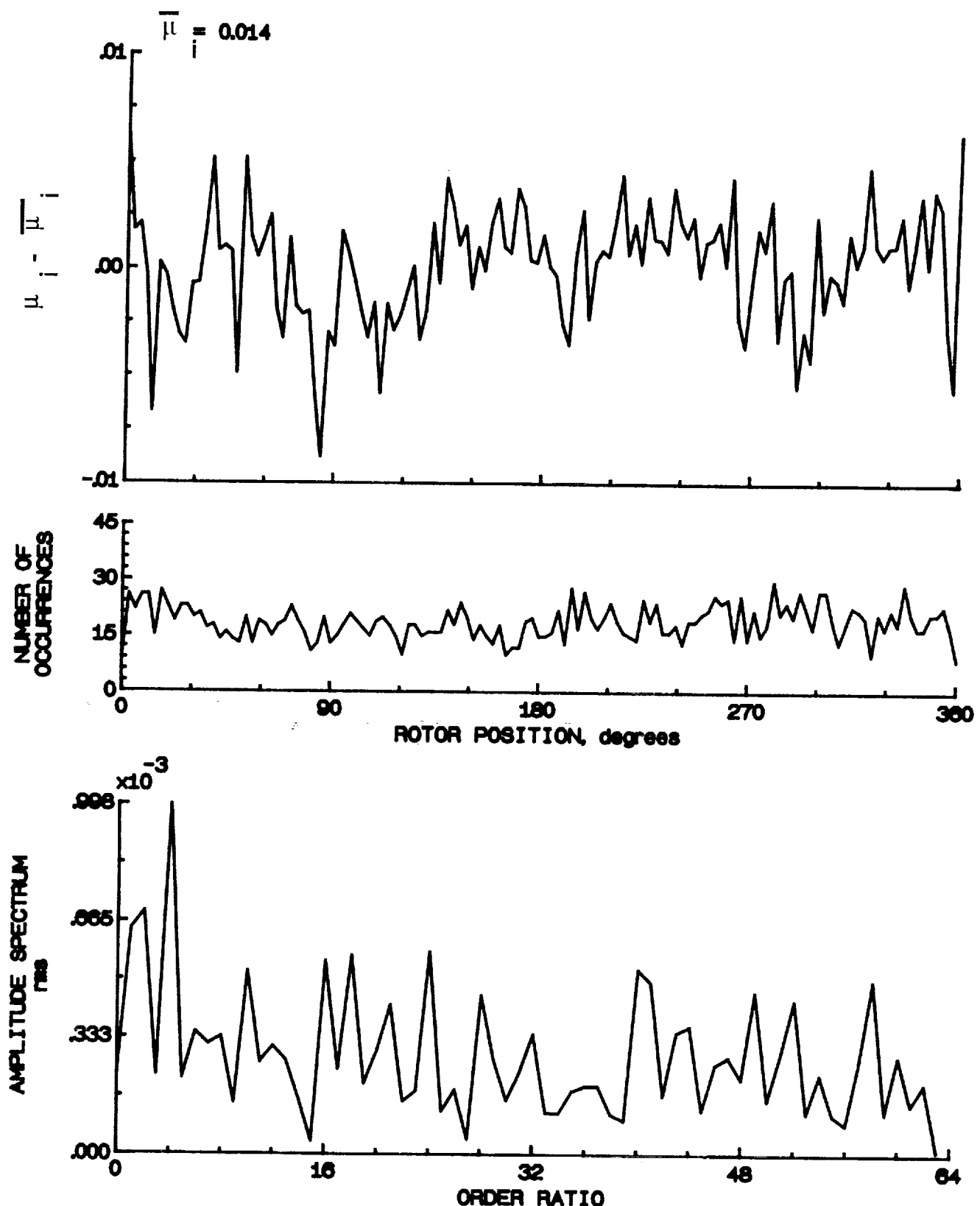


Figure 19.- Induced inflow velocity measured at 0 degrees and r/R of 0.82.

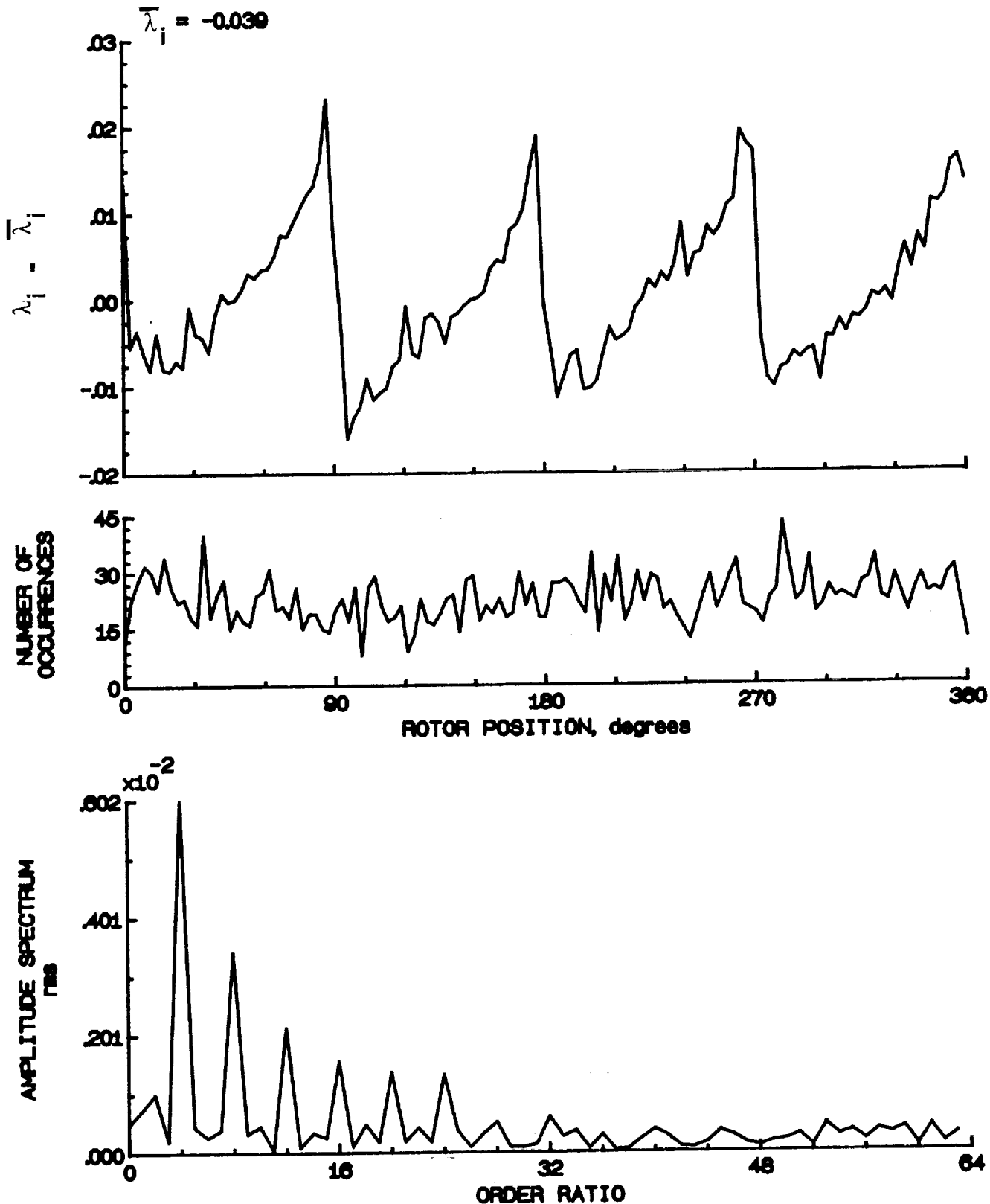


Figure 19.- Concluded.

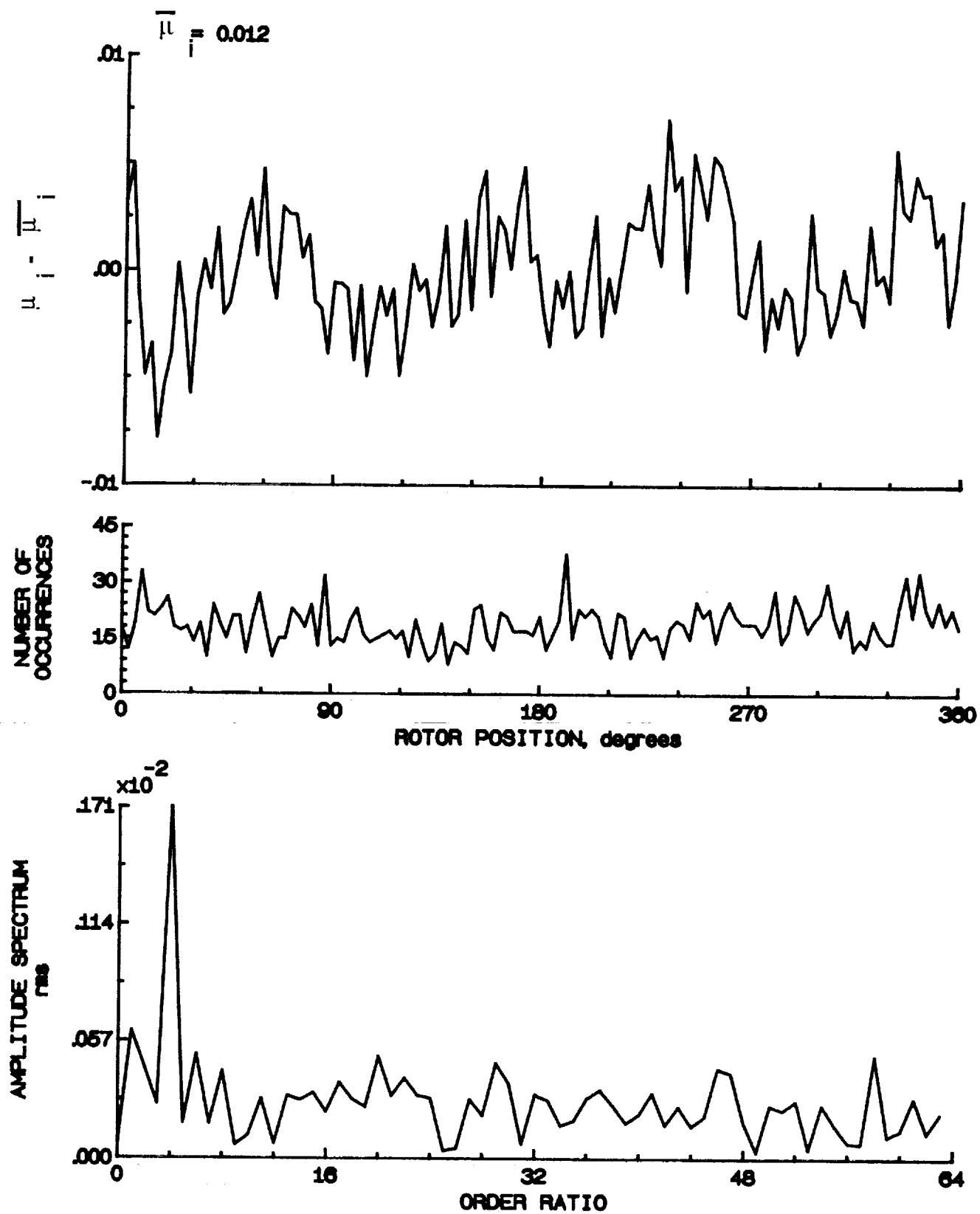


Figure 20.- Induced inflow velocity measured at 0 degrees and r/R of 0.86.

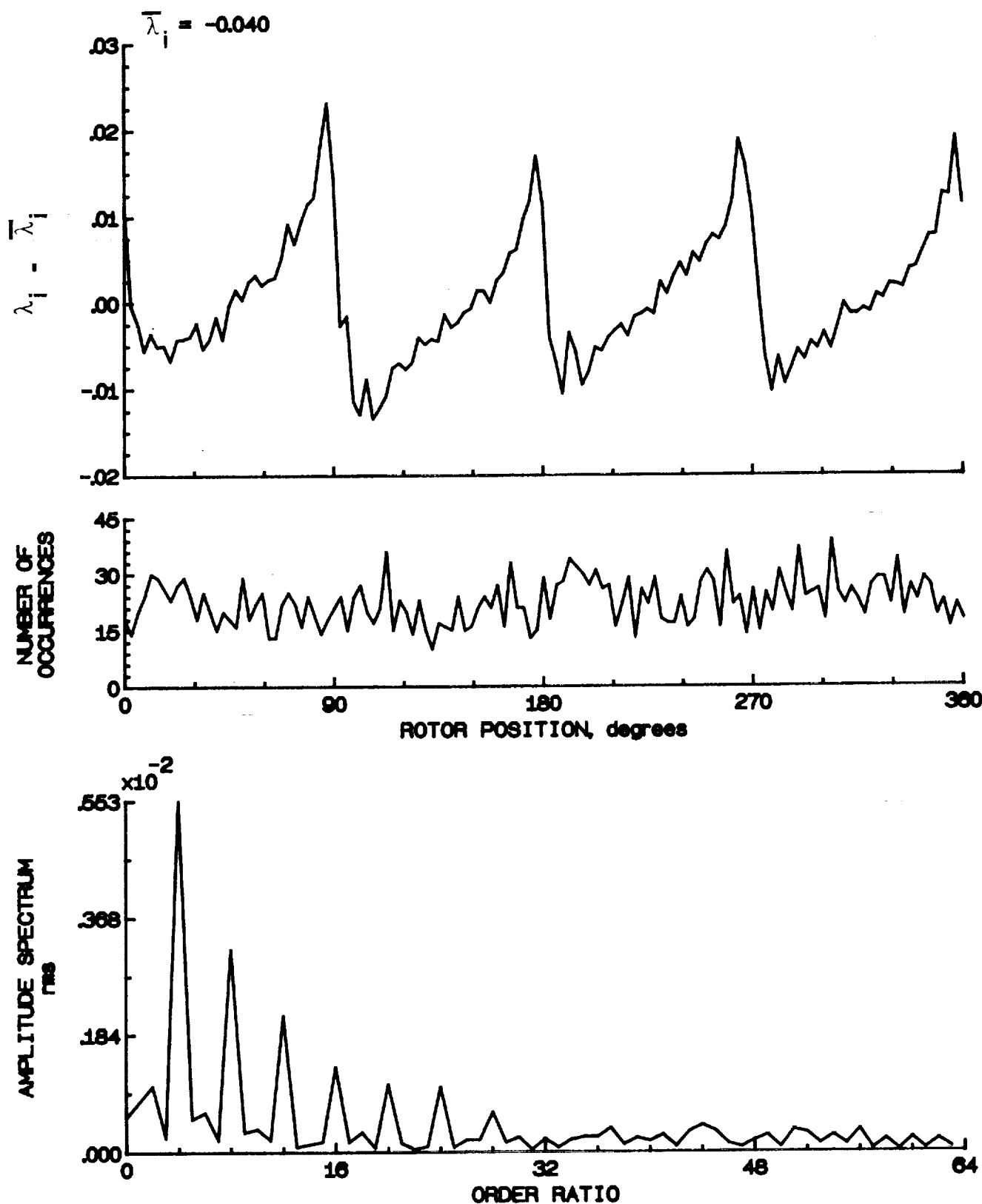


Figure 20.- Concluded.

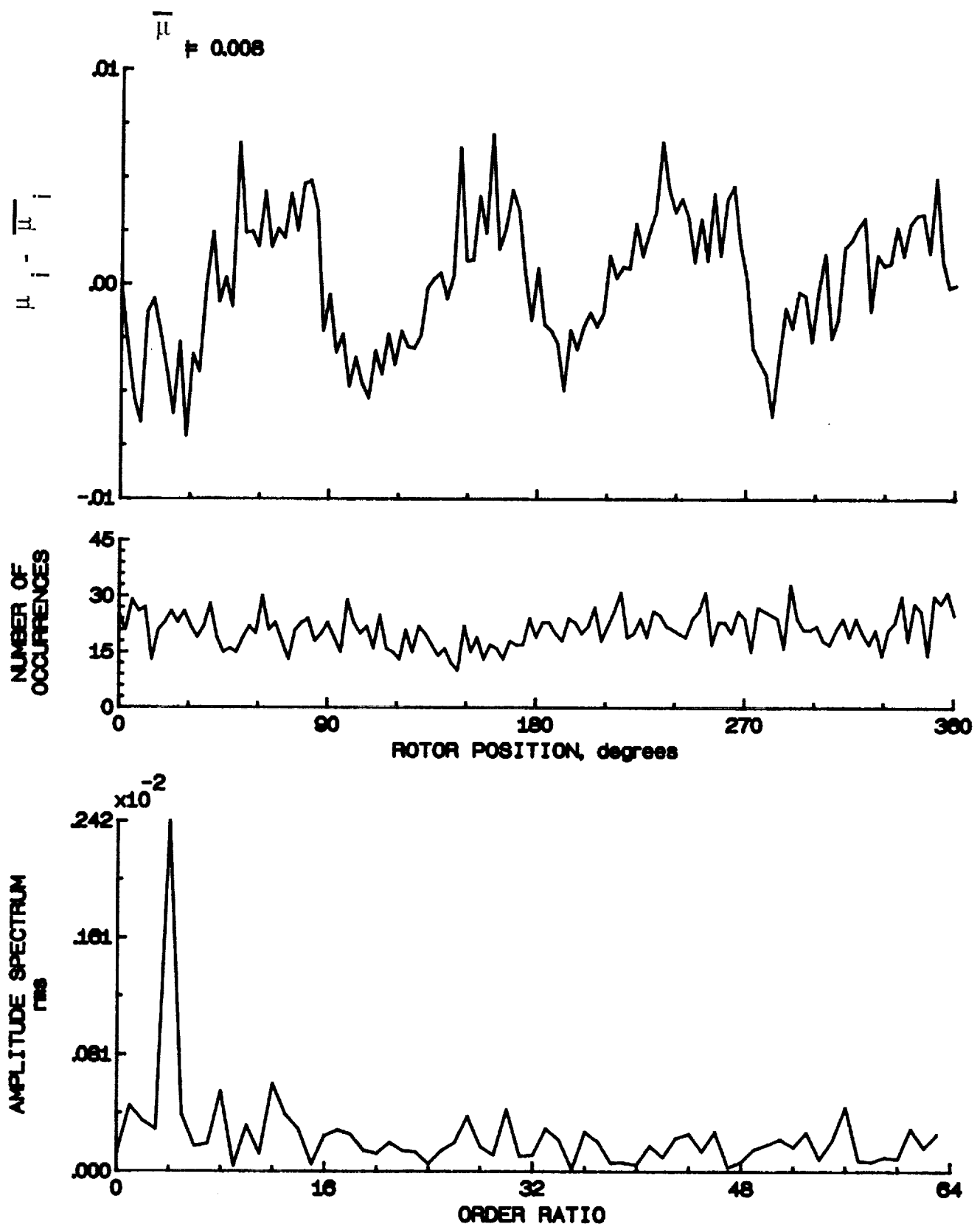


Figure 21.- Induced inflow velocity measured at 0 degrees and r/R of 0.90.

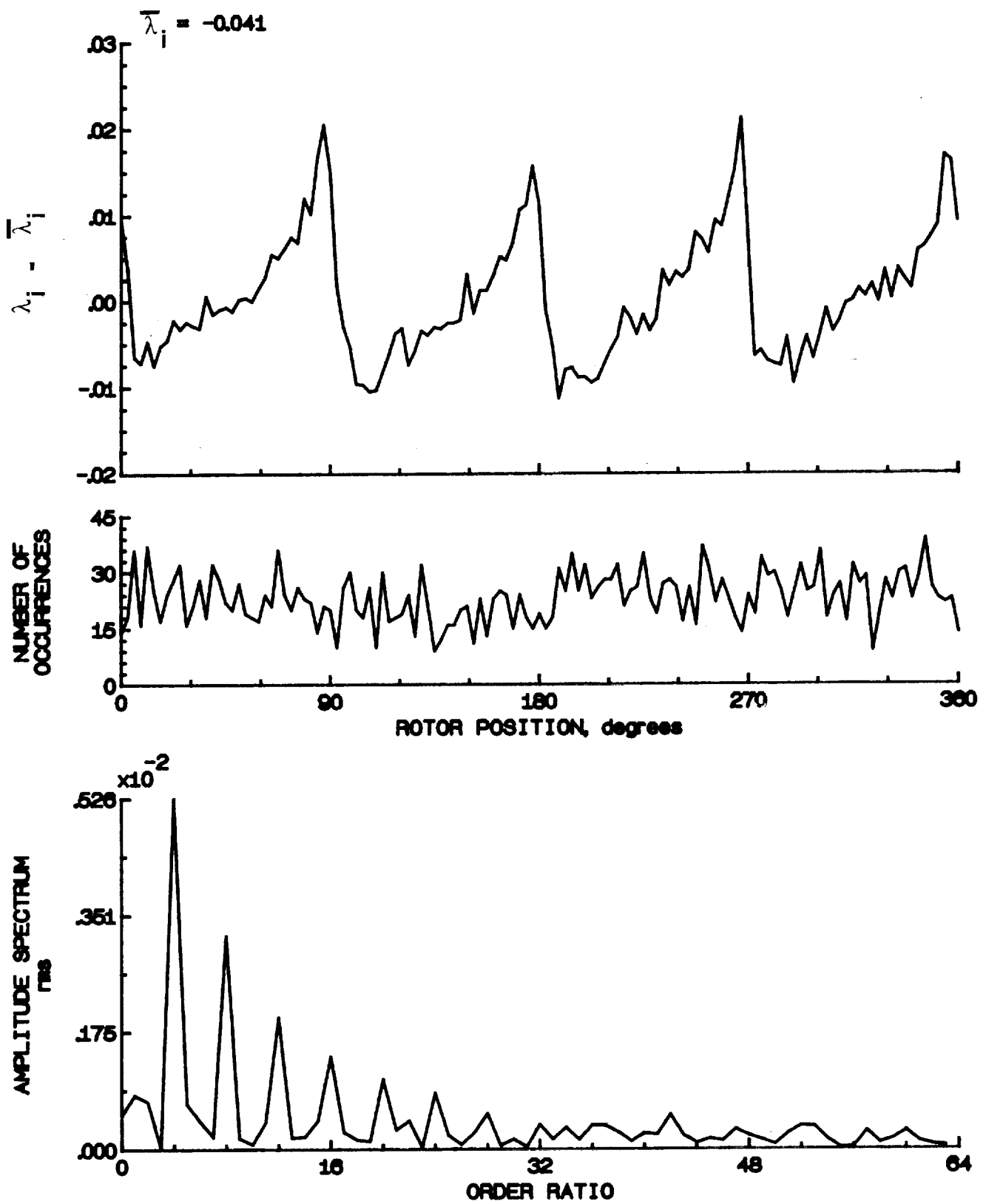


Figure 21.- Concluded.

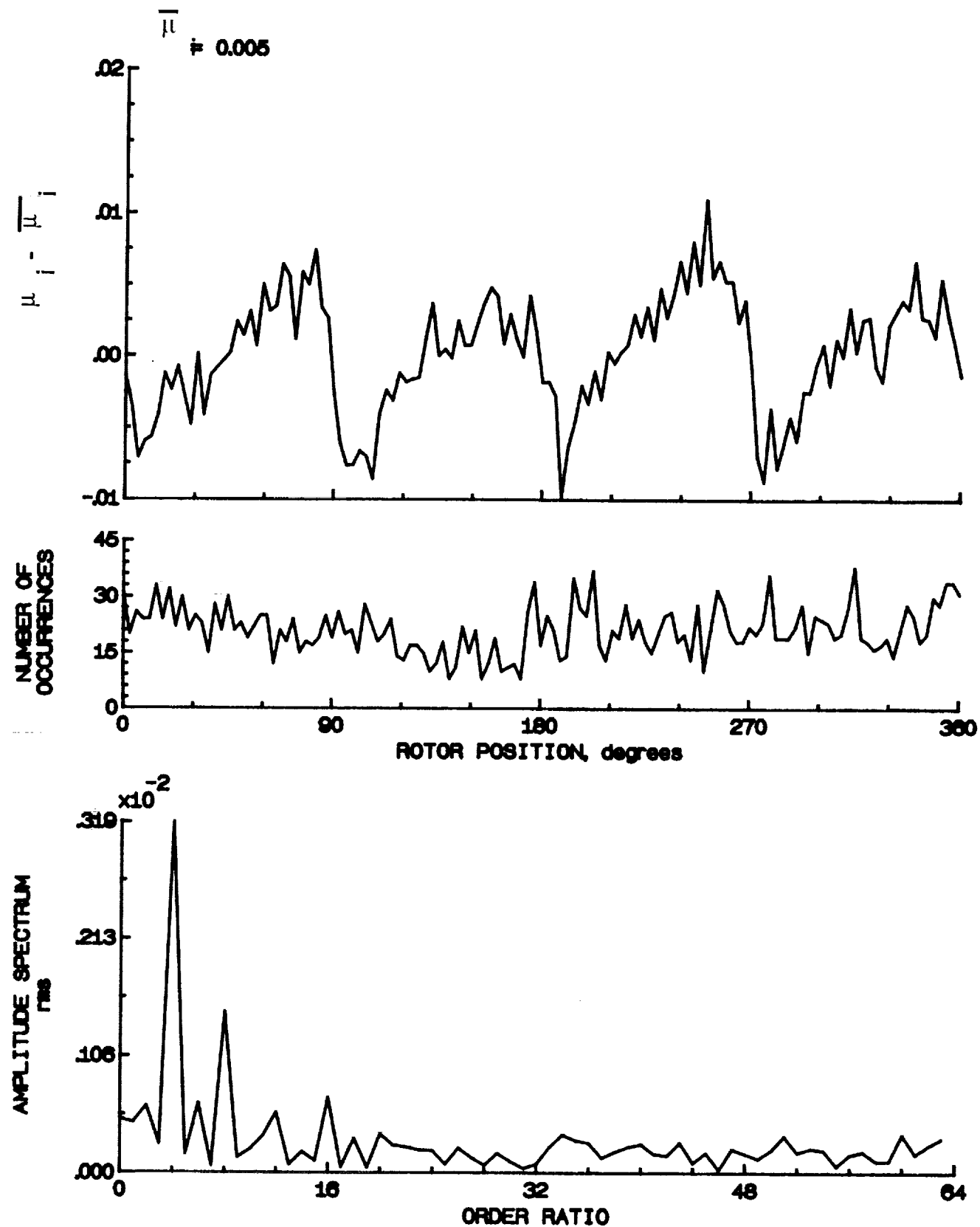


Figure 22.- Induced inflow velocity measured at 0 degrees and r/R of 0.94.

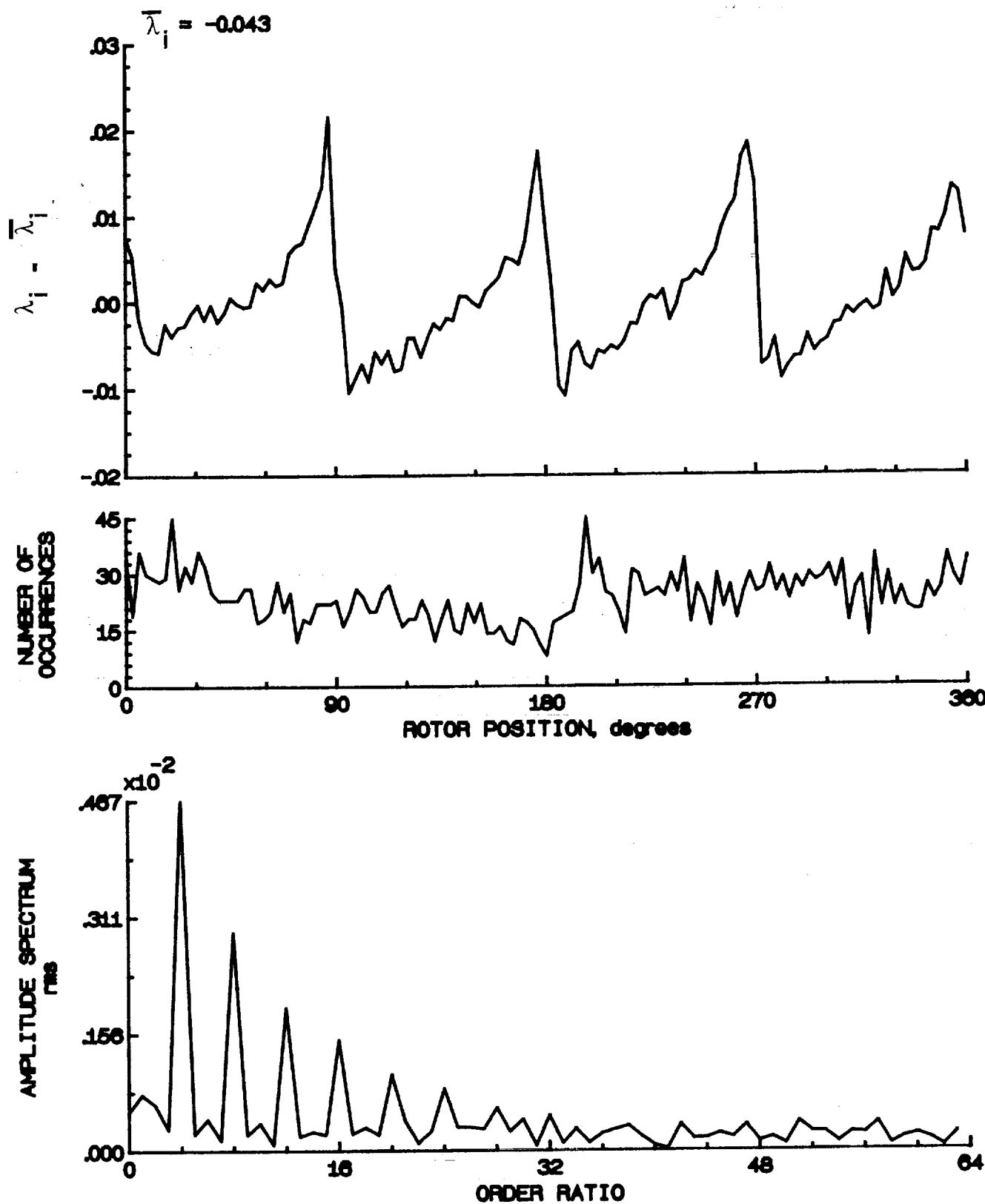


Figure 22.- Concluded.

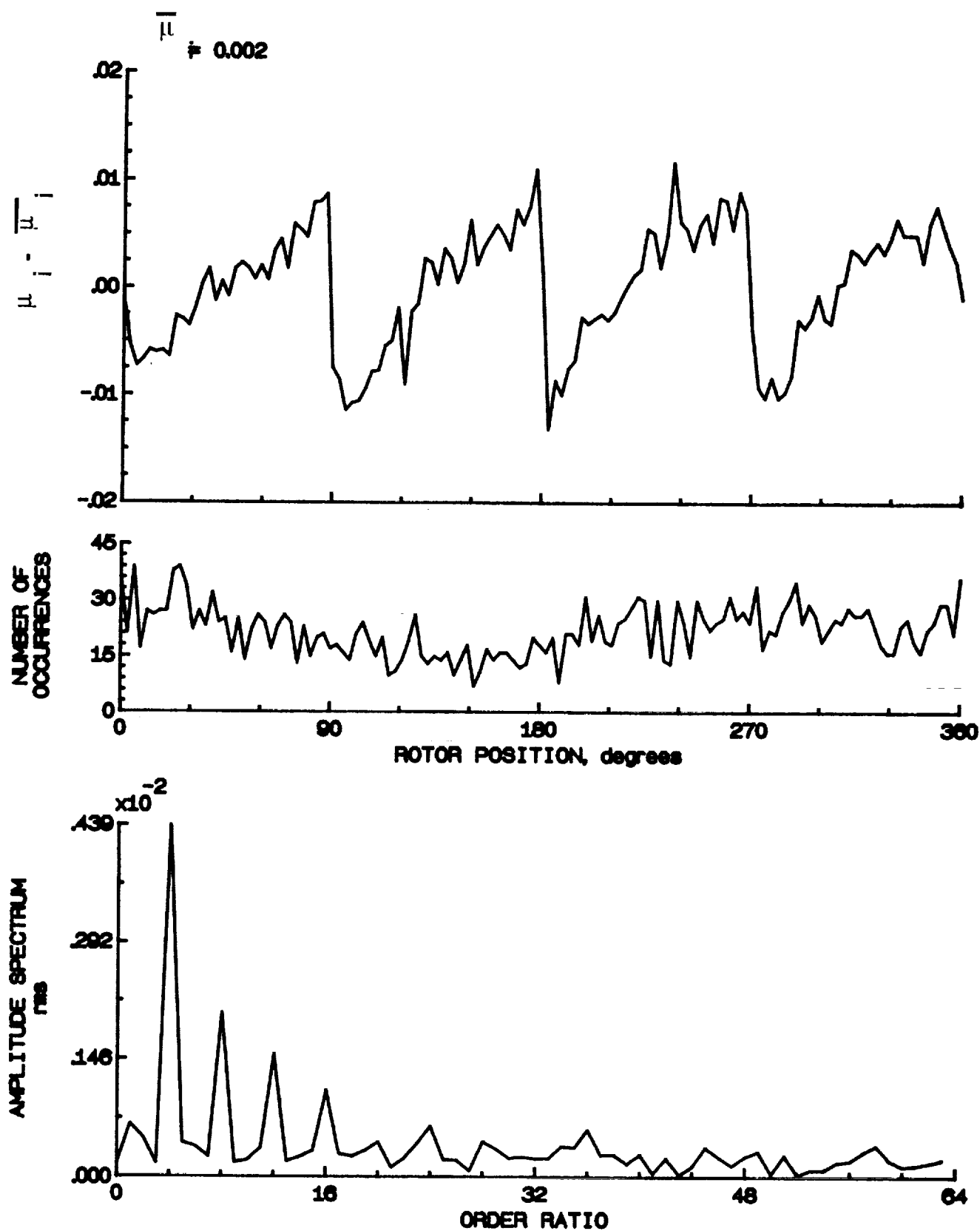


Figure 23.- Induced inflow velocity measured at 0 degrees and r/R of 0.98.

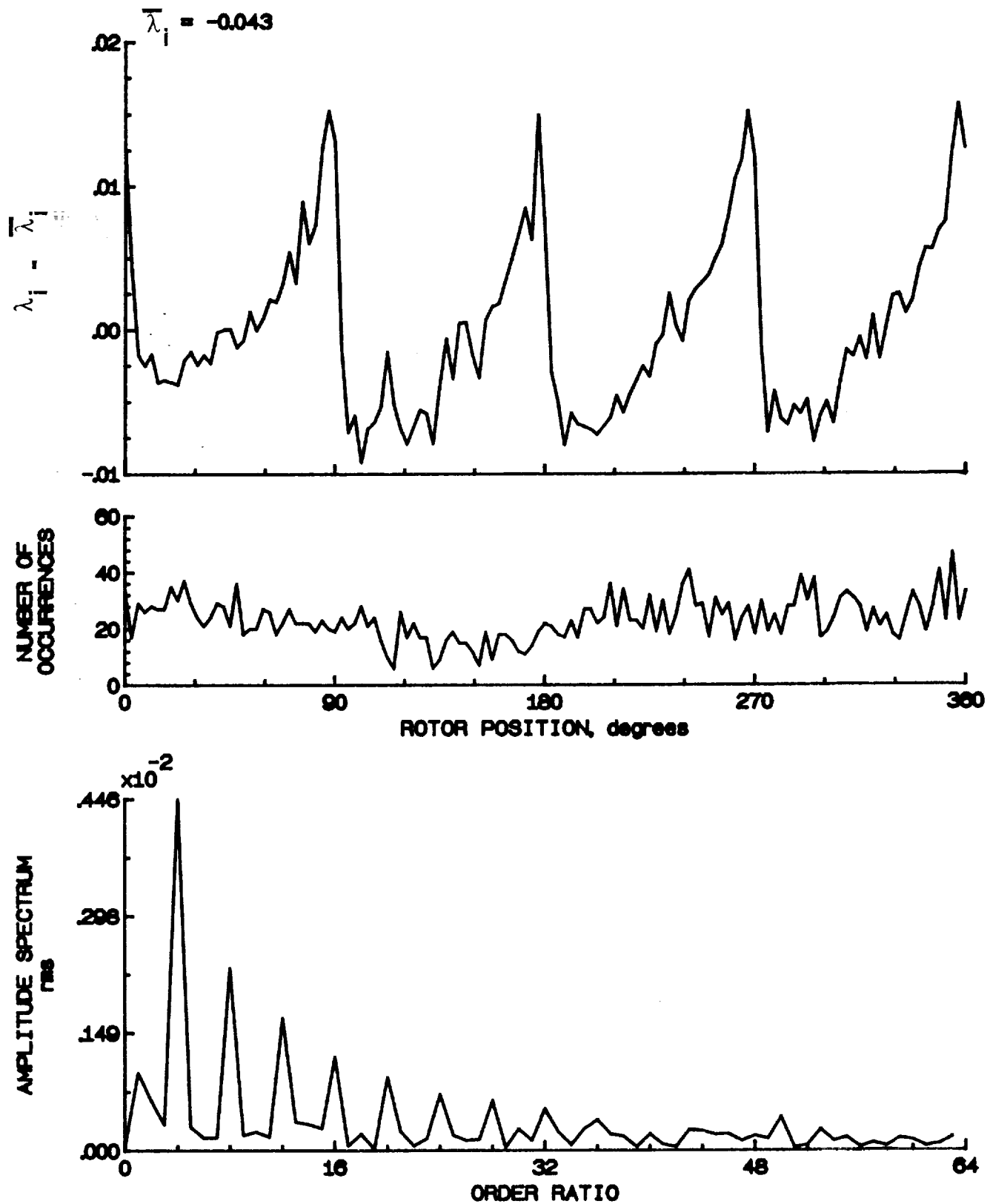


Figure 23.- Concluded.

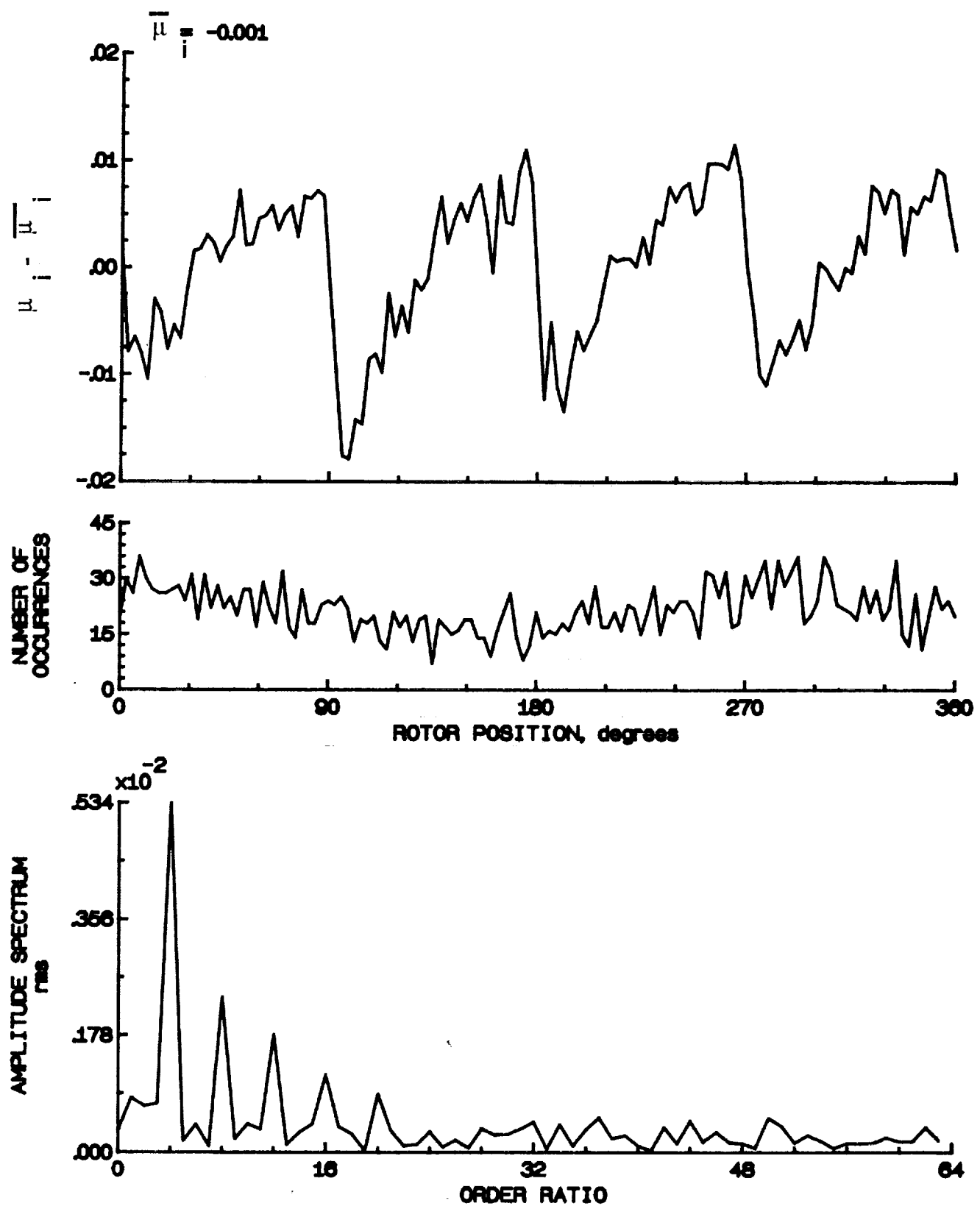


Figure 24.- Induced inflow velocity measured at 0 degrees and r/R of 1.02.

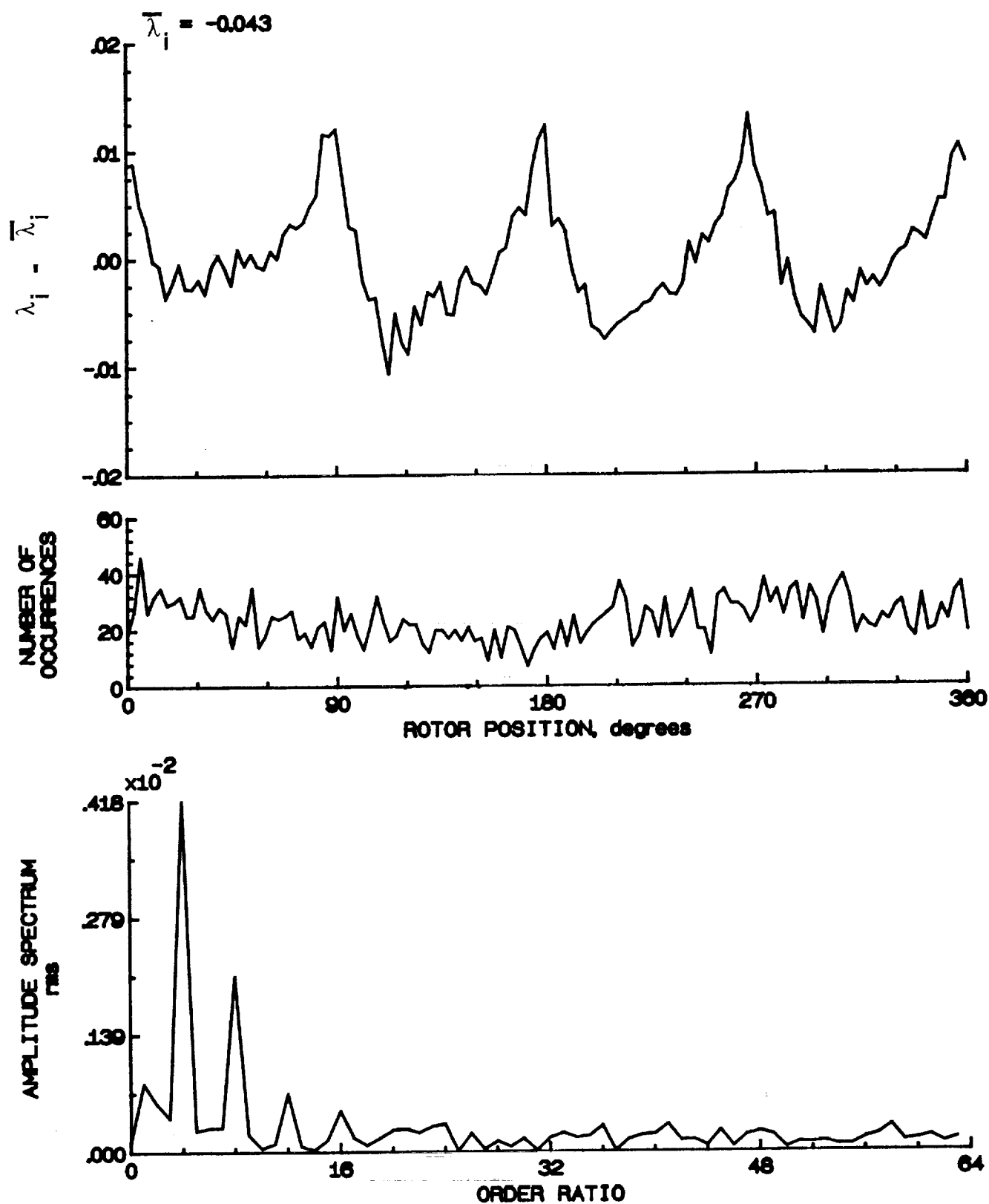


Figure 24.- Concluded.

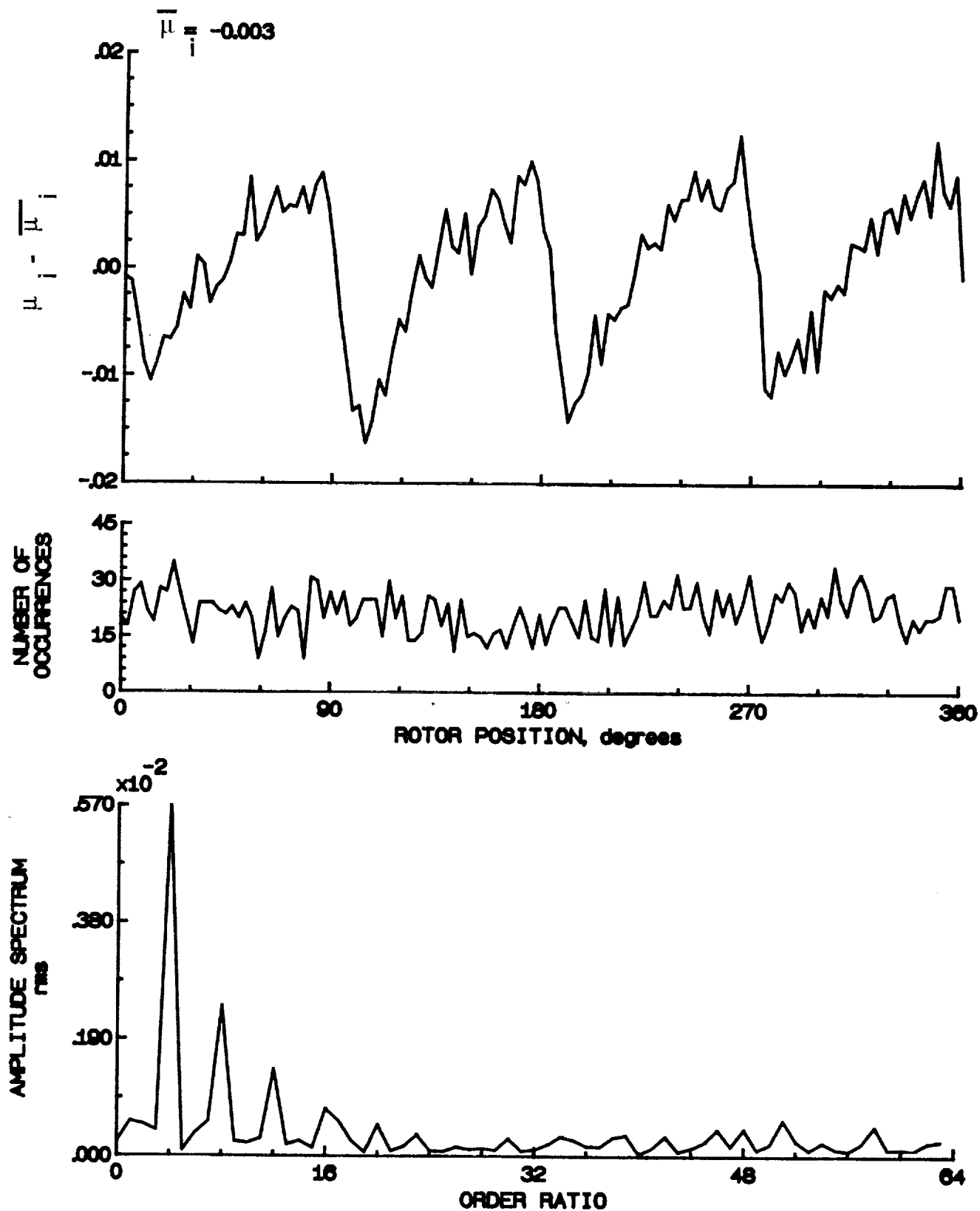


Figure 25.- Induced inflow velocity measured at 0 degrees and r/R of 1.04.

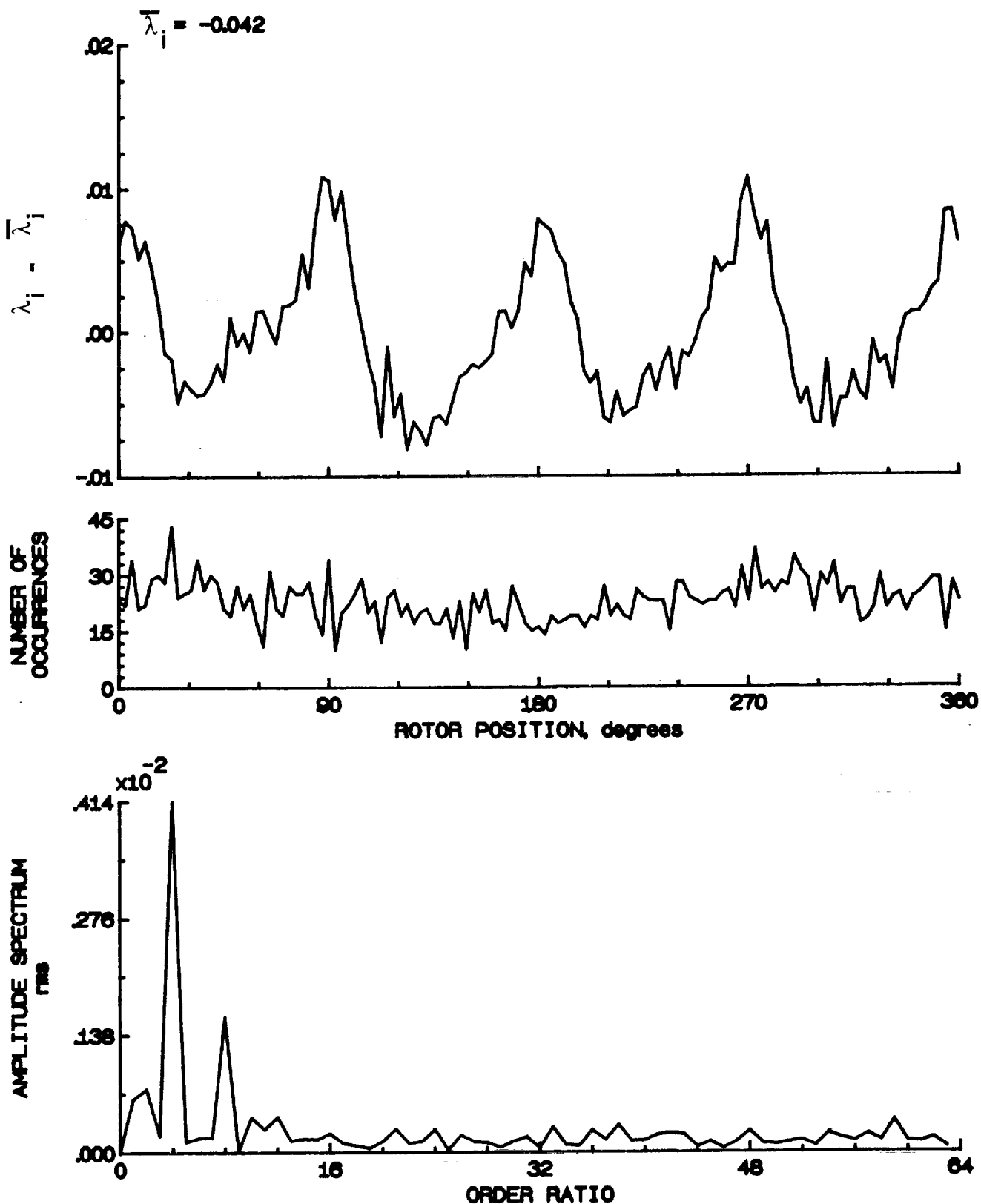


Figure 25.- Concluded.

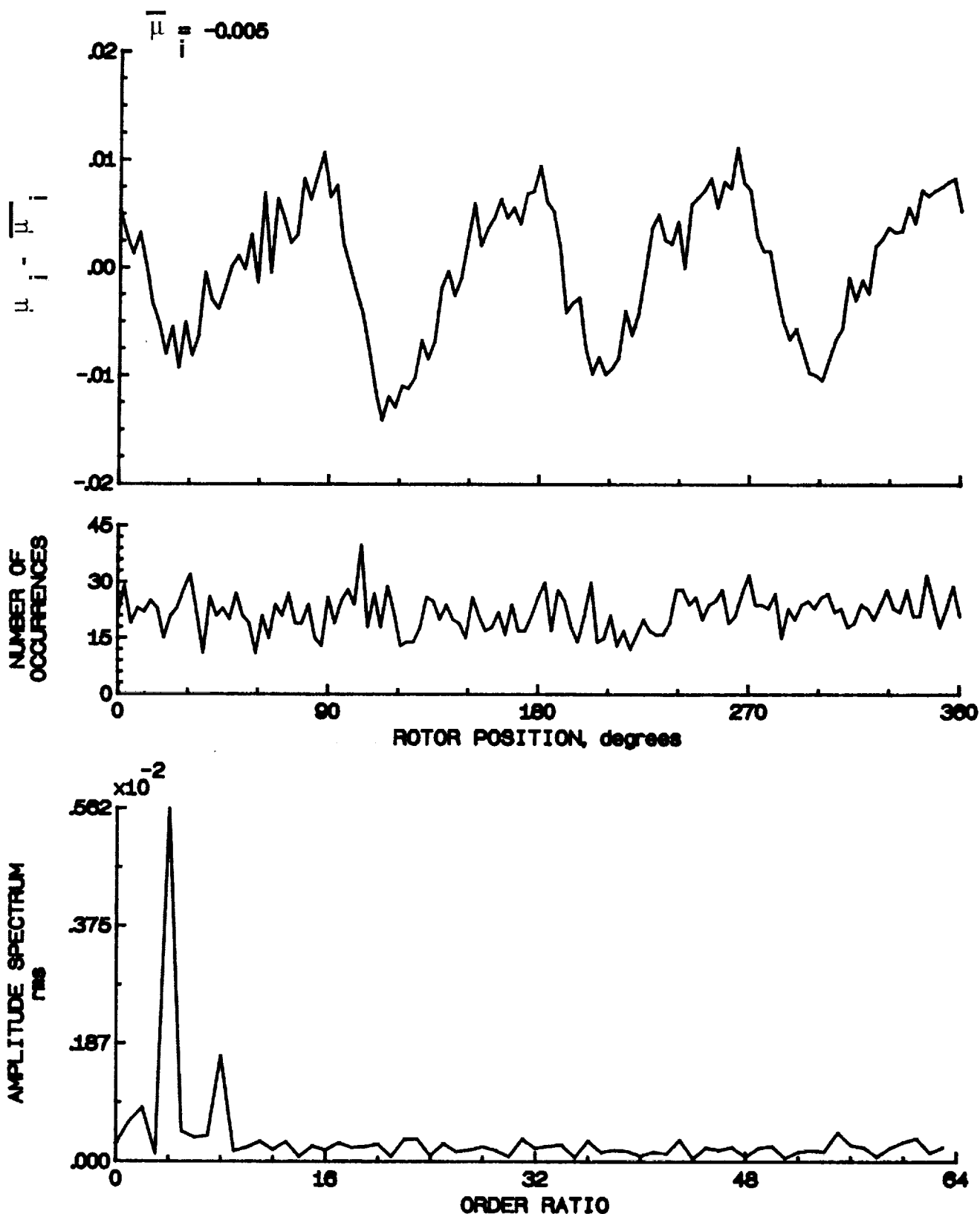


Figure 26.- Induced inflow velocity measured at 0 degrees and r/R of 1.10.

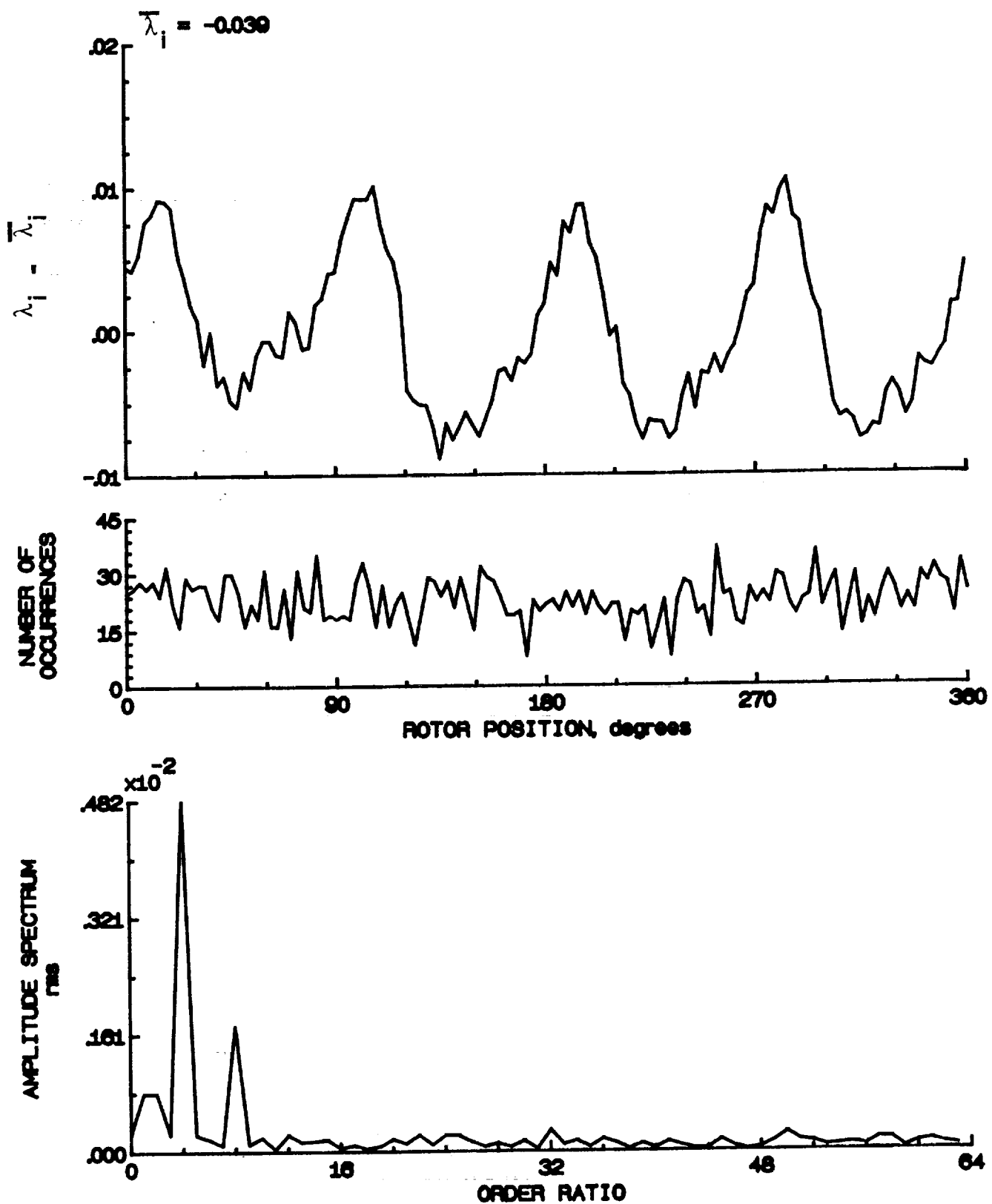


Figure 26.- Concluded.

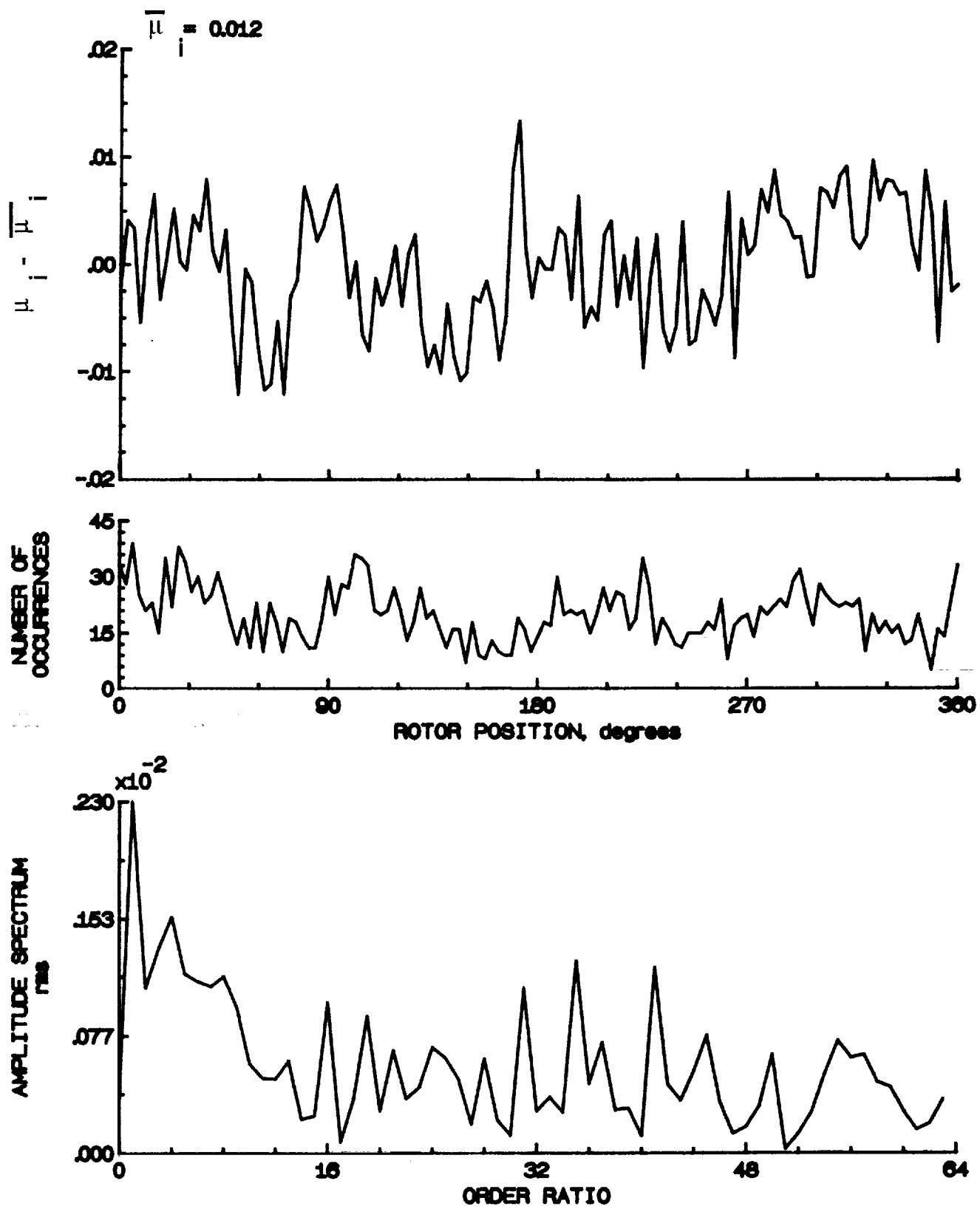


Figure 27.- Induced inflow velocity measured at 30 degrees and r/R of 0.20.

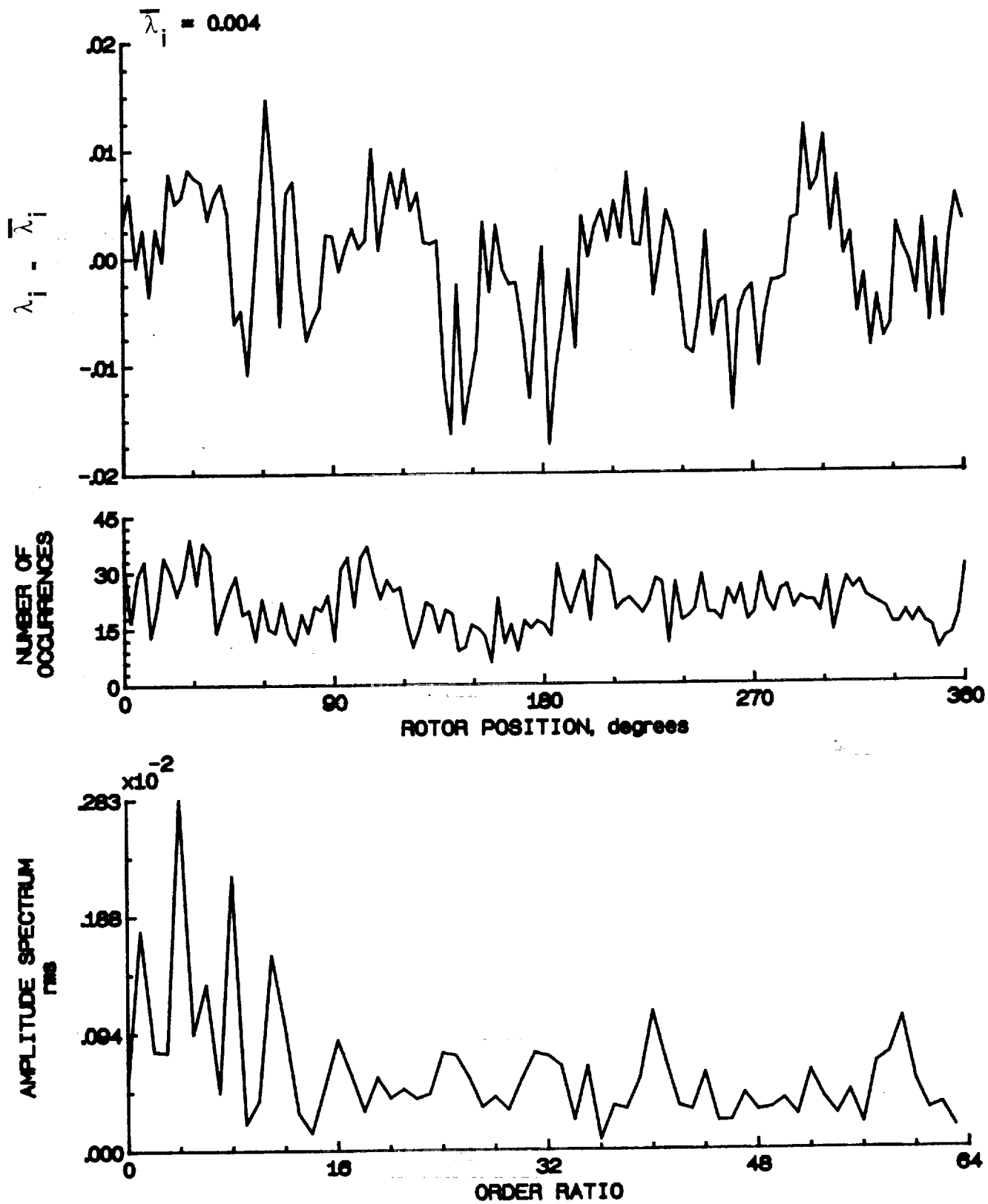


Figure 27.- Concluded.

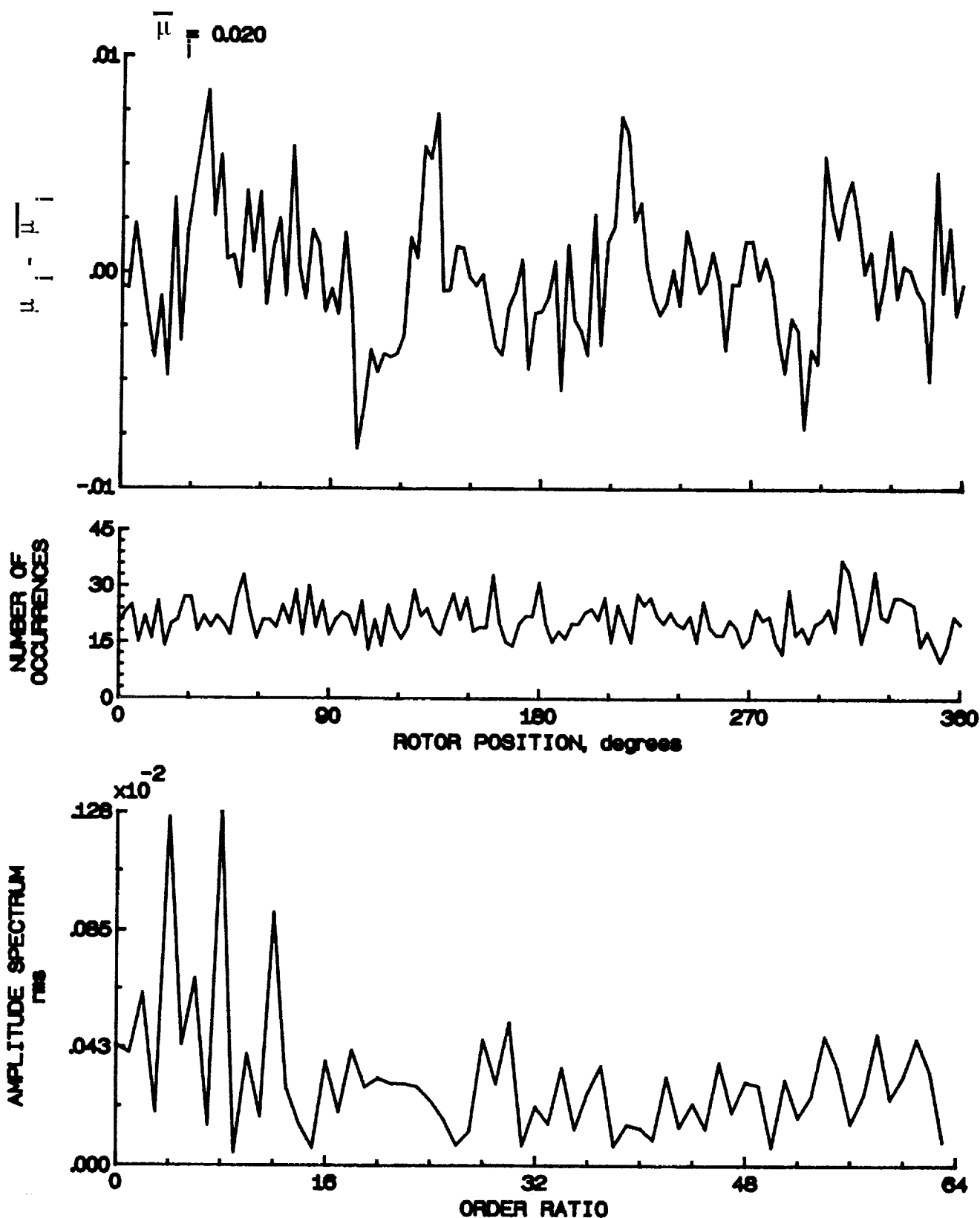


Figure 28.- Induced inflow velocity measured at 30 degrees and r/R of 0.40.

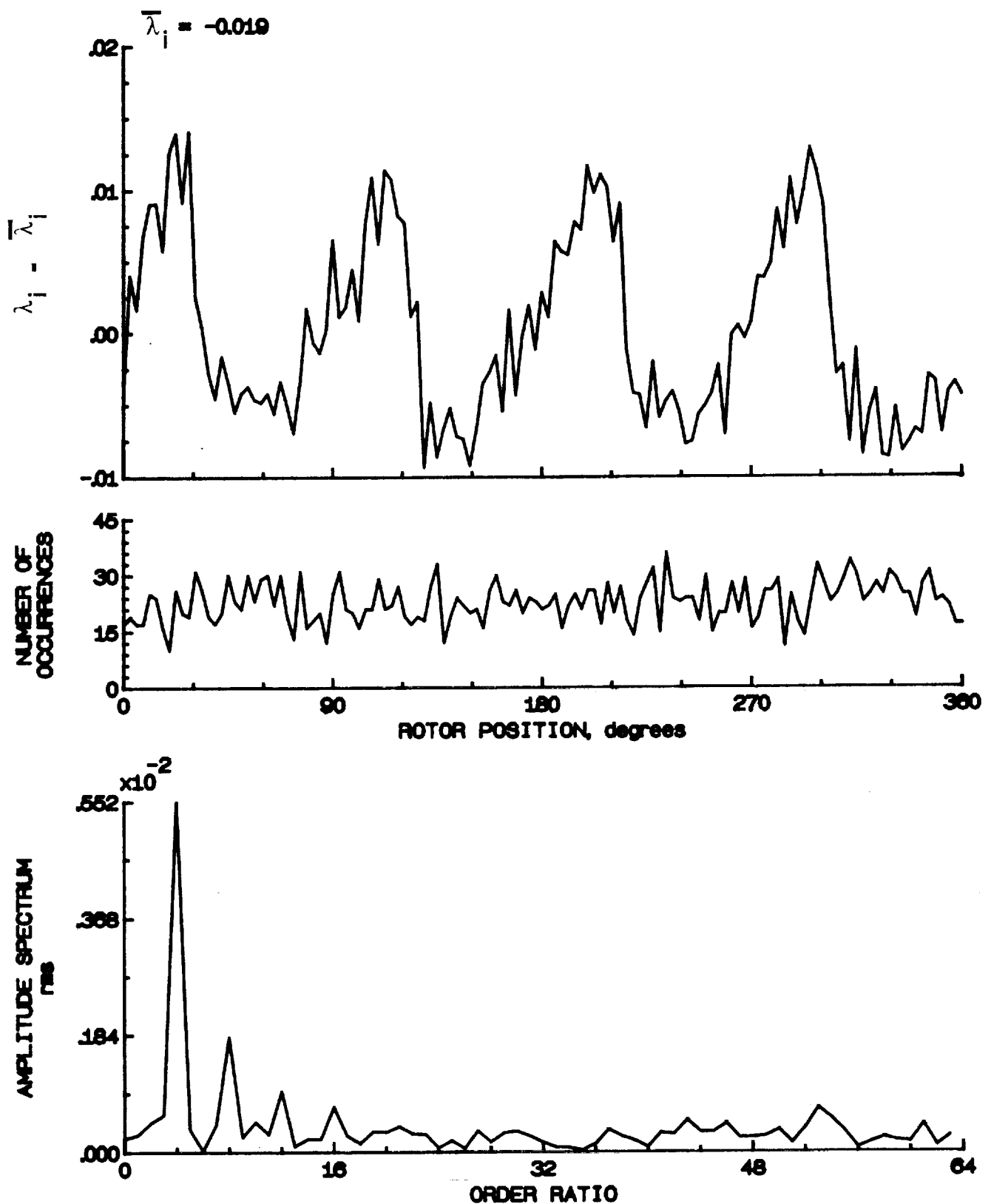


Figure 28.- Concluded.

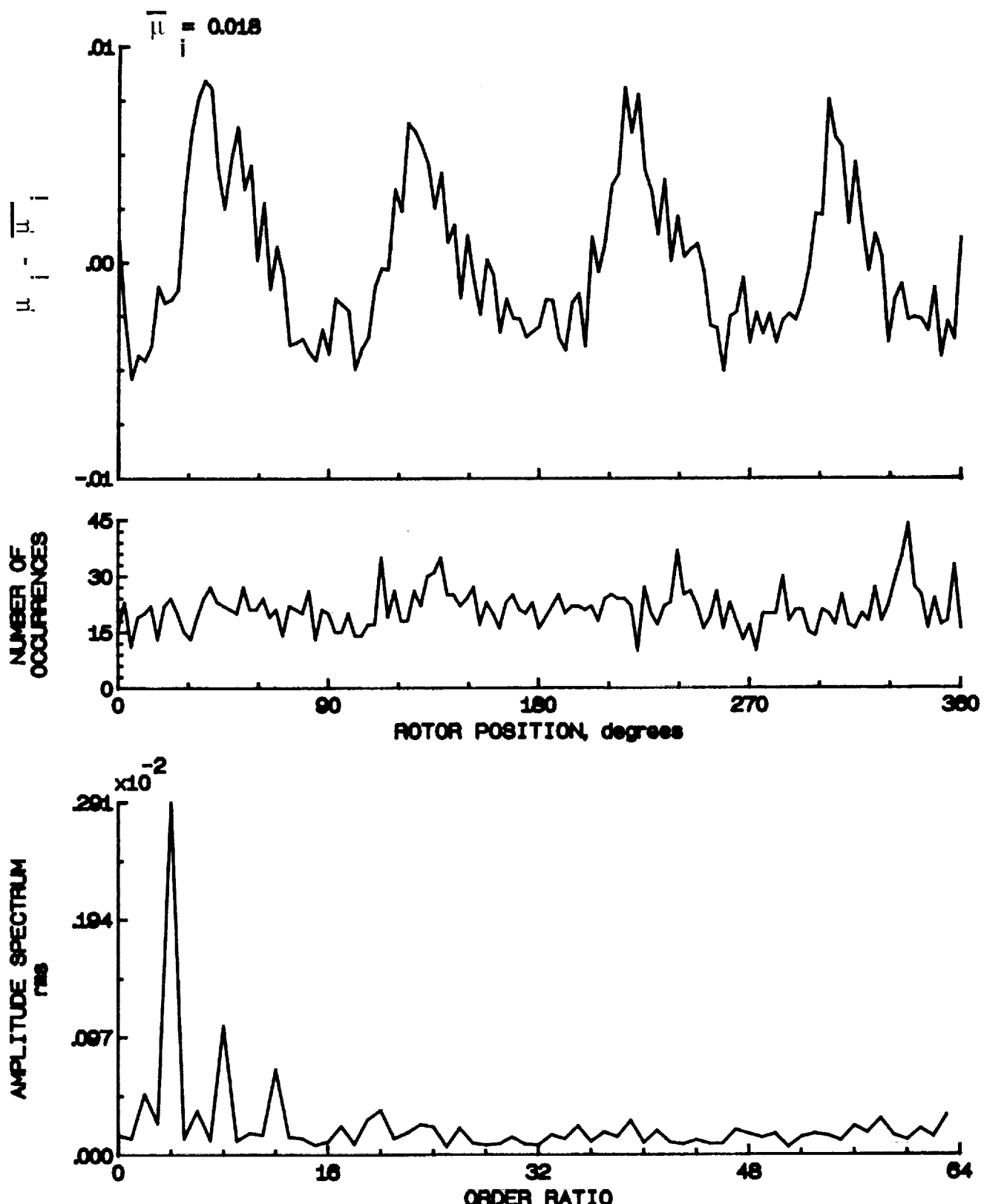


Figure 29.- Induced inflow velocity measured at 30 degrees and r/R of 0.50.

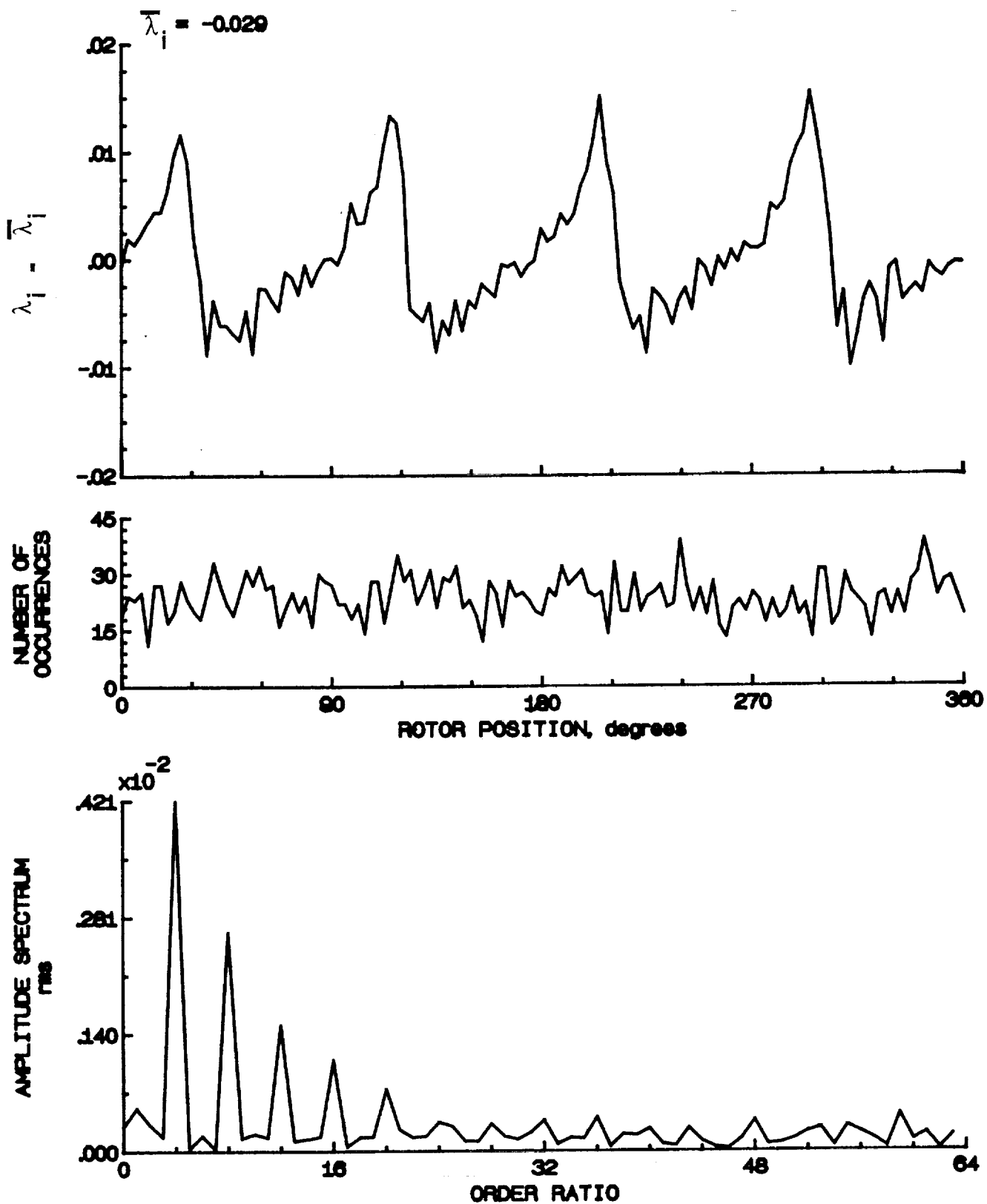


Figure 29.- Concluded.

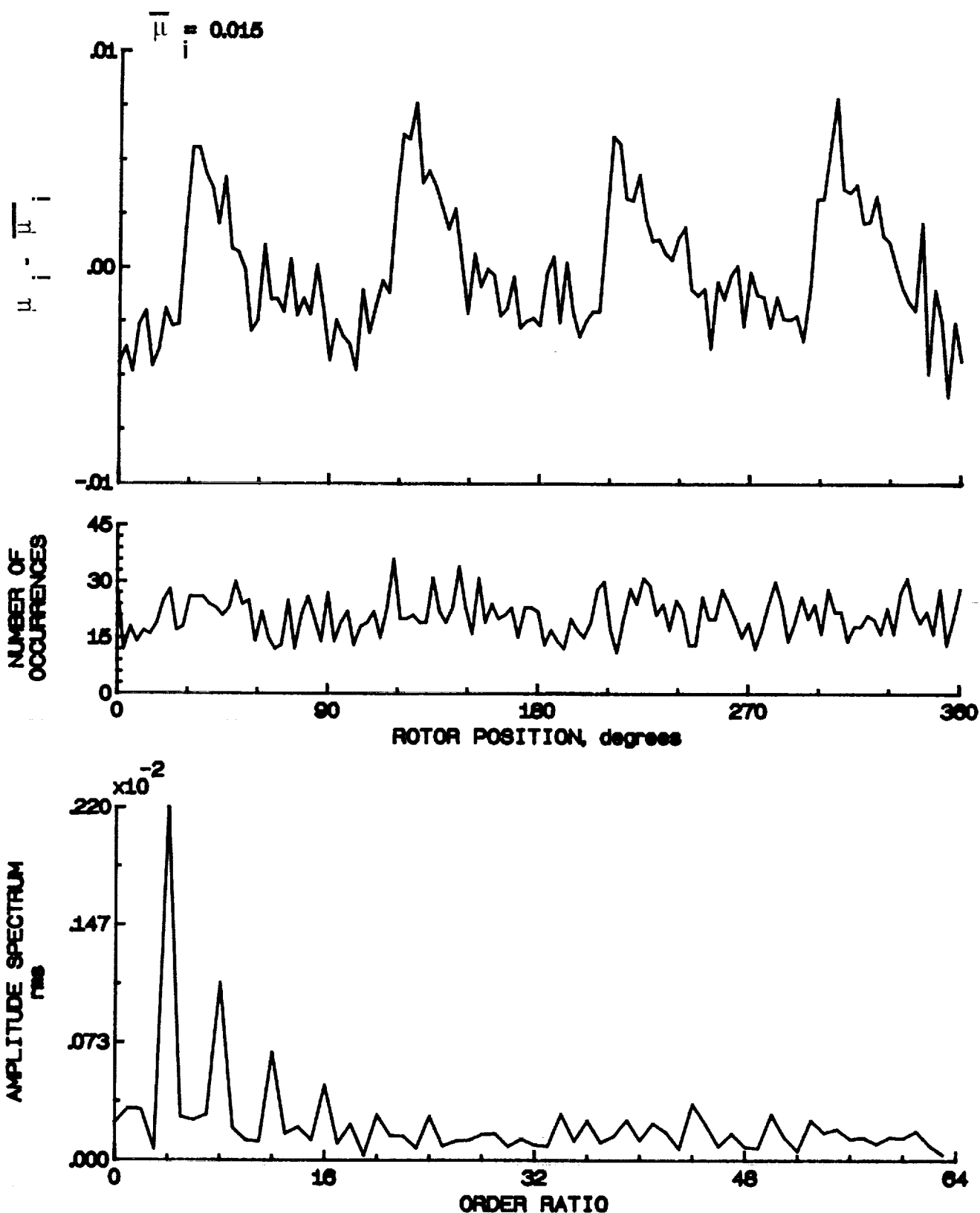


Figure 30.- Induced inflow velocity measured at 30 degrees and r/R of 0.50.

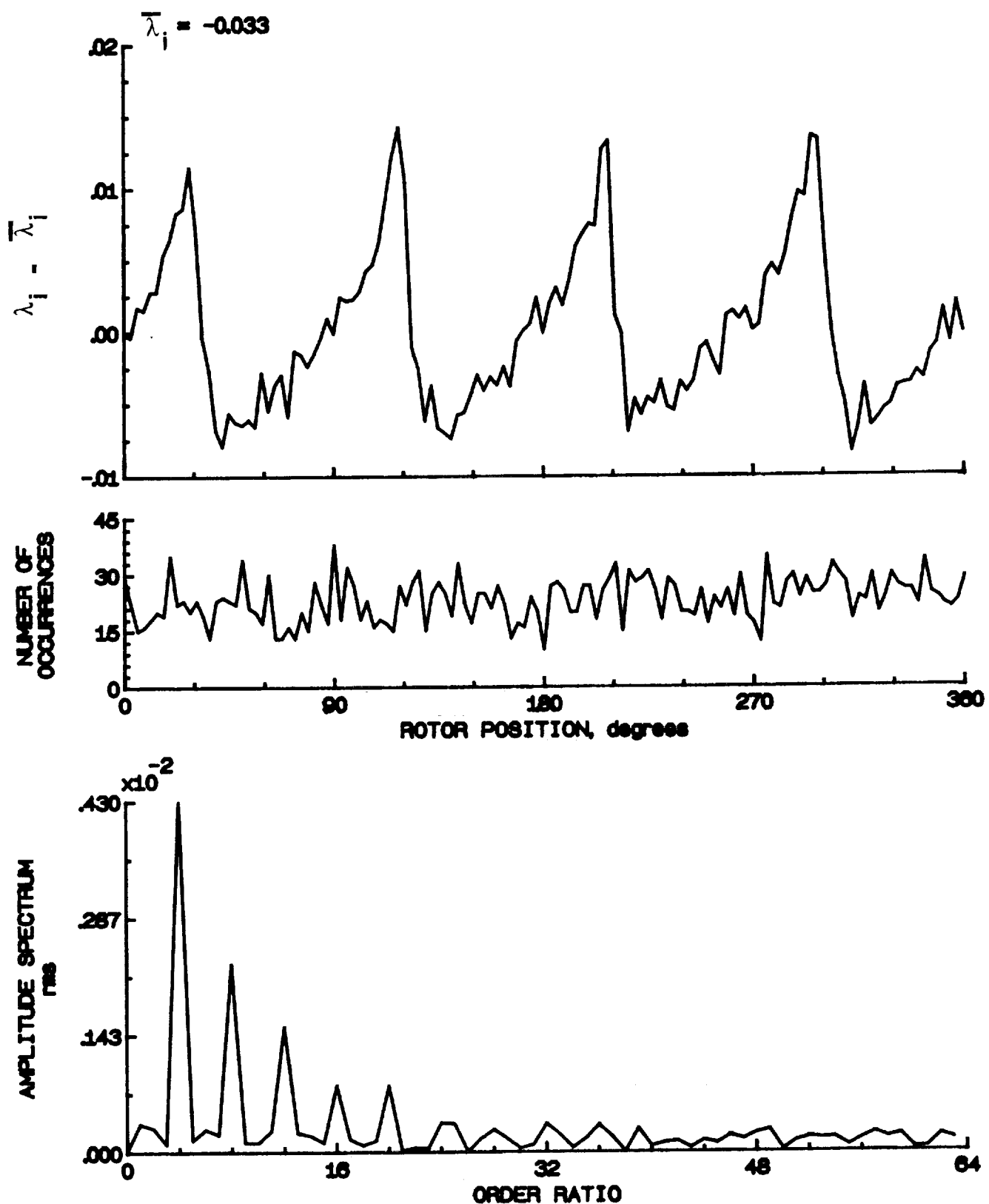


Figure 30.- Concluded.

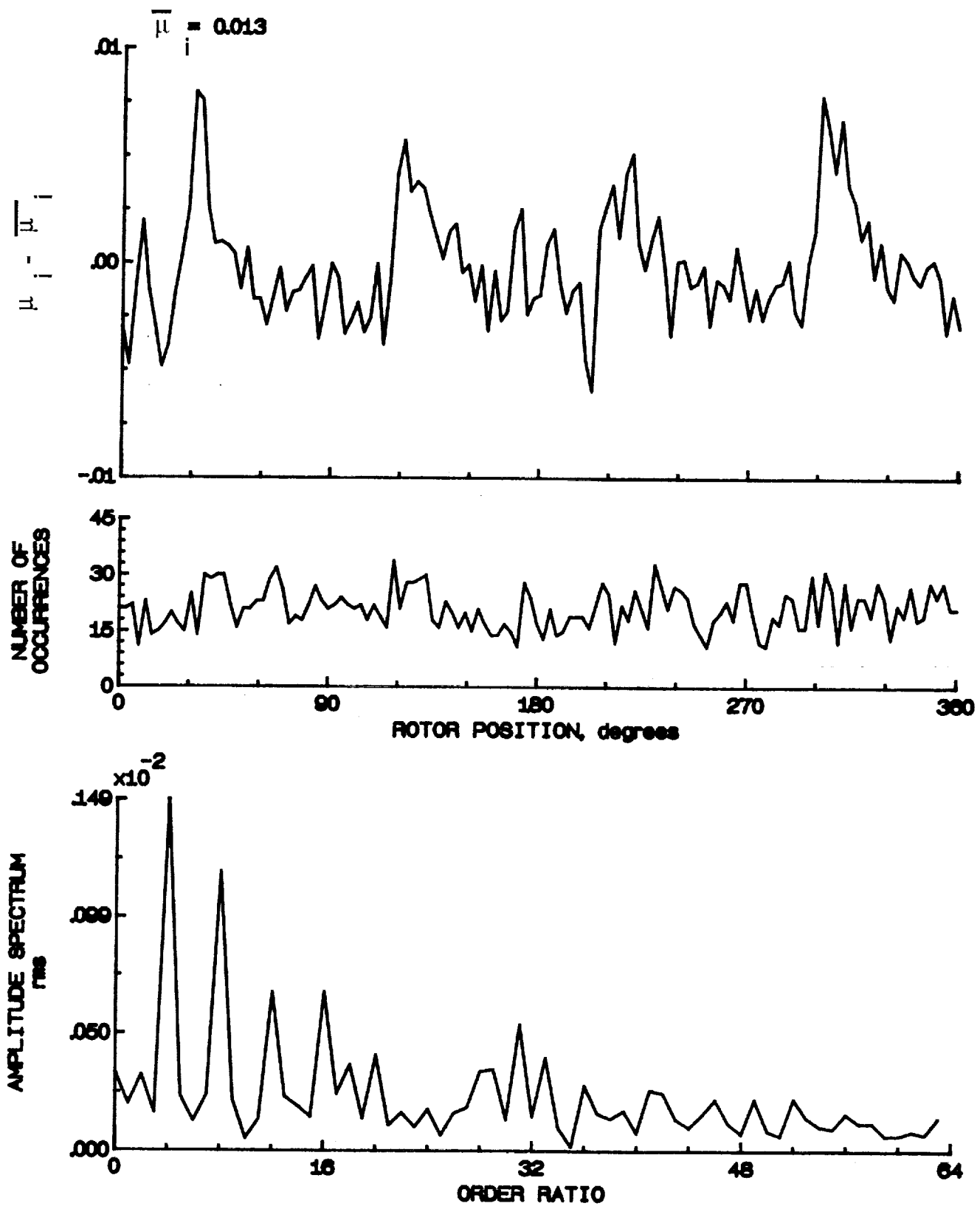


Figure 31.- Induced inflow velocity measured at 30 degrees and r/R of 0.70.

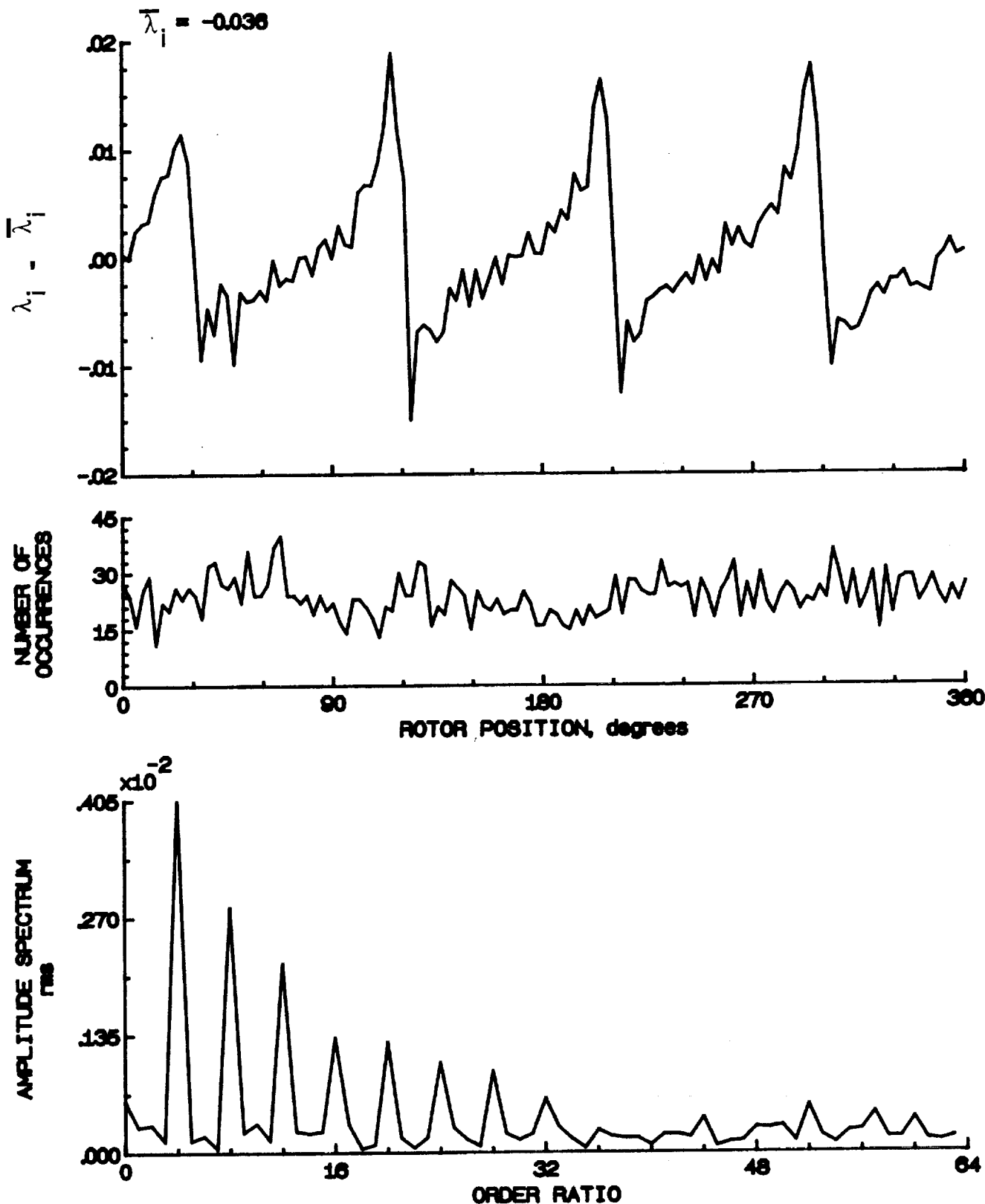


Figure 31- Concluded.

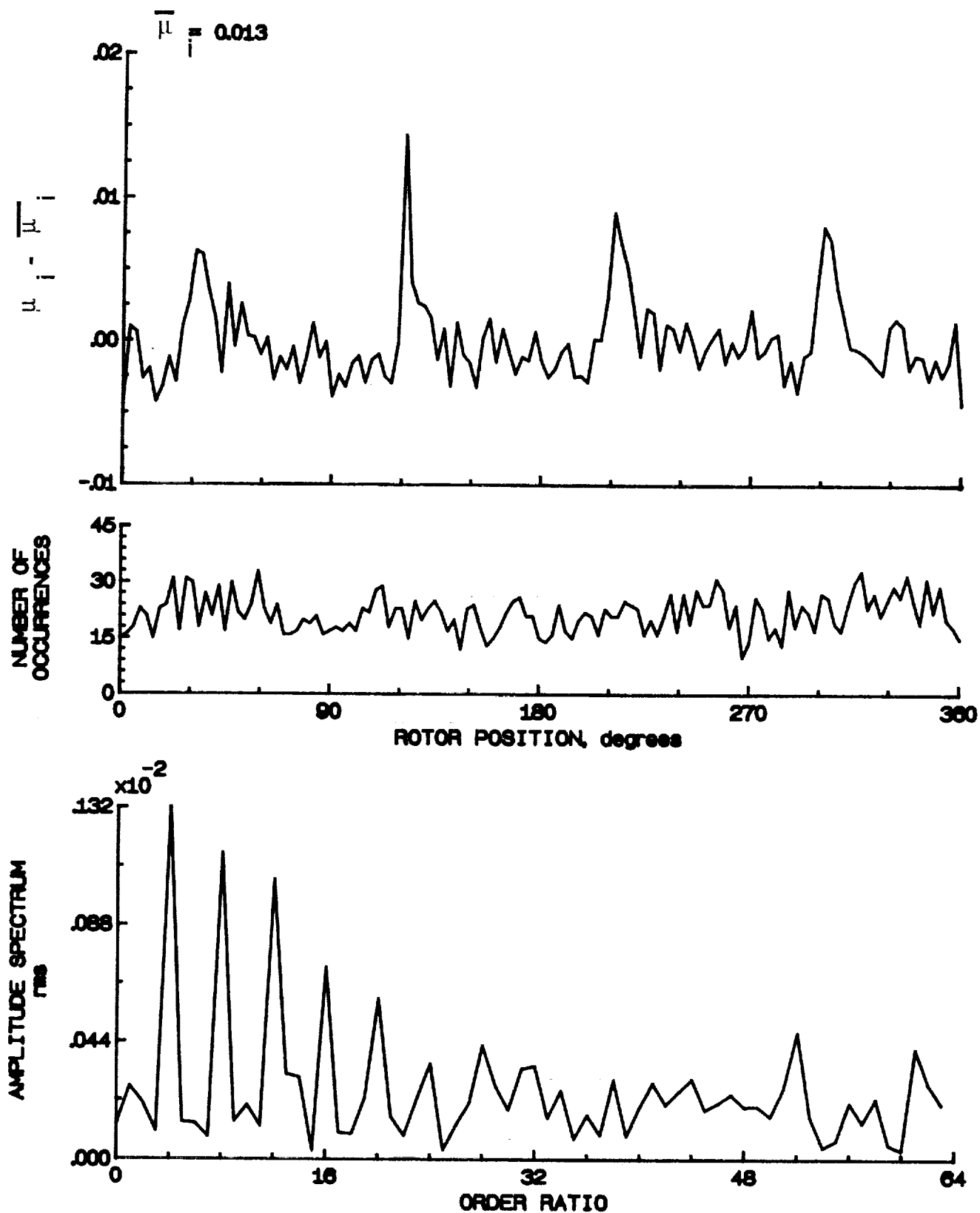


Figure 32.- Induced inflow velocity measured at 30 degrees and r/R of 0.74.

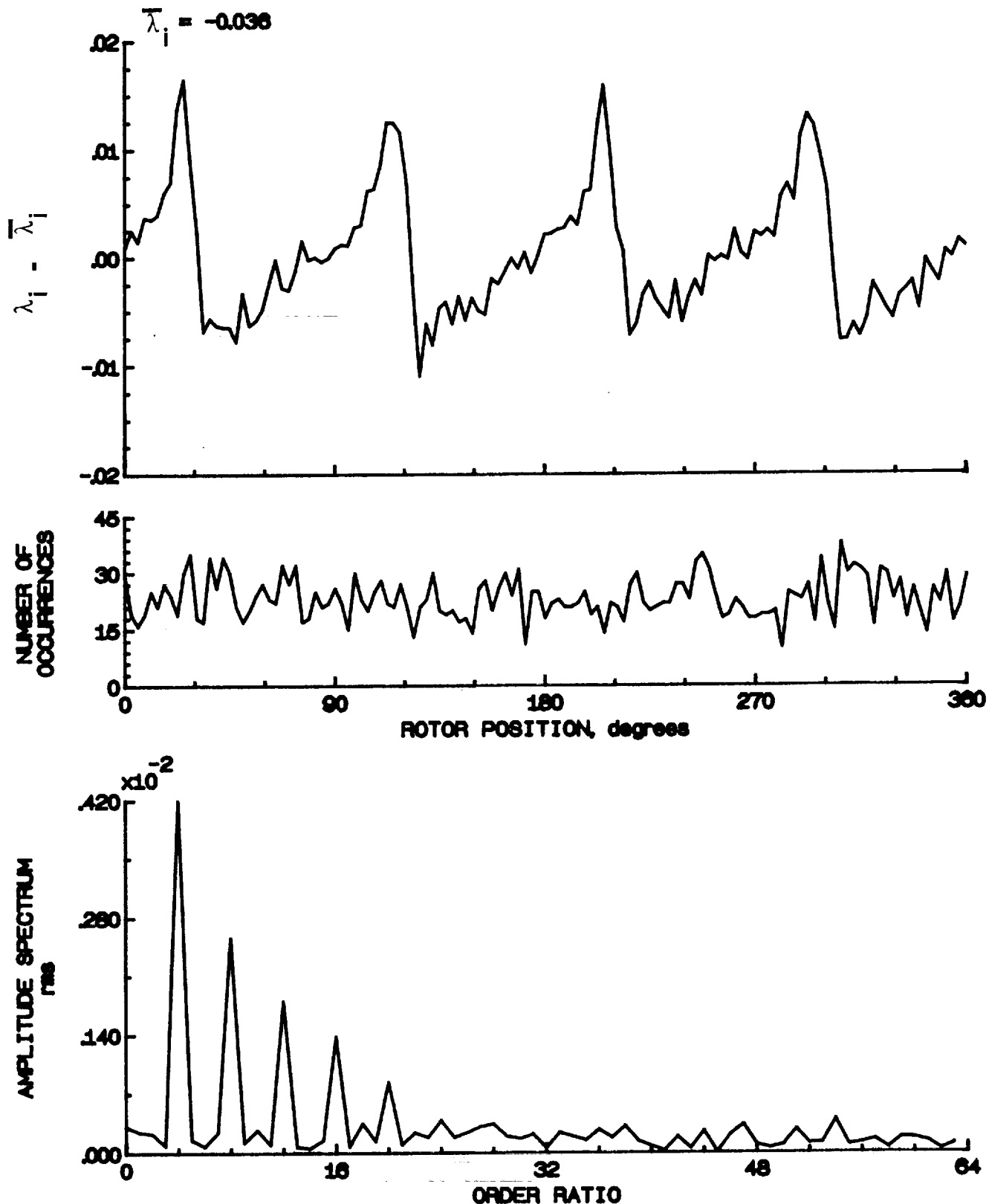


Figure 32.- Concluded.

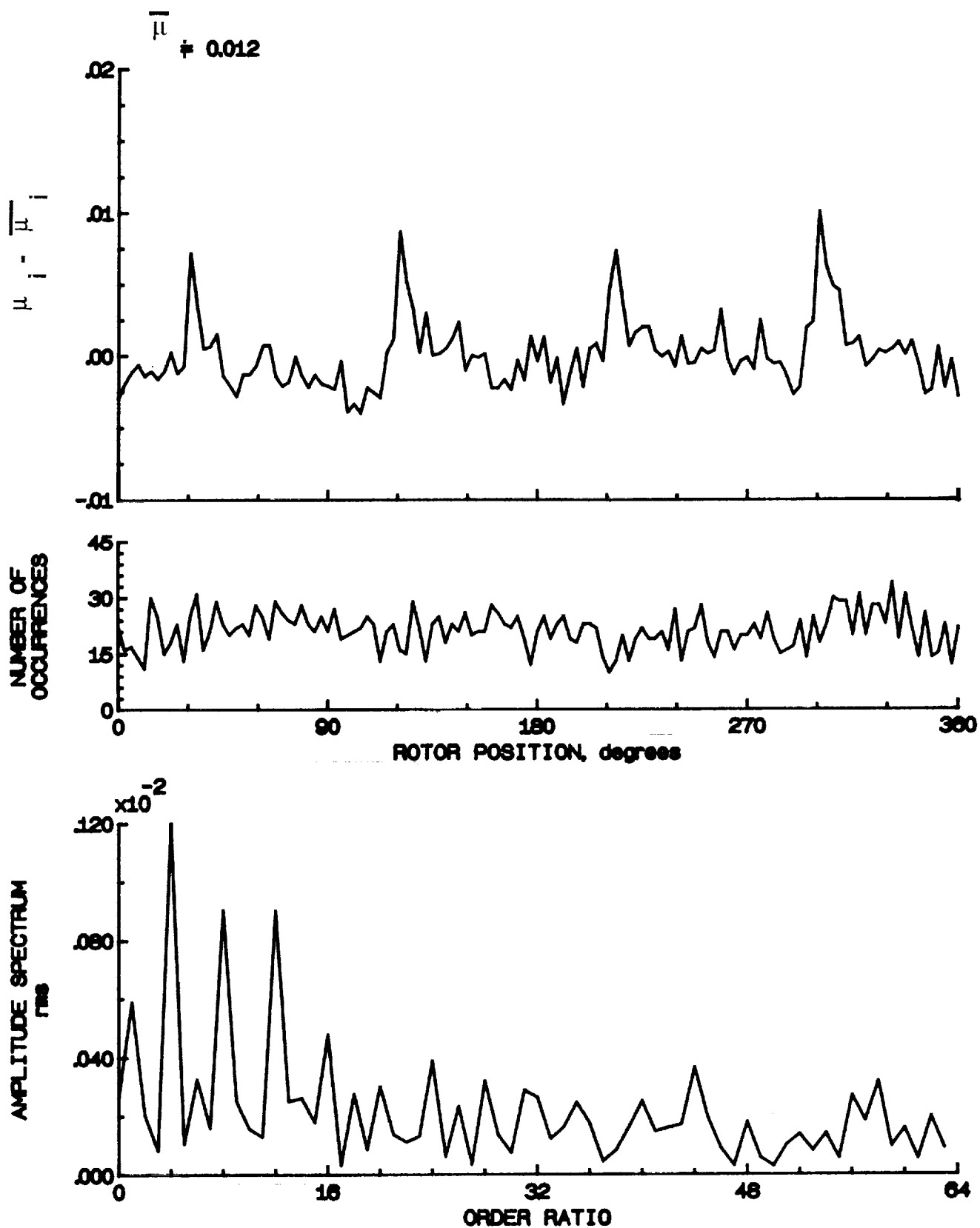


Figure 33.- Induced inflow velocity measured at 30 degrees and r/R of 0.78.

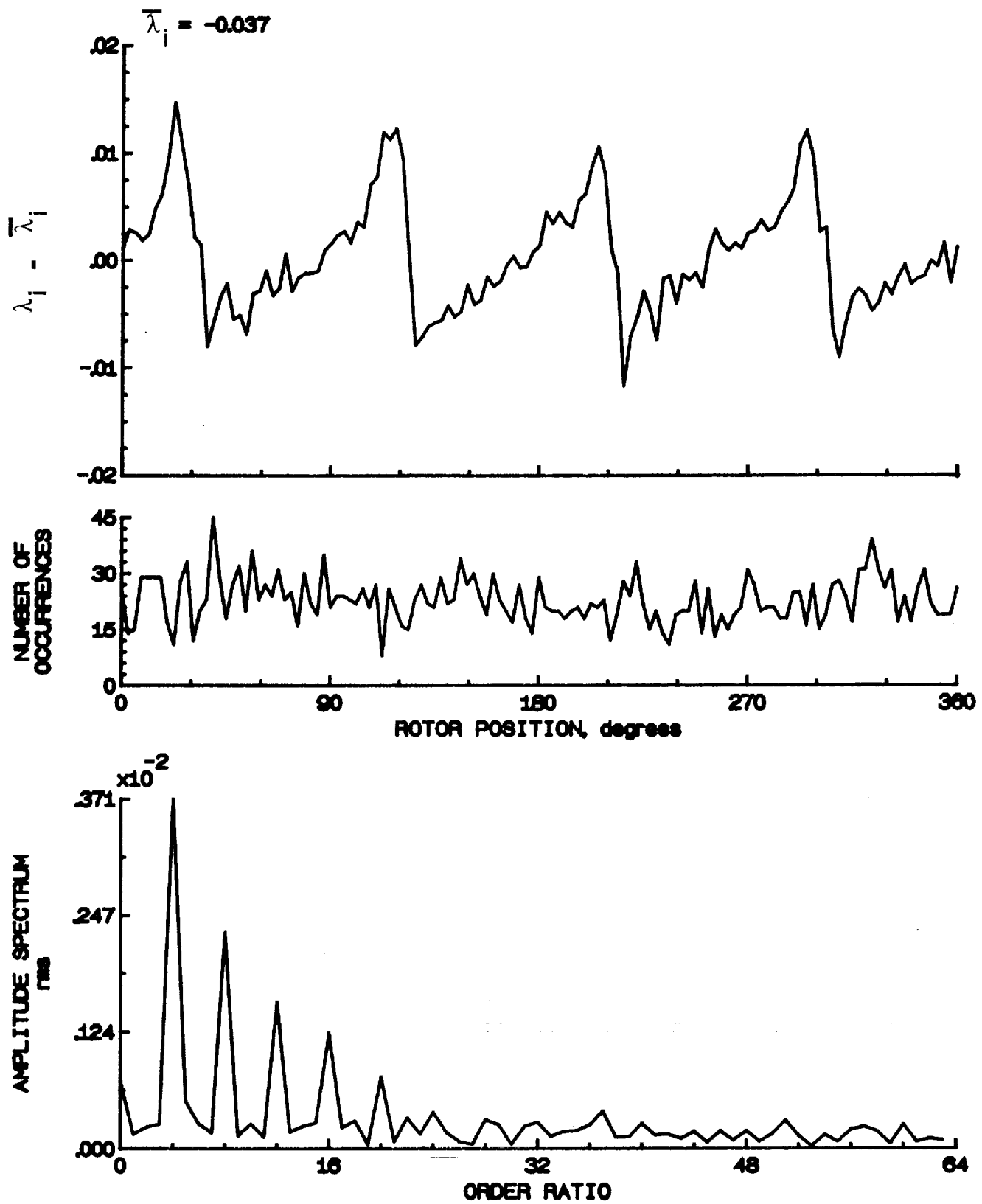


Figure 33.- Concluded.

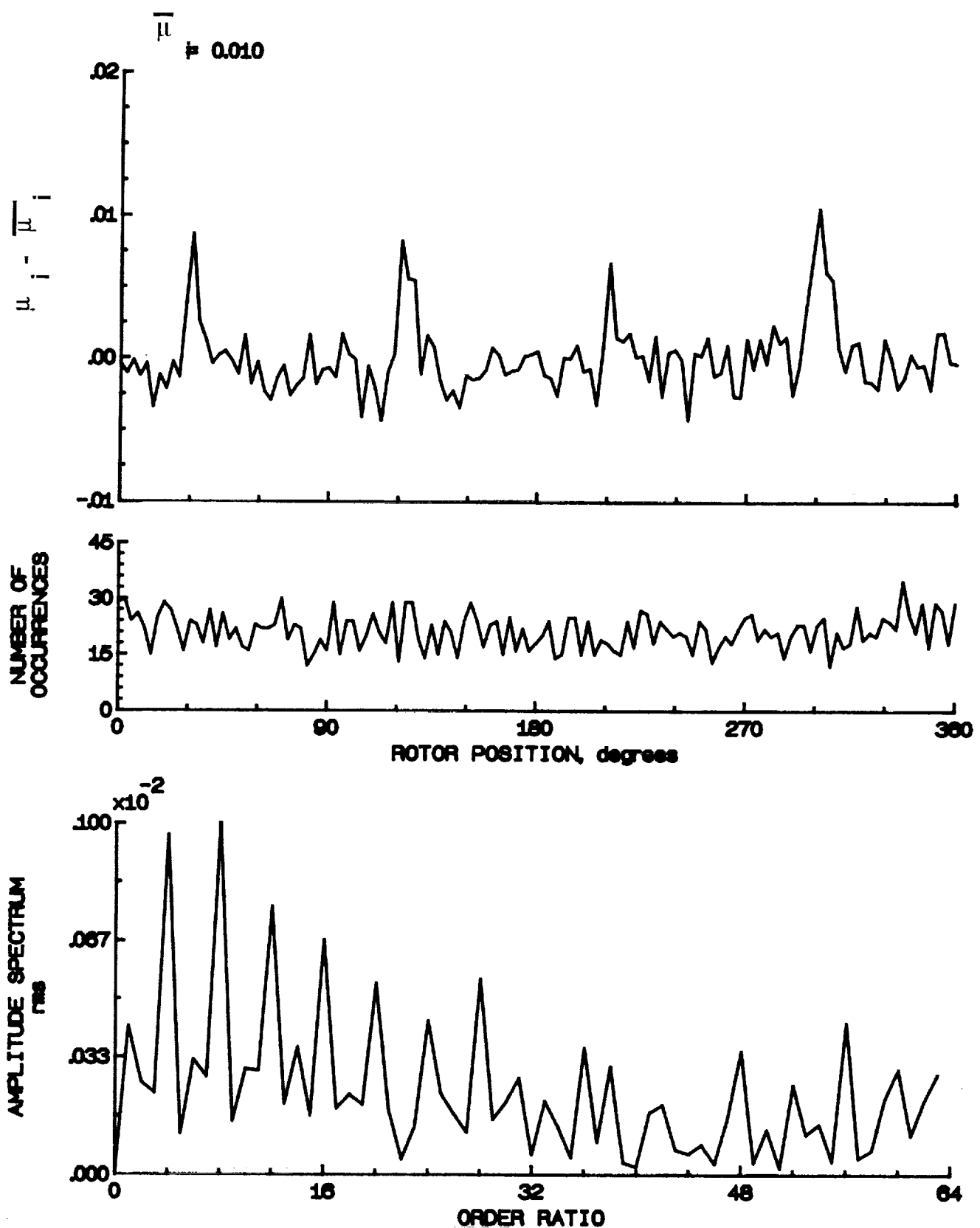


Figure 34.- Induced inflow velocity measured at 30 degrees and r/R of 0.82.

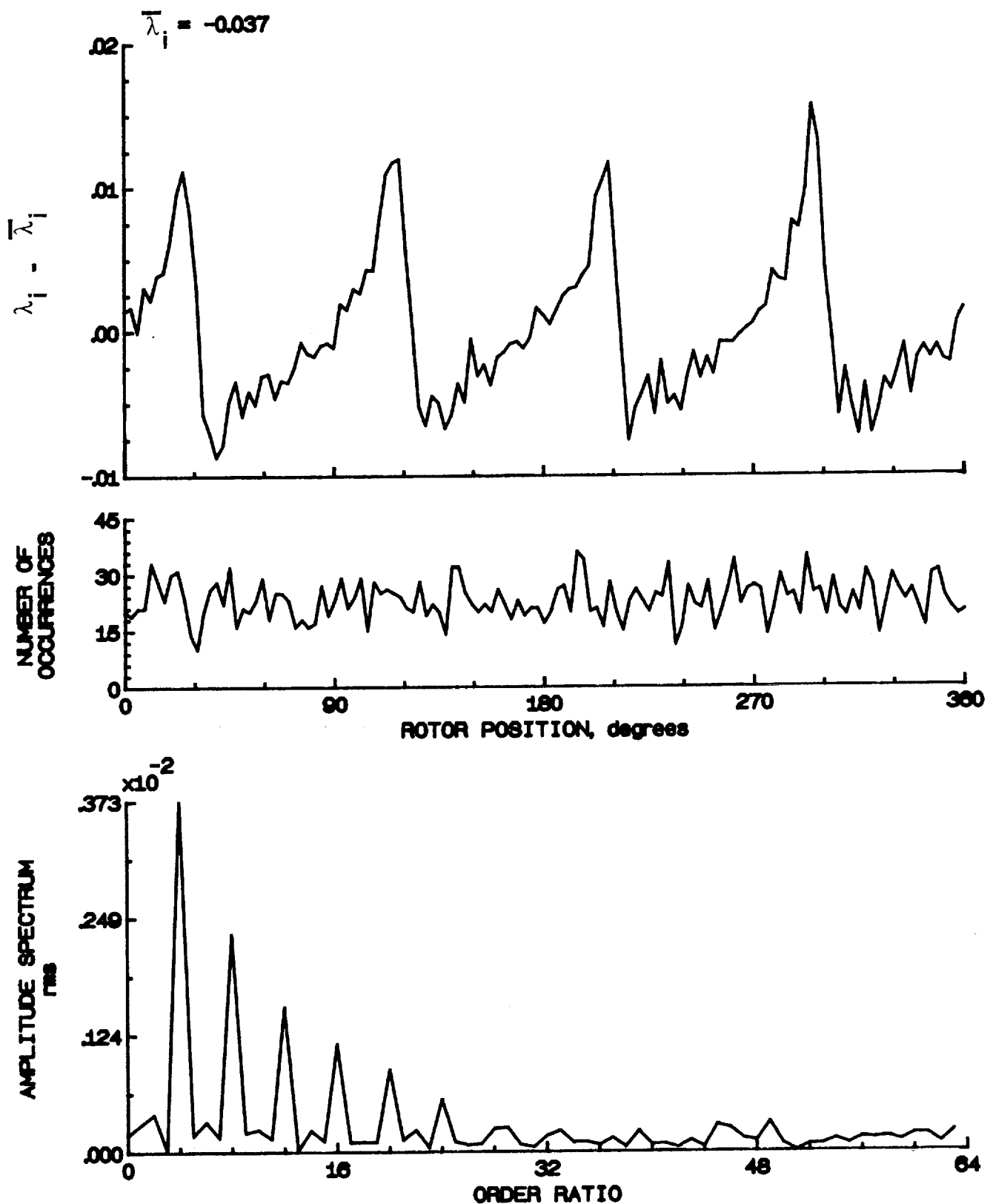


Figure 34.- Concluded.

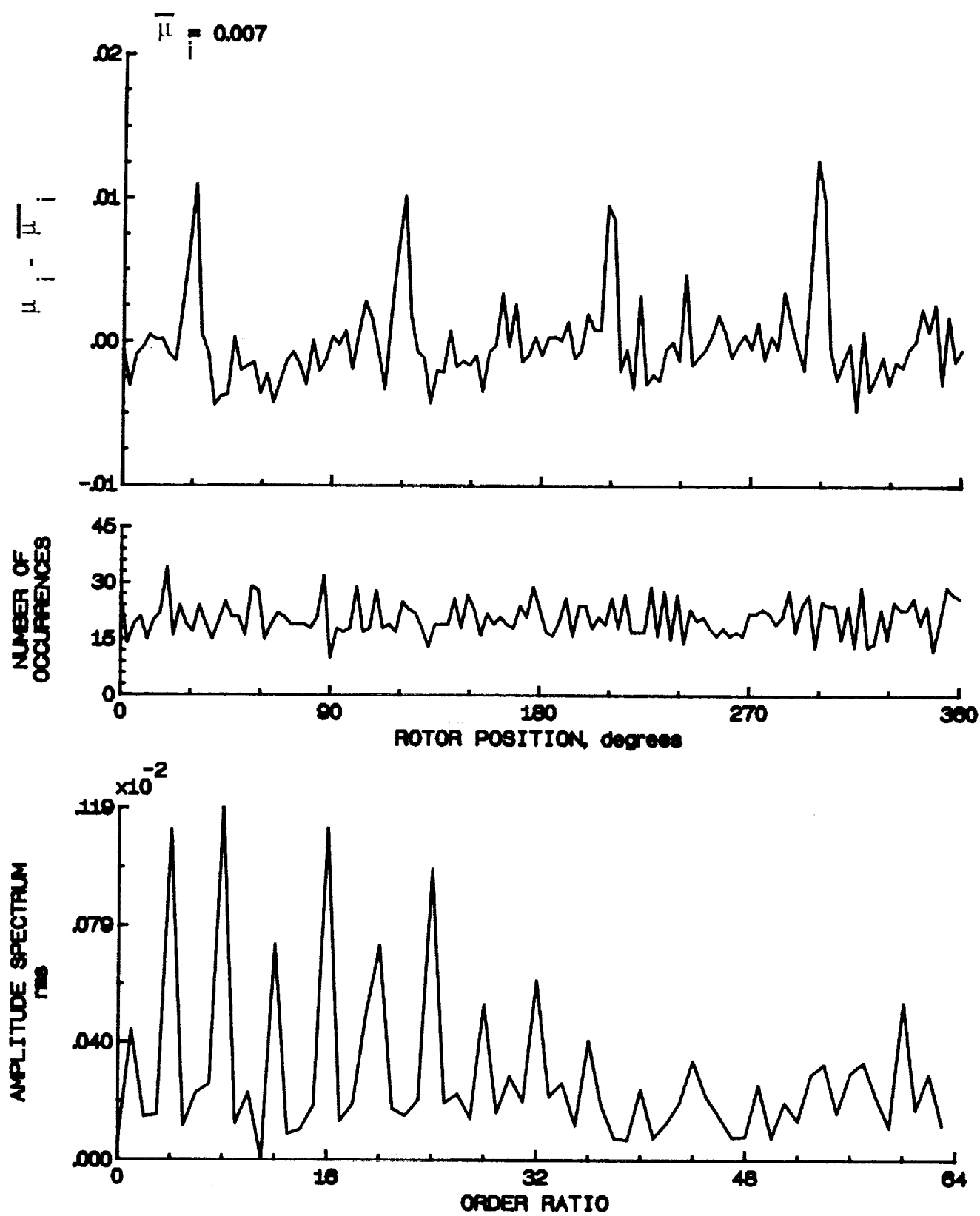


Figure 35.- Induced inflow velocity measured at 30 degrees and r/R of 0.86.

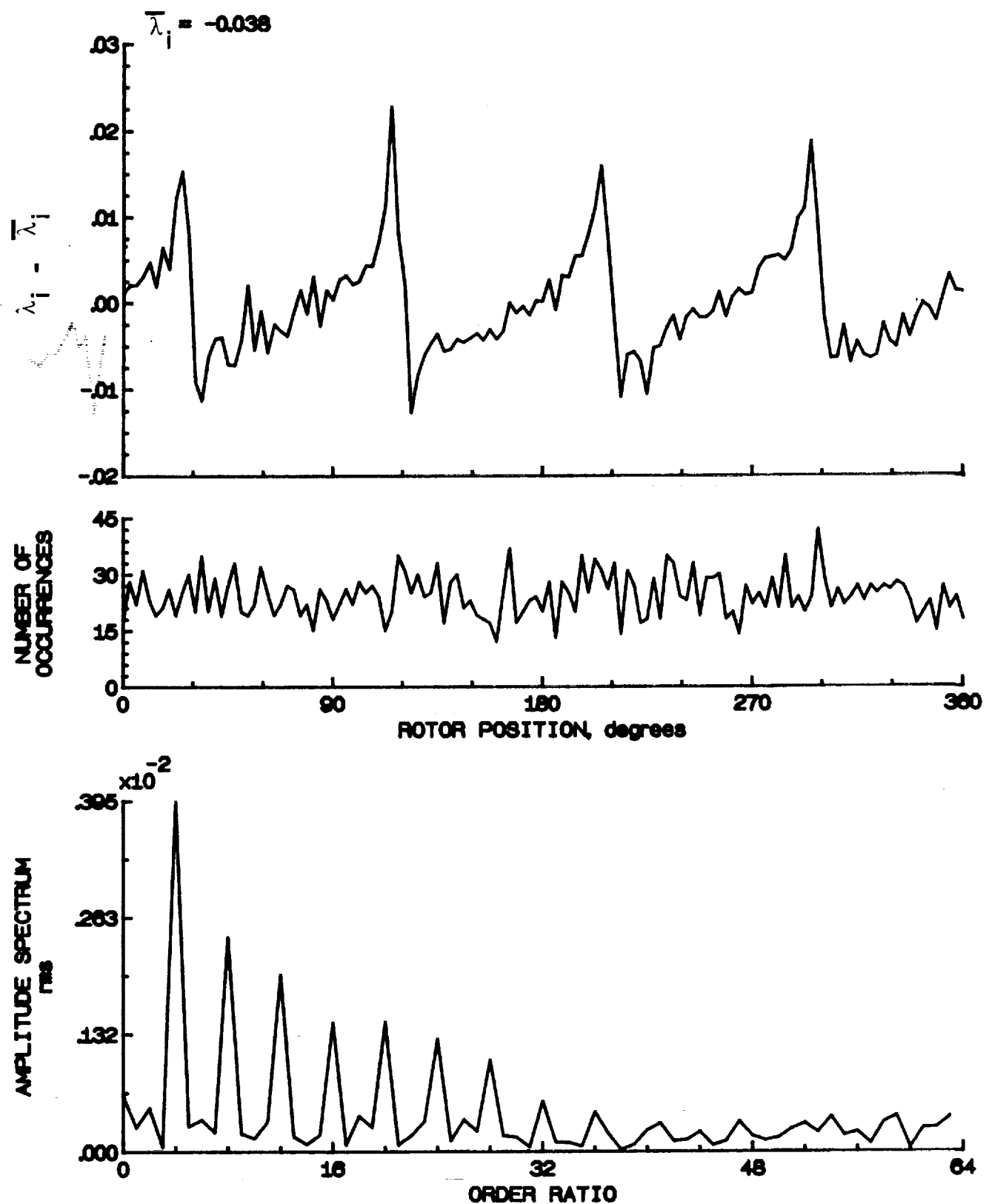


Figure 35.- Concluded.

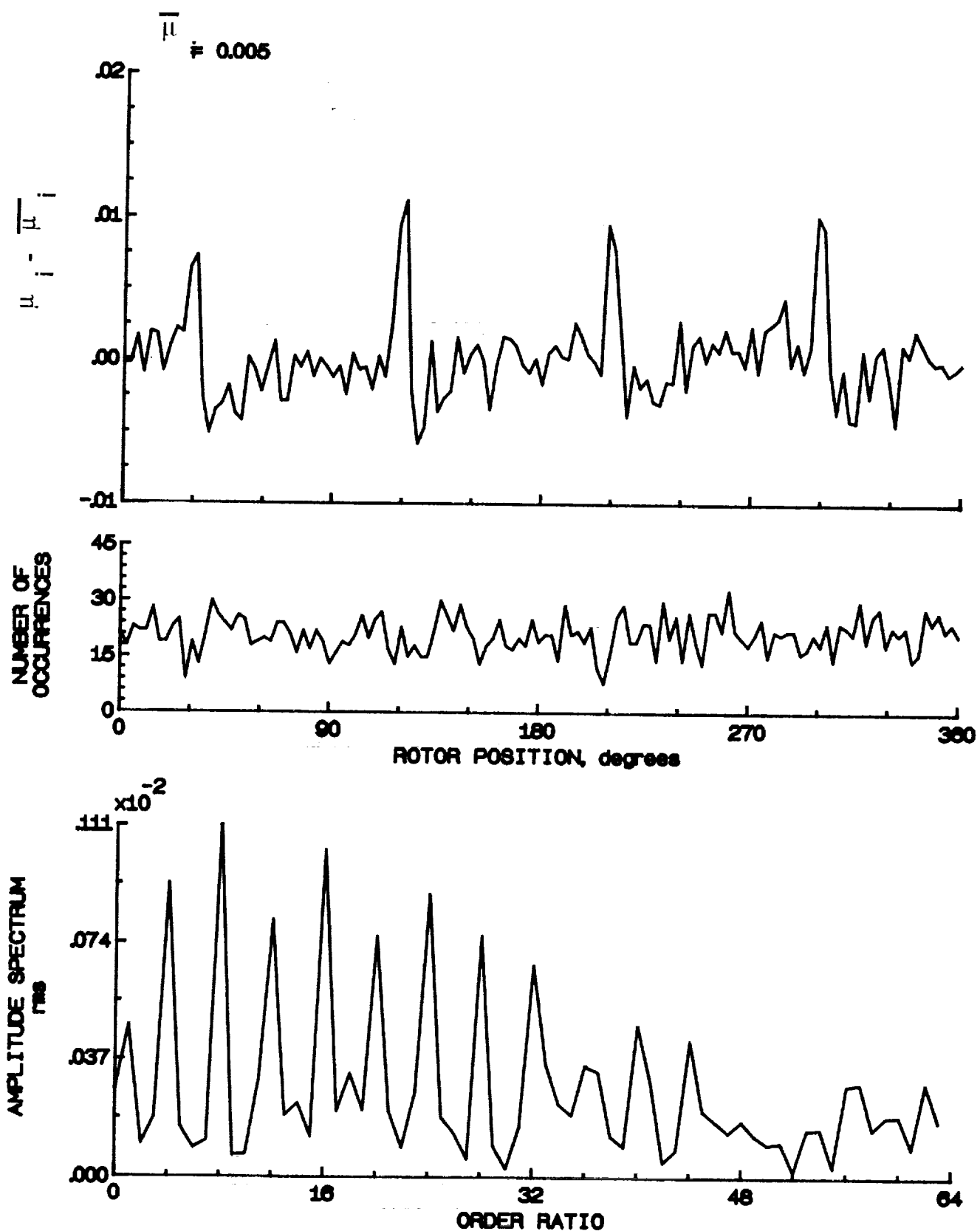


Figure 36.- Induced inflow velocity measured at 30 degrees and r/R of 0.90.

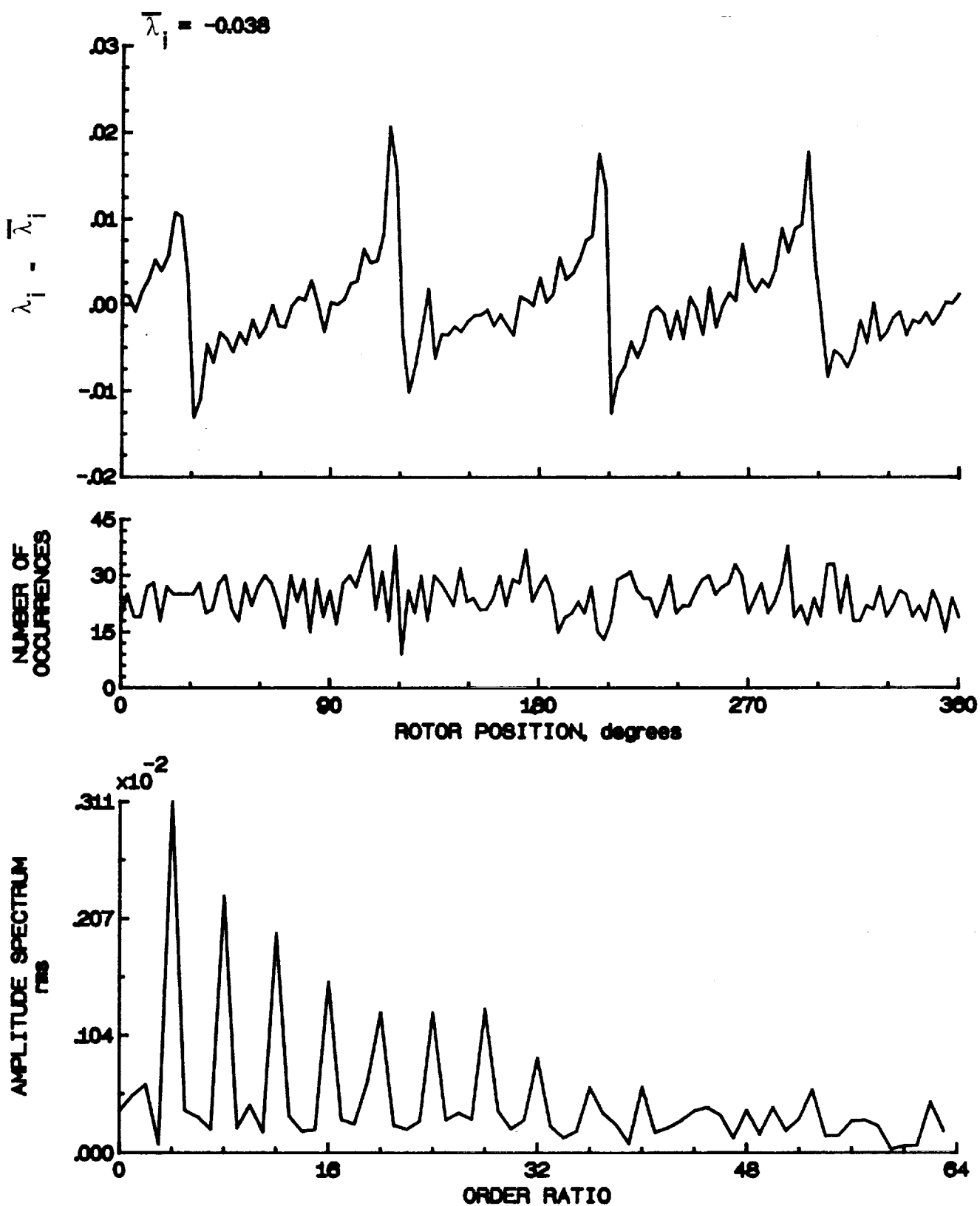


Figure 36.- Concluded.

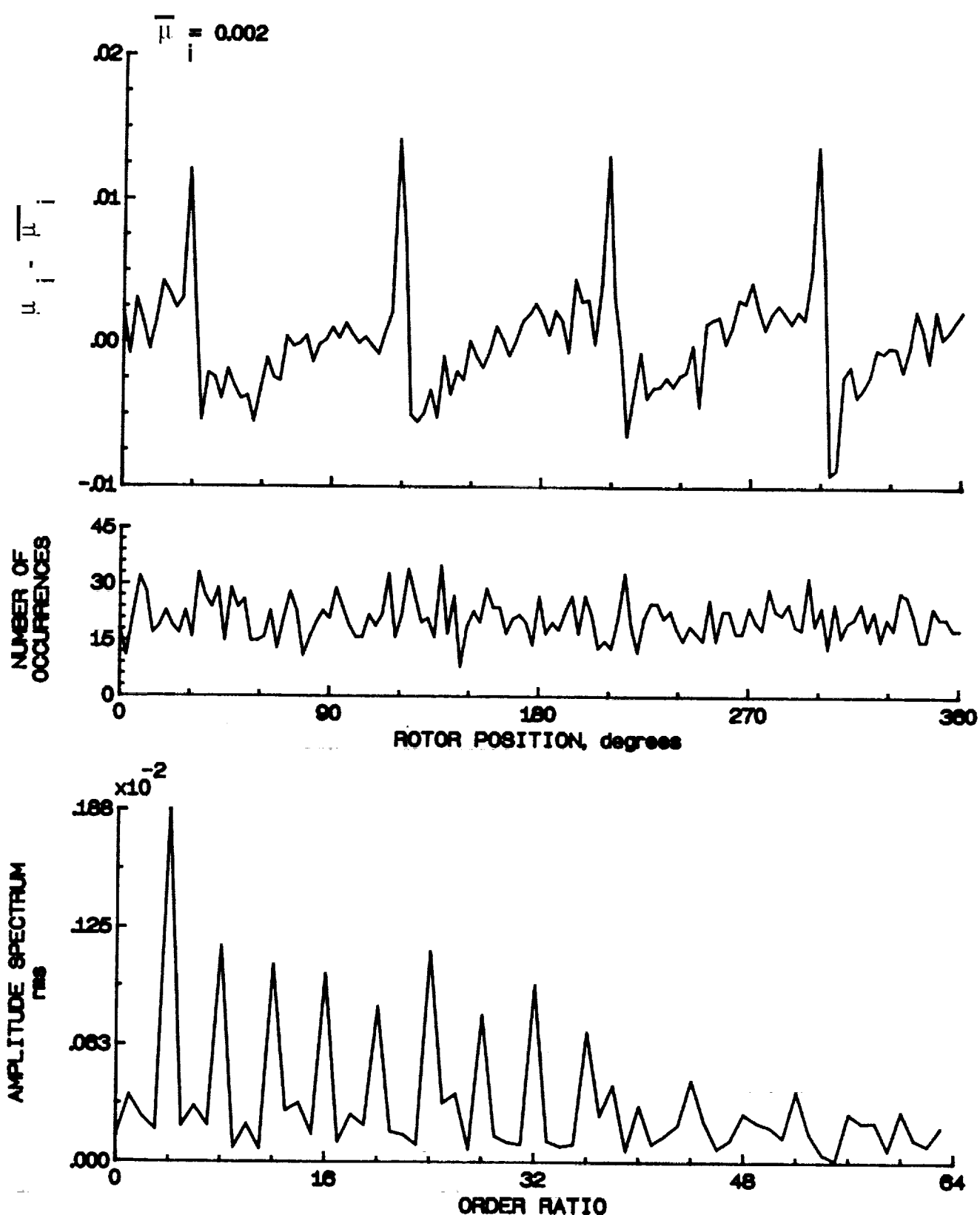


Figure 37.- Induced inflow velocity measured at 30 degrees and r/R of 0.94.

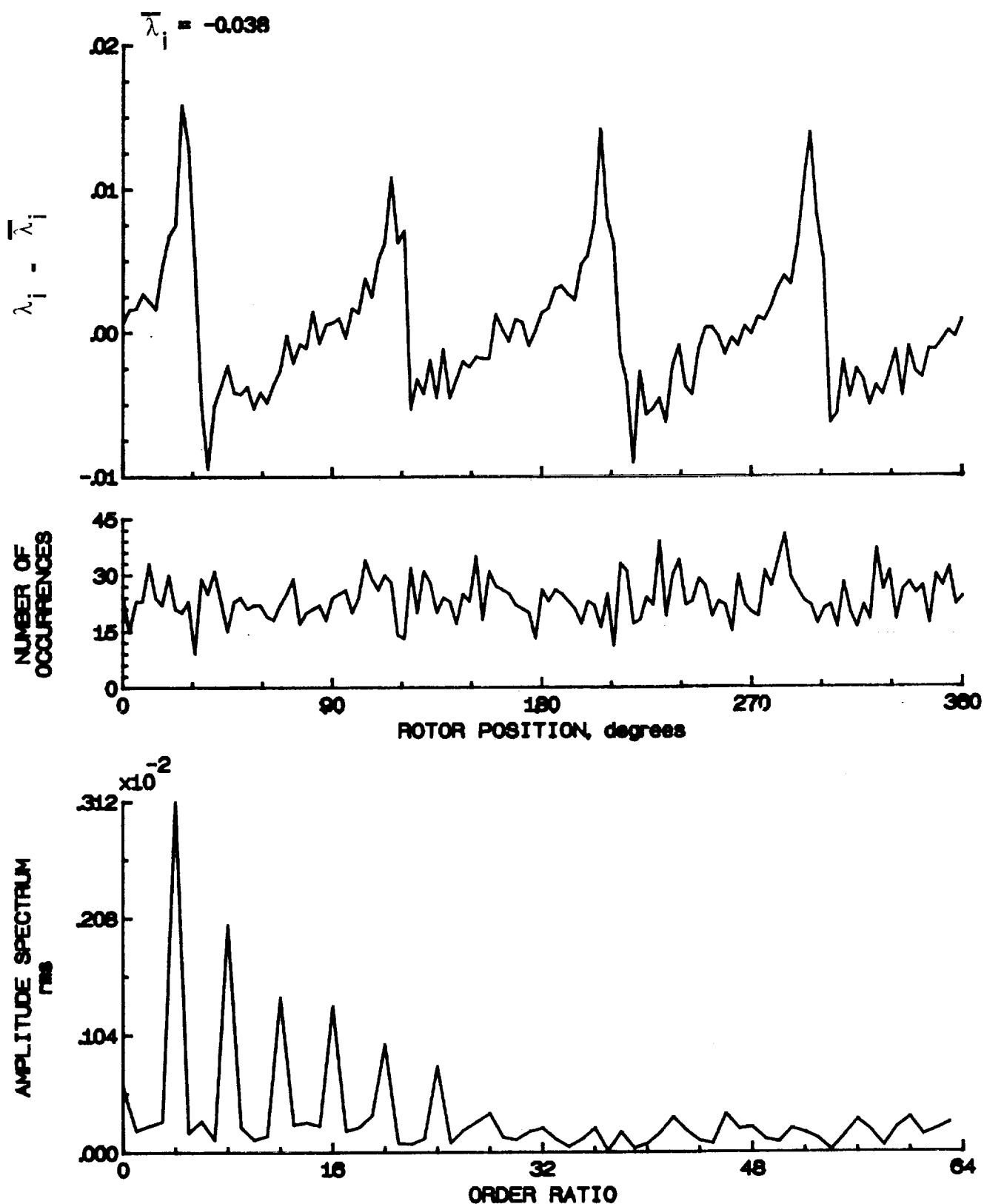


Figure 37.- Concluded.

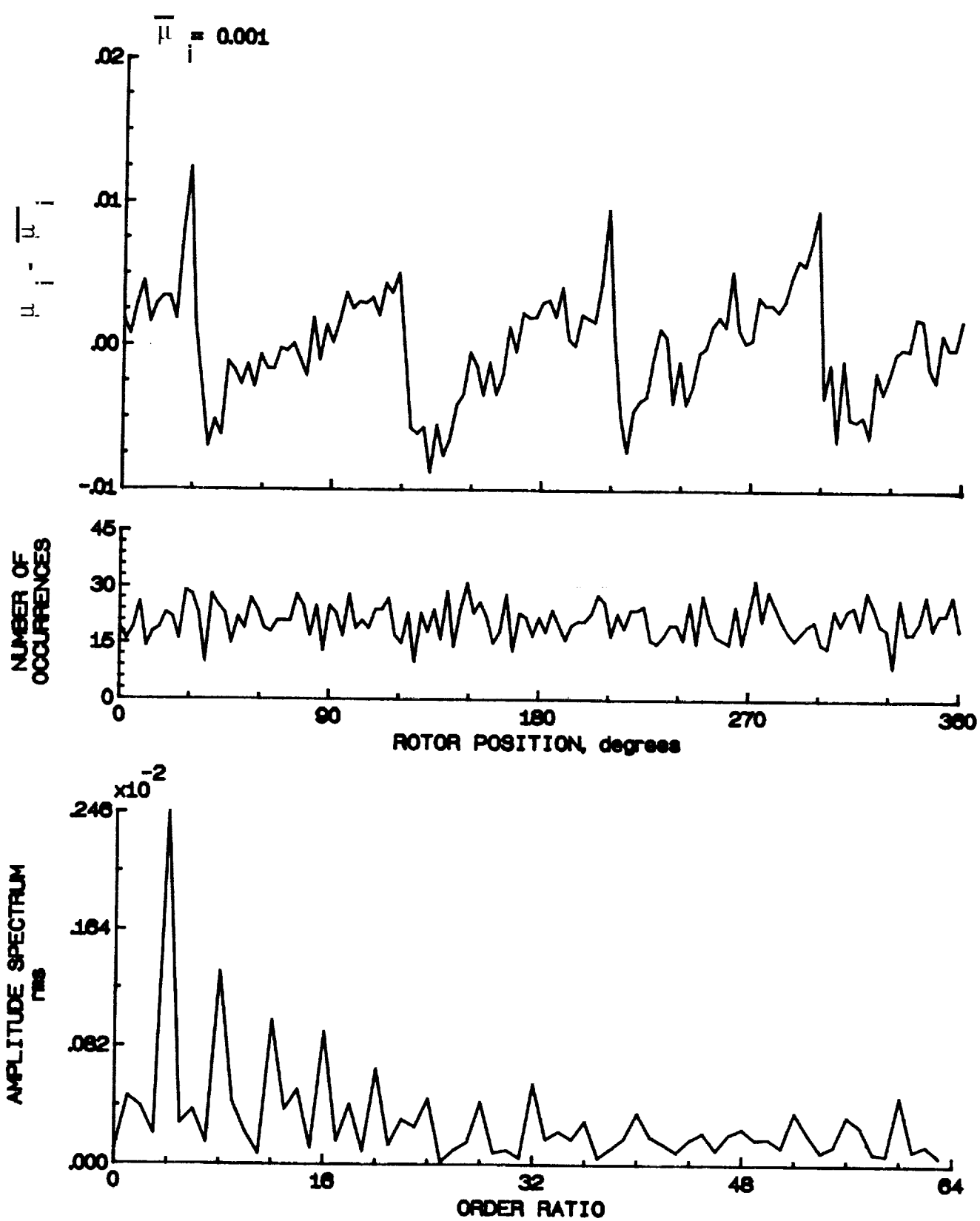


Figure 38.- Induced inflow velocity measured at 30 degrees and r/R of 0.98.

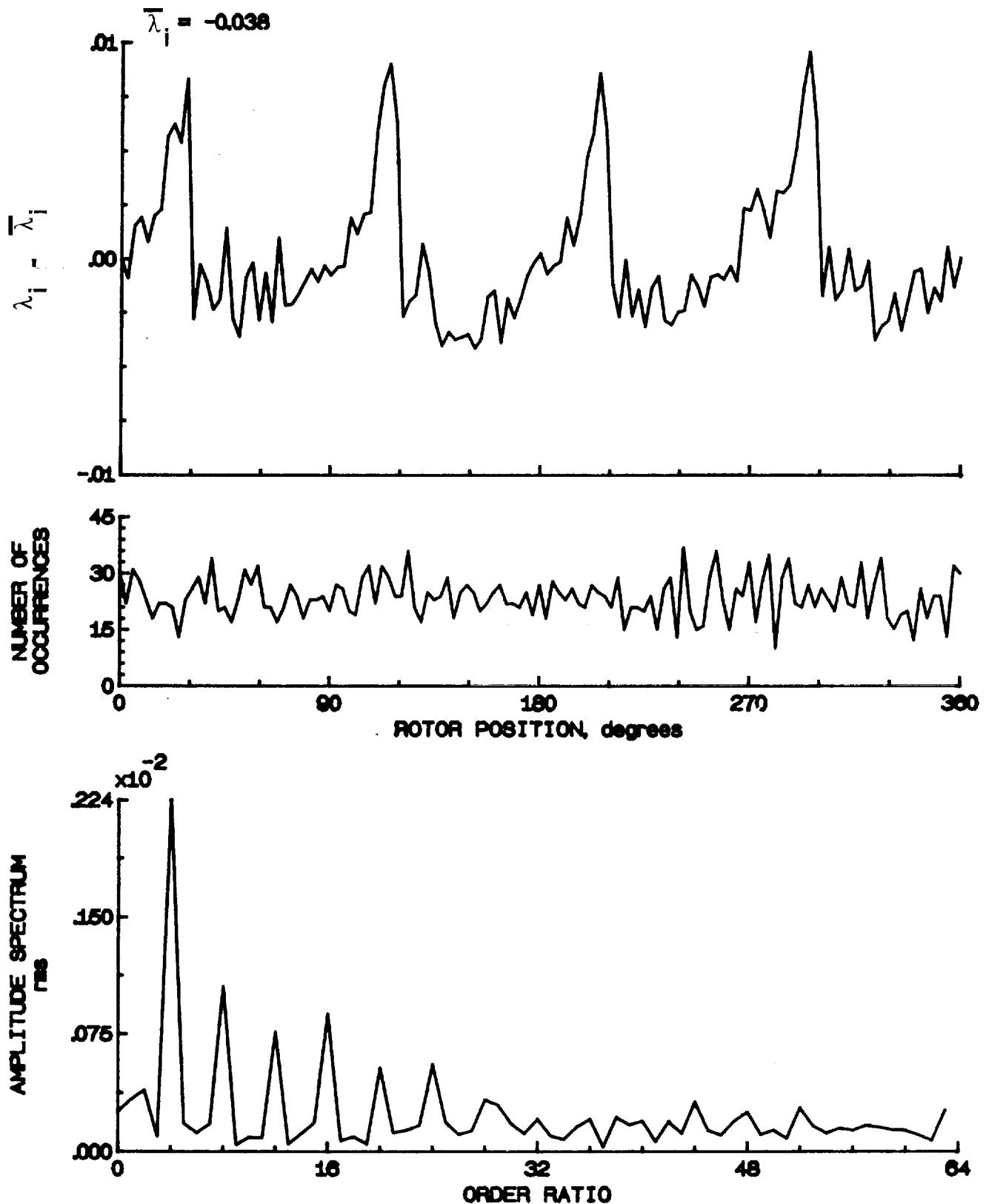


Figure 38.- Concluded.

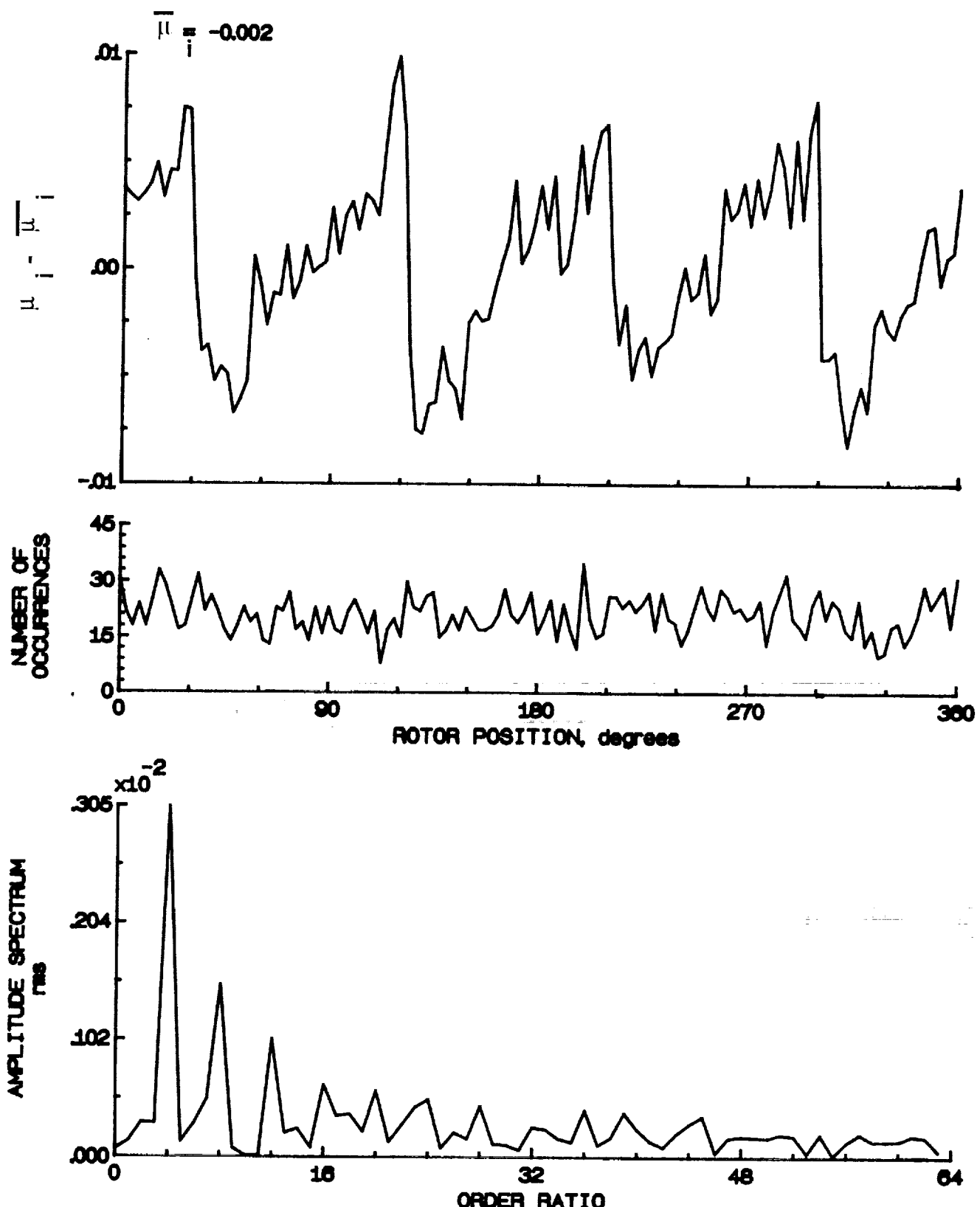


Figure 39.- Induced inflow velocity measured at 30 degrees and r/R of 102.

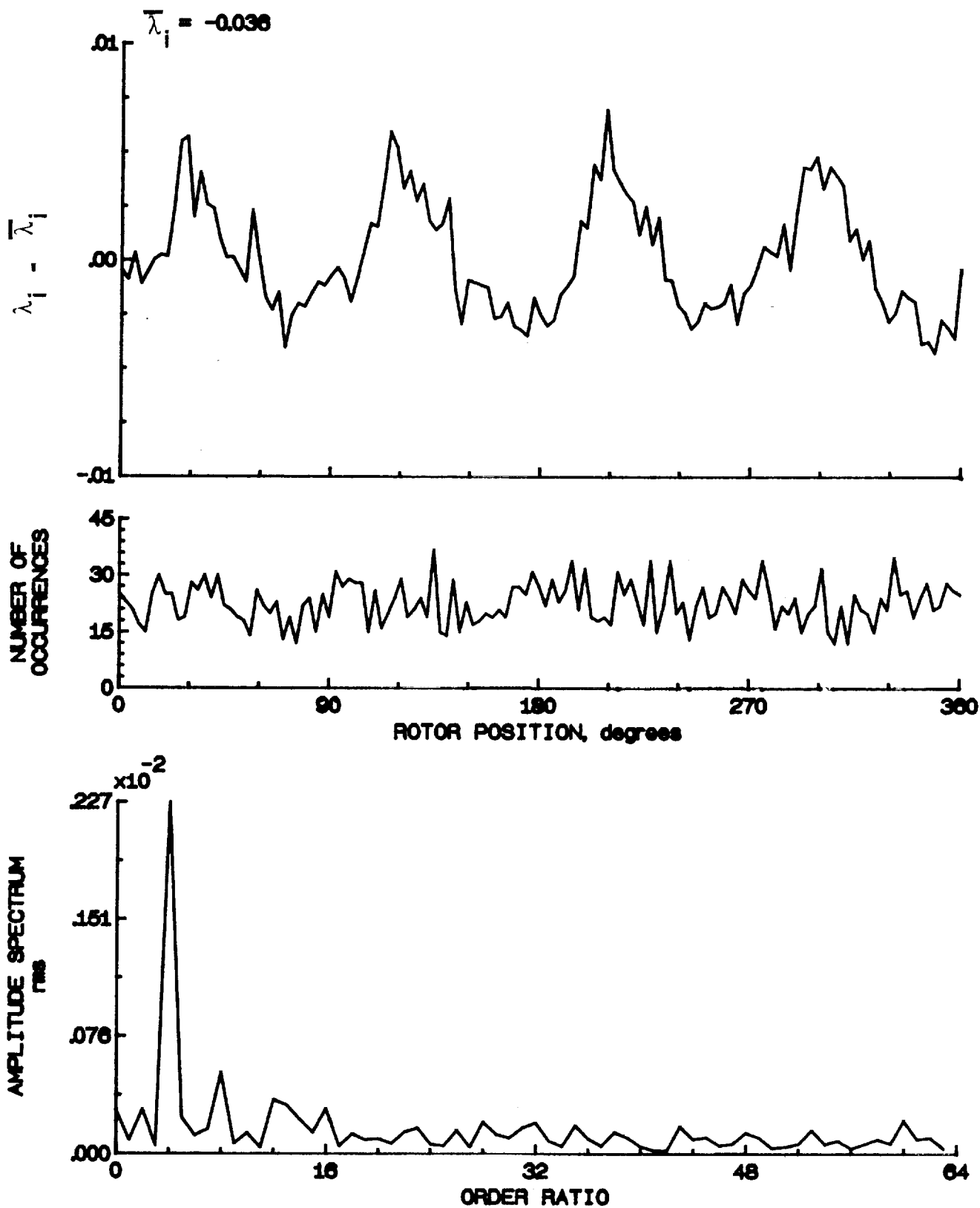


Figure 39.- Concluded.

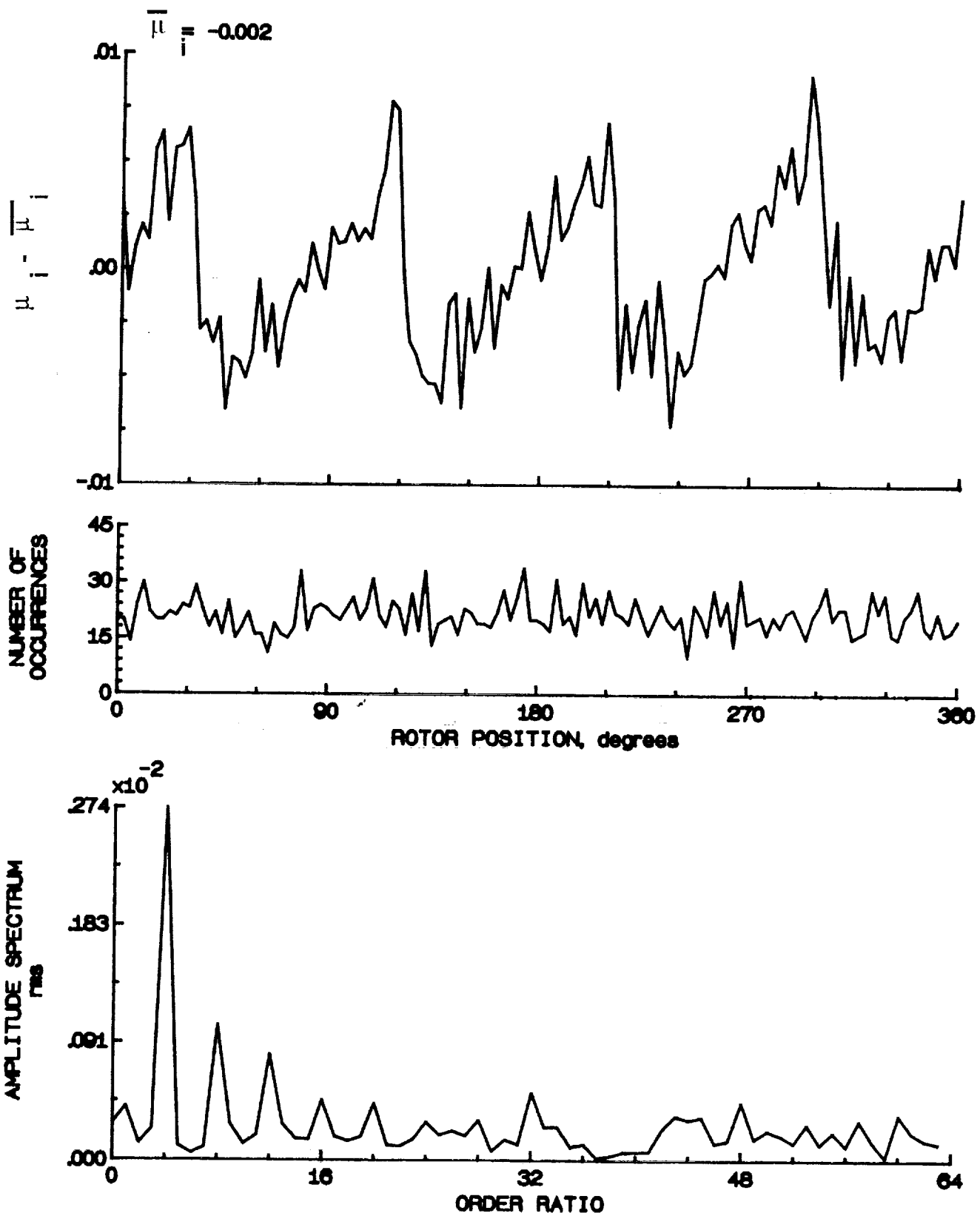


Figure 40.- Induced inflow velocity measured at 30 degrees and r/R of 1.04.

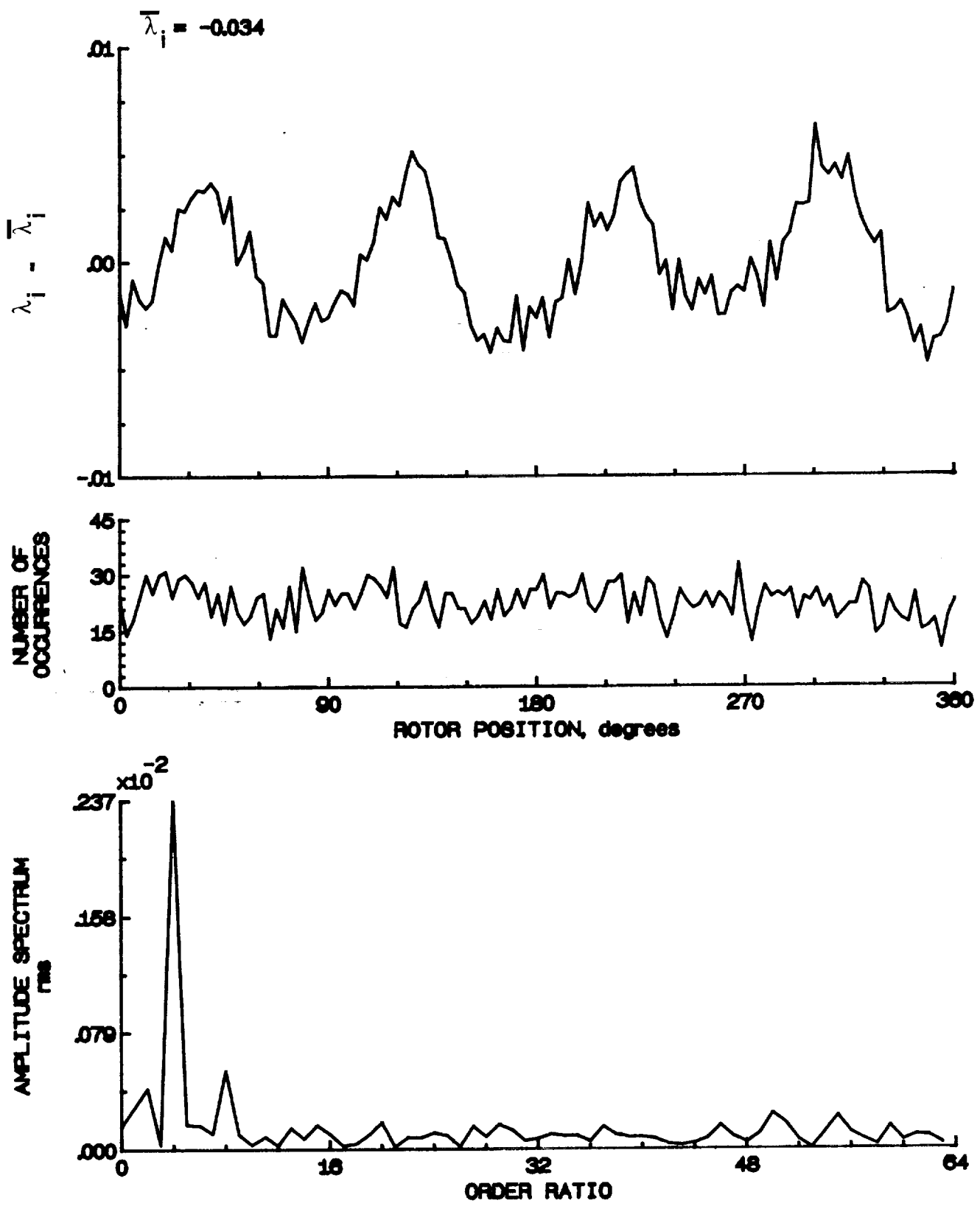


Figure 40.- Concluded.

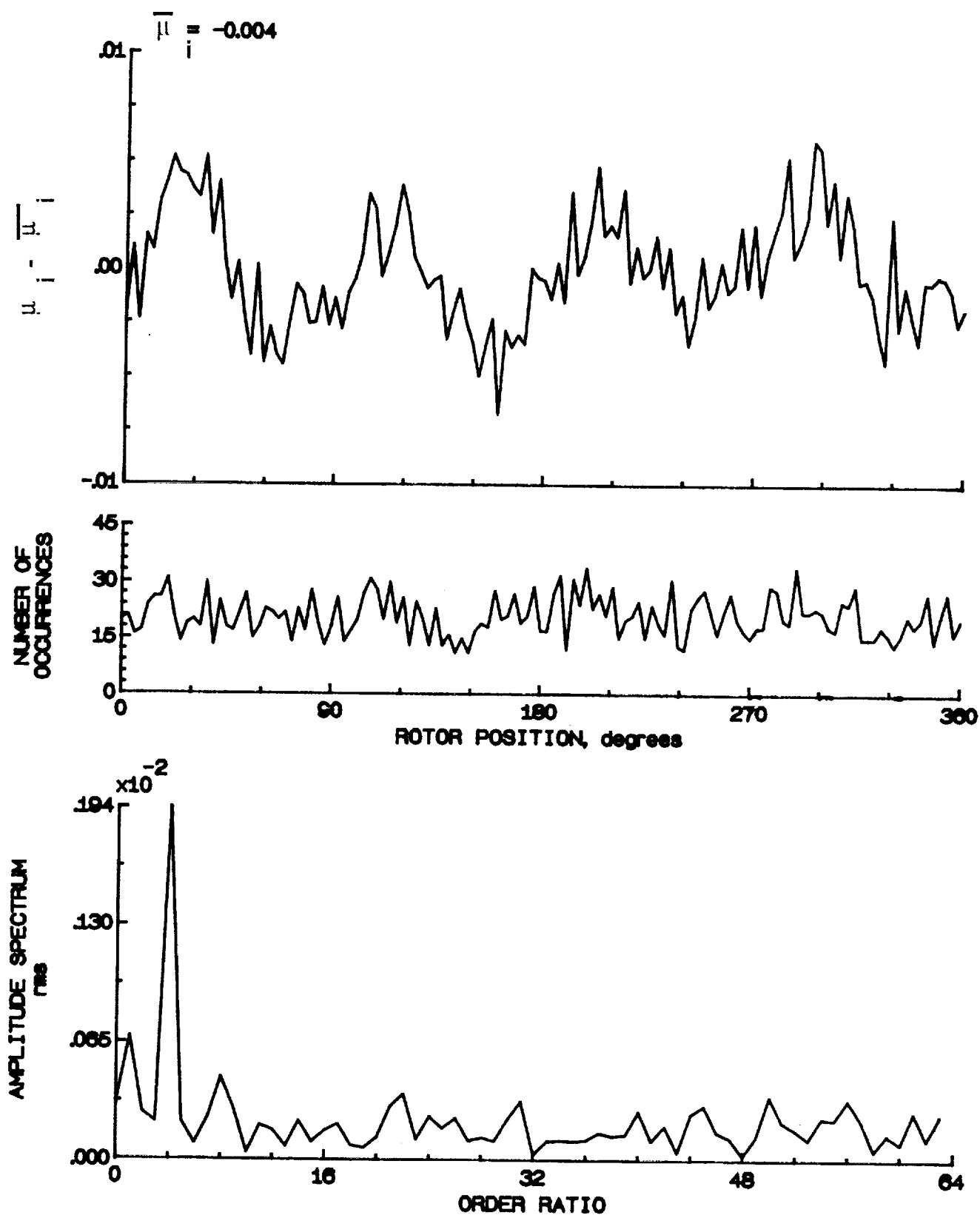


Figure 41.- Induced inflow velocity measured at 30 degrees and r/R of 1.10.

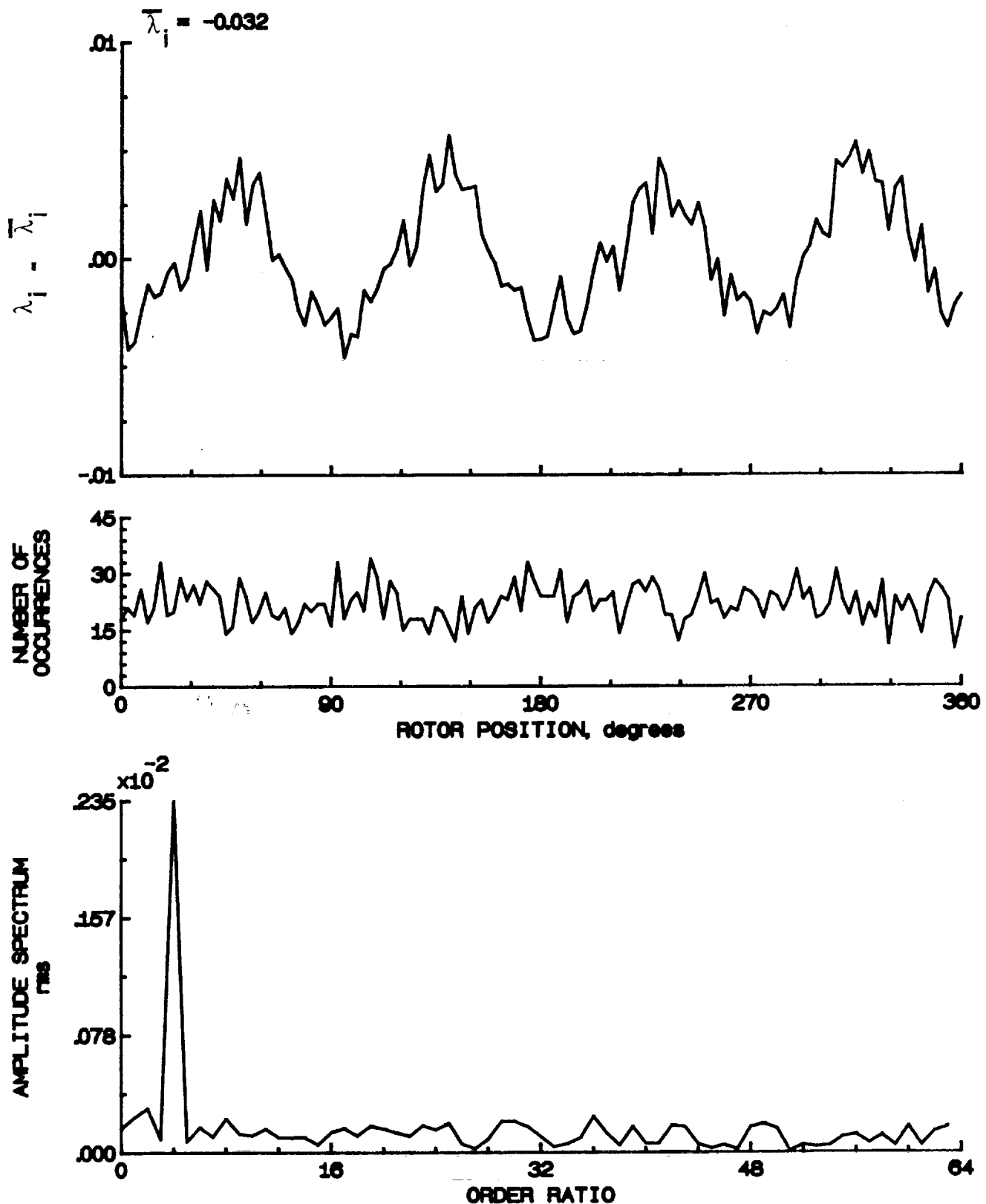


Figure 41.- Concluded.

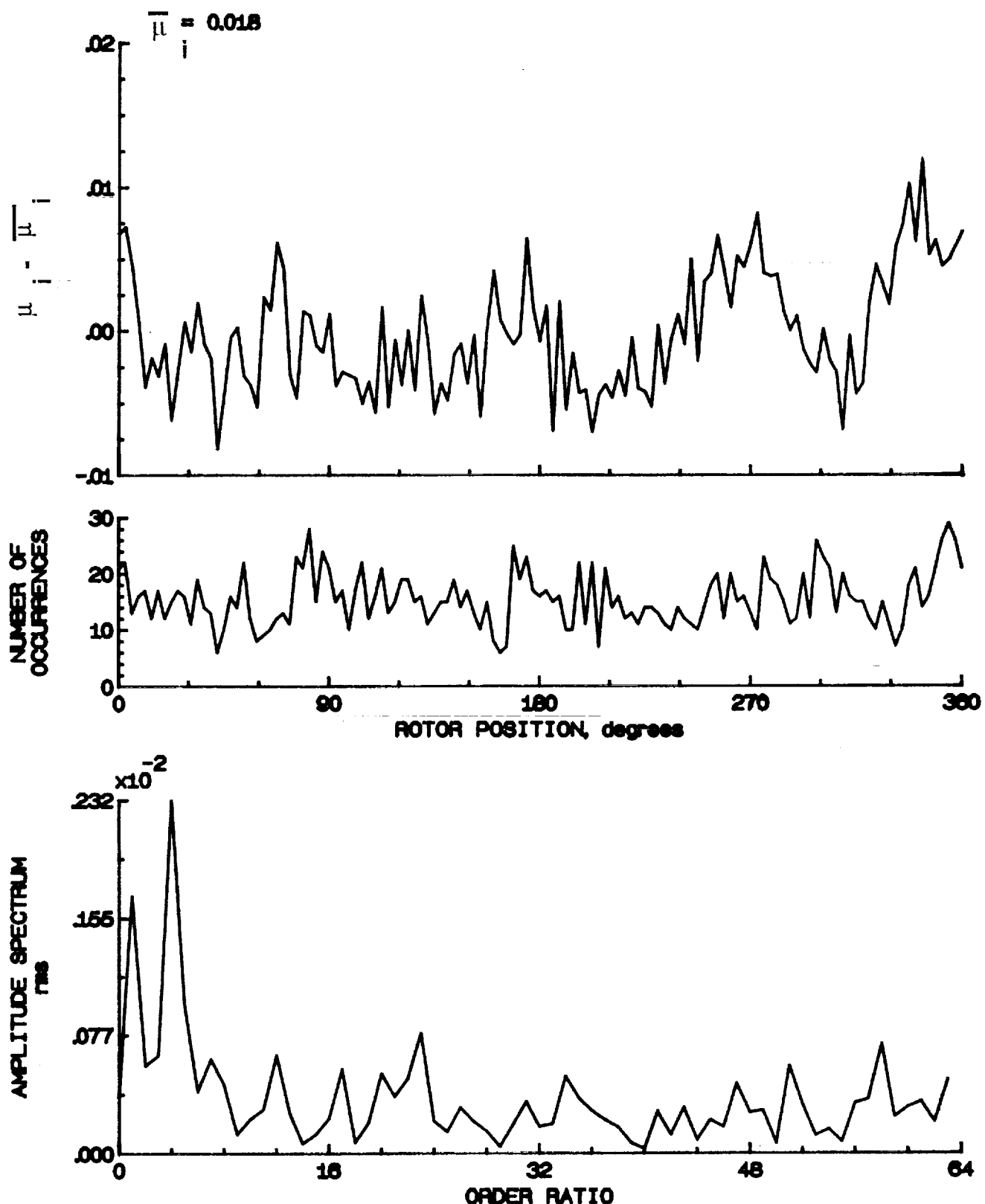


Figure 42.- Induced inflow velocity measured at 60 degrees and r/R of 0.20.

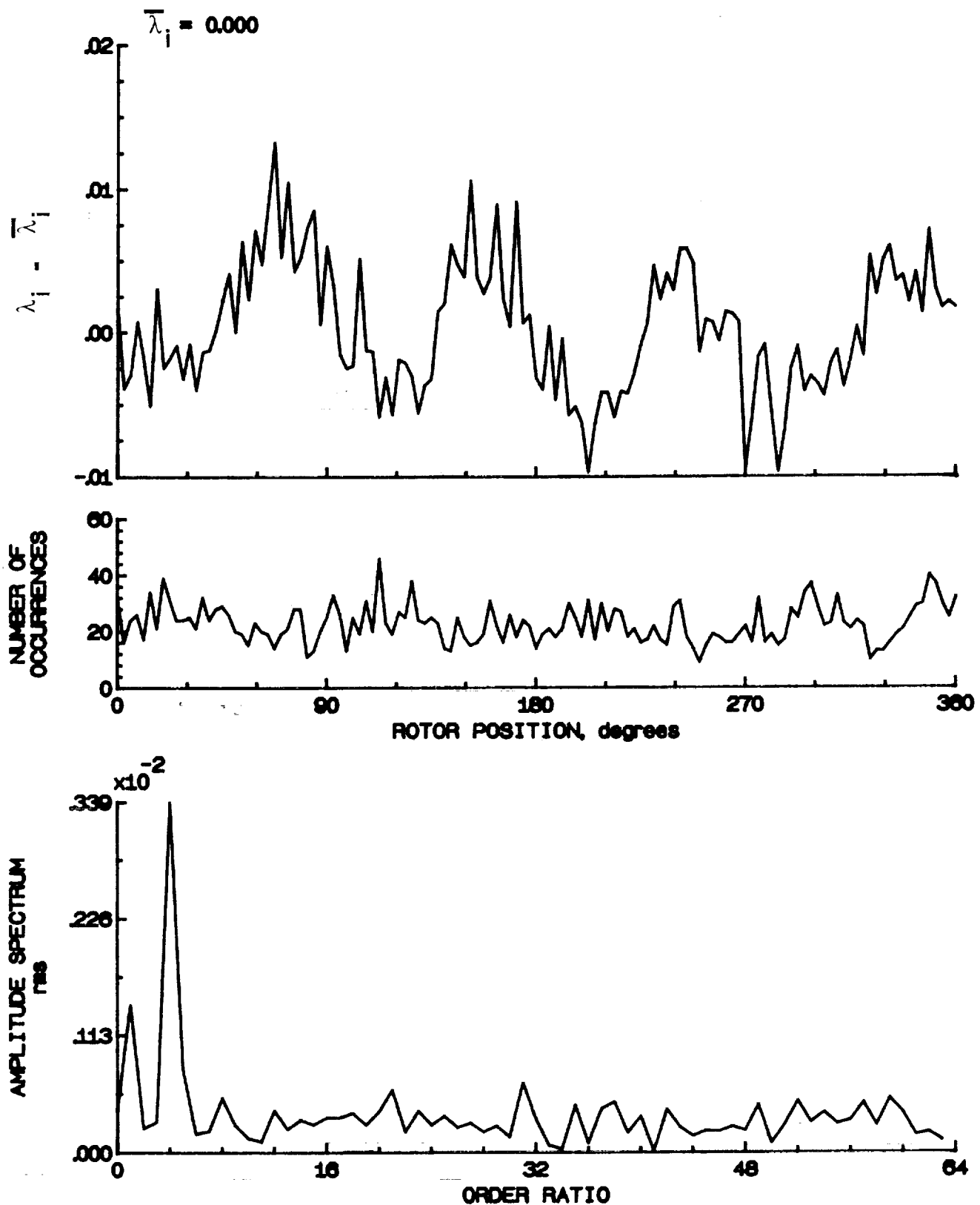


Figure 42.- Concluded.

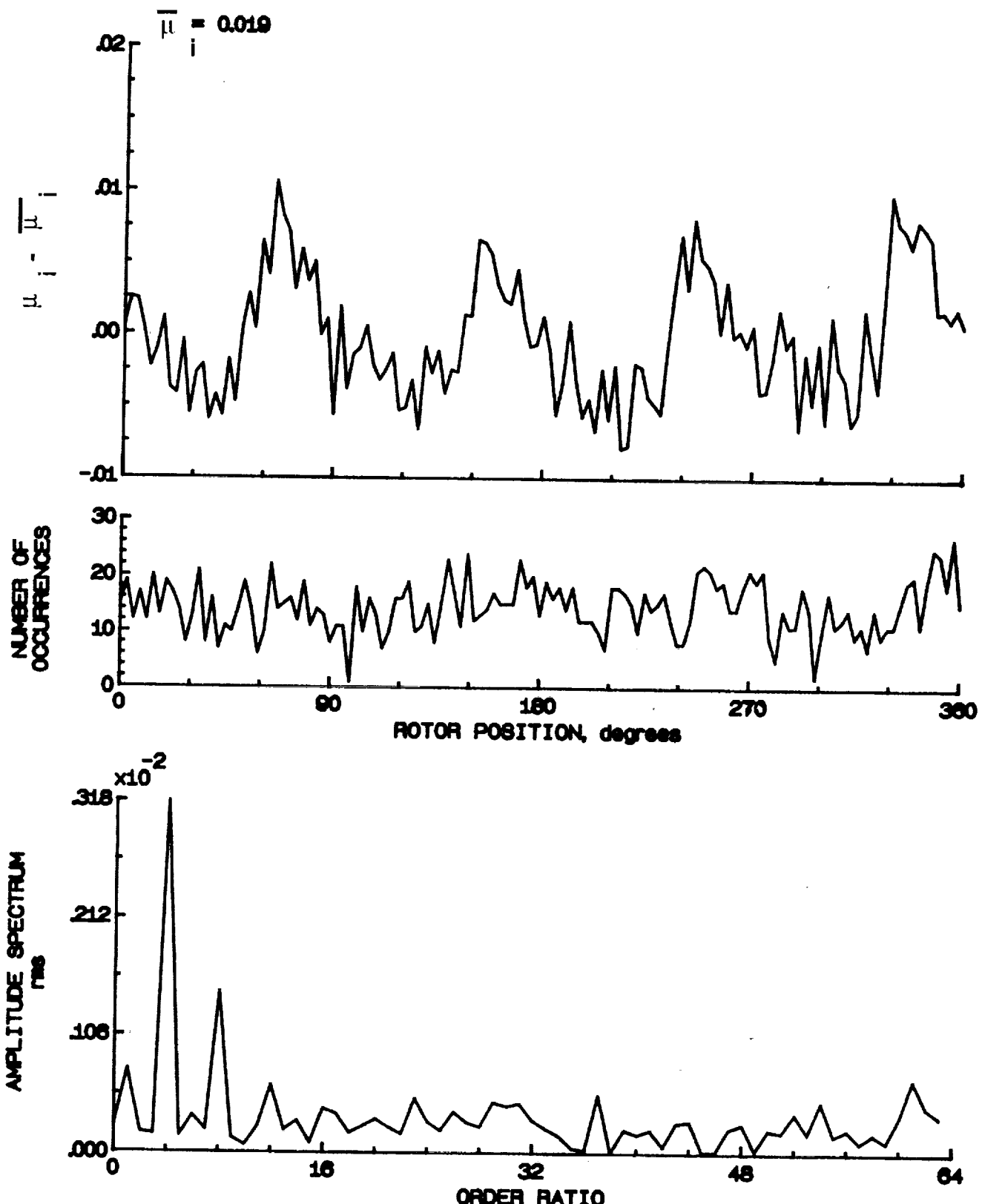


Figure 43.- Induced inflow velocity measured at 60 degrees and r/R of 0.40.

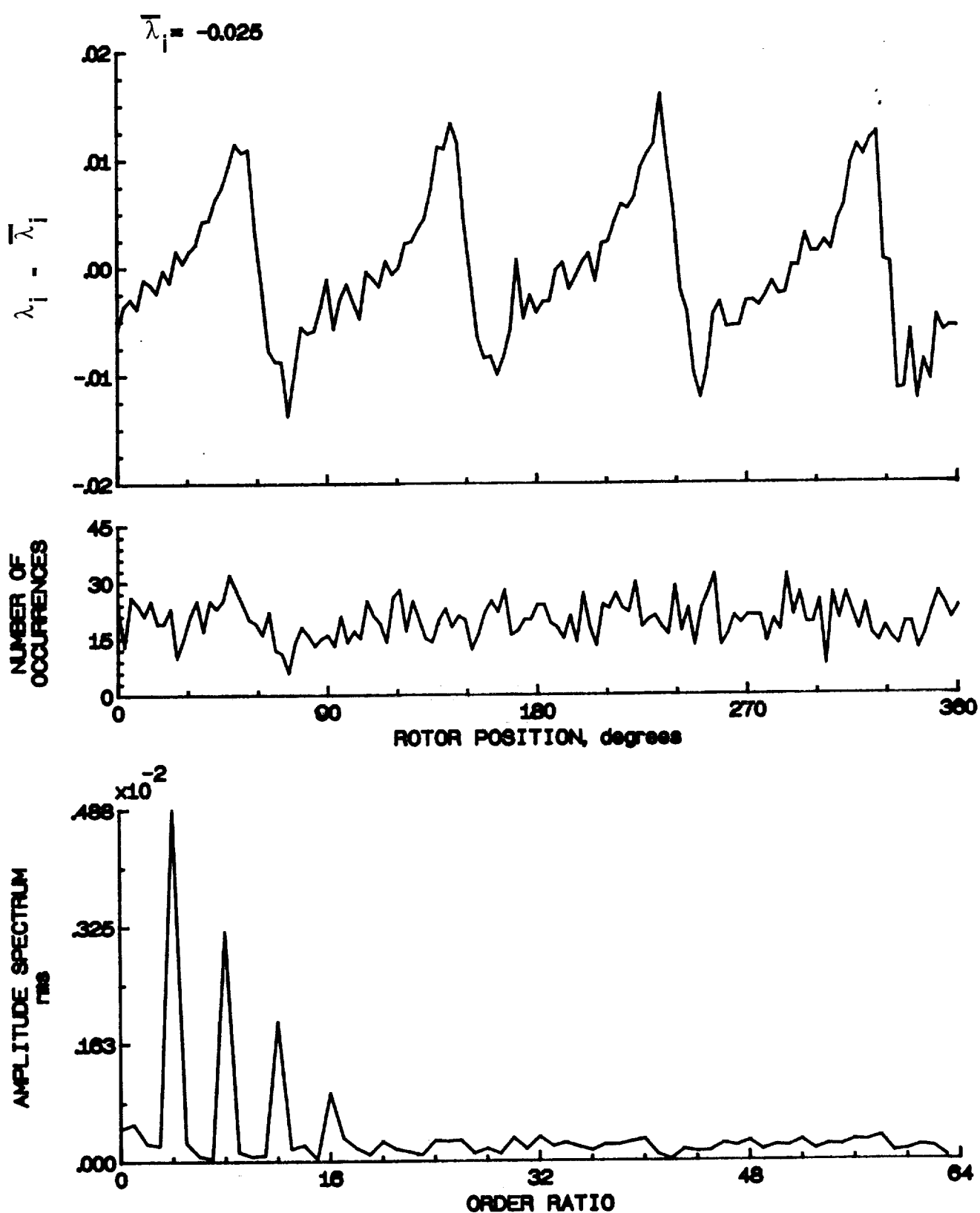


Figure 43.- Concluded.

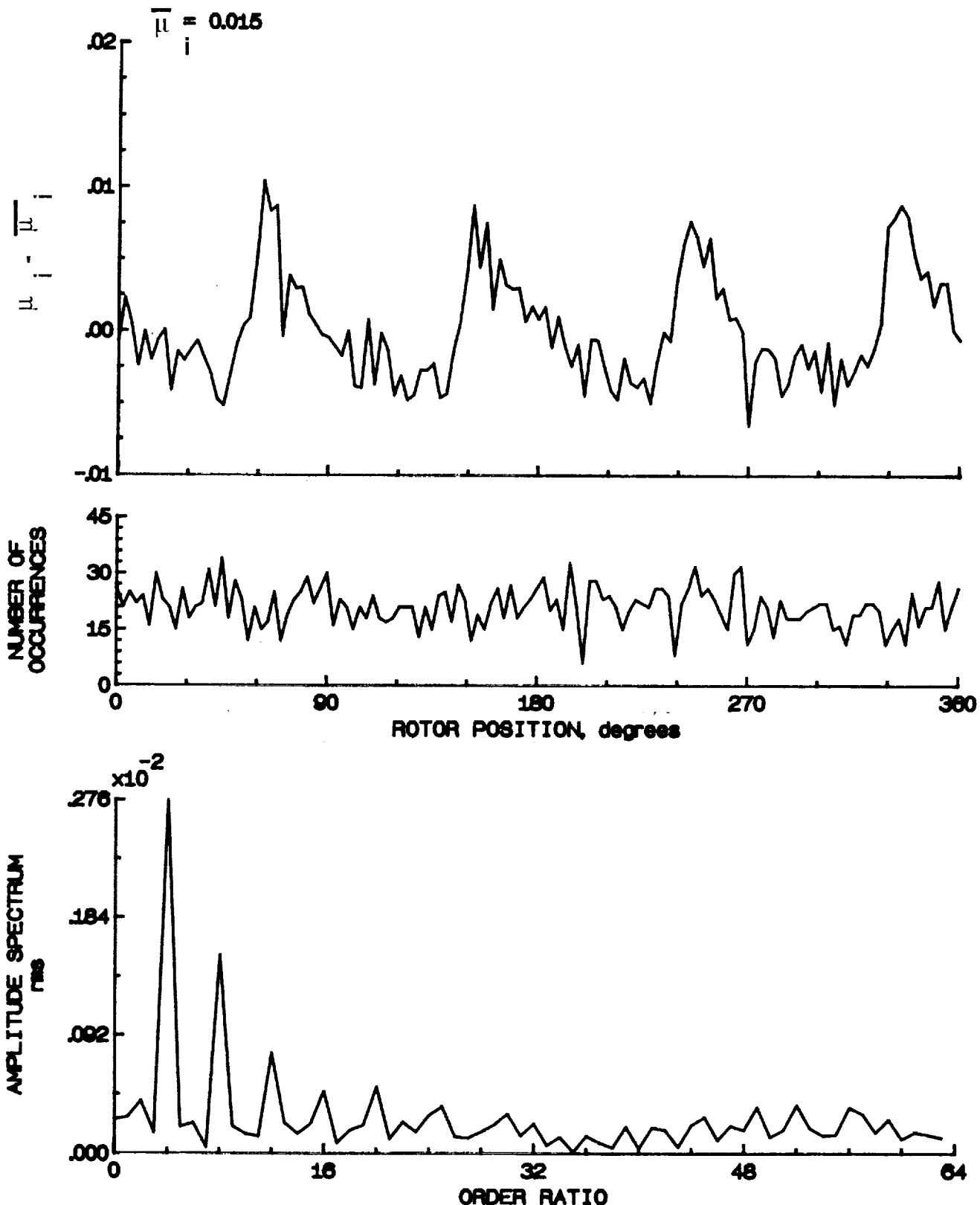


Figure 44.- Induced inflow velocity measured at 60 degrees and r/R of 0.50.

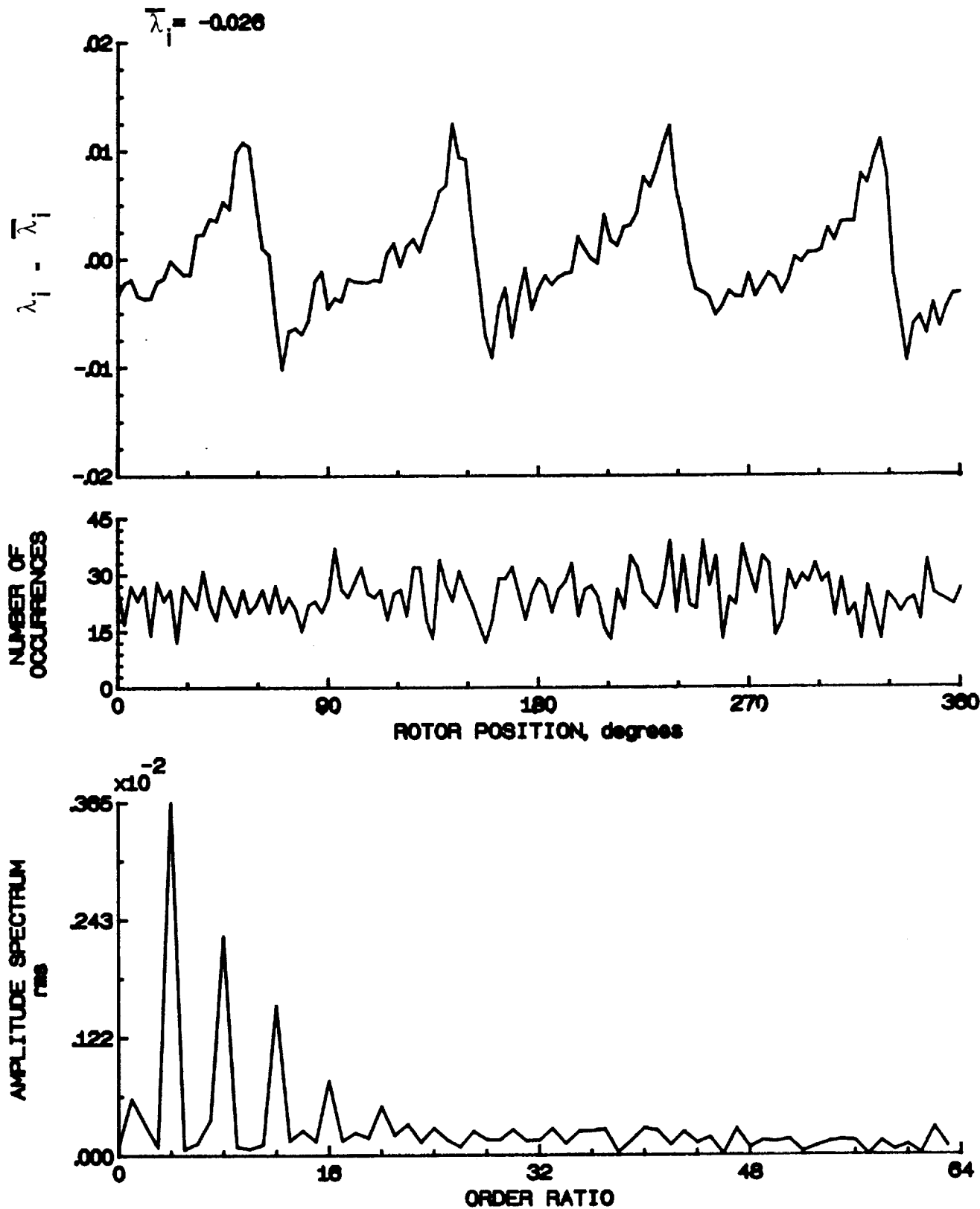


Figure 44.- Concluded.

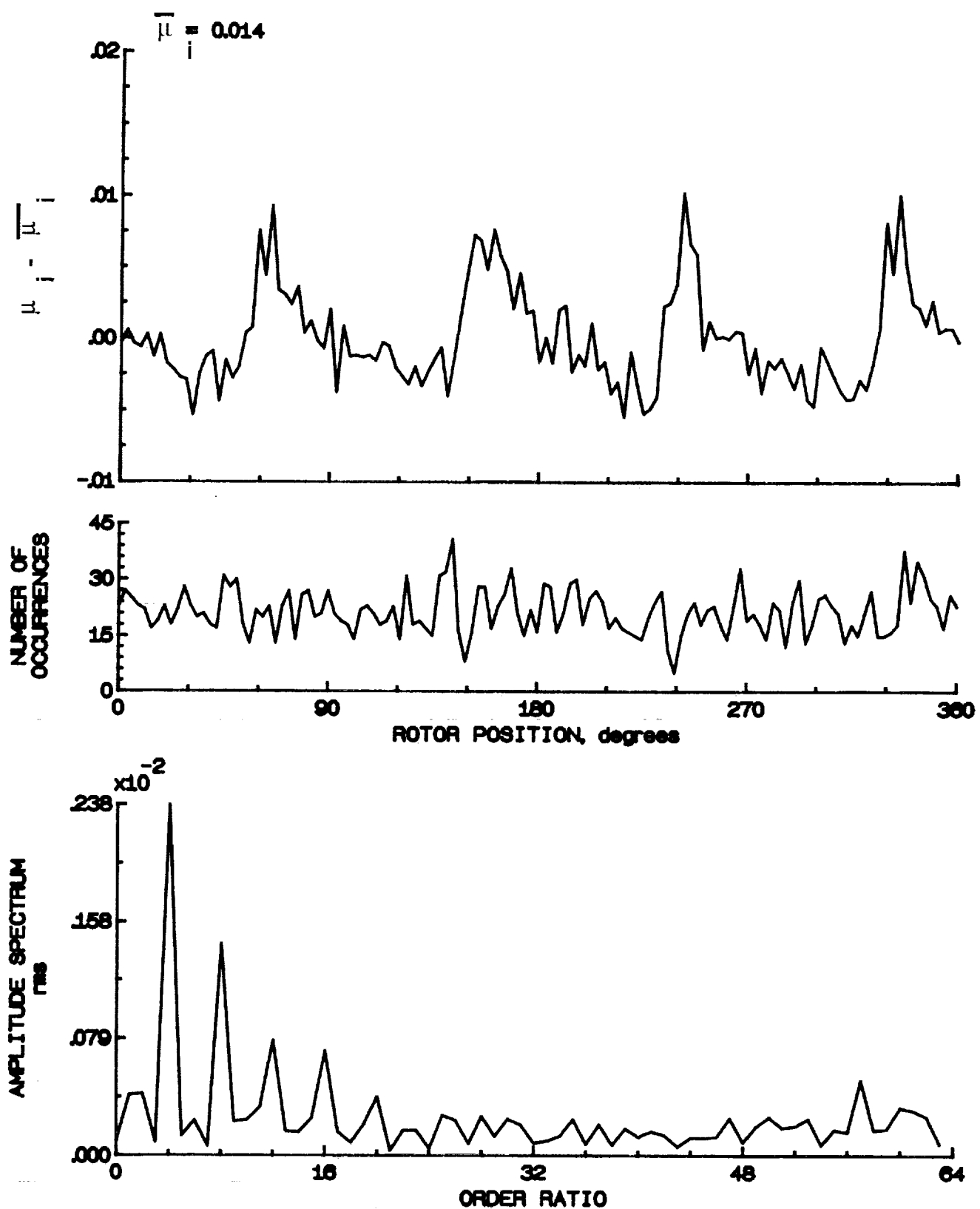


Figure 45.- Induced inflow velocity measured at 60 degrees and r/R of 0.00.

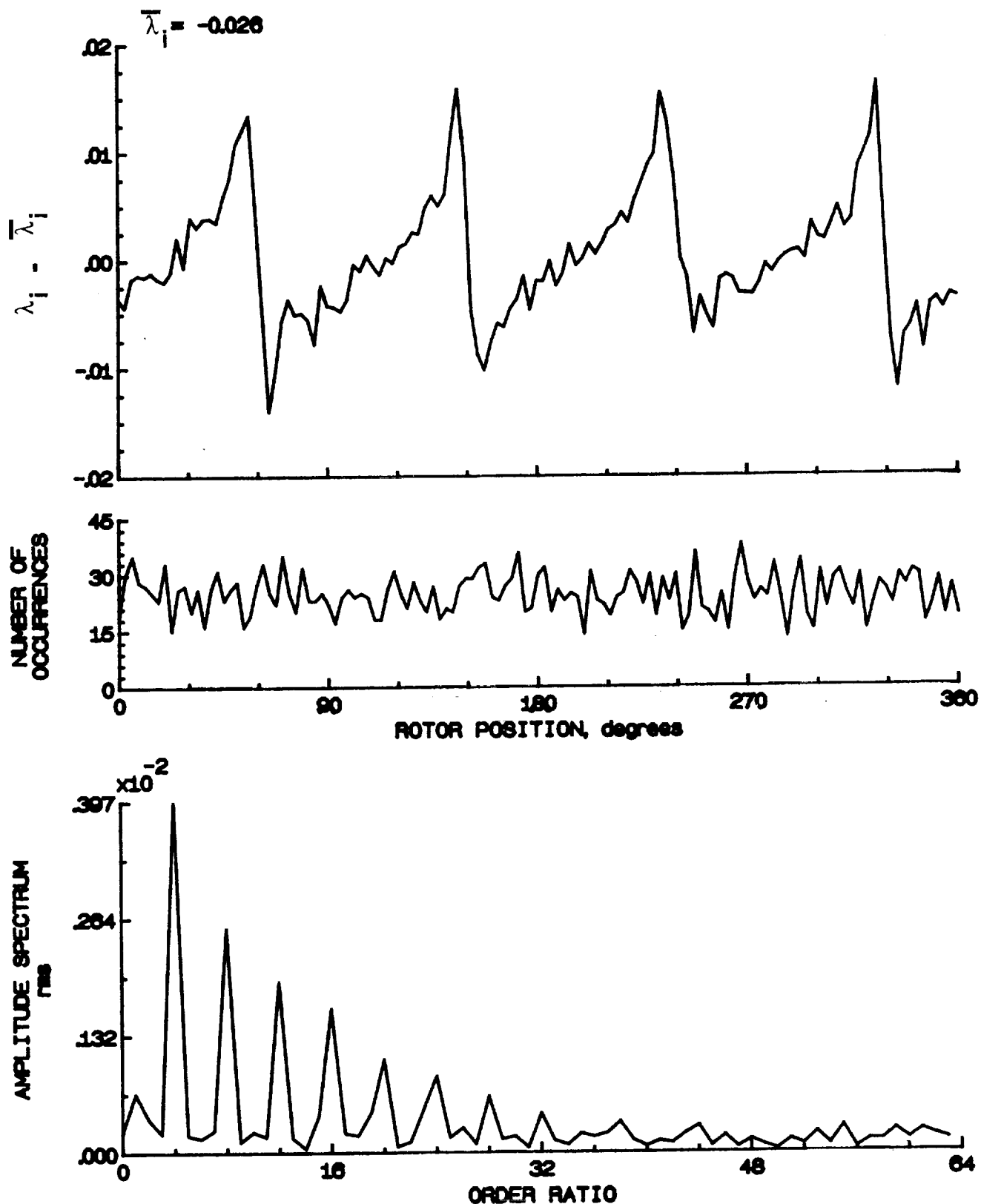


Figure 45.- Concluded.

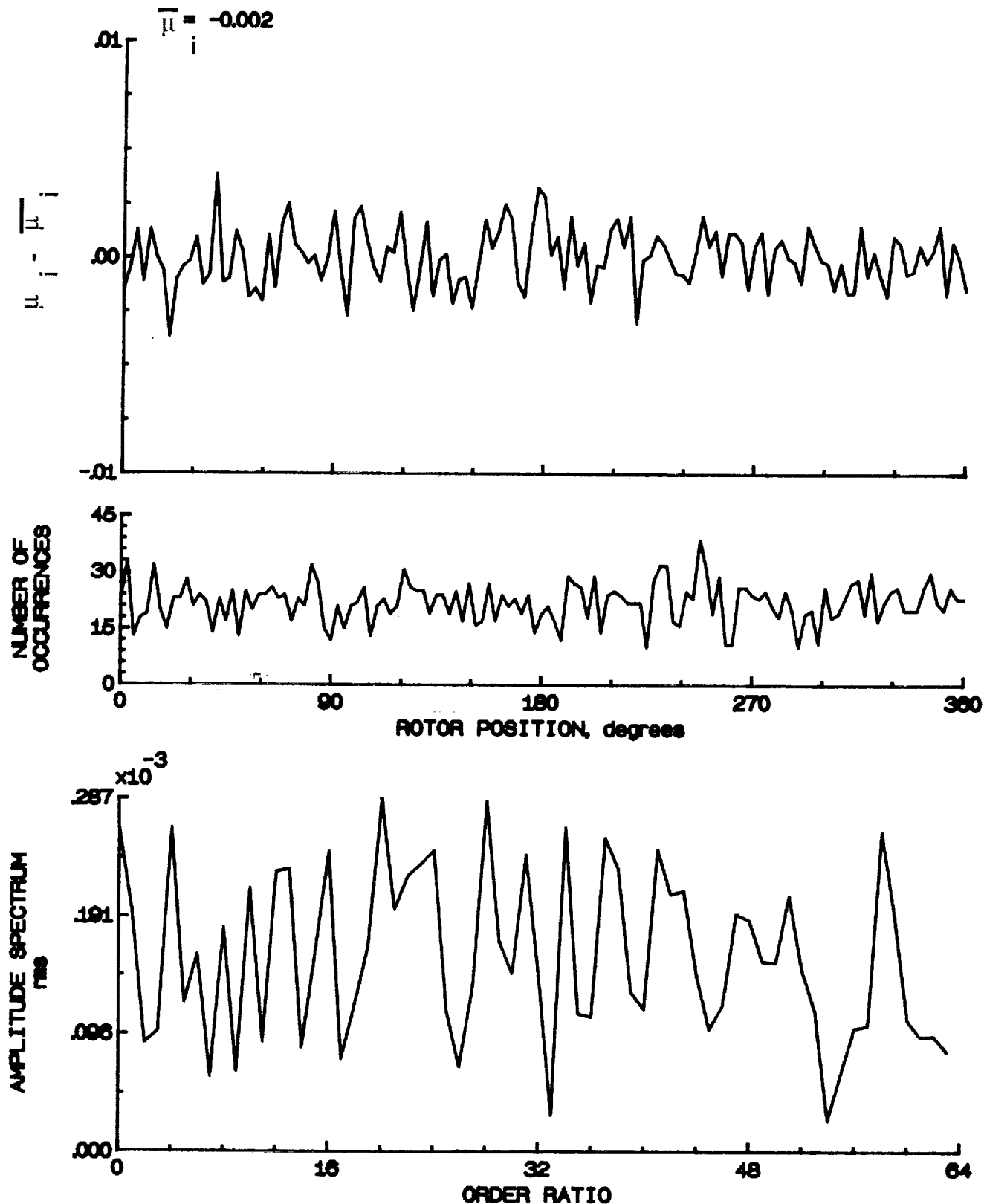


Figure 46.- Induced inflow velocity measured at 60 degrees and r/R of 0.70.

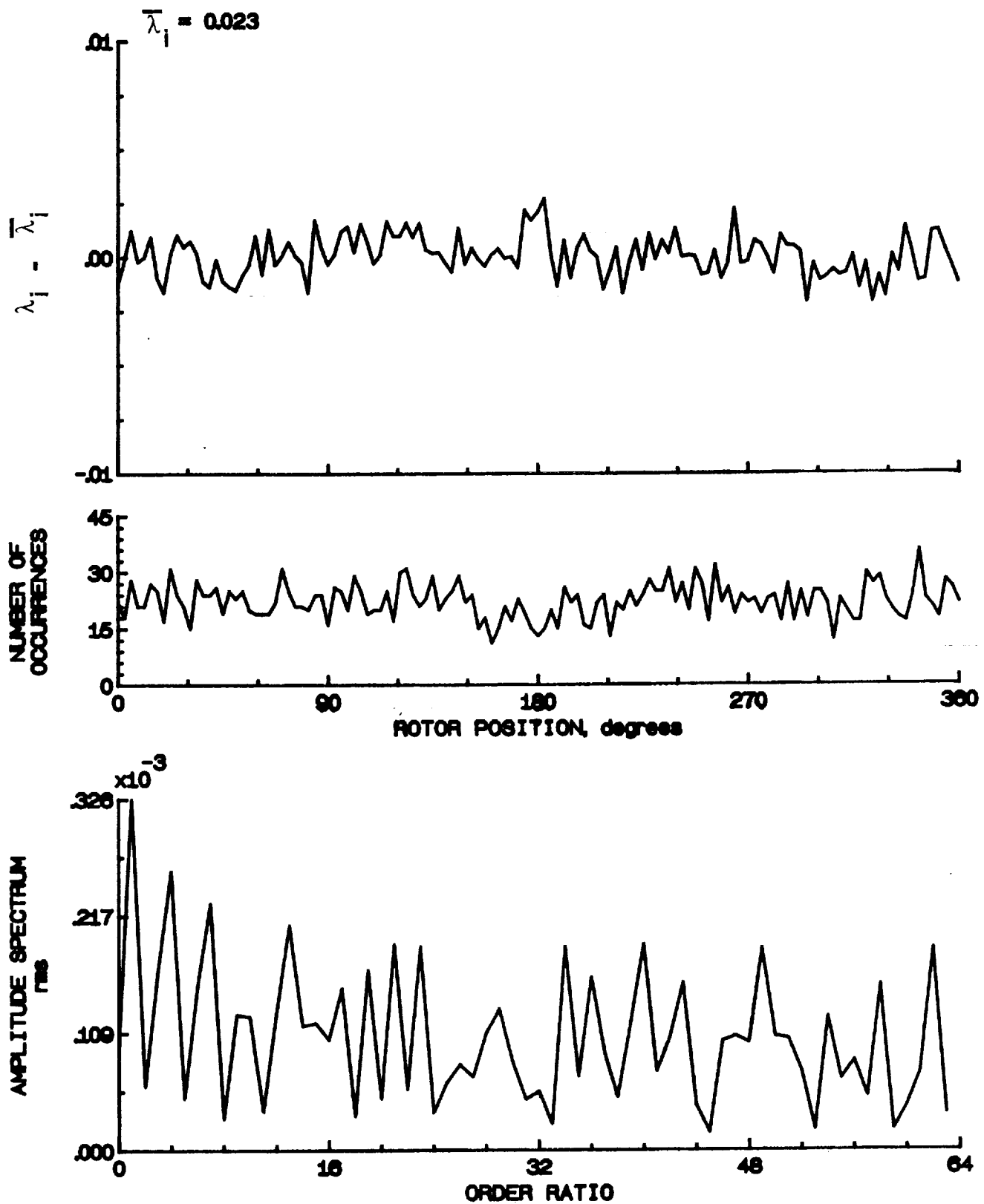


Figure 46.- Concluded.

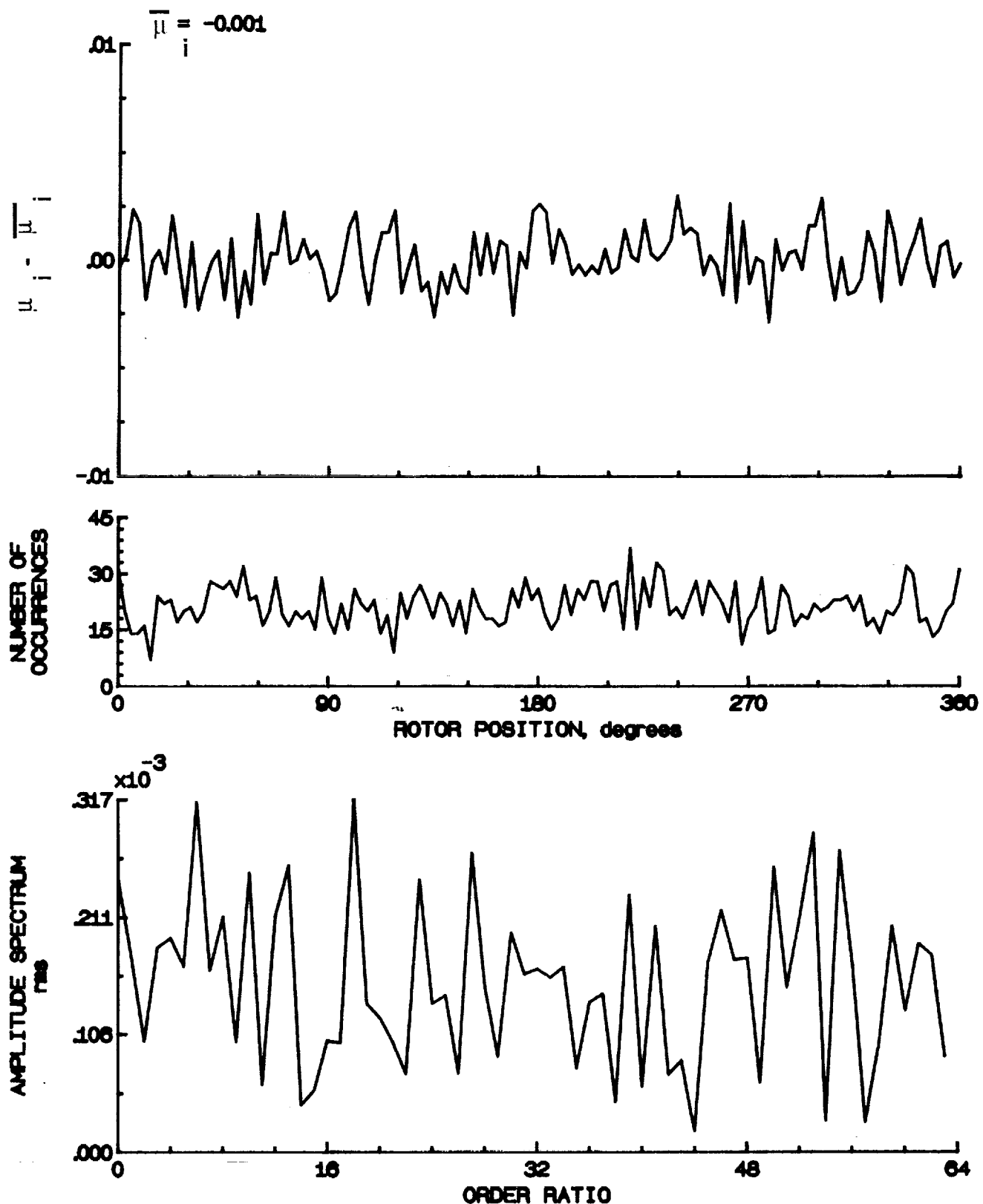


Figure 47.- Induced inflow velocity measured at 60 degrees and r/R of 0.74.

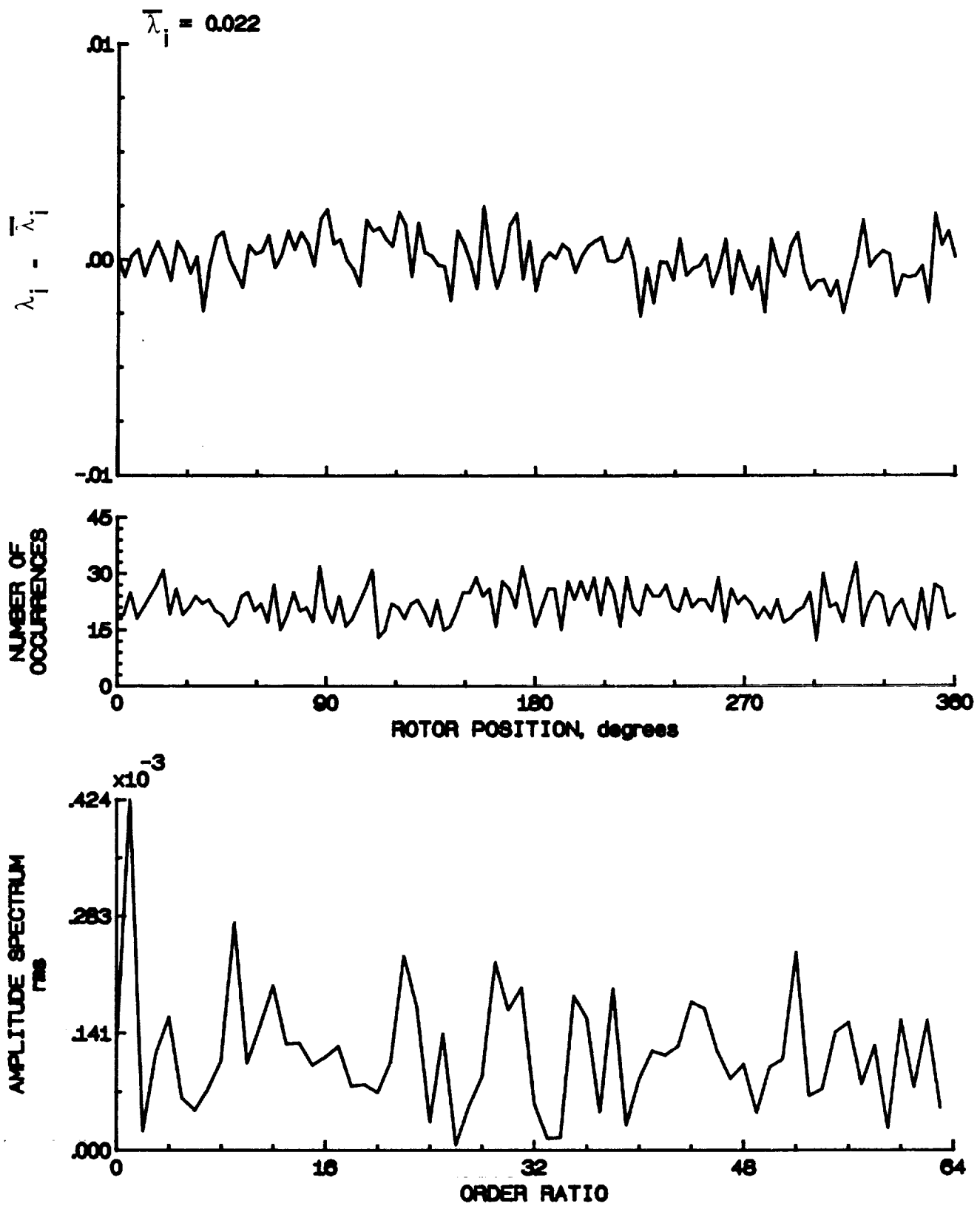


Figure 47.- Concluded.

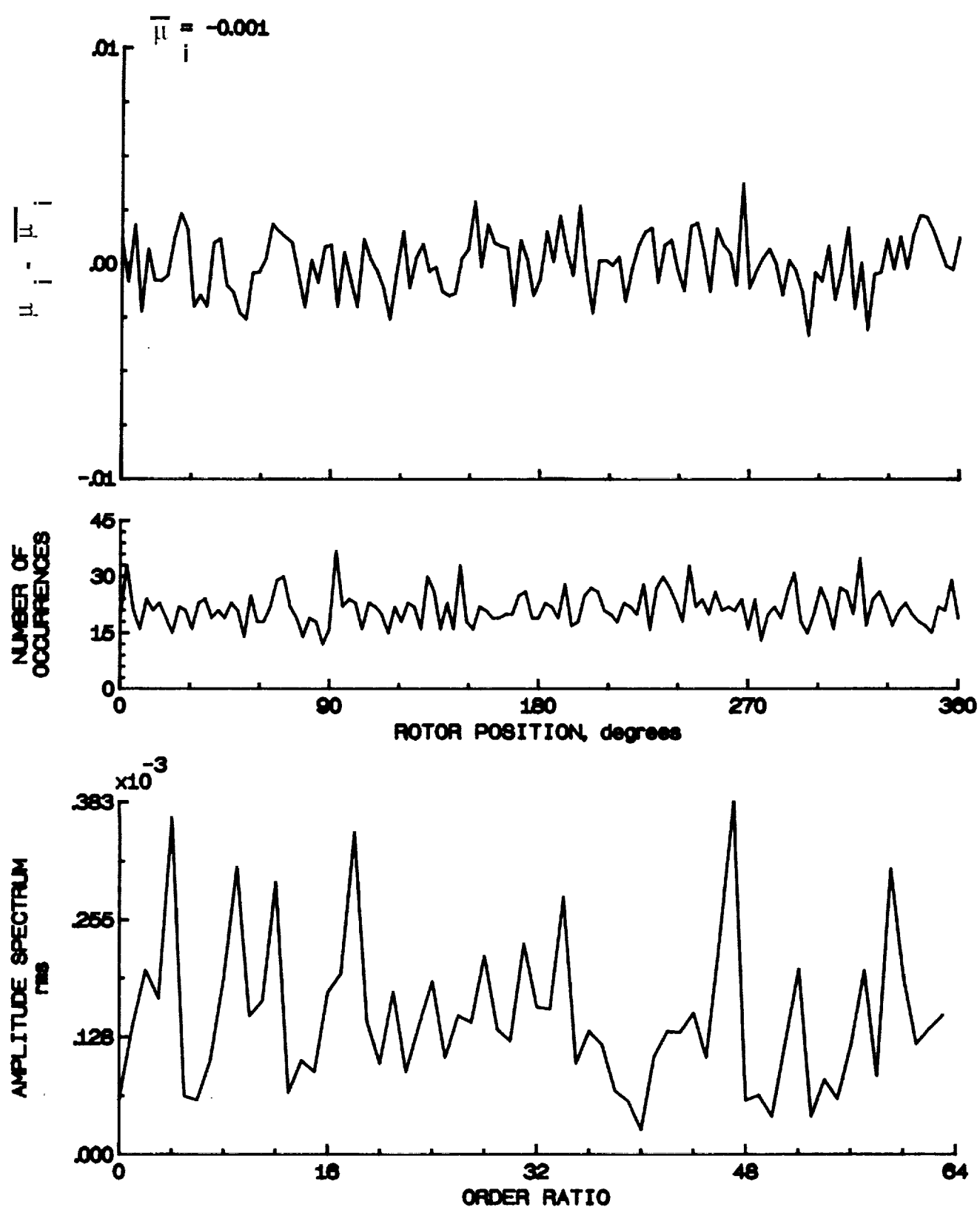


Figure 48.- Induced inflow velocity measured at 60 degrees and r/R of 0.78.

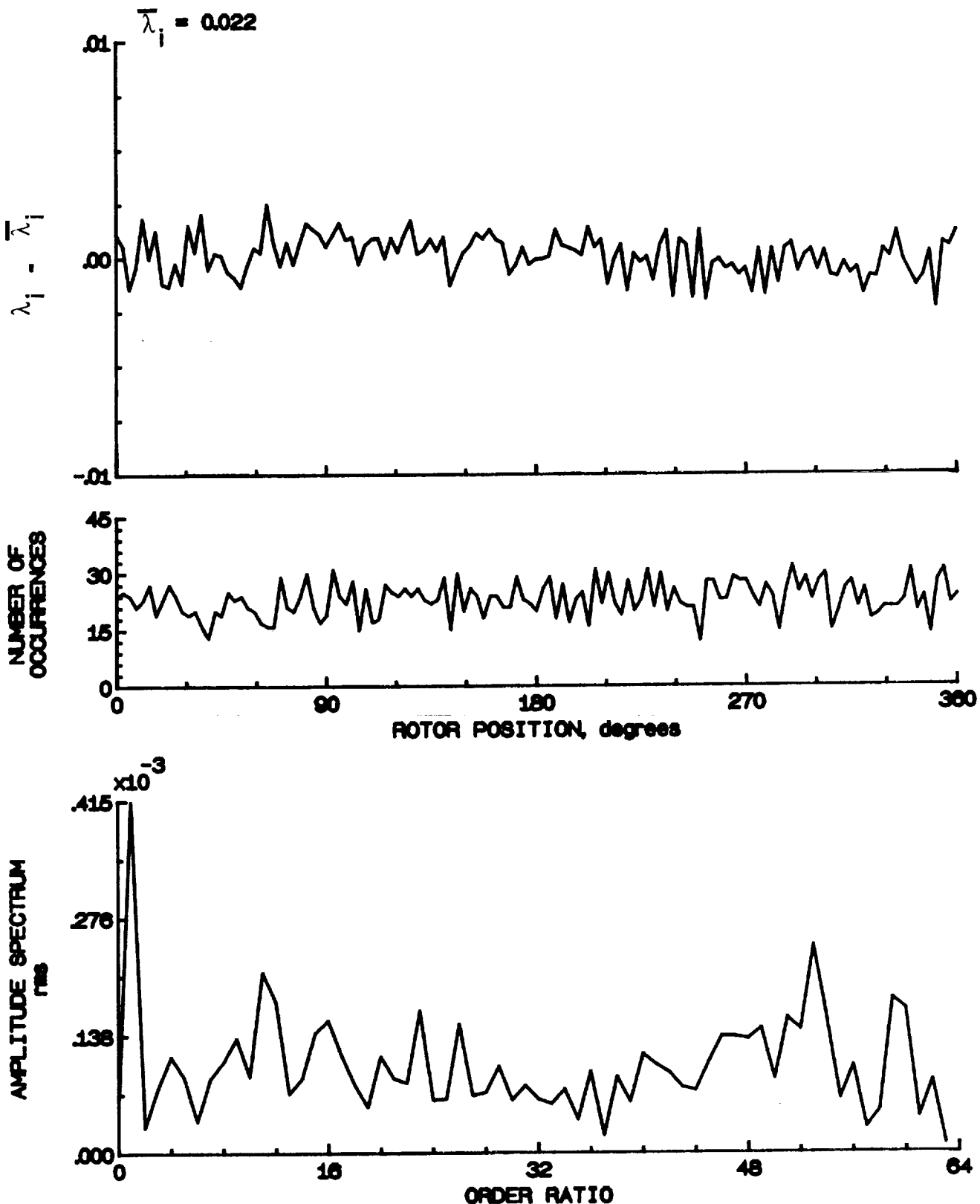


Figure 48.- Concluded.

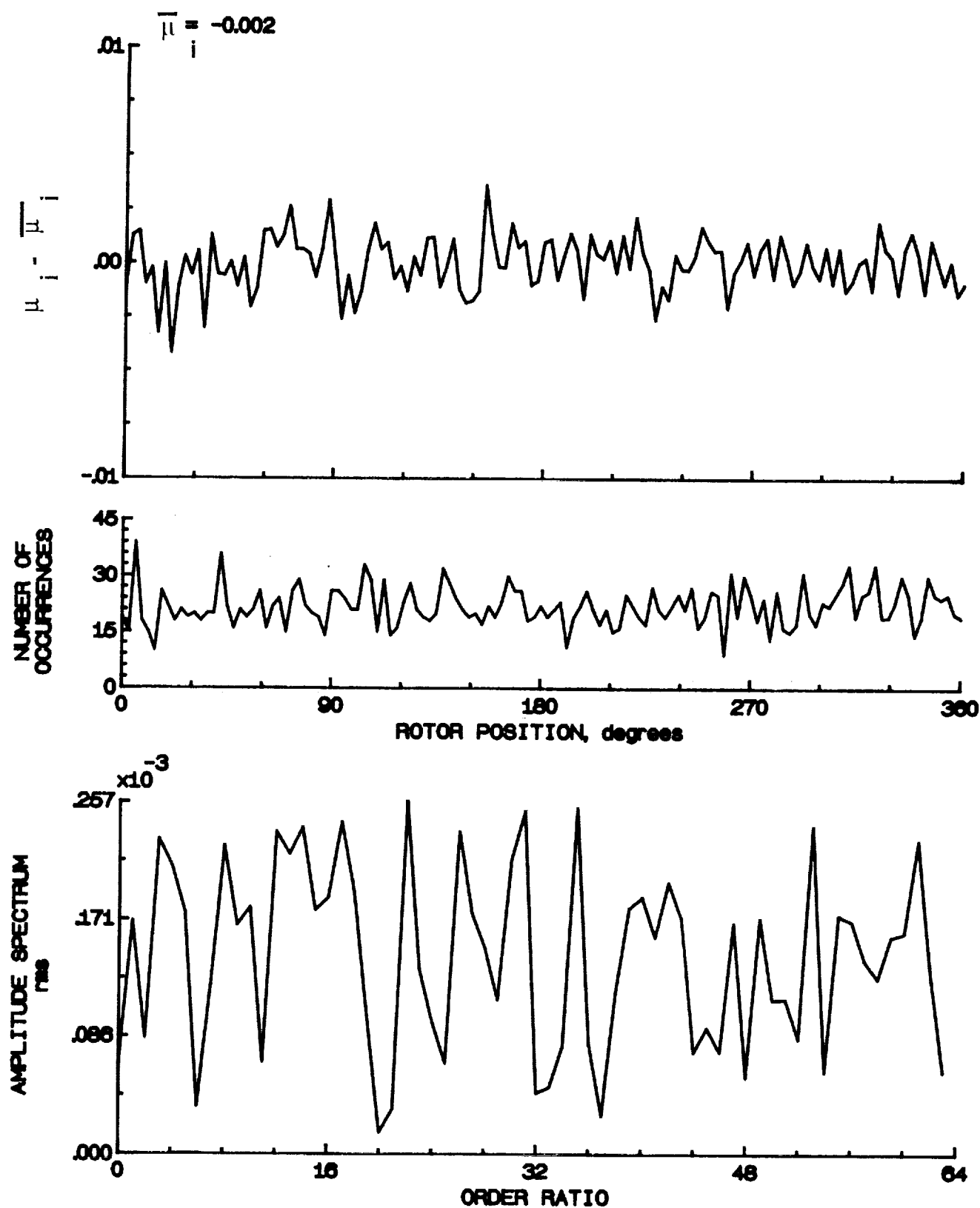


Figure 49.- Induced inflow velocity measured at 60 degrees and r/R of 0.82.

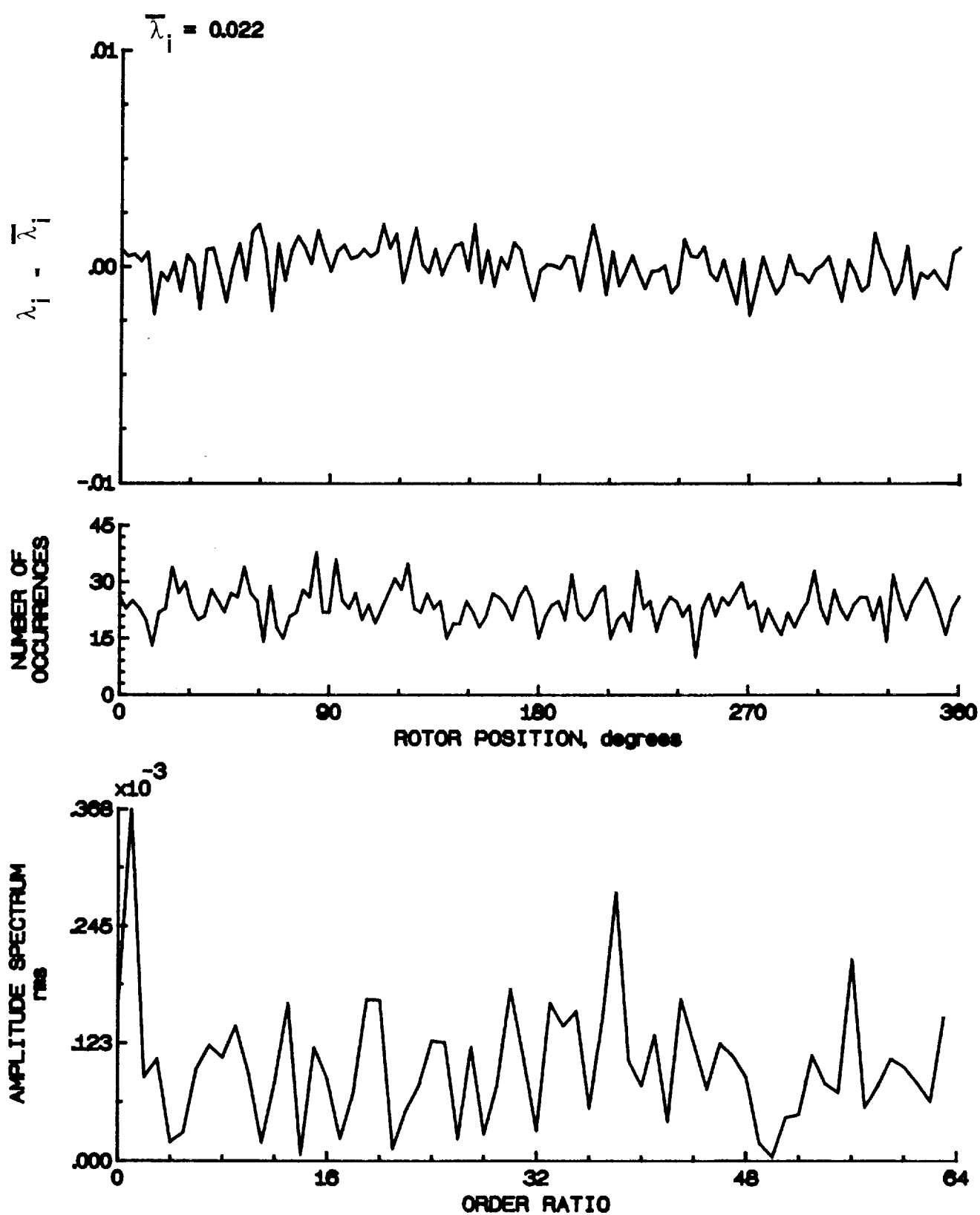


Figure 49.- Concluded.

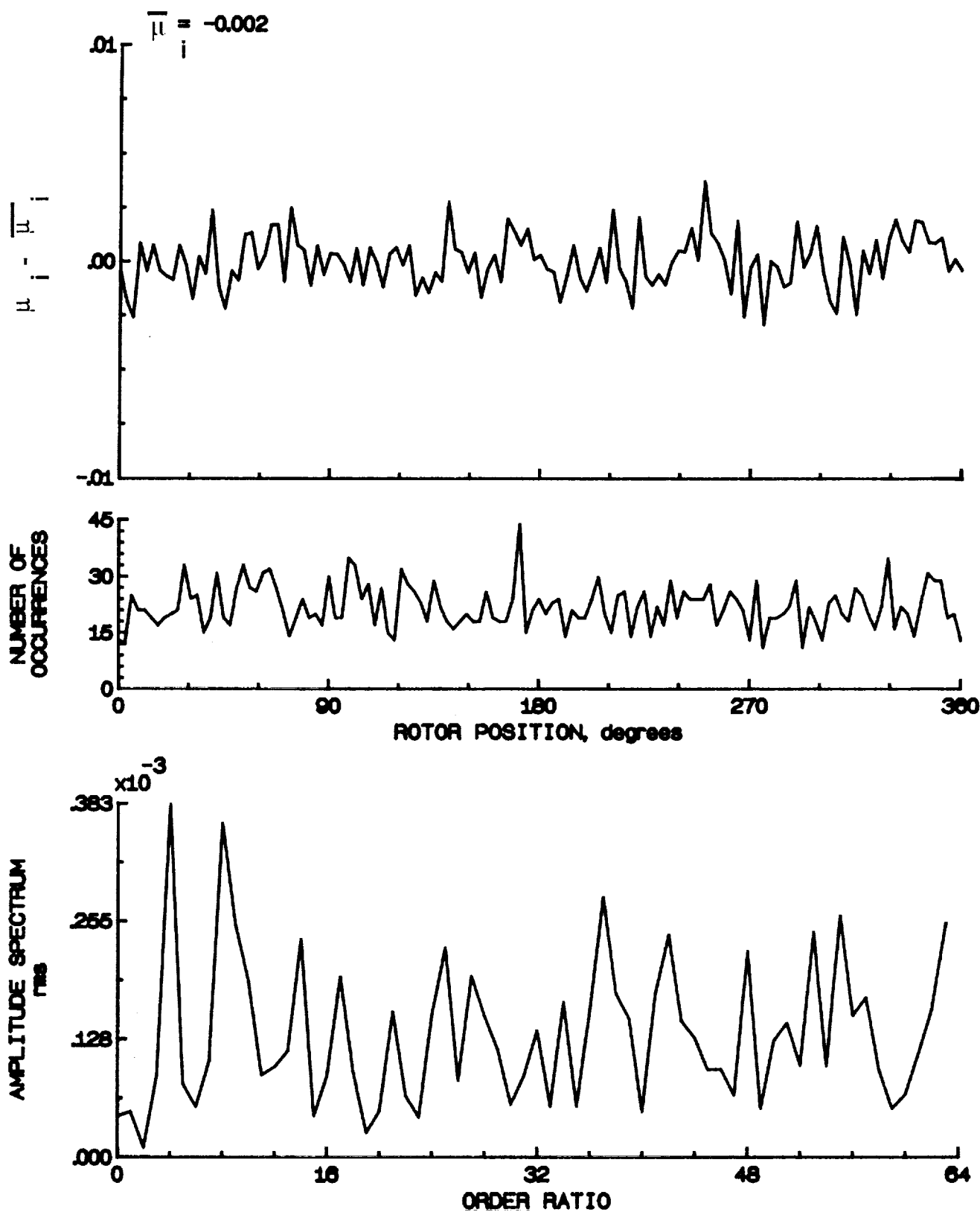


Figure 50.- Induced inflow velocity measured at 60 degrees and r/R of 0.86.

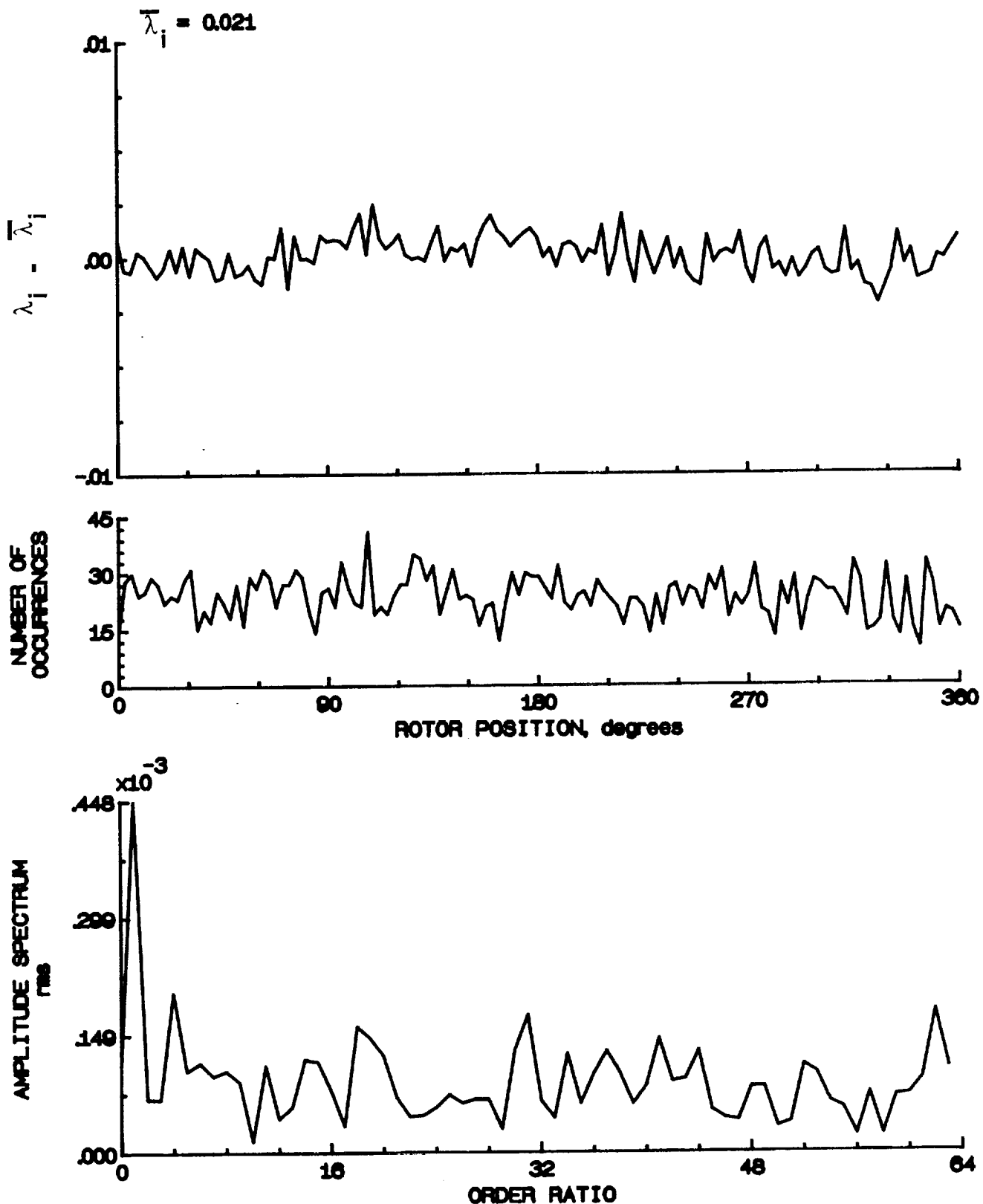


Figure 50.- Concluded.

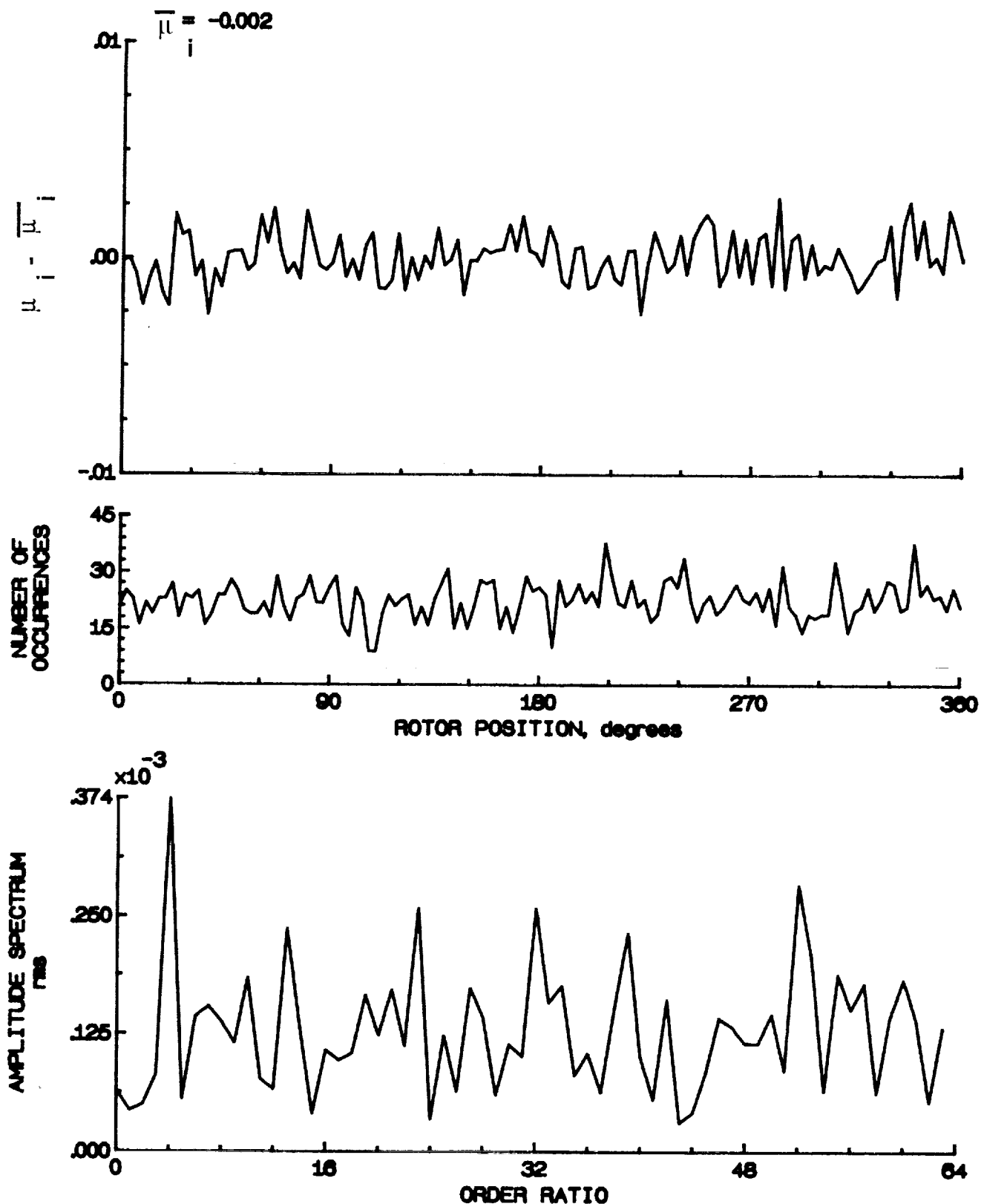


Figure 51.- Induced inflow velocity measured at 60 degrees and r/R of 0.90.

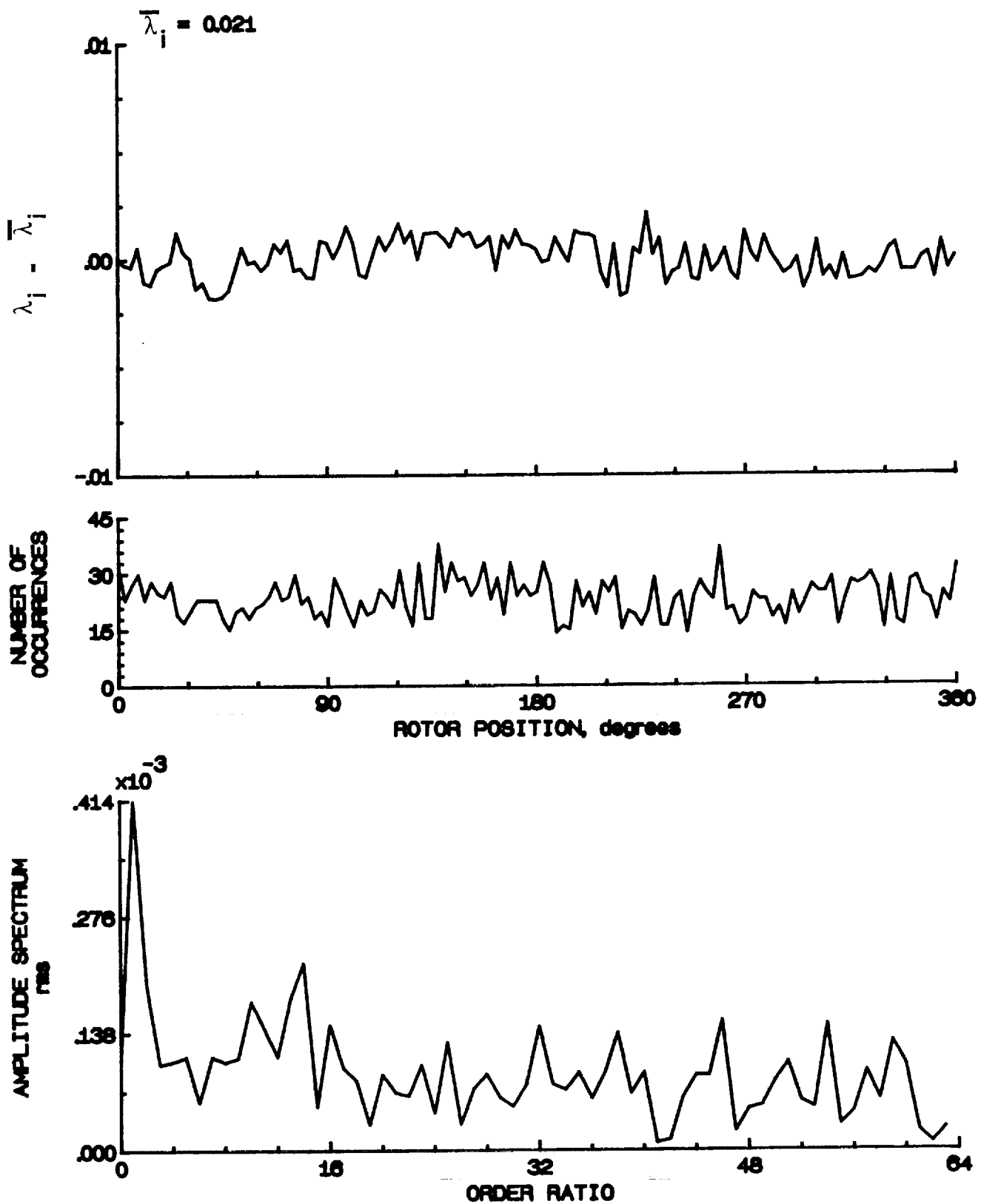


Figure 51.- Concluded.

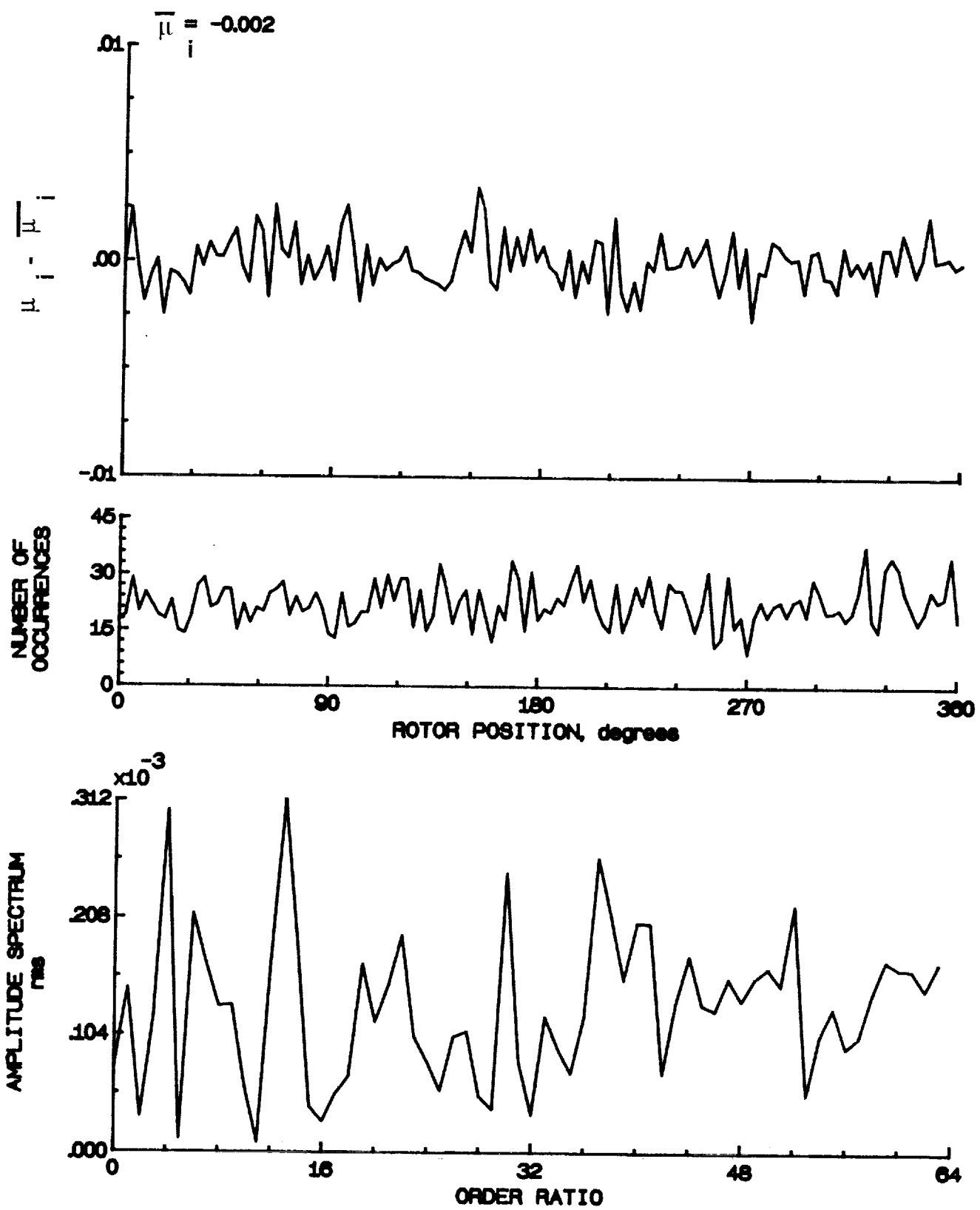


Figure 52.- Induced inflow velocity measured at 60 degrees and r/R of 0.94.

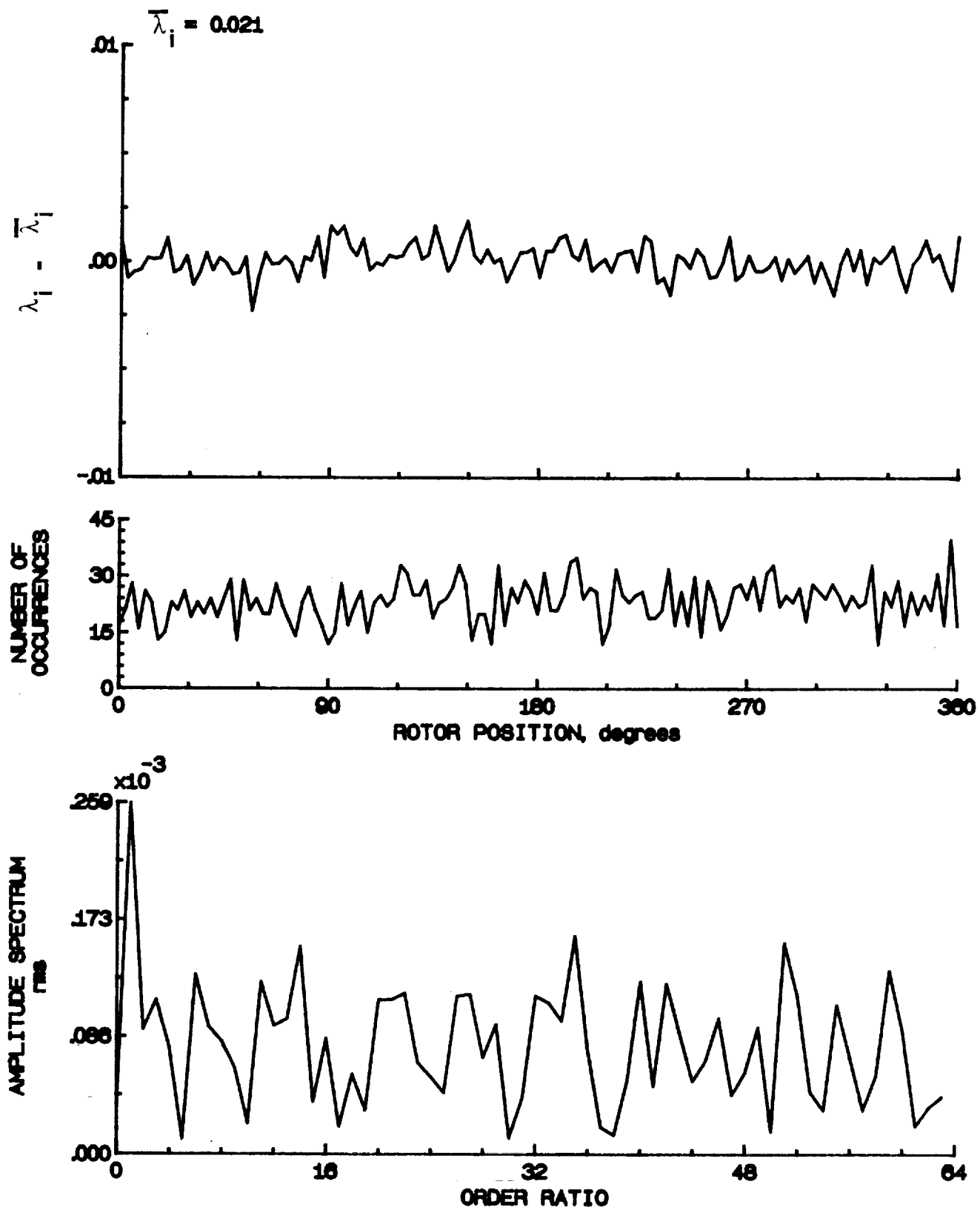


Figure 52.- Concluded.

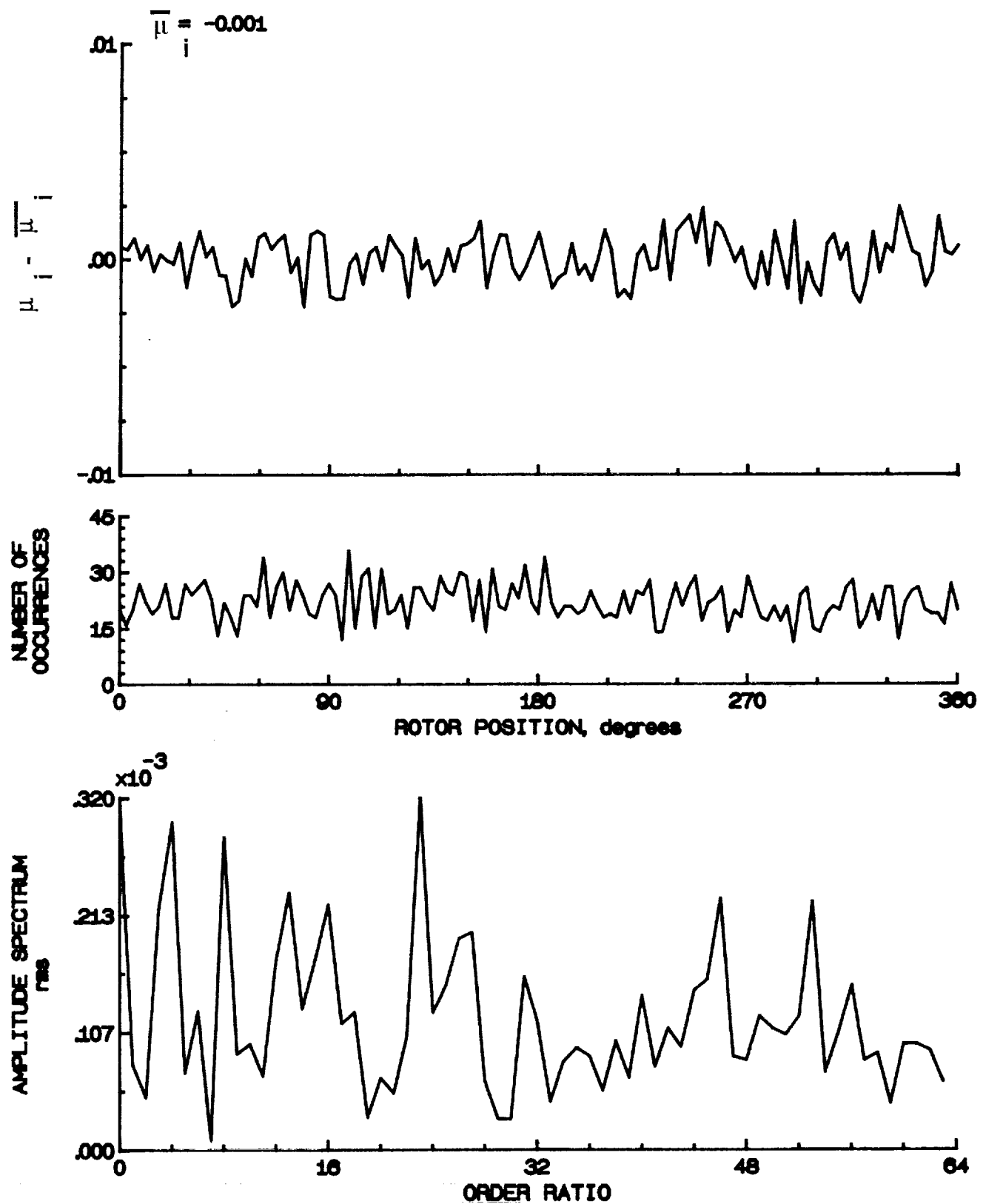


Figure 53.- Induced inflow velocity measured at 60 degrees and r/R of 0.98.

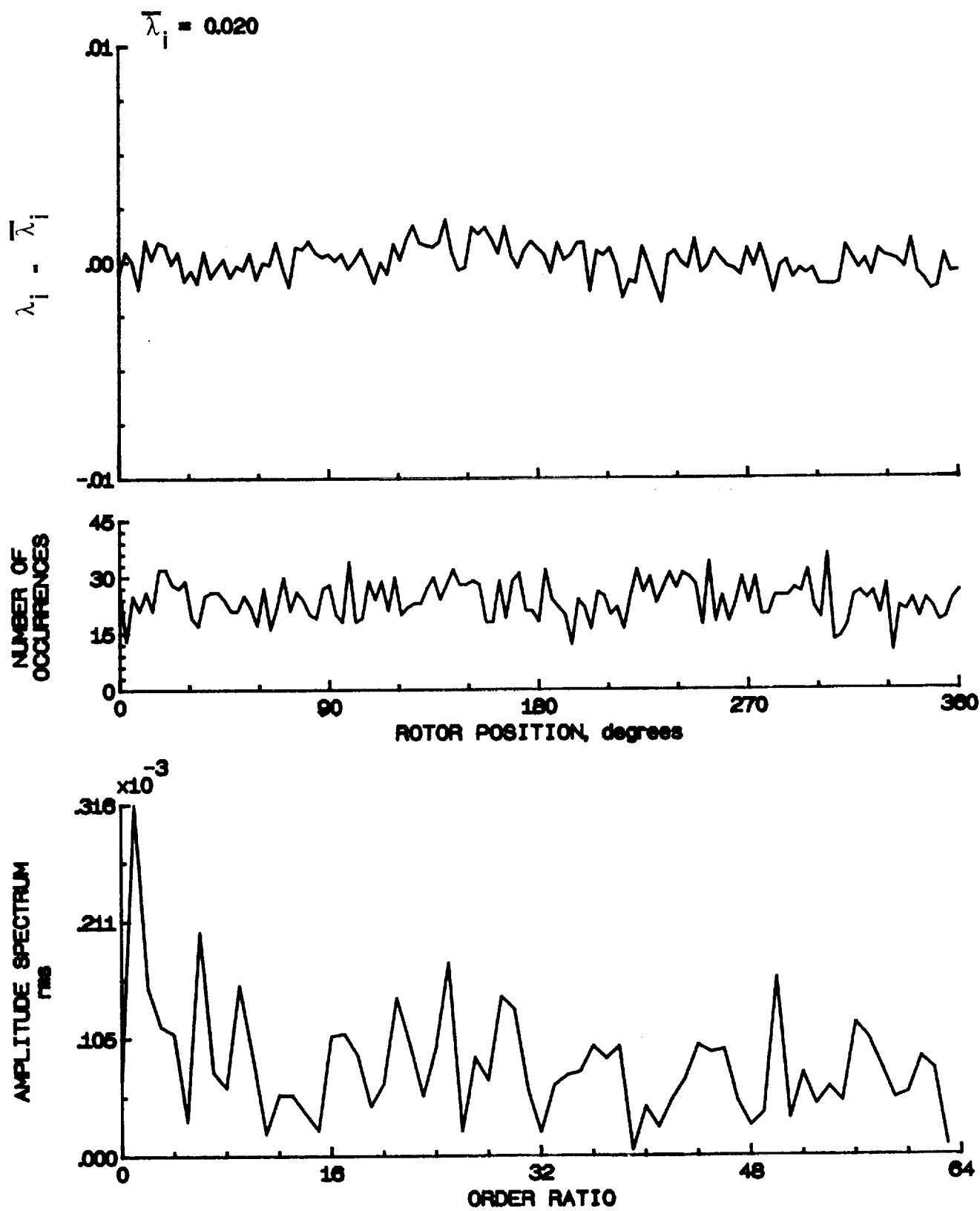


Figure 53.- Concluded.

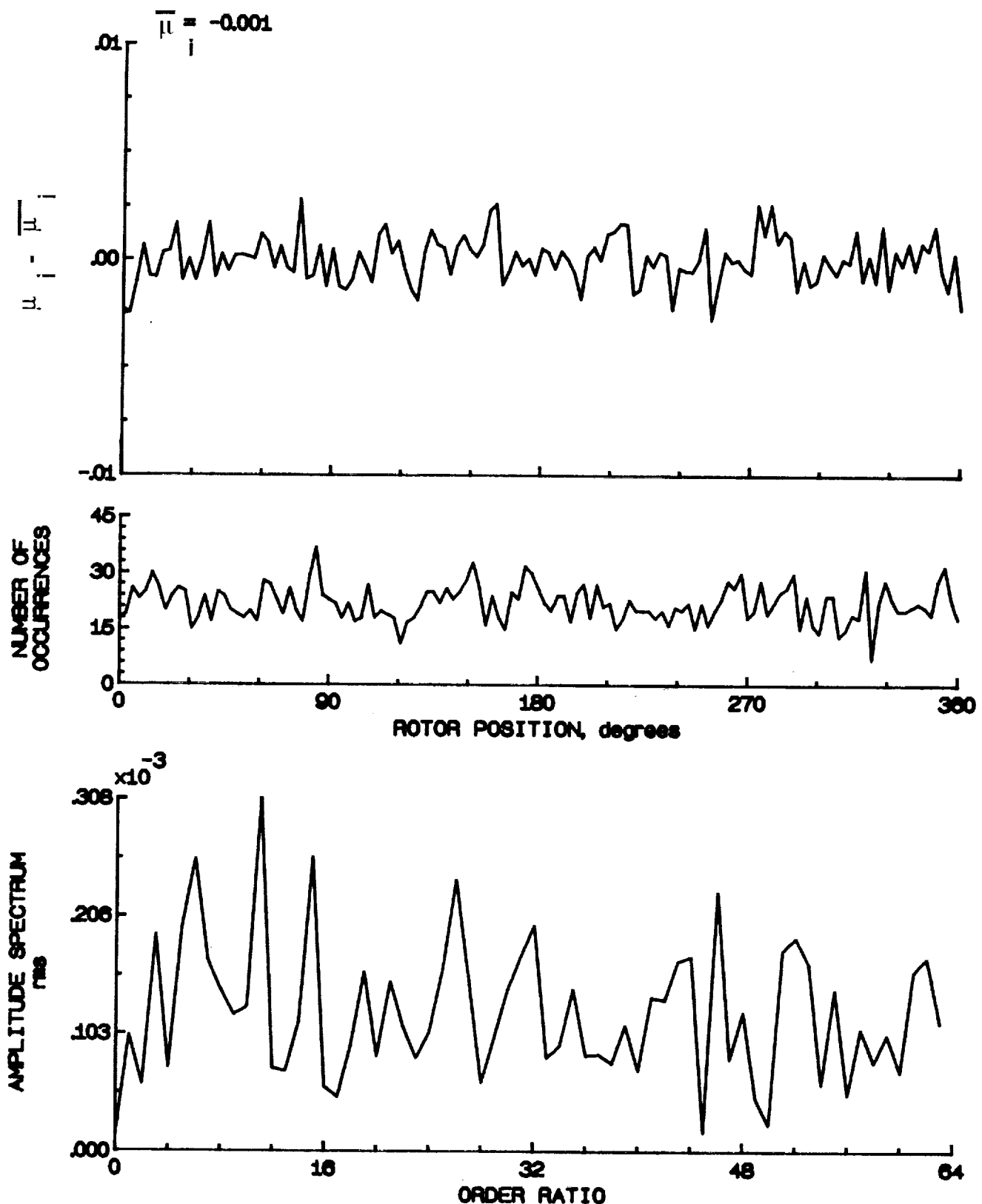


Figure 54.- Induced inflow velocity measured at 60 degrees and r/R of 1.02.

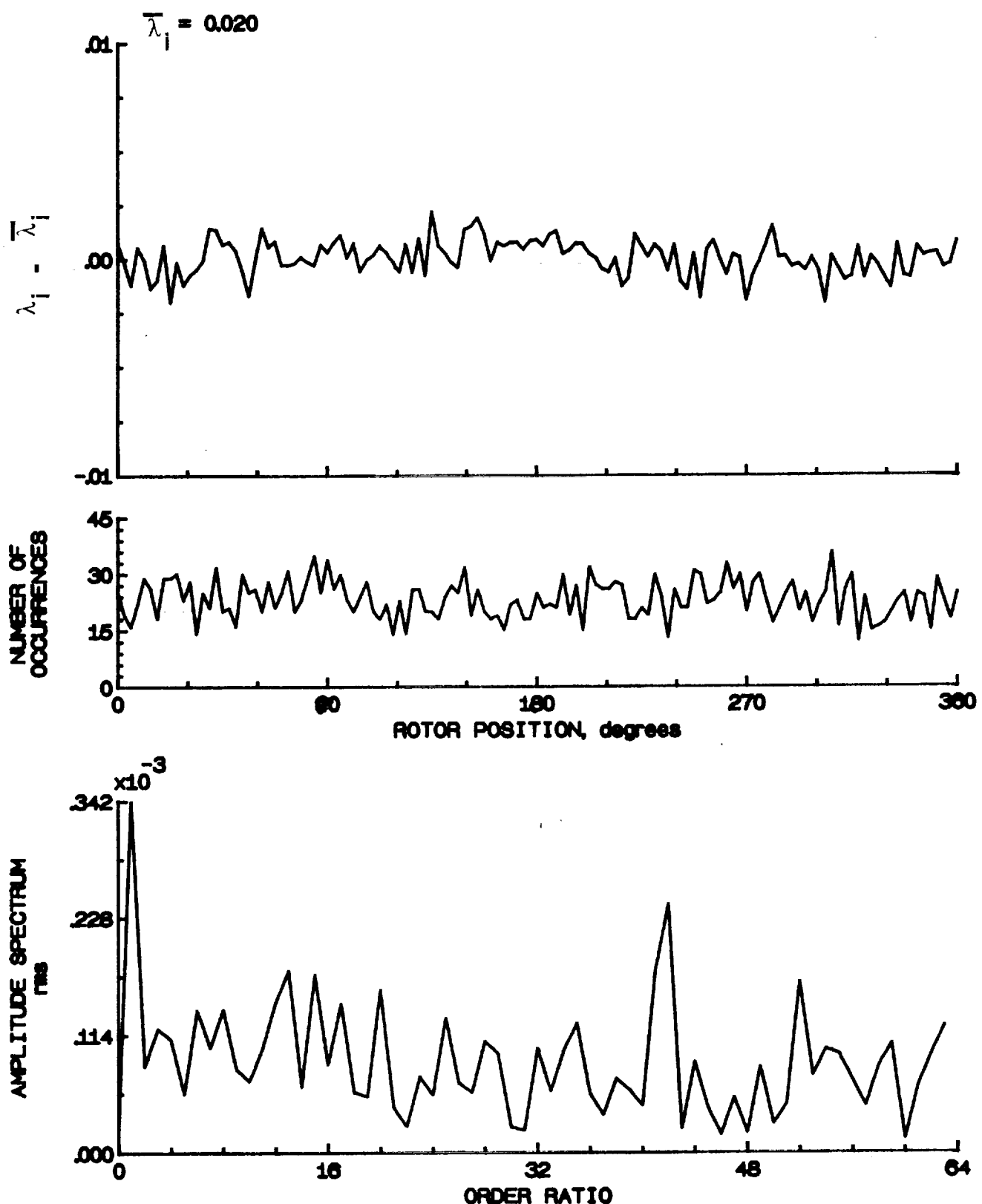


Figure 54.- Concluded.

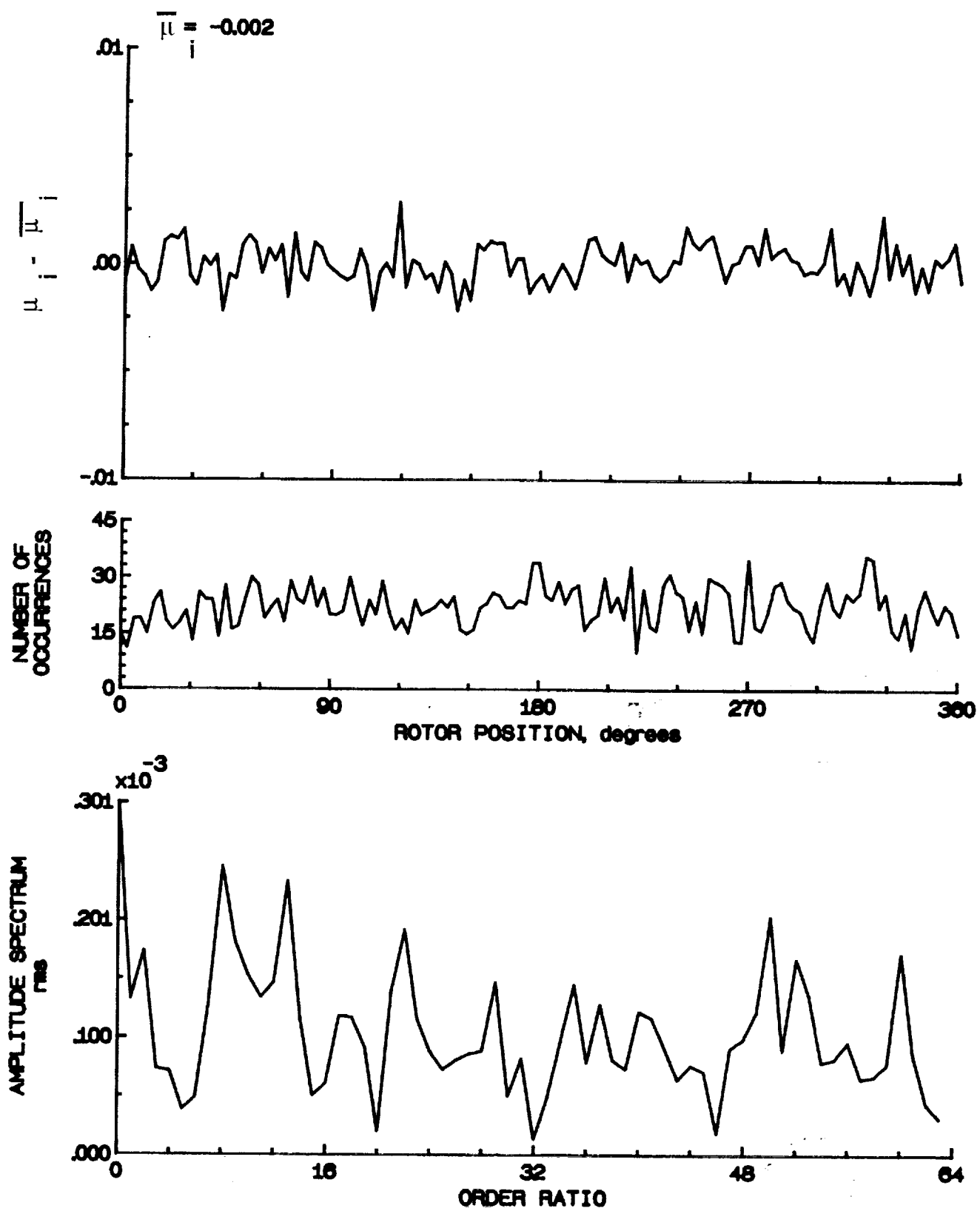


Figure 55.- Induced inflow velocity measured at 60 degrees and r/R of 1.04.

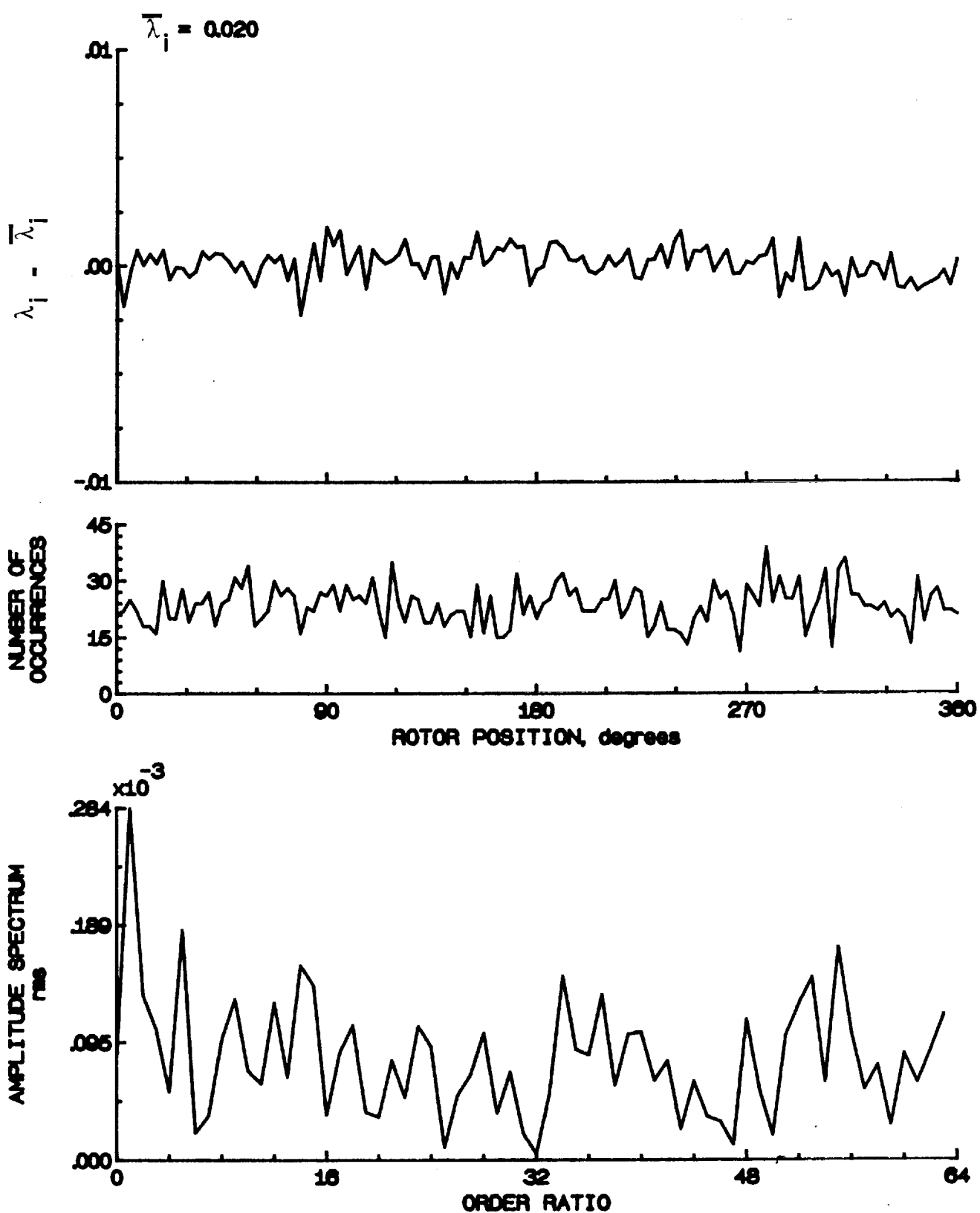


Figure 55.- Concluded.

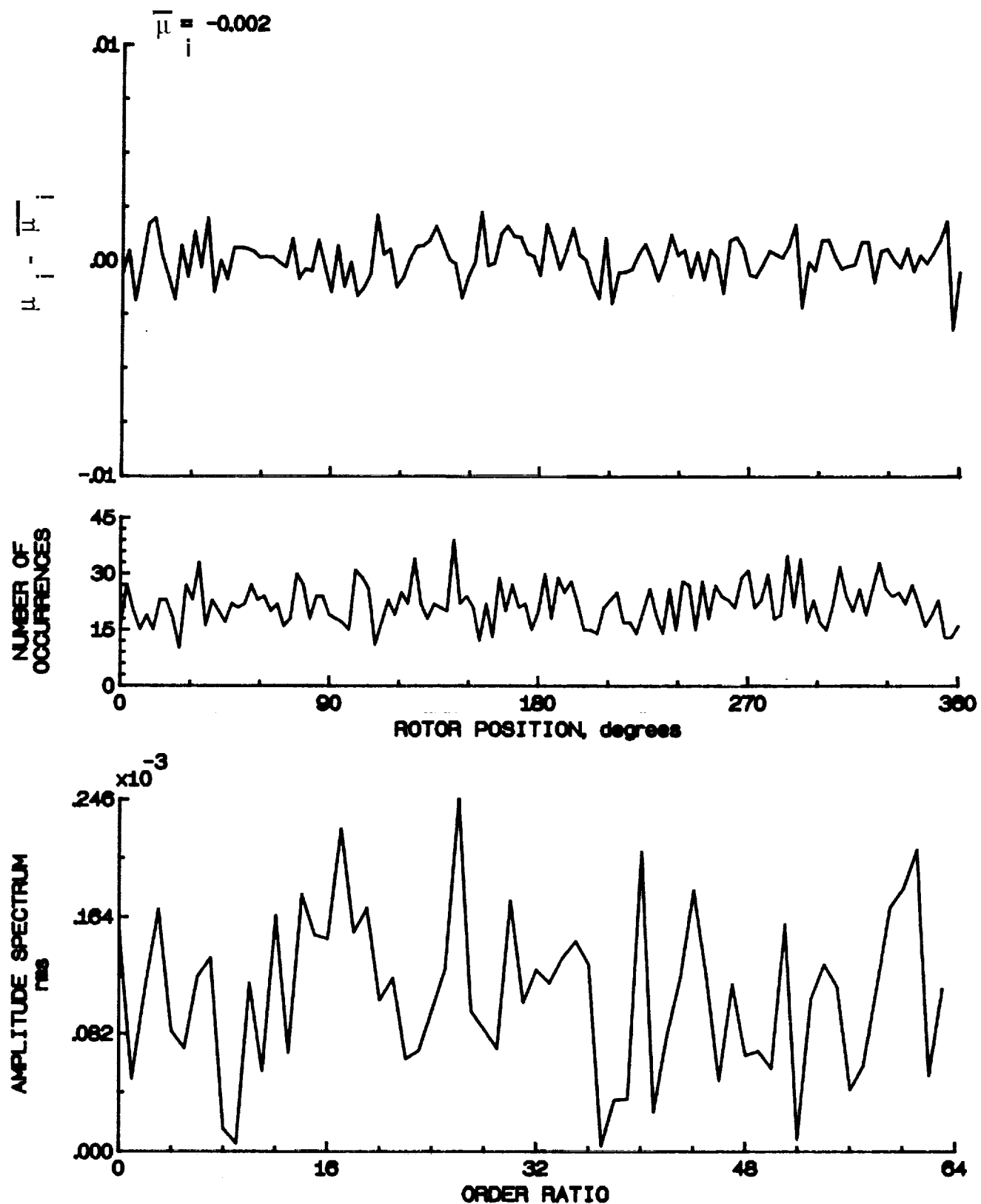


Figure 56.- Induced inflow velocity measured at 60 degrees and r/R of 1.10.

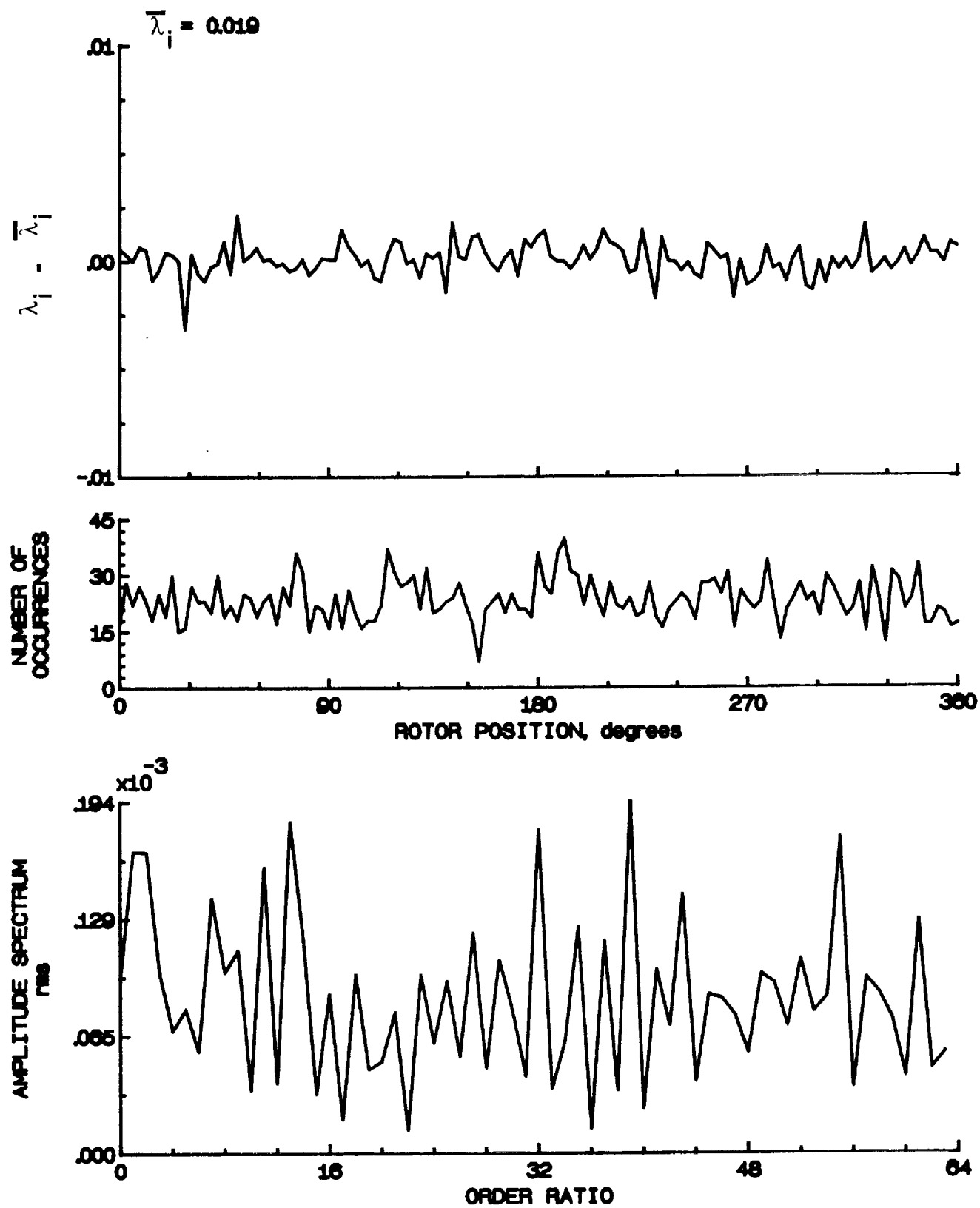


Figure 56.- Concluded.

This page intentionally left blank.

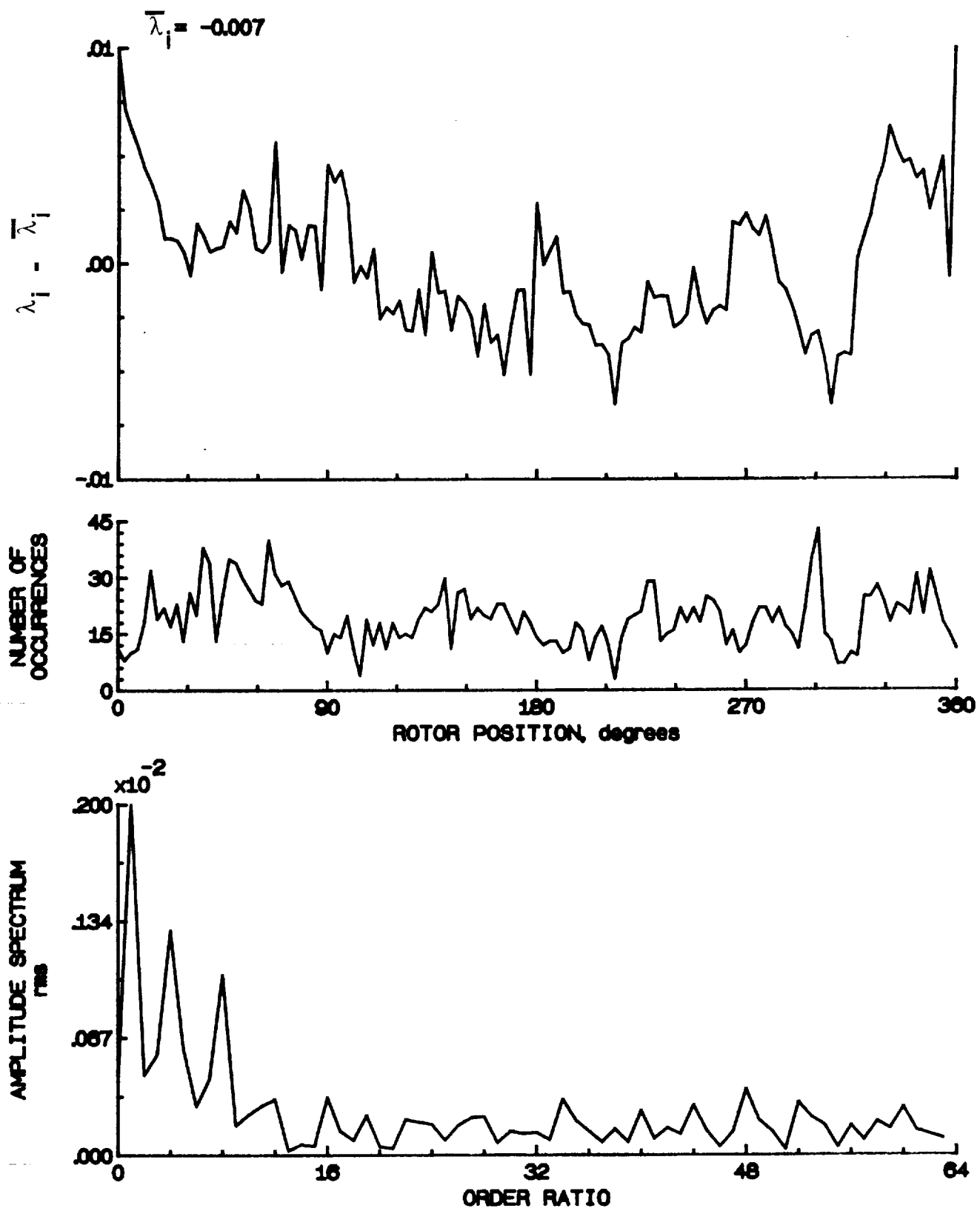


Figure 57.- Induced inflow velocity measured at 90 degrees and r/R of 0.20.

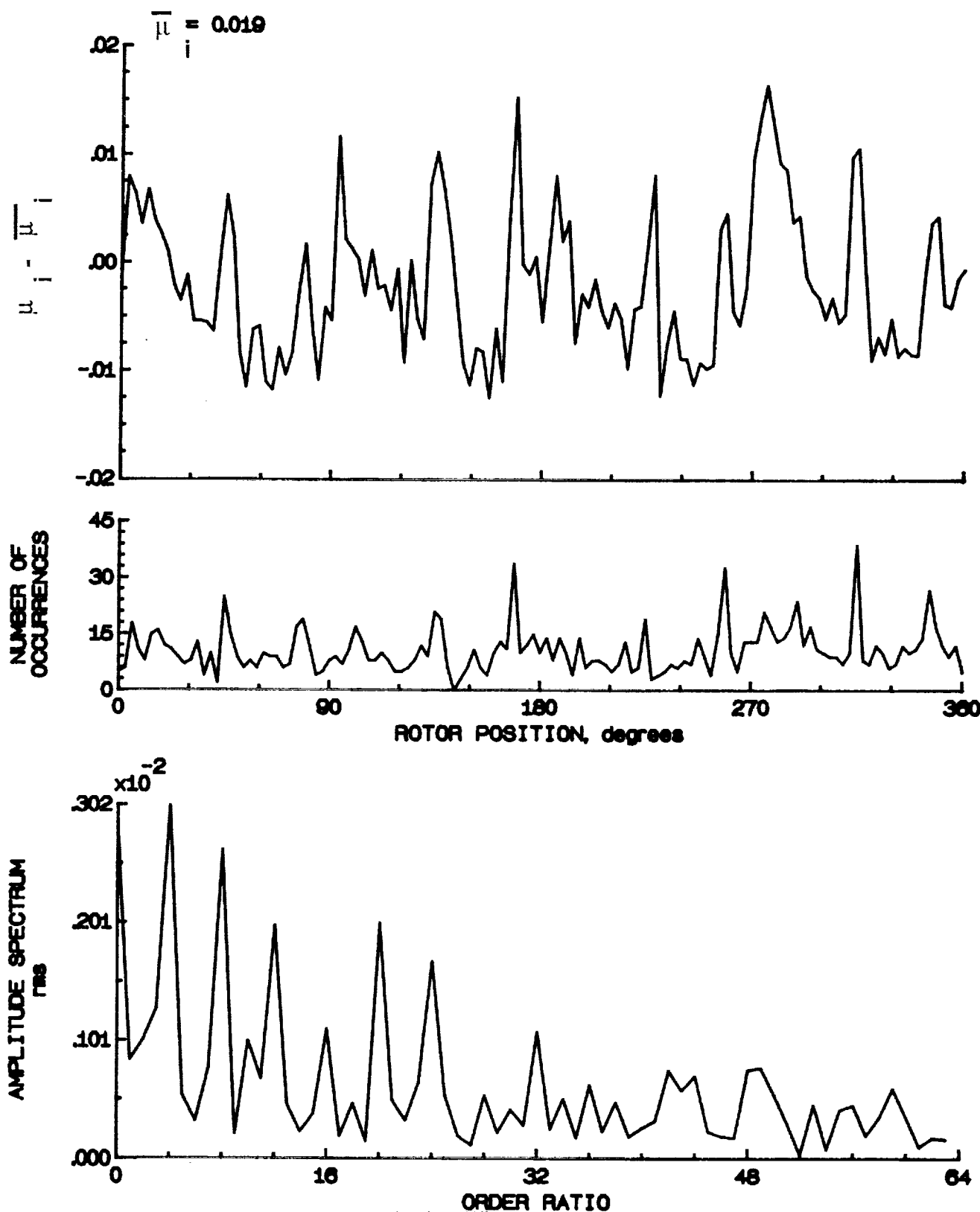


Figure 58.- Induced inflow velocity measured at 90 degrees and r/R of 0.40.

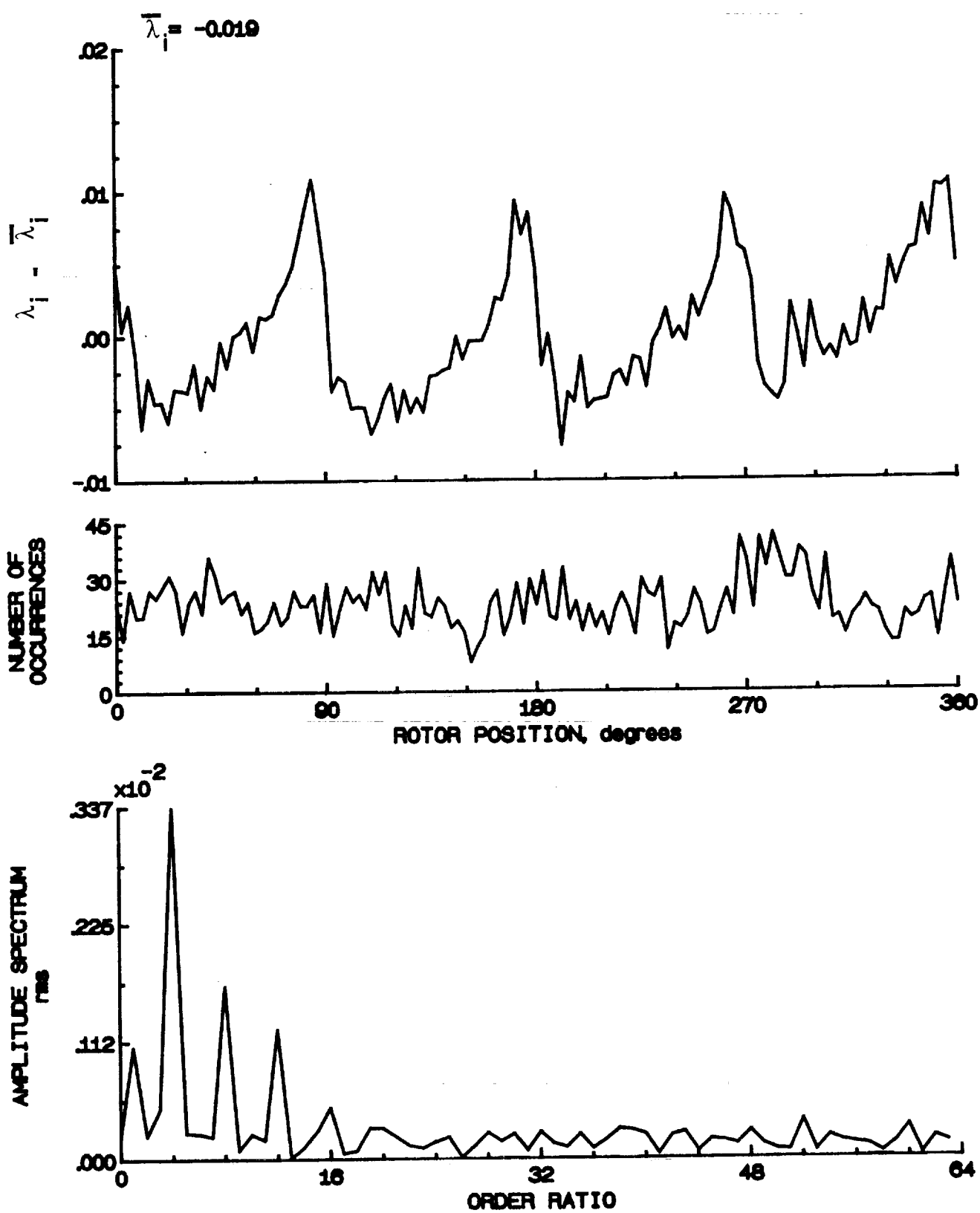


Figure 58.- Concluded.

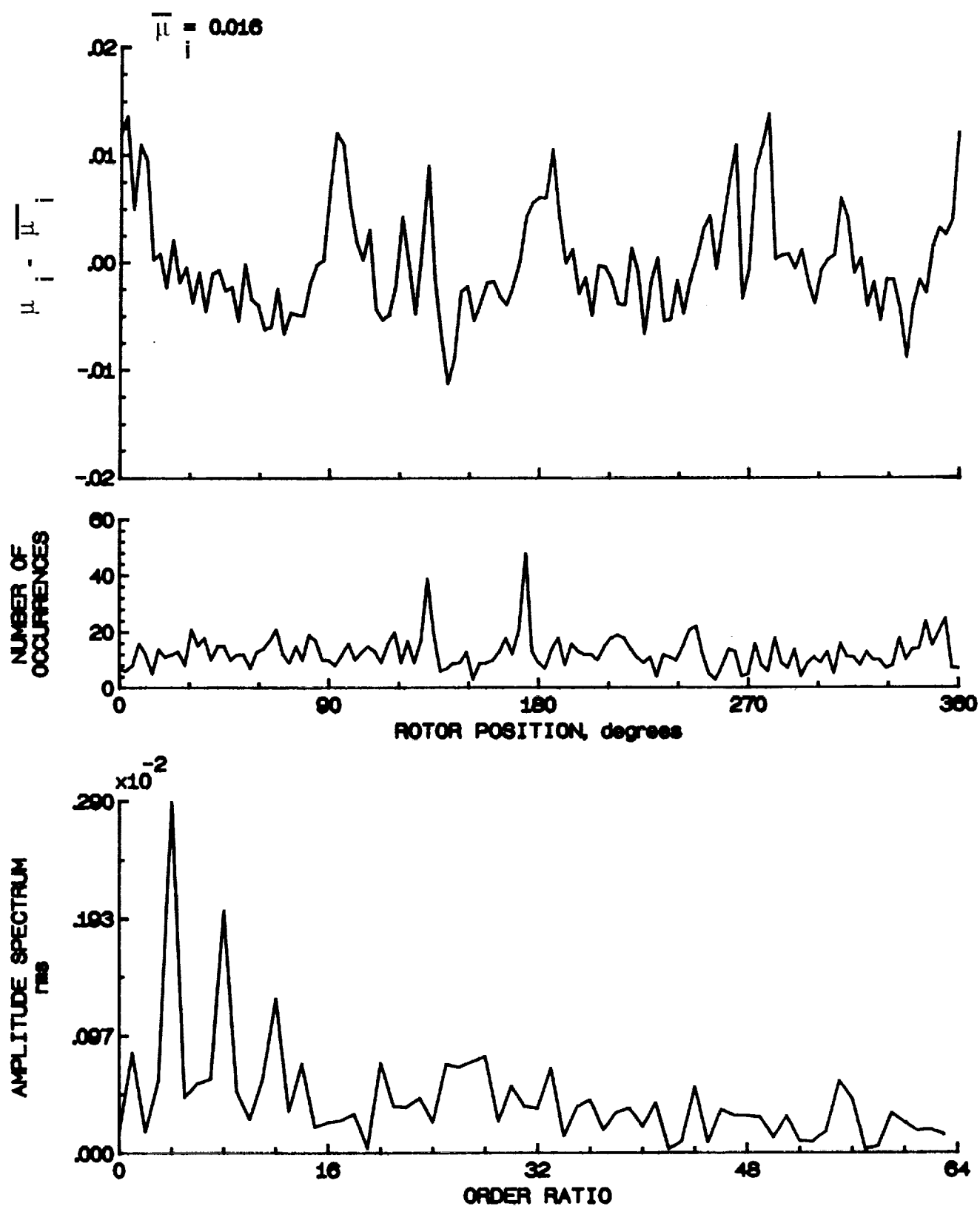


Figure 59.- Induced inflow velocity measured at 90 degrees and r/R of 0.50.

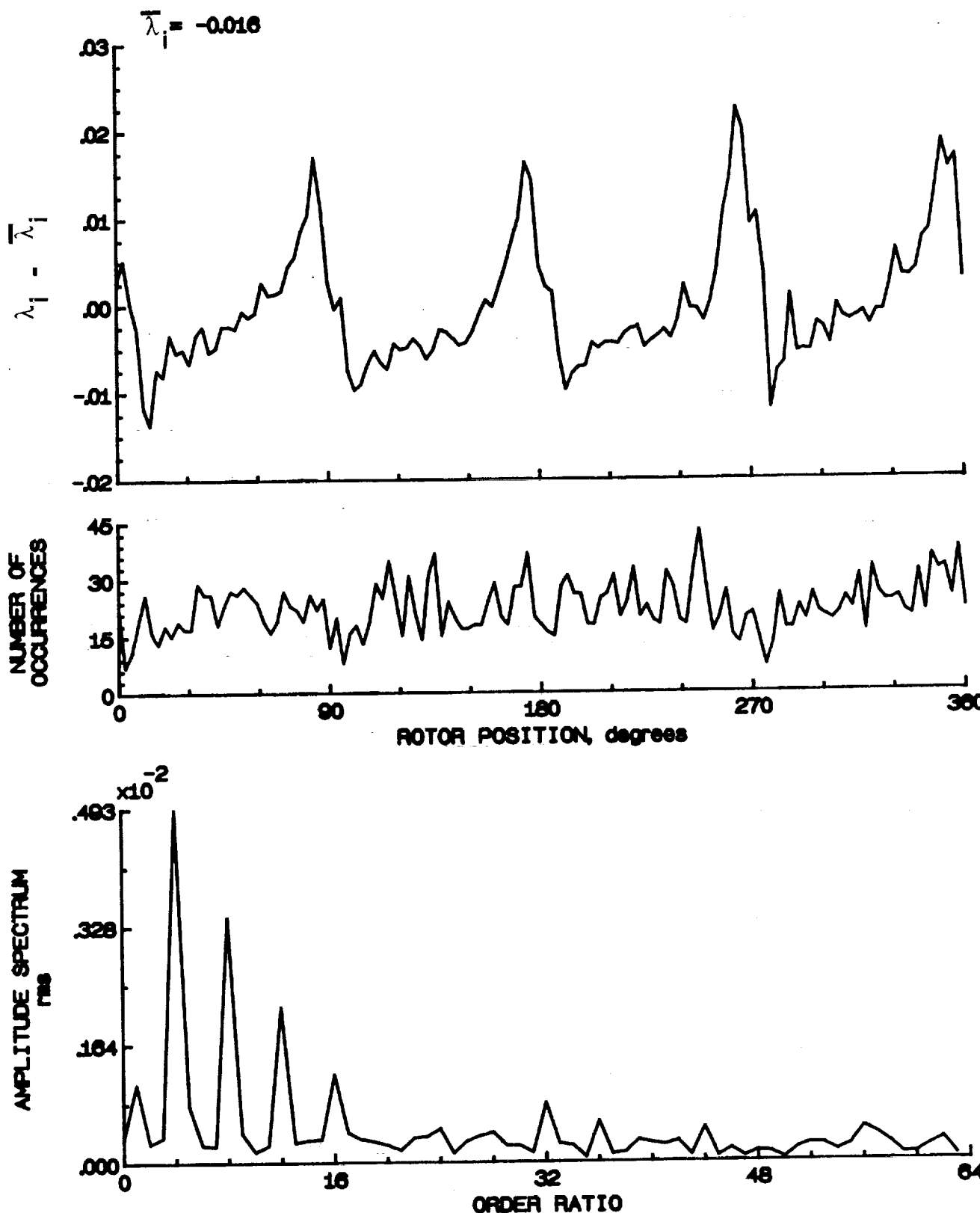


Figure 50.- Concluded.

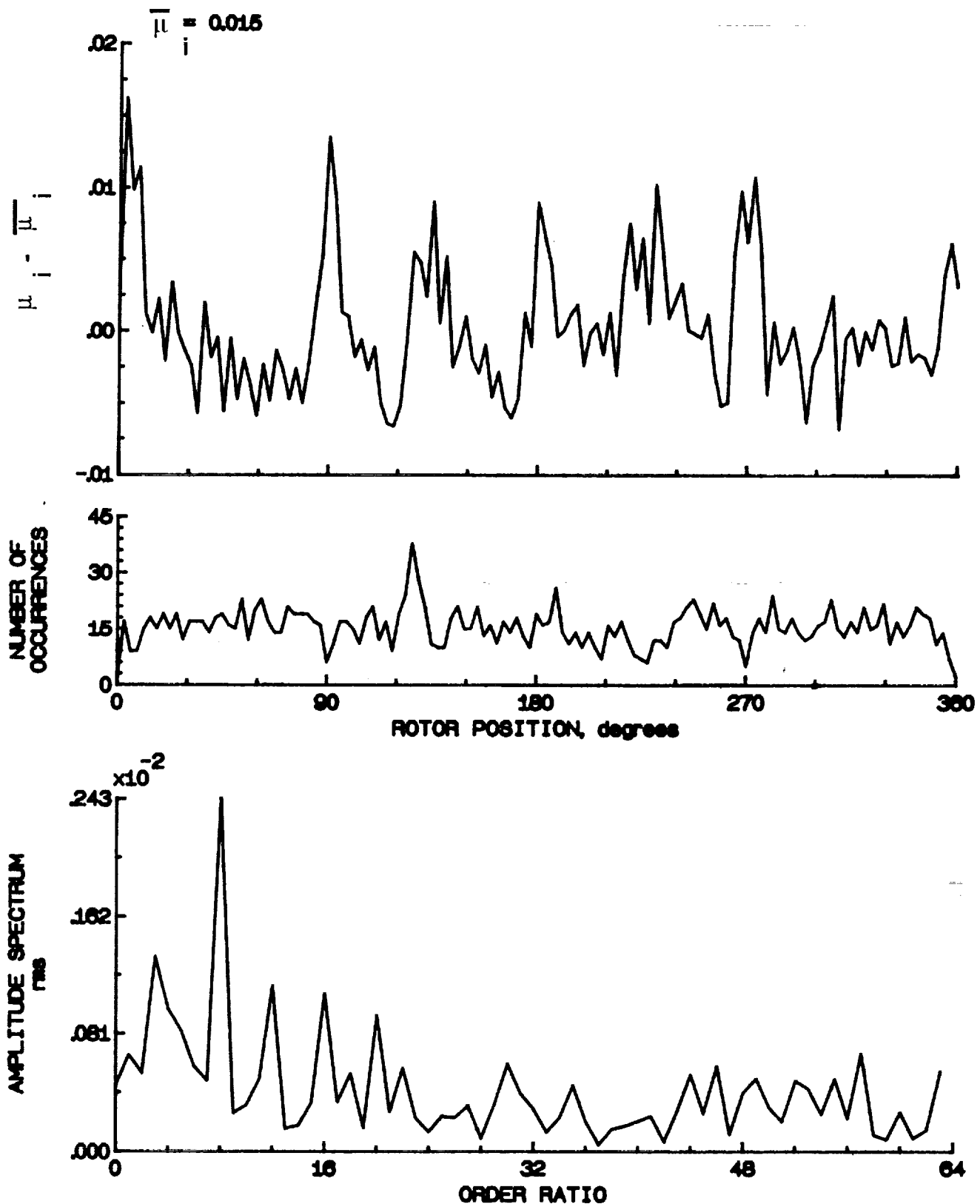


Figure 60.- Induced inflow velocity measured at 90 degrees and  $r/R$  of 0.80.

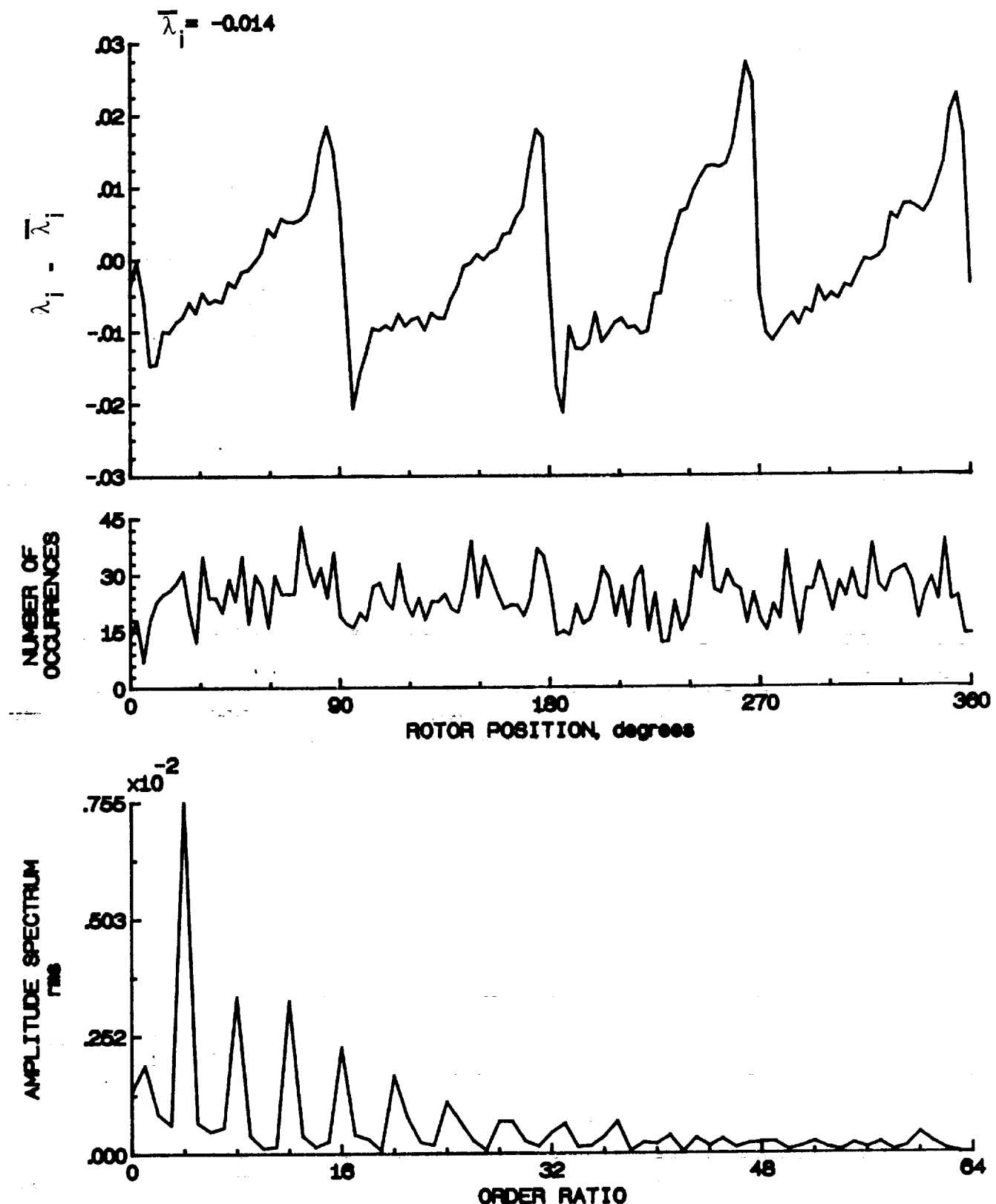


Figure 60.- Concluded.

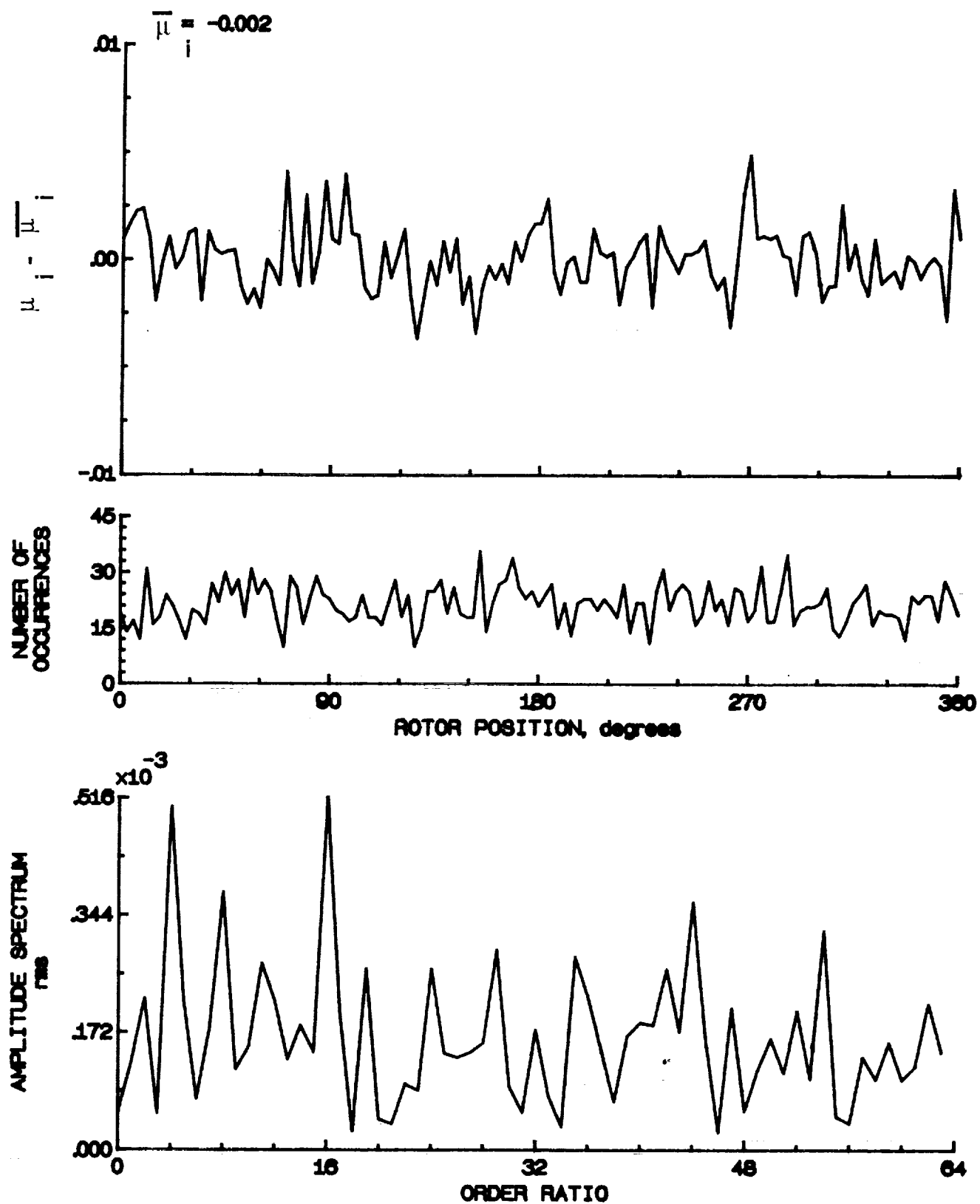


Figure 61- Induced inflow velocity measured at 90 degrees and r/R of 0.70.

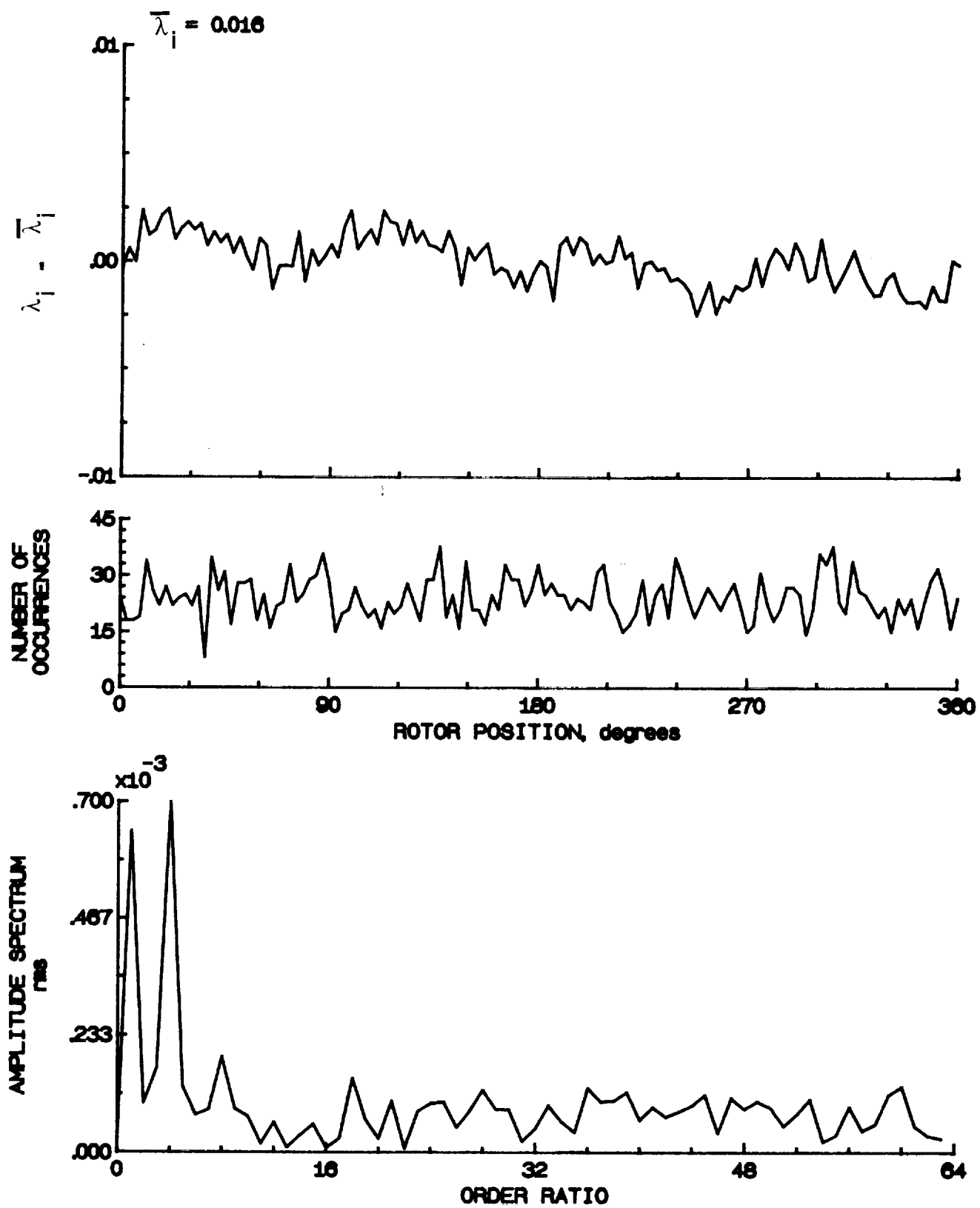


Figure 61.- Concluded.

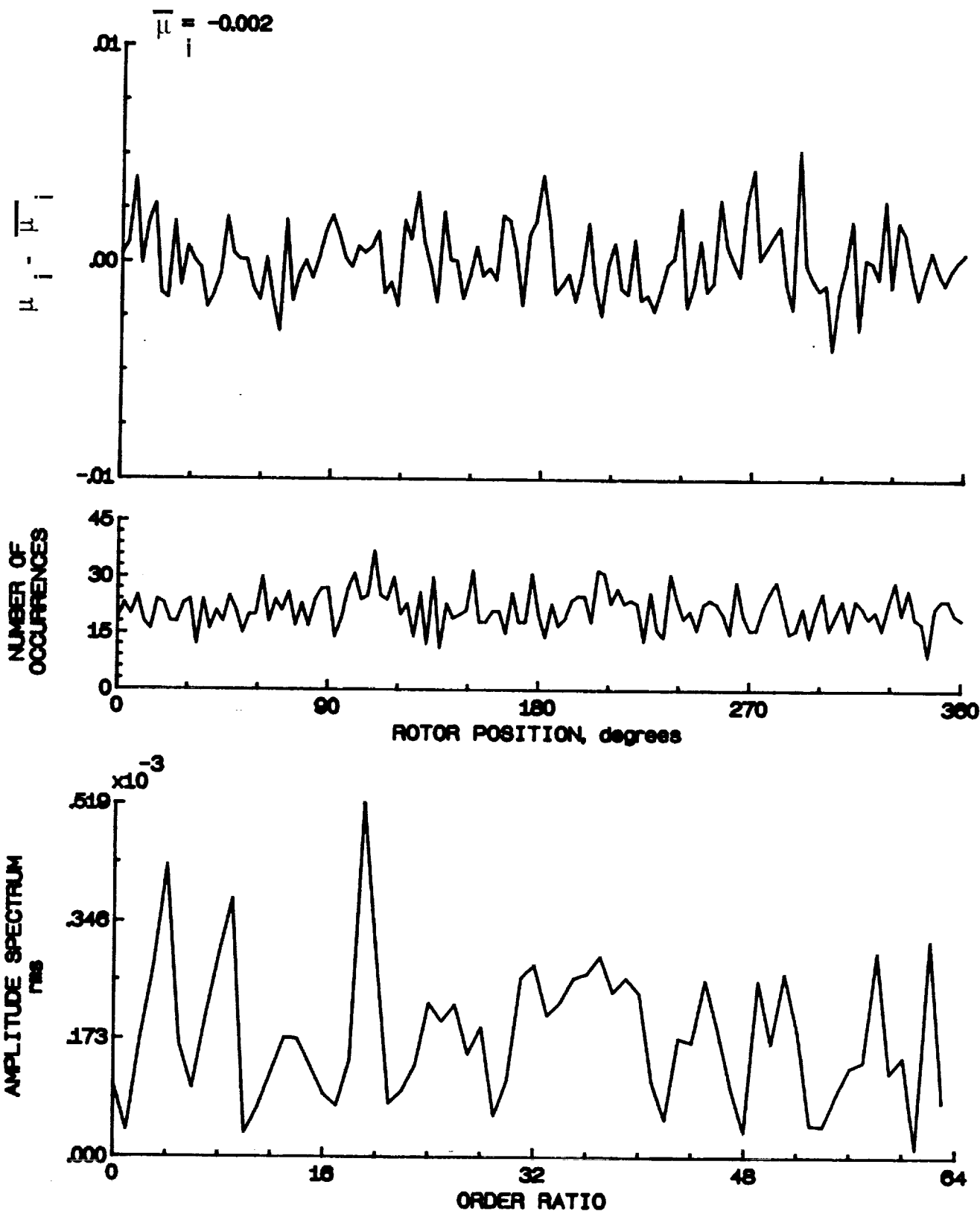


Figure 62.- Induced inflow velocity measured at 90 degrees and r/R of 0.74.

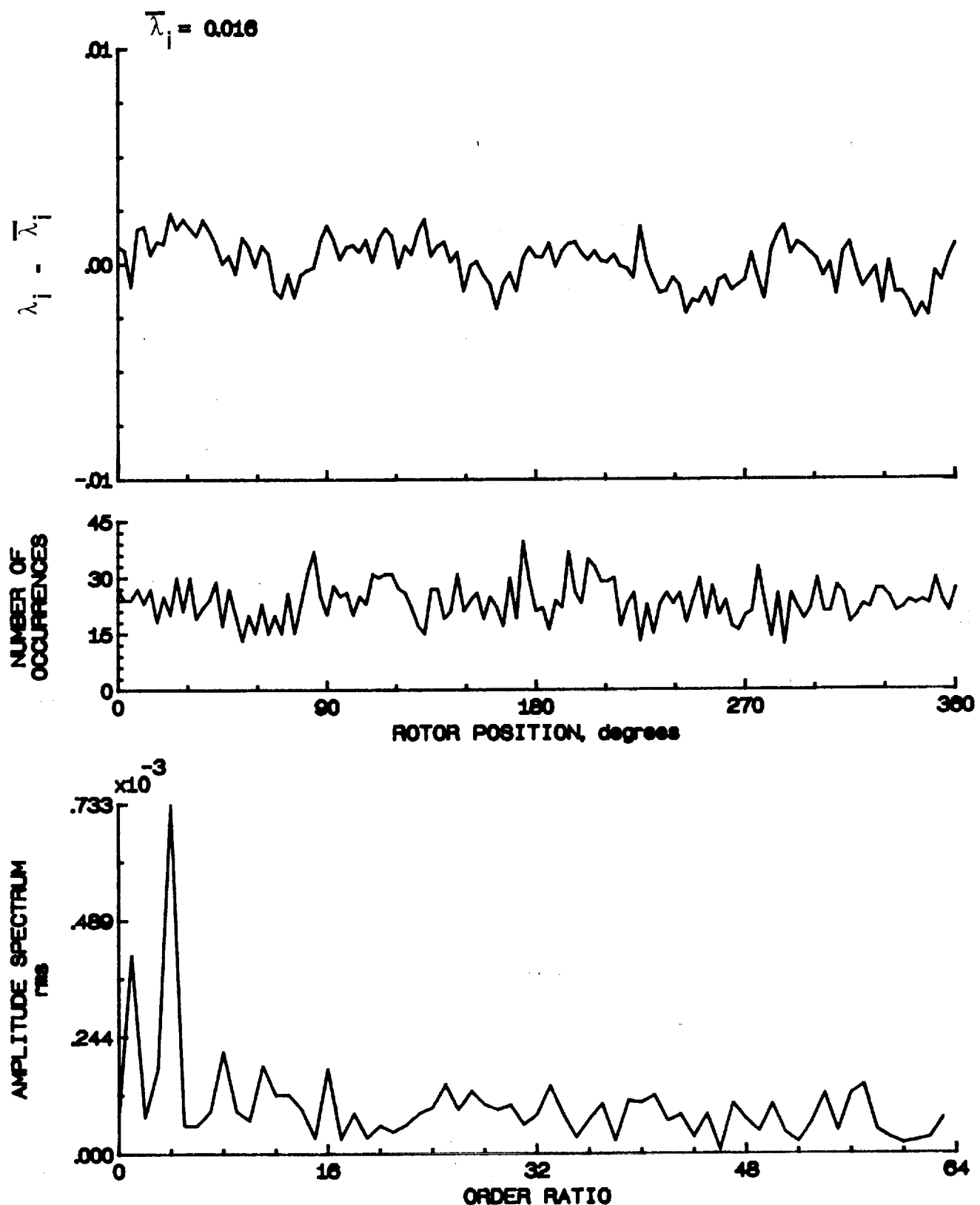


Figure 62.- Concluded.

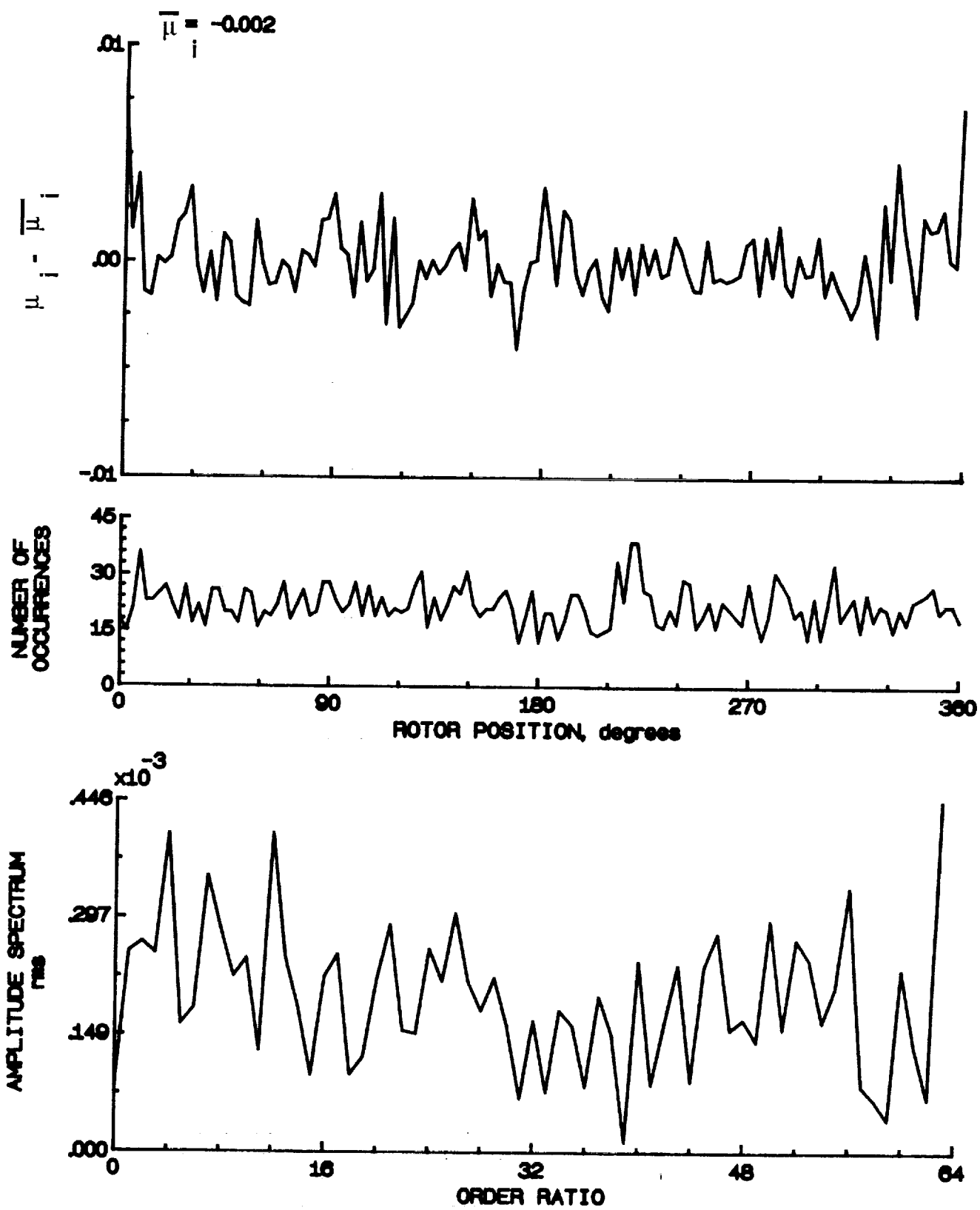


Figure 63.- Induced inflow velocity measured at 90 degrees and r/R of 0.78.

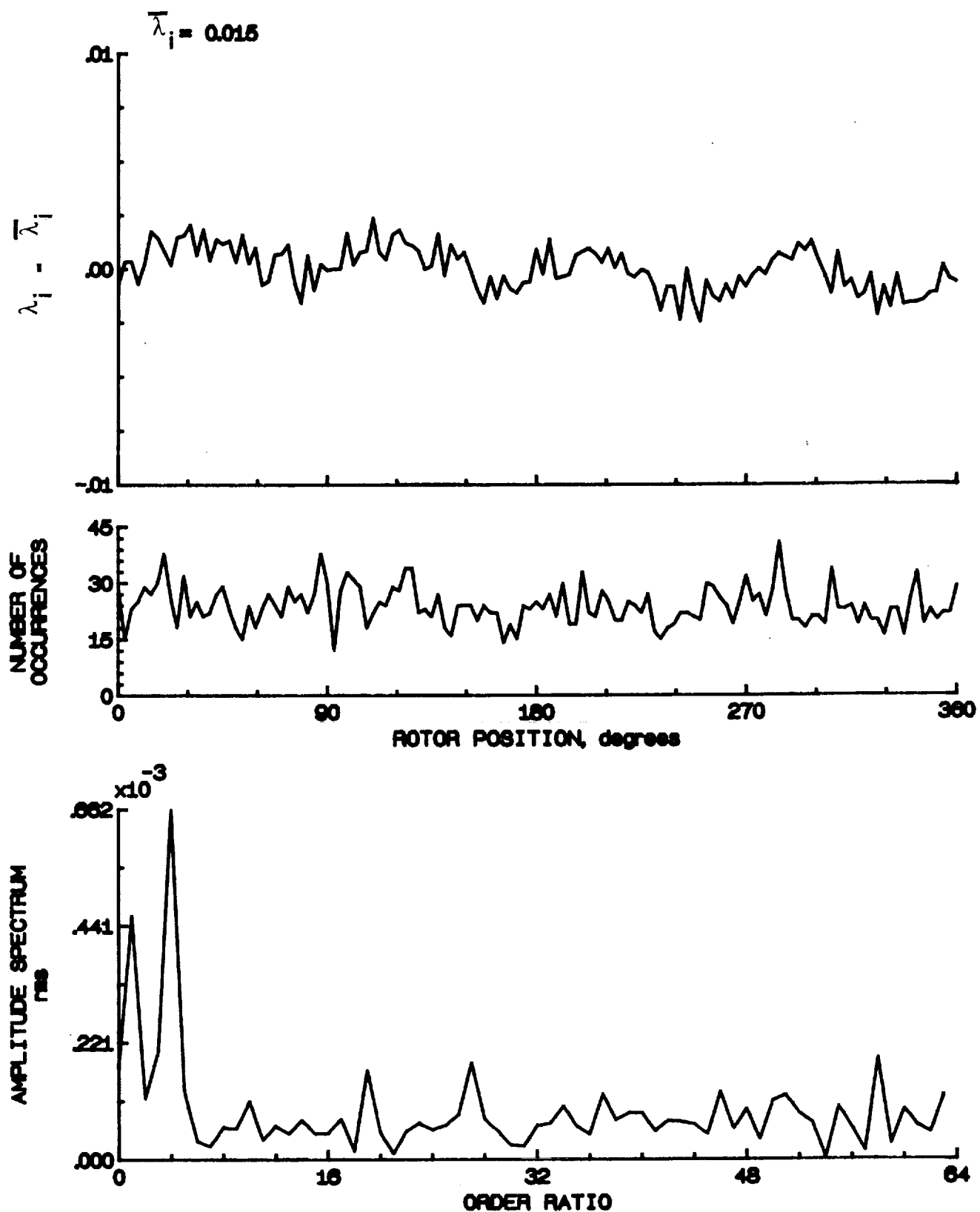


Figure 63.- Concluded.

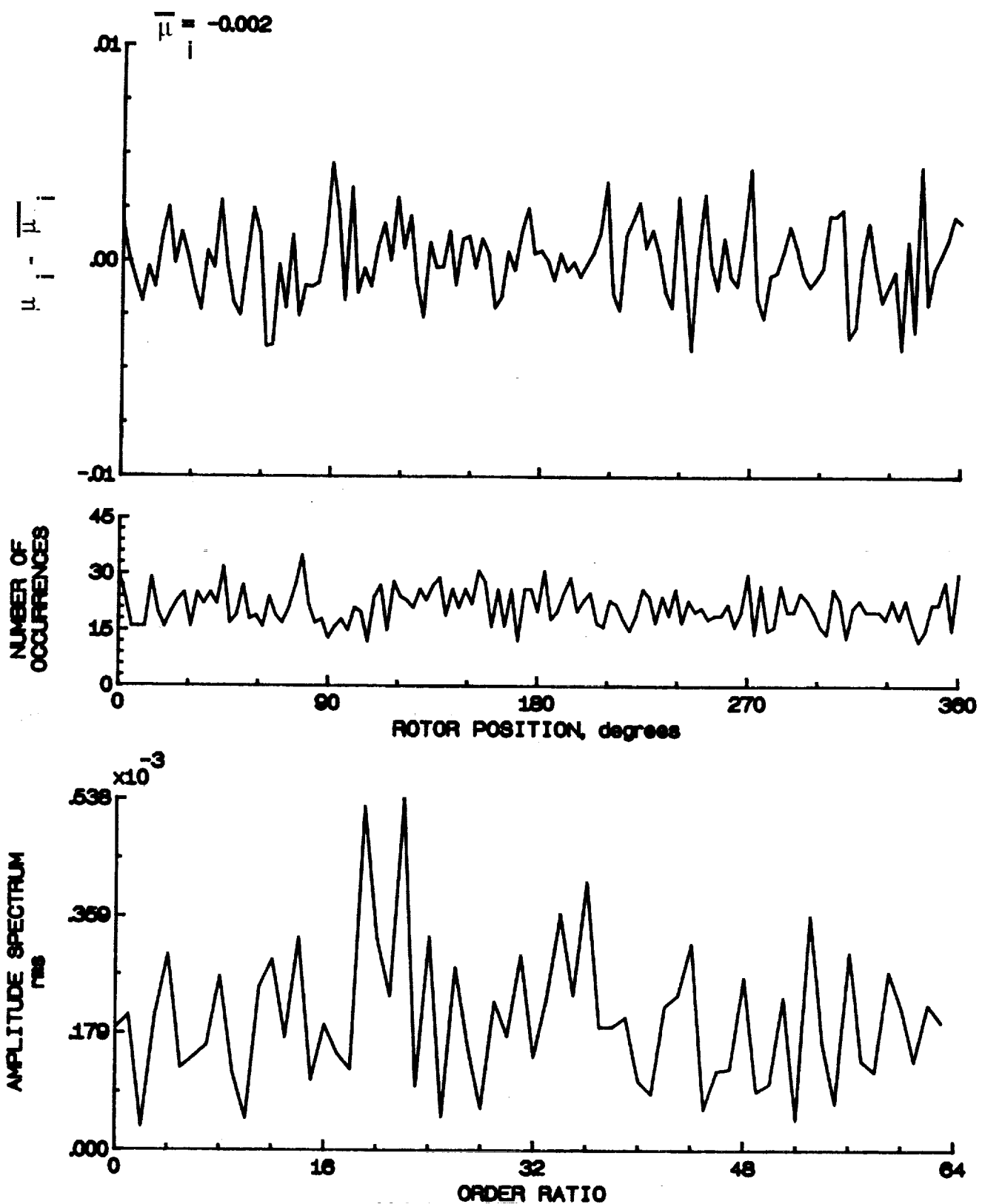


Figure 64.- Induced inflow velocity measured at 90 degrees and r/R of 0.82.

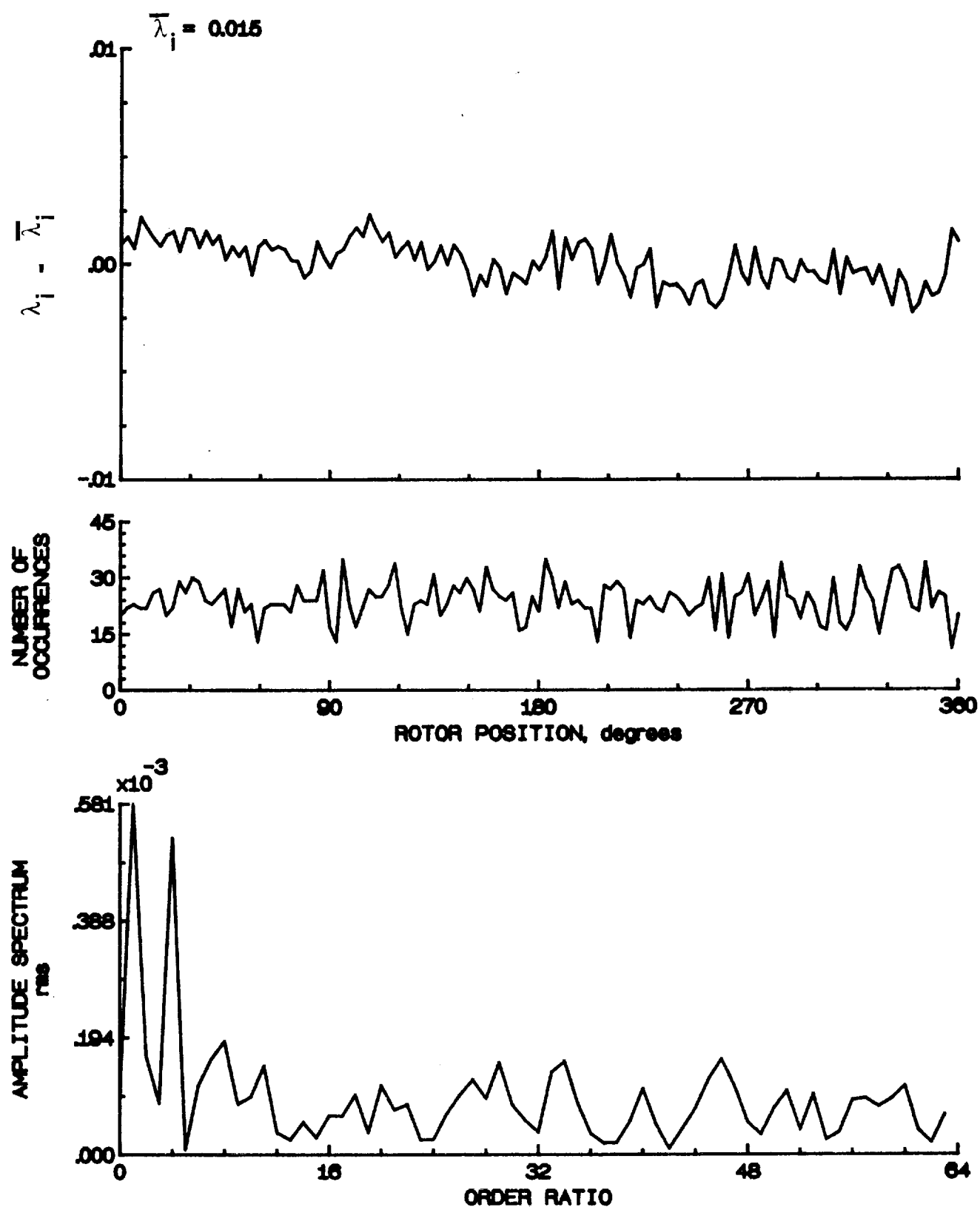


Figure 64.- Concluded.

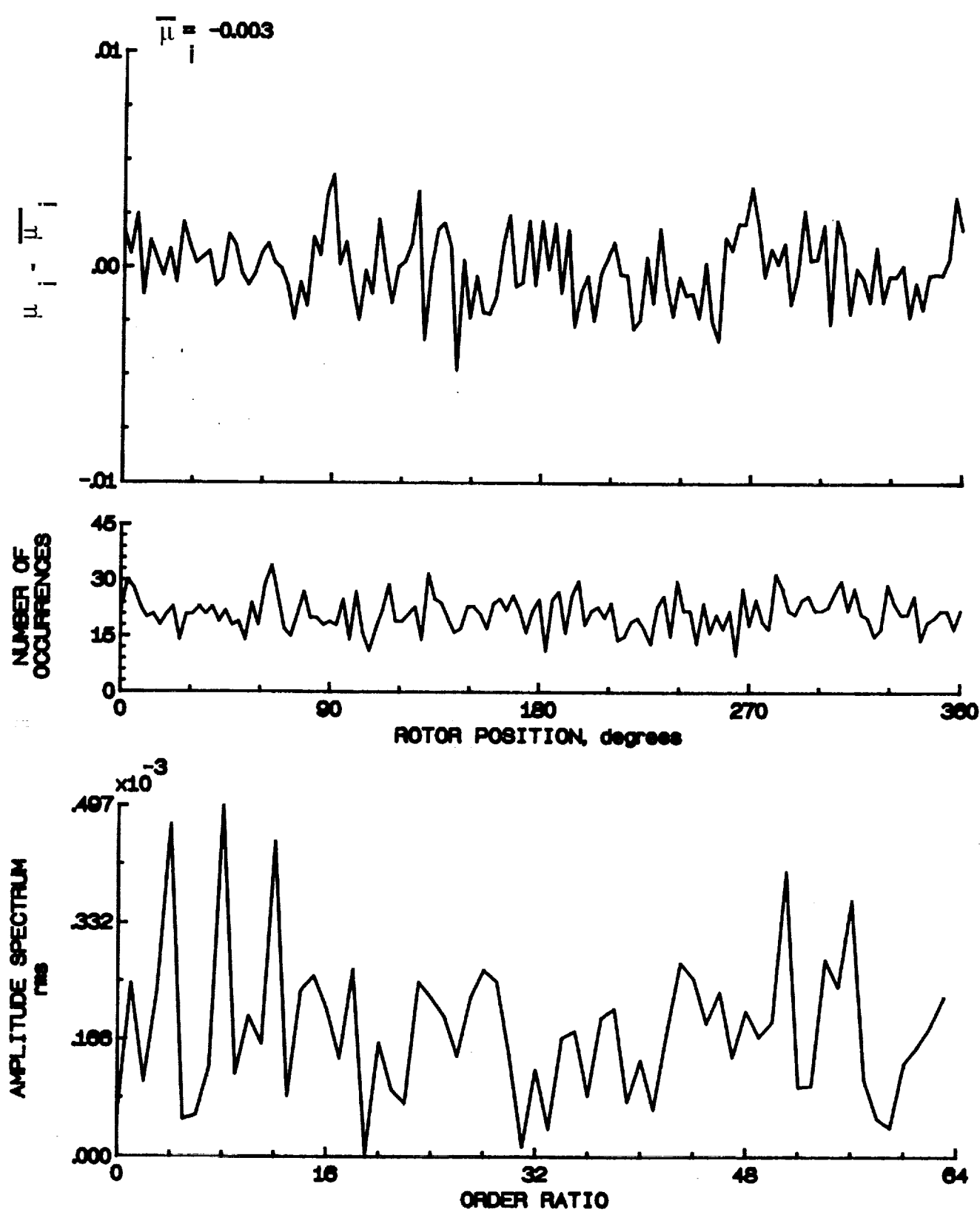


Figure 65.- Induced inflow velocity measured at 90 degrees and r/R of 0.86.

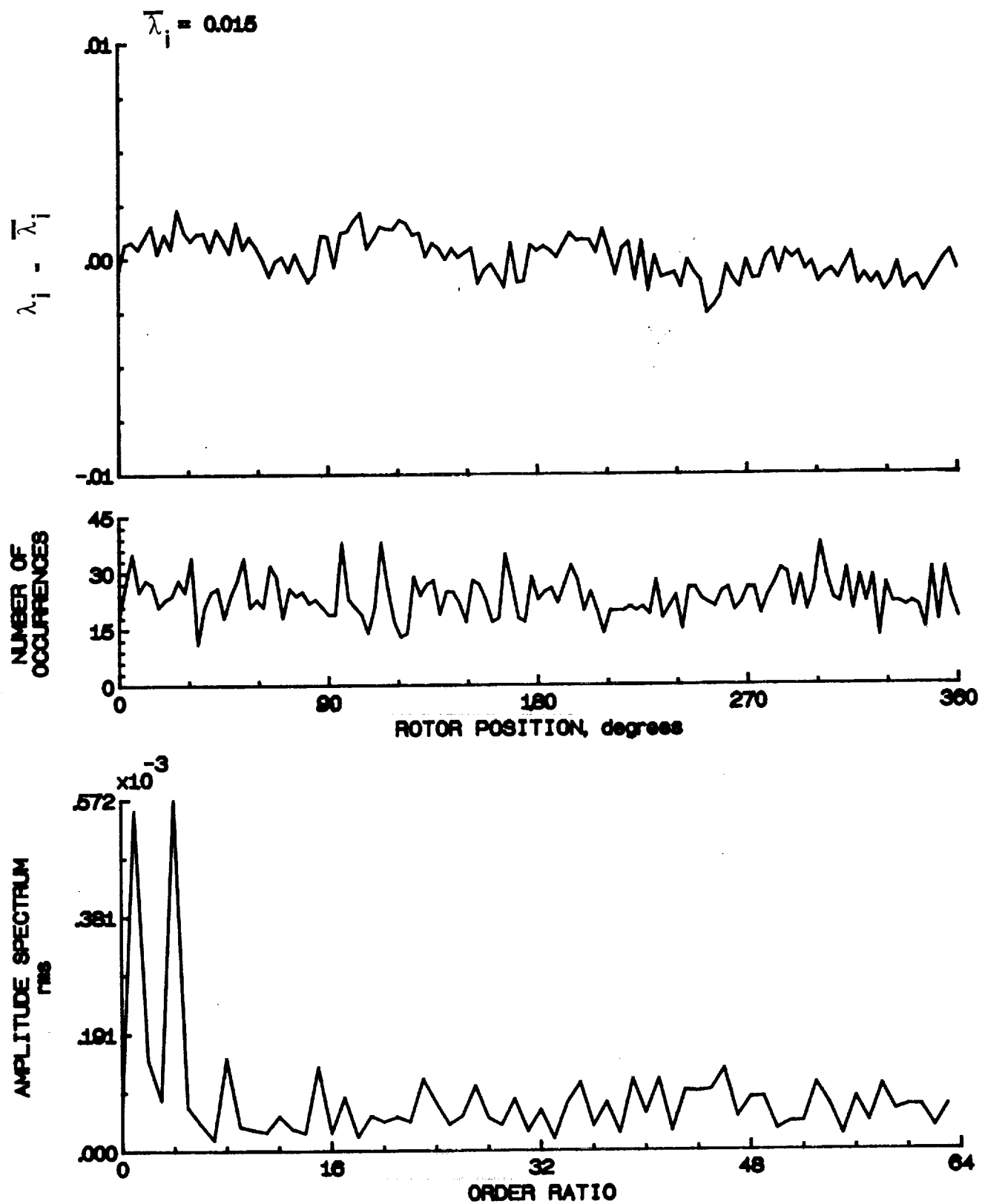


Figure 65.- Concluded.

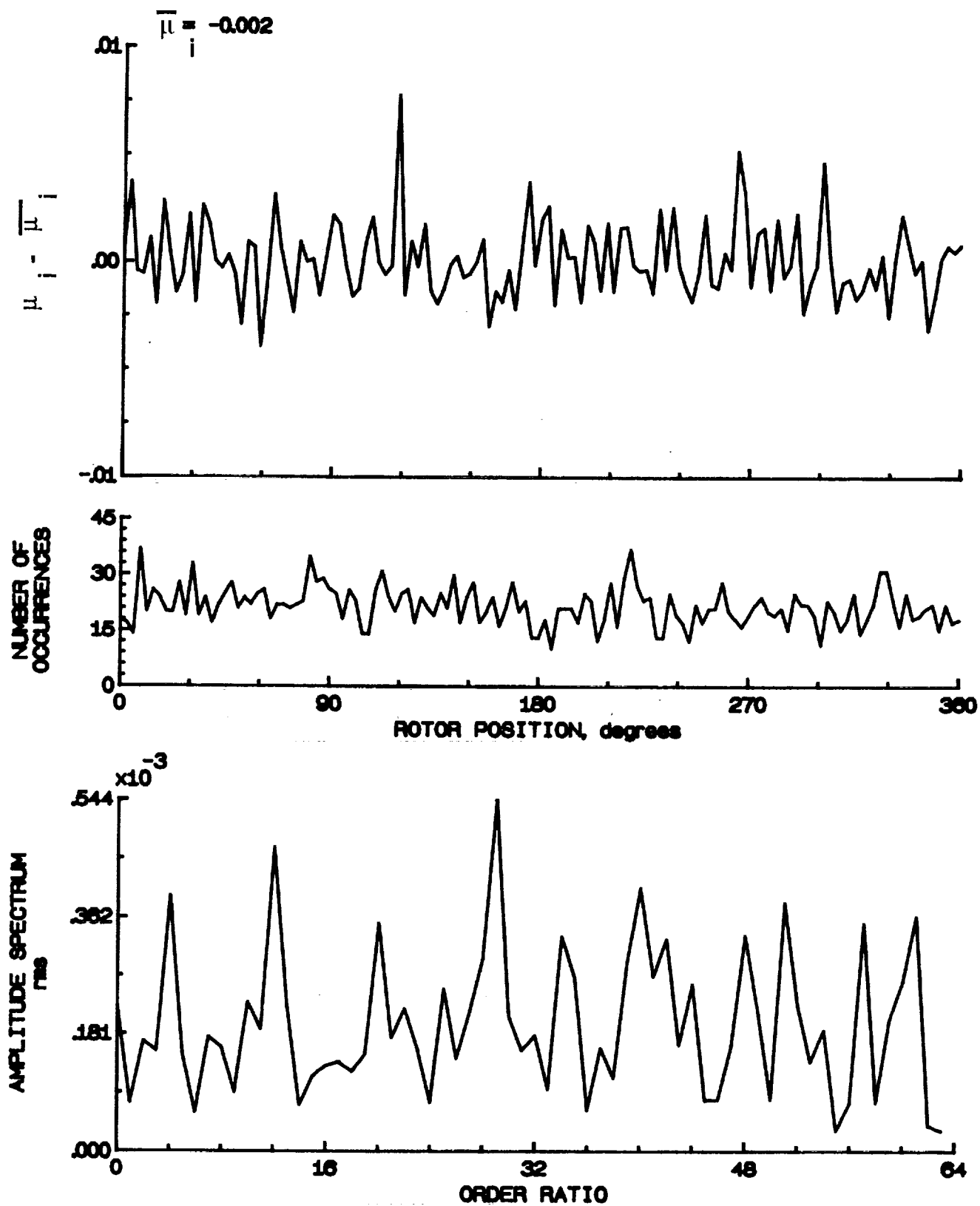


Figure 66.- Induced inflow velocity measured at 90 degrees and r/R of 0.90.

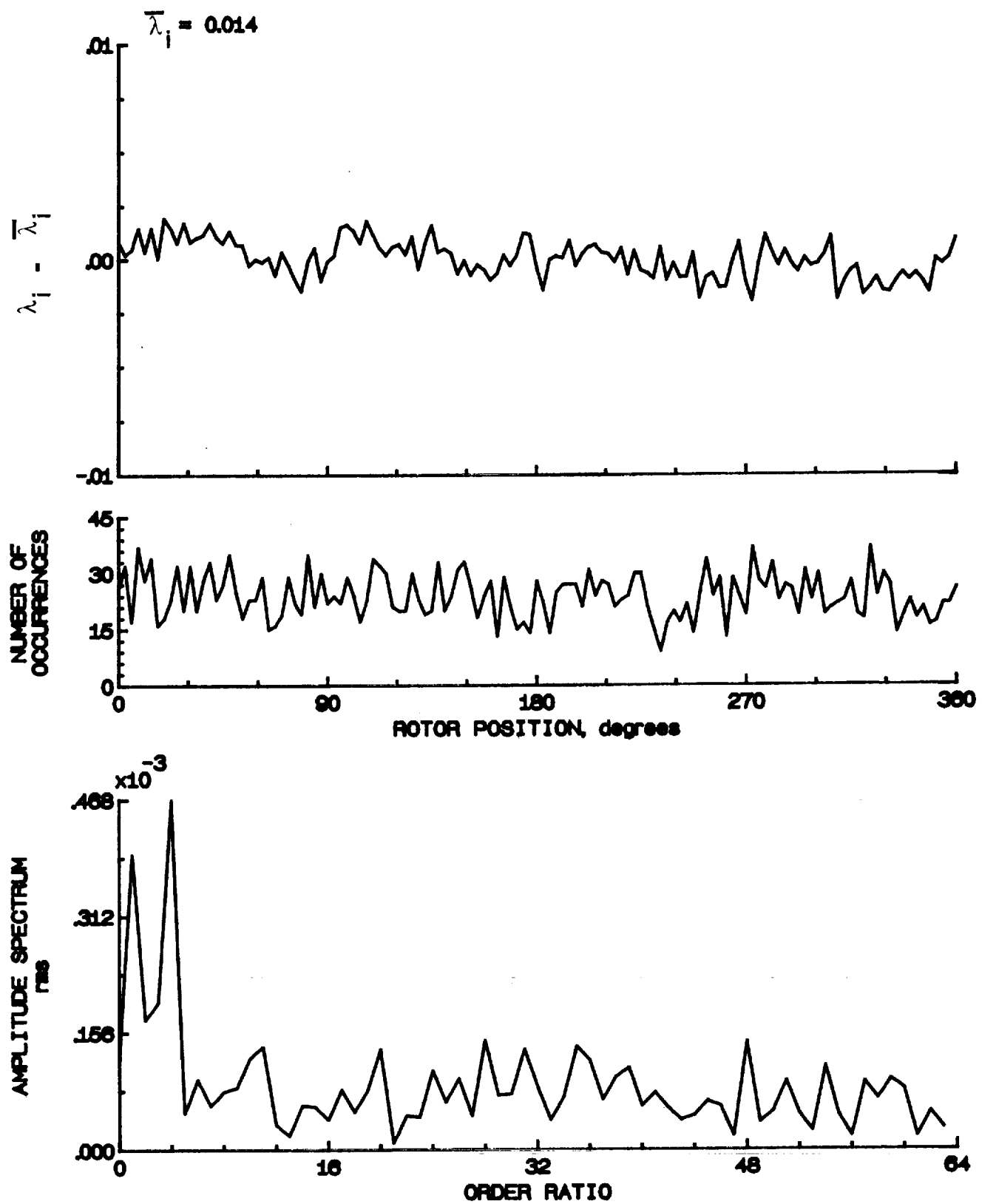


Figure 66.- Concluded.

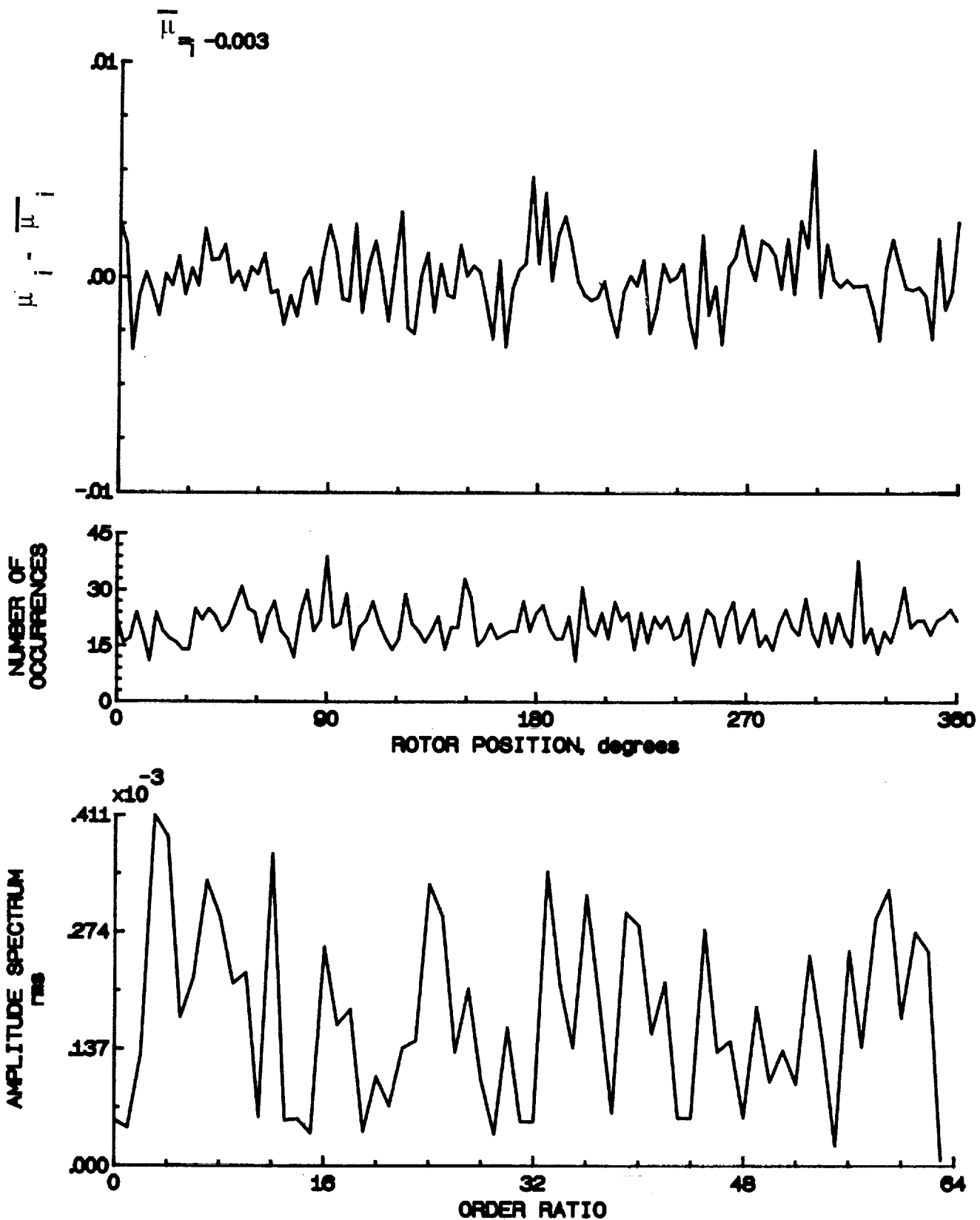


Figure 67.- Induced inflow velocity measured at 90 degrees and r/R of 0.94.

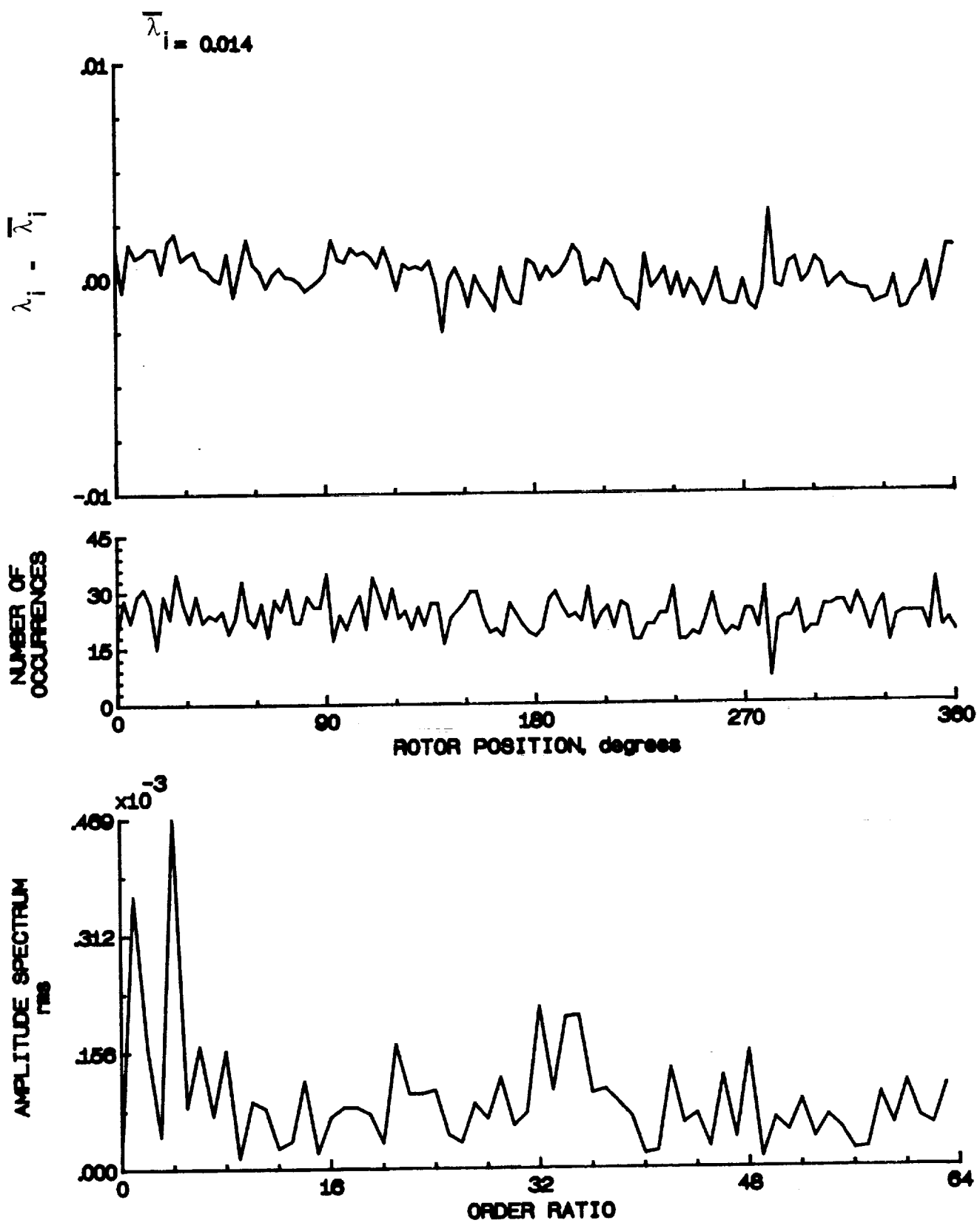


Figure 67.- Concluded.

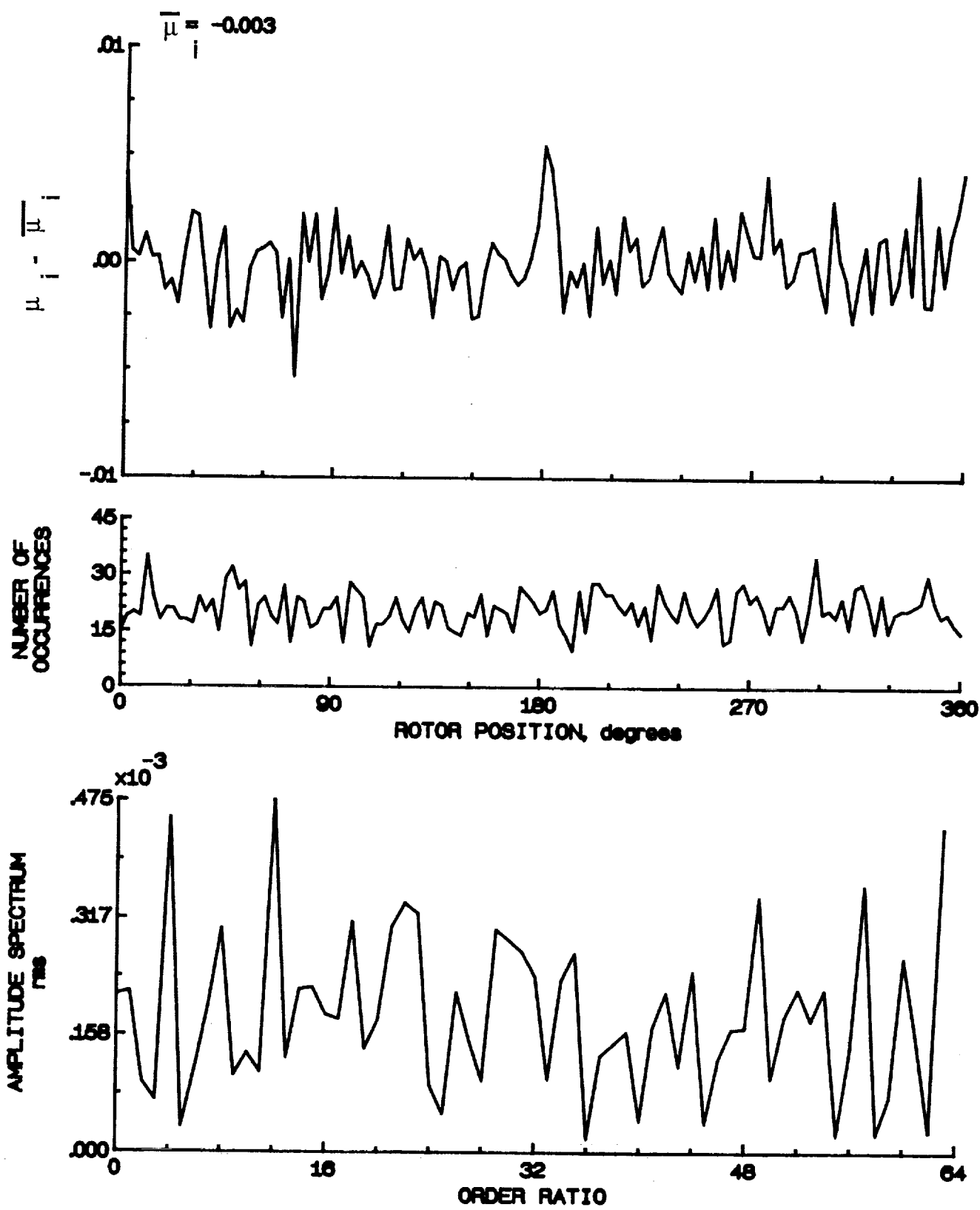


Figure 68.- Induced inflow velocity measured at 90 degrees and r/R of 0.98.

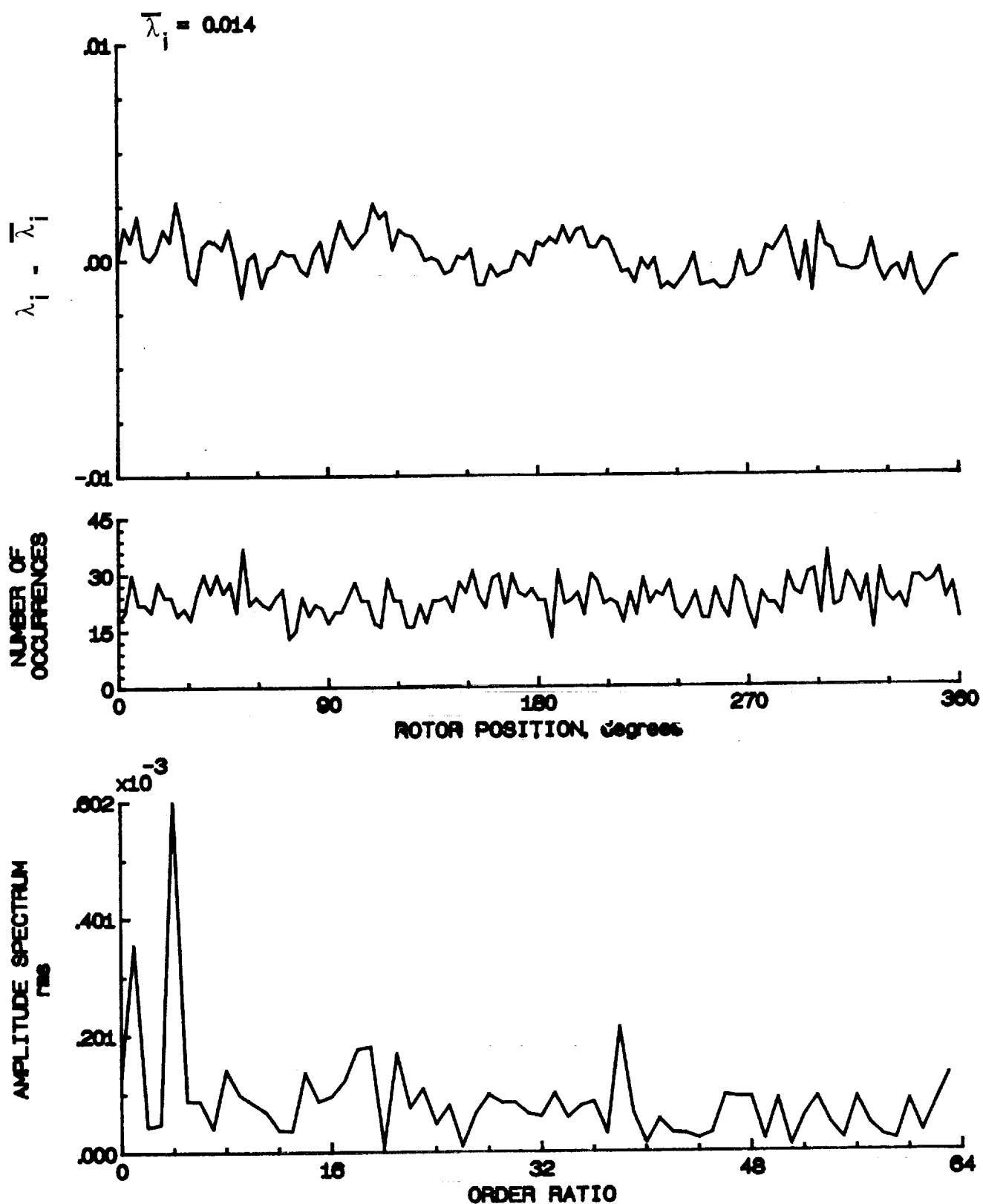


Figure 68.- Concluded.

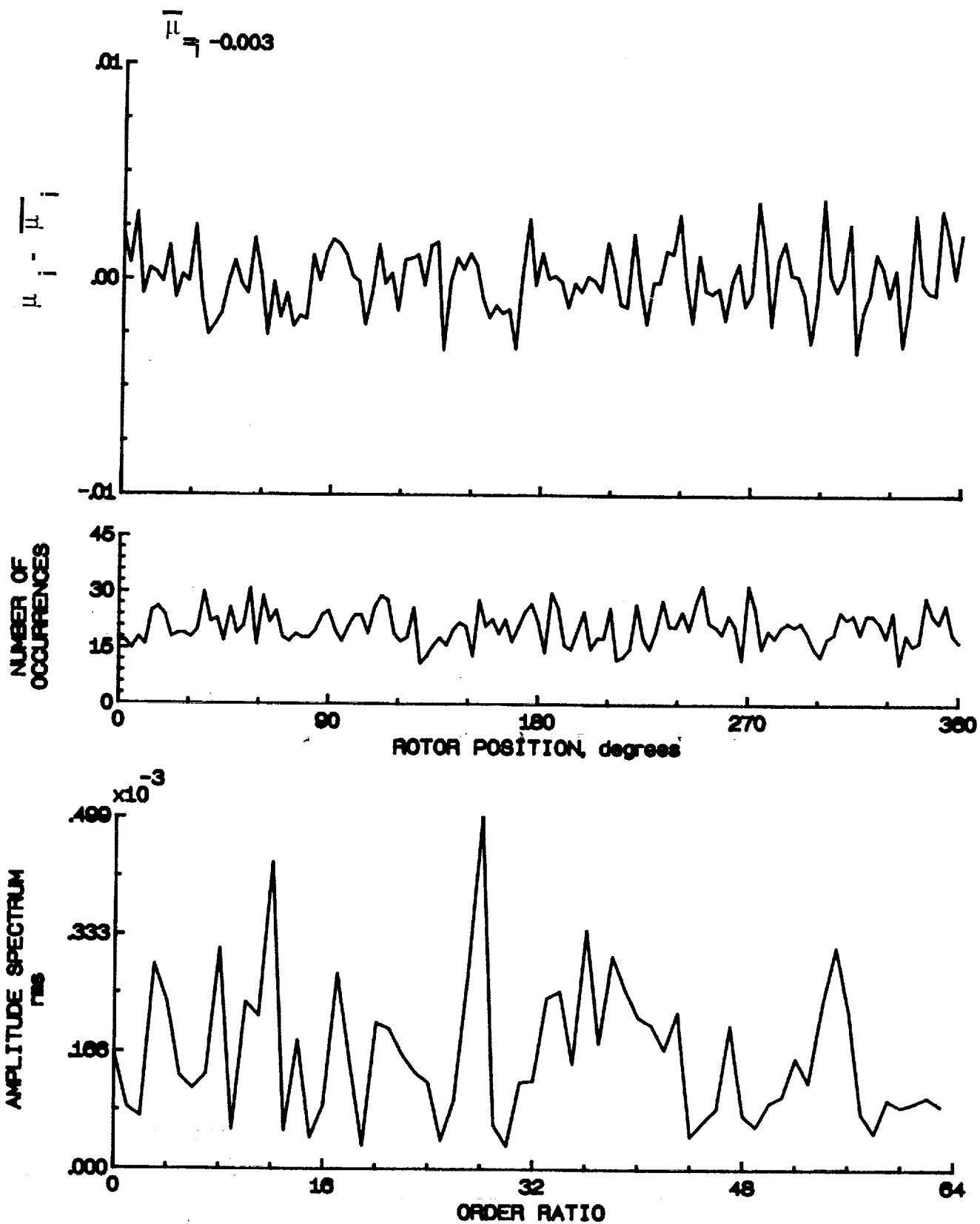


Figure 69.- Induced inflow velocity measured at 90 degrees and r/R of 1.02.

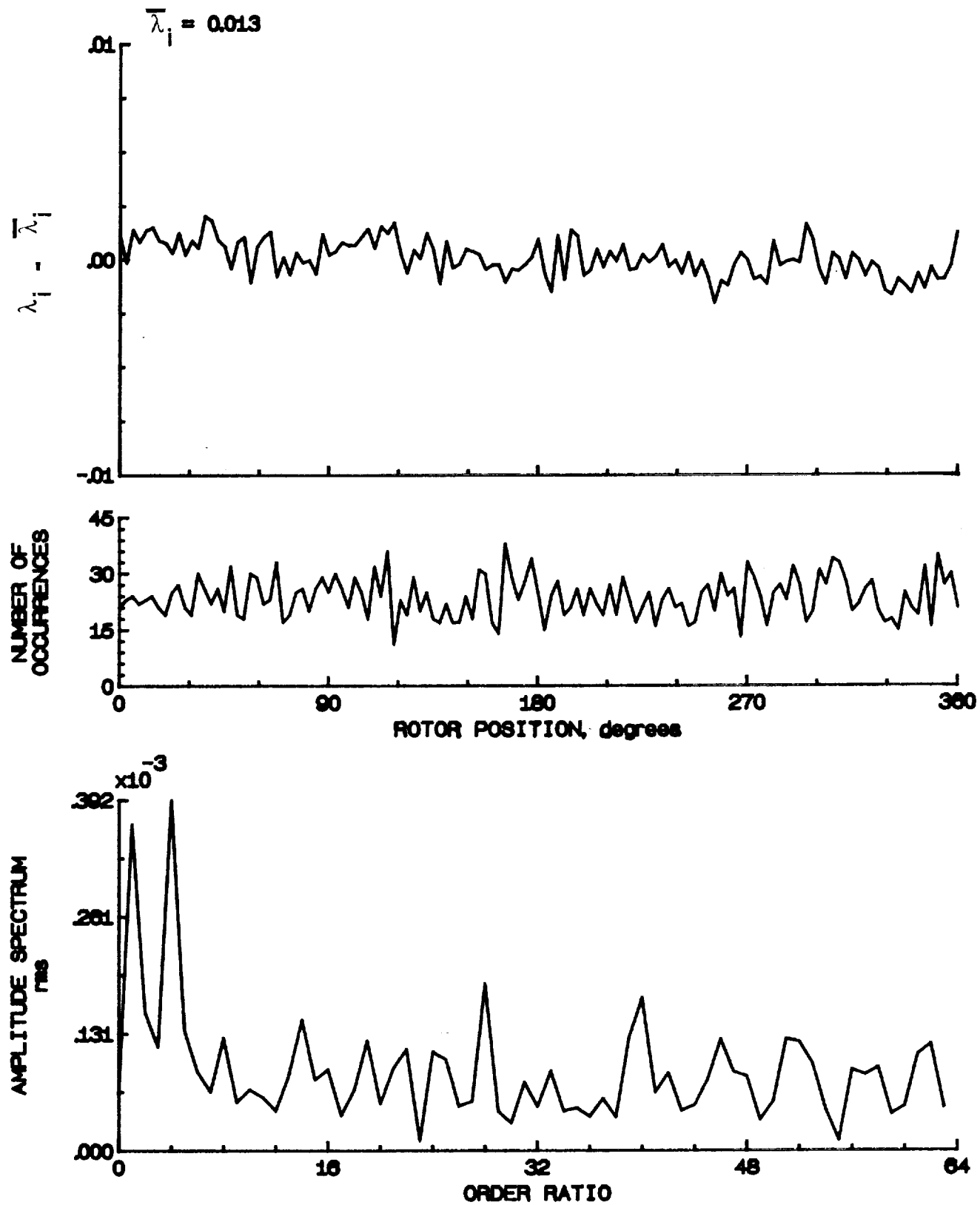


Figure 69.- Concluded.

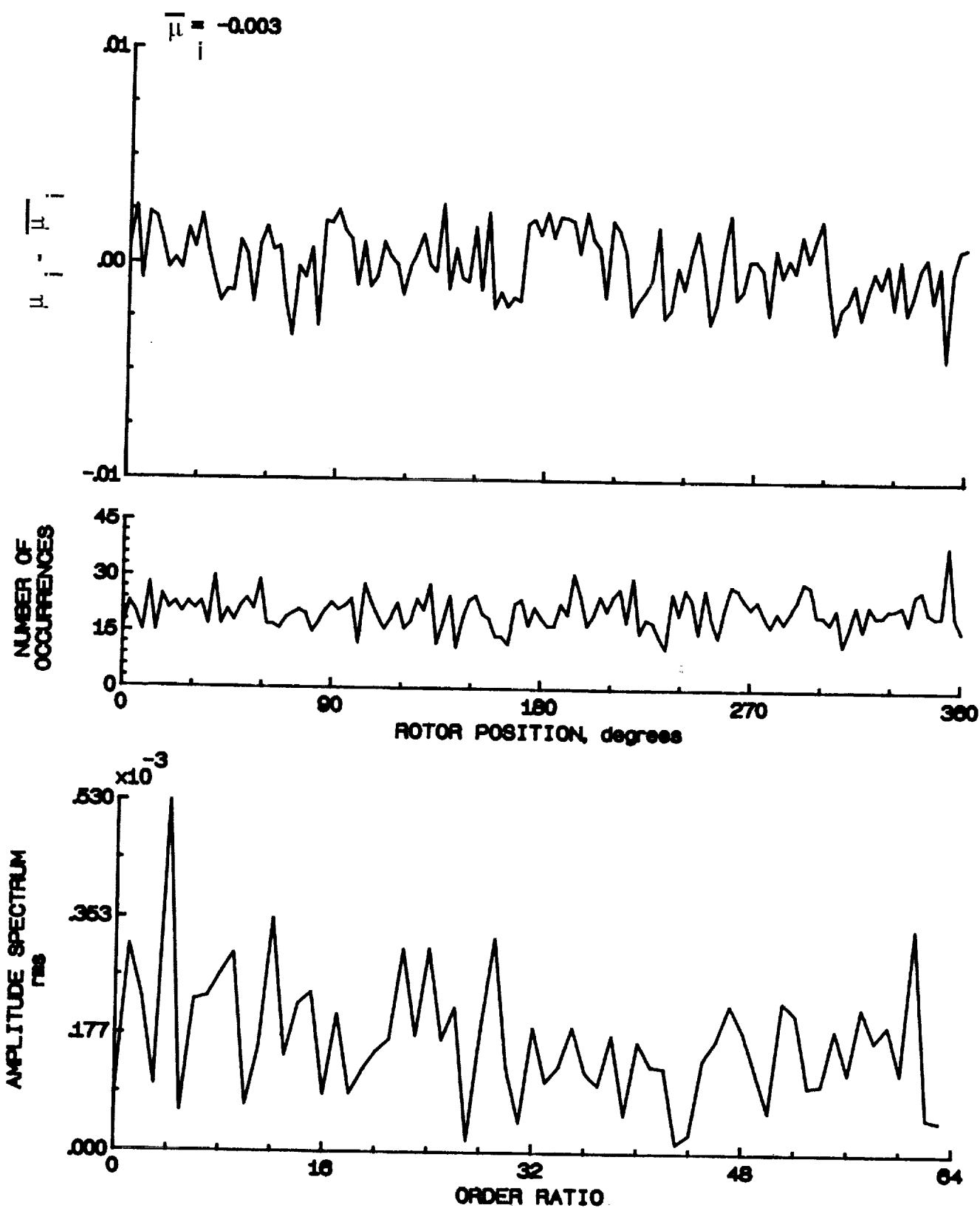


Figure 70.- Induced inflow velocity measured at 90 degrees and r/R of 1.04.

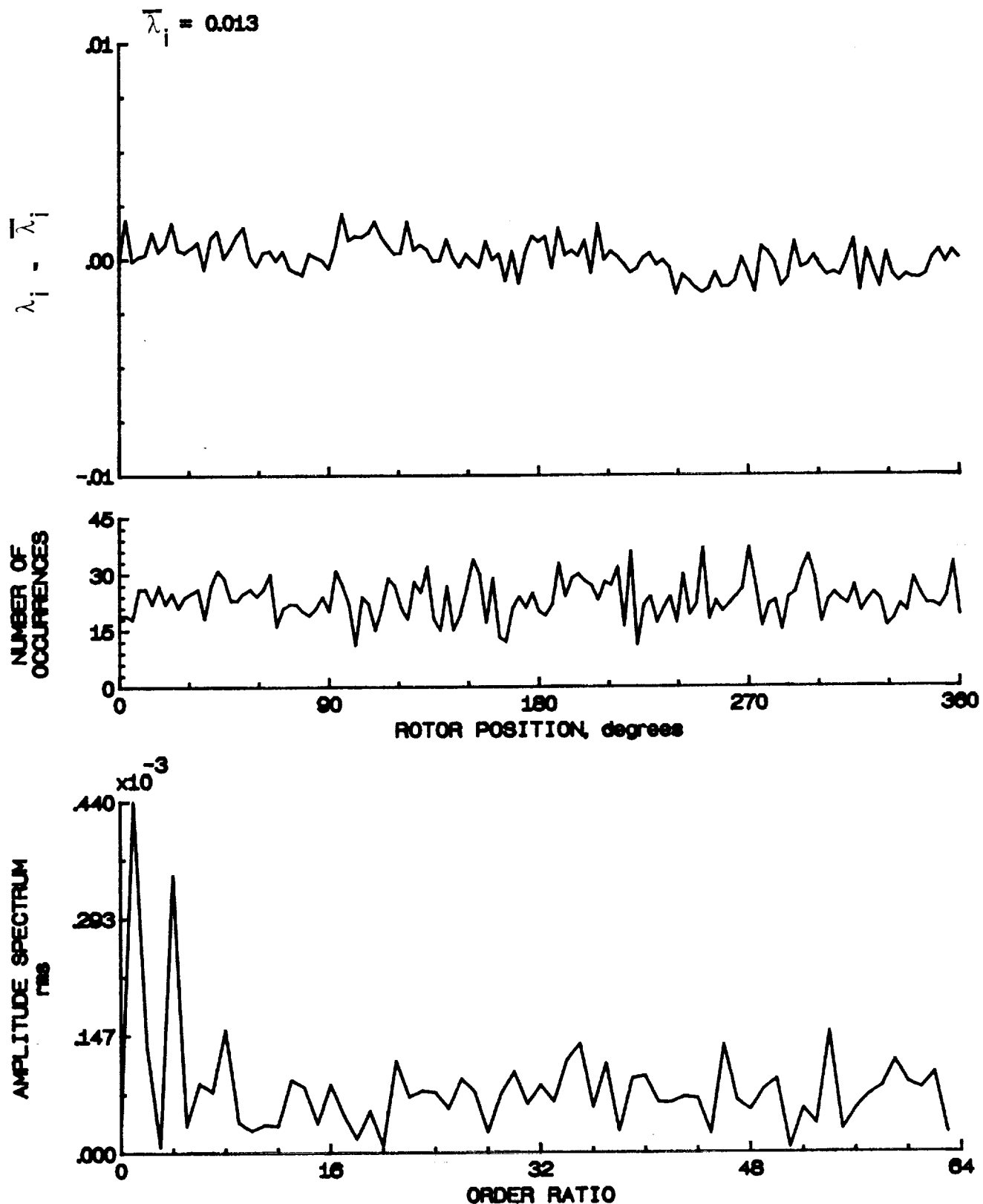


Figure 70.- Concluded.

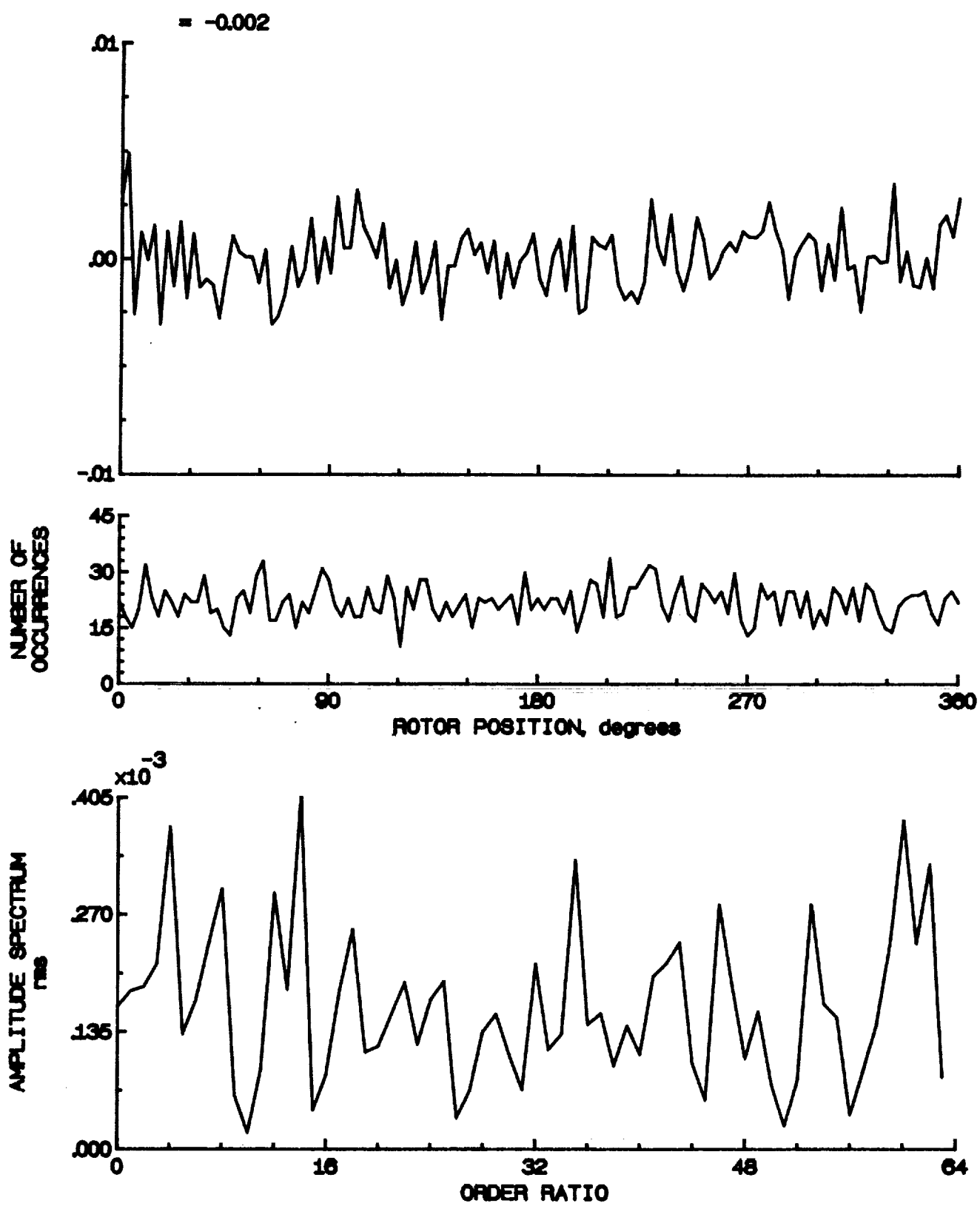


Figure 71.- Induced inflow velocity measured at 90 degrees and r/R of 1.10.

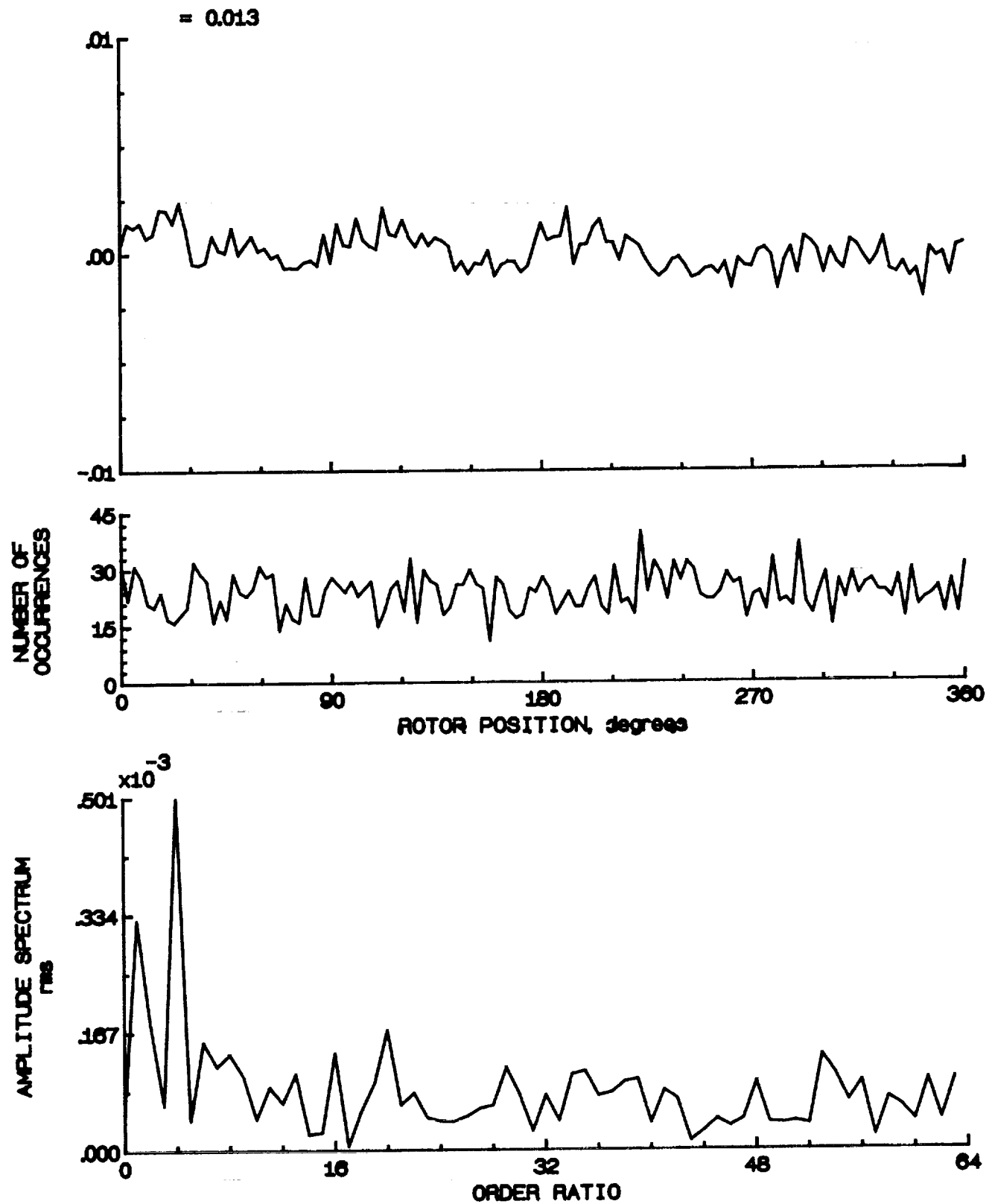


Figure 71.- Concluded.

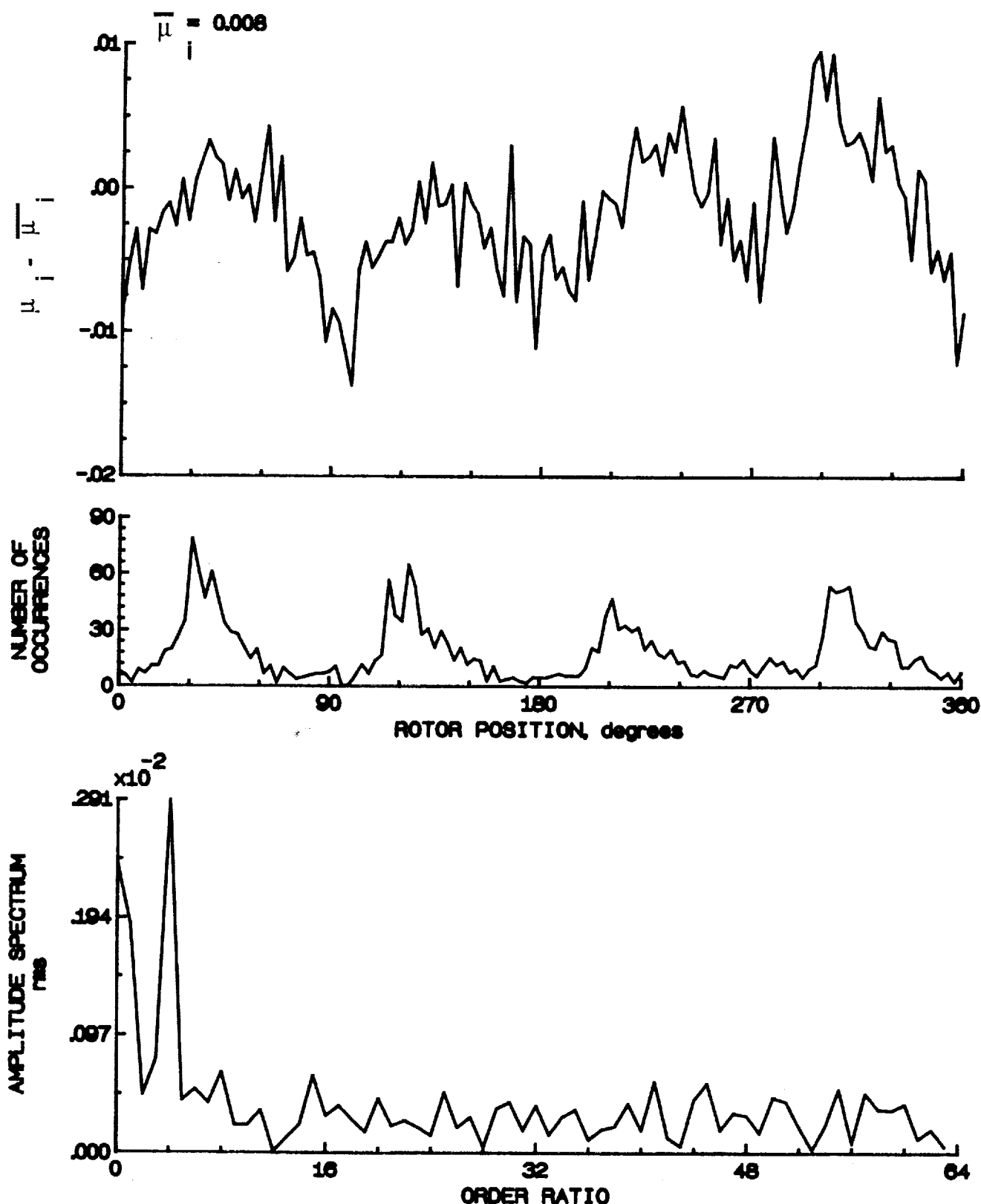


Figure 72.- Induced inflow velocity measured at 120 degrees and r/R of 0.20.

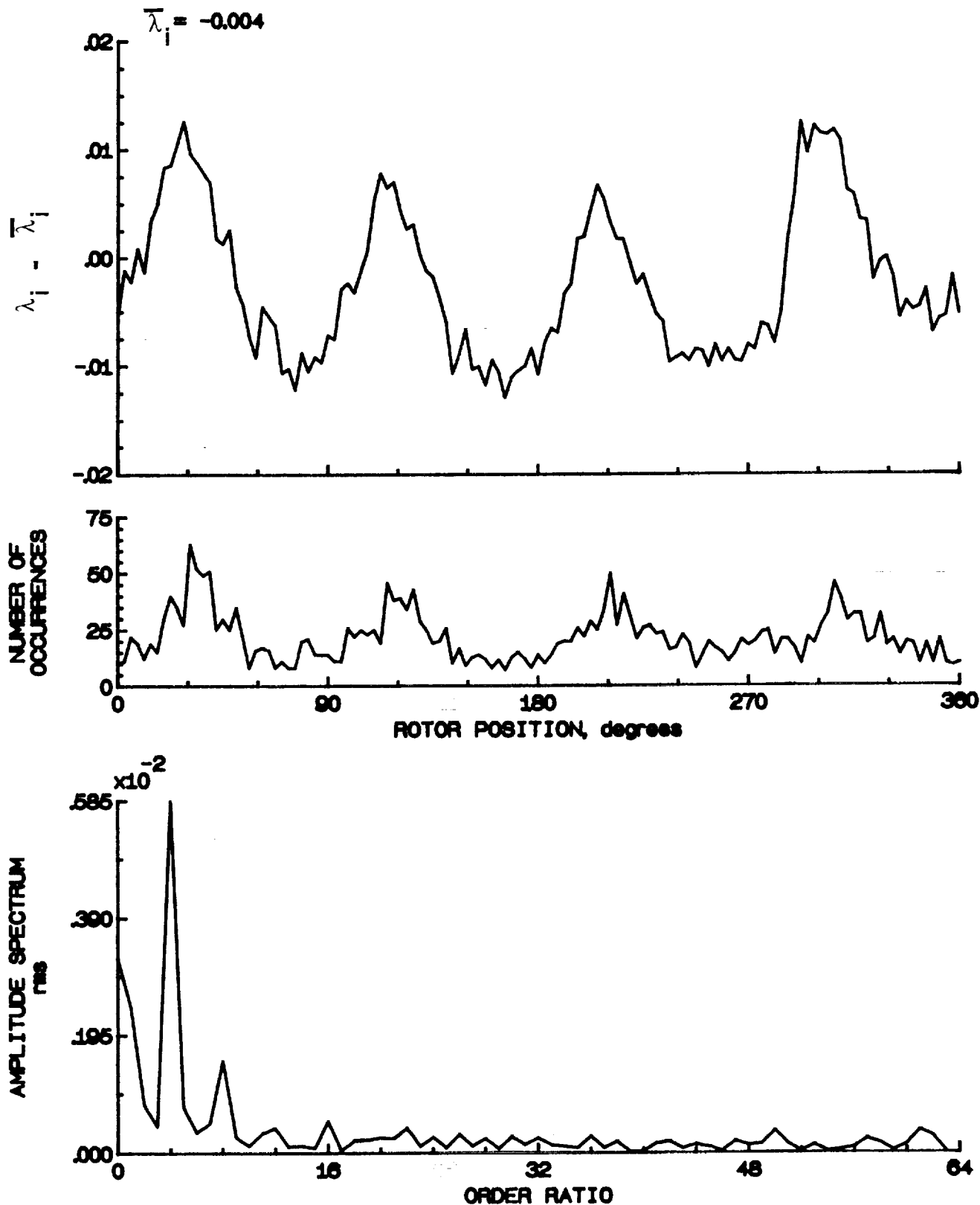


Figure 72.- Concluded.

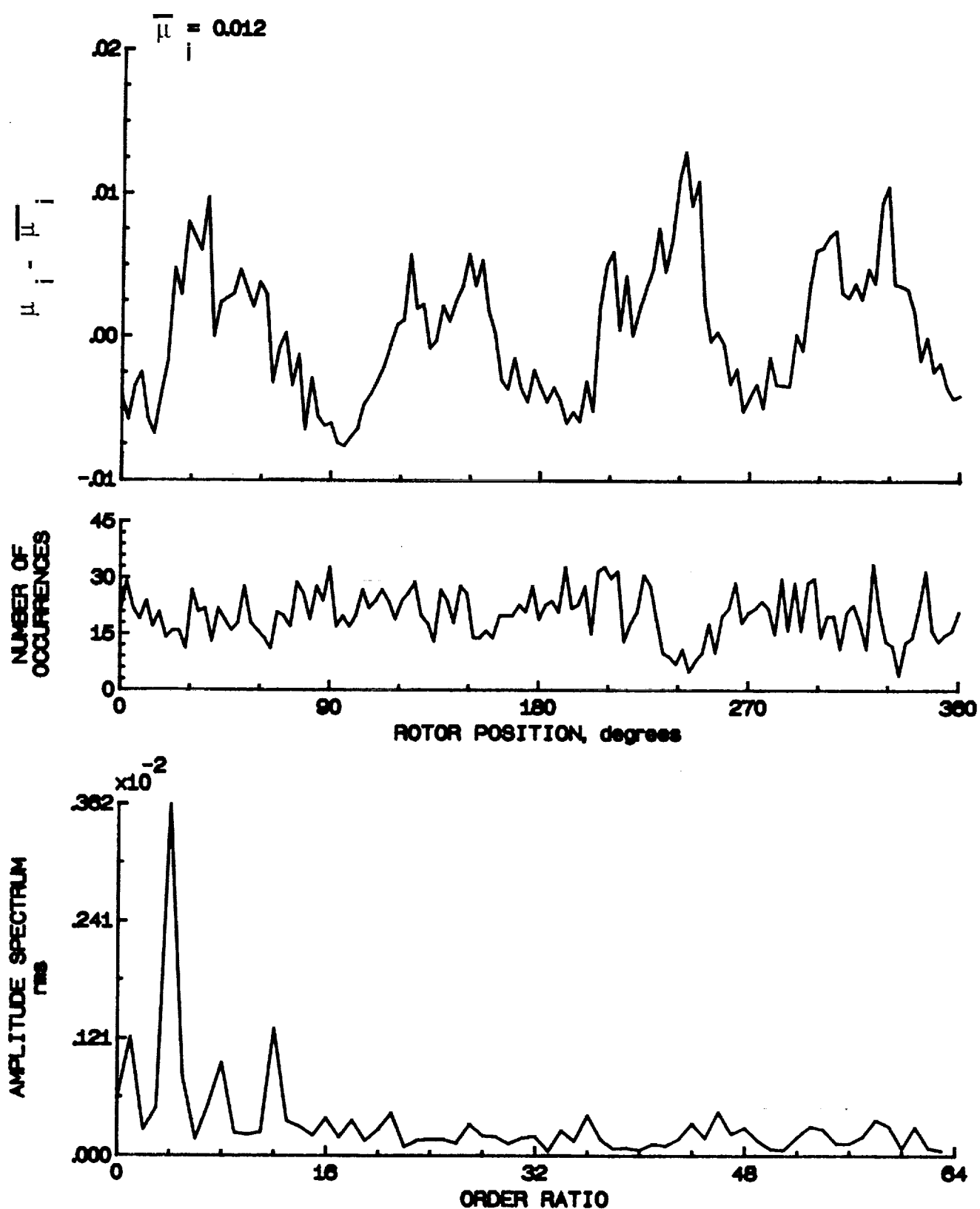


Figure 73.- Induced inflow velocity measured at 120 degrees and r/R of 0.40.

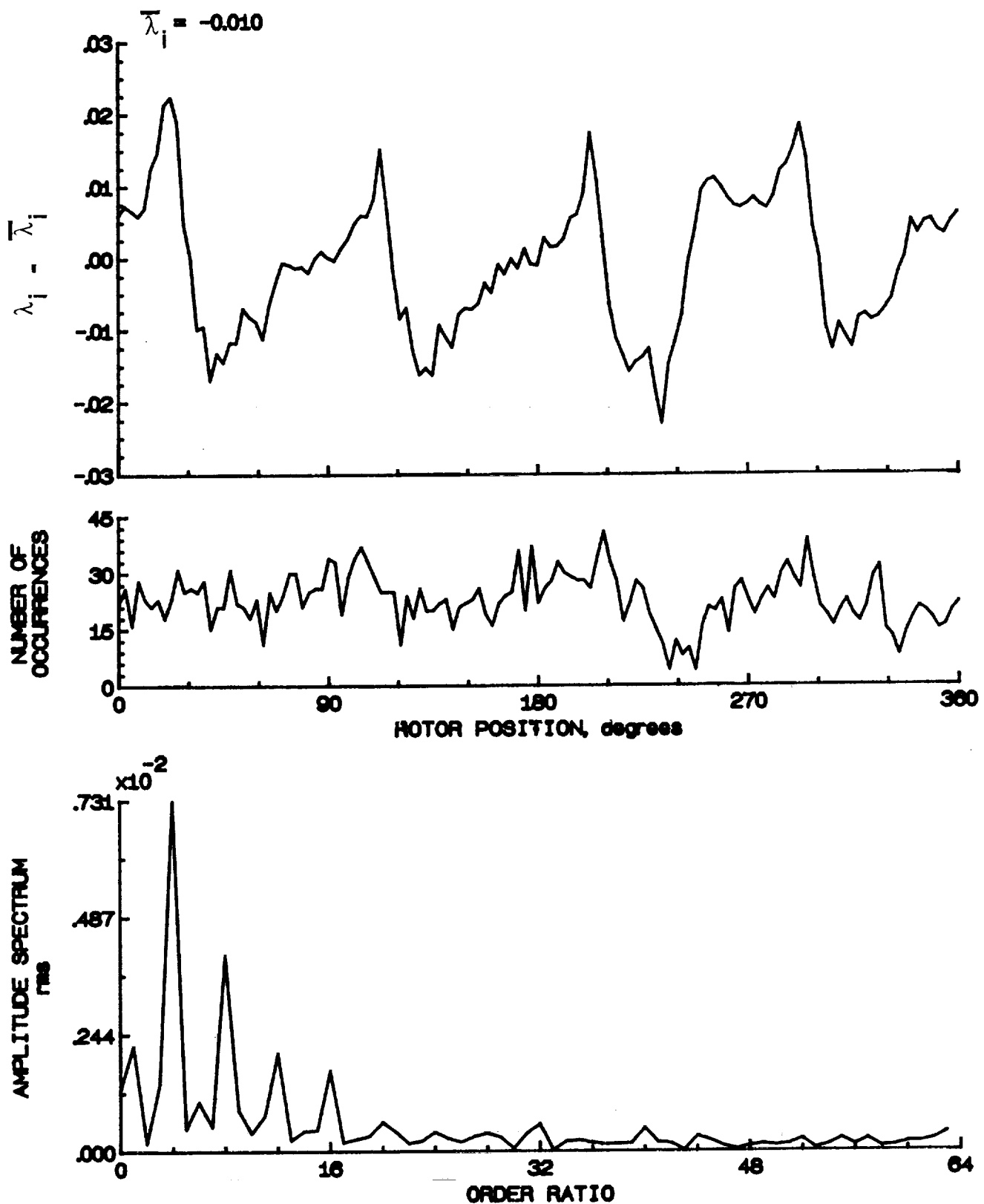


Figure 73.- Concluded.

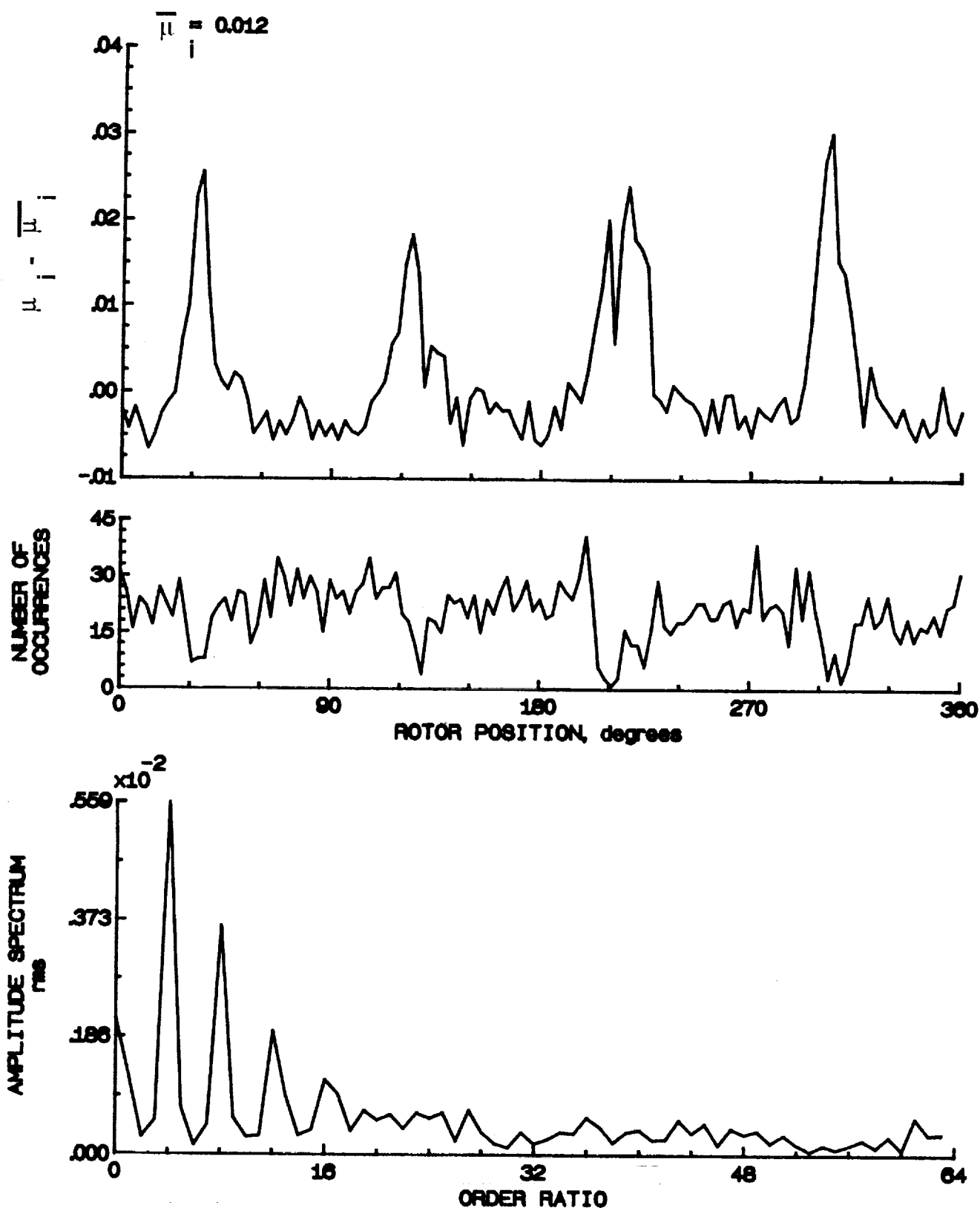


Figure 74.- Induced inflow velocity measured at 120 degrees and r/R of 0.50.

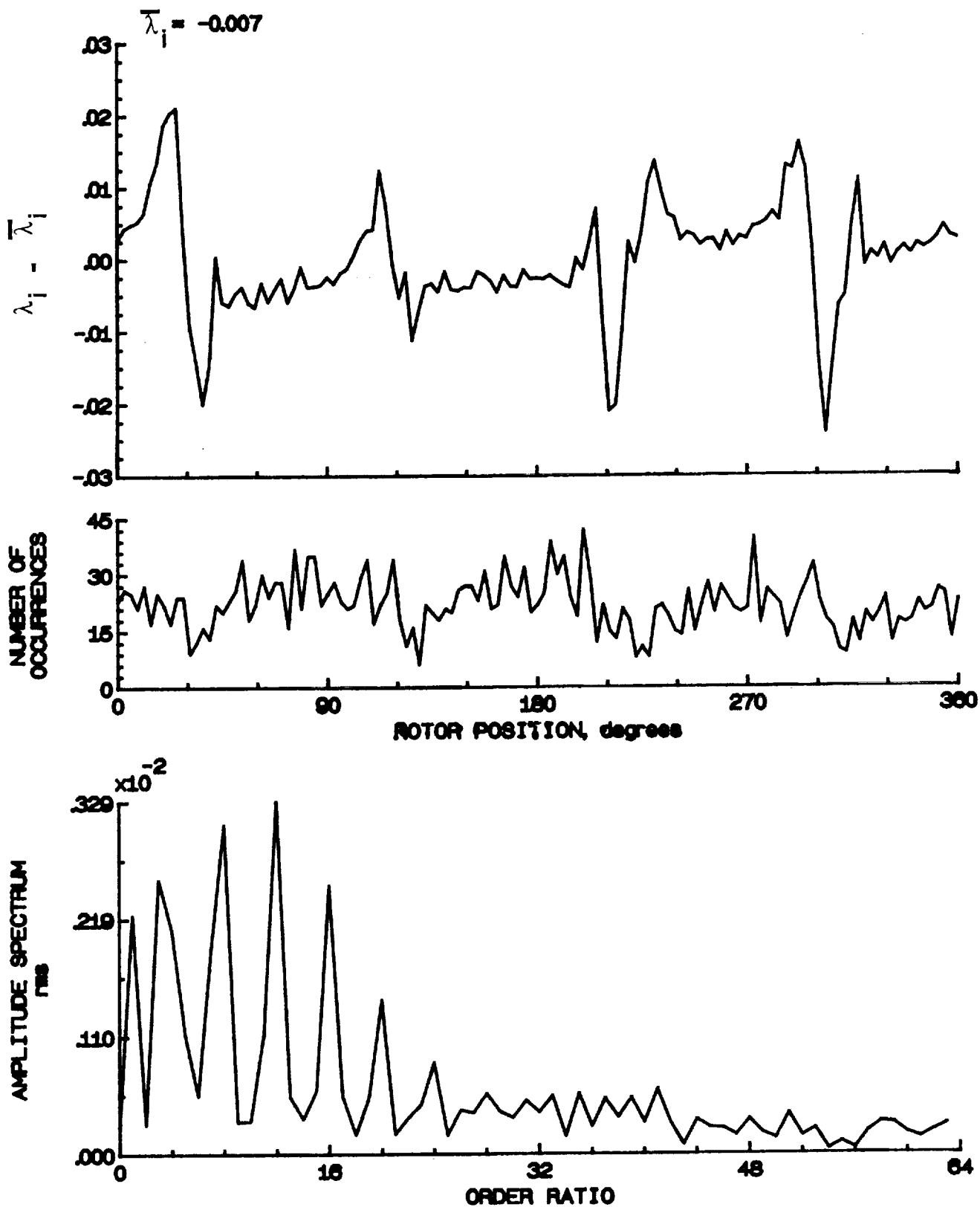


Figure 74.- Concluded.

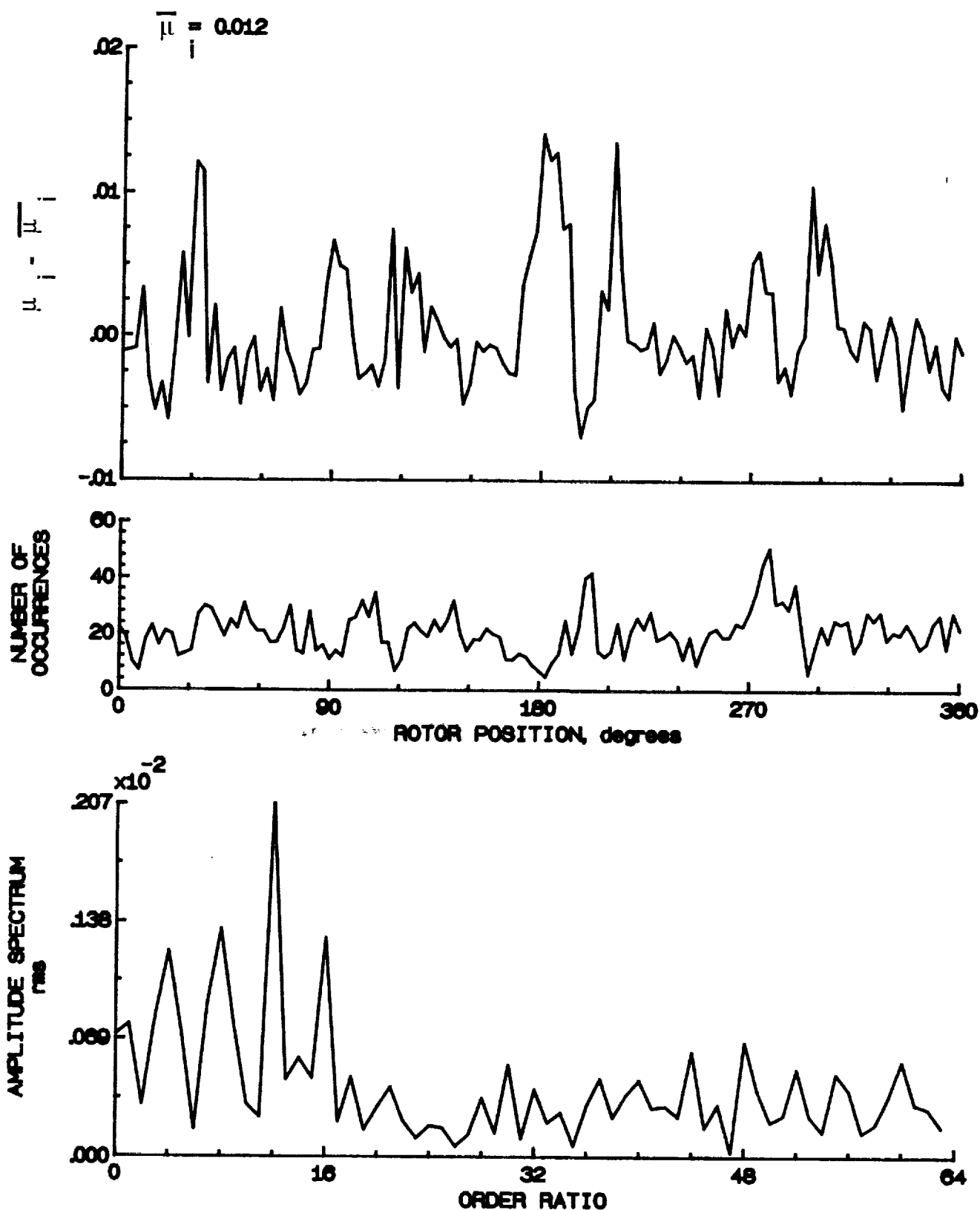


Figure 75.- Induced inflow velocity measured at 120 degrees and r/R of 0.60.

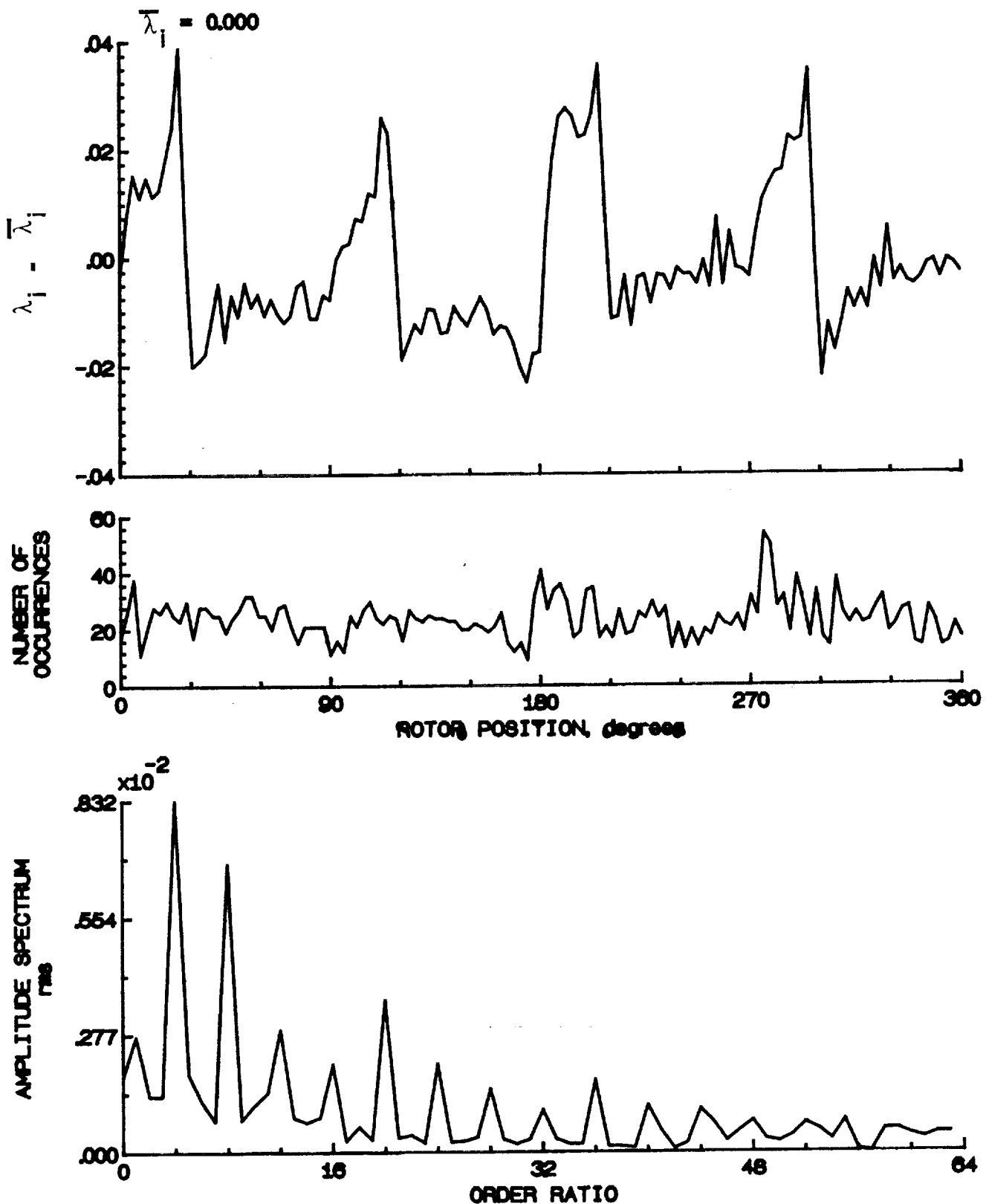


Figure 75.- Concluded.

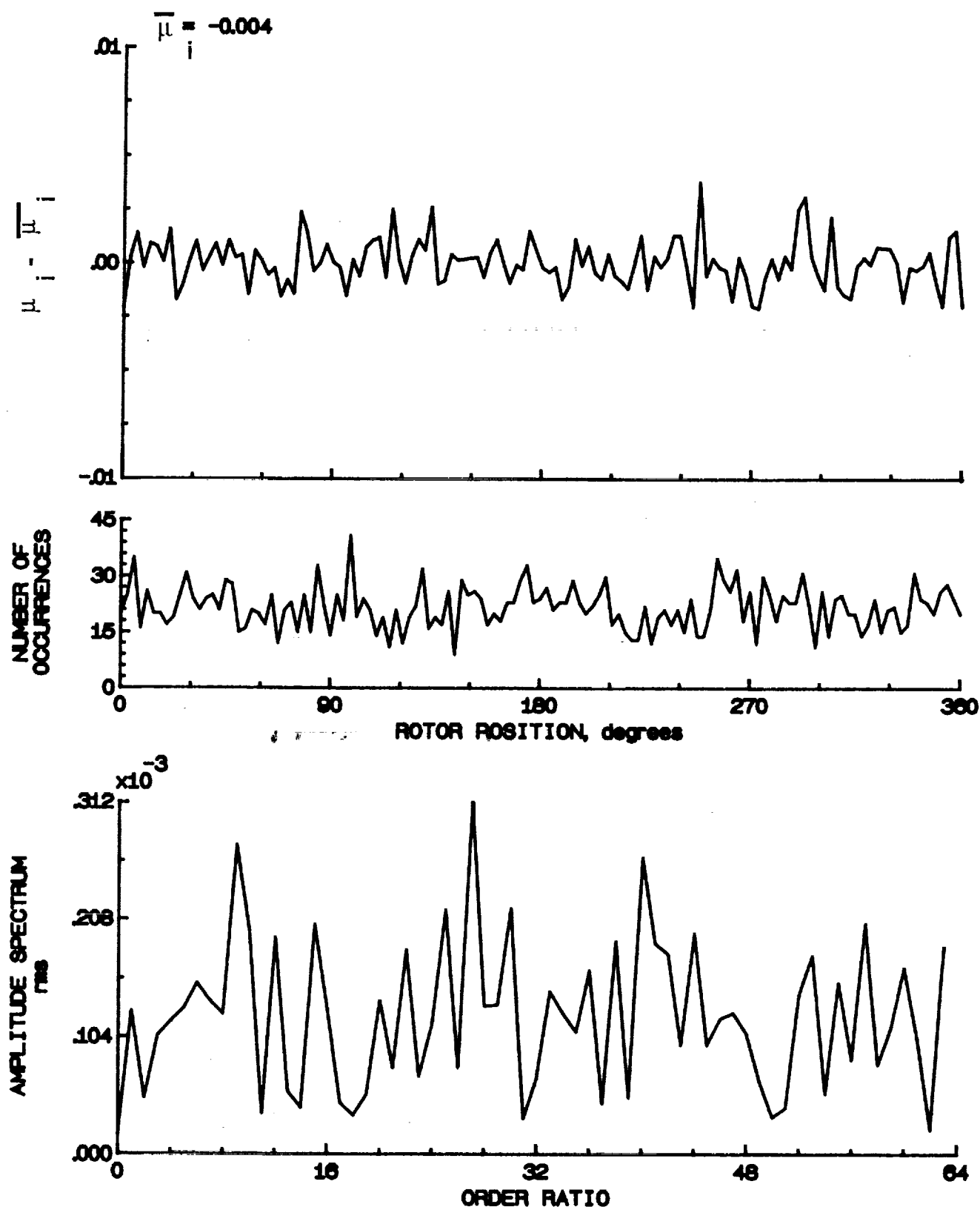


Figure 76.- Induced inflow velocity measured at 120 degrees and r/R of 0.70.

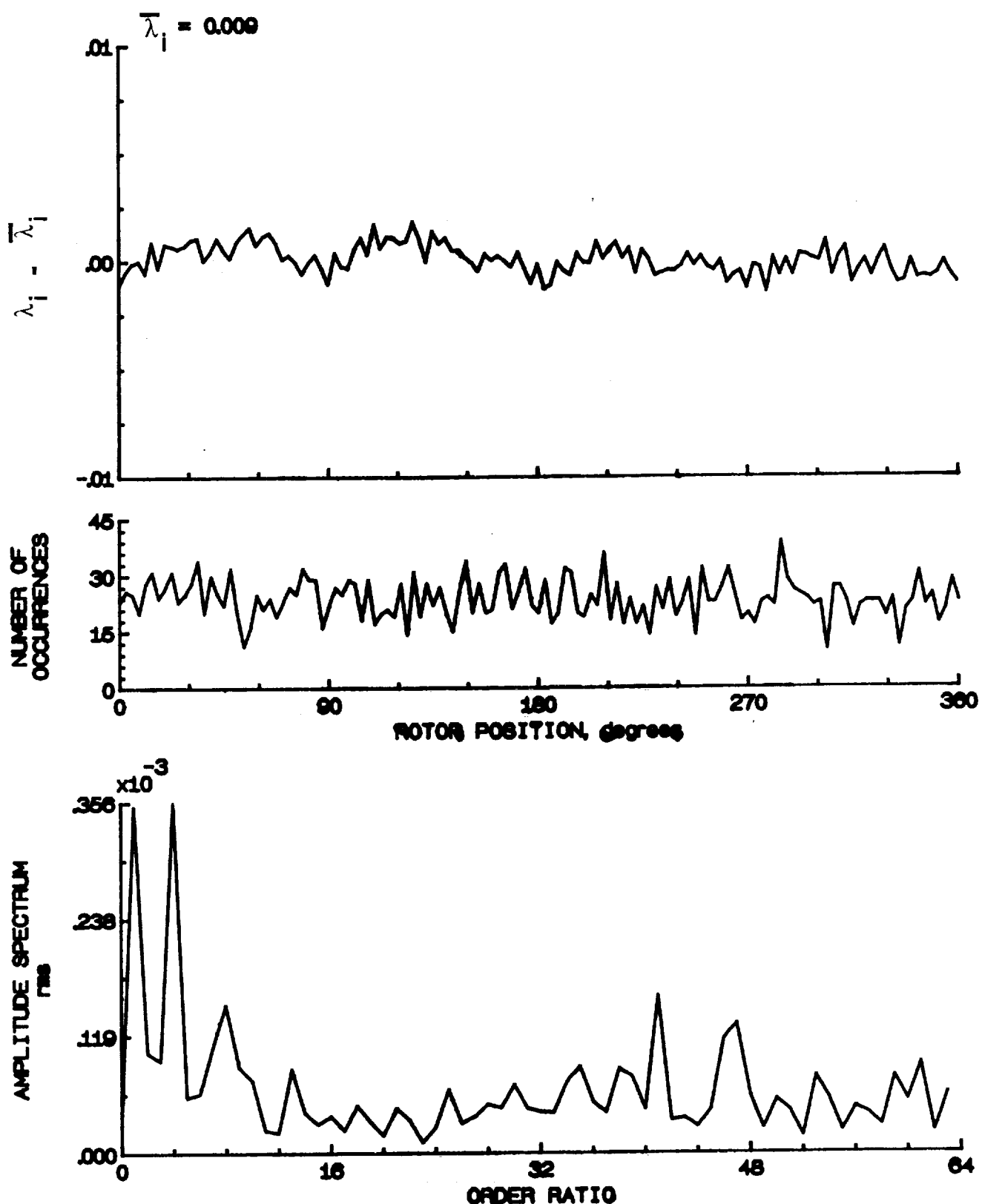


Figure 7a.- Concluded.

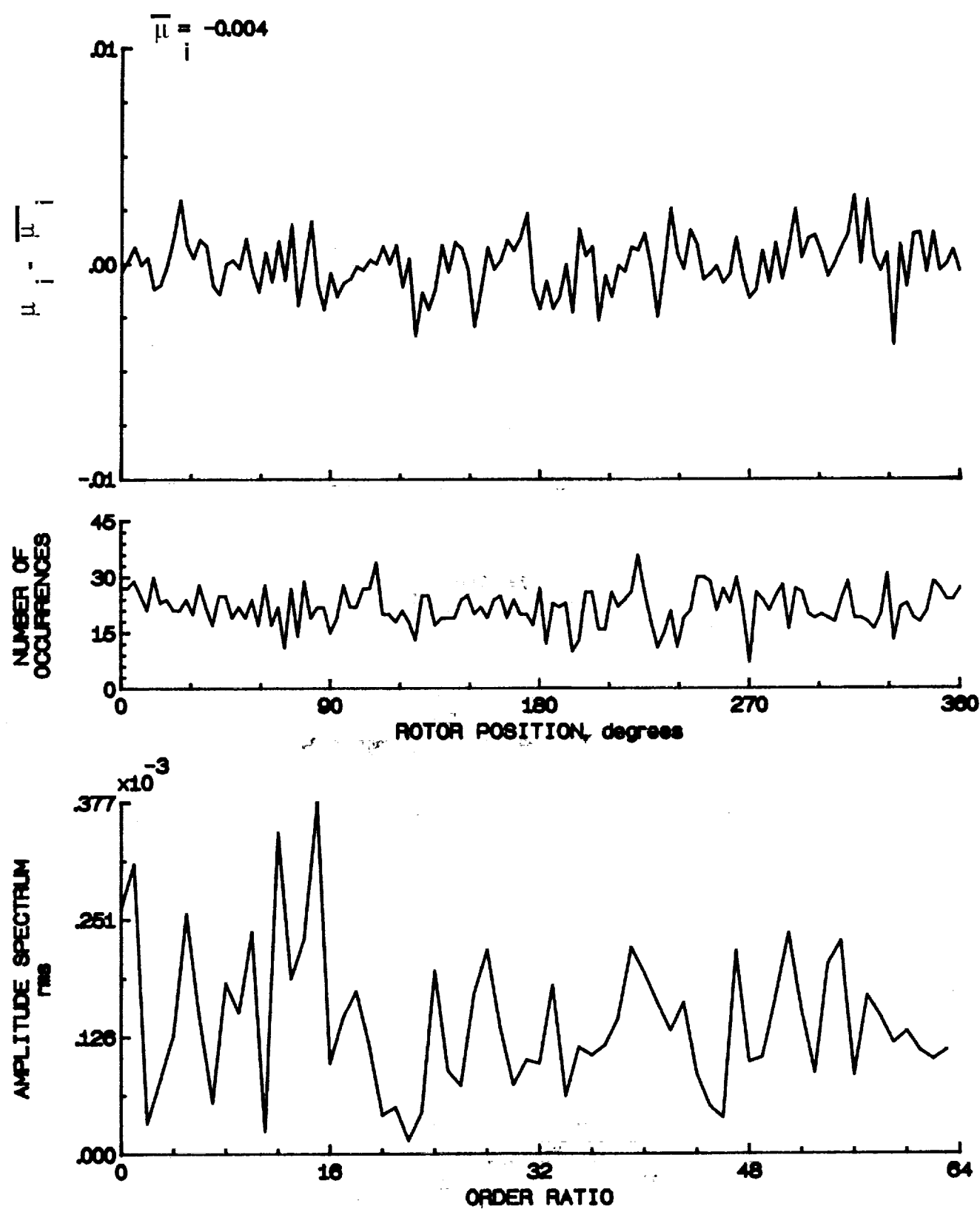


Figure 77.- Induced inflow velocity measured at 120 degrees and r/R of 0.74.

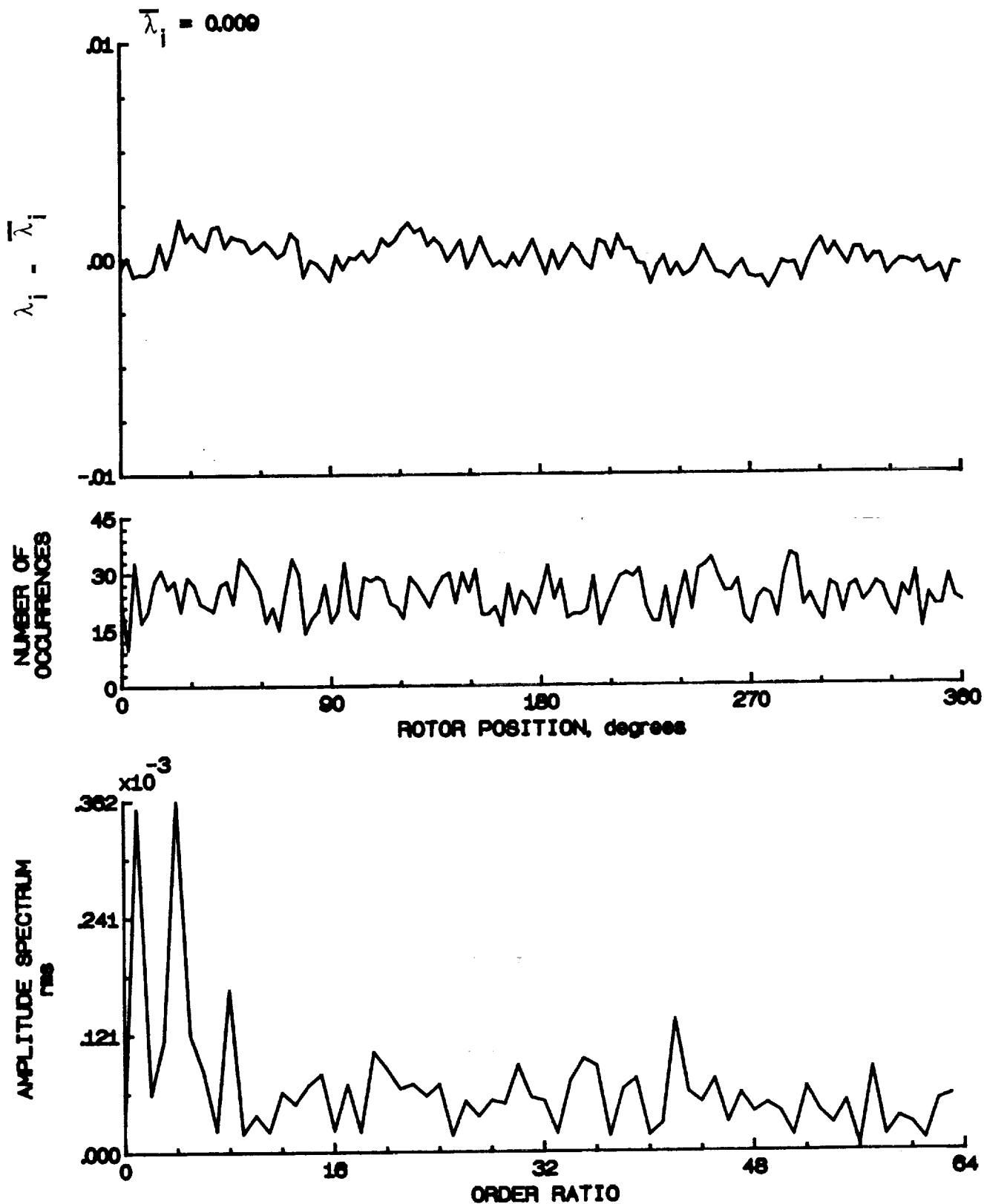


Figure 77.- Concluded.

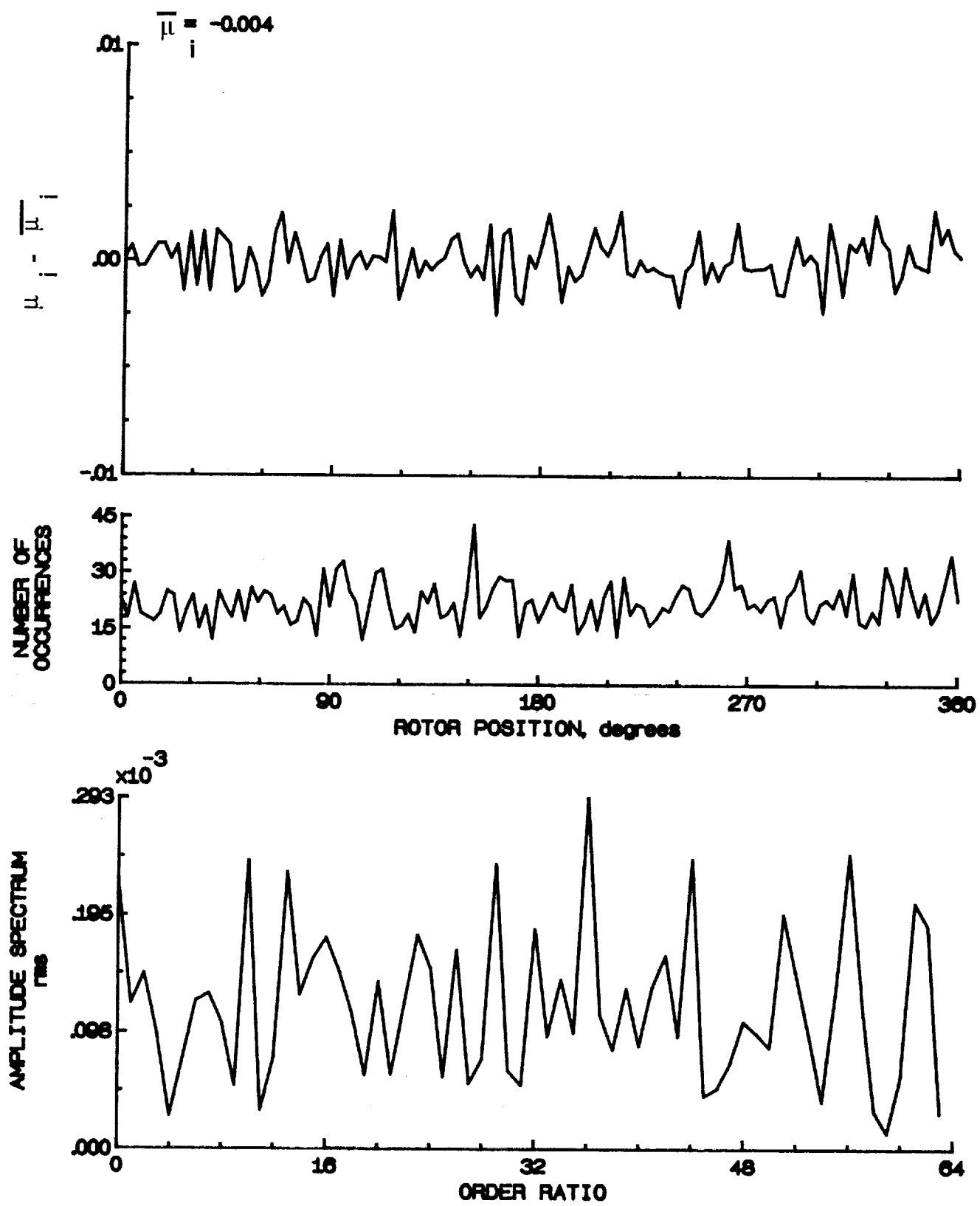


Figure 78.- Induced inflow velocity measured at 120 degrees and r/R of 0.78.

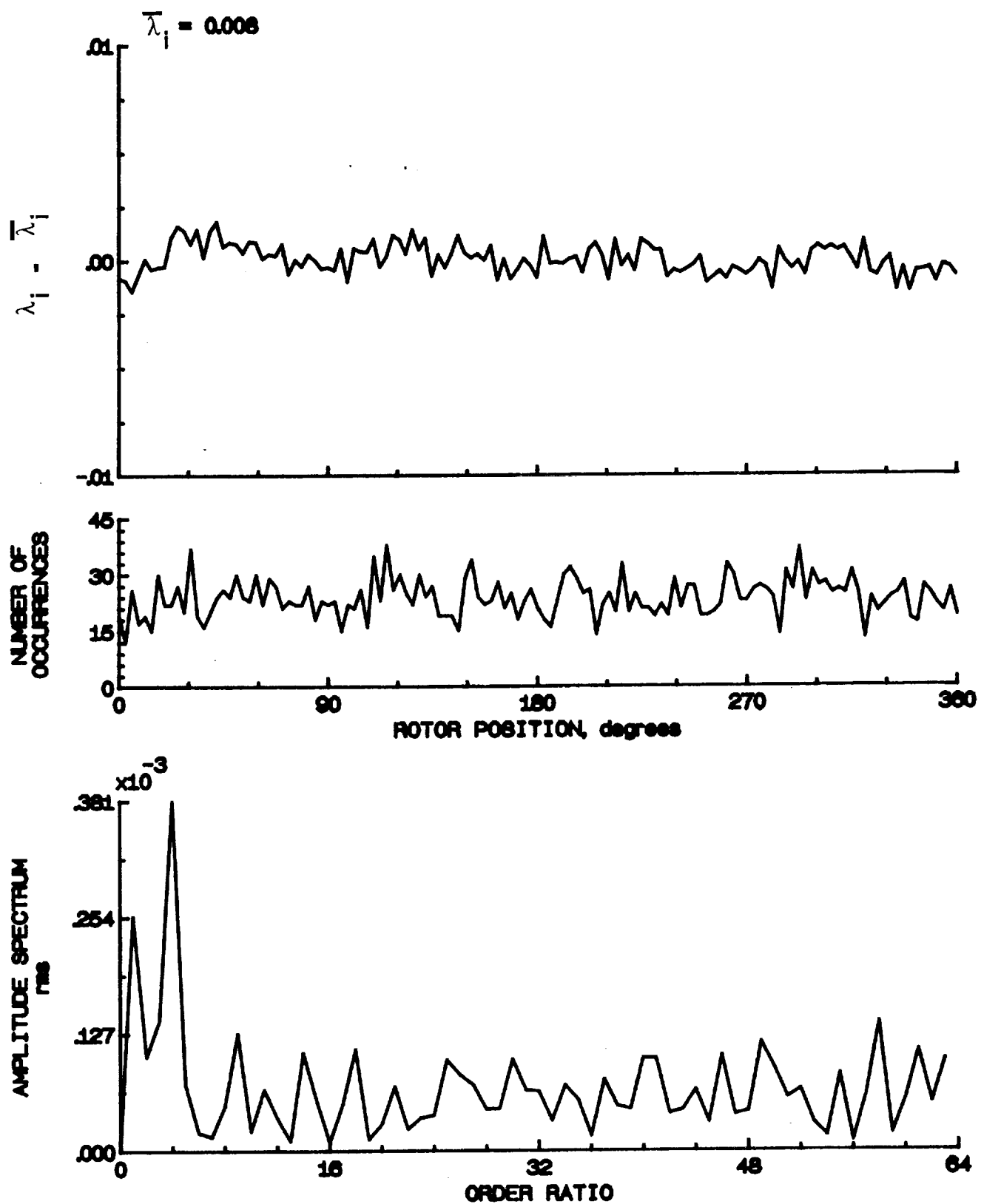


Figure 78.- Concluded.

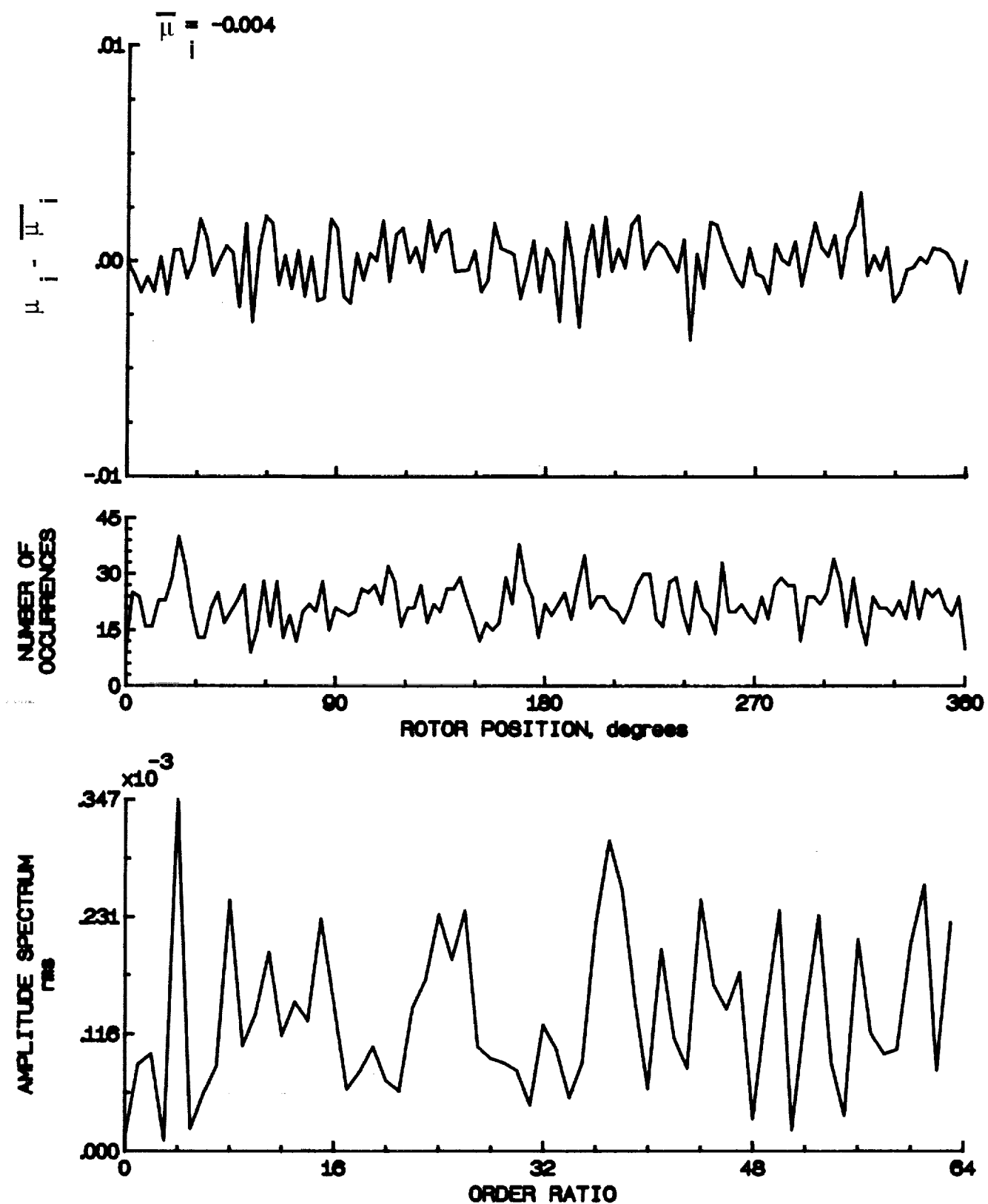


Figure 79.- Induced inflow velocity measured at 120 degrees and r/R of 0.82.

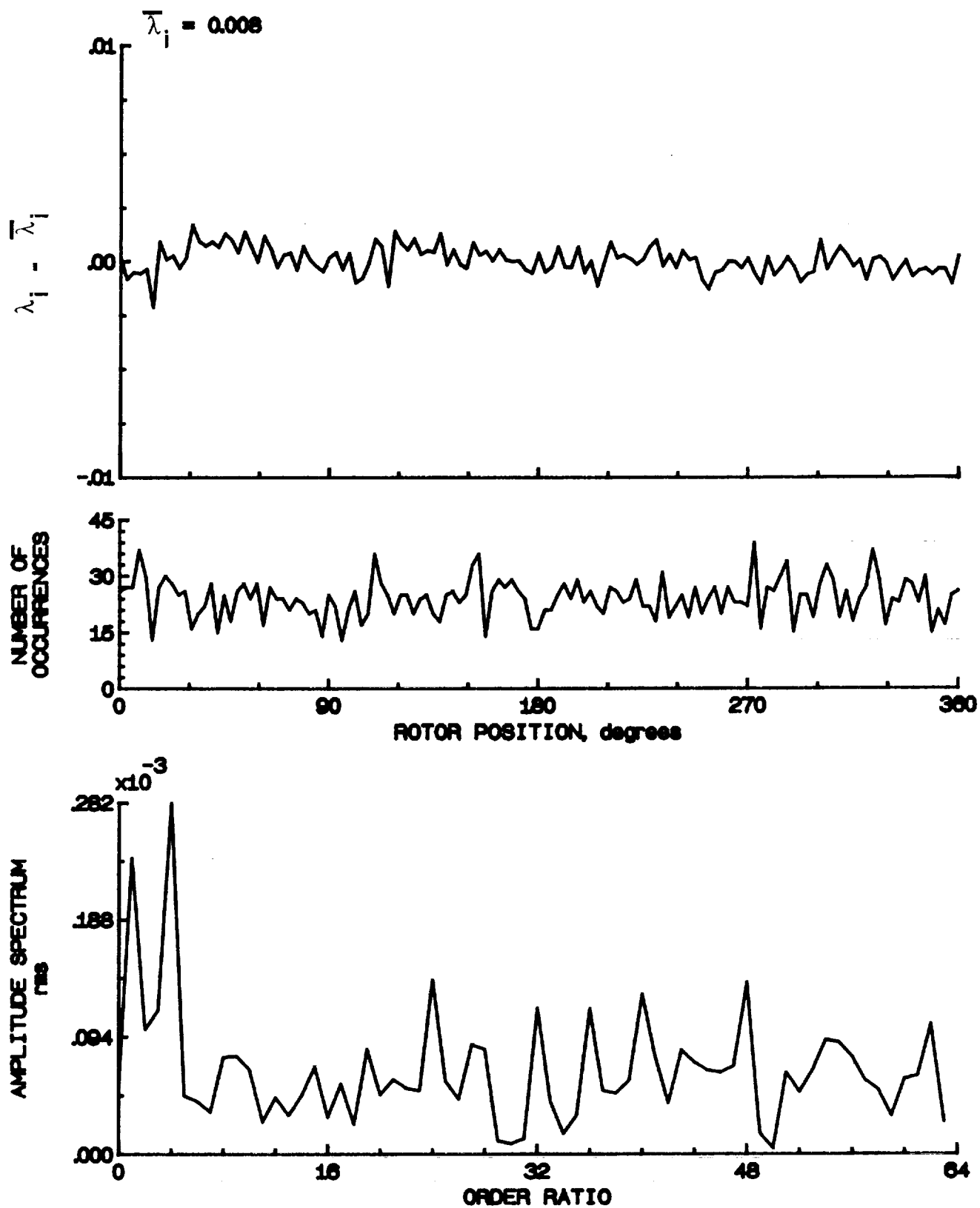


Figure 79.- Concluded.

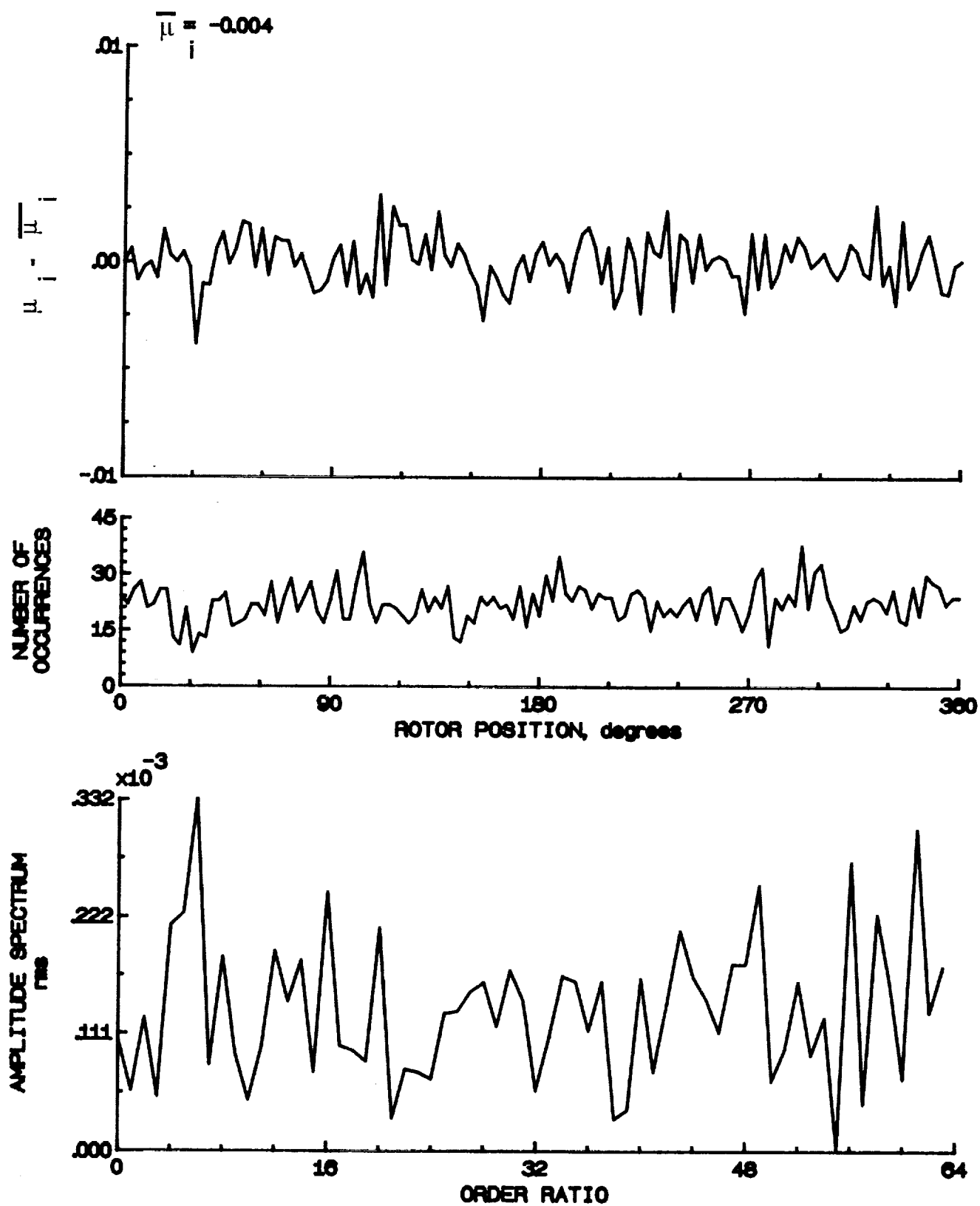


Figure 80.- Induced inflow velocity measured at 120 degrees and r/R of 0.86.

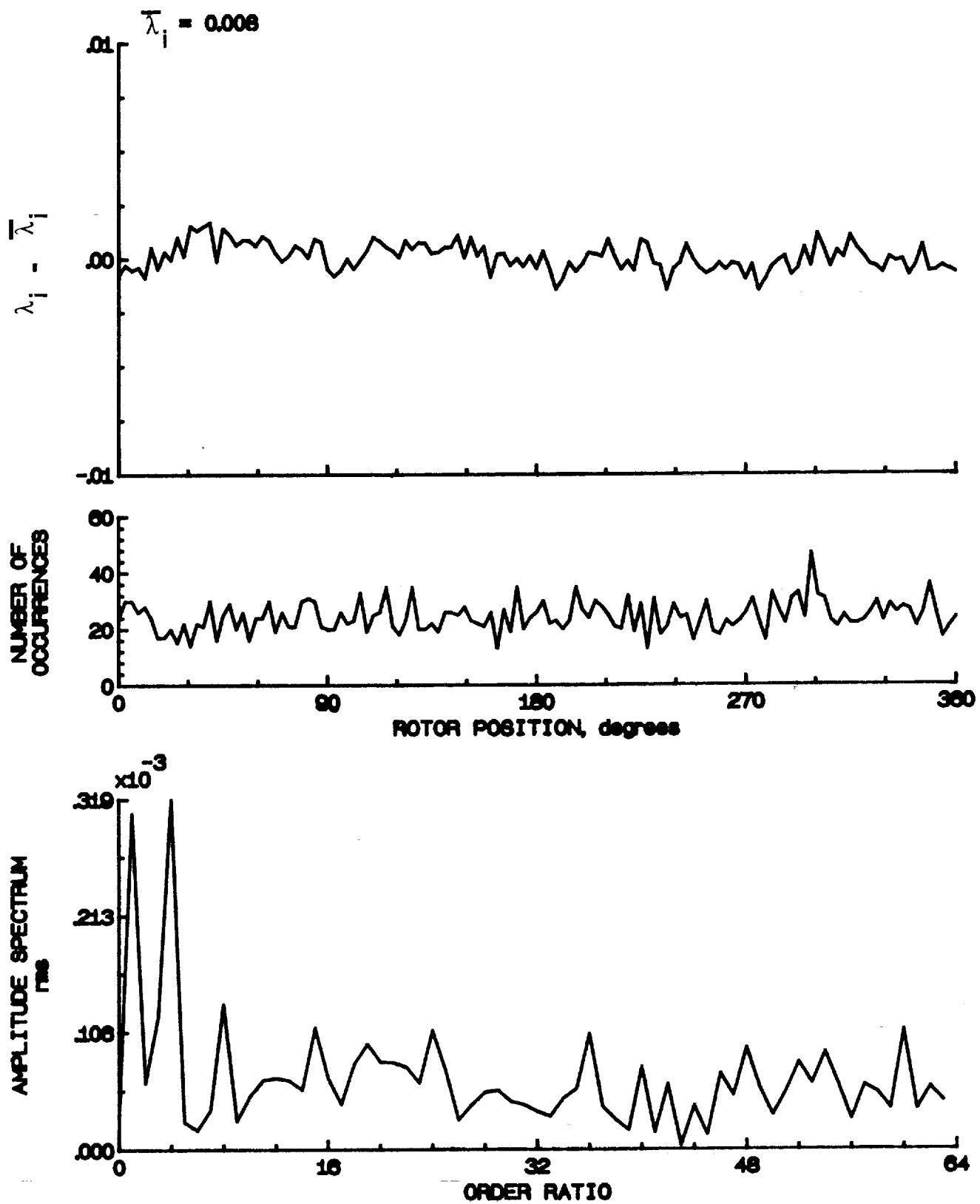


Figure 80.- Concluded.

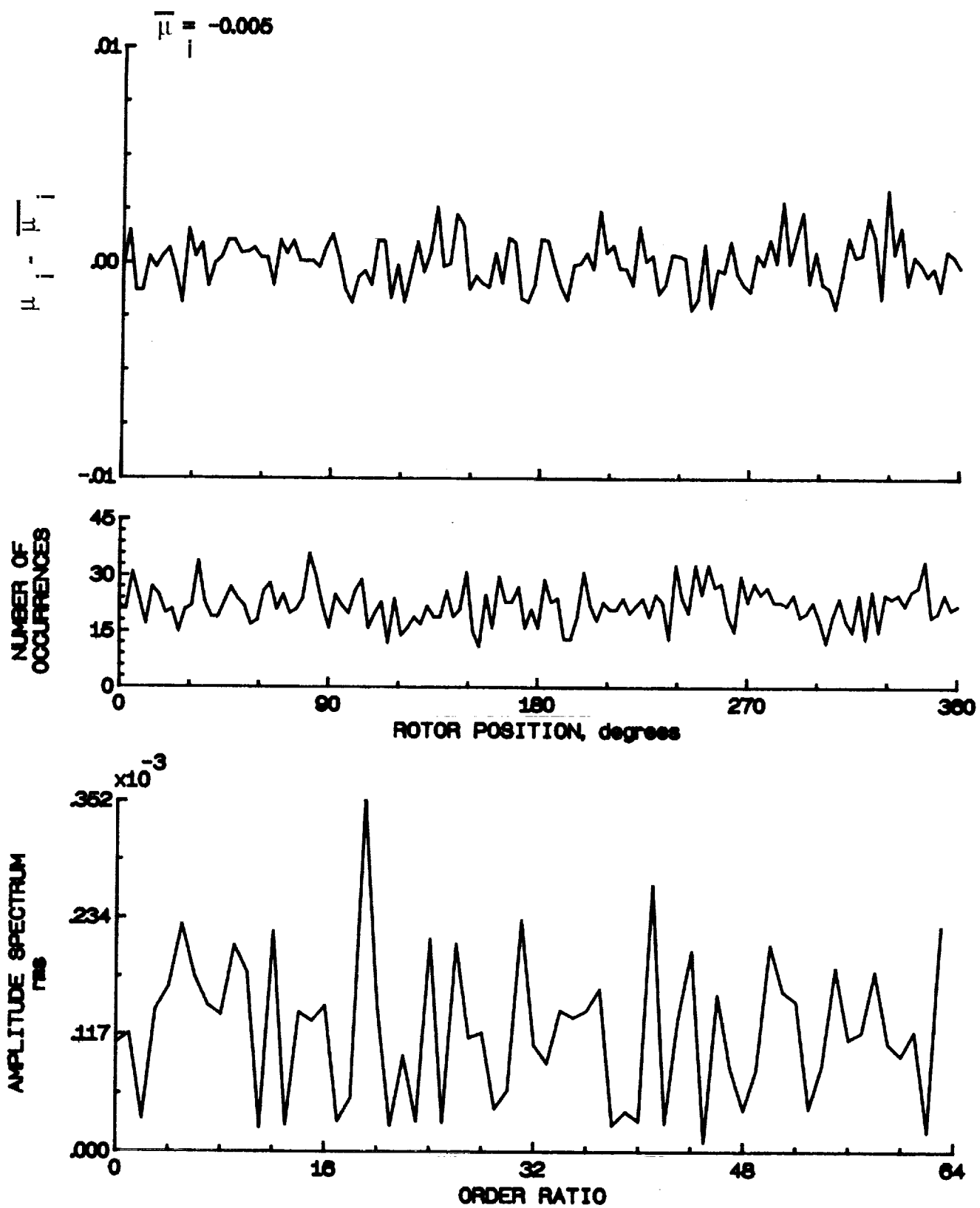


Figure 81.- Induced inflow velocity measured at 120 degrees and r/R of 0.90.

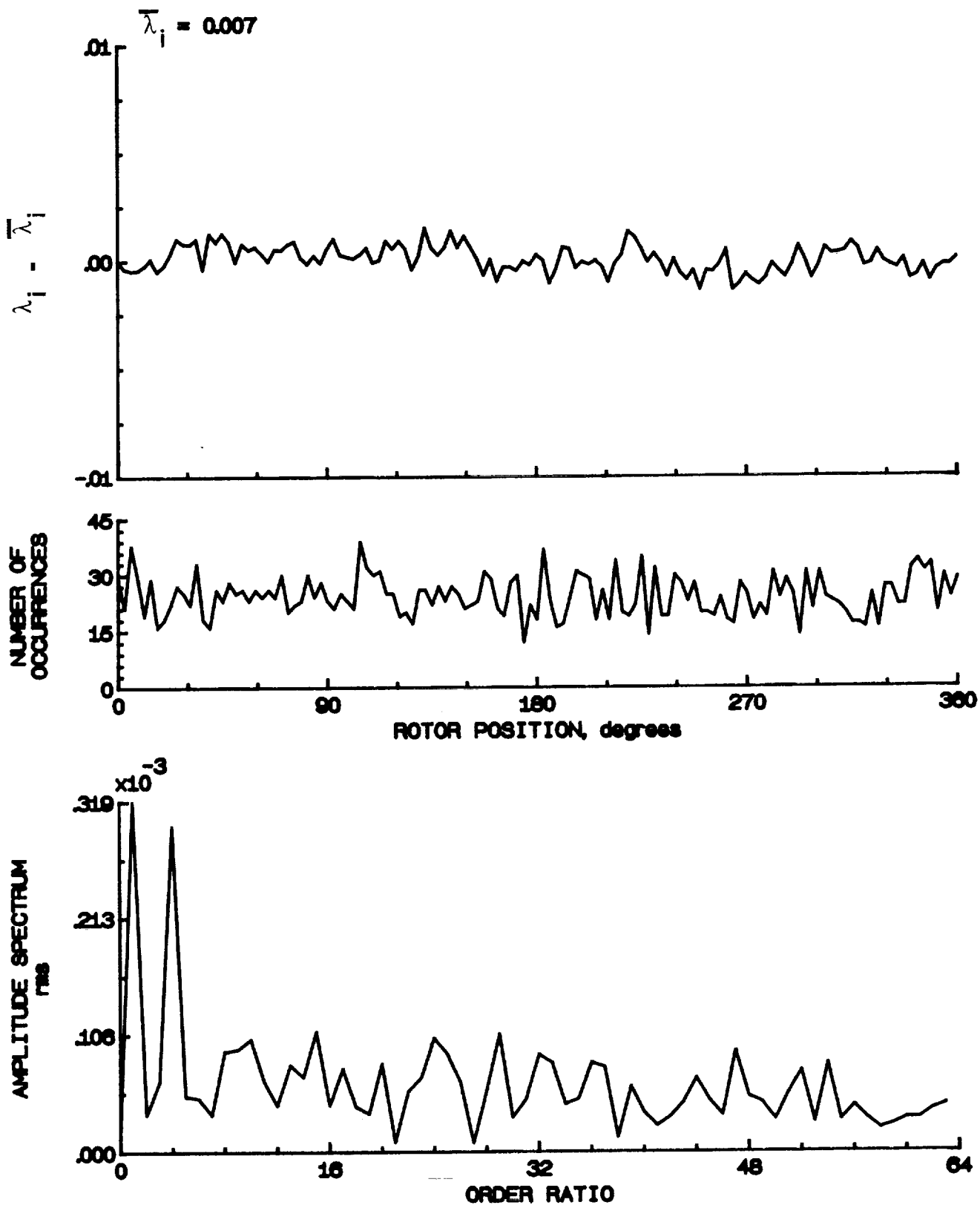


Figure 81.- Concluded.

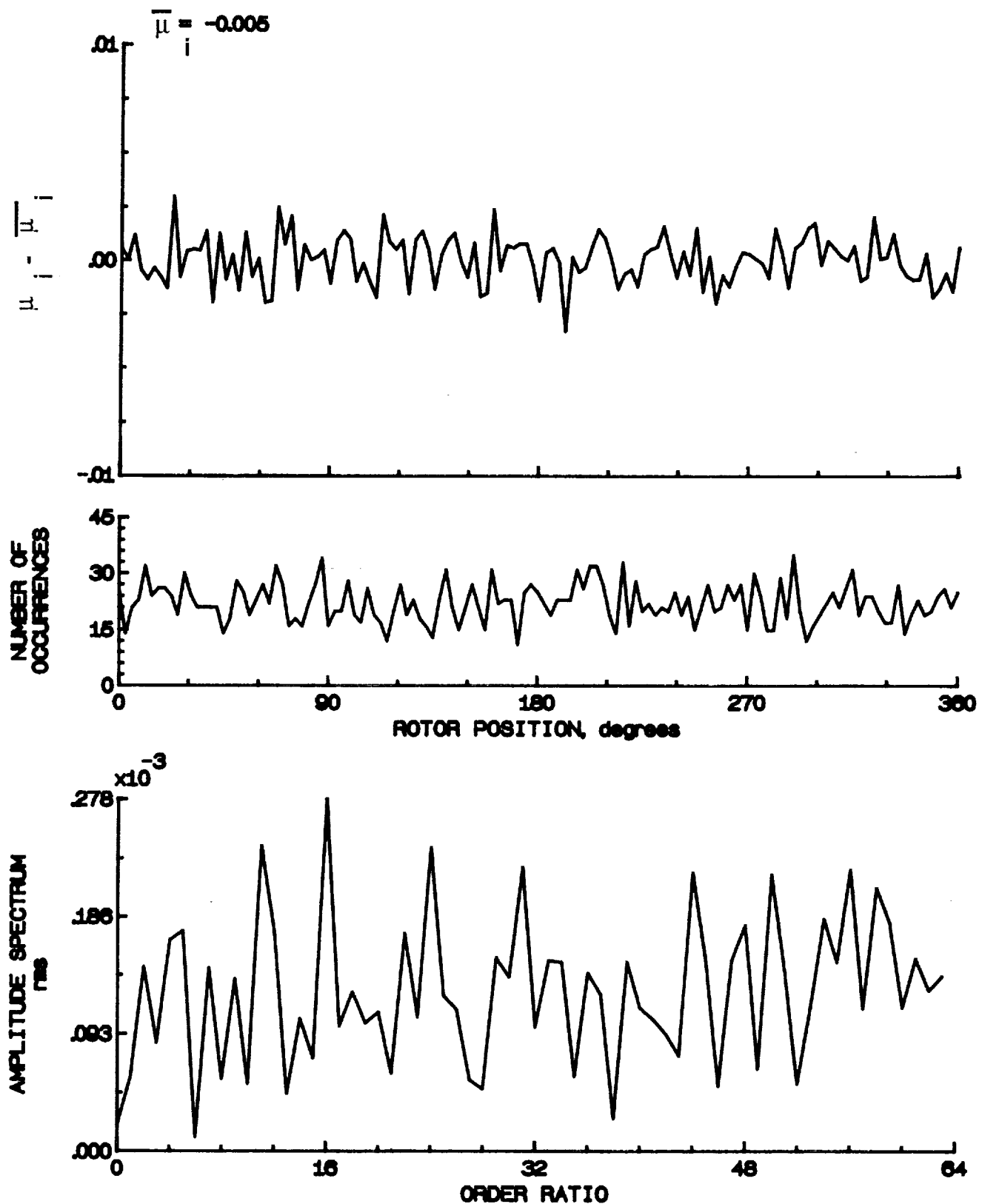


Figure 82.- Induced inflow velocity measured at 120 degrees and r/R of 0.94.

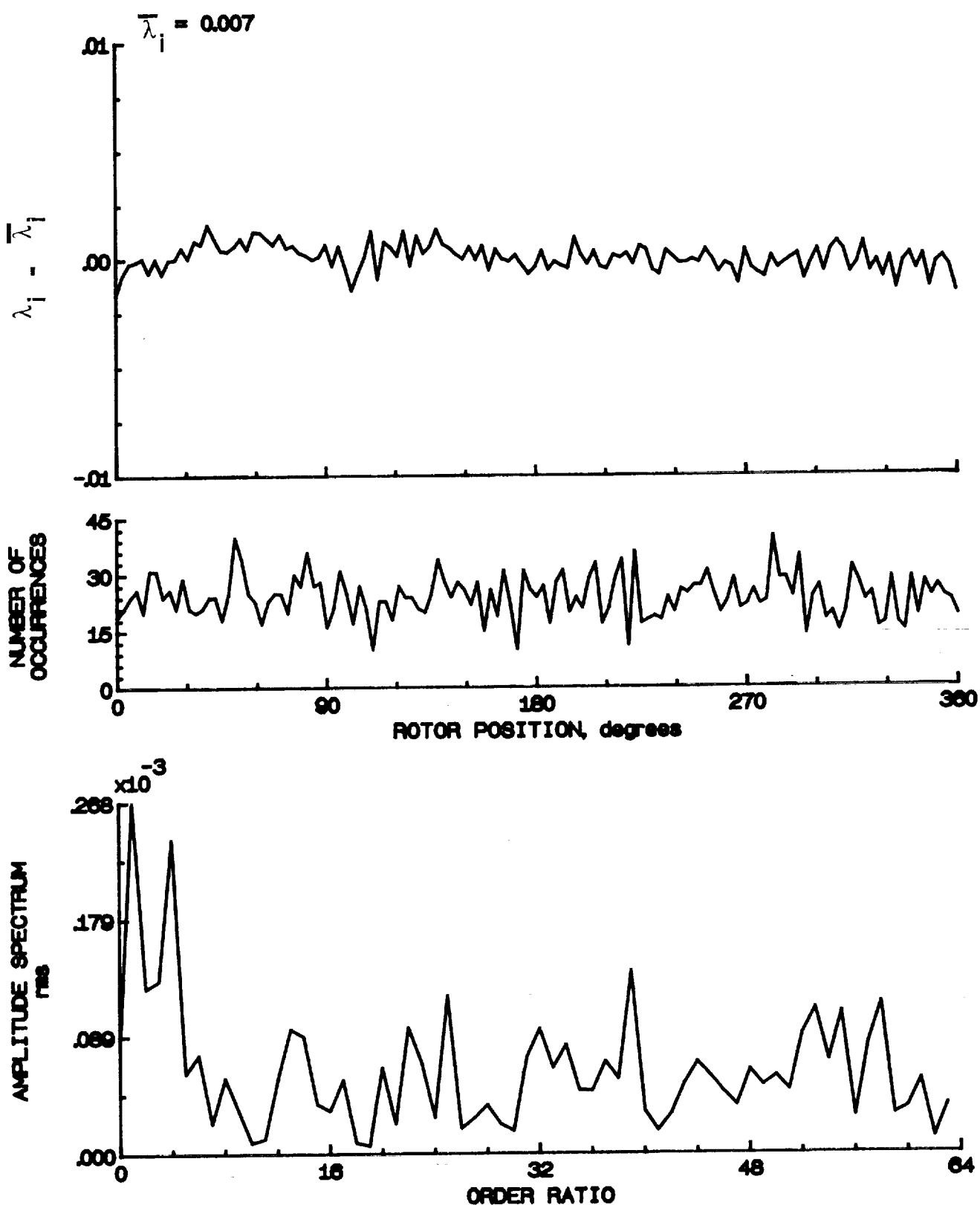


Figure 82.- Concluded.

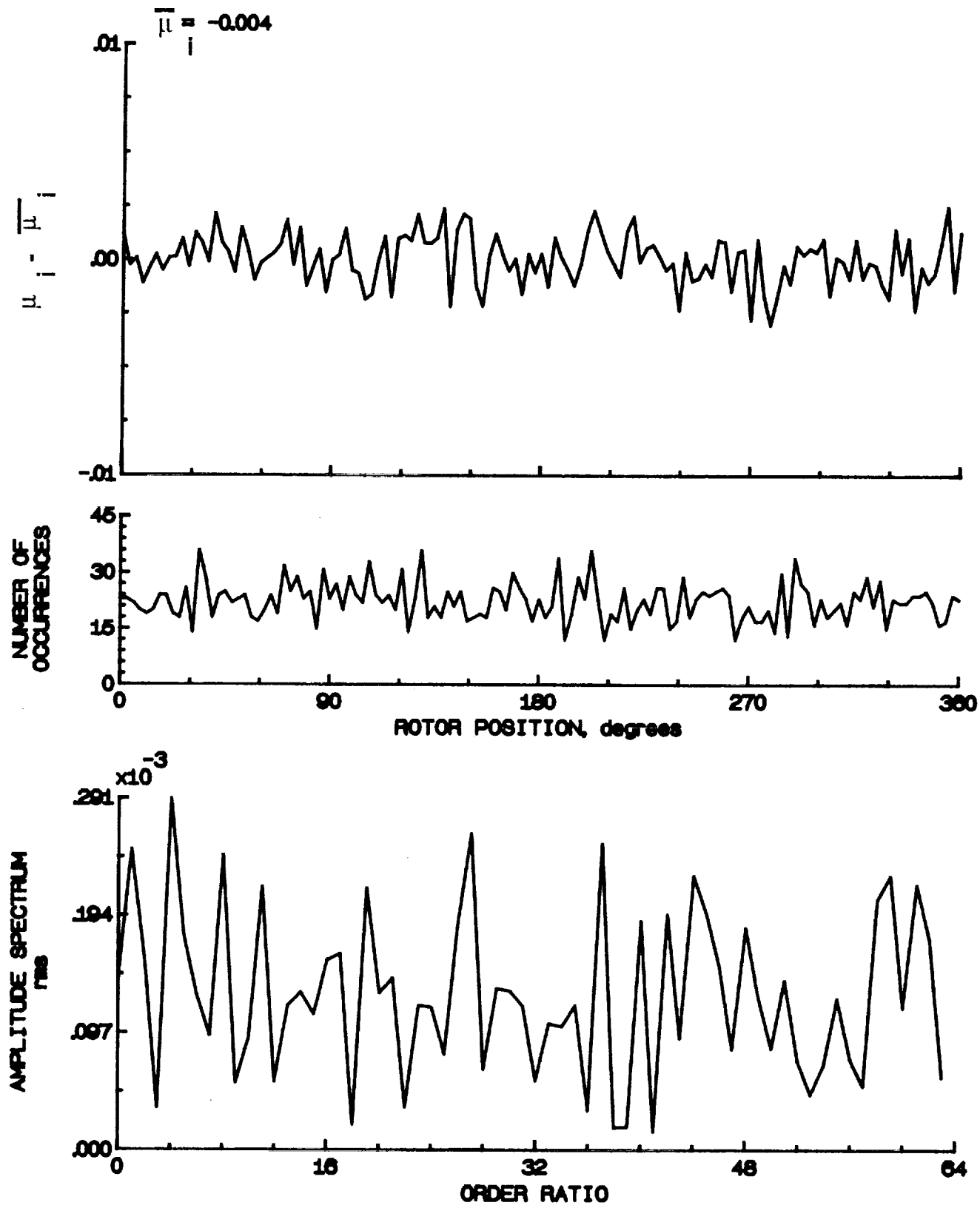


Figure 83.- Induced inflow velocity measured at 120 degrees and r/R of 0.98.

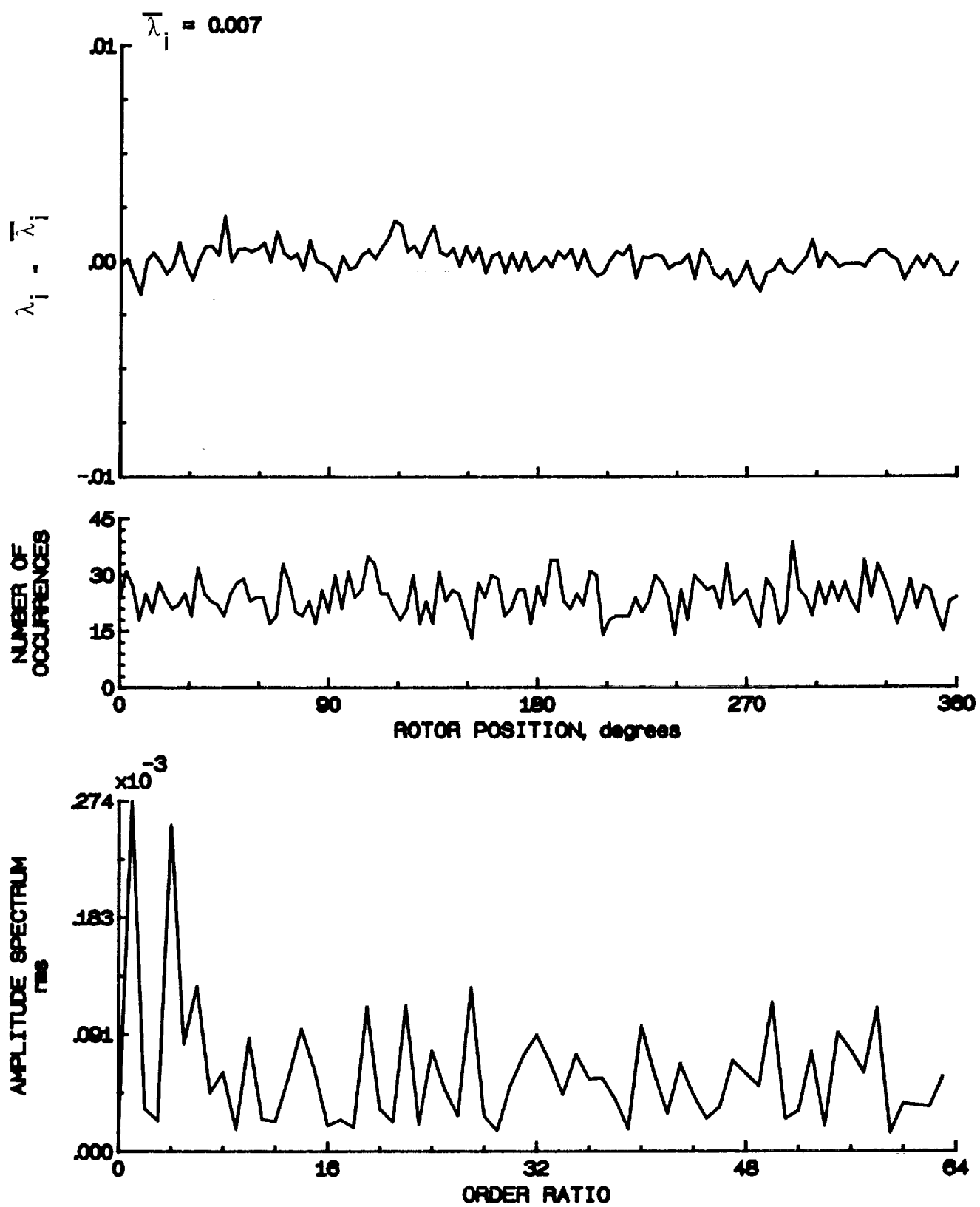


Figure 83.- Concluded.

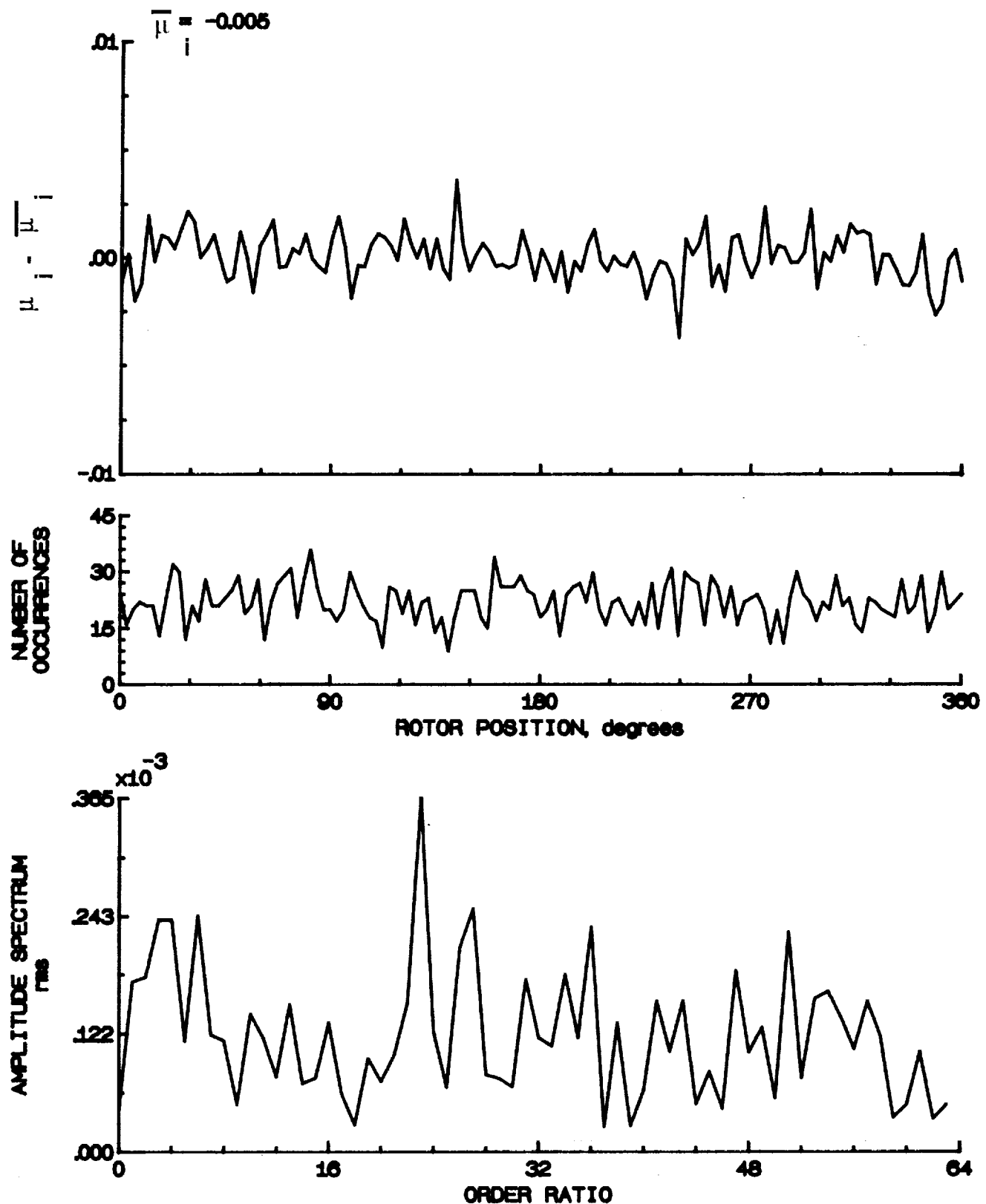


Figure 84.- Induced inflow velocity measured at 120 degrees and r/R of 1.02.

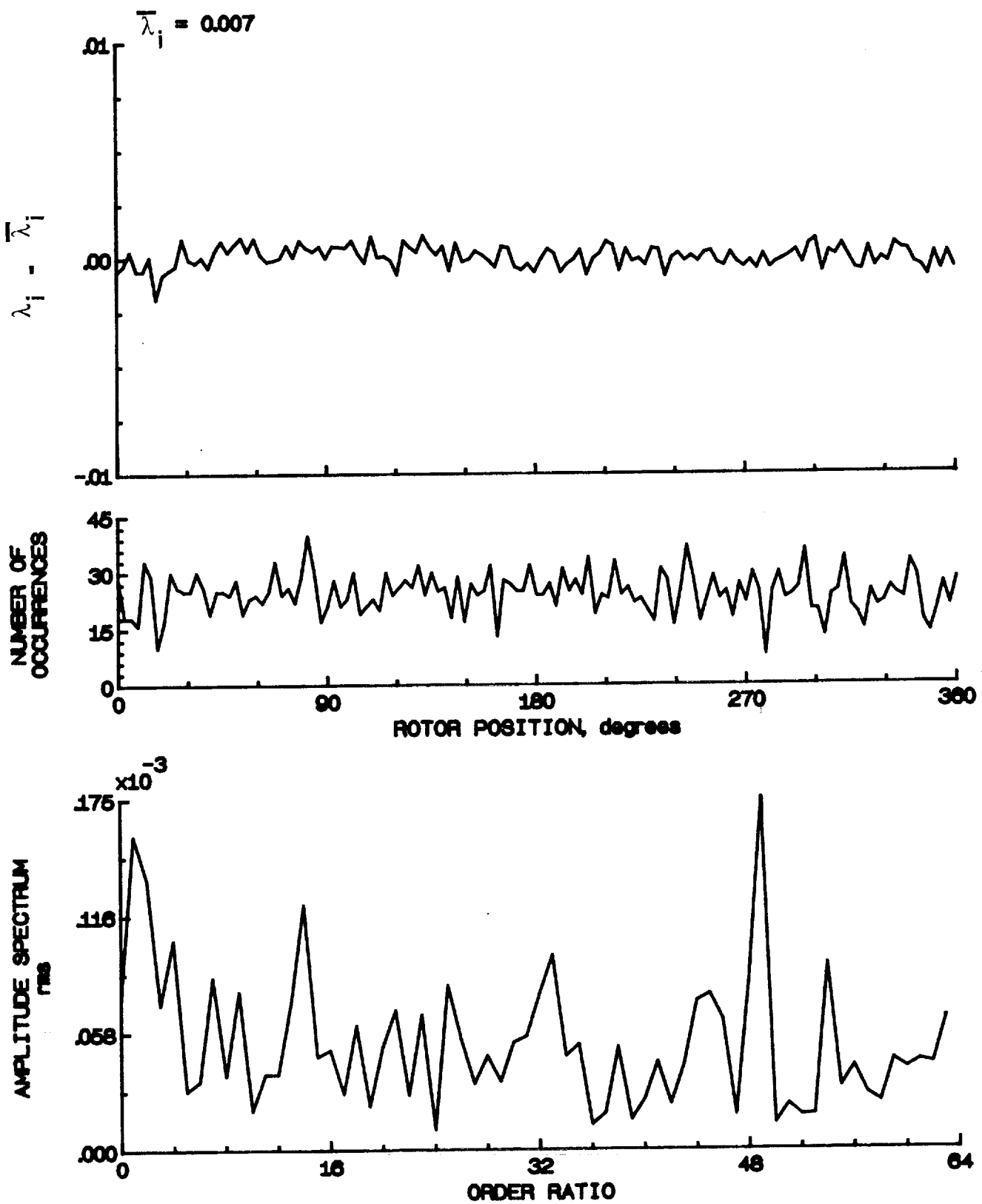


Figure 84.- Concluded.

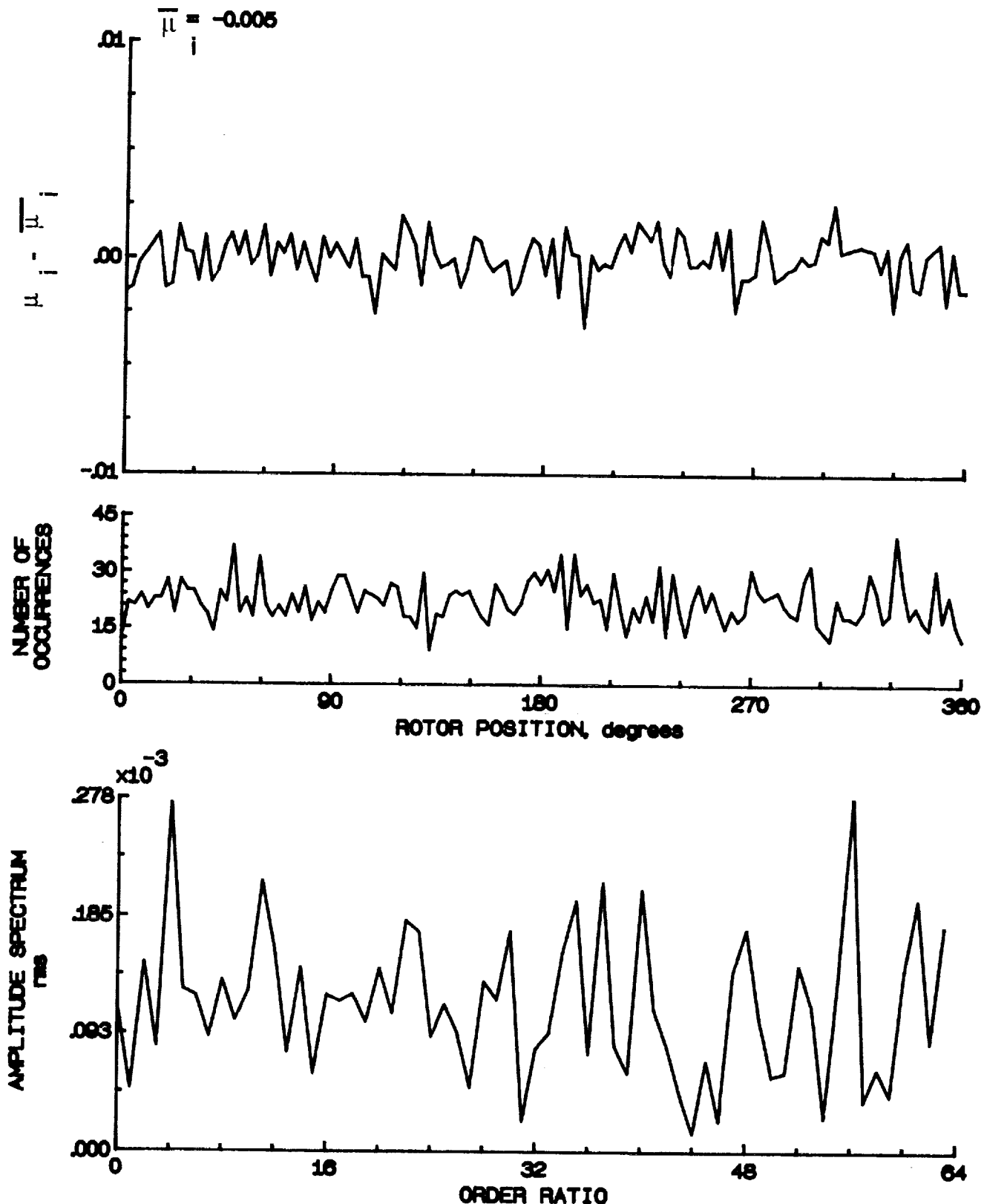


Figure 85.- Induced inflow velocity measured at 120 degrees and r/R of 1.04.

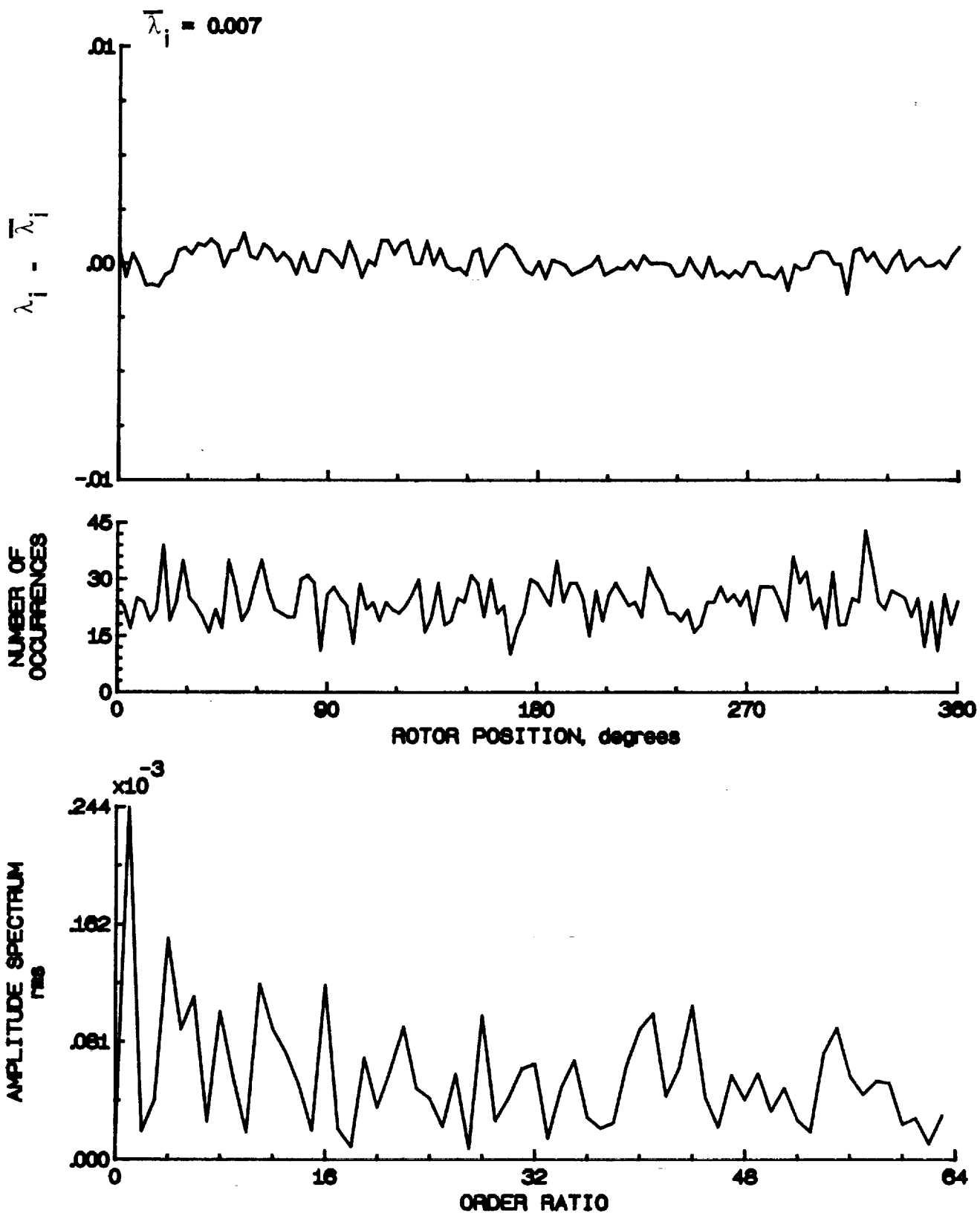


Figure 85.- Concluded.

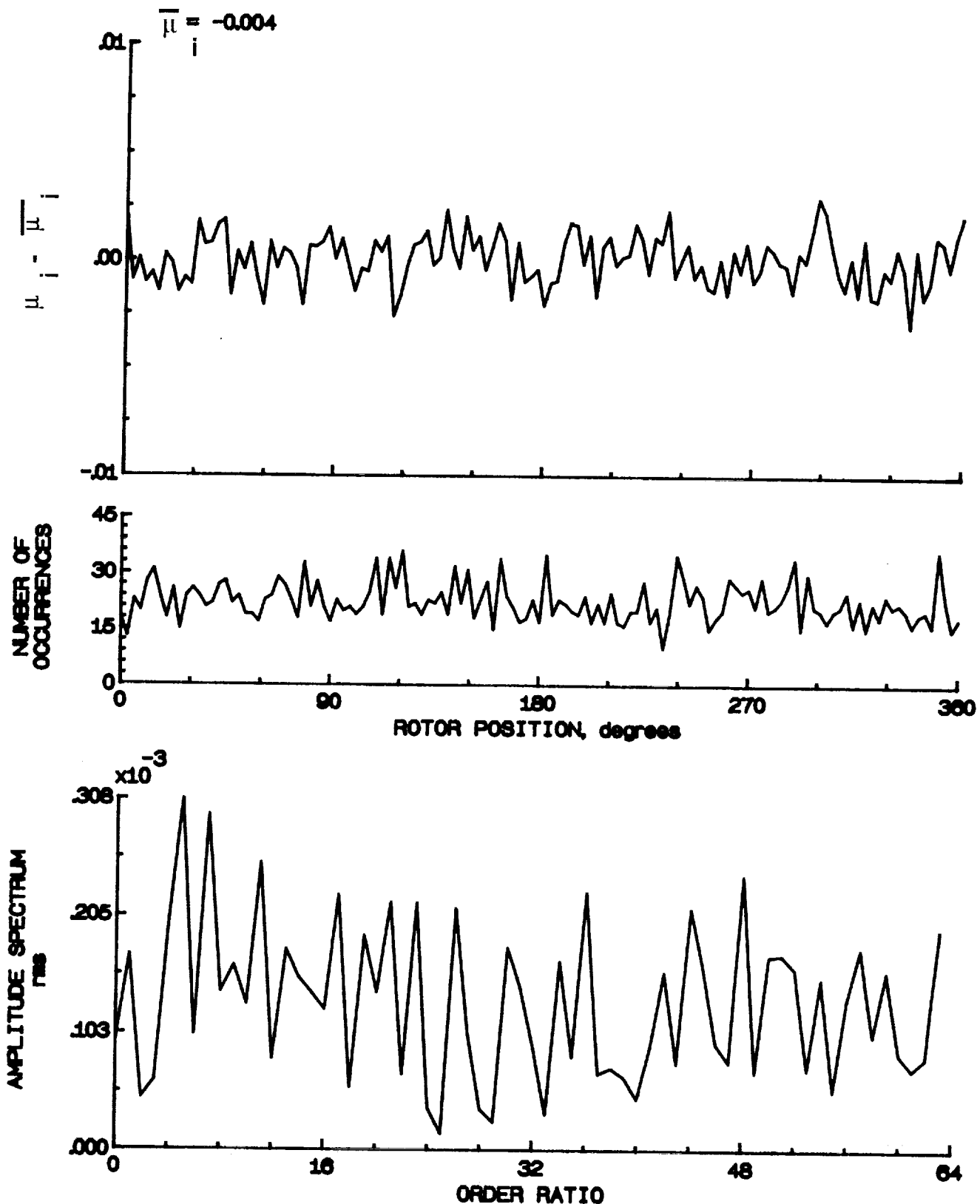


Figure 86.- Induced inflow velocity measured at 120 degrees and r/R of 1.10.

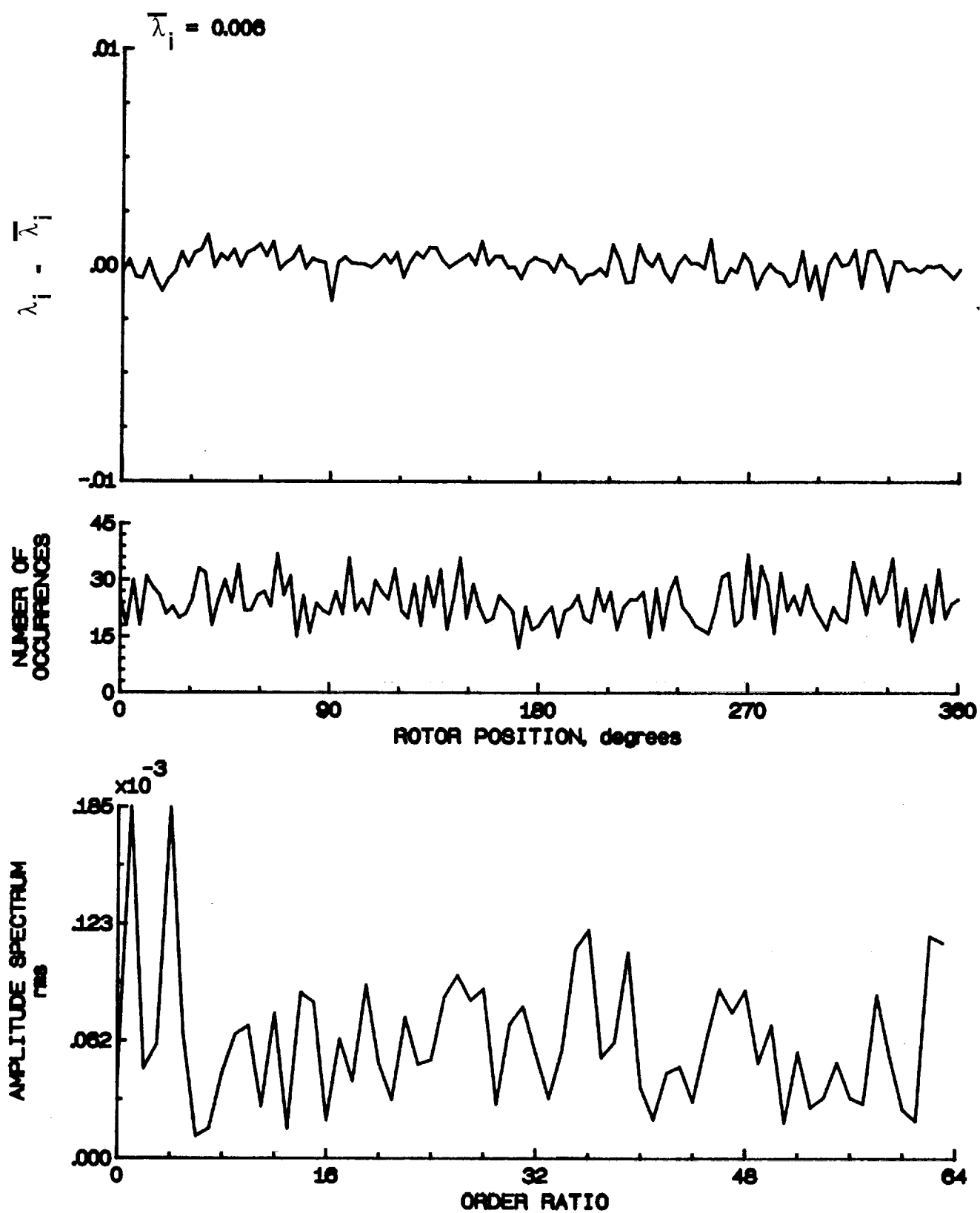


Figure 86.- Concluded.

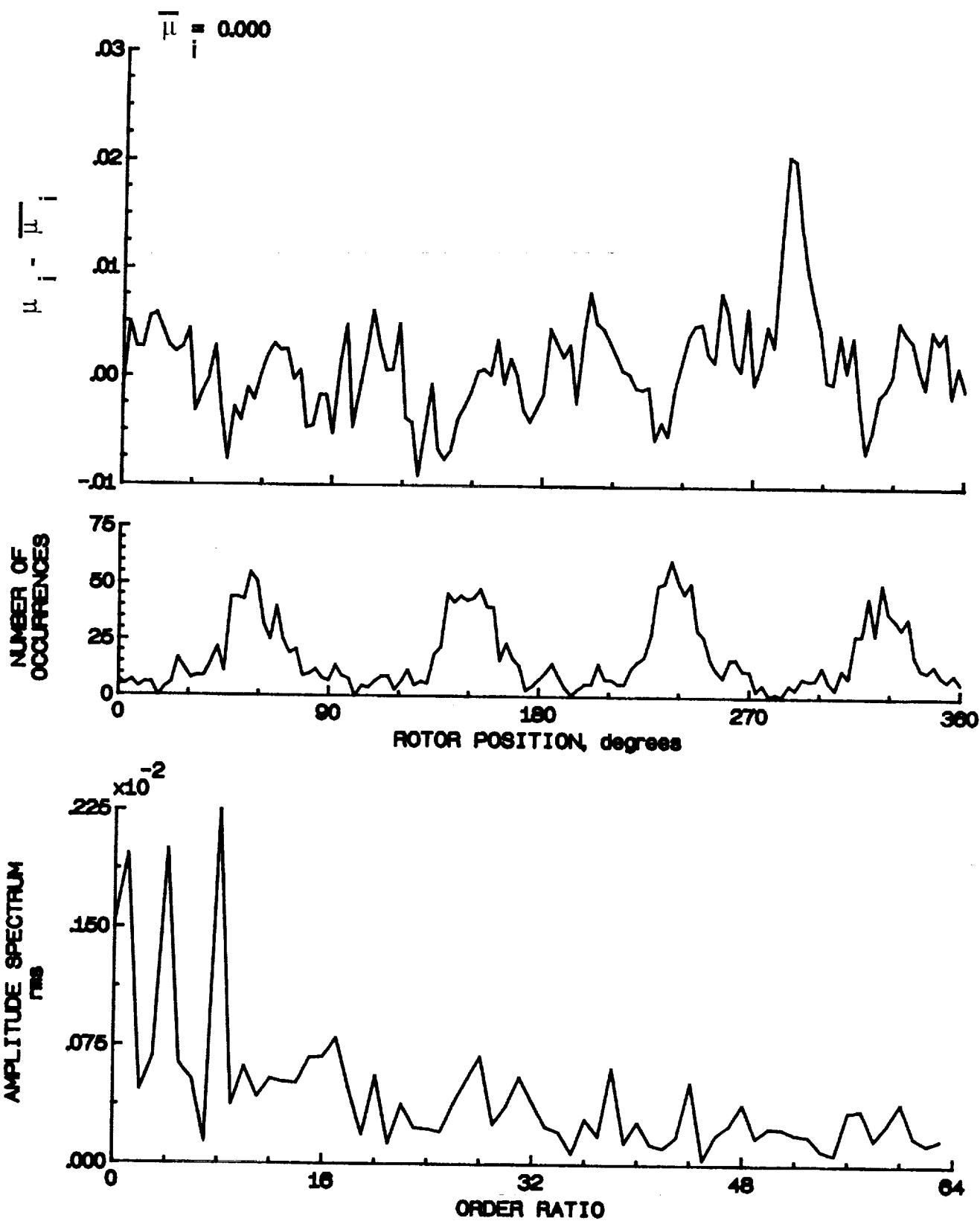


Figure 87.- Induced inflow velocity measured at 150 degrees and r/R of 0.20.

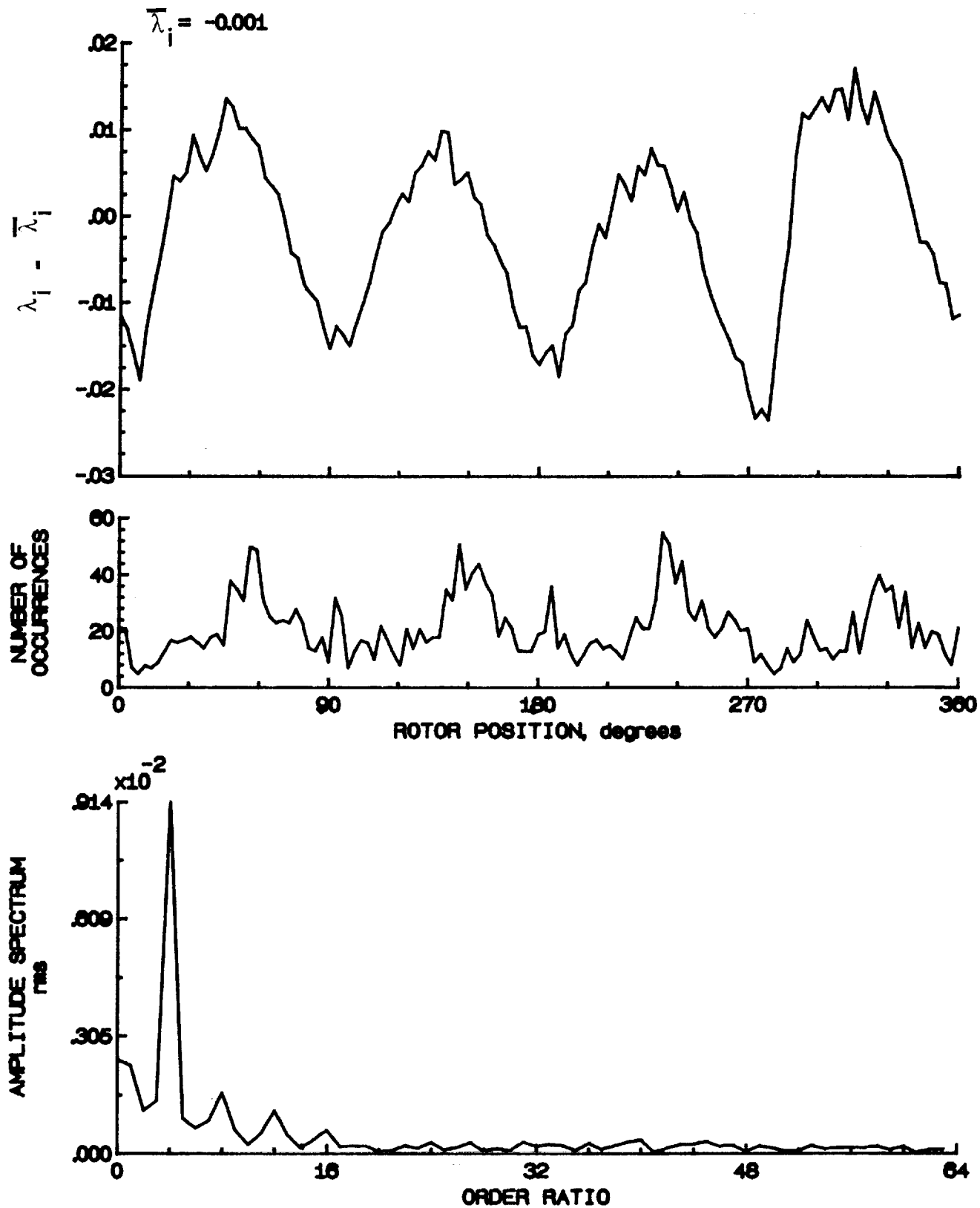


Figure 87.- Concluded.

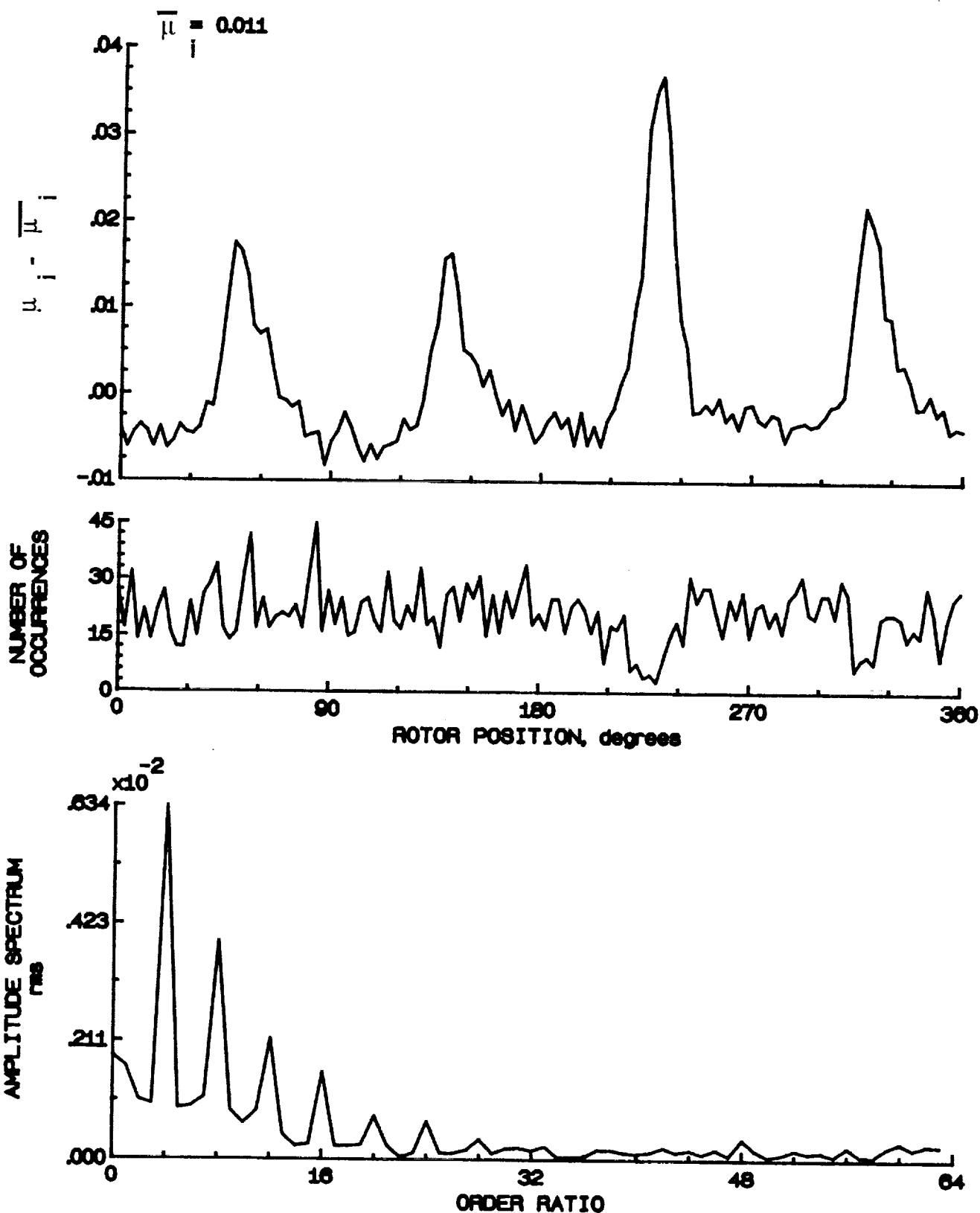


Figure 88.- Induced inflow velocity measured at 150 degrees and r/R of 0.40.

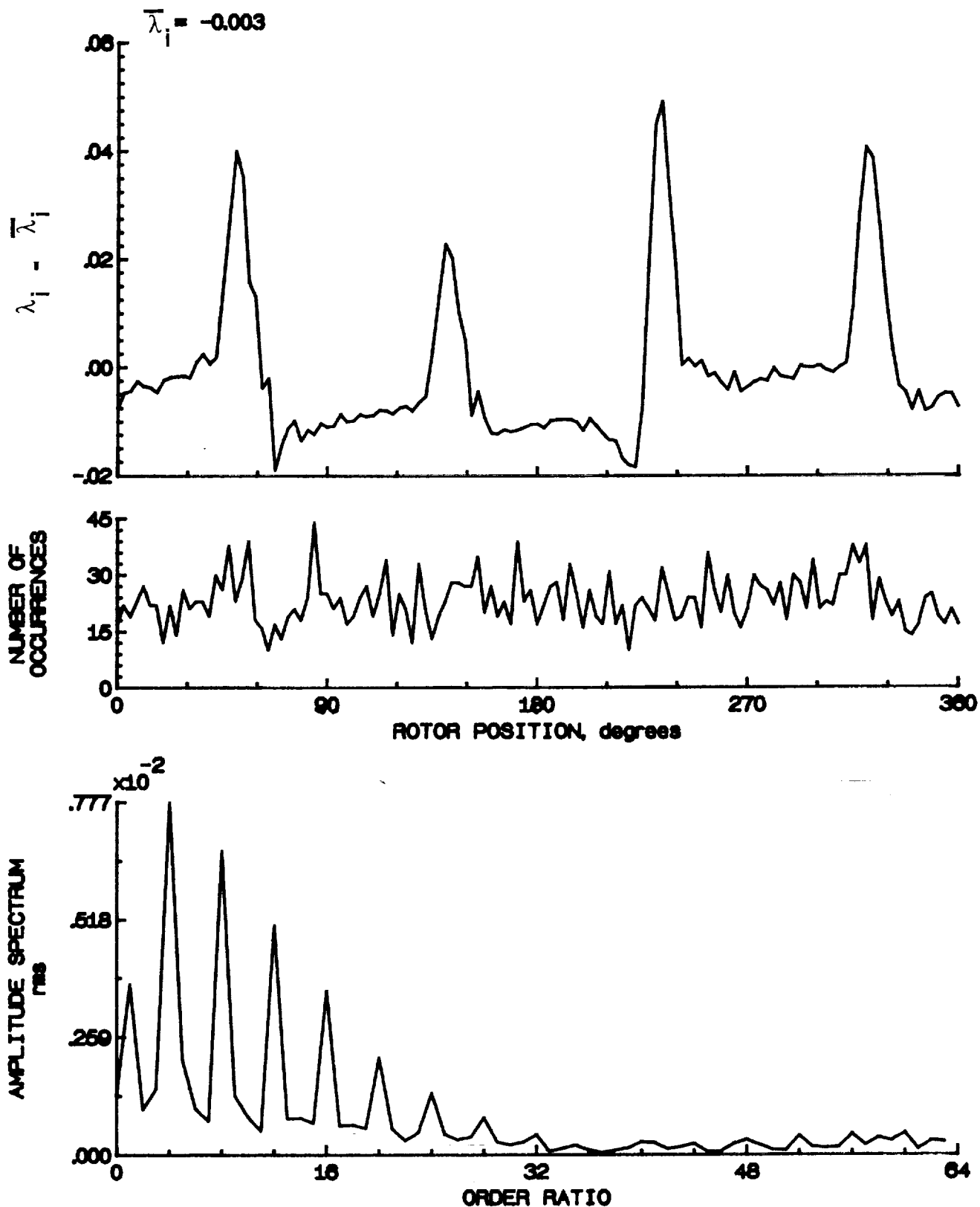


Figure 88.- Concluded.

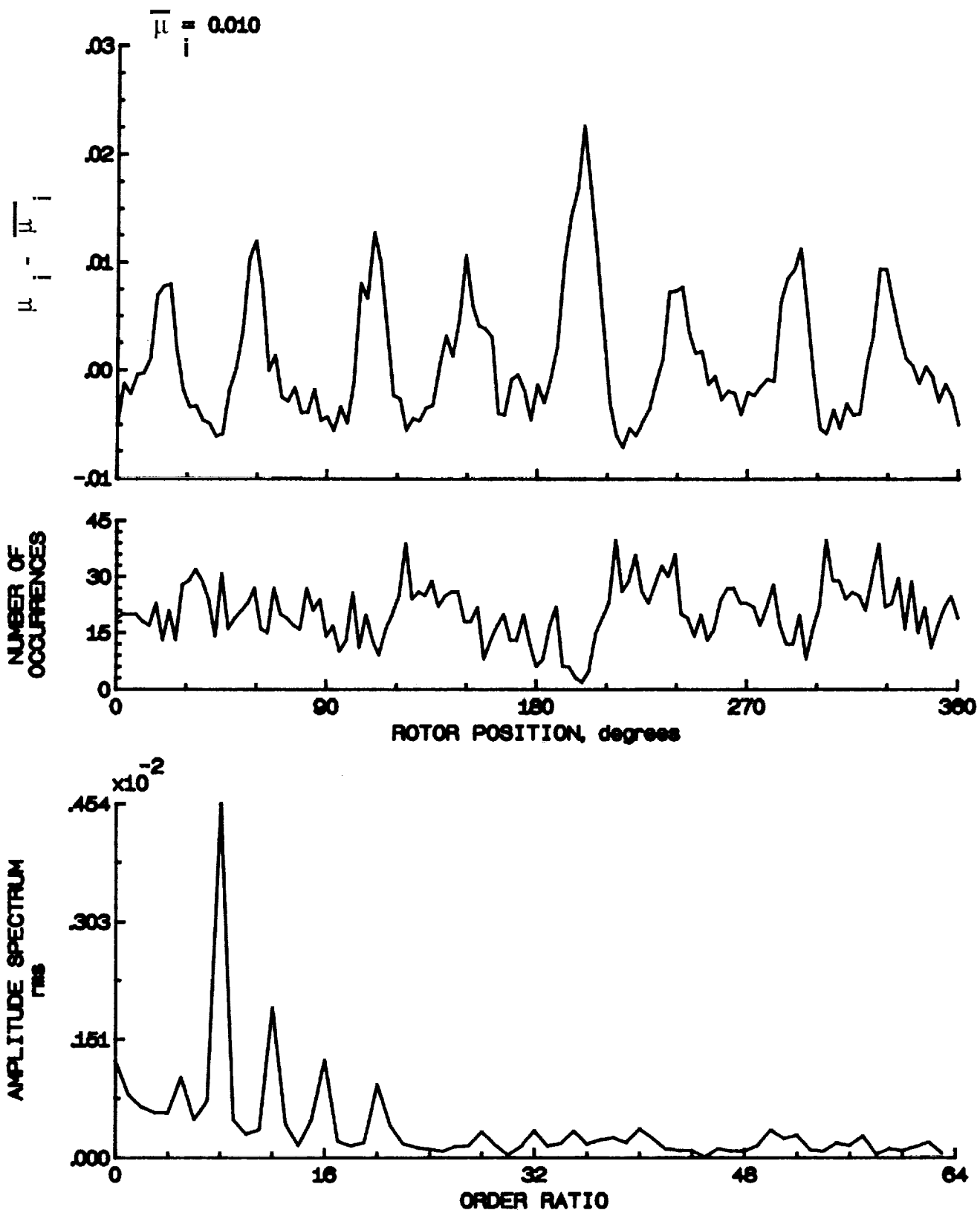


Figure 80.- Induced inflow velocity measured at 150 degrees and r/R of 0.50.

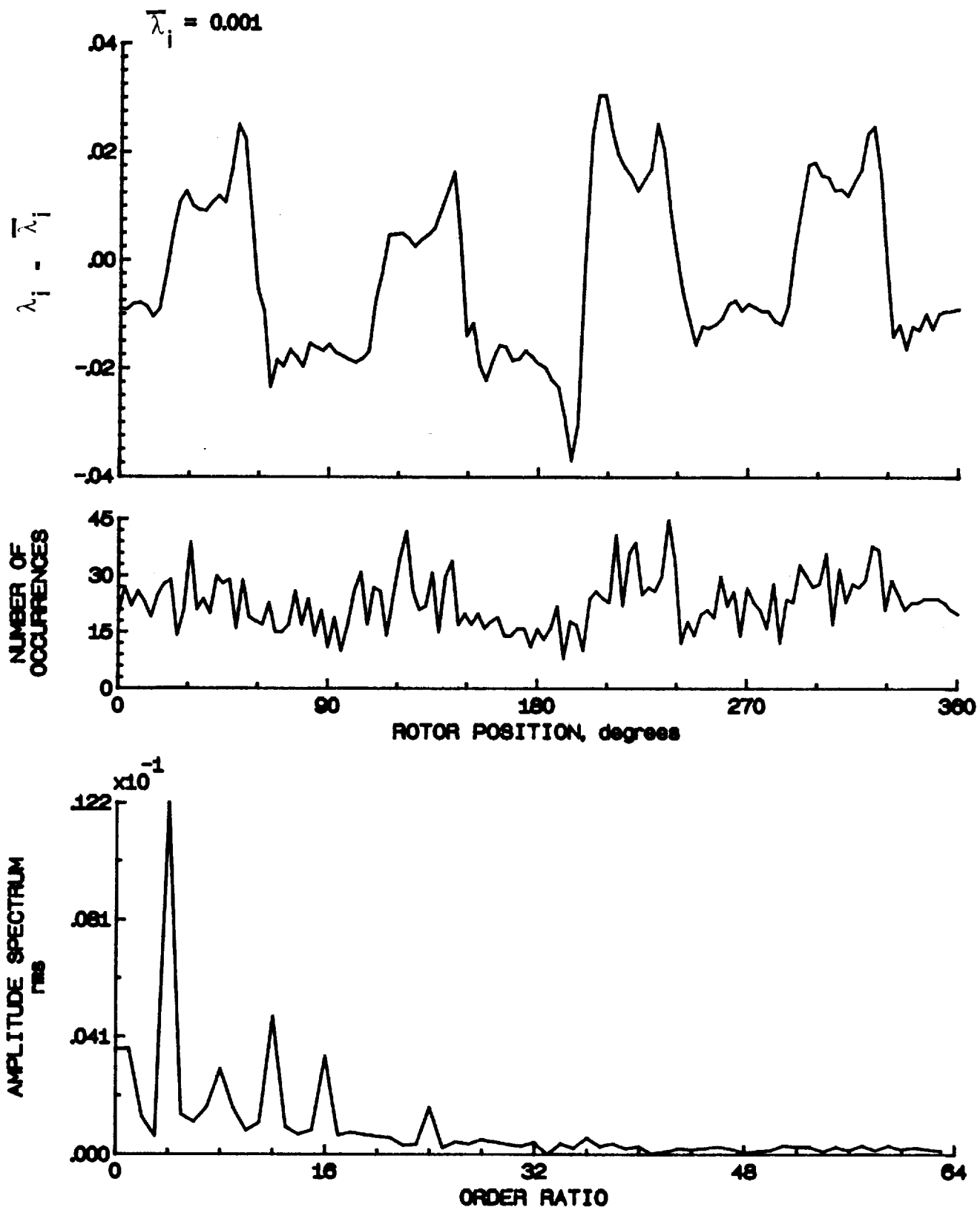


Figure 89.- Concluded.

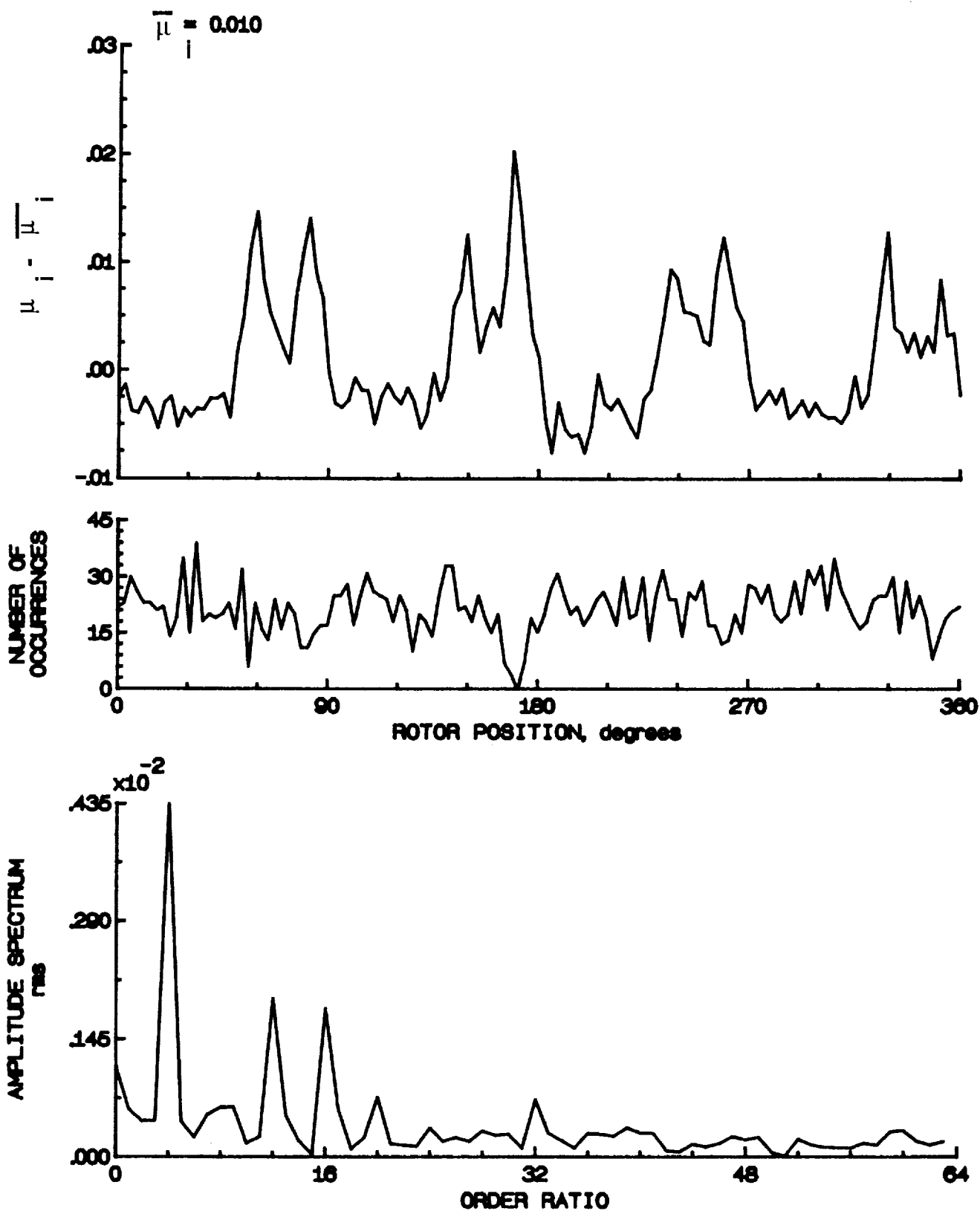


Figure 90.- Induced inflow velocity measured at 150 degrees and r/R of 0.60.

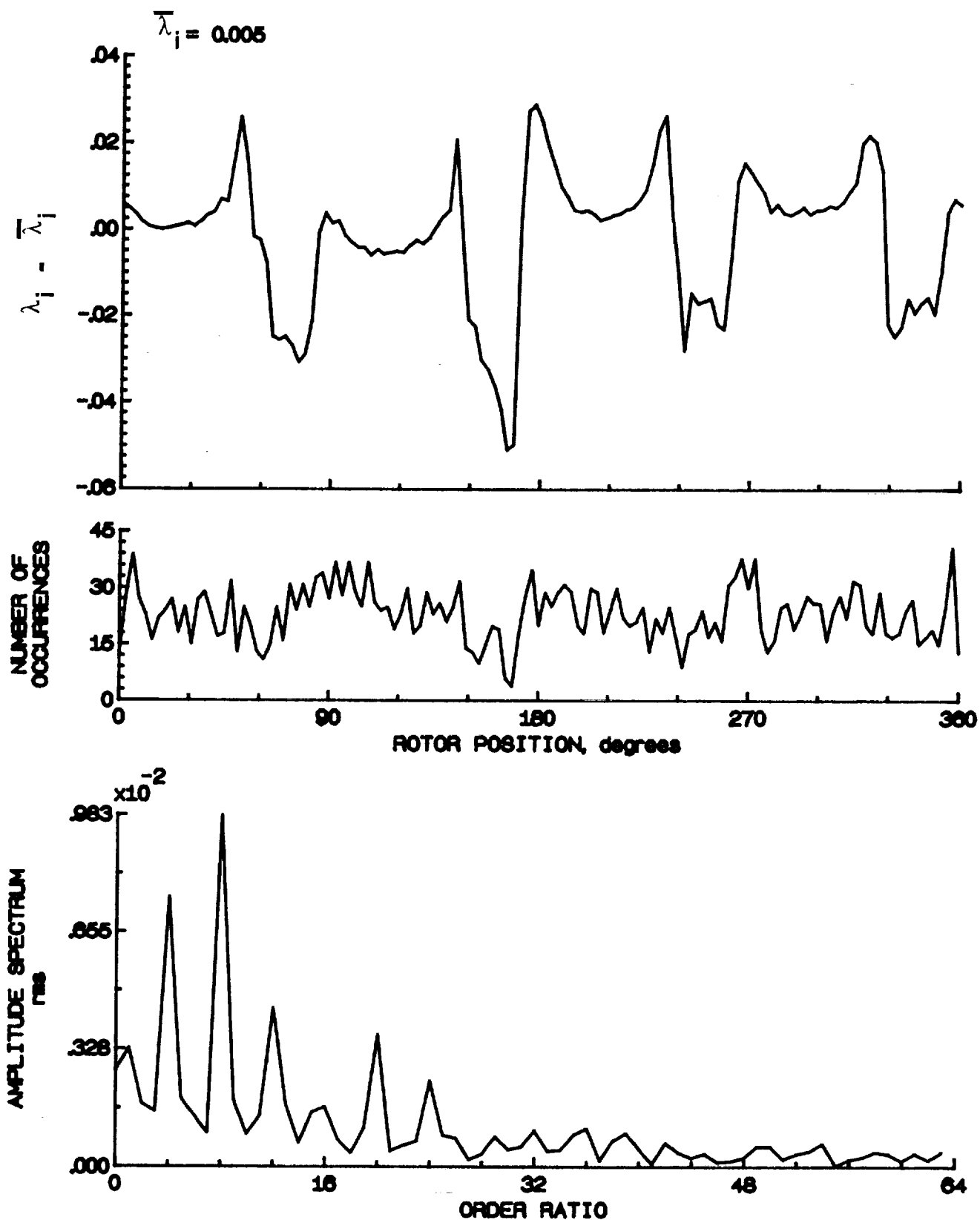


Figure 90.- Concluded.

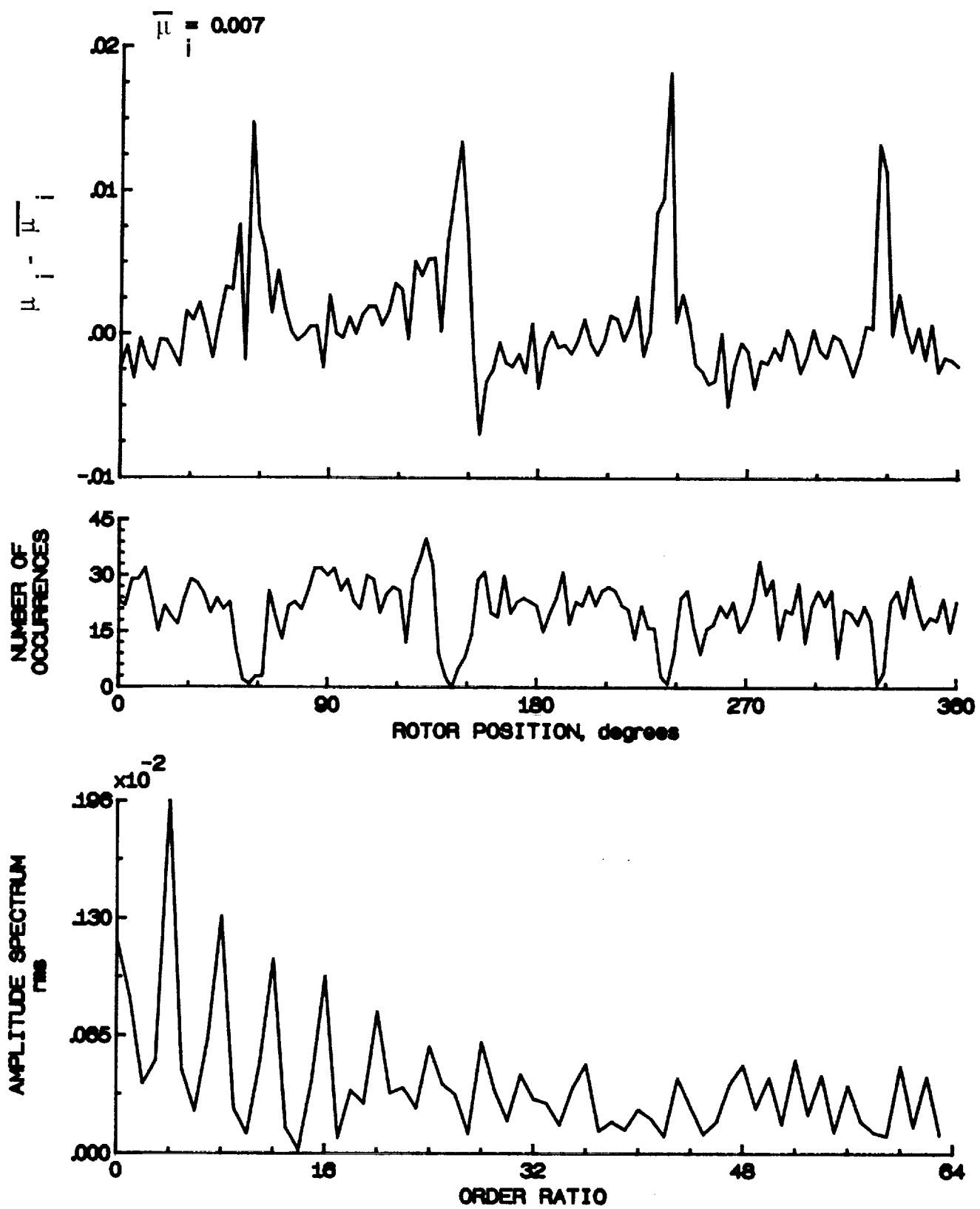


Figure 91.- Induced inflow velocity measured at 150 degrees and r/R of 0.70.

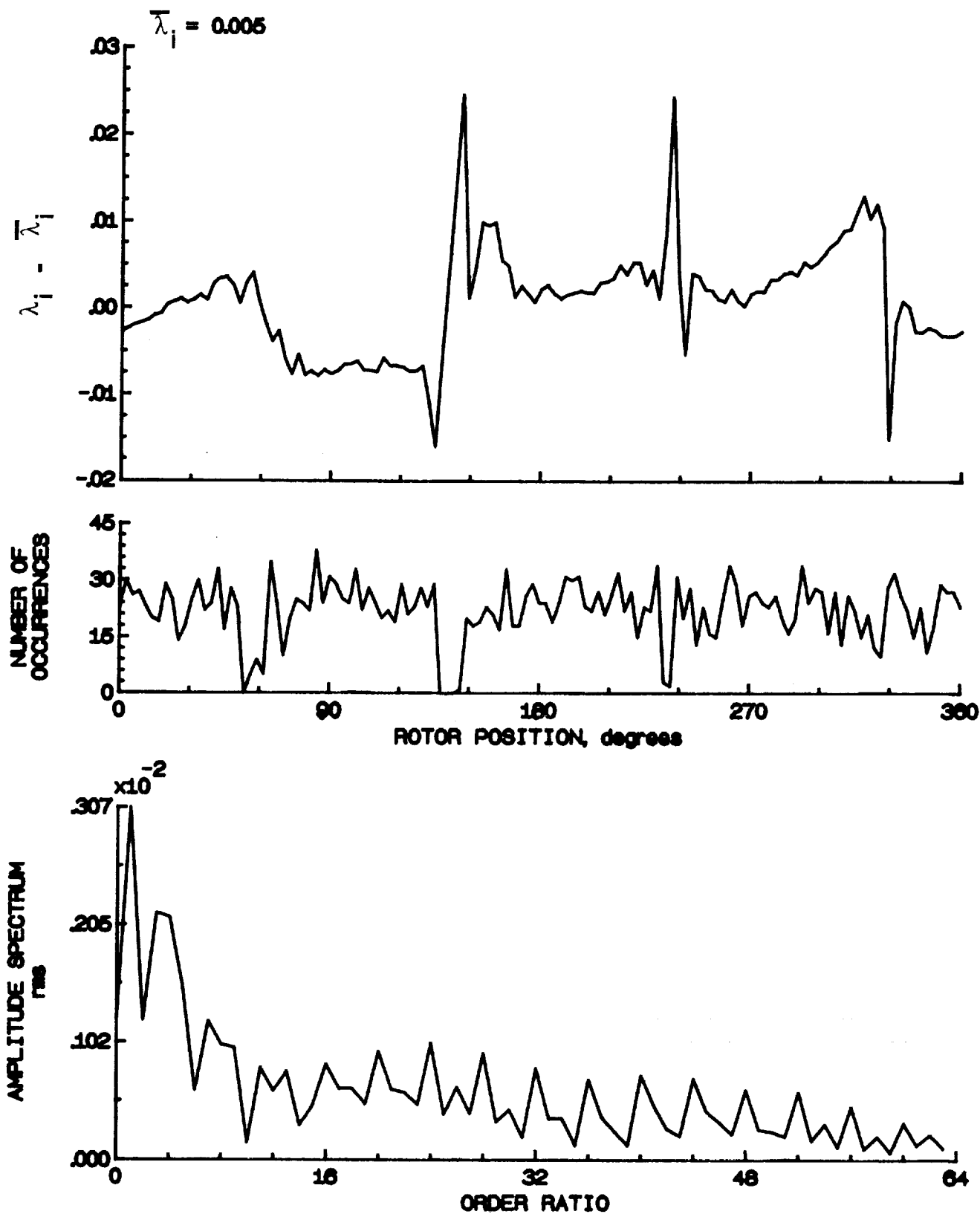


Figure 91.- Concluded.

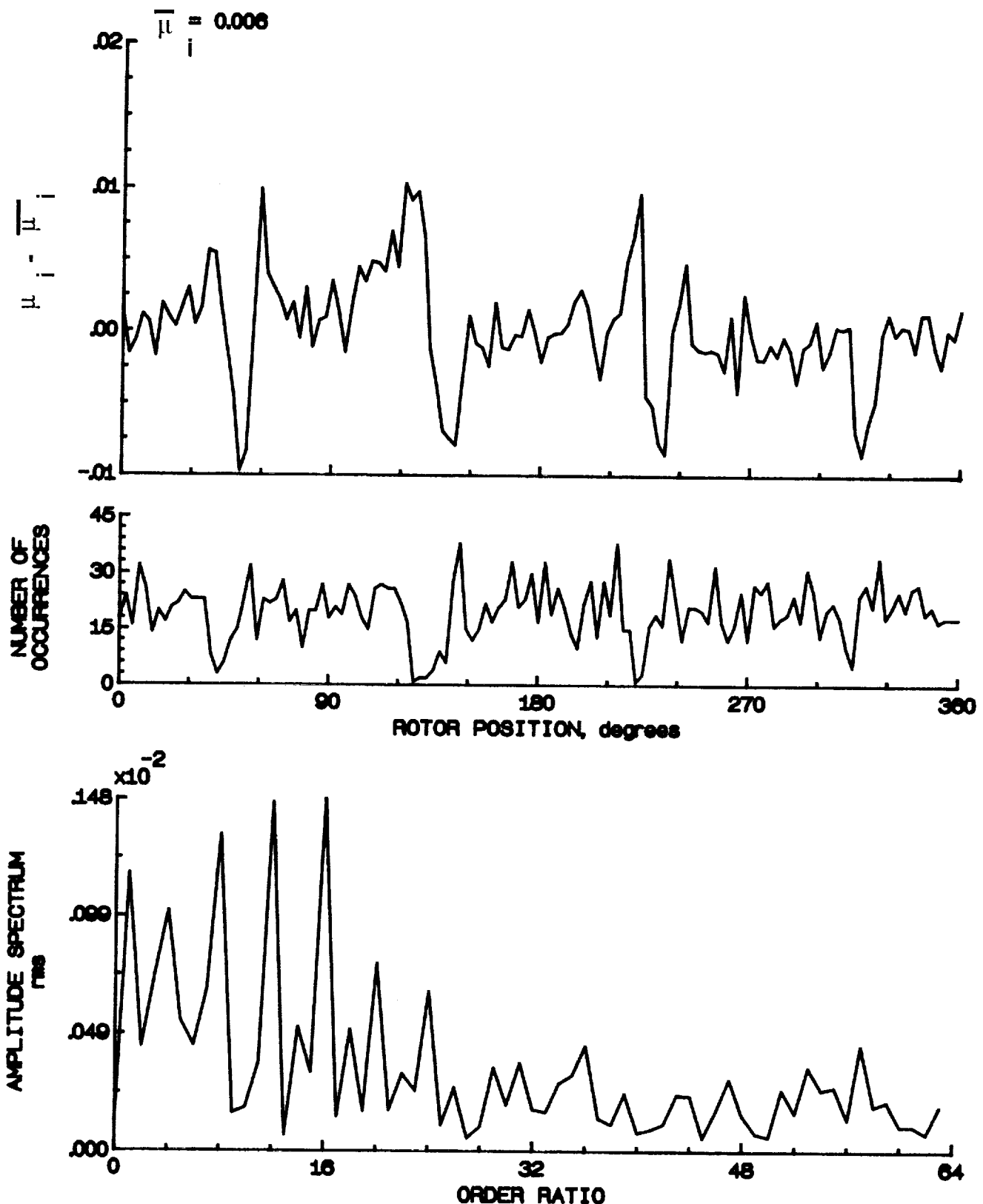


Figure 92.- Induced inflow velocity measured at 150 degrees and r/R of 0.74.

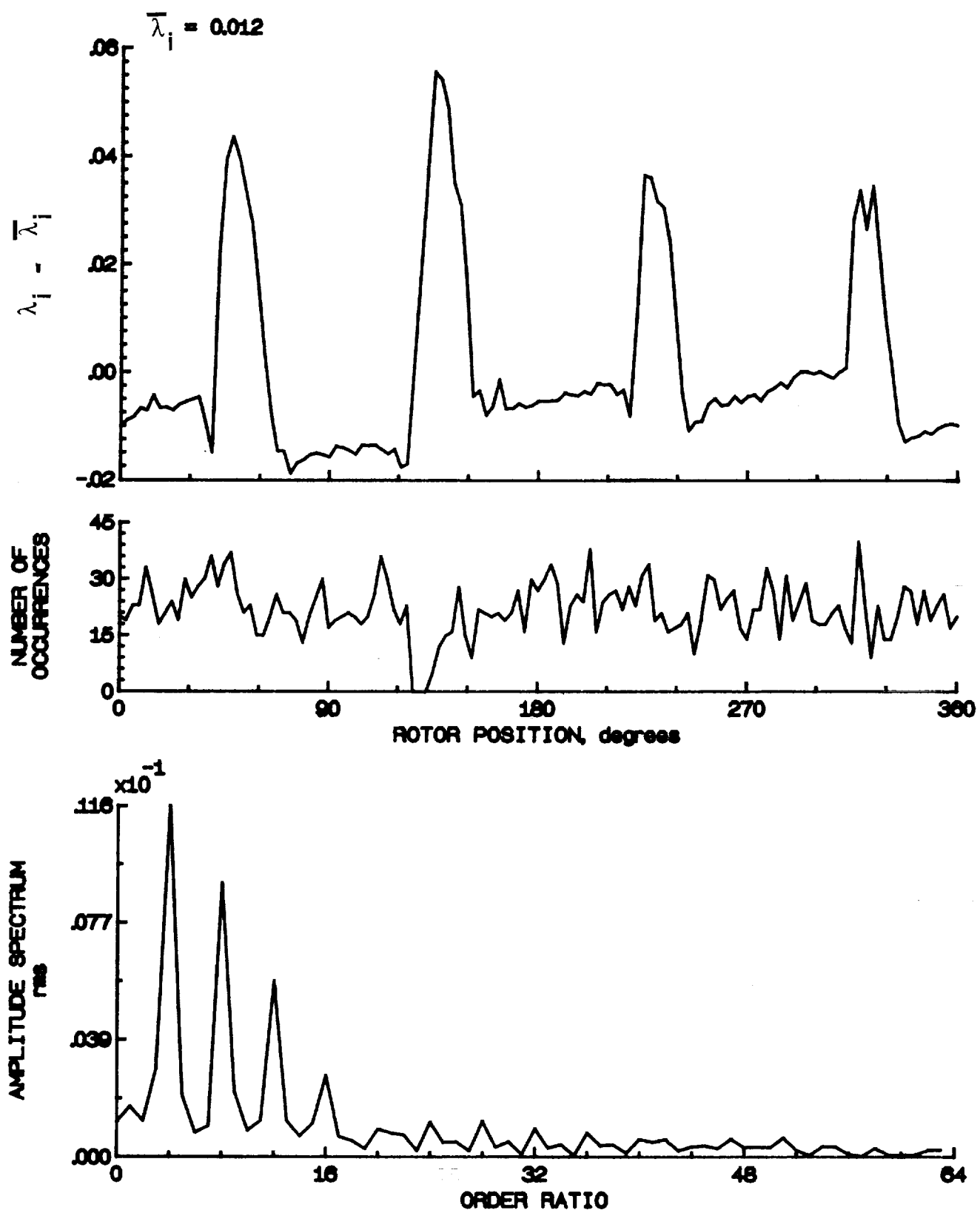


Figure 92.- Concluded.

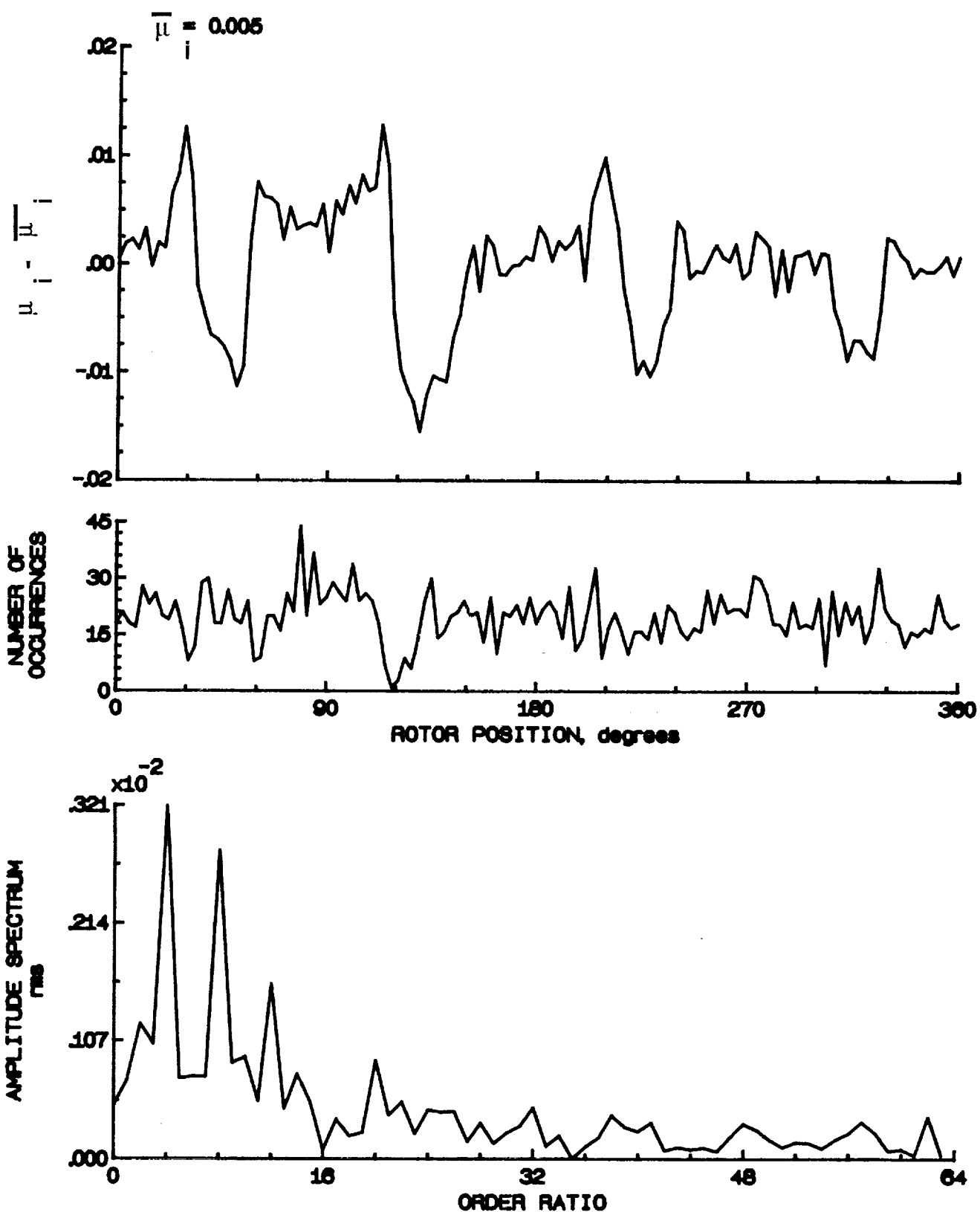


Figure 93.- Induced inflow velocity measured at 150 degrees and r/R of 0.78.

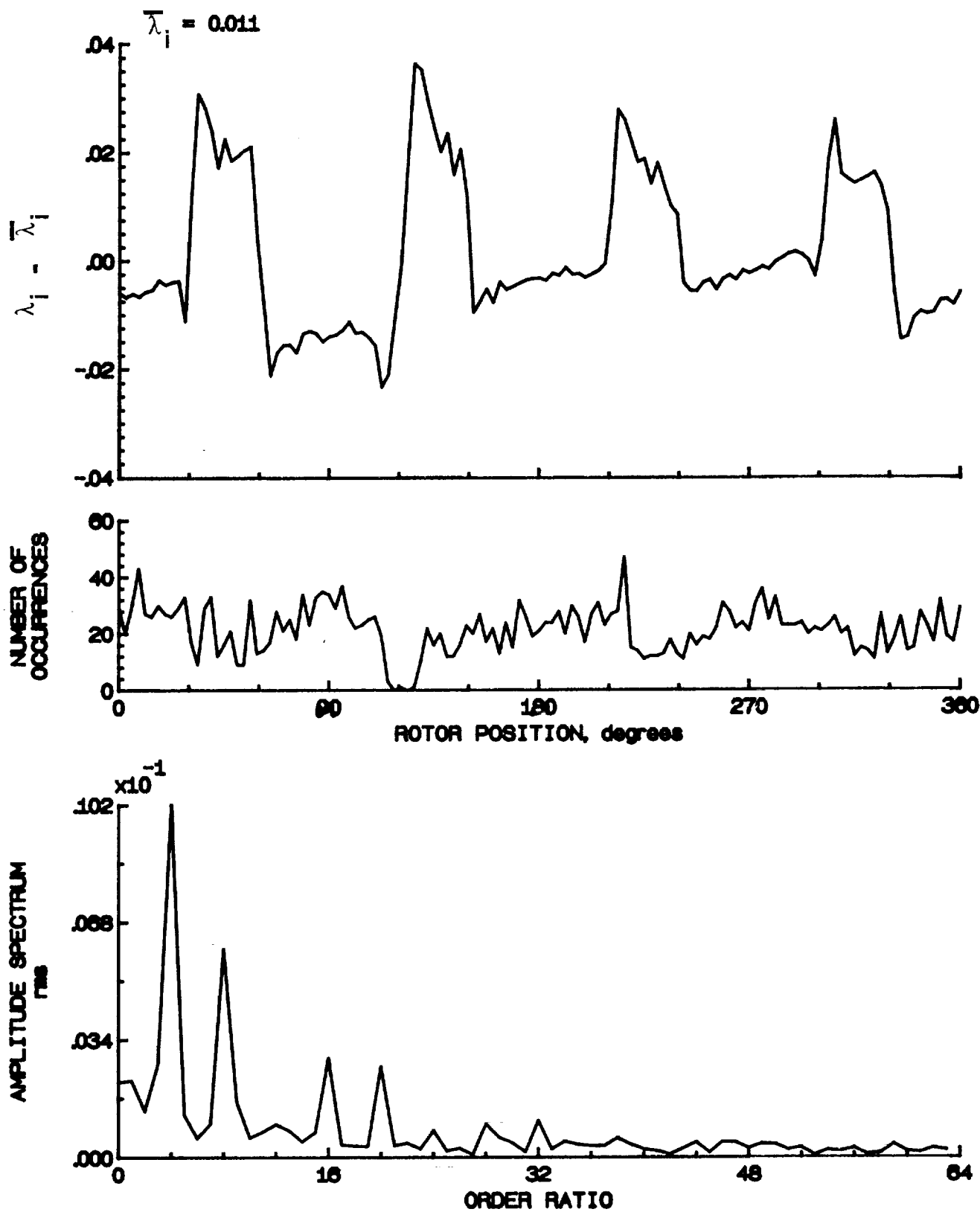


Figure 93.- Concluded.

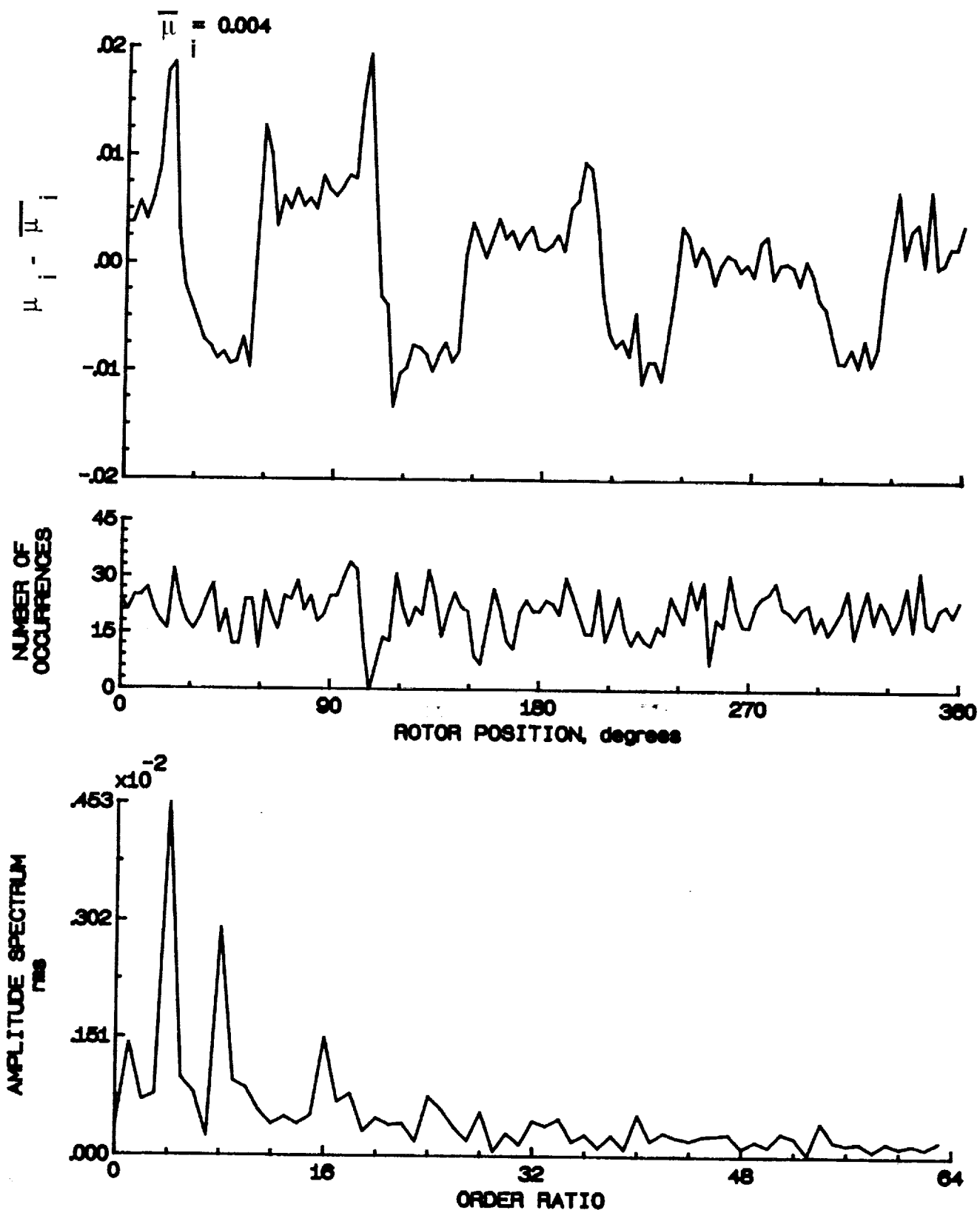


Figure 94.- Induced inflow velocity measured at 150 degrees and r/R of 0.82.

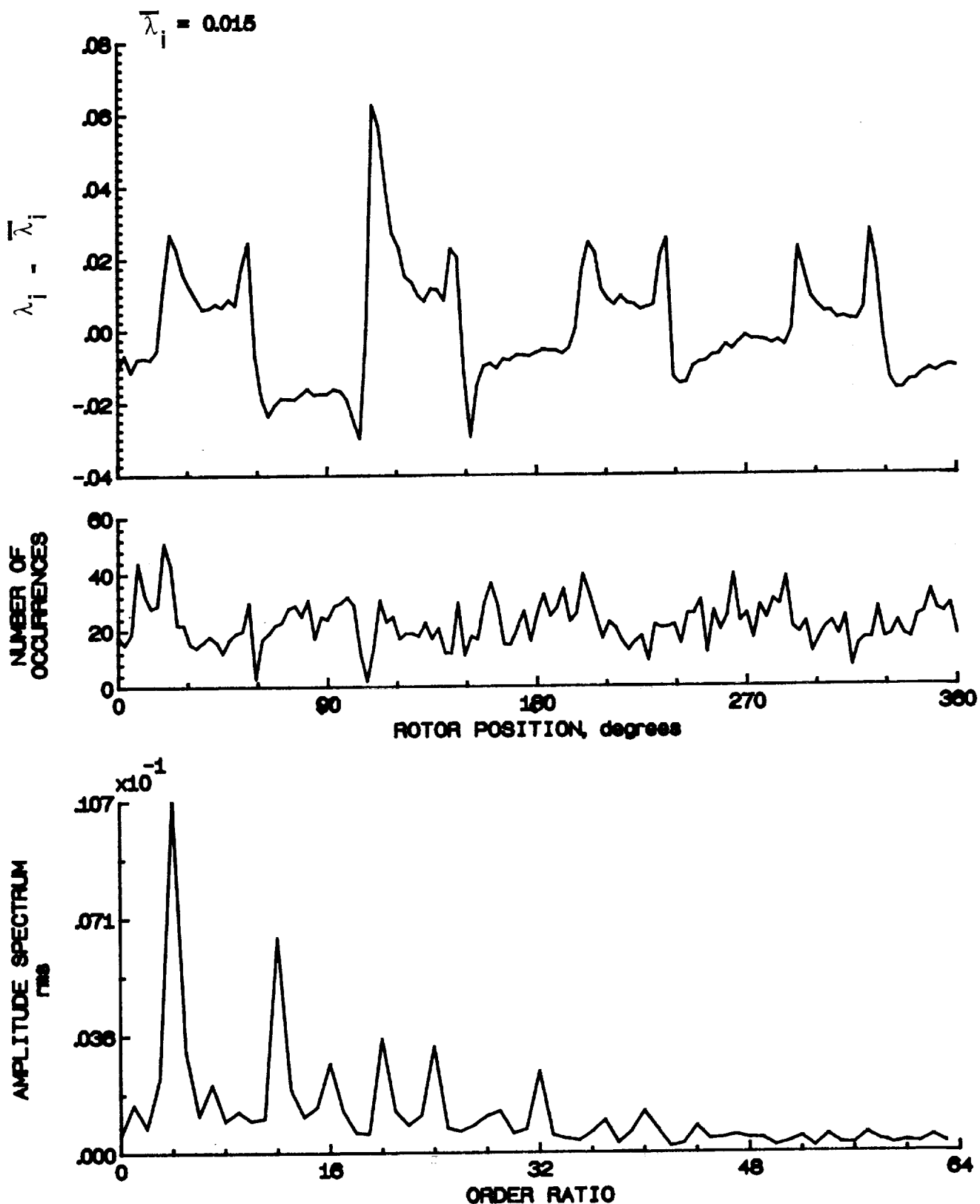


Figure 94.- Concluded.

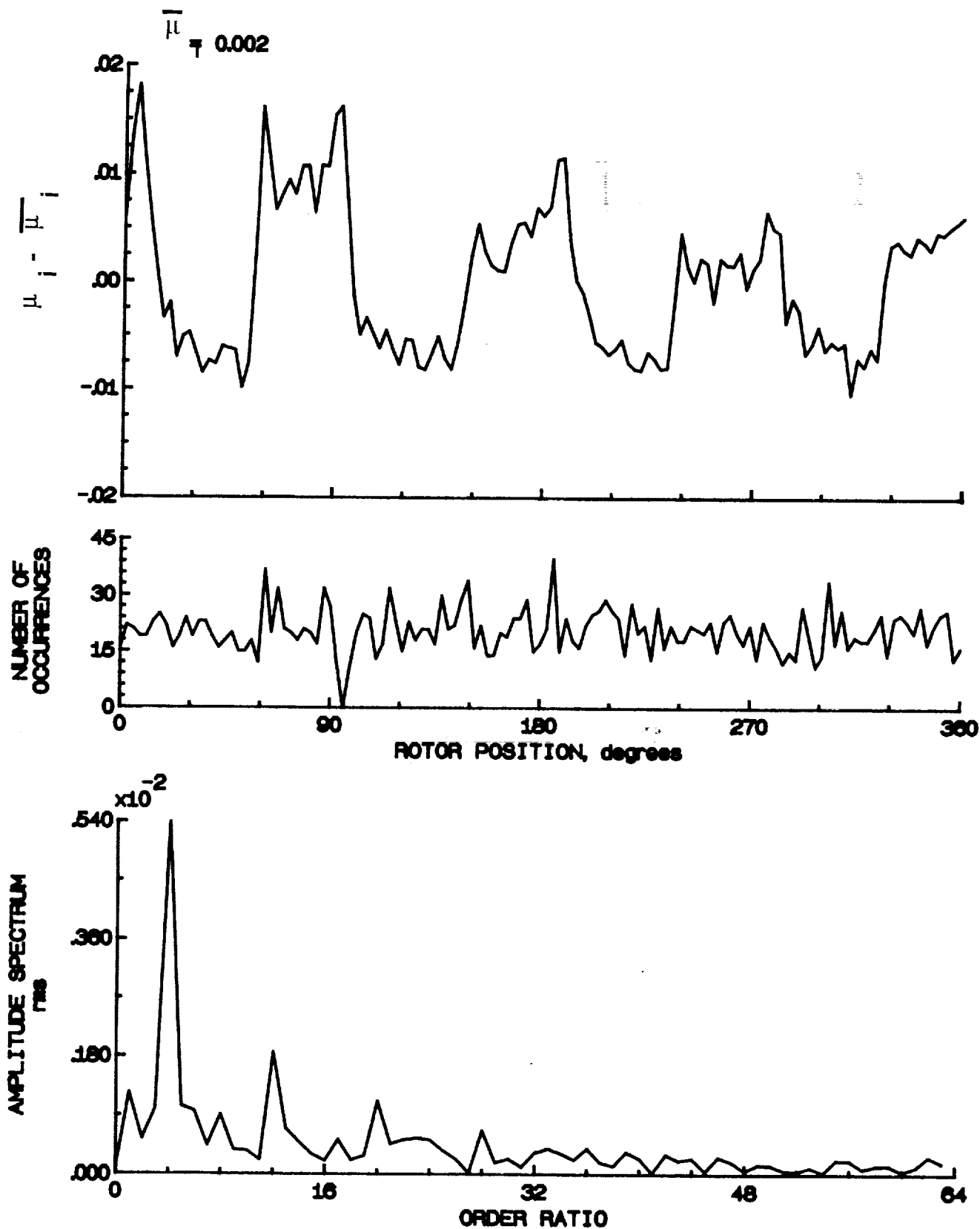


Figure 95.- Induced inflow velocity measured at 150 degrees and r/R of 0.86.

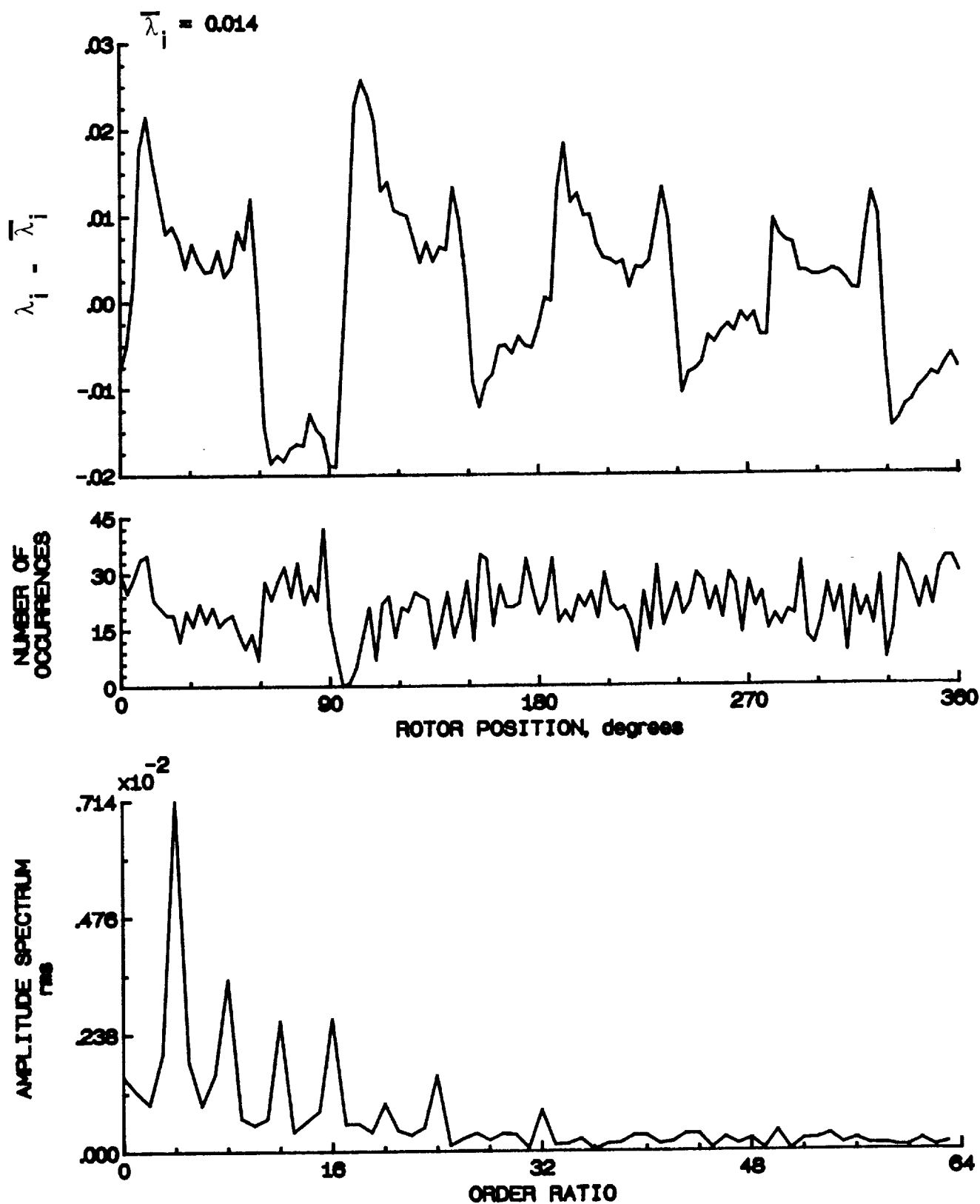


Figure 95.- Concluded.

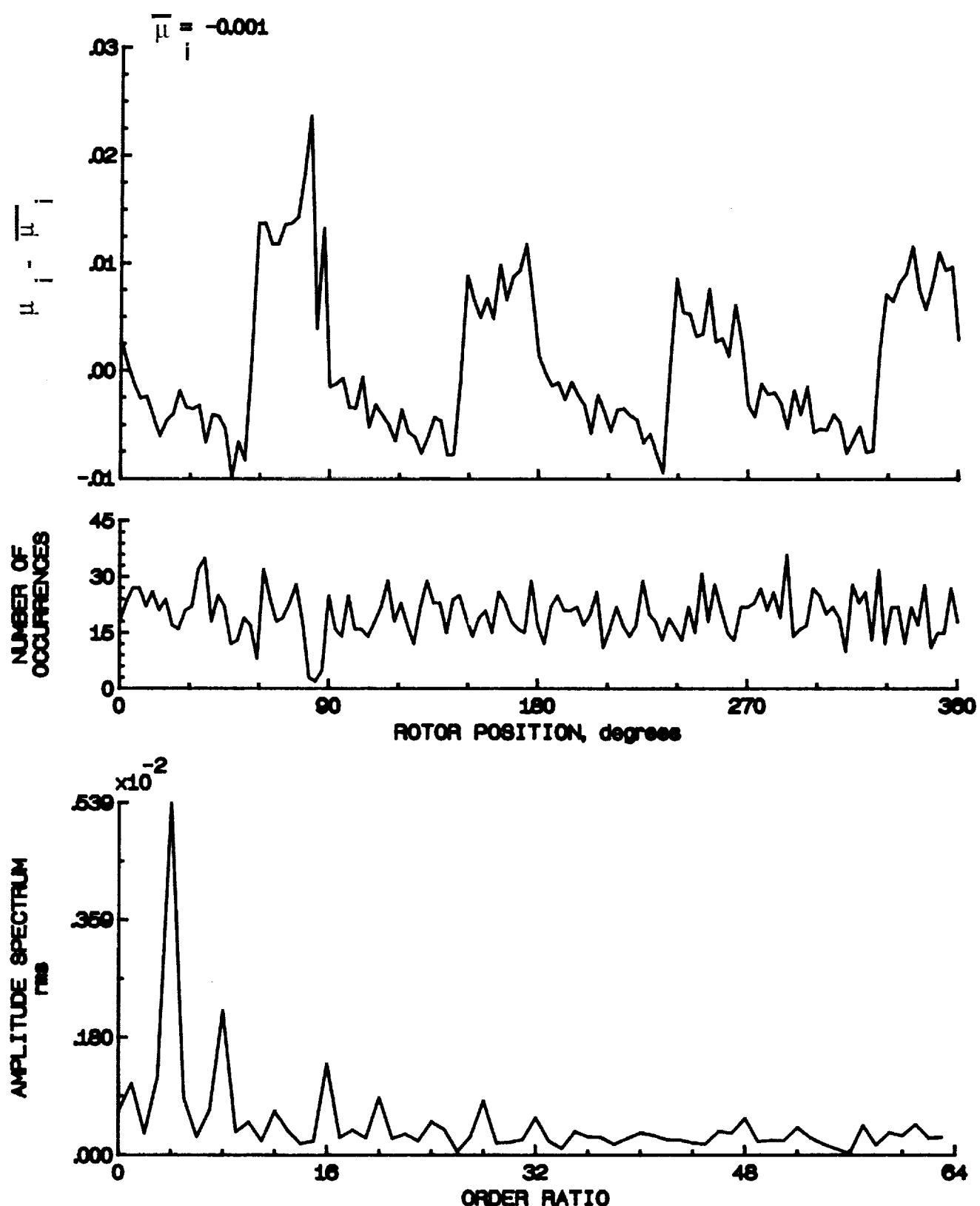


Figure 96.- Induced inflow velocity measured at 150 degrees and r/R of 0.90.

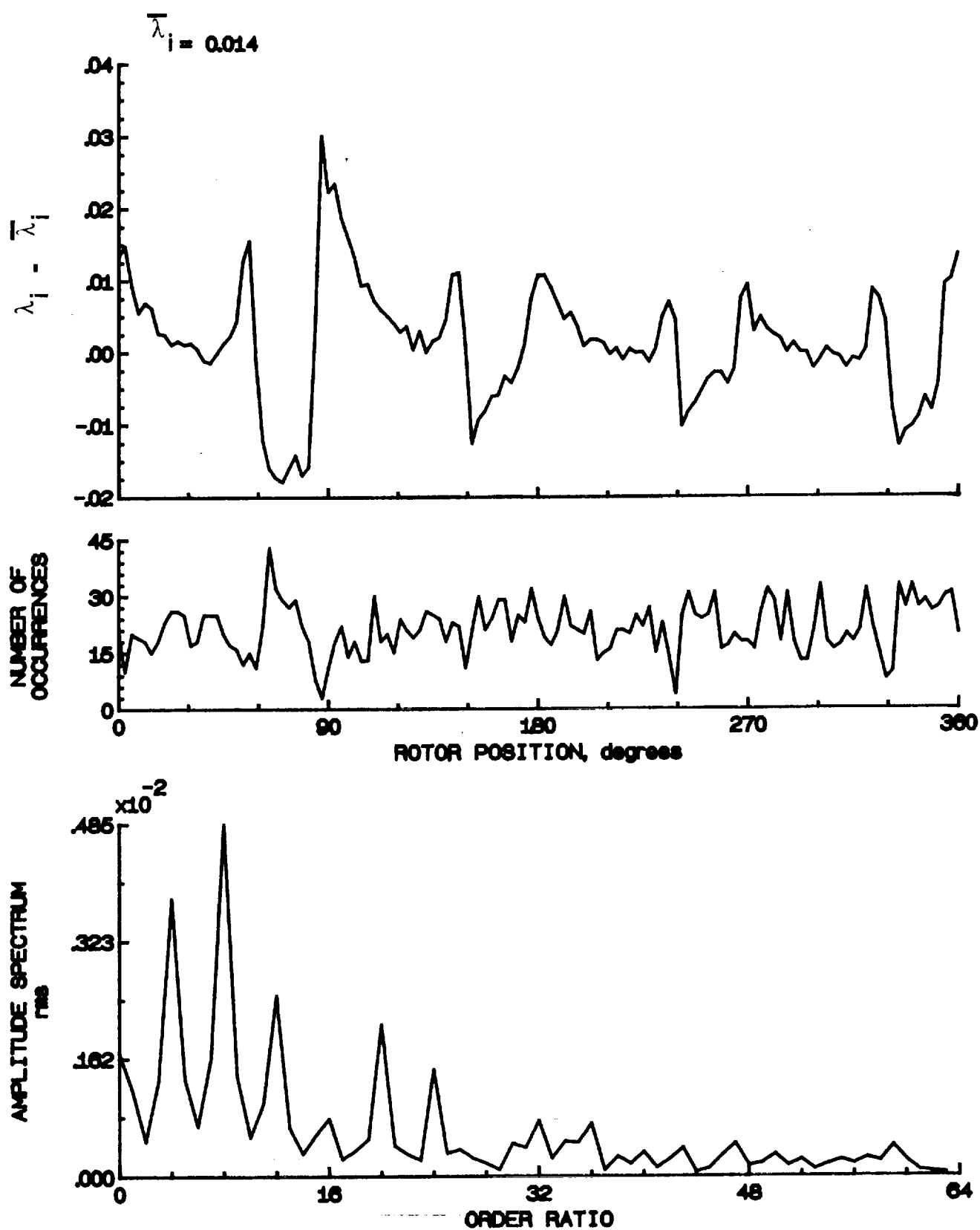


Figure 96.- Concluded.

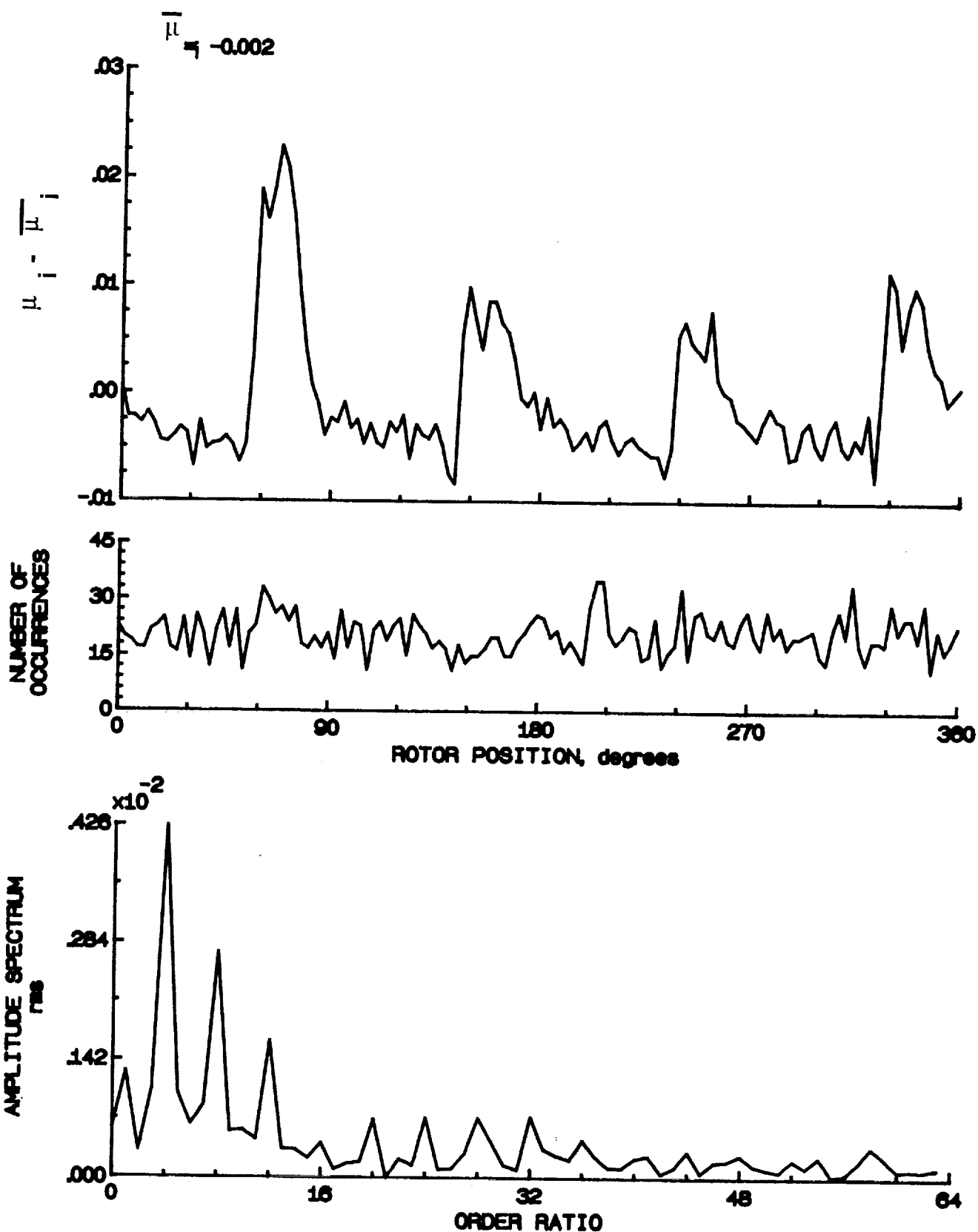


Figure 97.- Induced inflow velocity measured at 150 degrees and r/R of 0.94.

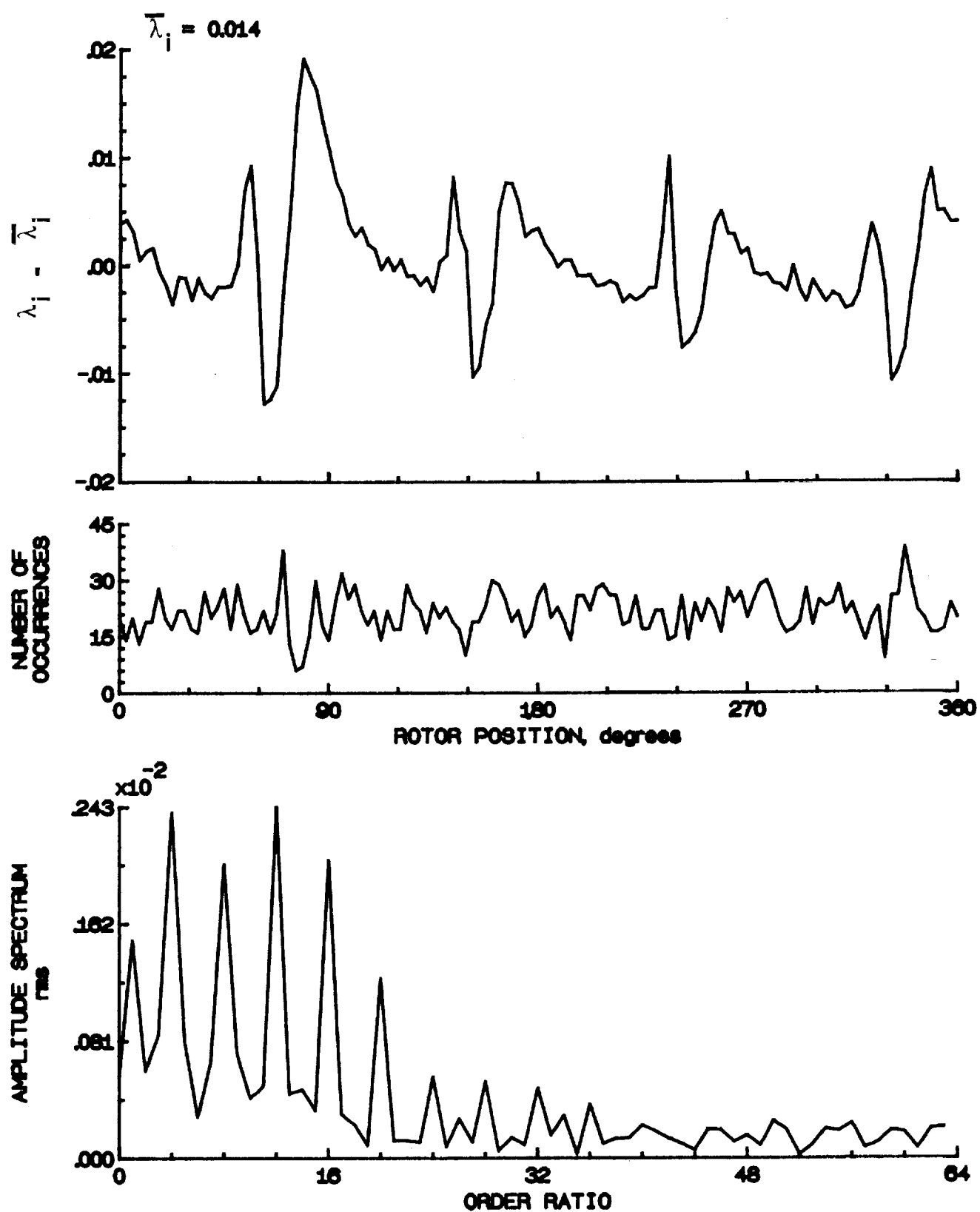


Figure 97.- Concluded.

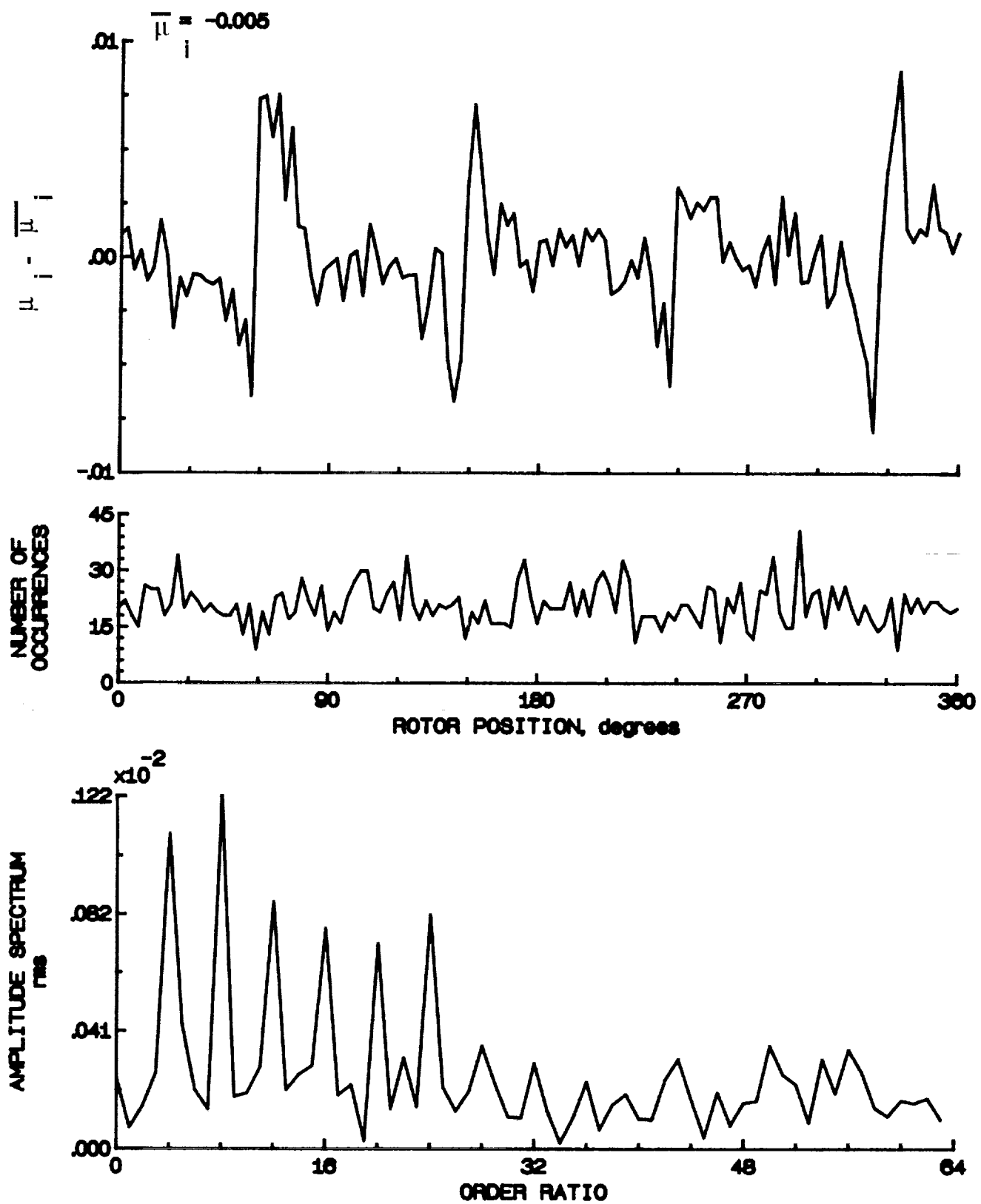


Figure 98.- Induced inflow velocity measured at 150 degrees and r/R of 0.98.

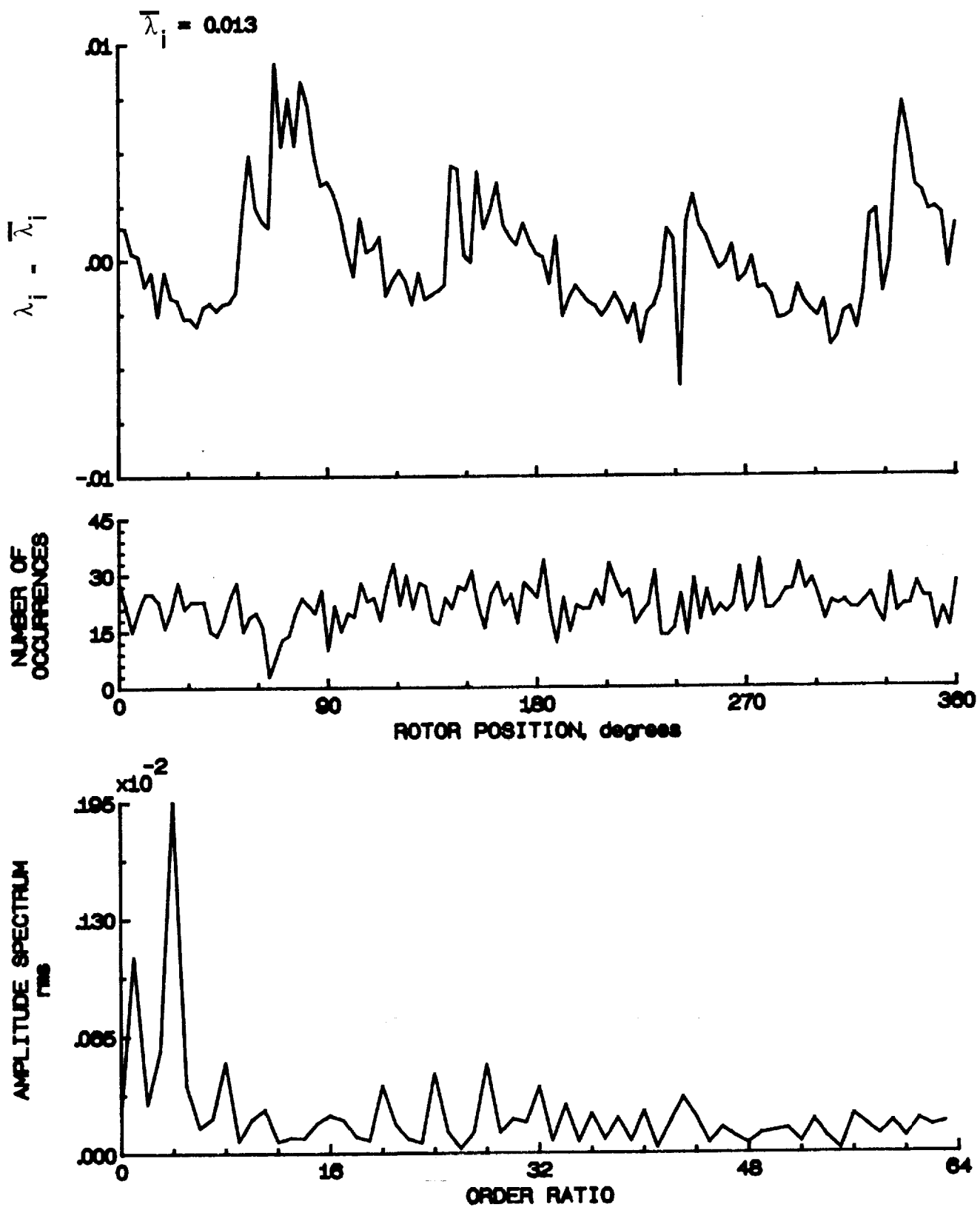


Figure 98.- Concluded.

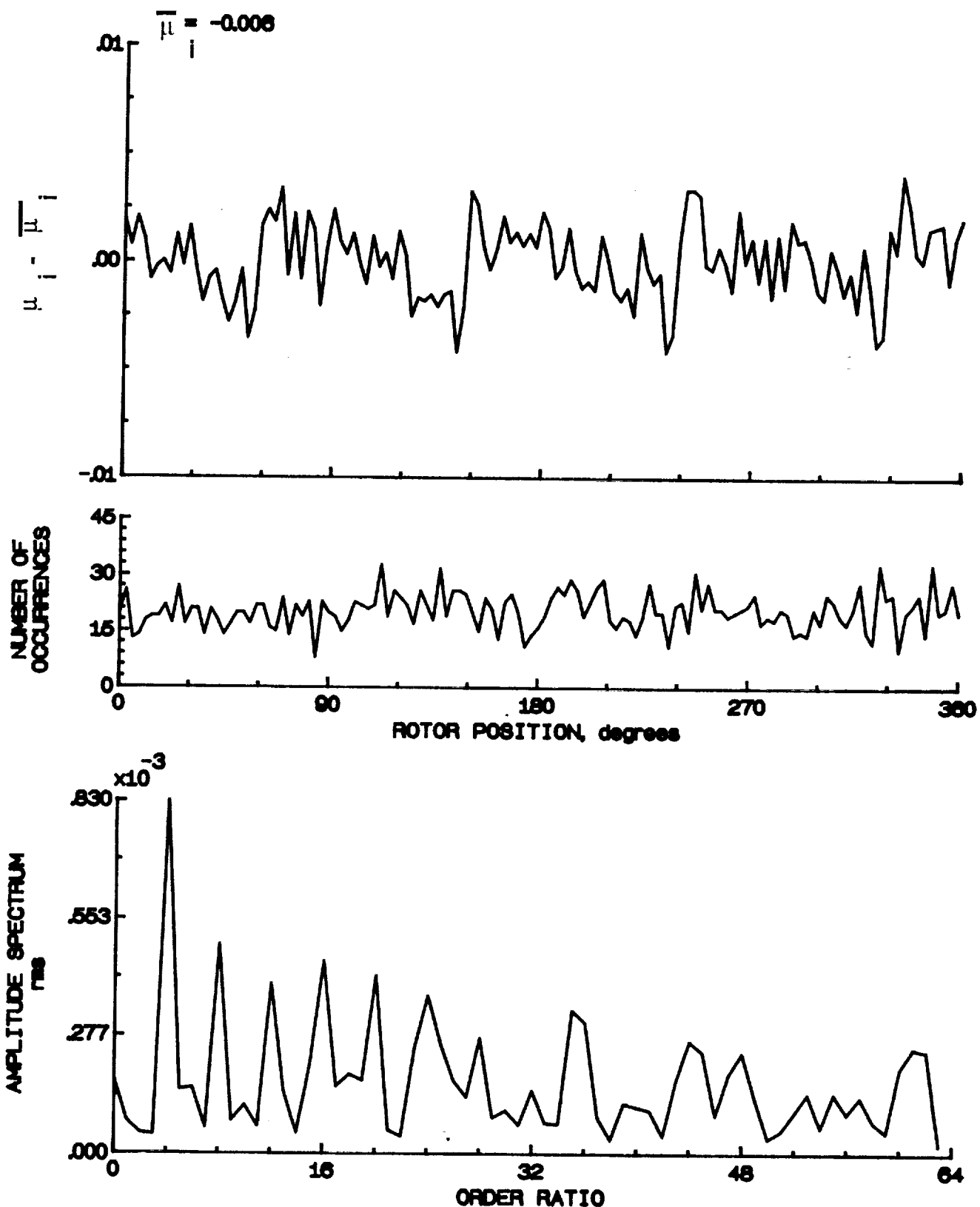


Figure 99.- Induced inflow velocity measured at 150 degrees and r/R of 1.02.

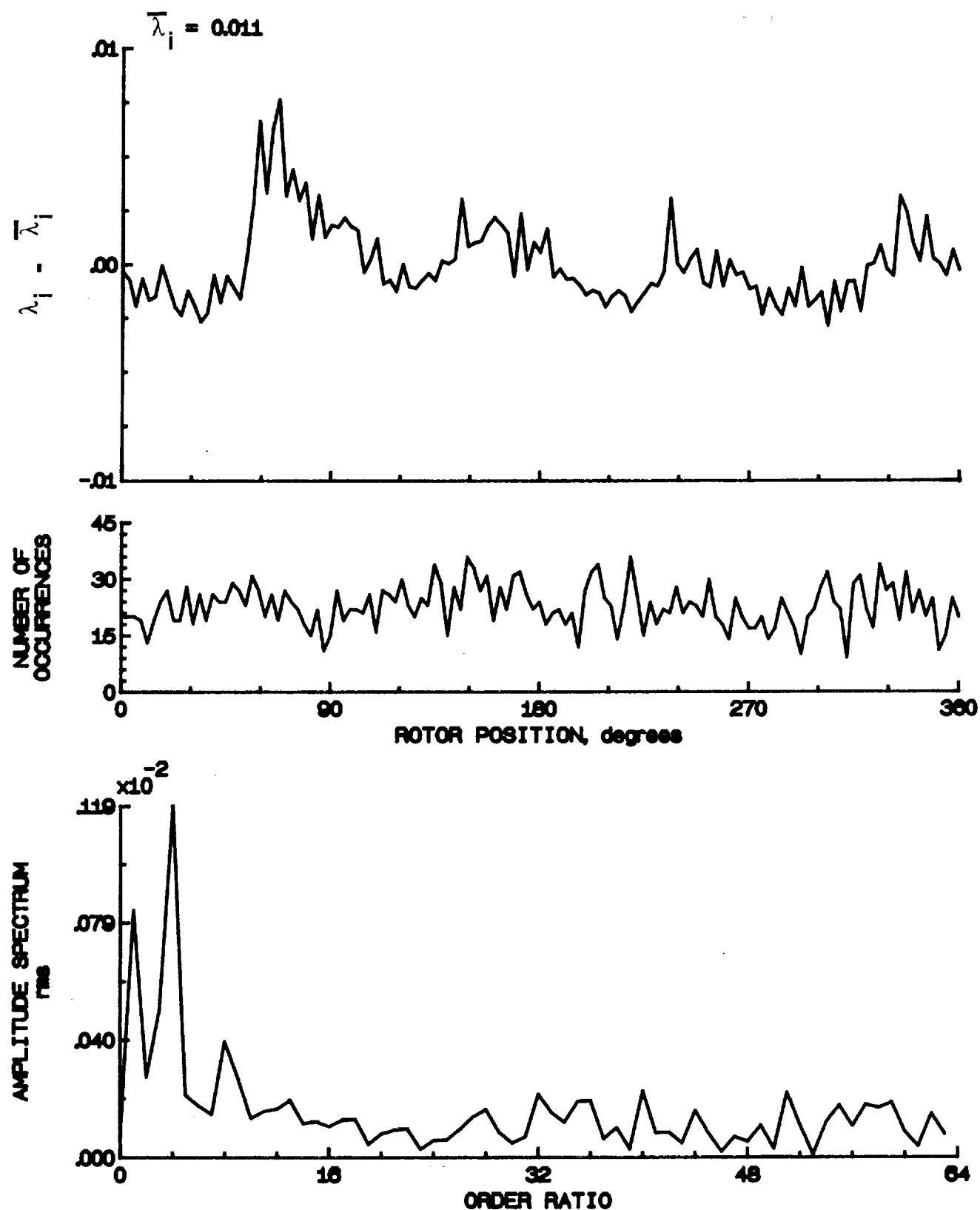


Figure 99.- Concluded.

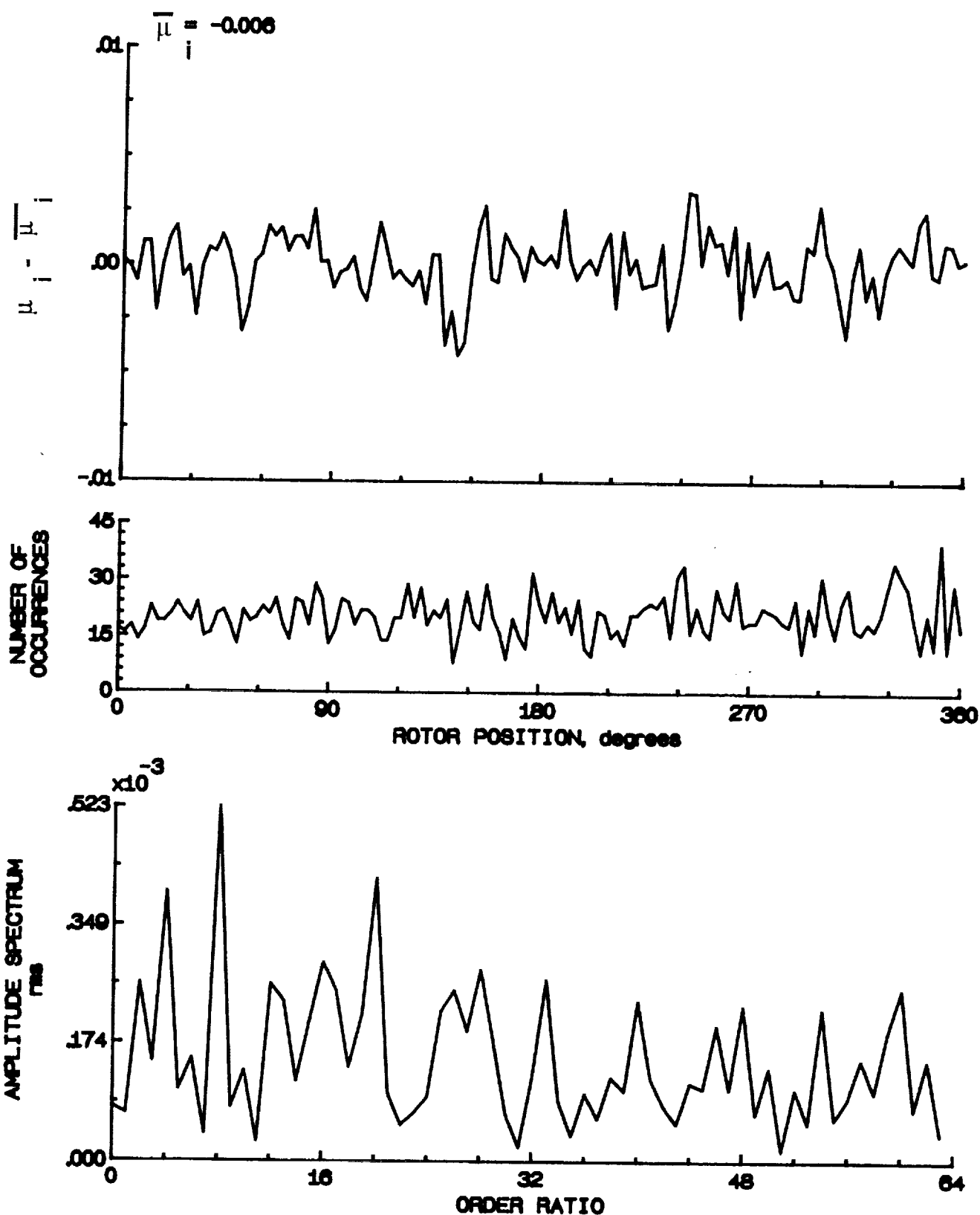


Figure 100.- Induced inflow velocity measured at 150 degrees and r/R of 1.04.

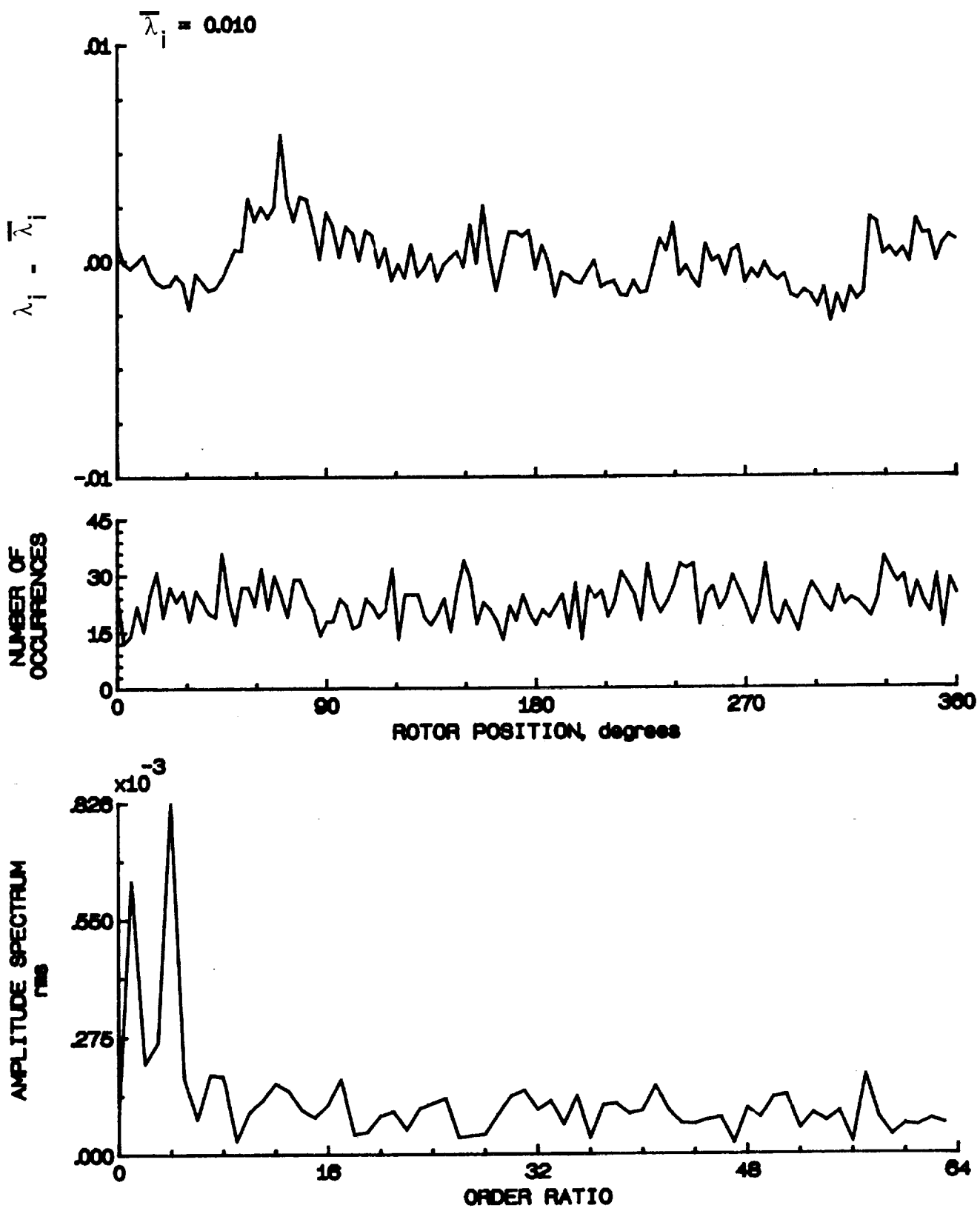


Figure 100.- Concluded.

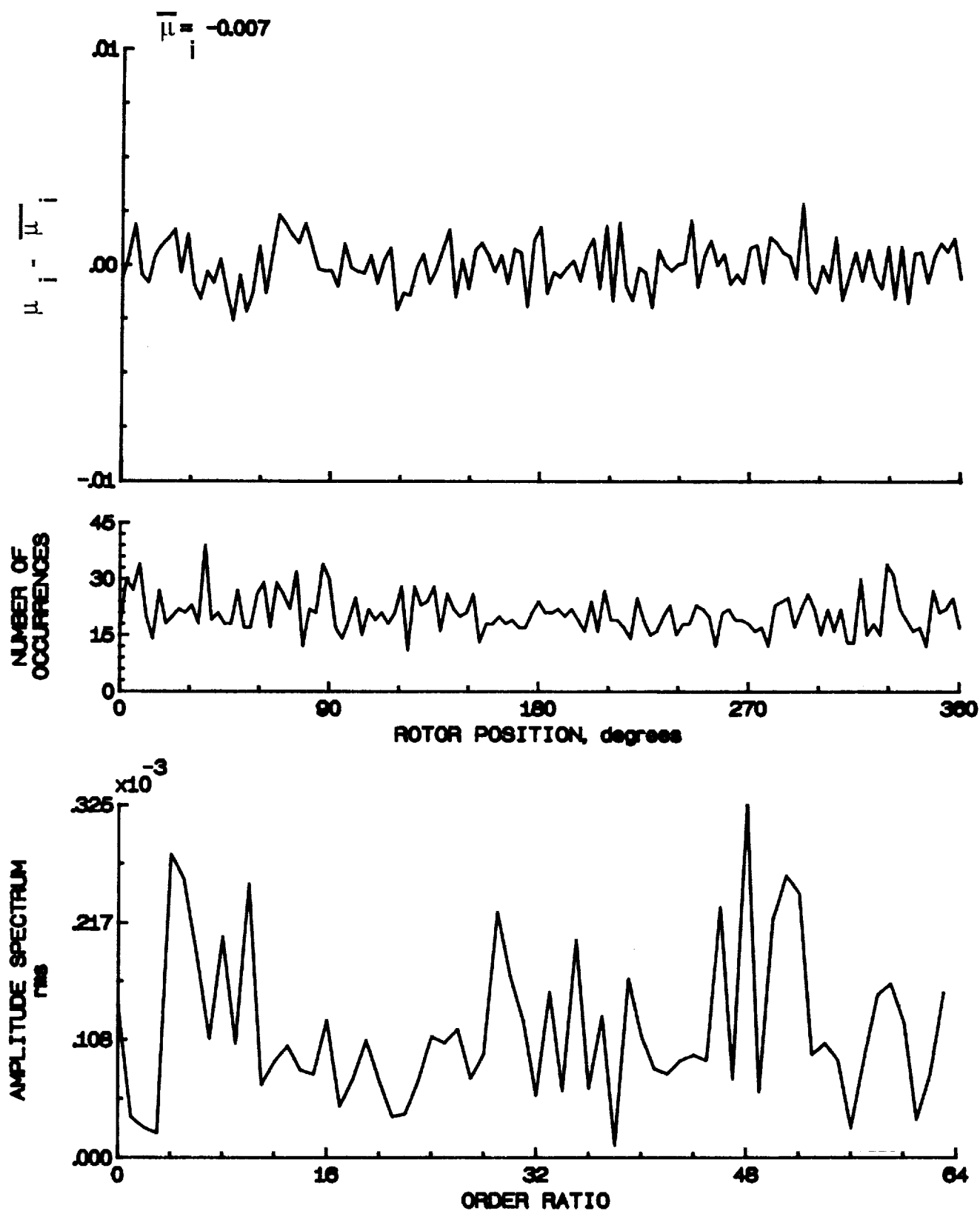


Figure 101- Induced inflow velocity measured at 150 degrees and r/R of 1.10.

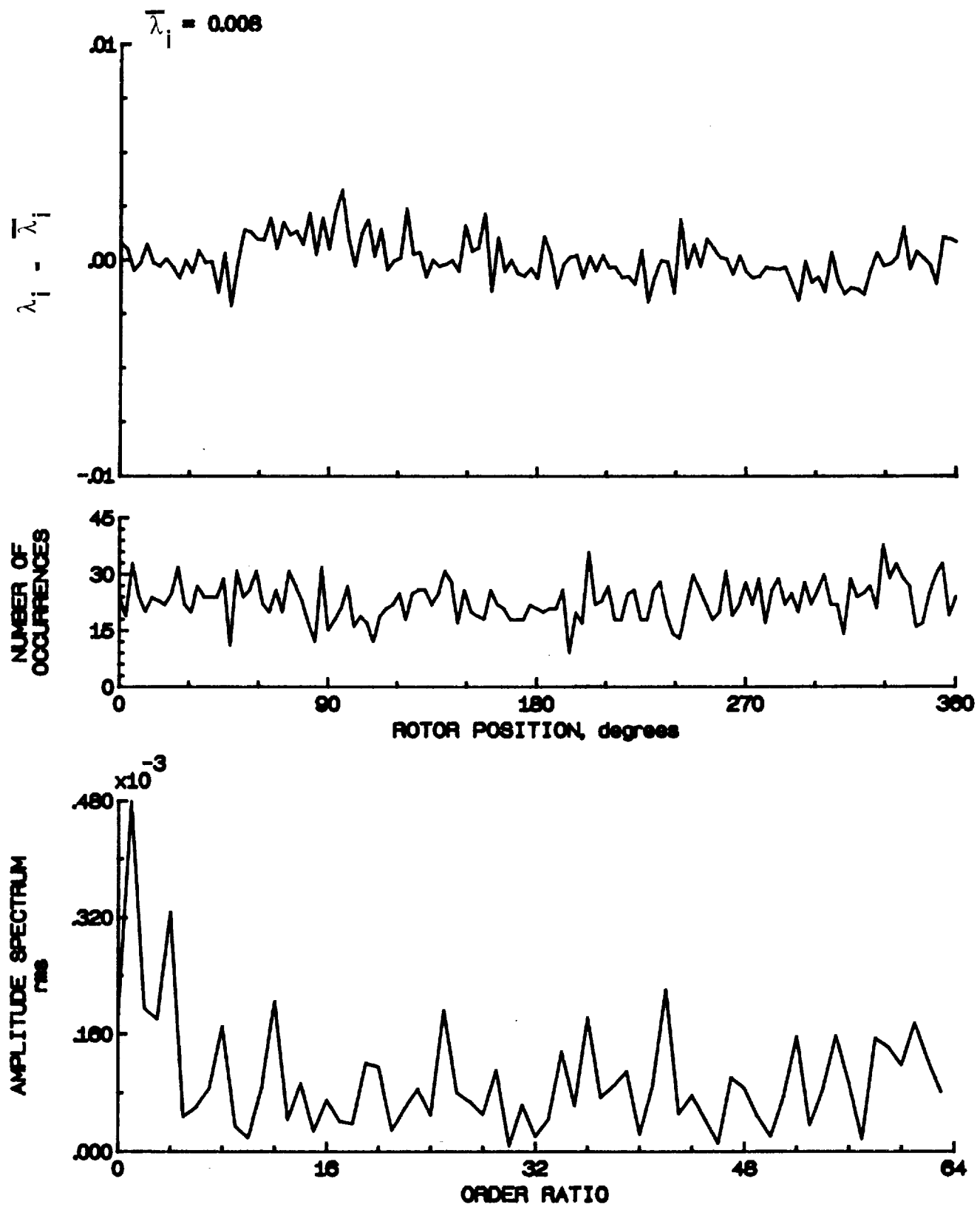


Figure 101.- Concluded.

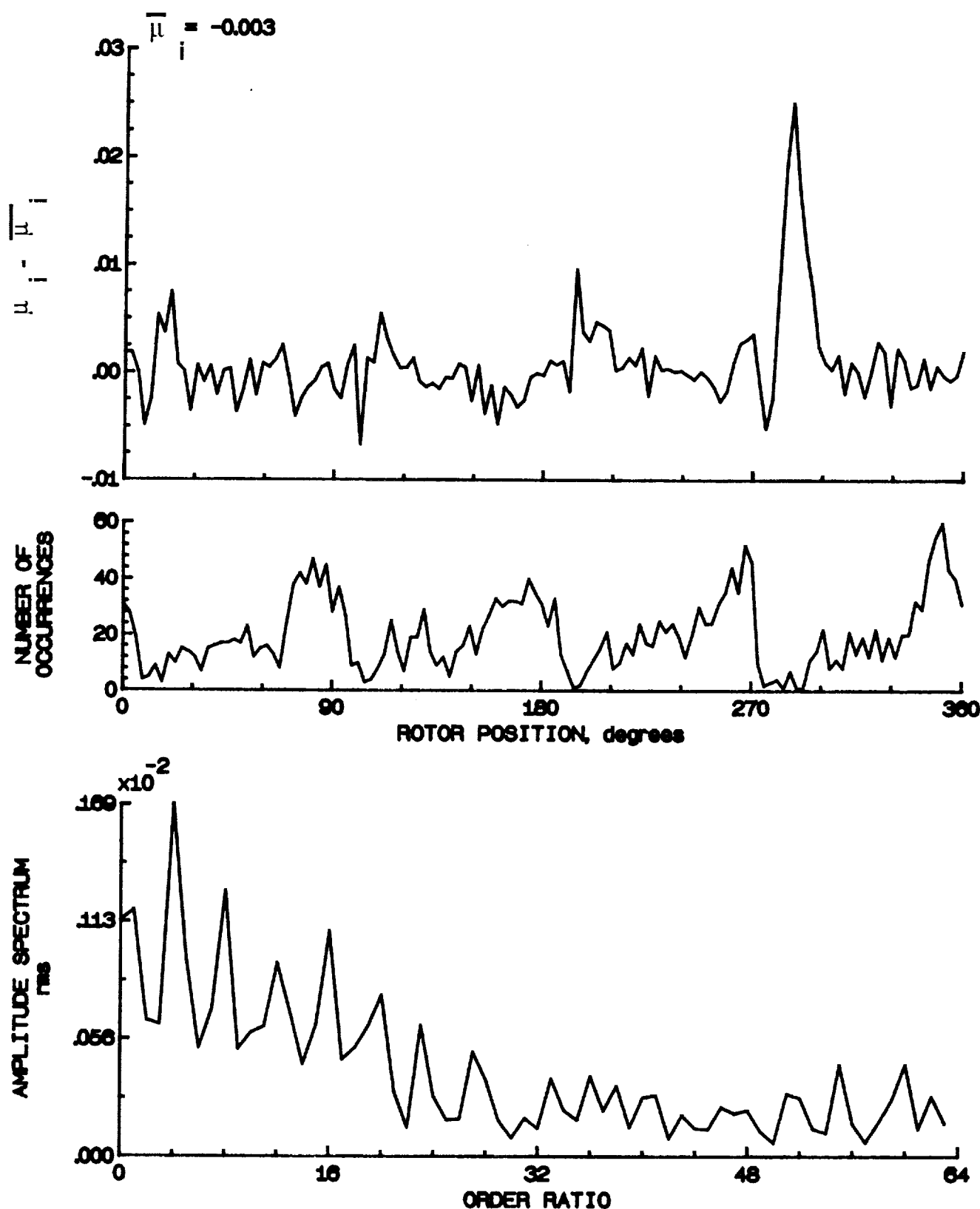


Figure 102.- Induced inflow velocity measured at 180 degrees and r/R of 0.20.

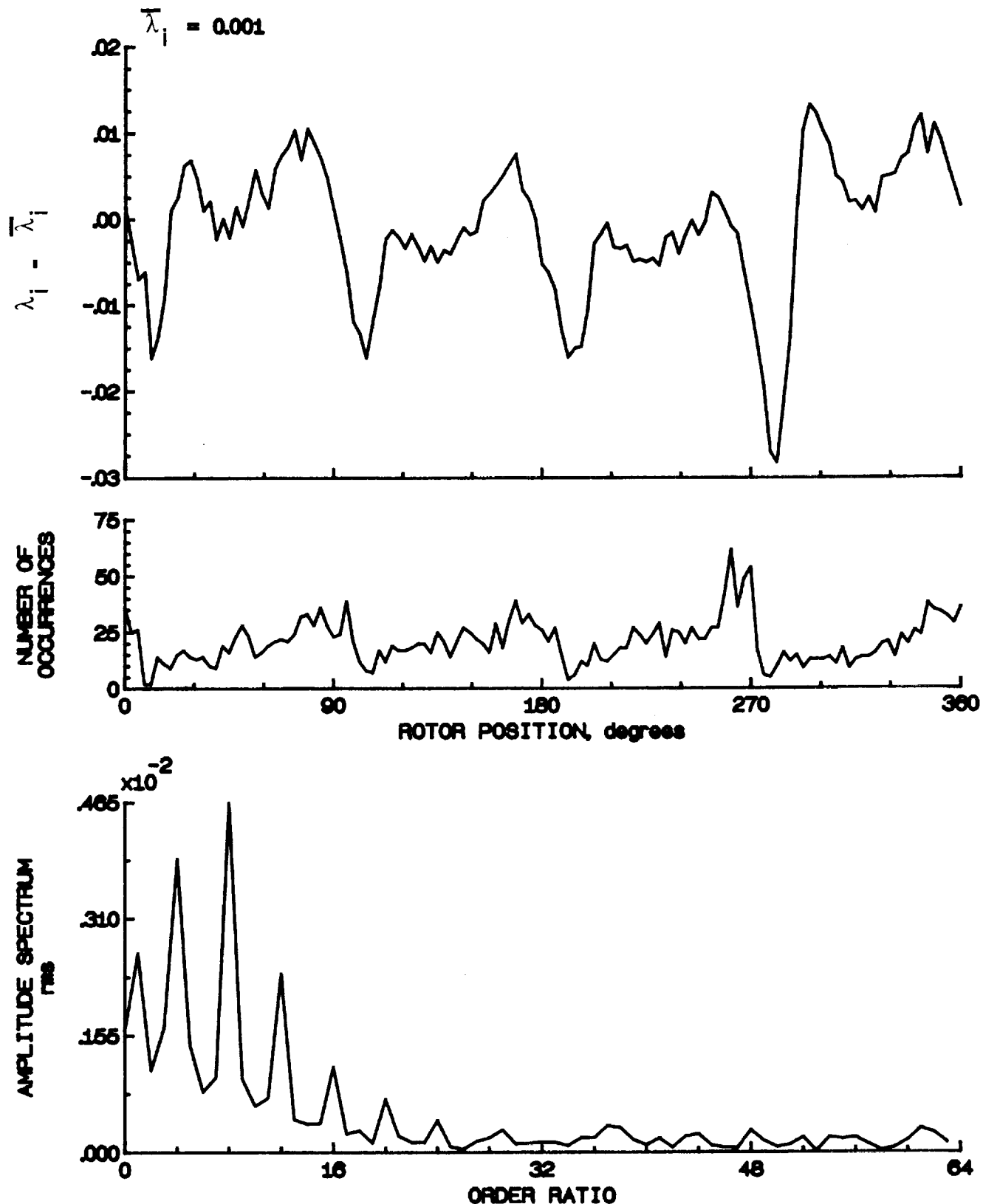


Figure 102.- Concluded.

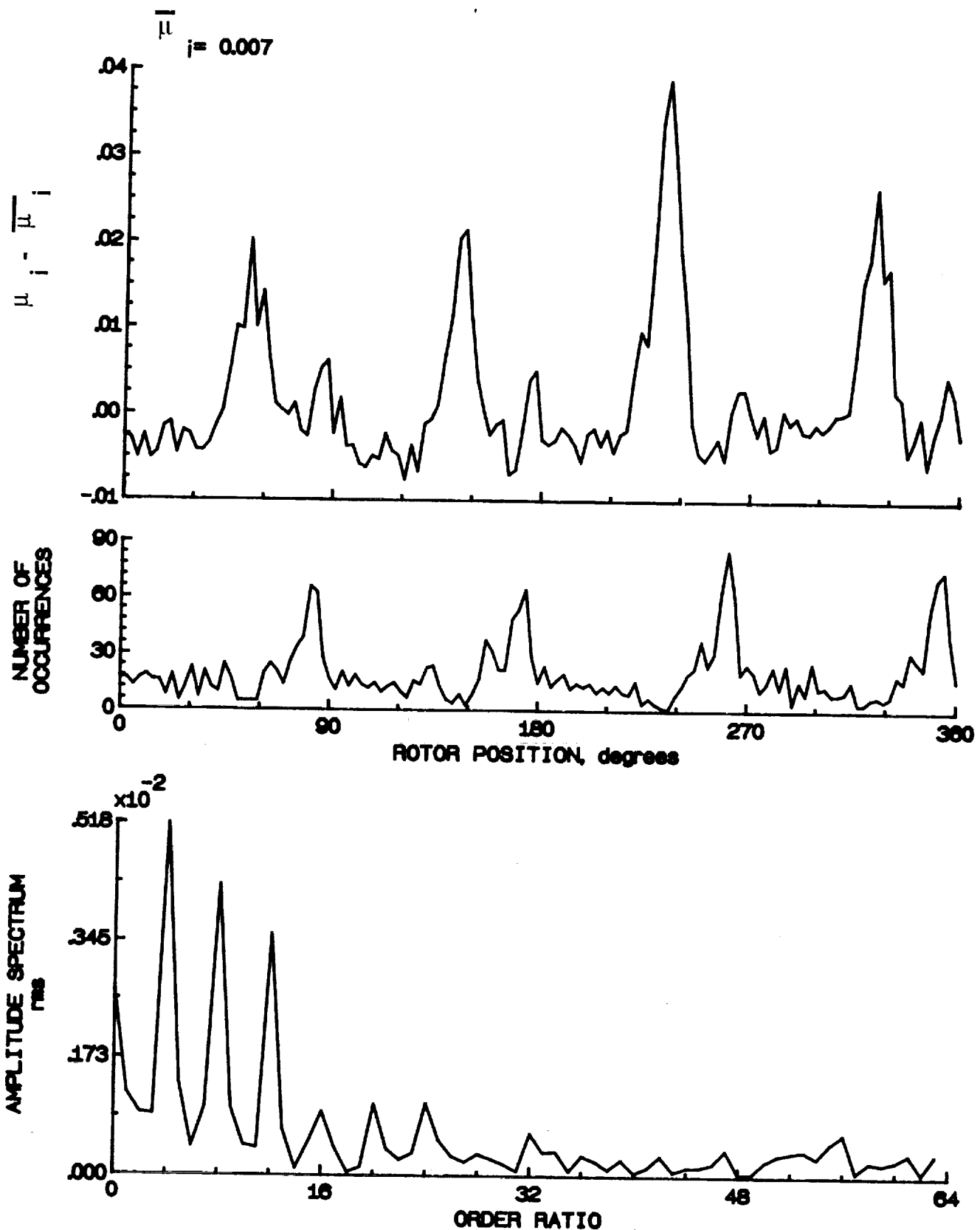


Figure 103.- Induced inflow velocity measured at 180 degrees and r/R of 0.40.

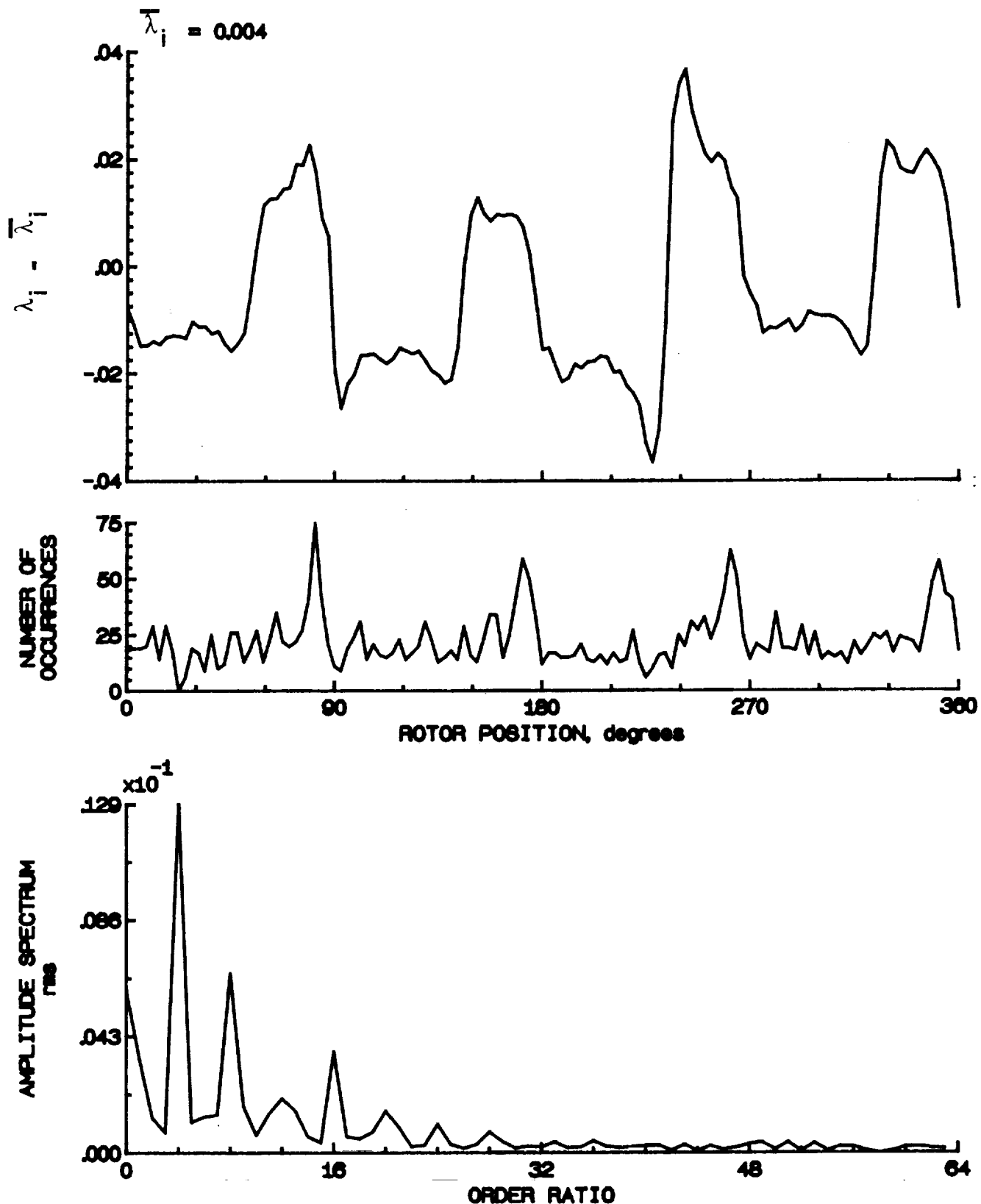


Figure 103.- Concluded.

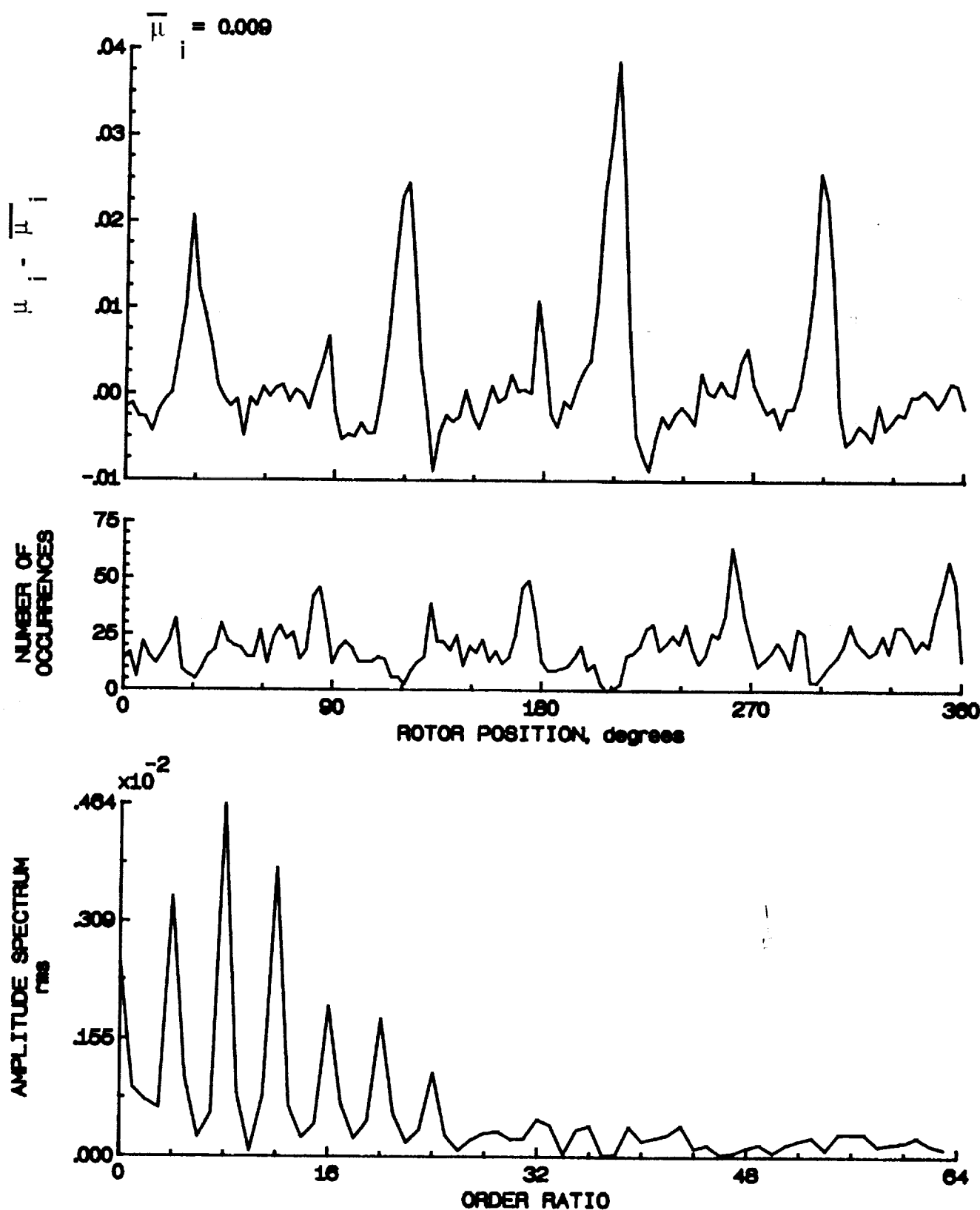


Figure 104.- Induced inflow velocity measured at 180 degrees and r/R of 0.50.

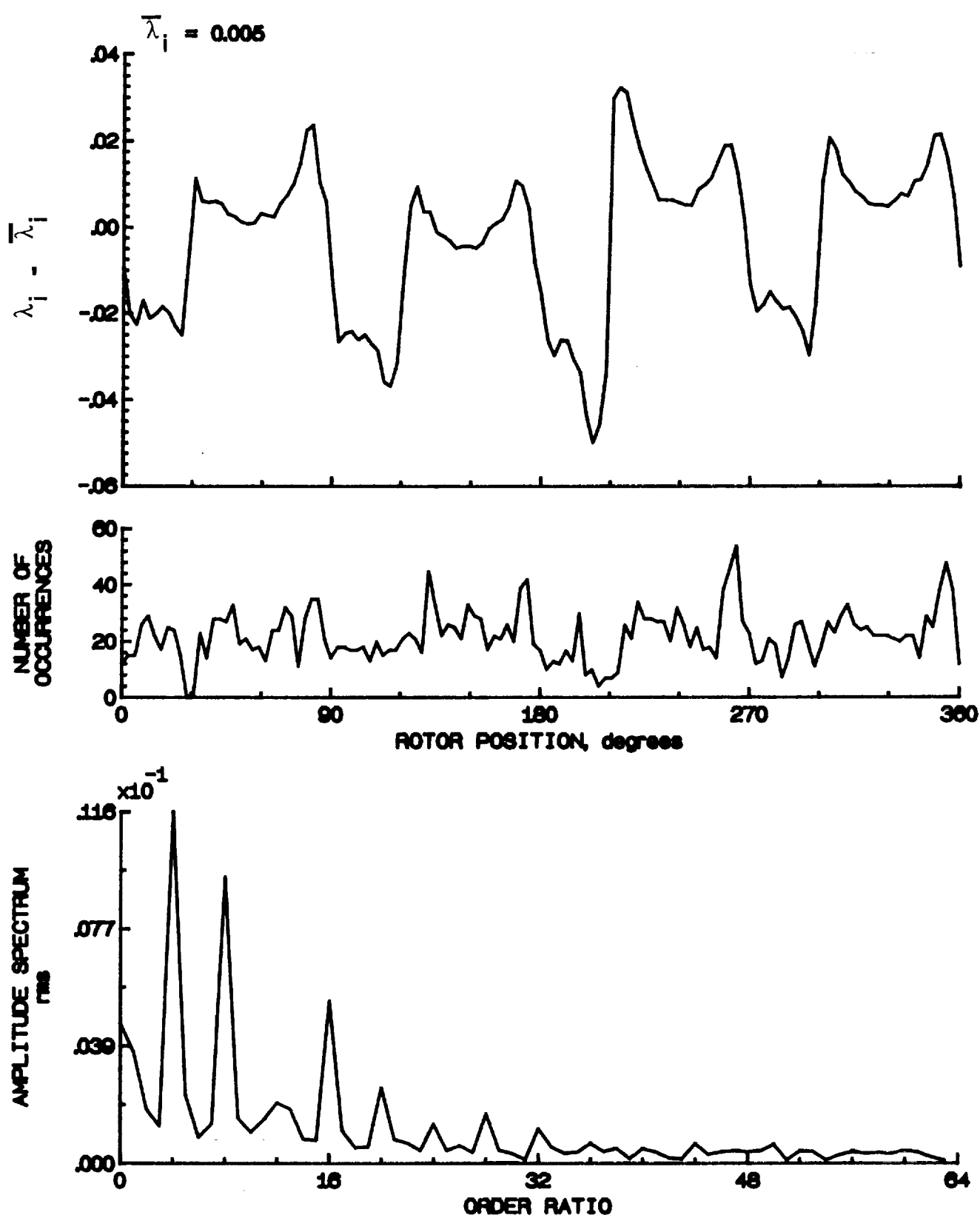


Figure 104.- Concluded.

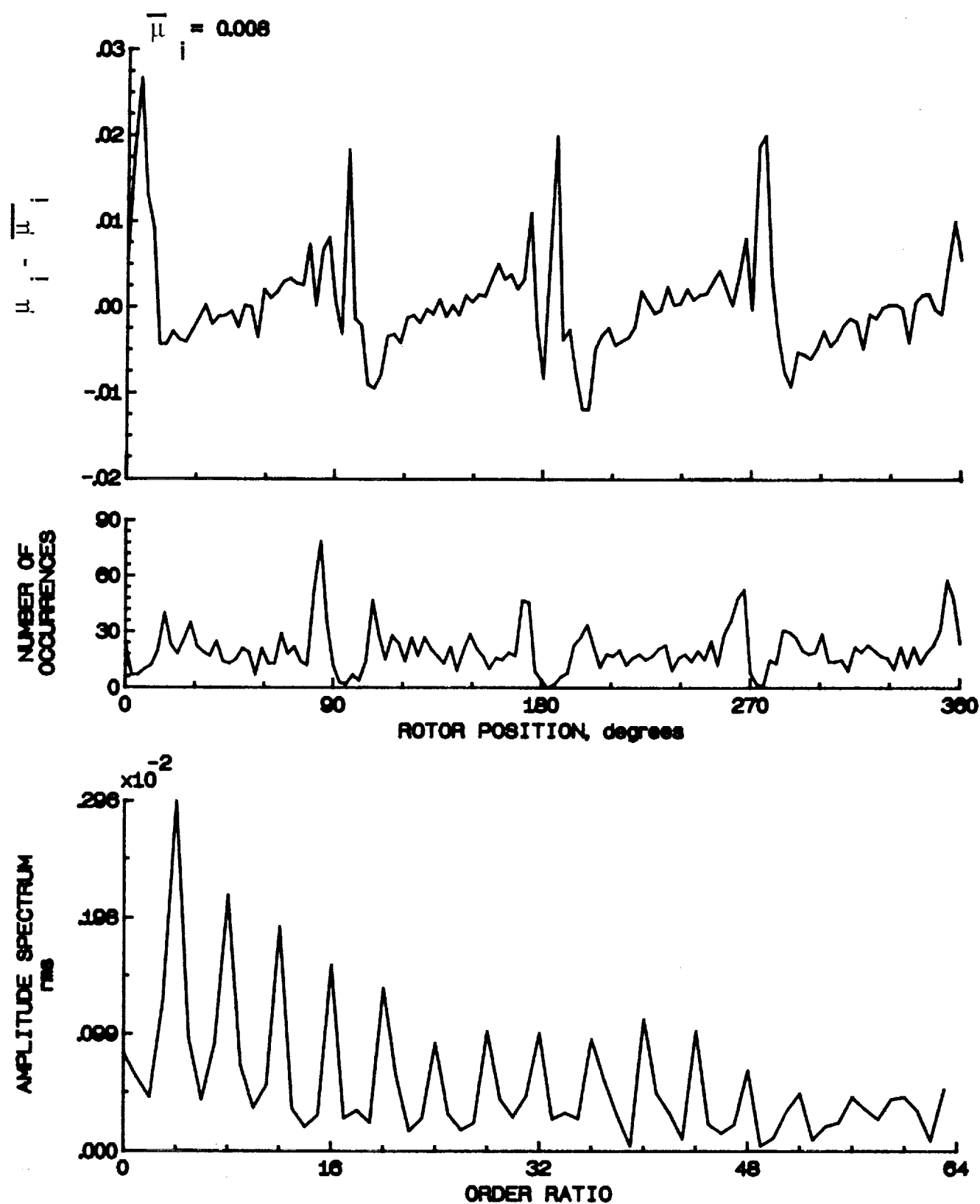


Figure 105.- Induced inflow velocity measured at 180 degrees and r/R of 0.60.

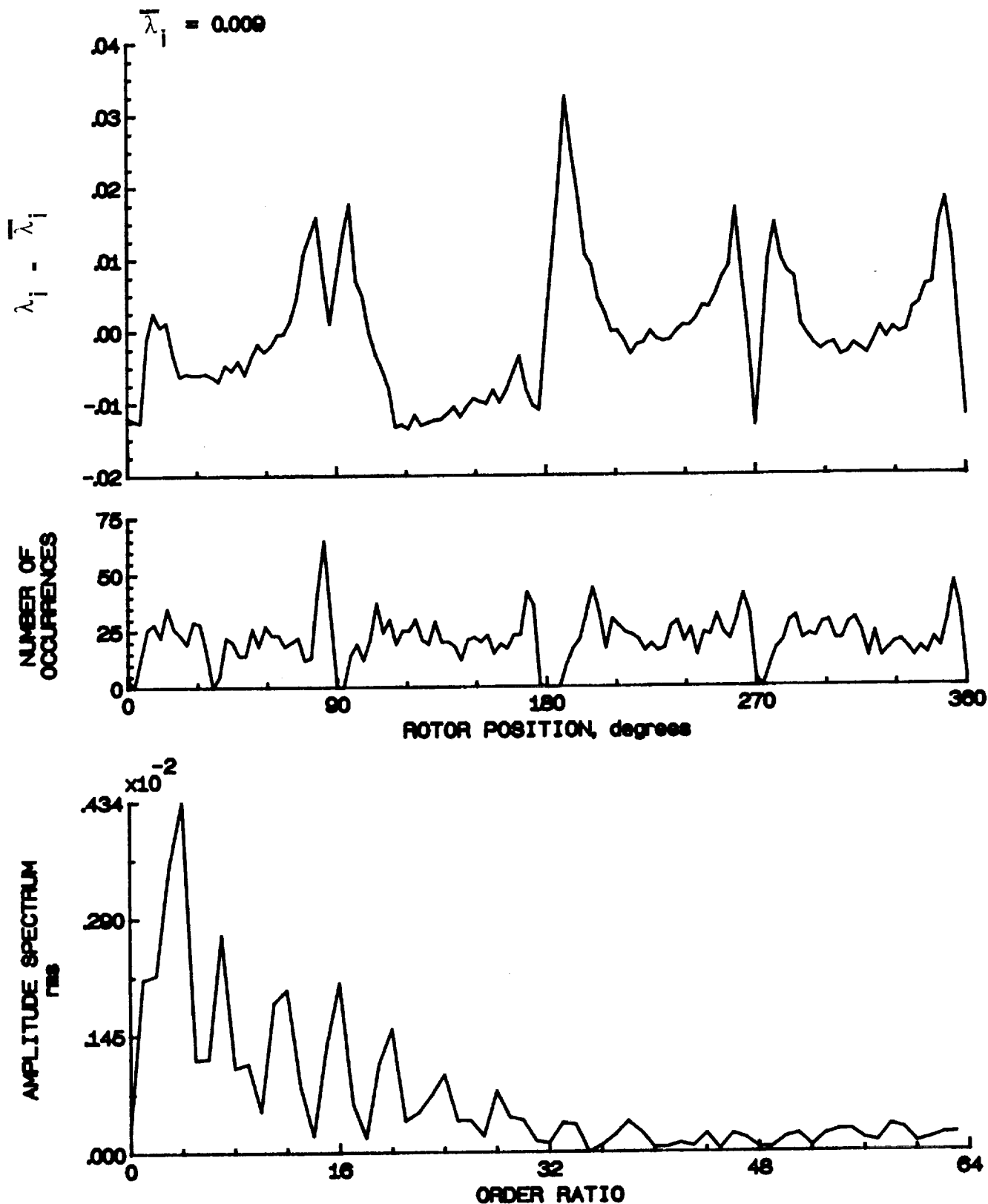


Figure 105.- Concluded.

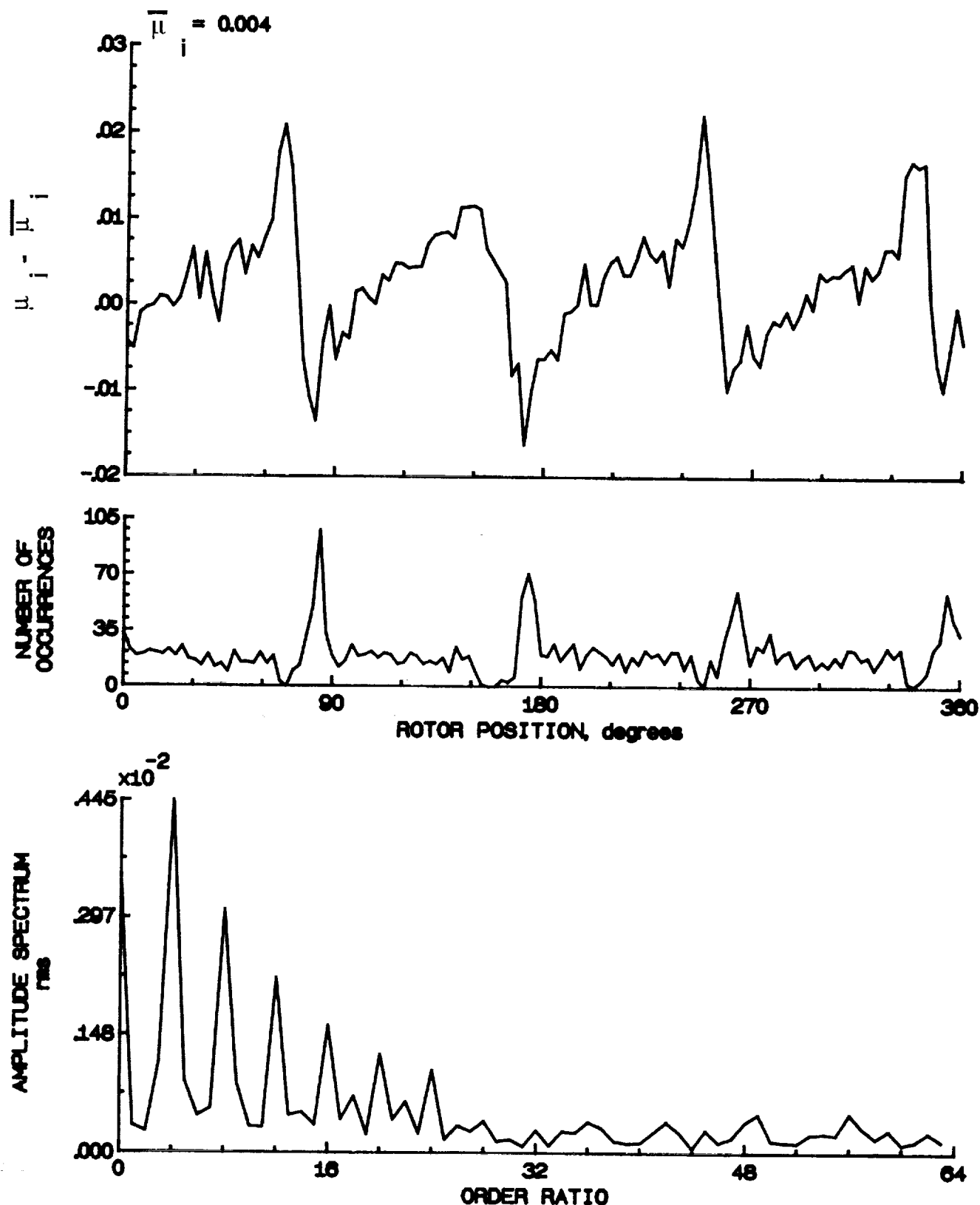


Figure 106.- Induced inflow velocity measured at 180 degrees and r/R of 0.70.

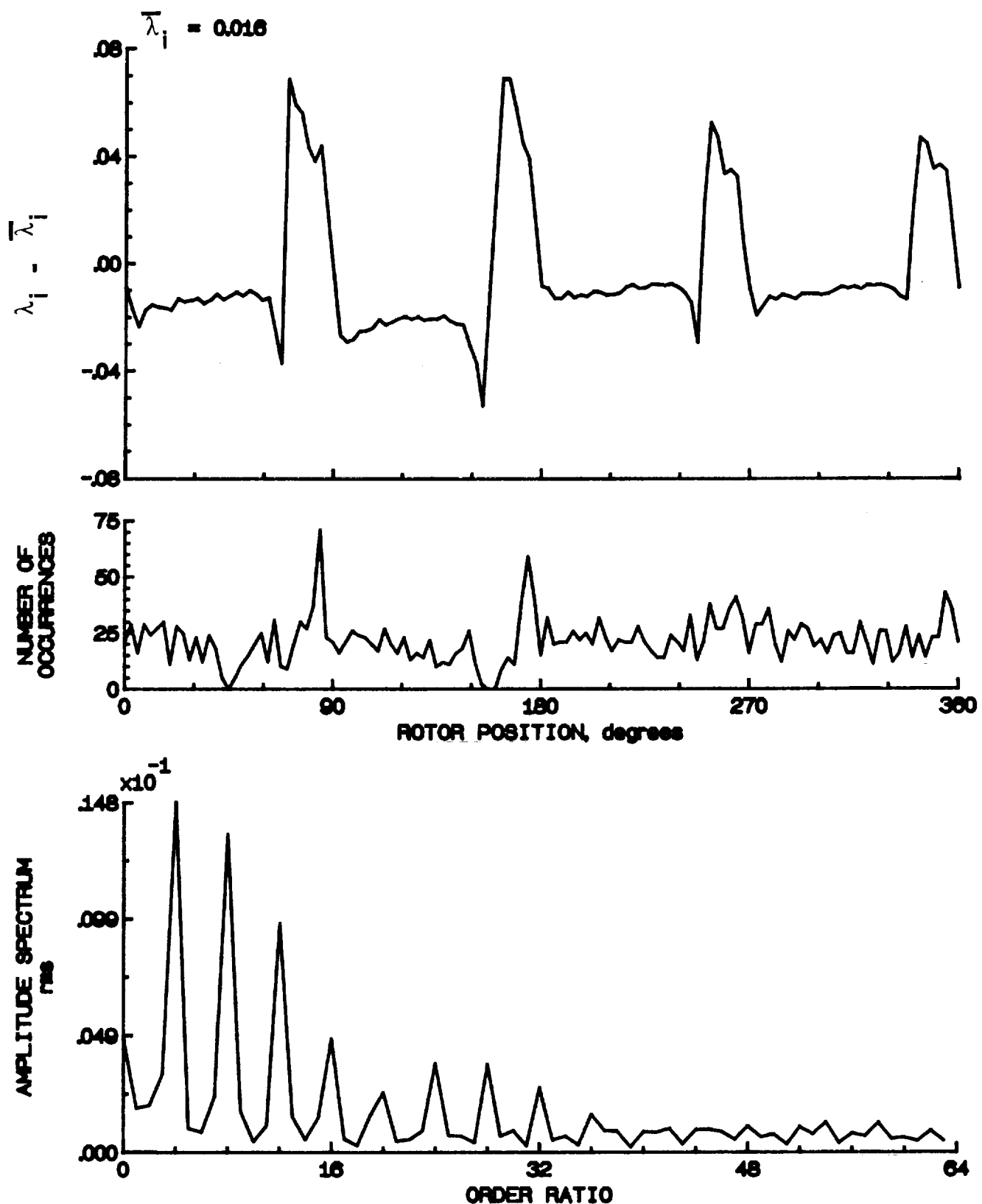


Figure 106.- Concluded.

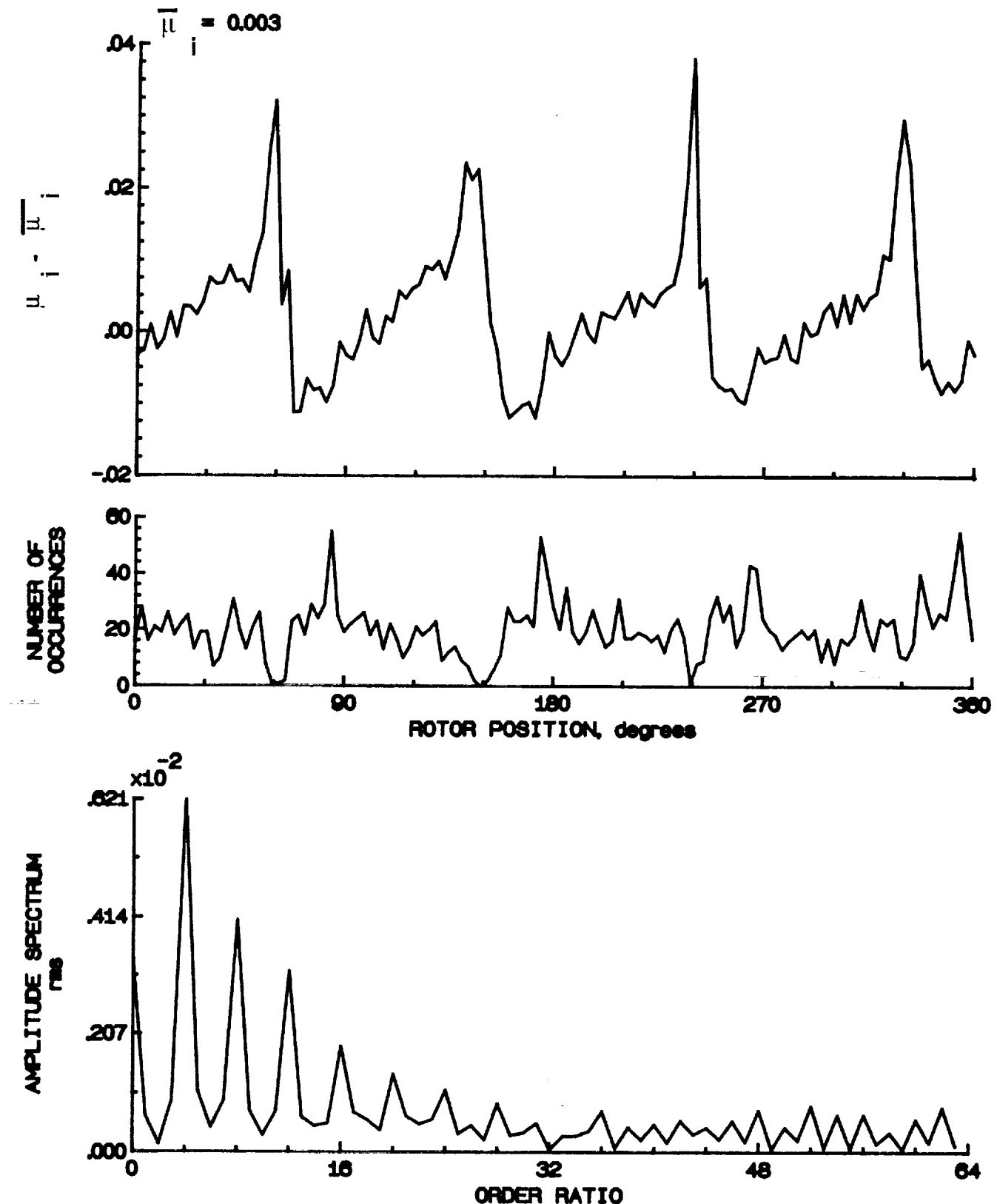


Figure 107.- Induced inflow velocity measured at 180 degrees and r/R of 0.74.

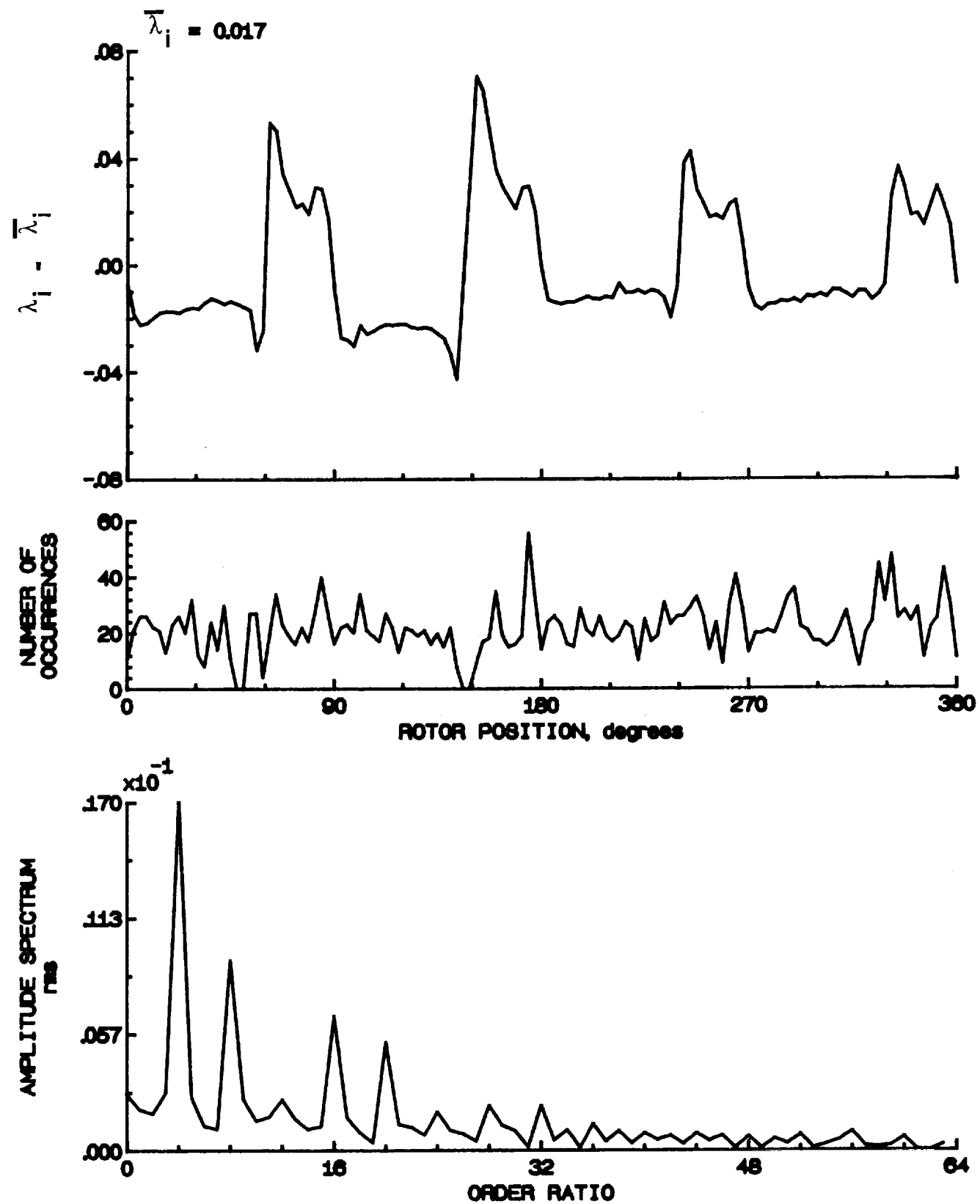


Figure 107.- Concluded.

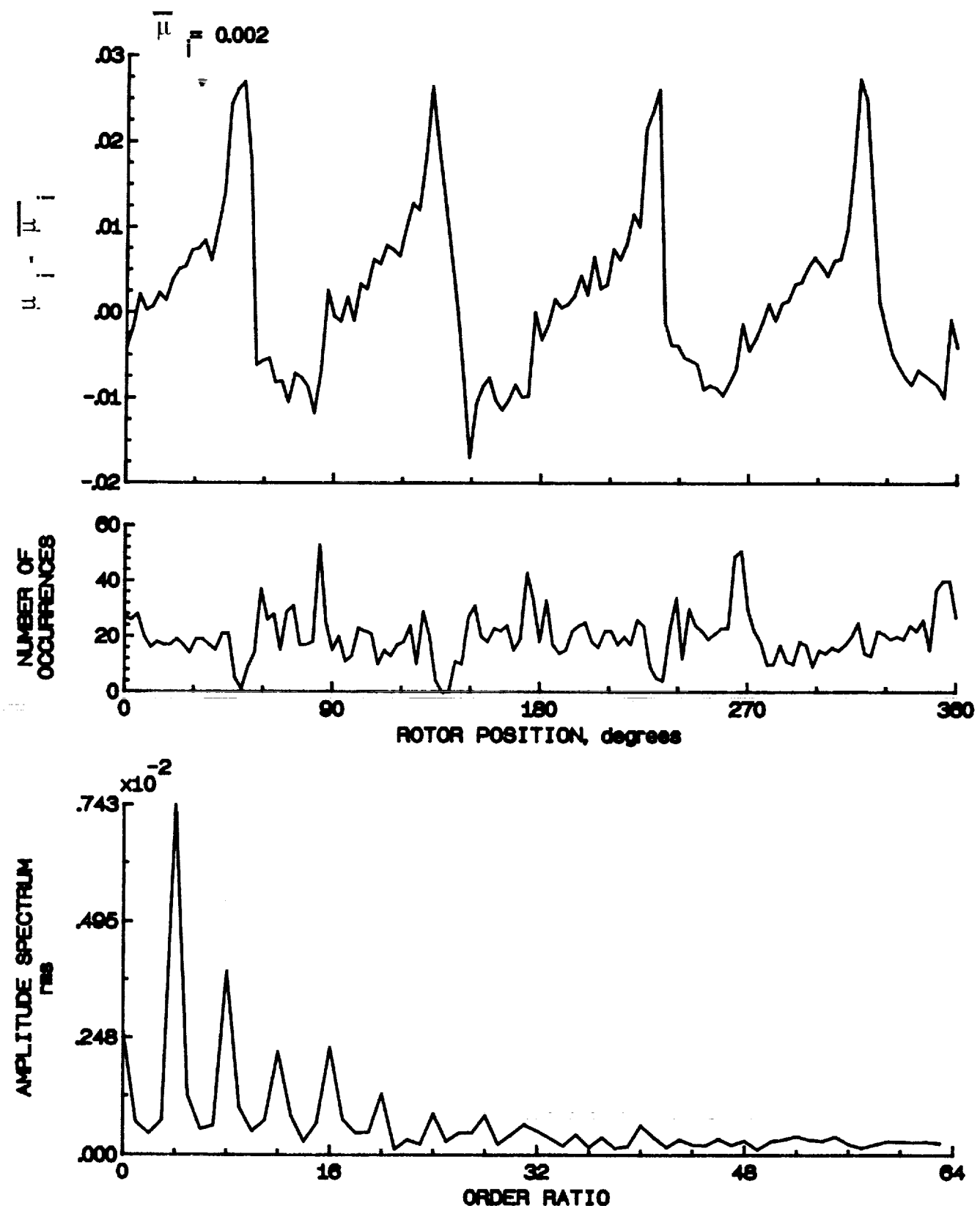


Figure 108.- Induced inflow velocity measured at 180 degrees and r/R of 0.75.

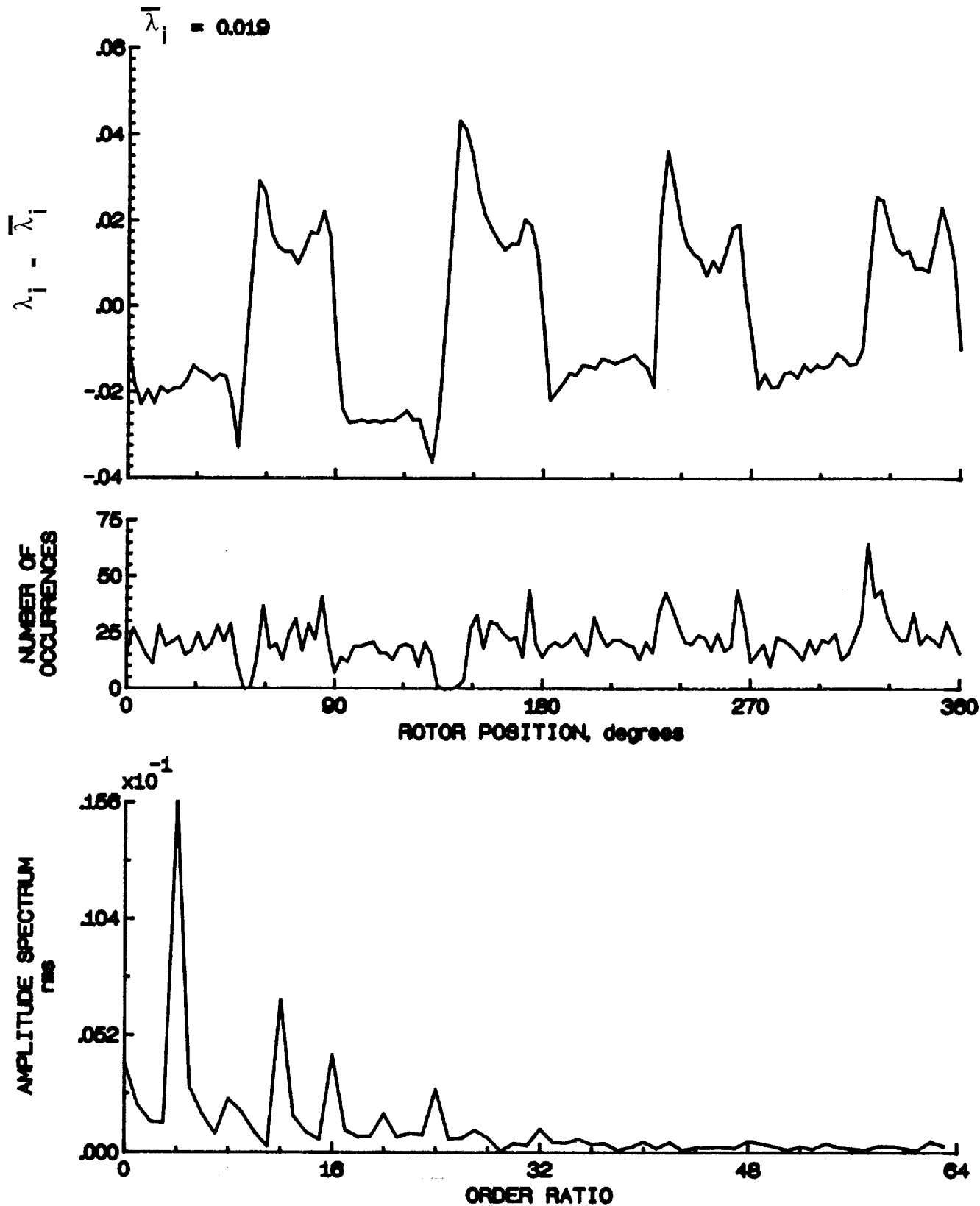


Figure 108.- Concluded.

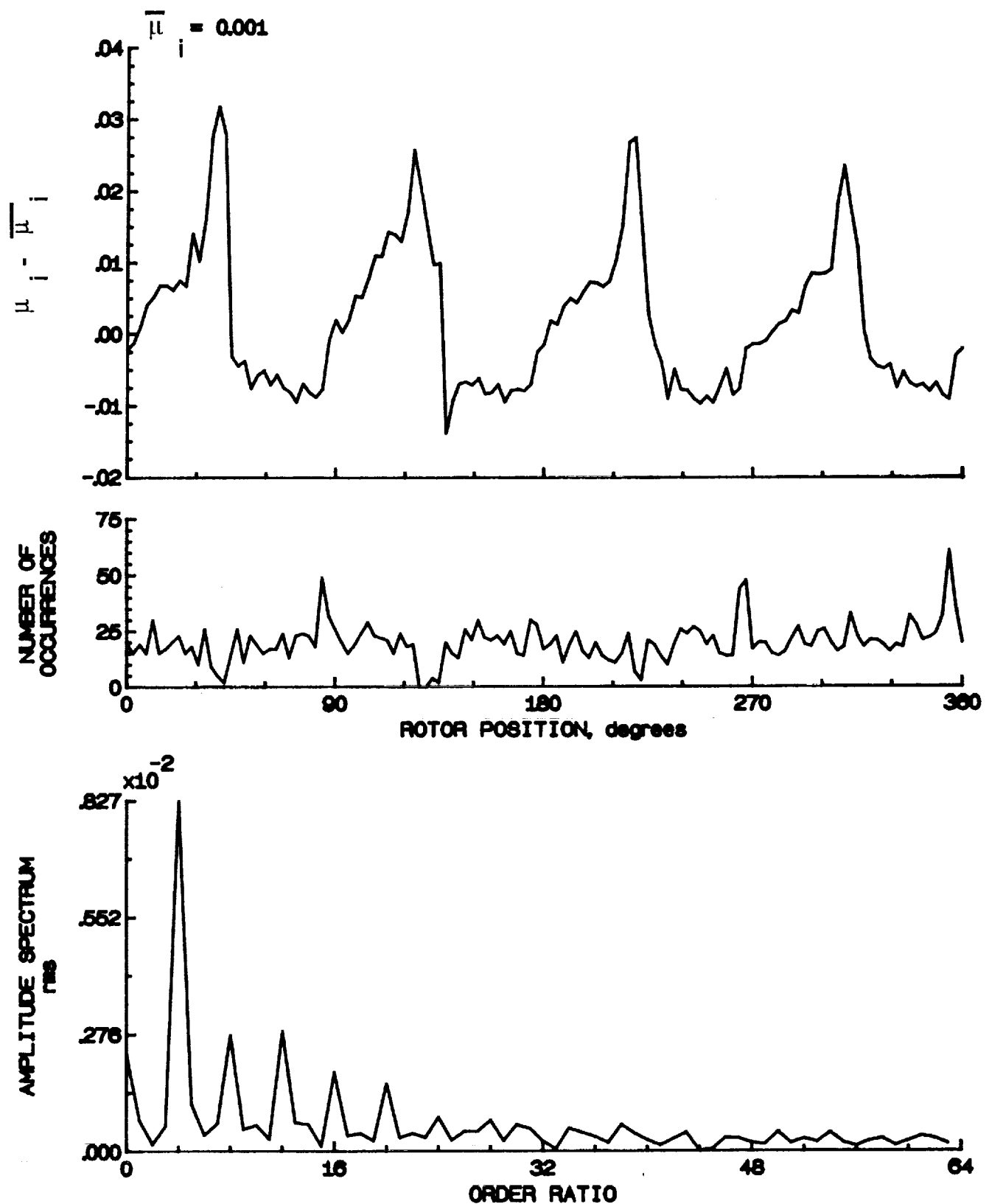


Figure 109.- Induced inflow velocity measured at 180 degrees and r/R of 0.82.

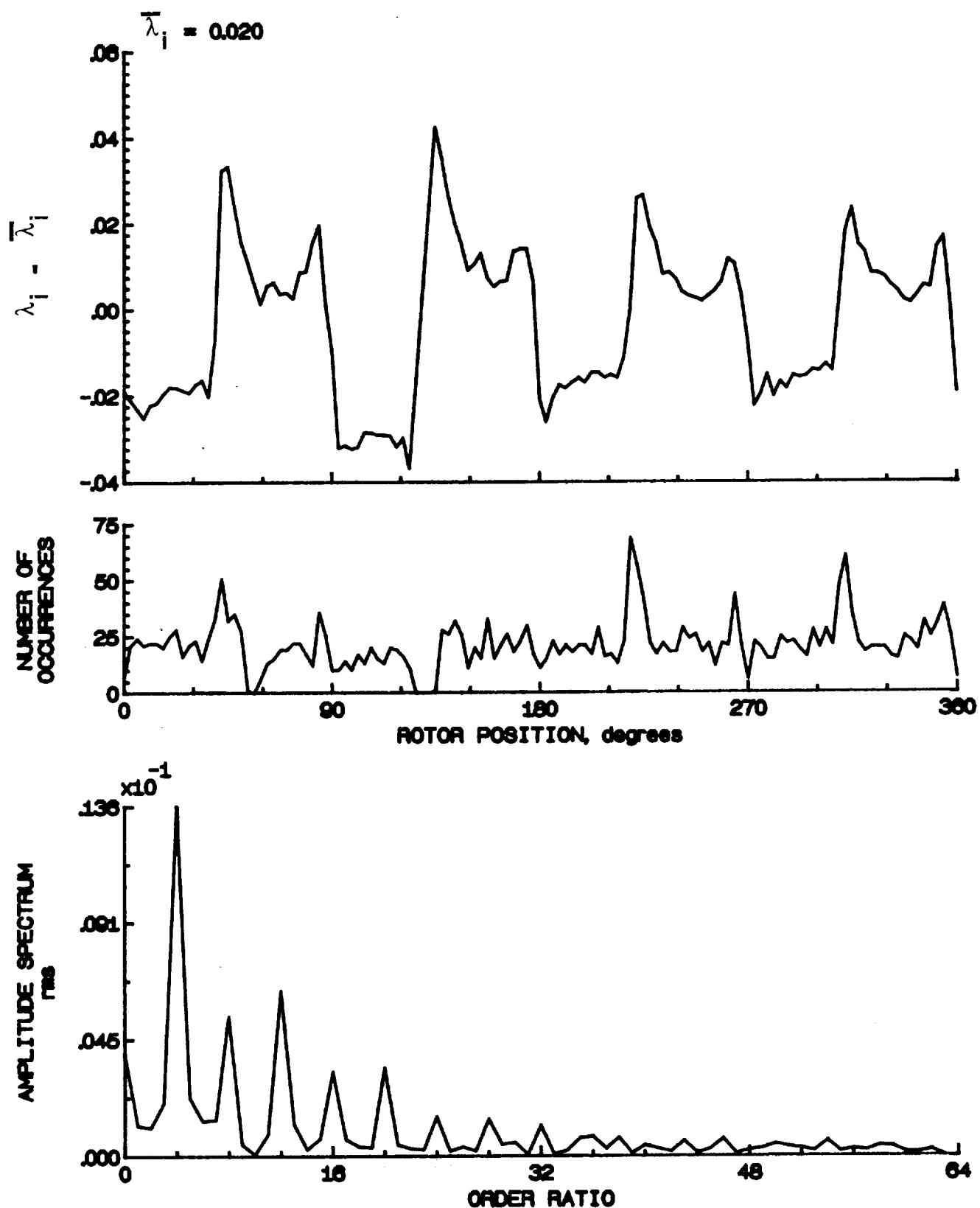


Figure 100.- Concluded.

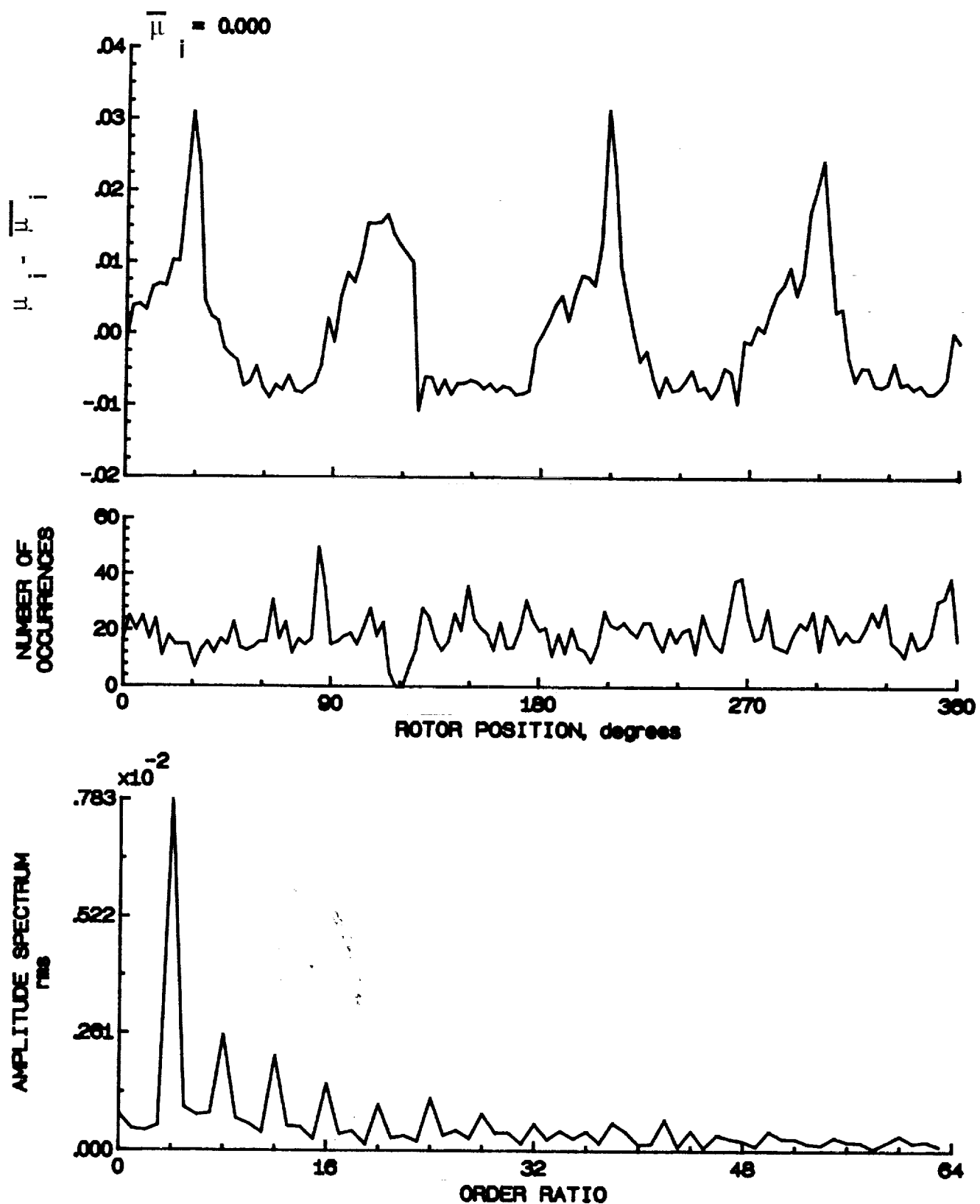


Figure 110.- Induced inflow velocity measured at 180 degrees and r/R of 0.86.

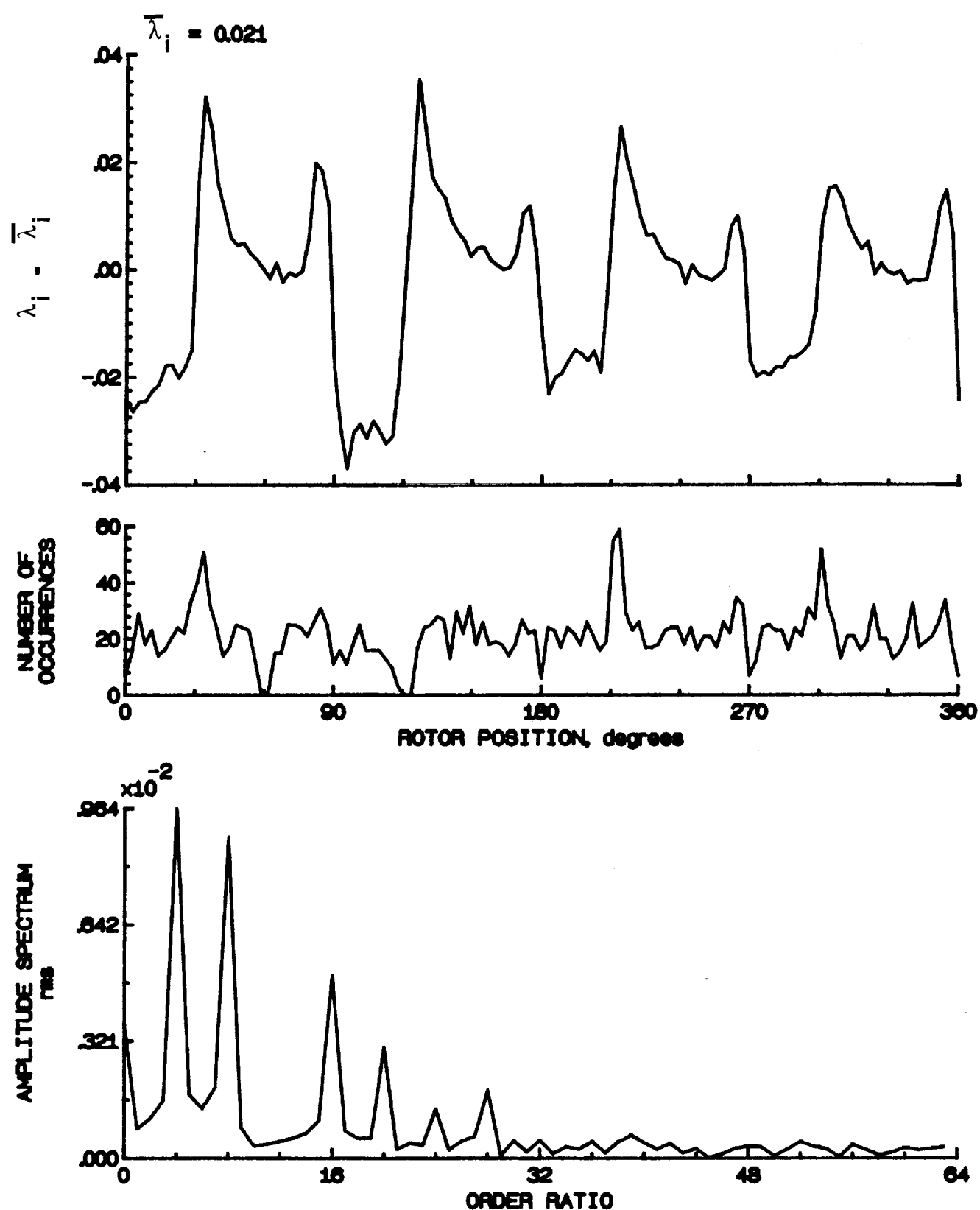


Figure 110.- Concluded.

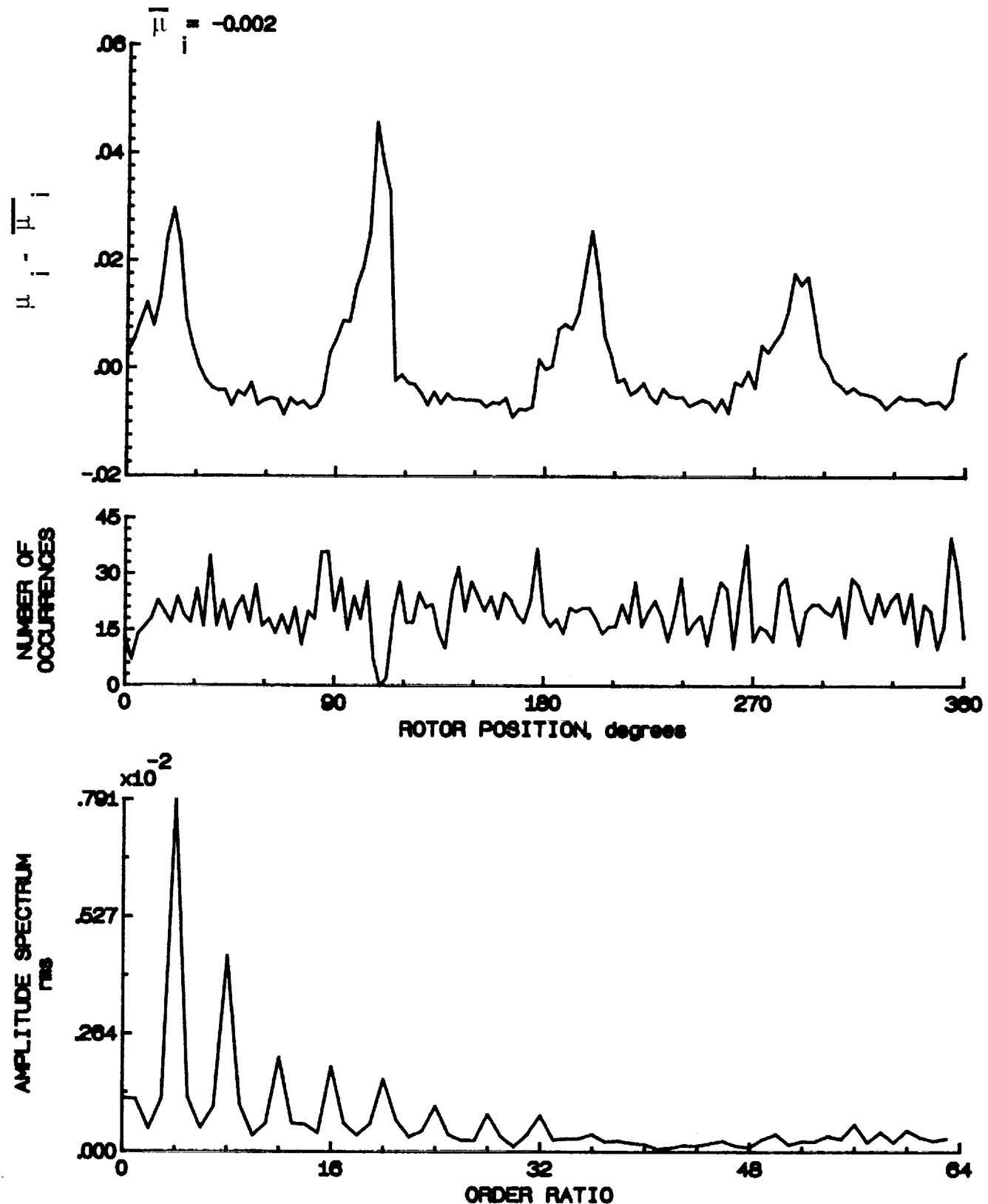


Figure iii.- Induced inflow velocity measured at 180 degrees and r/R of 0.90.

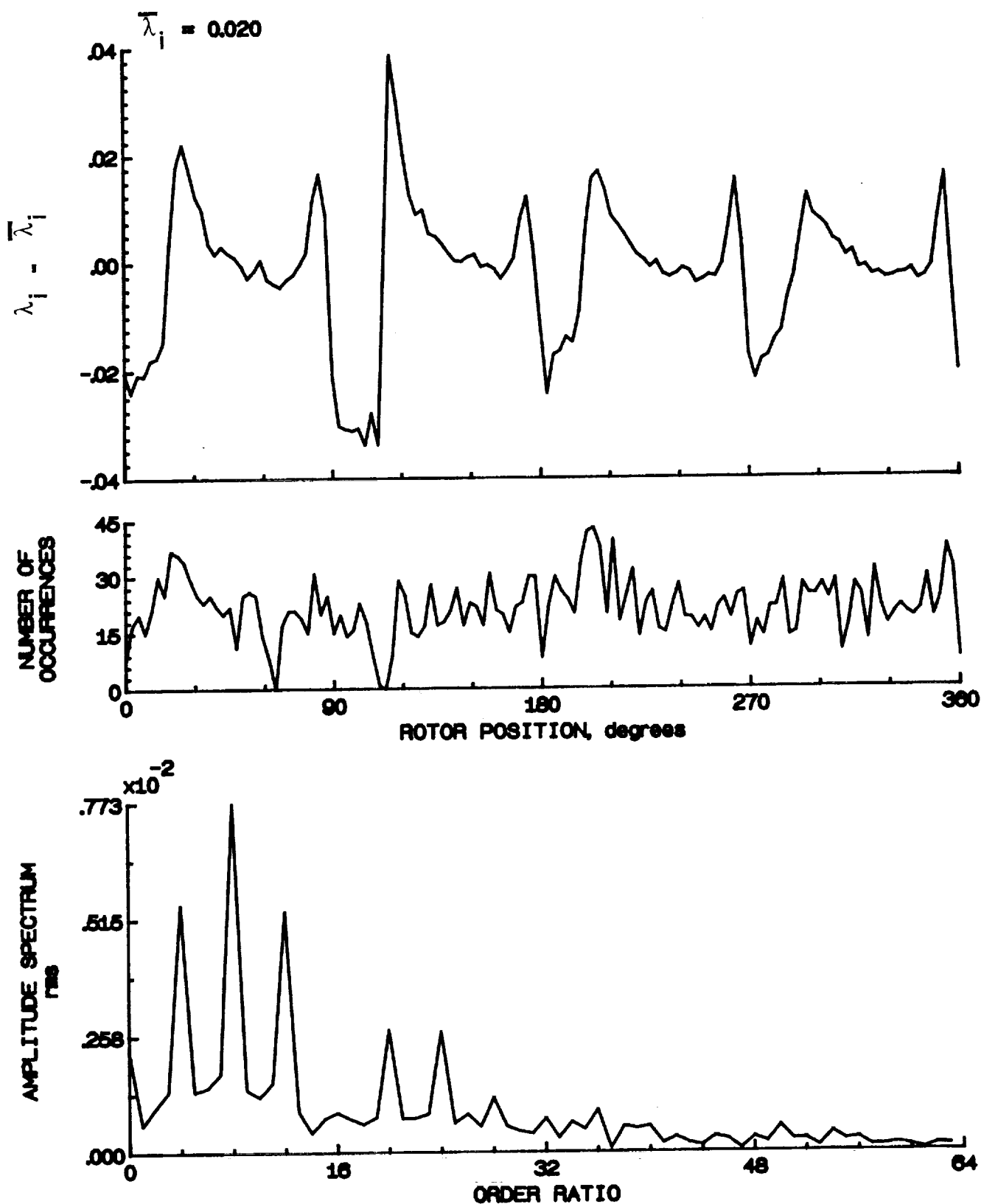


Figure 111.- Concluded.

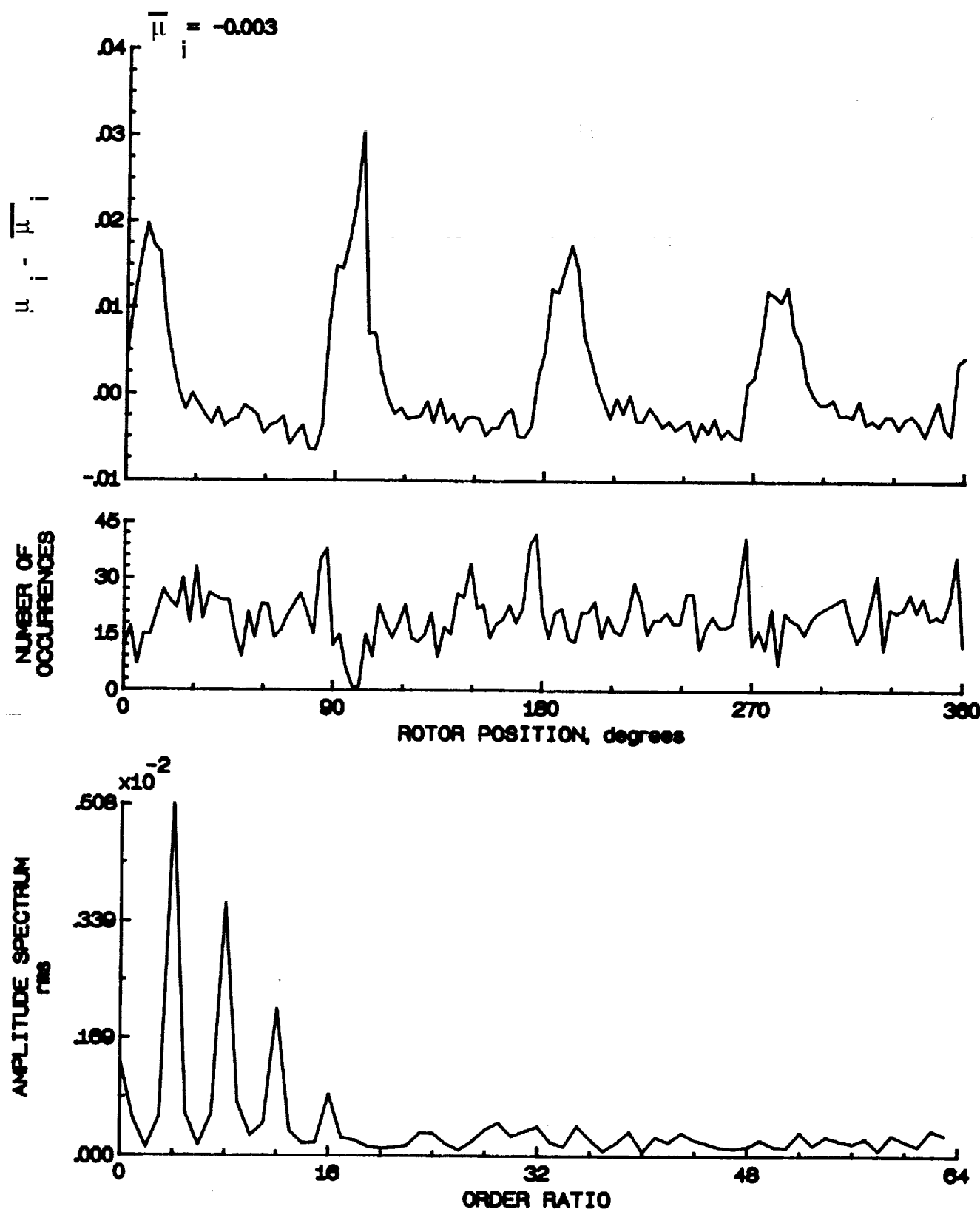


Figure 112.- Induced inflow velocity measured at 180 degrees and r/R of 0.94.

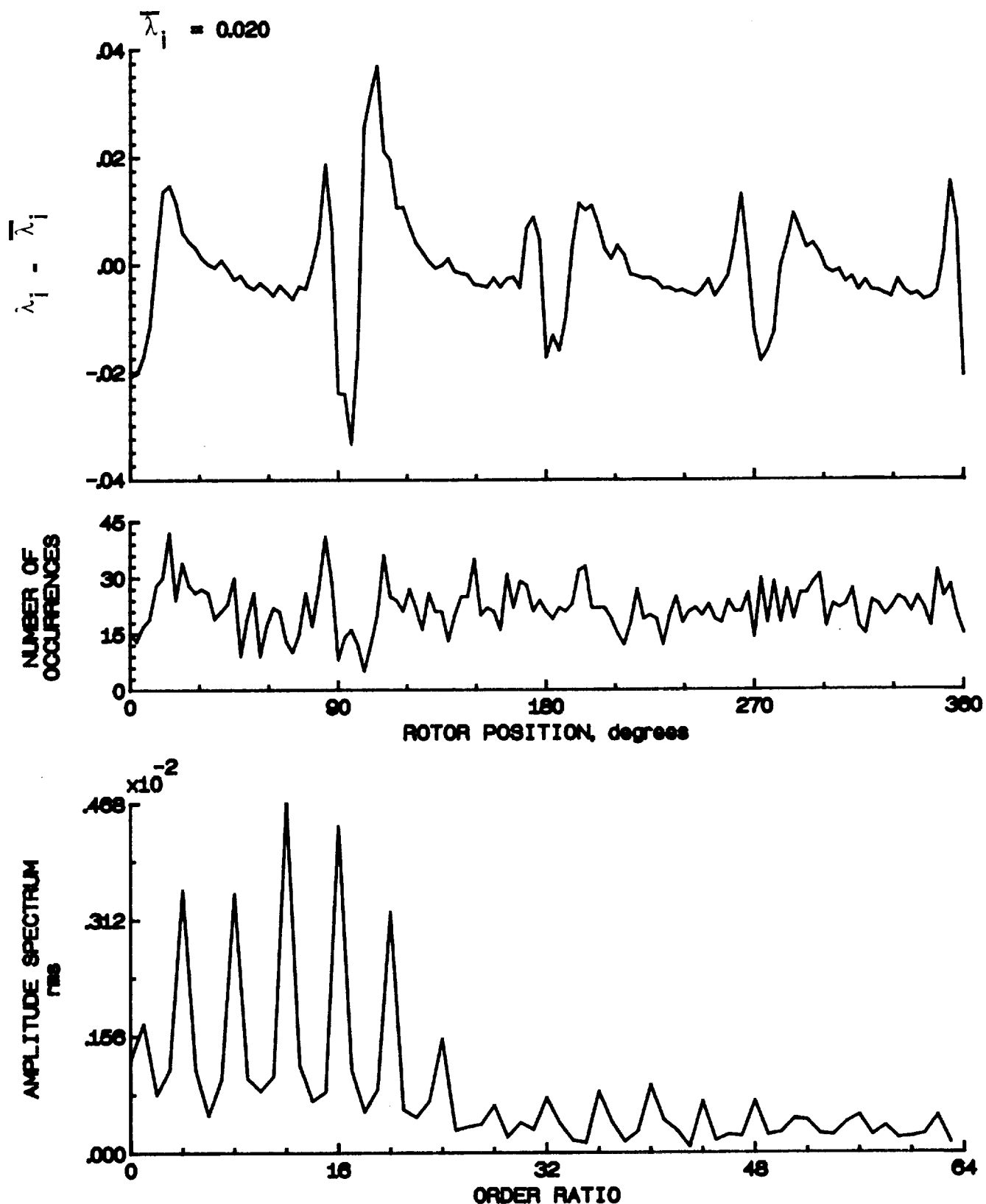


Figure 112.- Concluded.

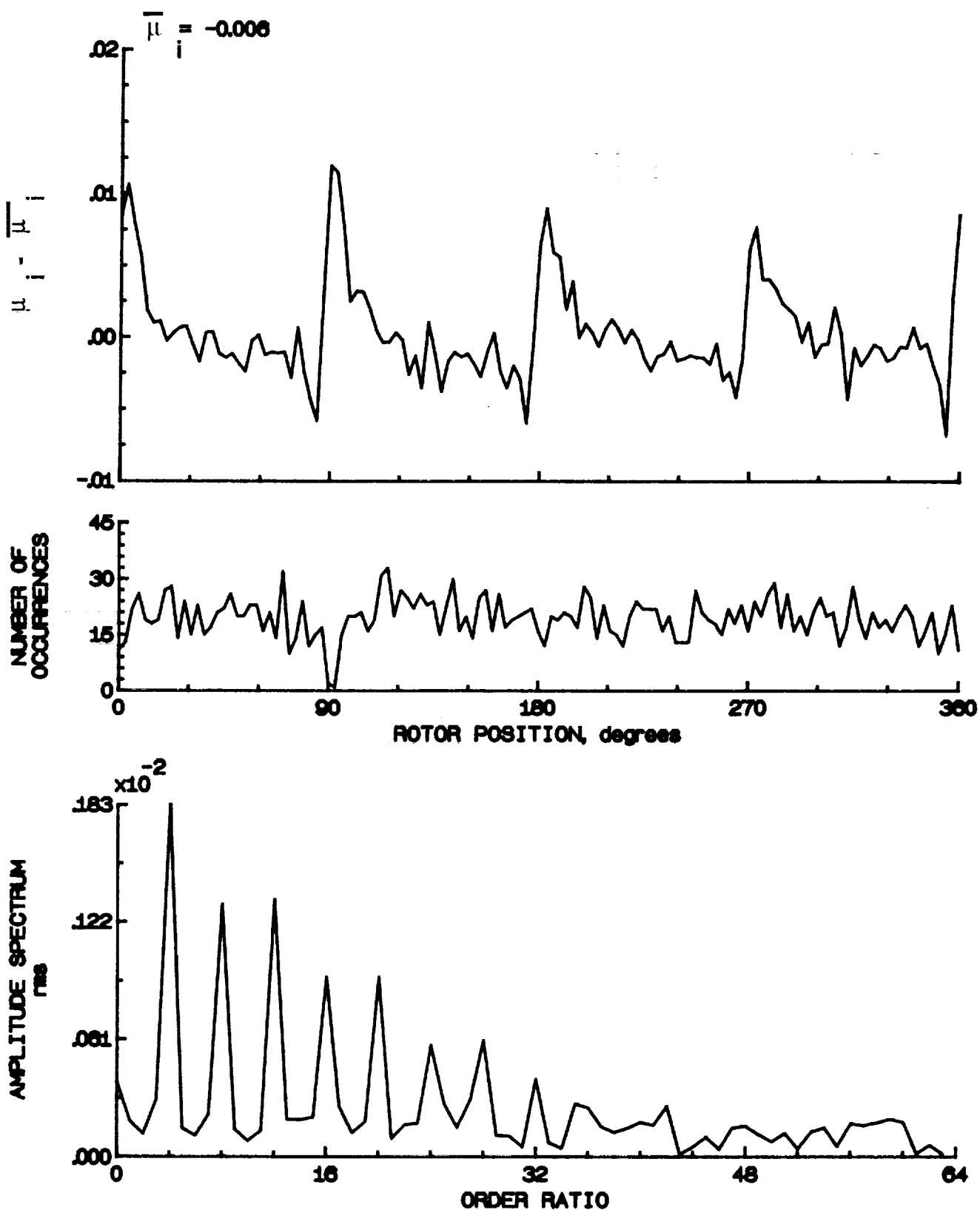


Figure 113.- Induced inflow velocity measured at 180 degrees and r/R of 0.96.

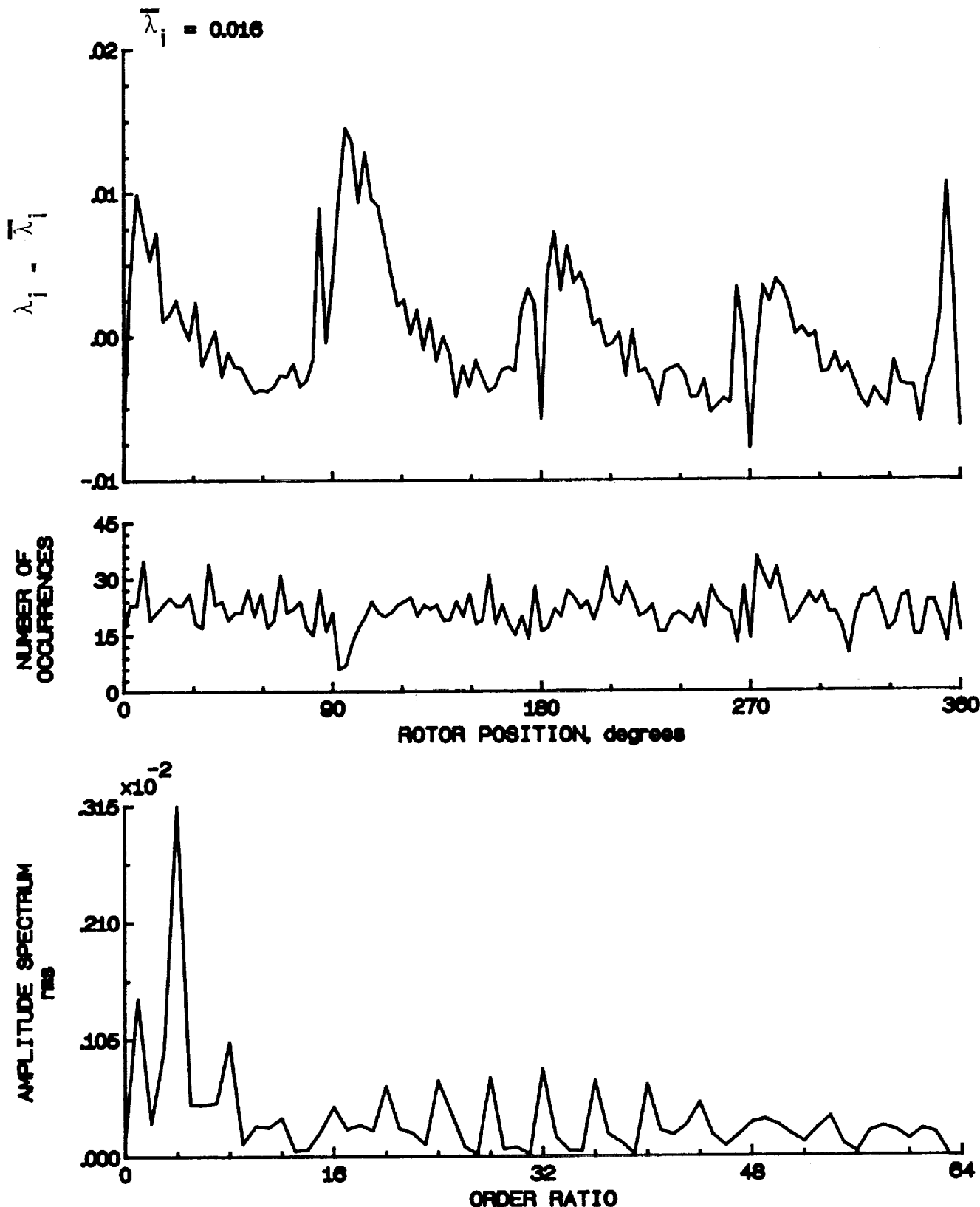


Figure 113.- Concluded.

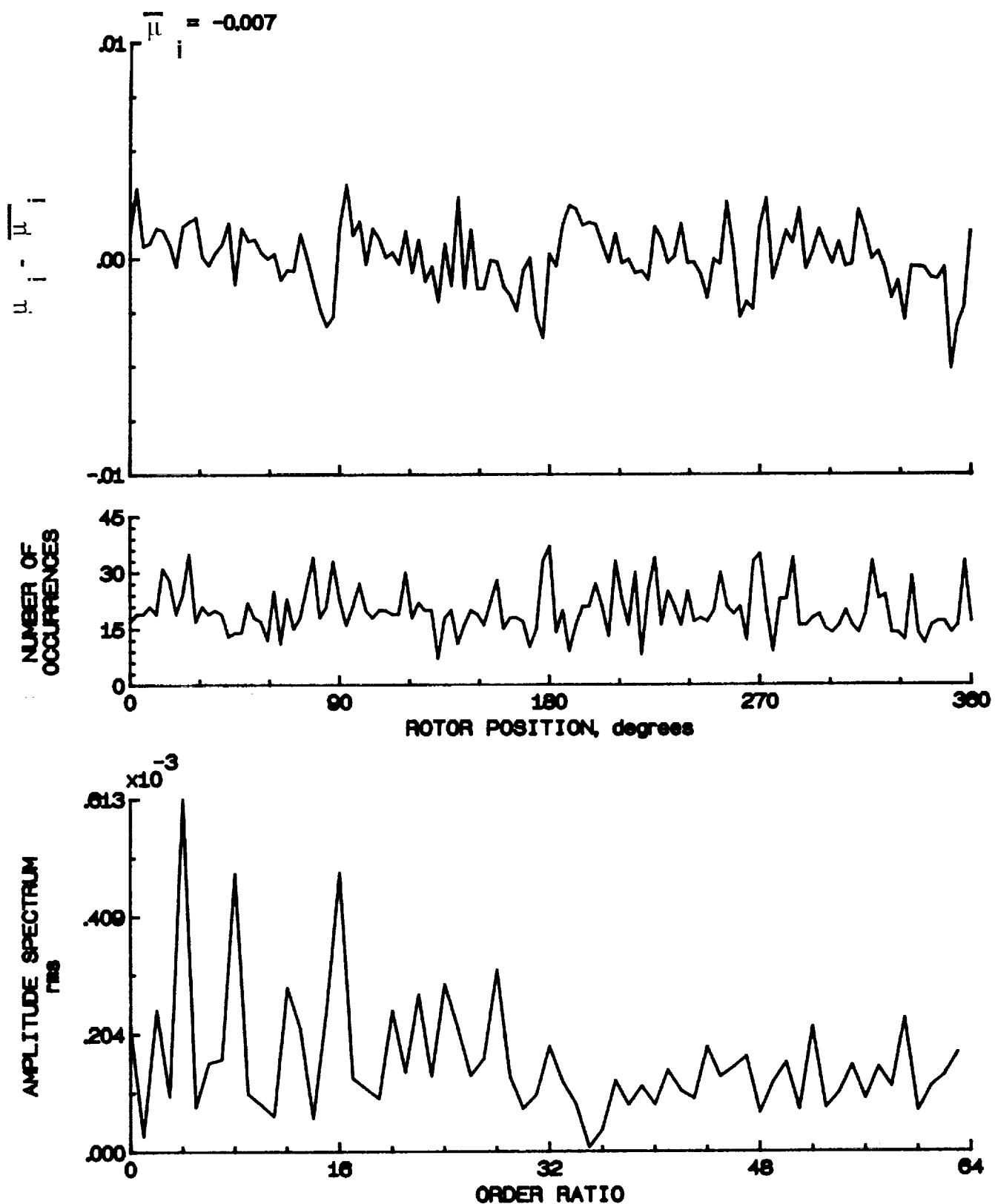


Figure 114.- Induced inflow velocity measured at 180 degrees and r/R of 1.02.

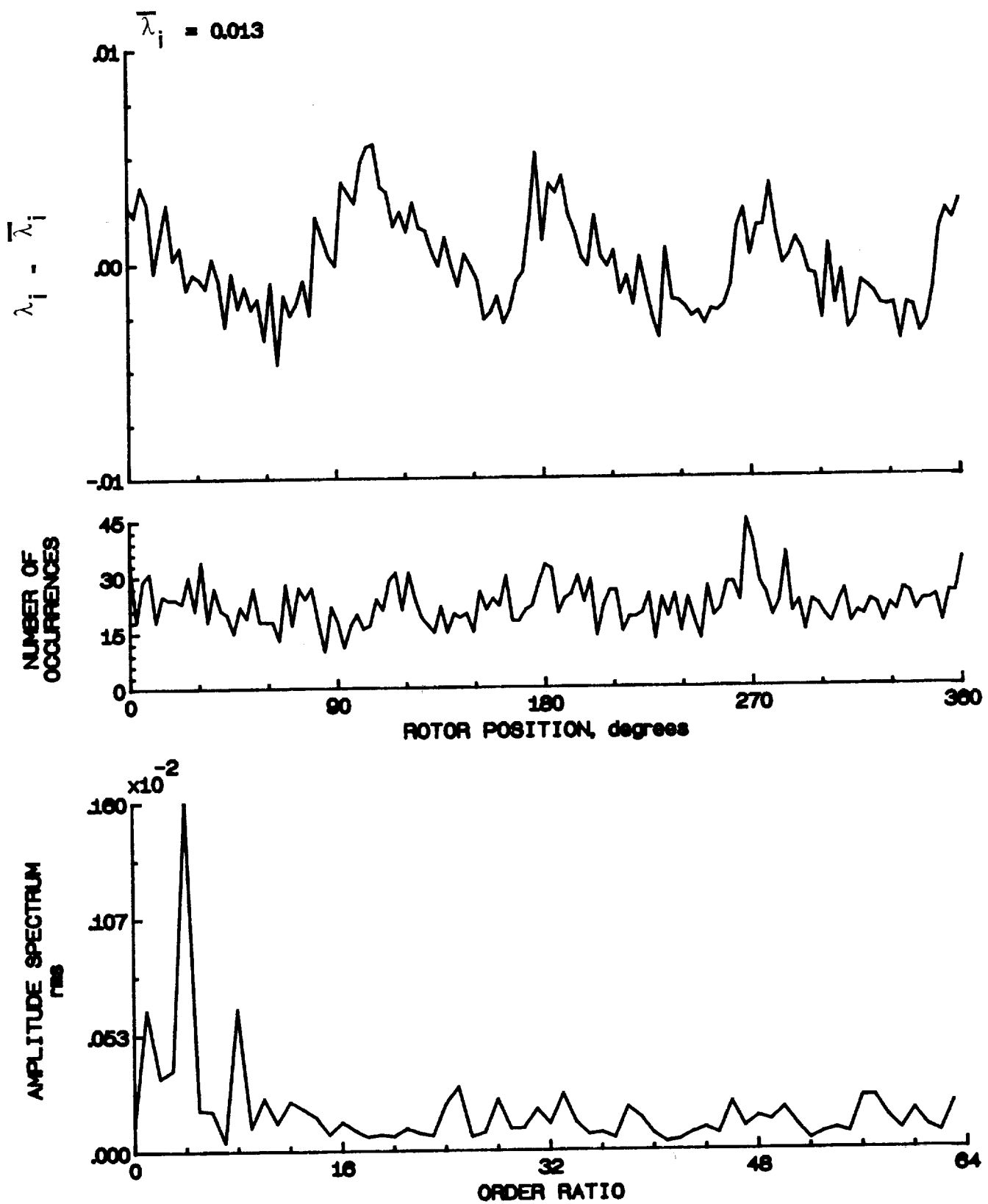


Figure 114.- Concluded.

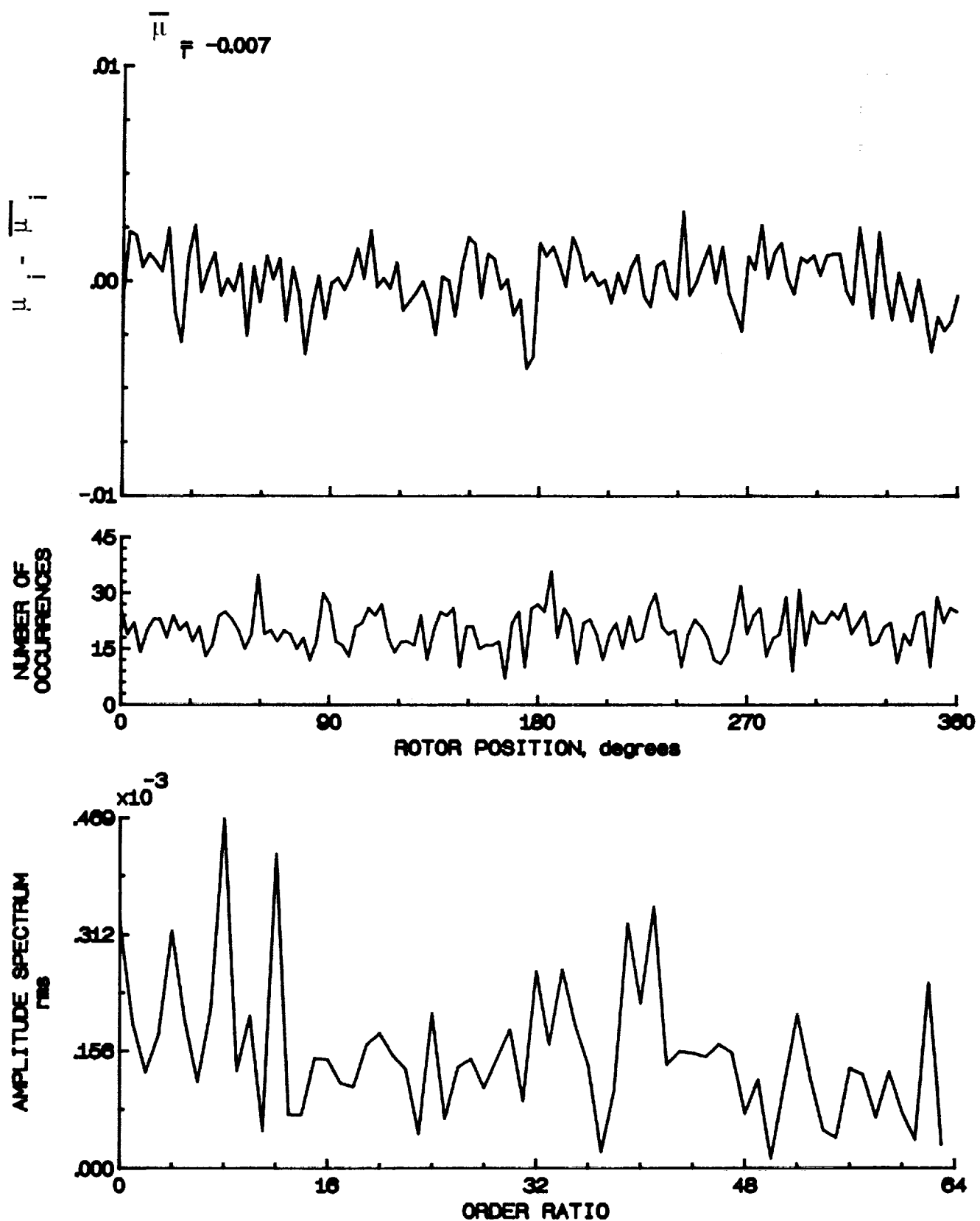


Figure 115.- Induced inflow velocity measured at 180 degrees and r/R of 1.04.

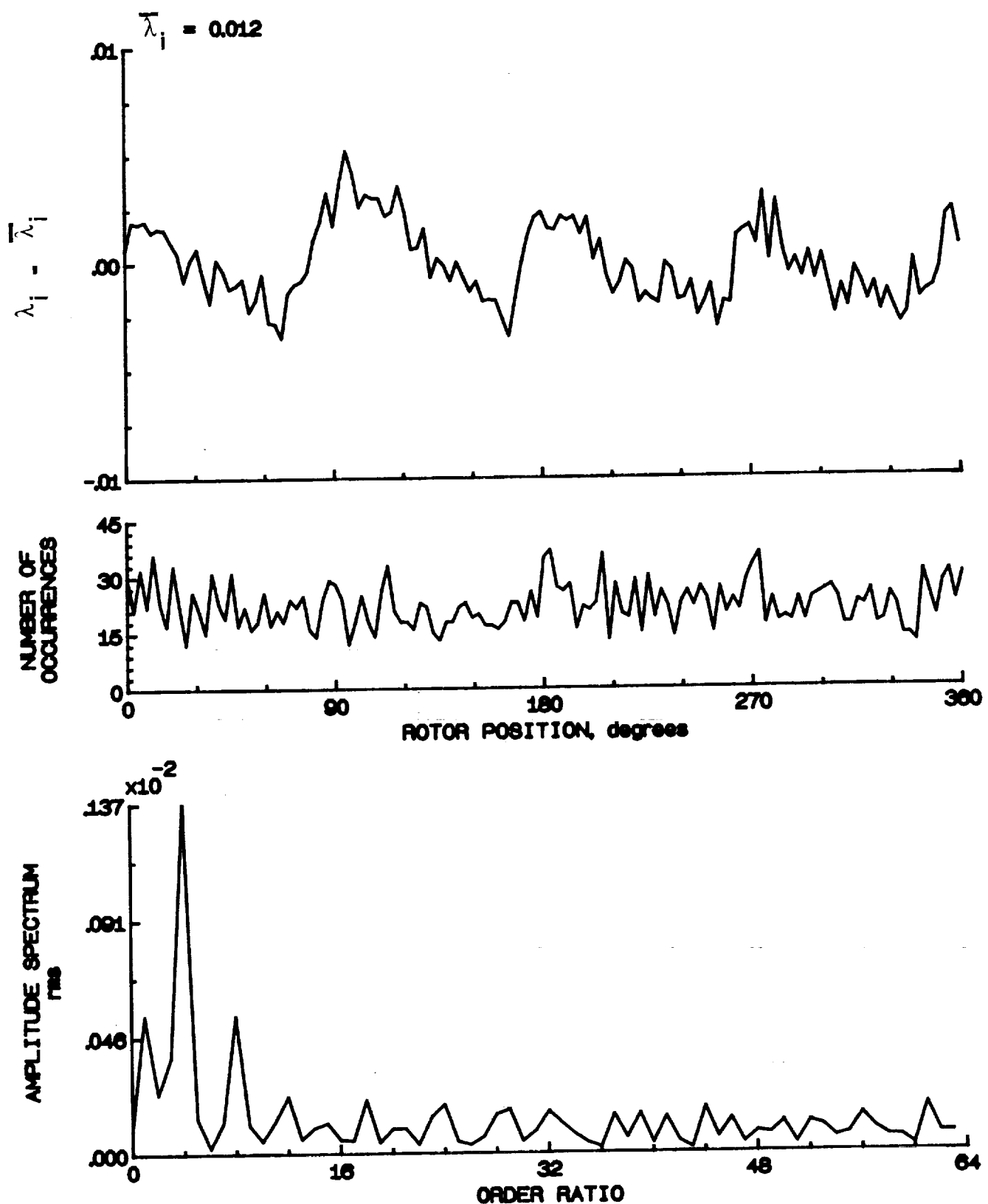


Figure 115.- Concluded.

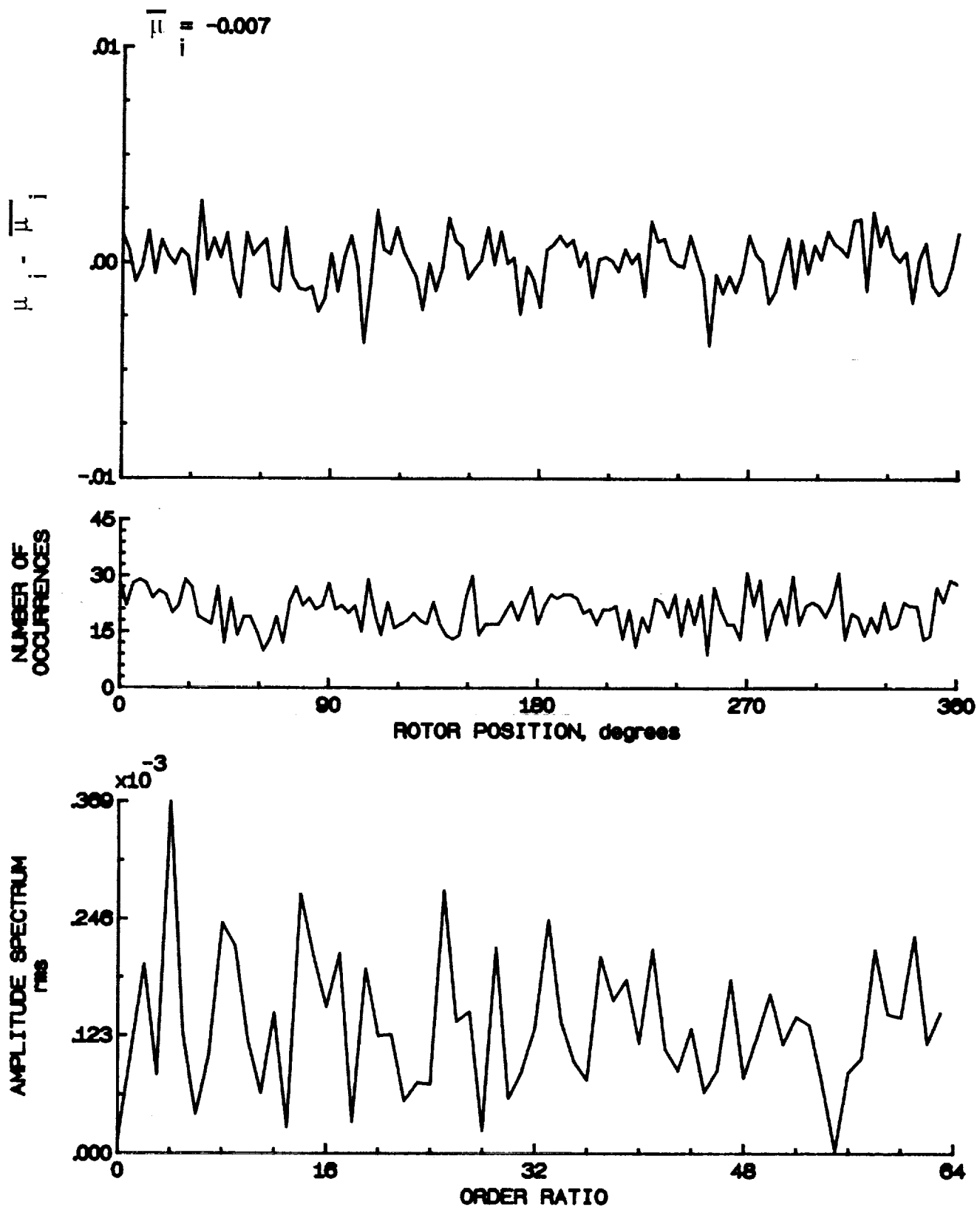


Figure 116.- Induced inflow velocity measured at 180 degrees and r/R of 1.10.

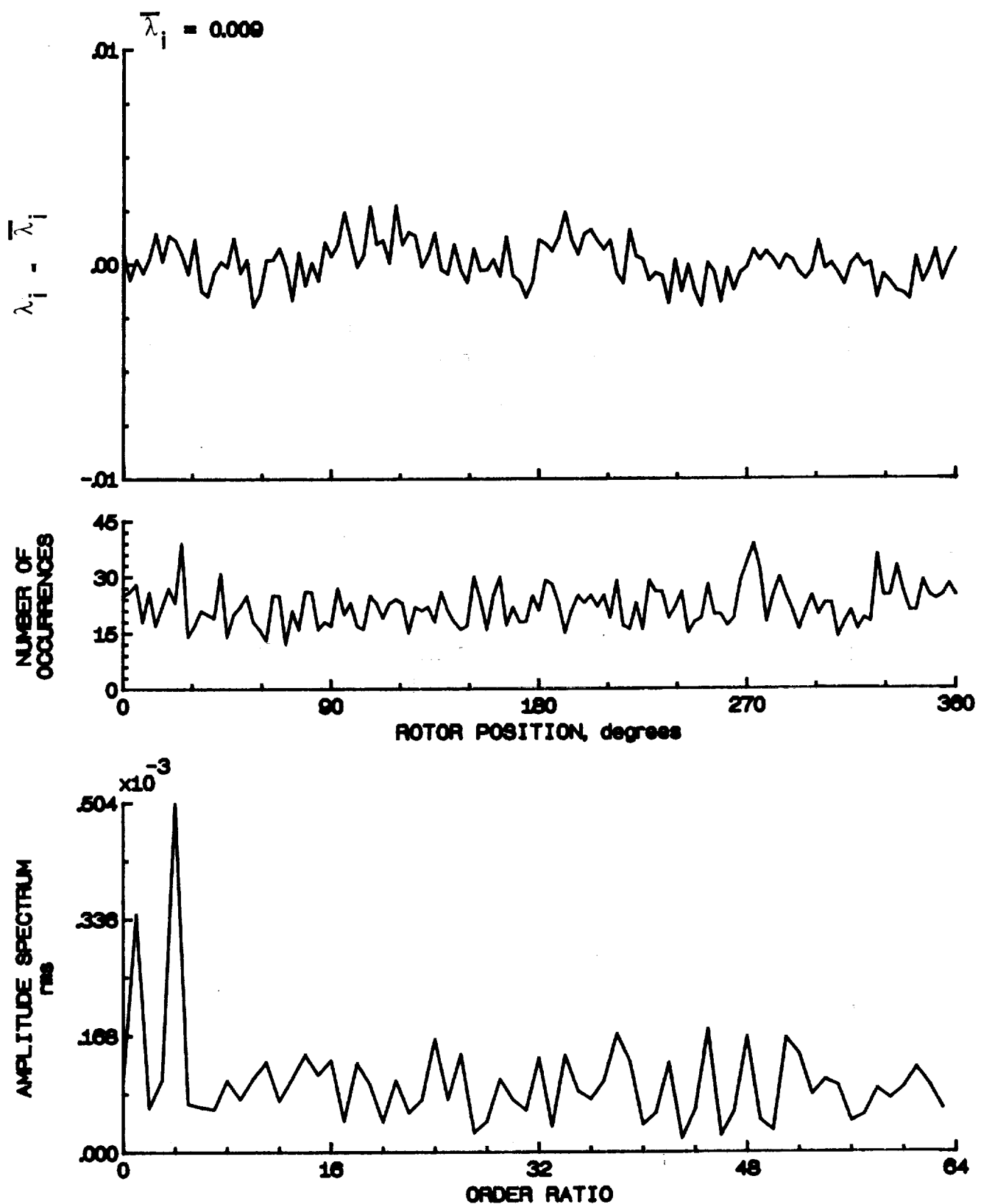


Figure 116.- Concluded.

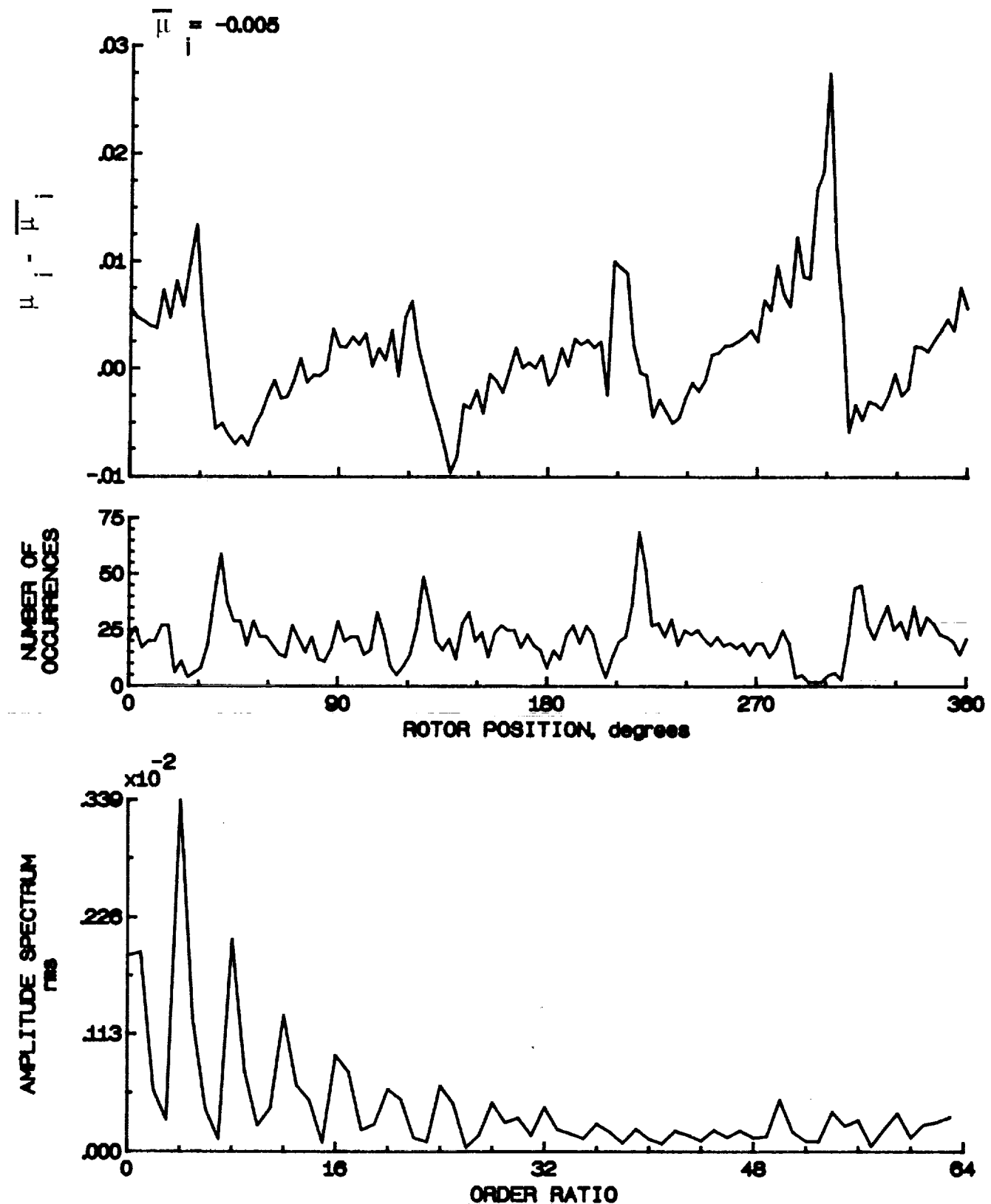


Figure 117.- Induced inflow velocity measured at 210 degrees and r/R of 0.20.

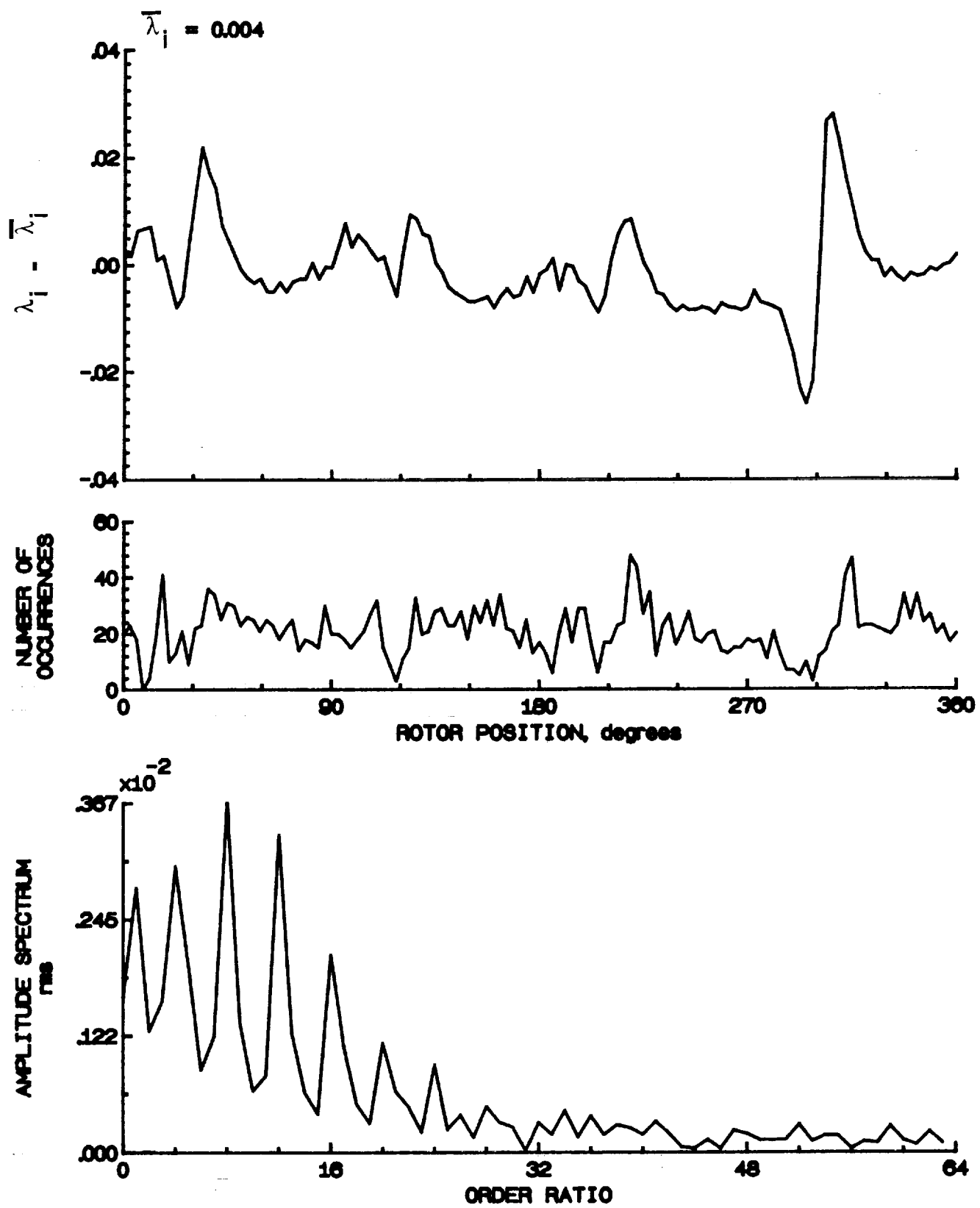


Figure 117.- Concluded.

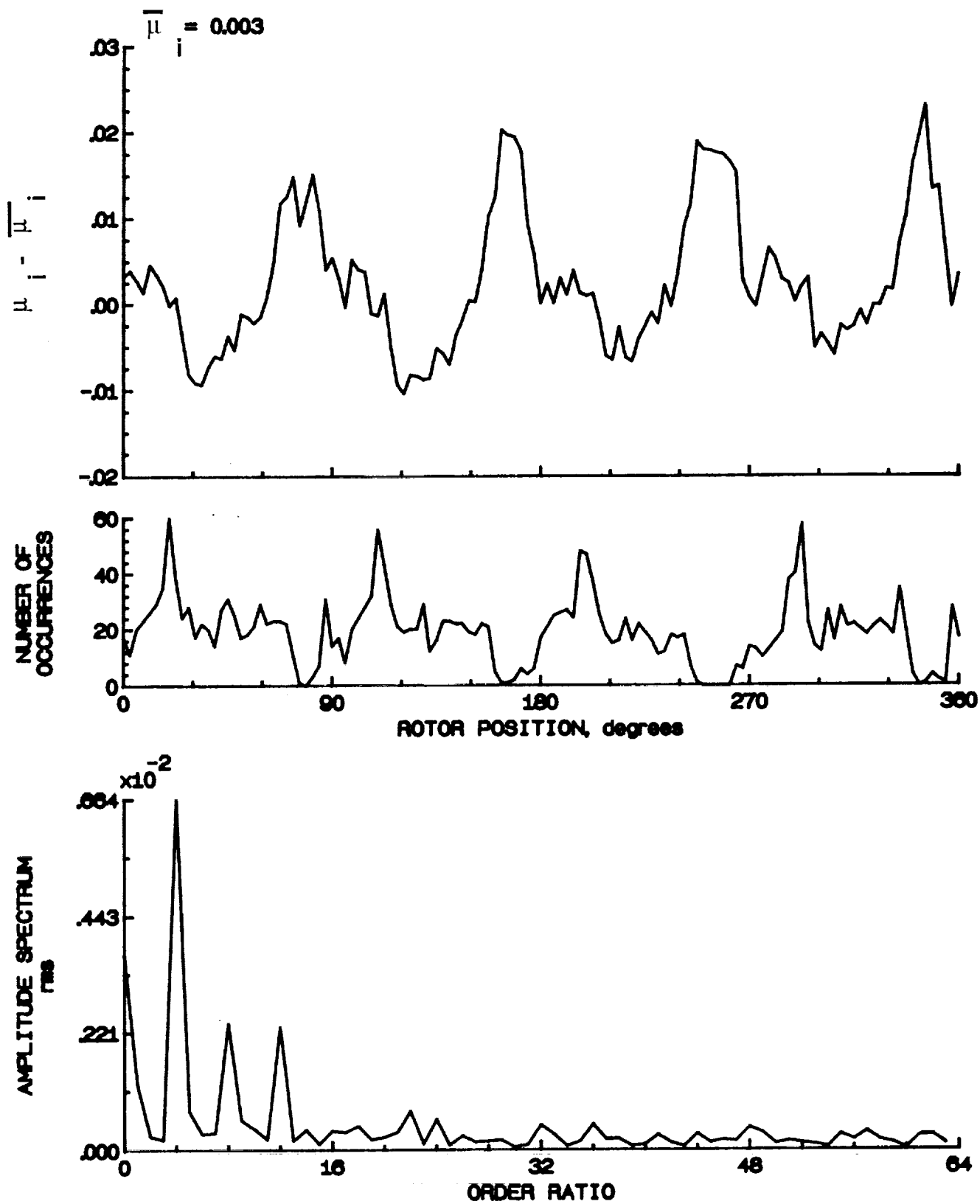


Figure 118.- Induced inflow velocity measured at 210 degrees and r/R of 0.40.

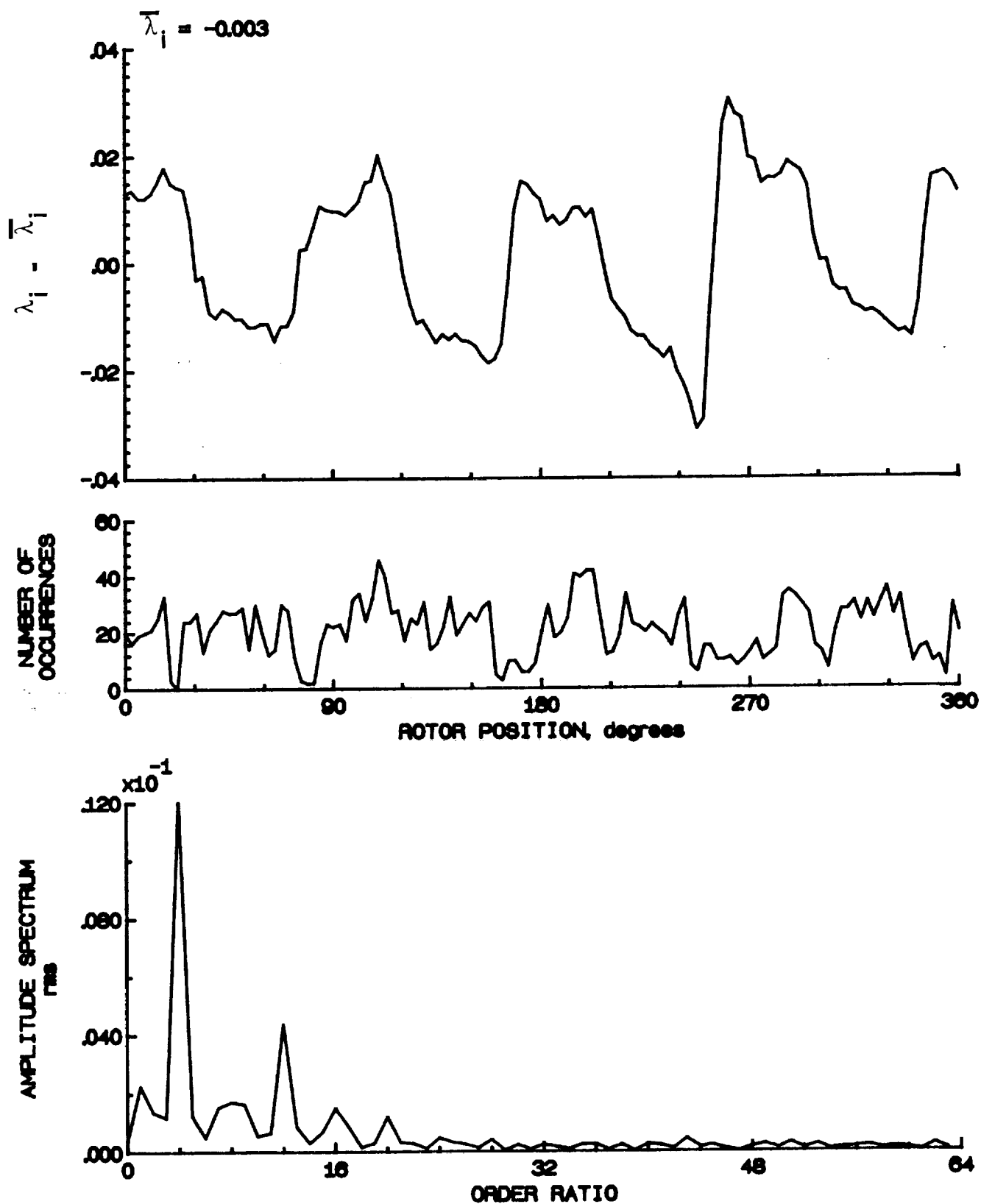


Figure 118.- Concluded.

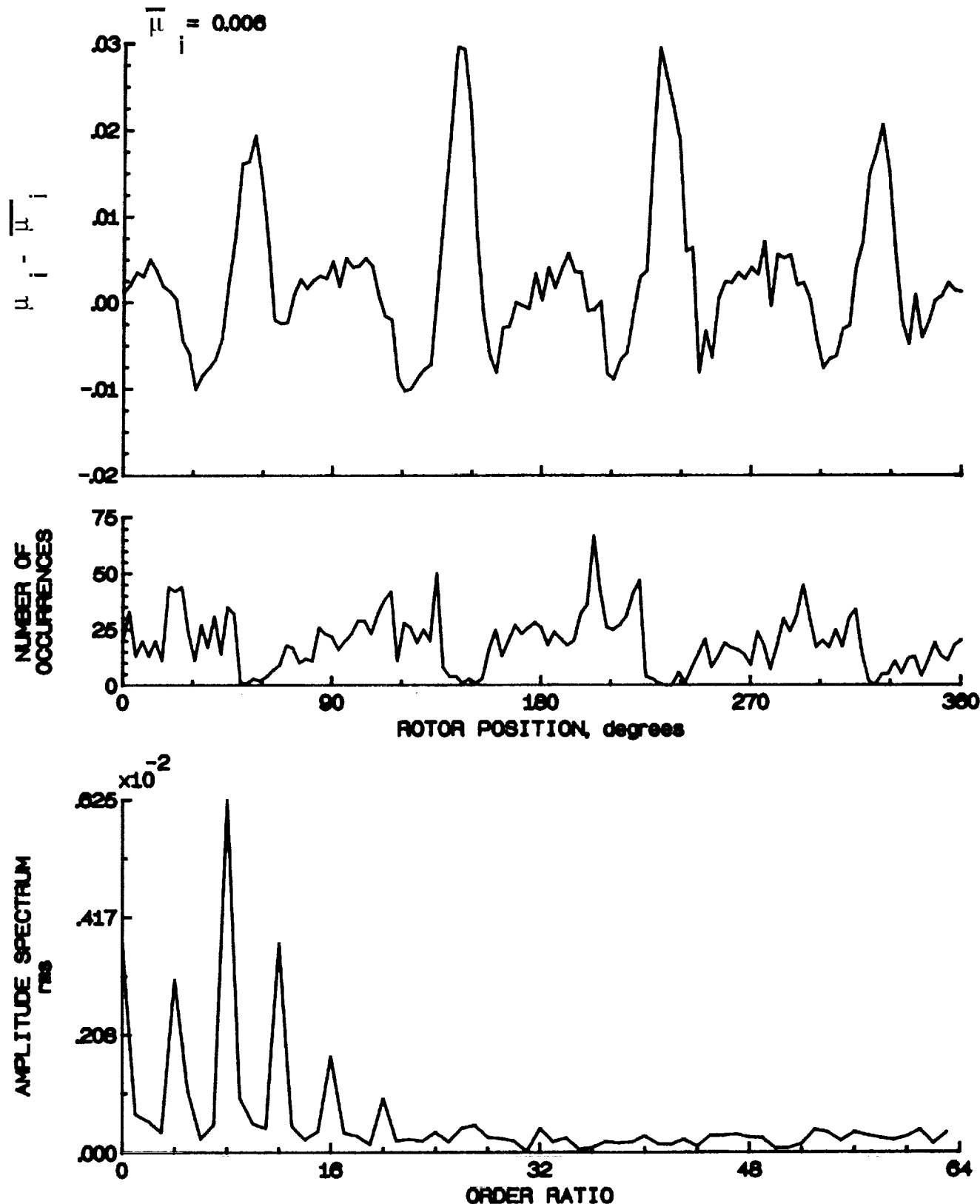


Figure 119.- Induced inflow velocity measured at 210 degrees and r/R of 0.50.

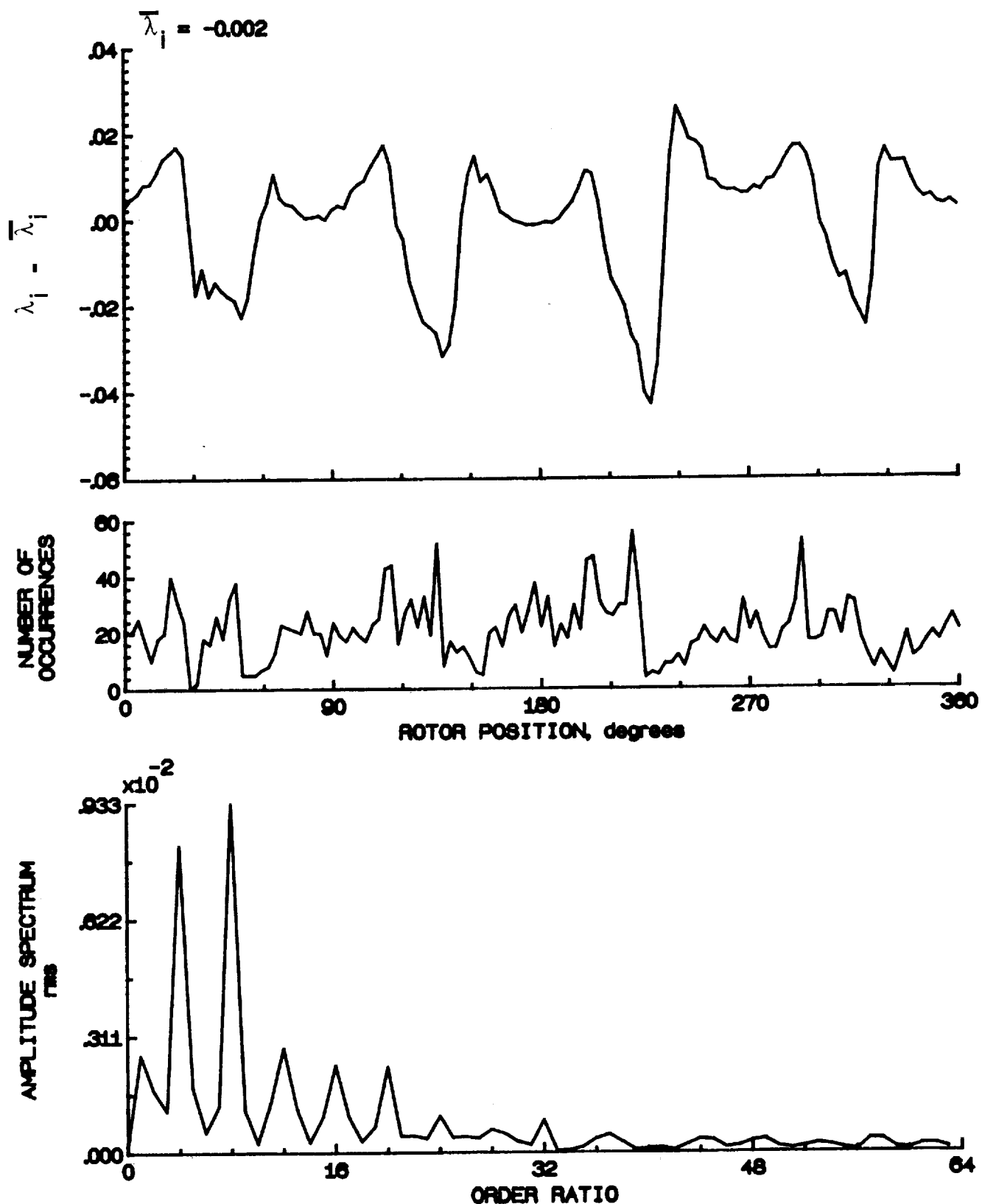


Figure 119.- Concluded.

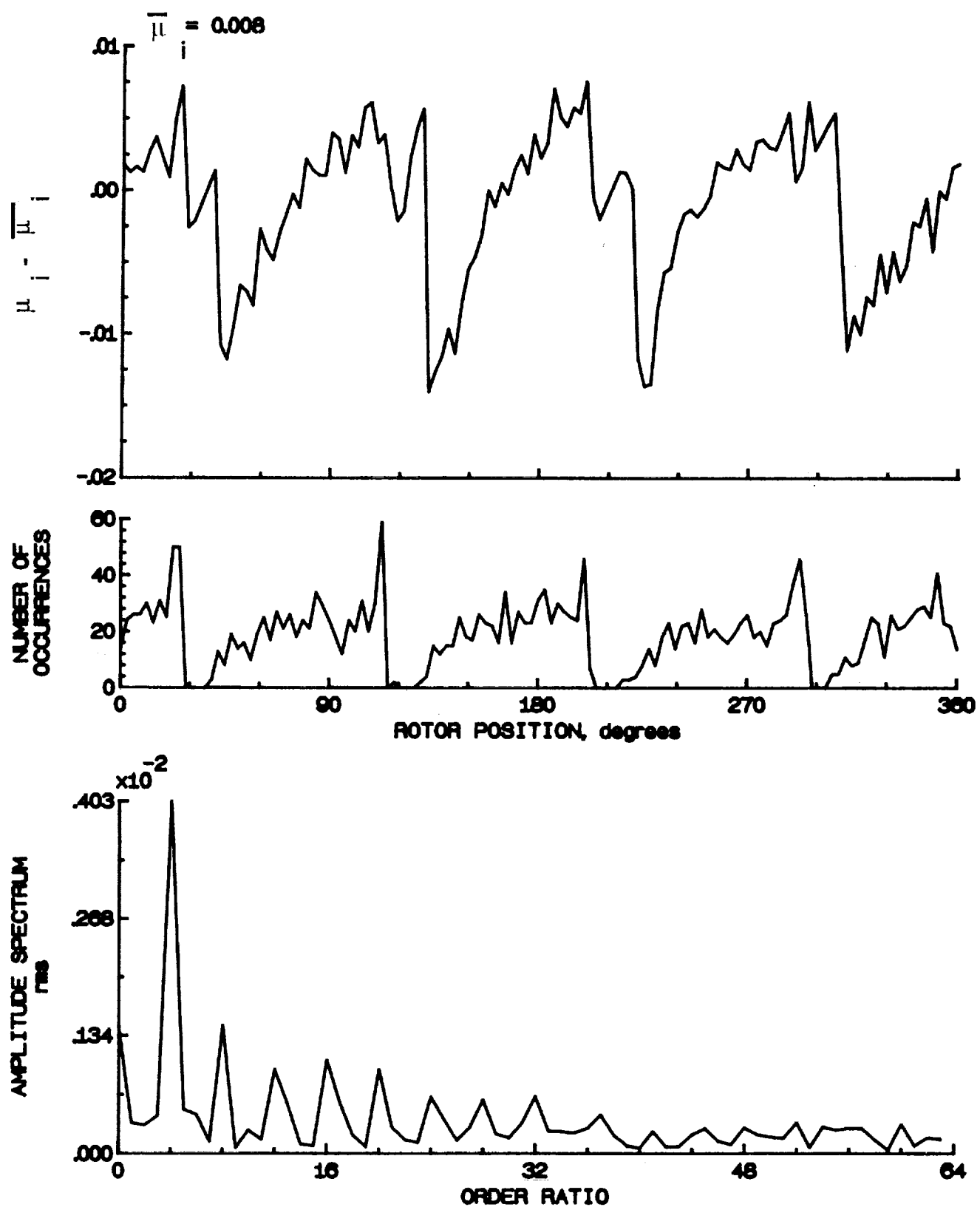


Figure 120.- Induced inflow velocity measured at 210 degrees and r/R of 0.60.

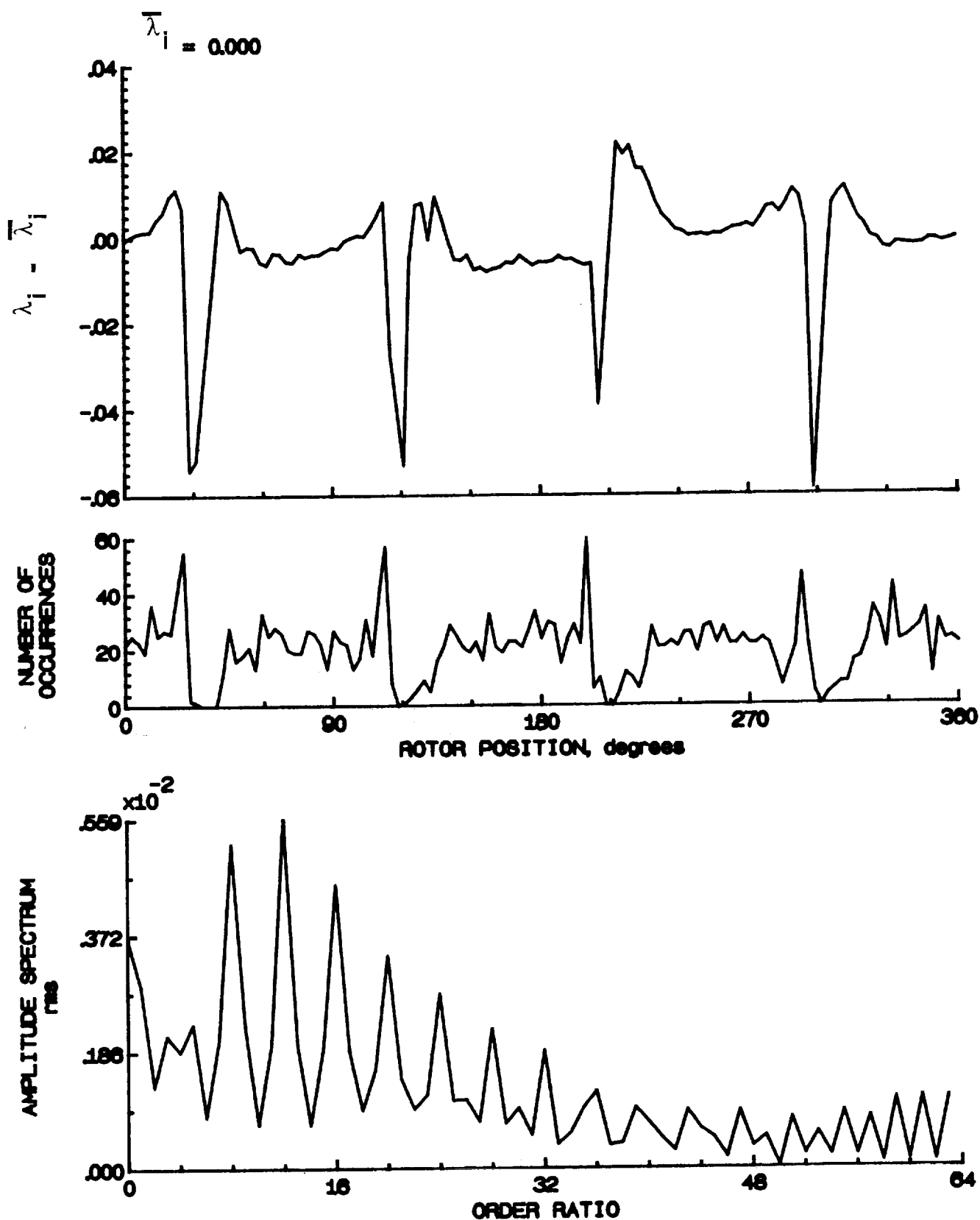


Figure 120.- Concluded.

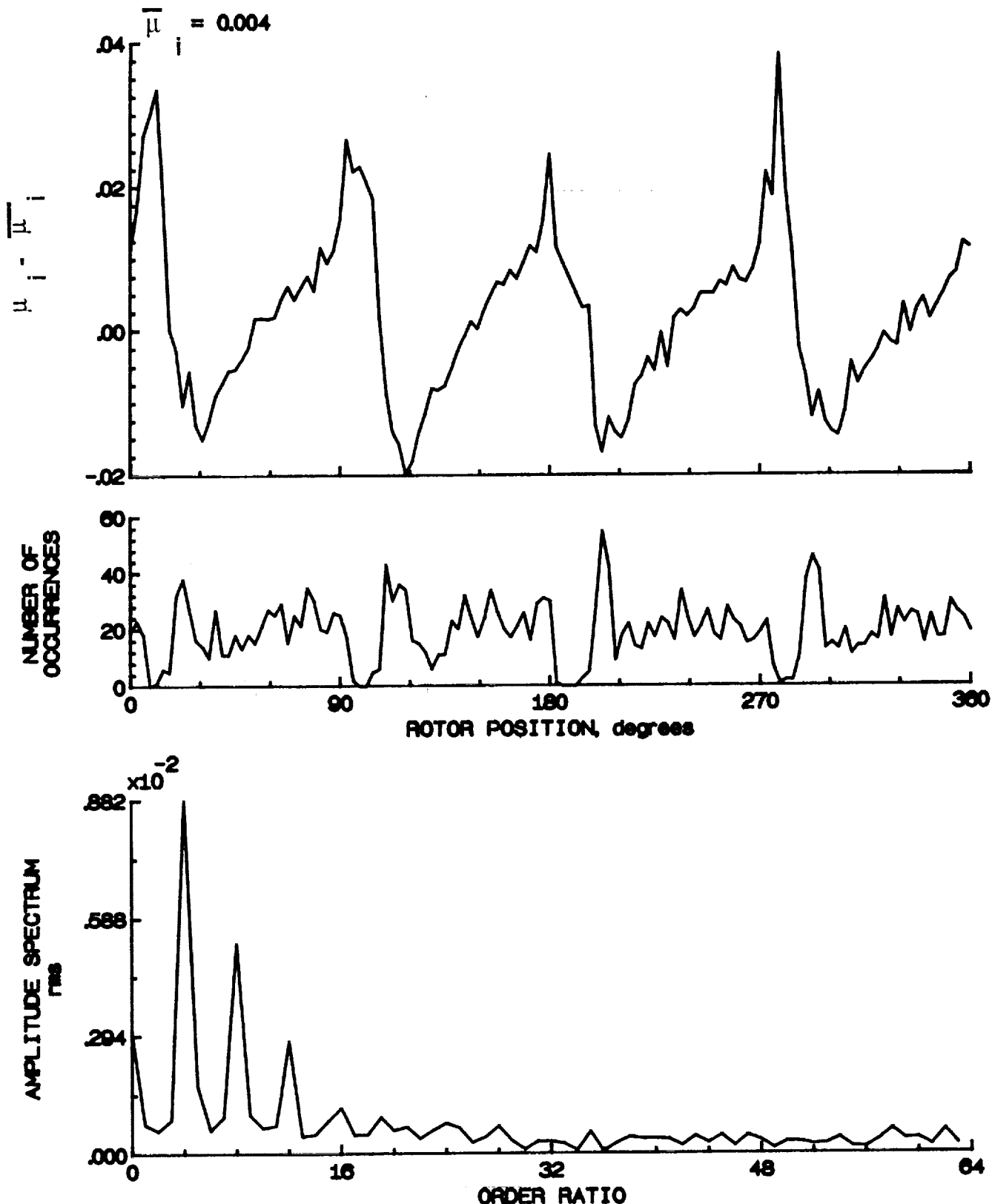


Figure 121.- Induced inflow velocity measured at 210 degrees and r/R of 0.70.

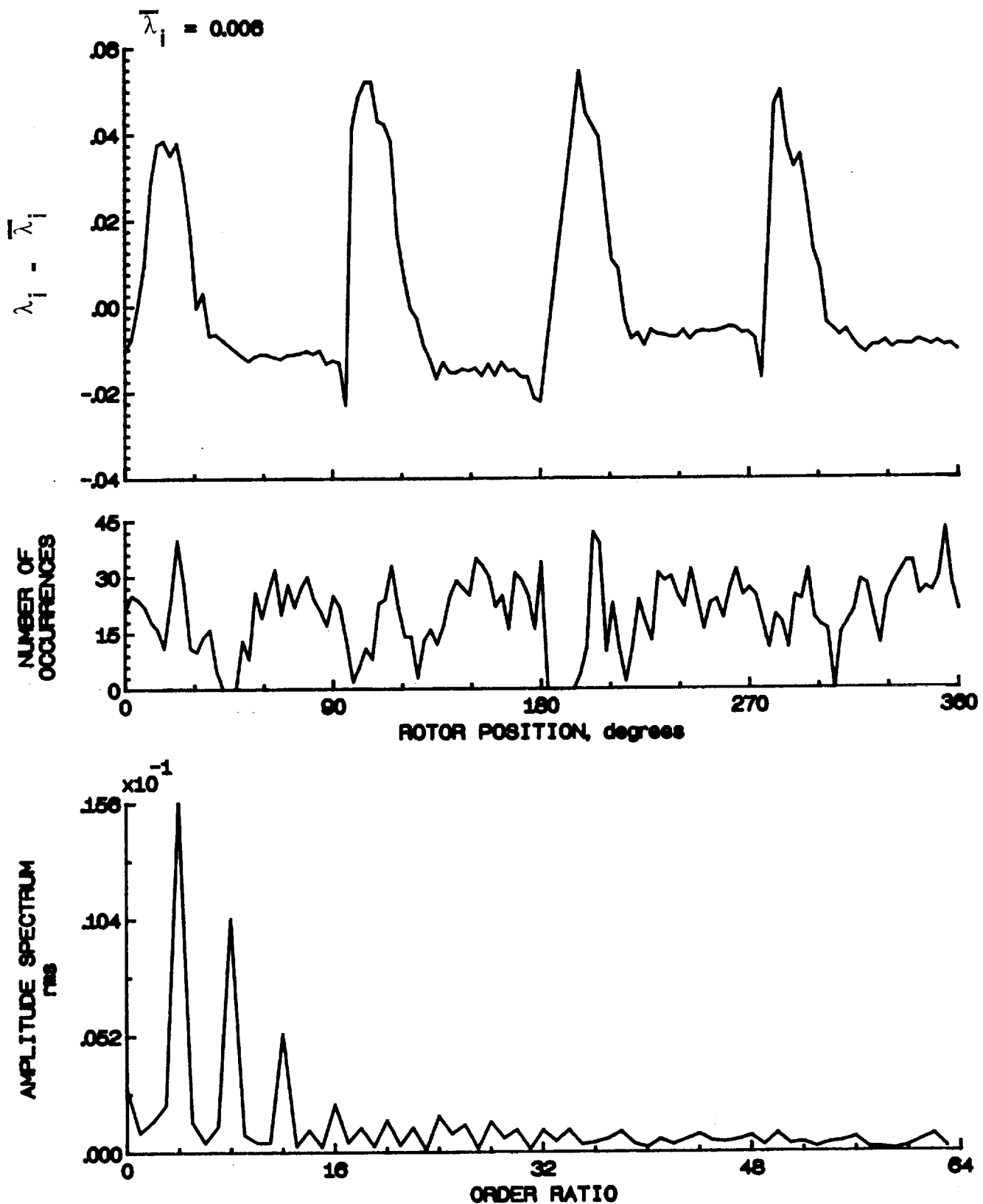


Figure 121.- Concluded.

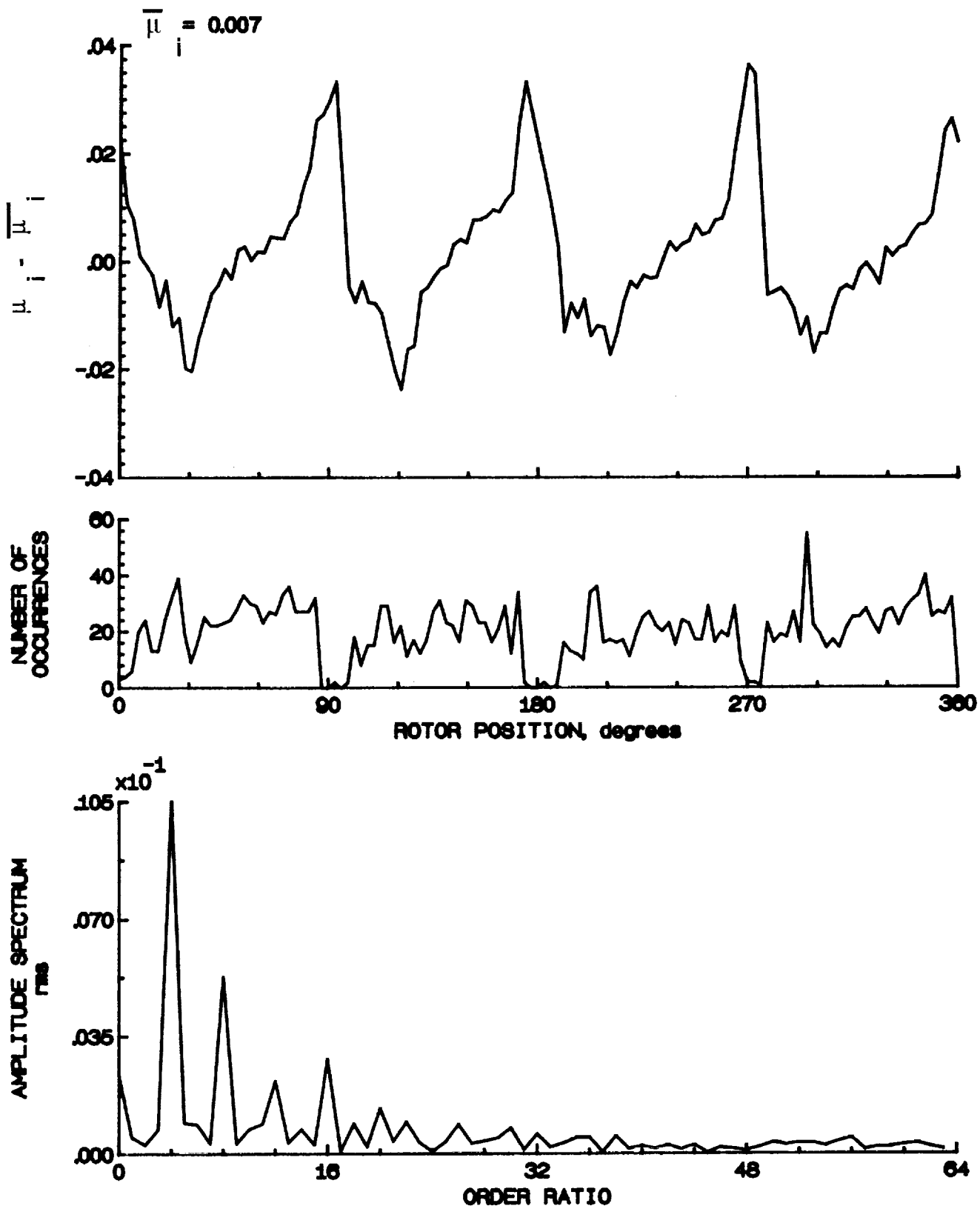


Figure 122.- Induced inflow velocity measured at 210 degrees and r/R of 0.74.

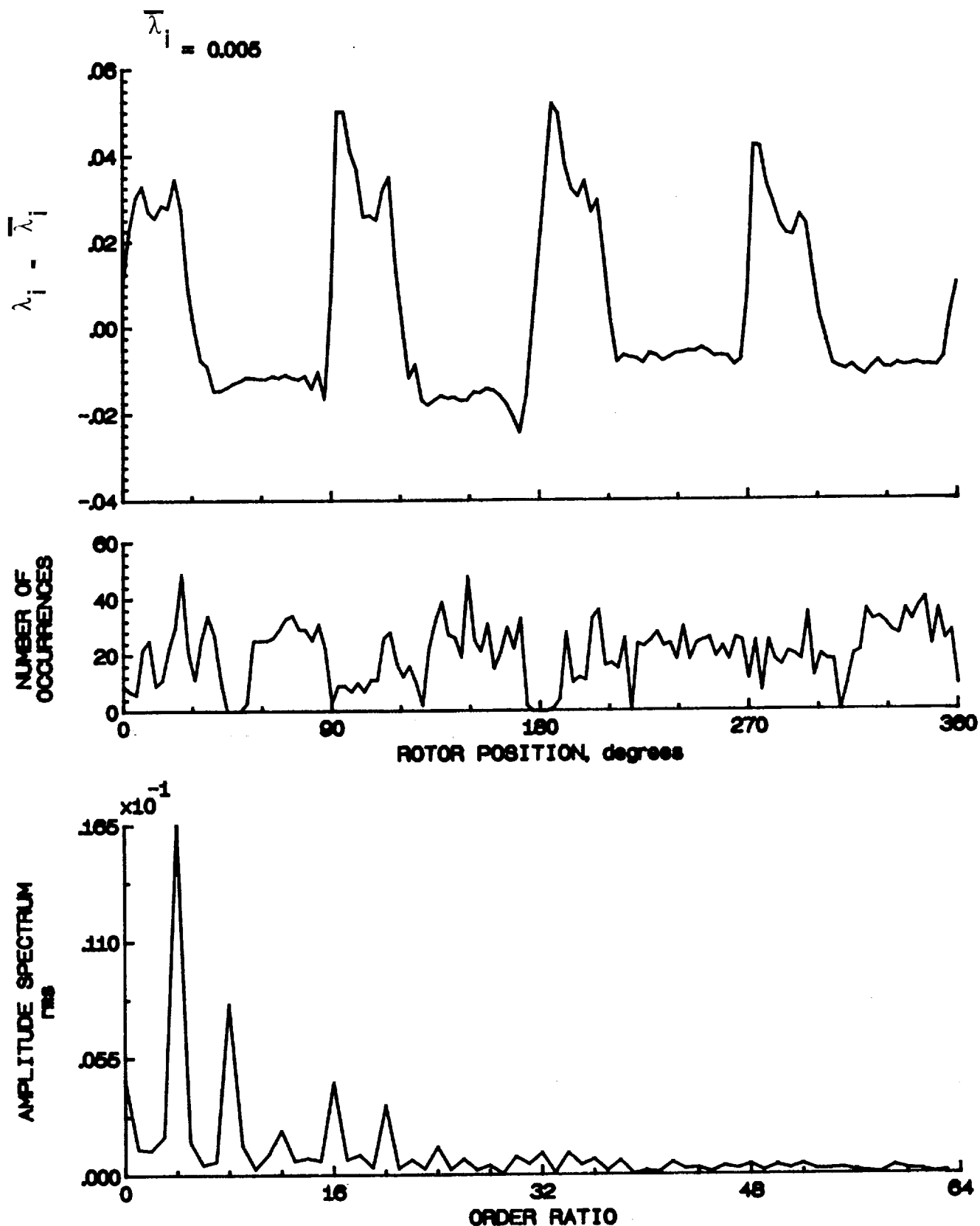


Figure 122.- Concluded.

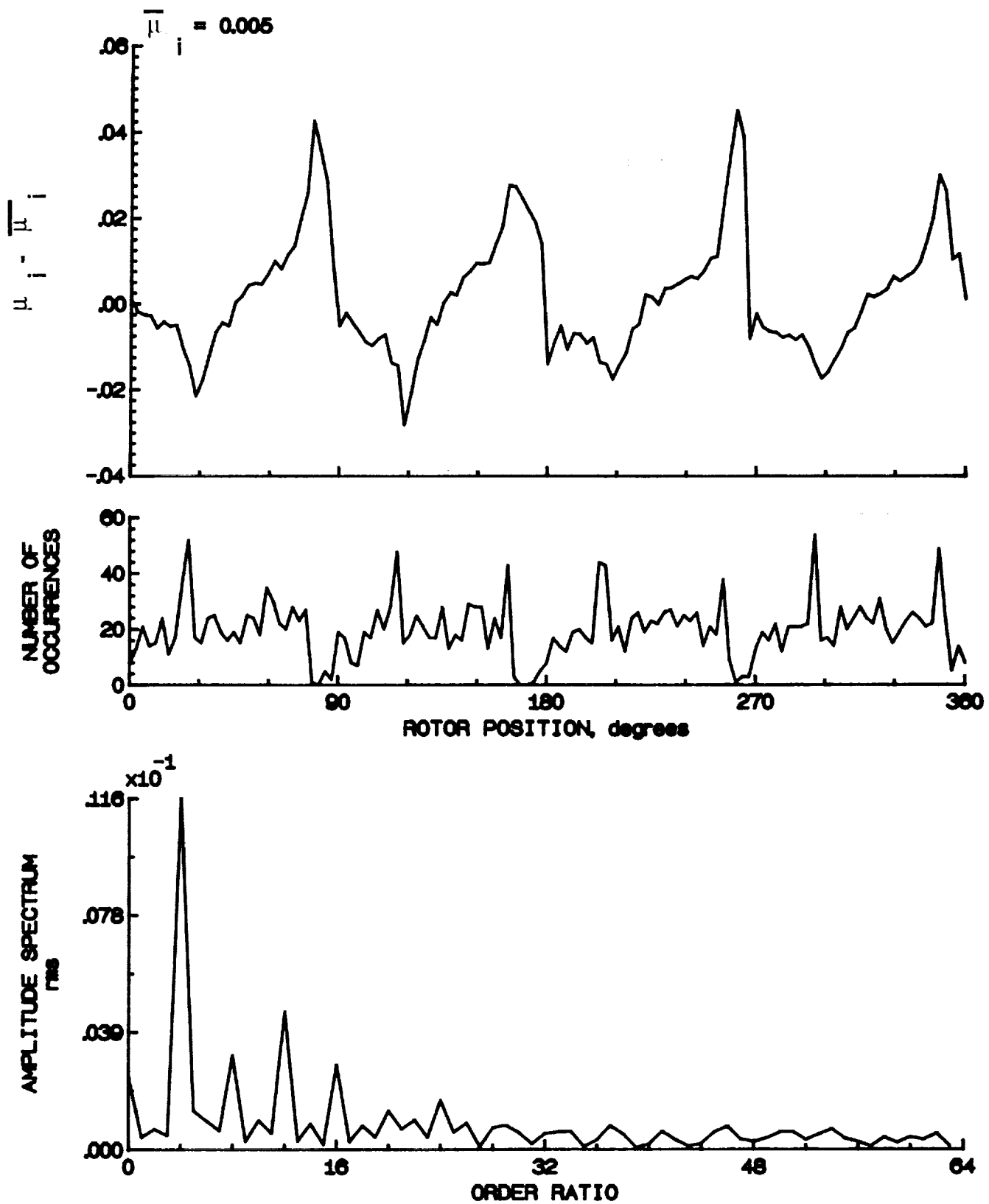


Figure 123.- Induced inflow velocity measured at 210 degrees and r/R of 0.78.

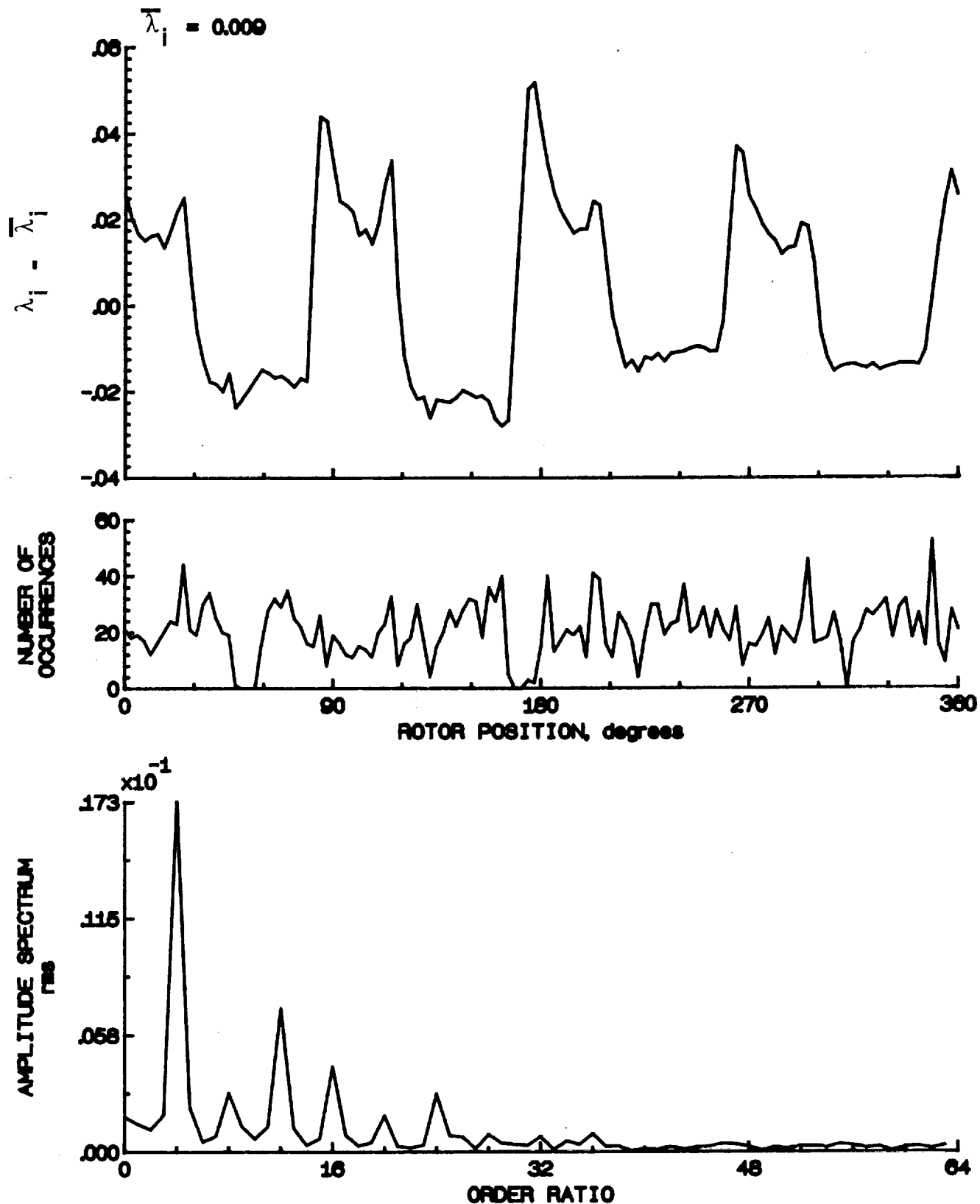


Figure 123.- Concluded.

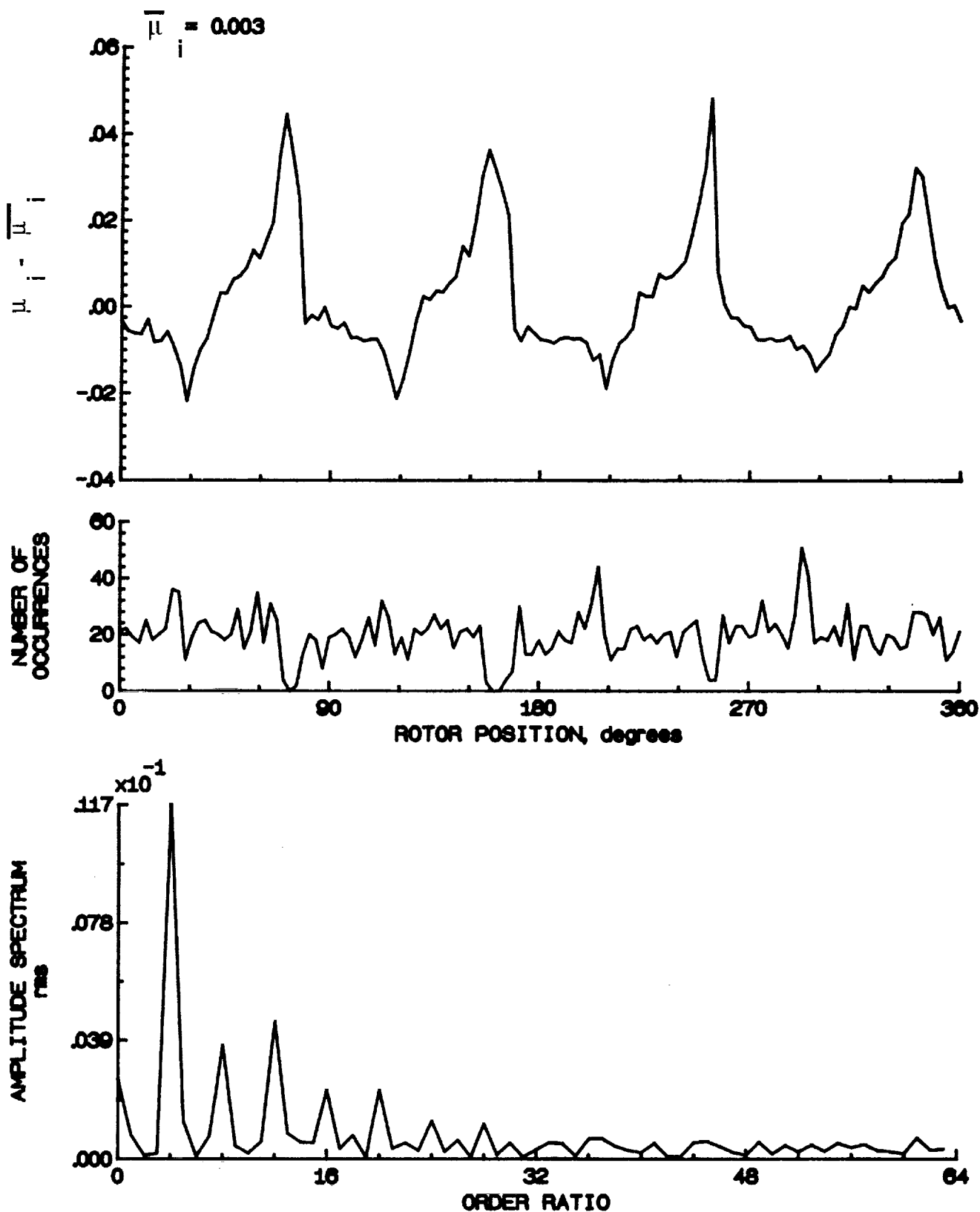


Figure 124.- Induced inflow velocity measured at 210 degrees and r/R of 0.82.

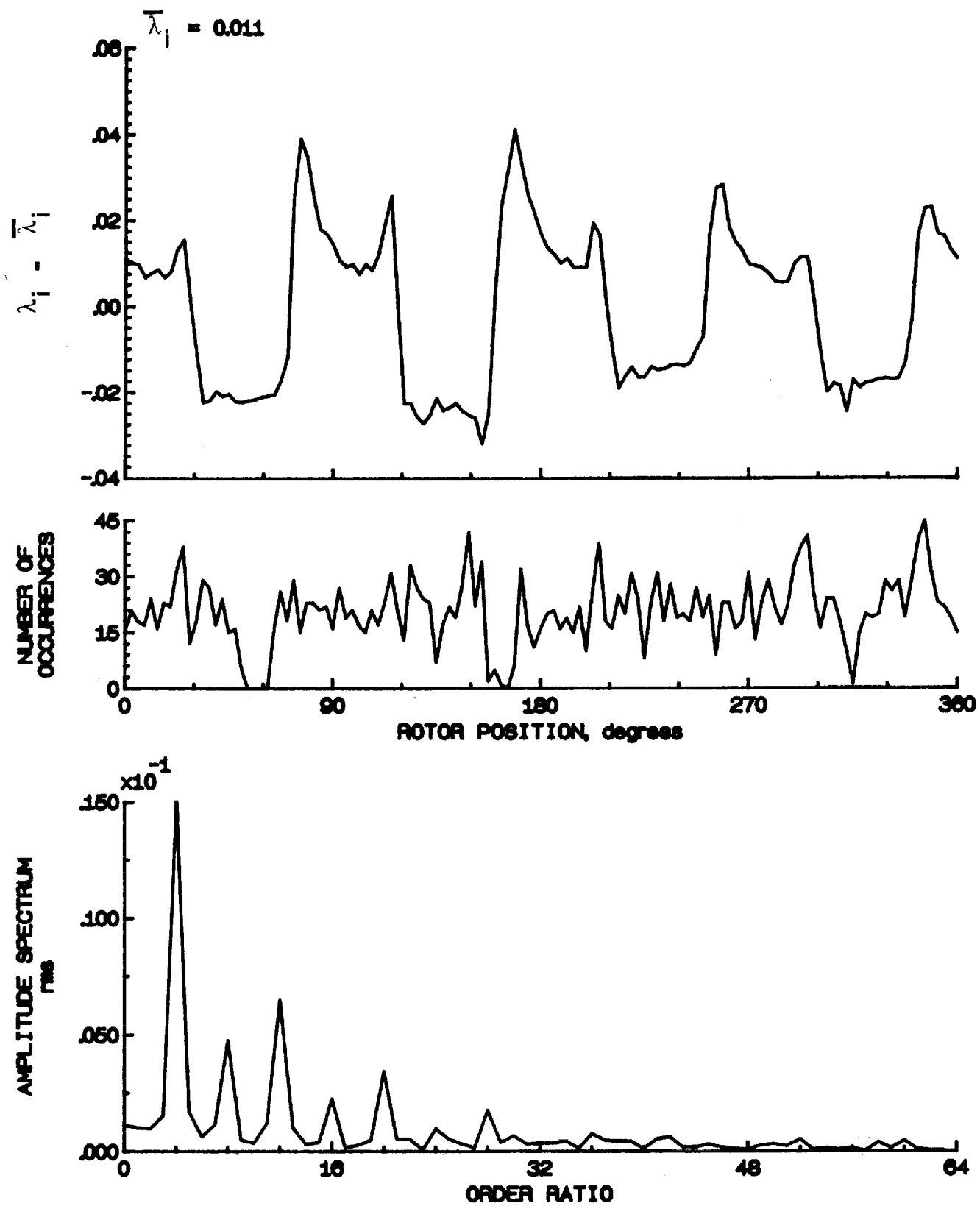


Figure 124.- Concluded.

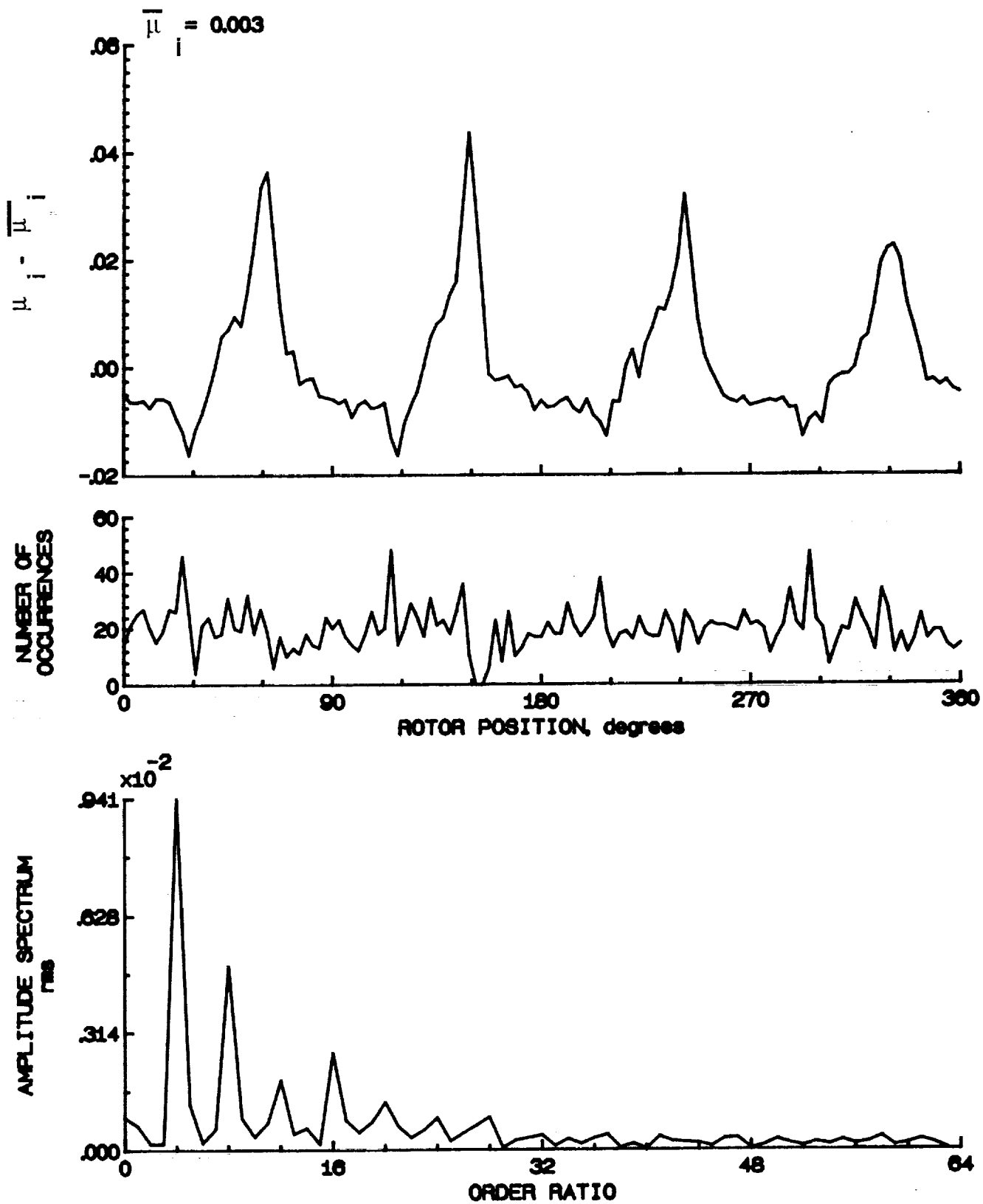


Figure 125.- Induced inflow velocity measured at 210 degrees and r/R of 0.86.

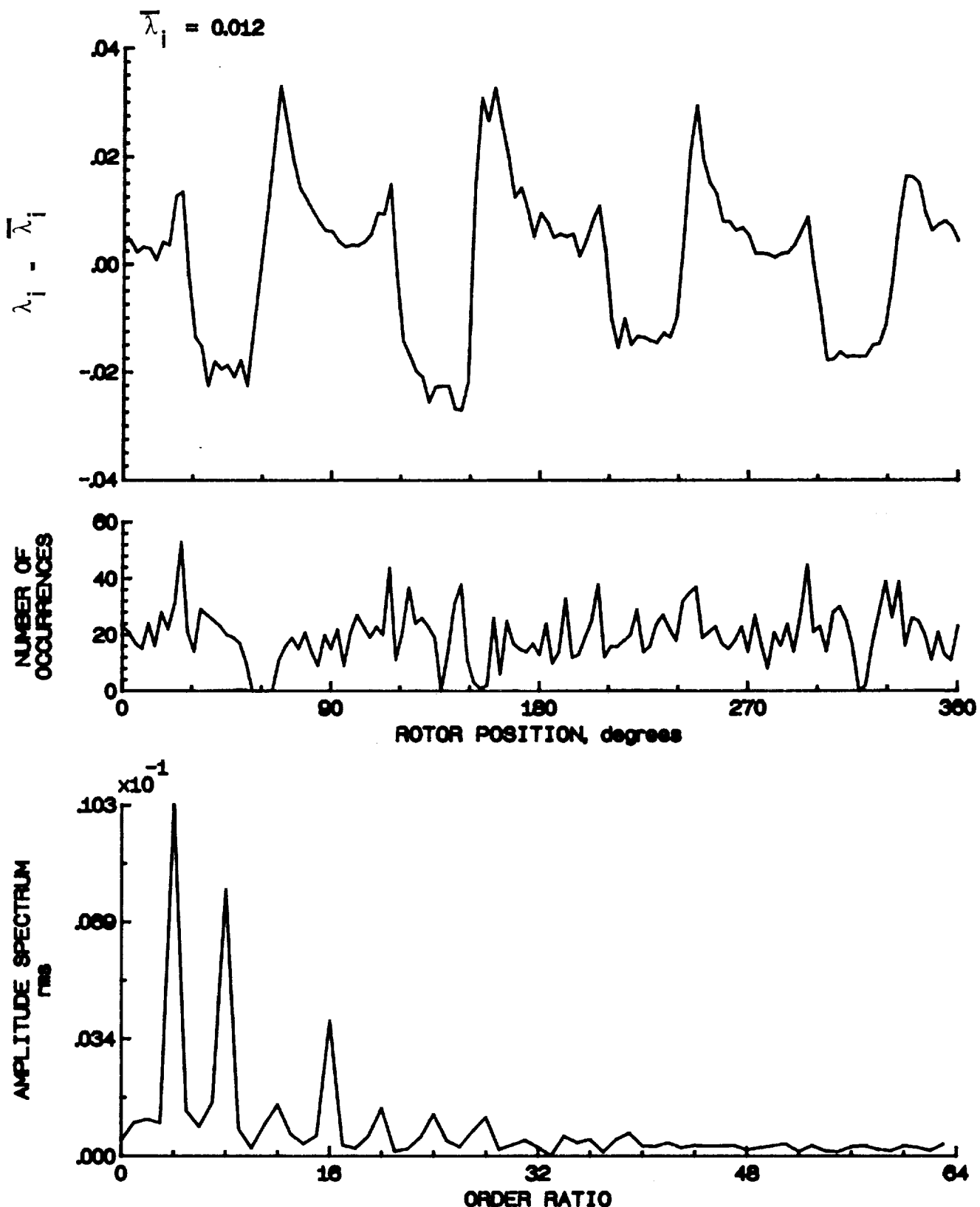


Figure 125.- Concluded.

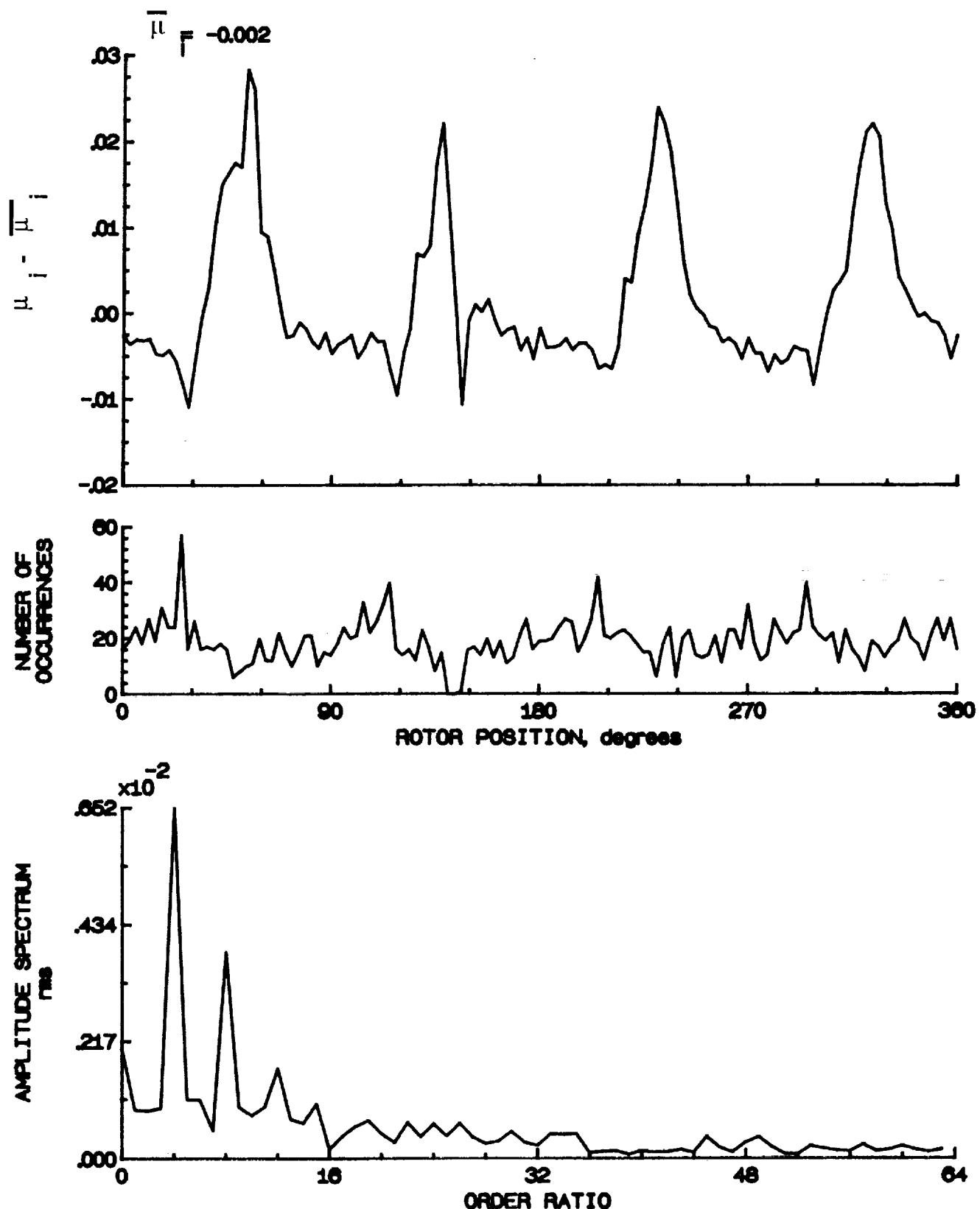


Figure 126.- Induced inflow velocity measured at 210 degrees and r/R of 0.90.

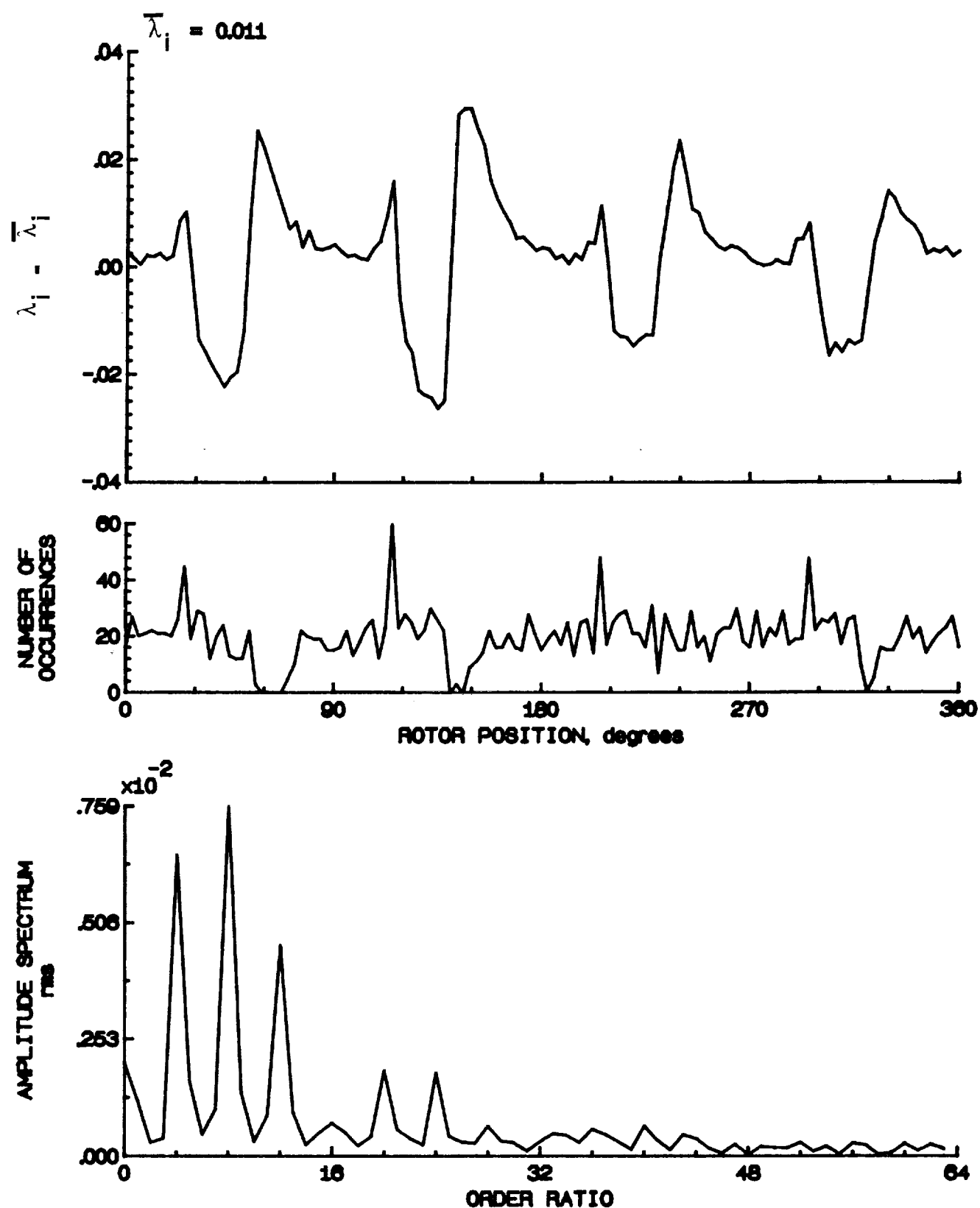


Figure 126.- Concluded.

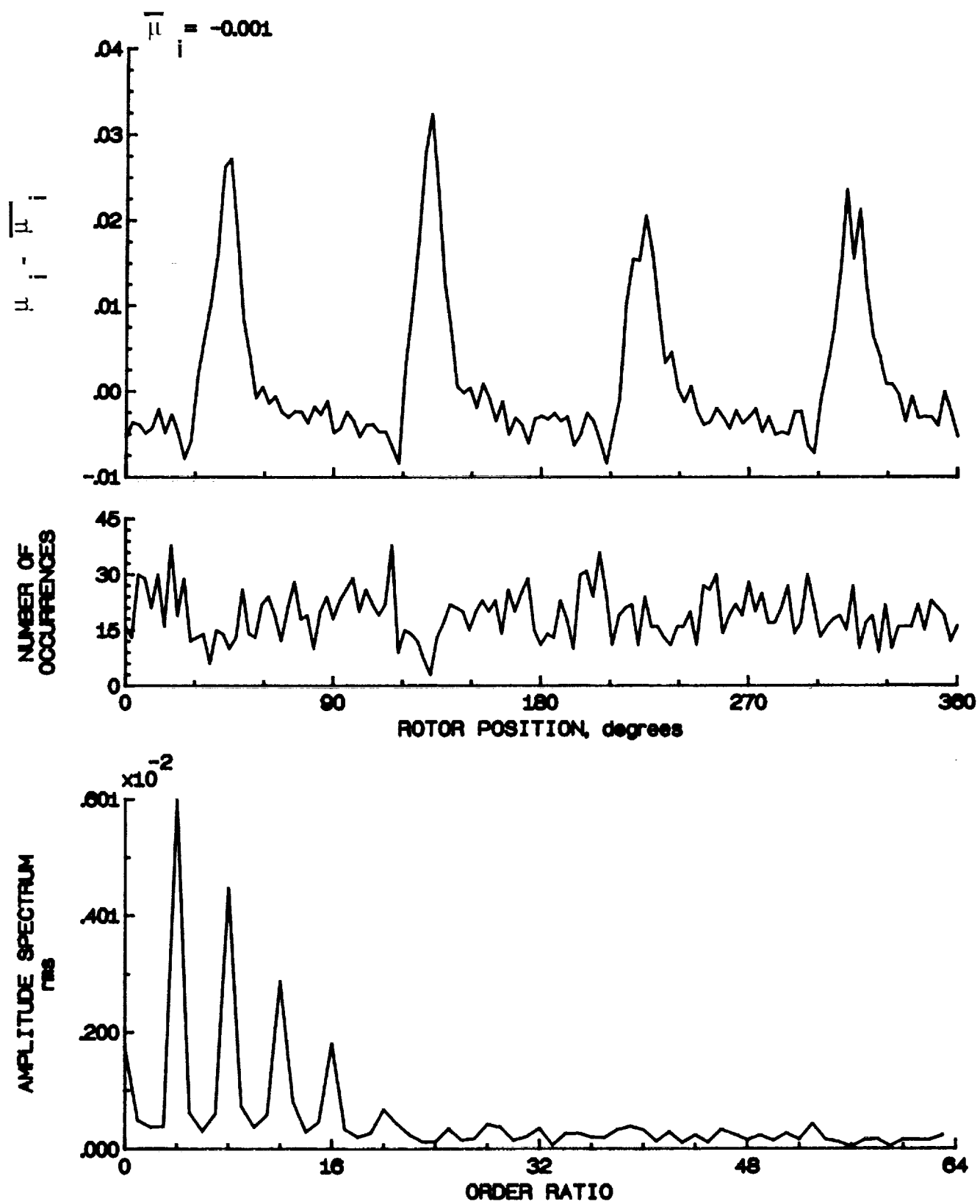


Figure 127.- Induced inflow velocity measured at 210 degrees and r/R of 0.94.

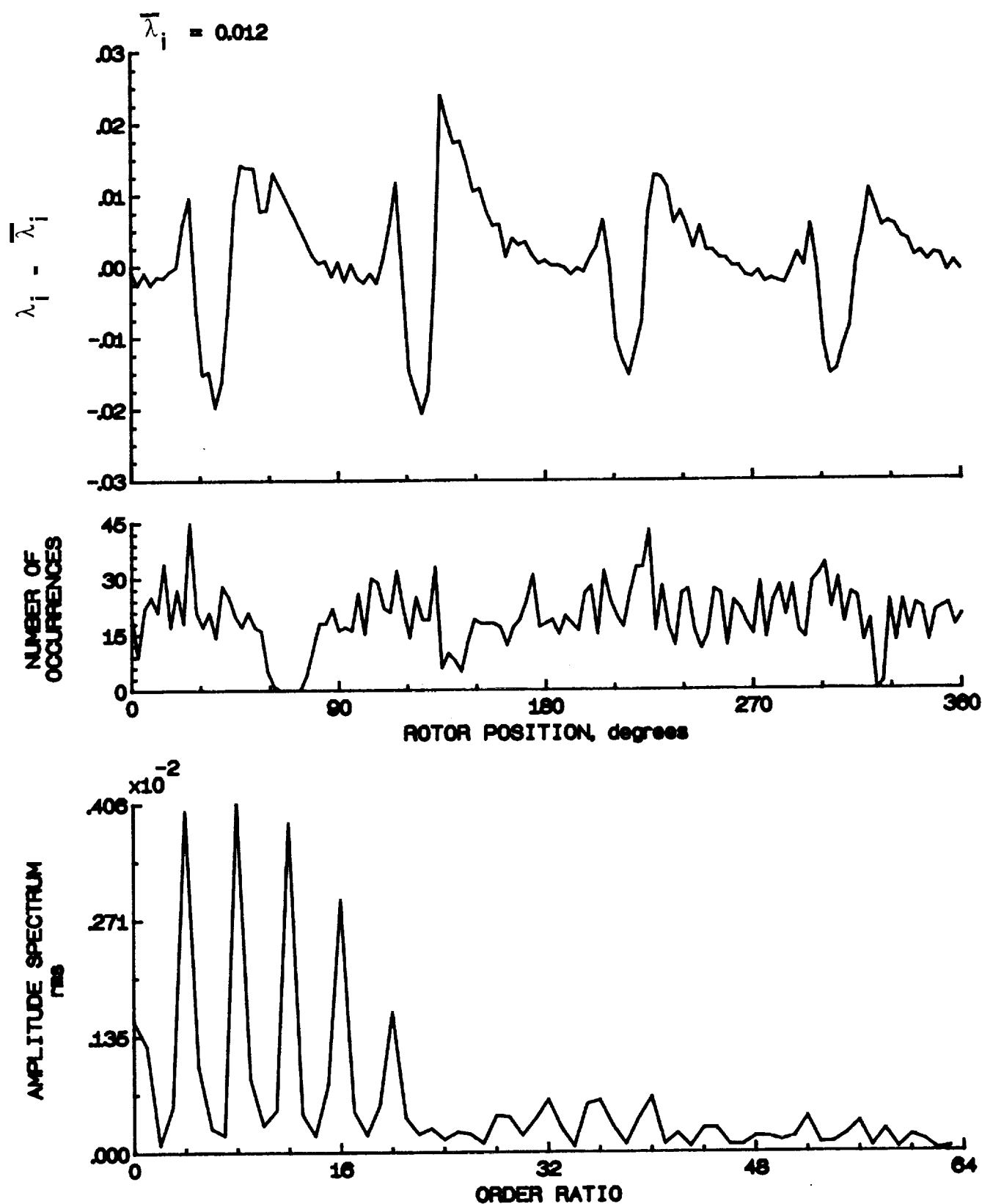


Figure 127.- Concluded.

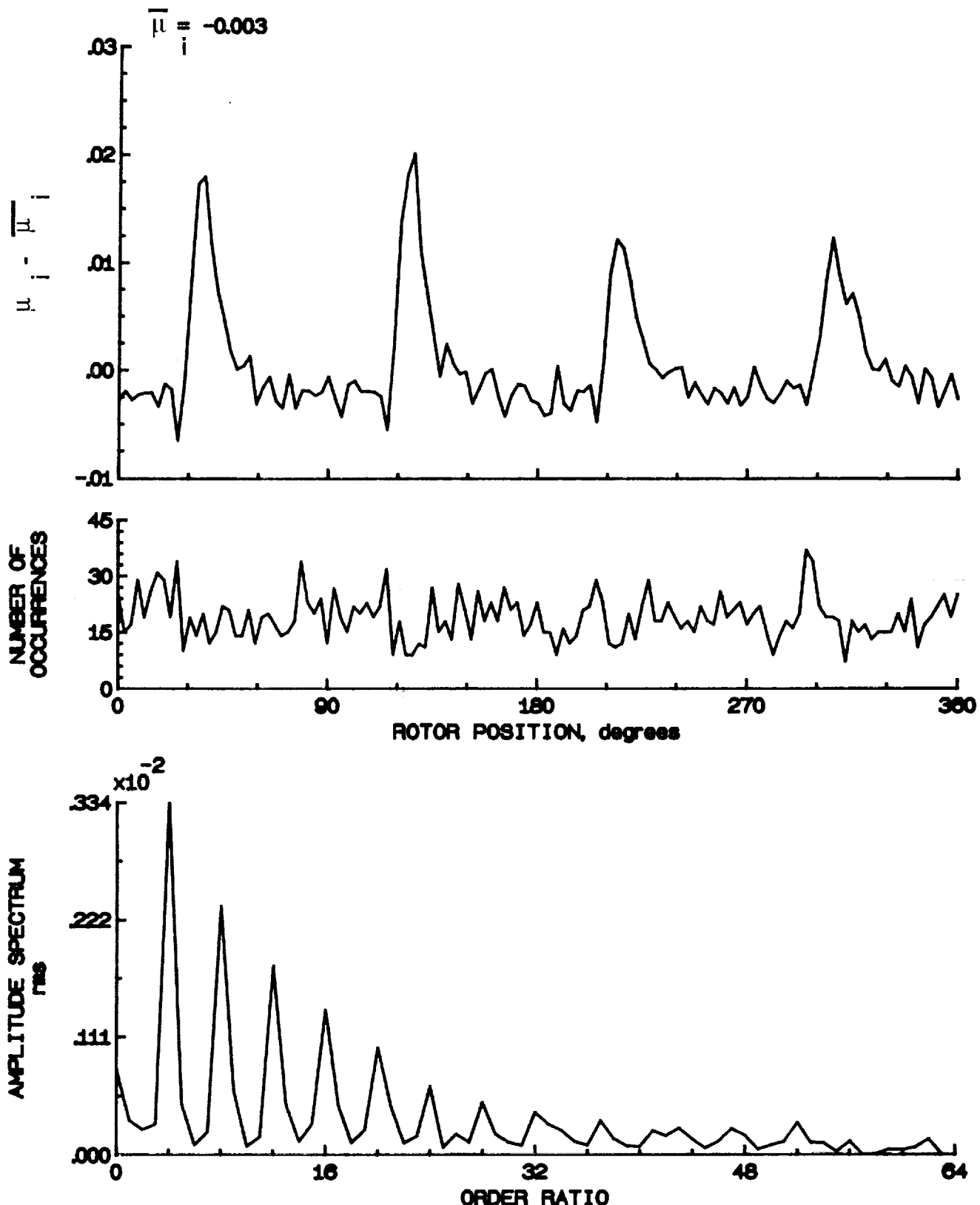


Figure 128.- Induced inflow velocity measured at 210 degrees and r/R of 0.98.

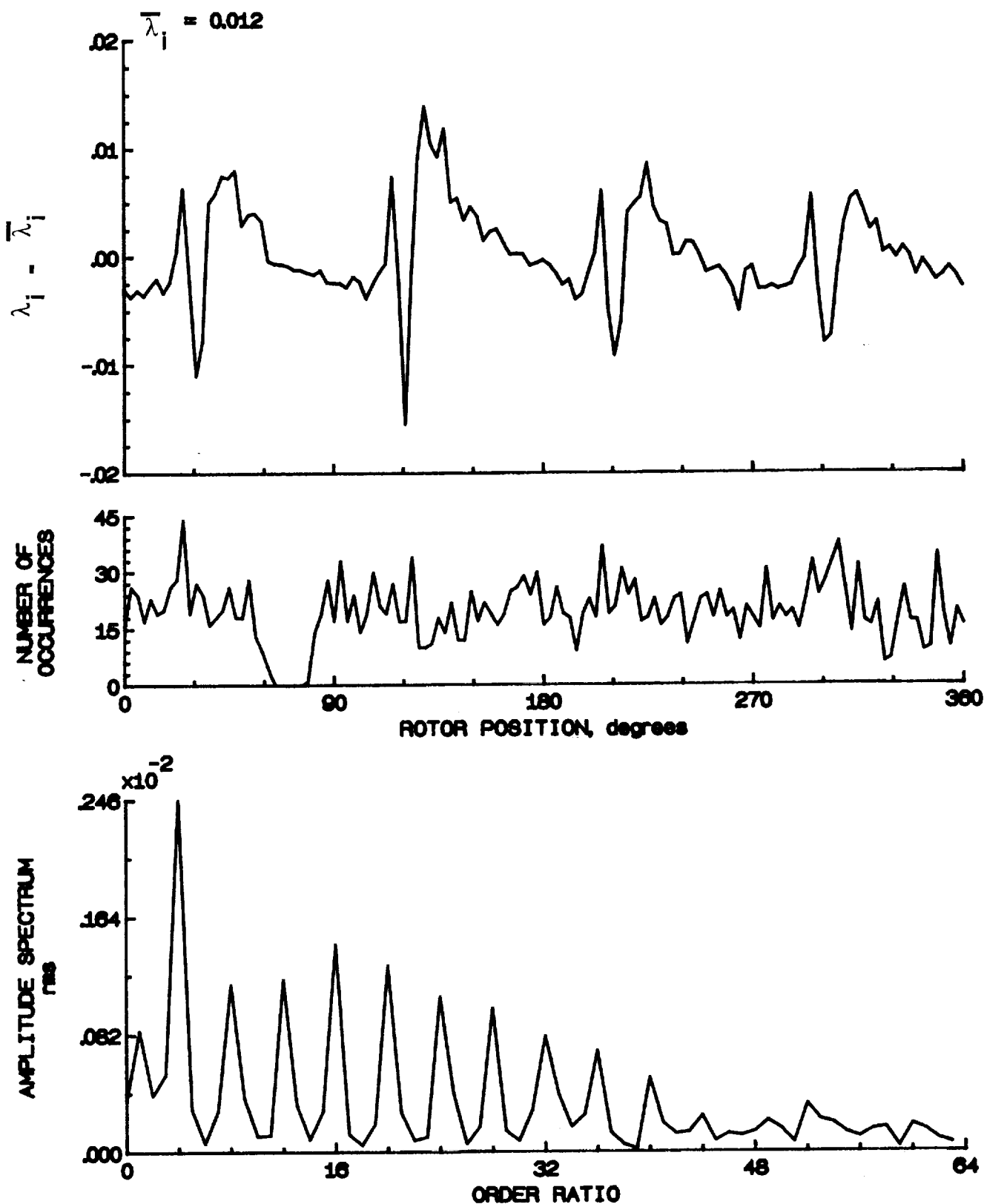


Figure 128.- Concluded.

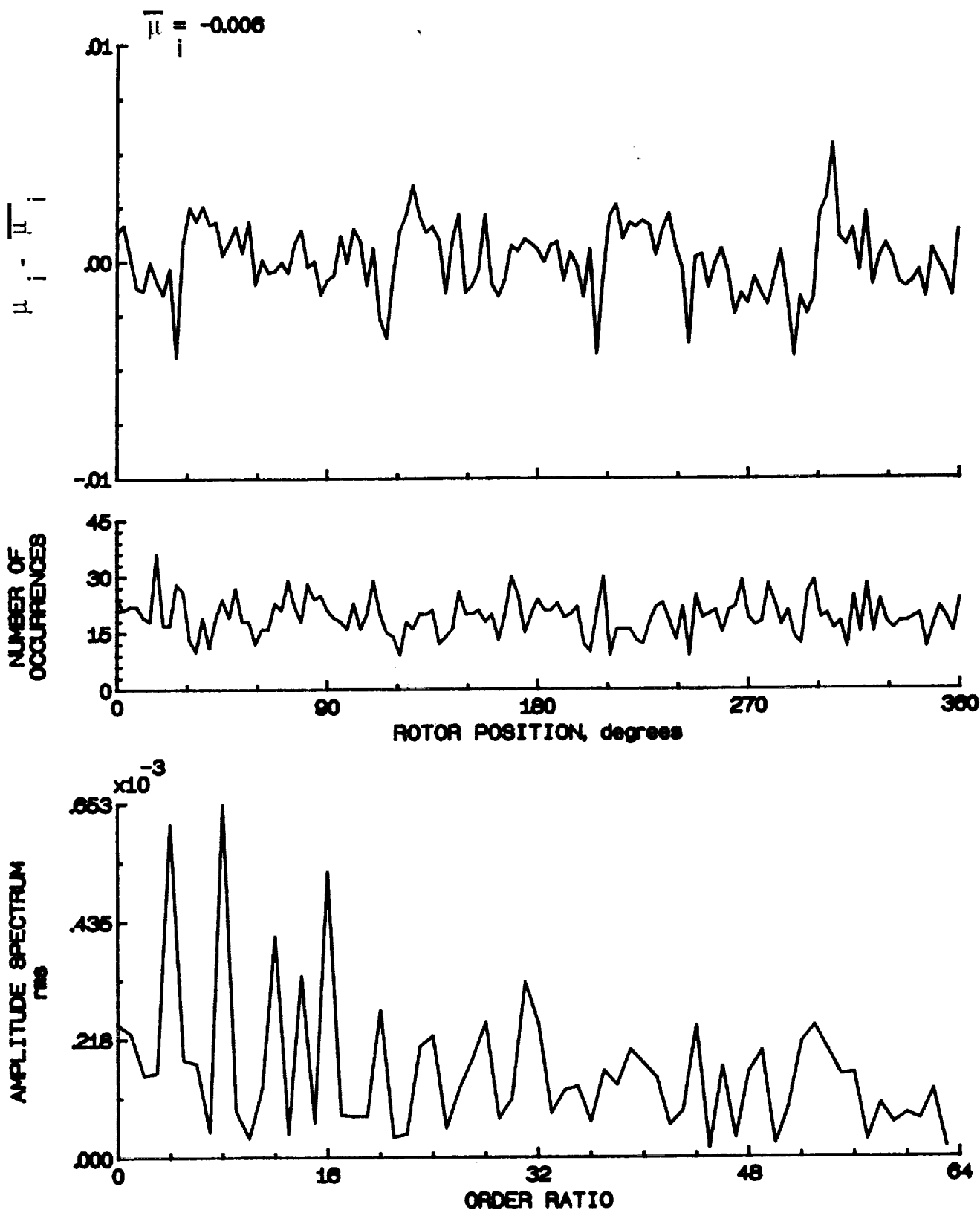


Figure 129.- Induced inflow velocity measured at 210 degrees and r/R of 1.02.

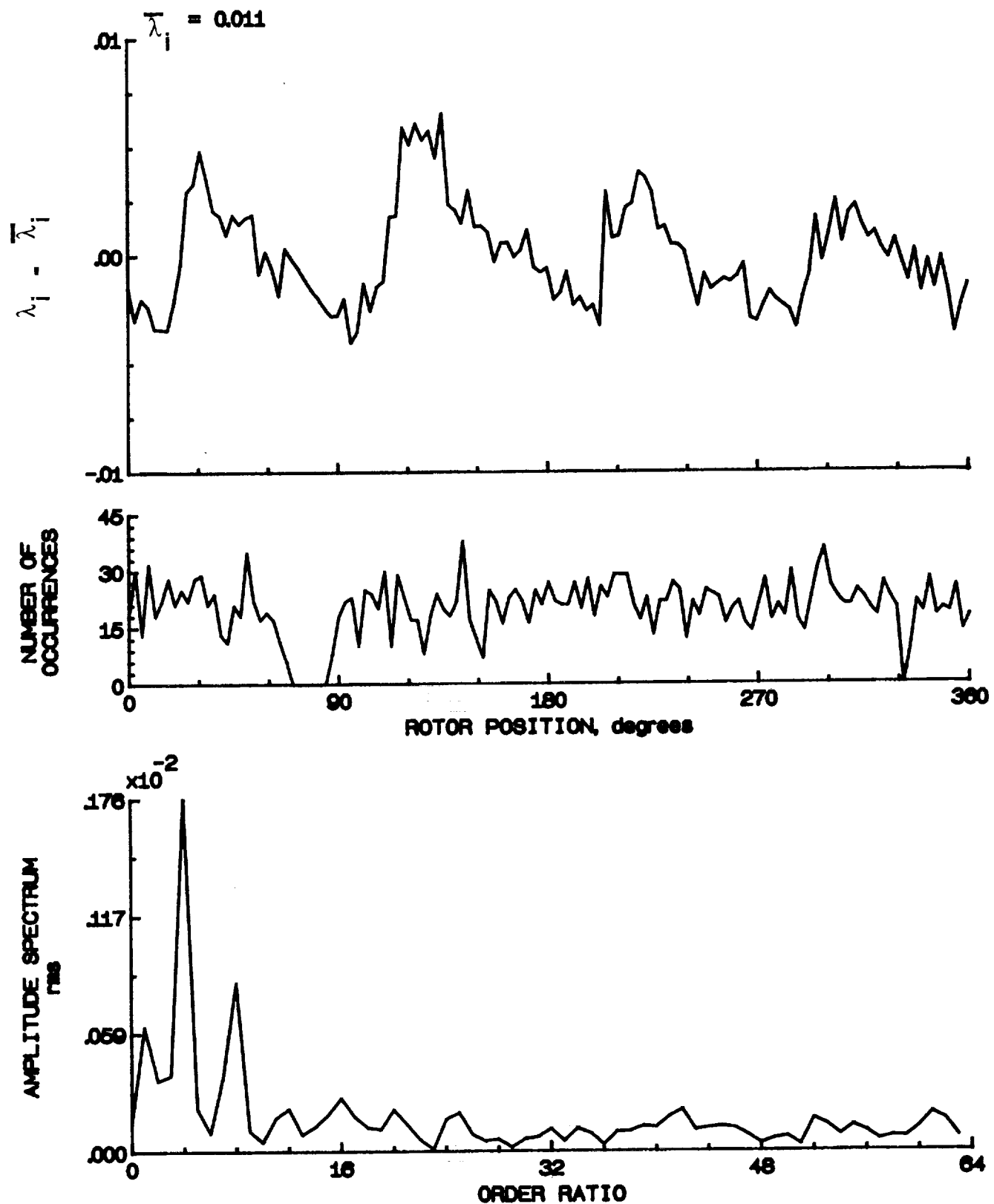


Figure 129.- Concluded.

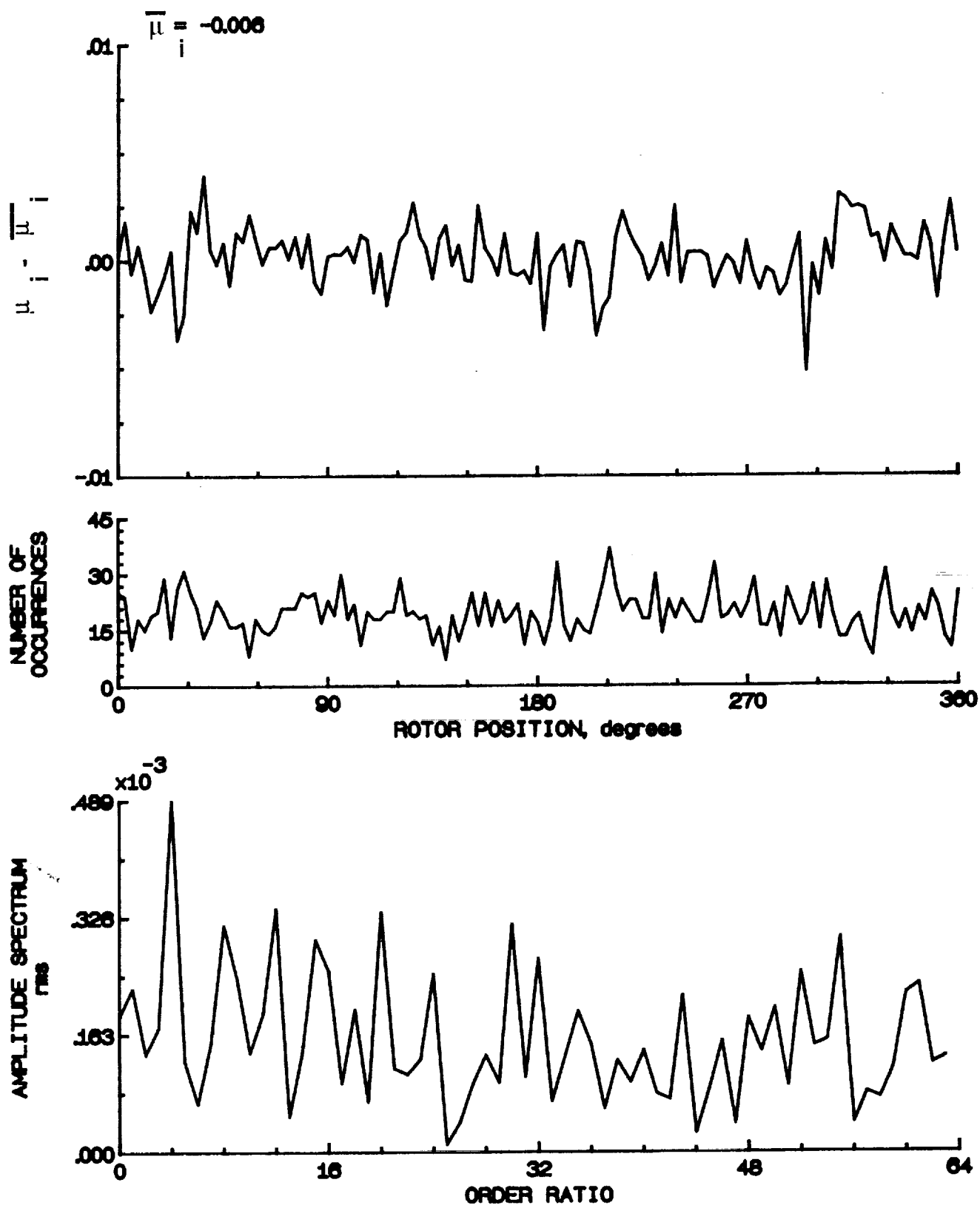


Figure 130.- Induced inflow velocity measured at 210 degrees and r/R of 1.04.

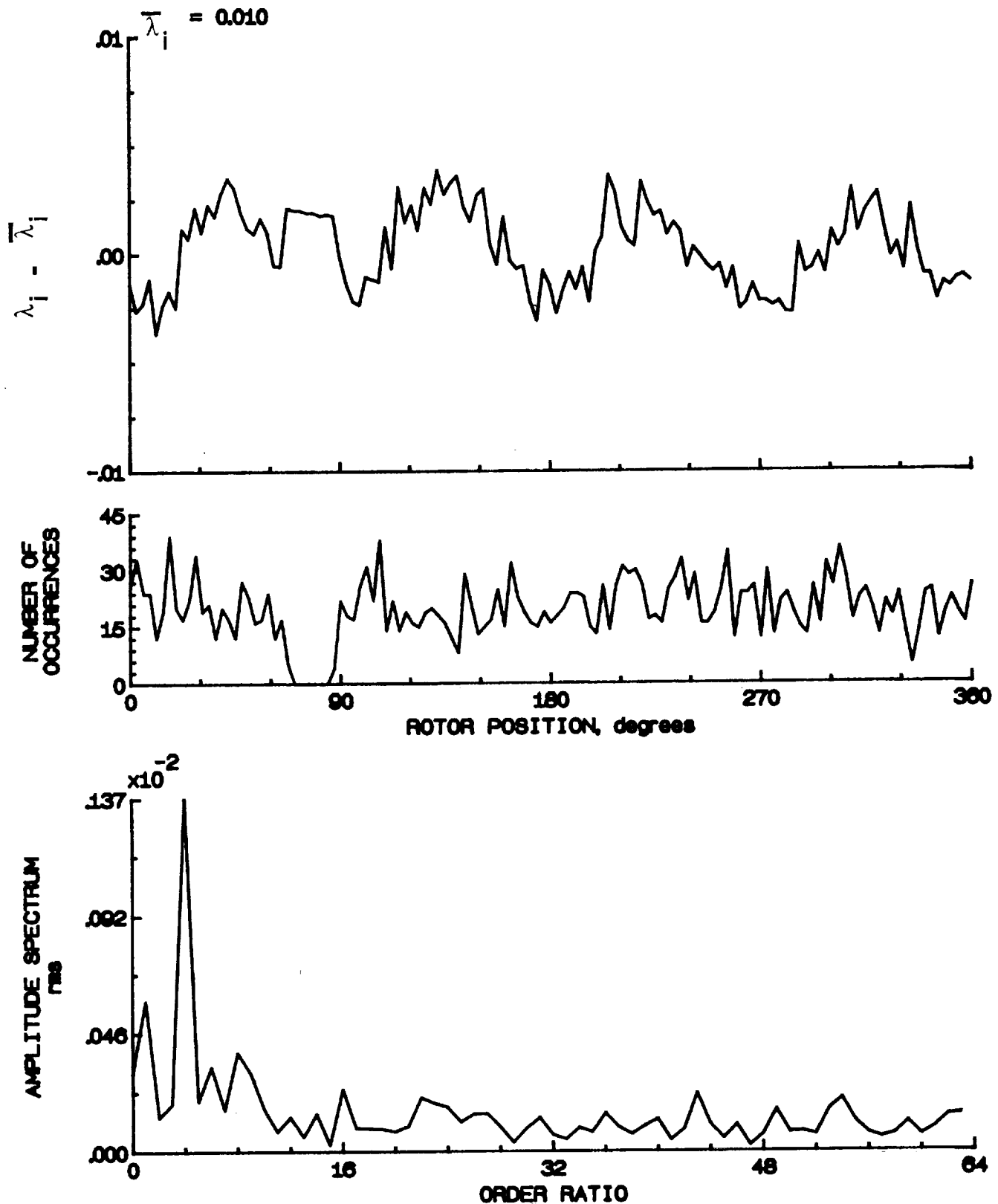


Figure 130.- Concluded.

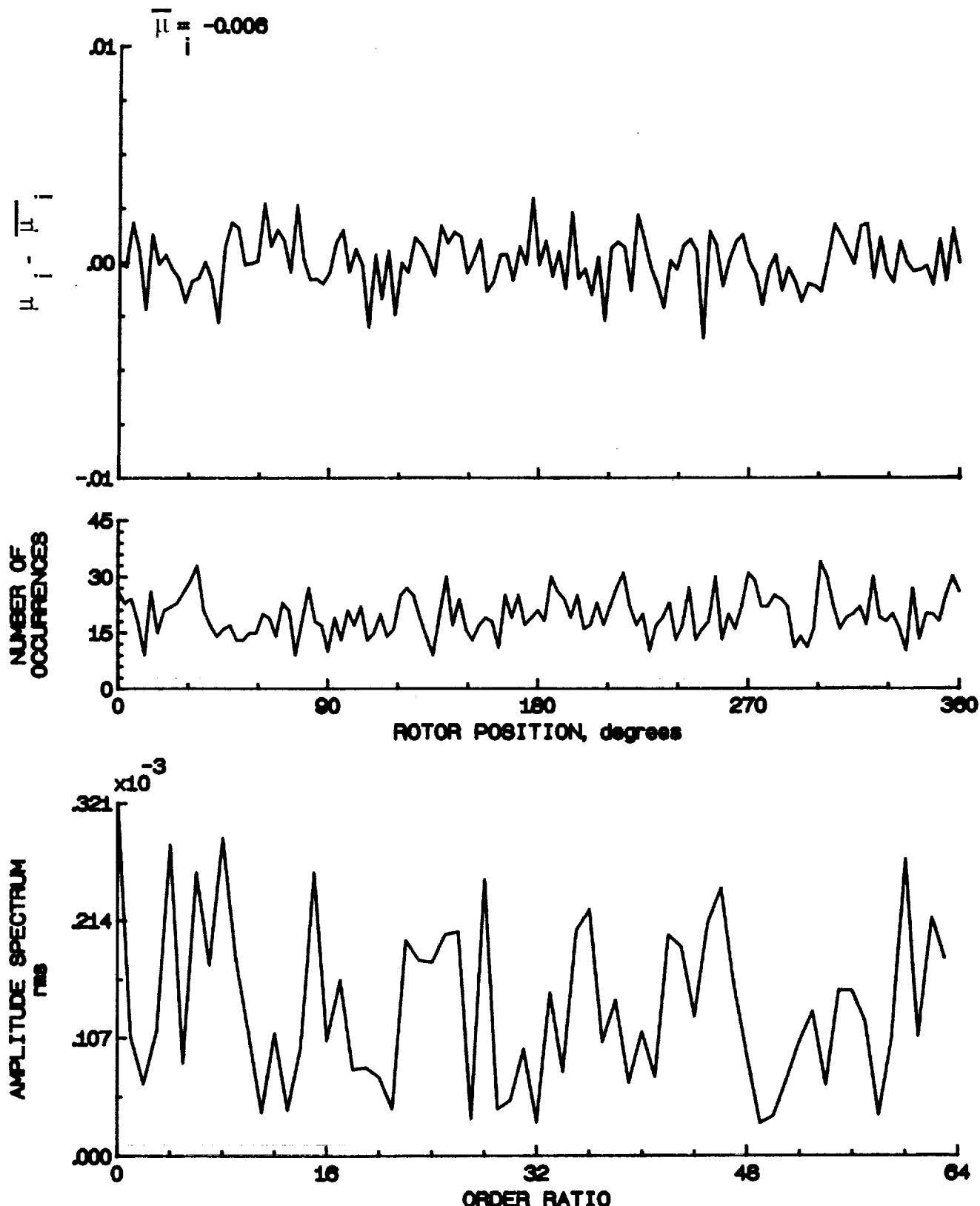


Figure 131.- Induced inflow velocity measured at 210 degrees and r/R of 1.10.

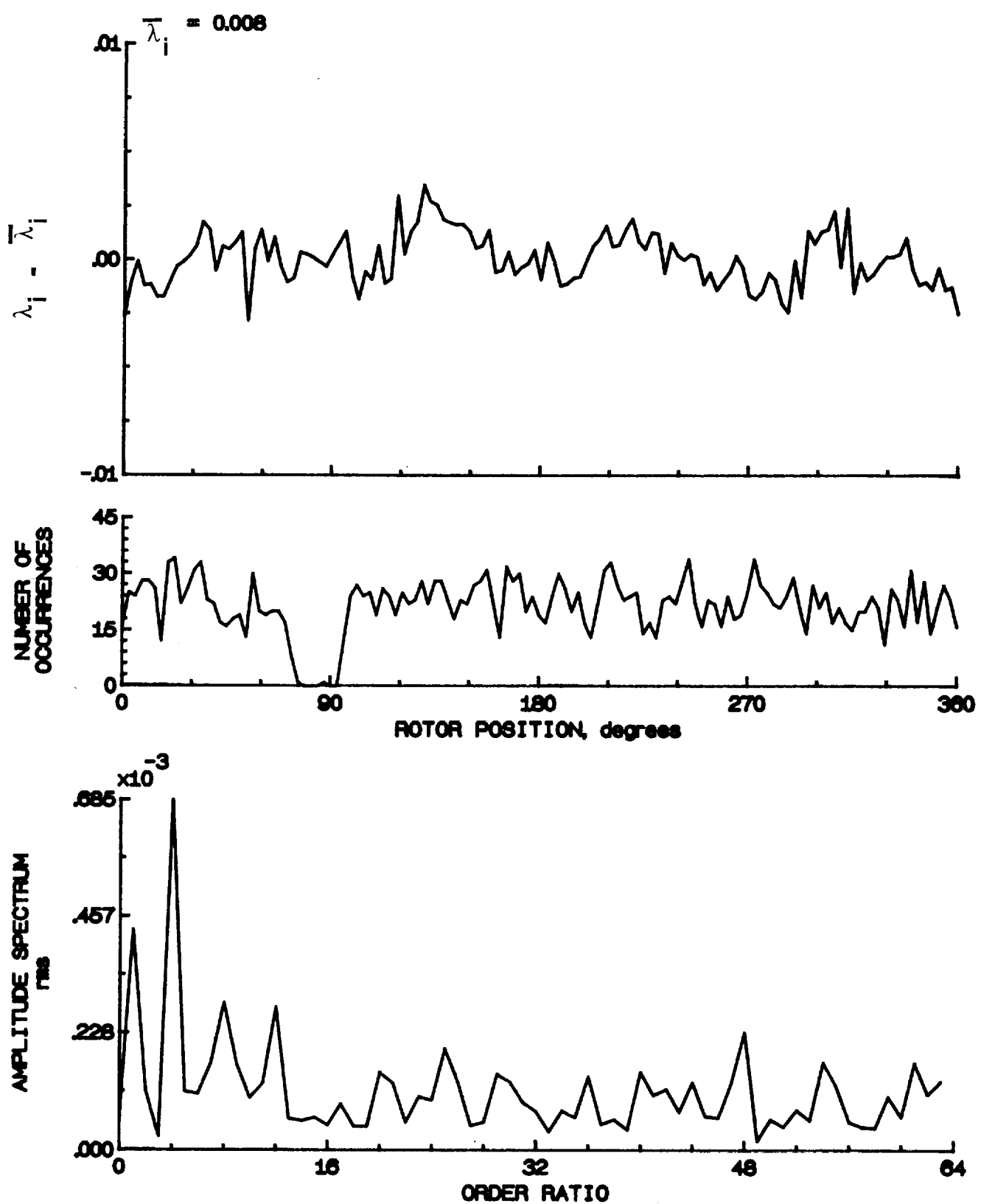


Figure 131.- Concluded.

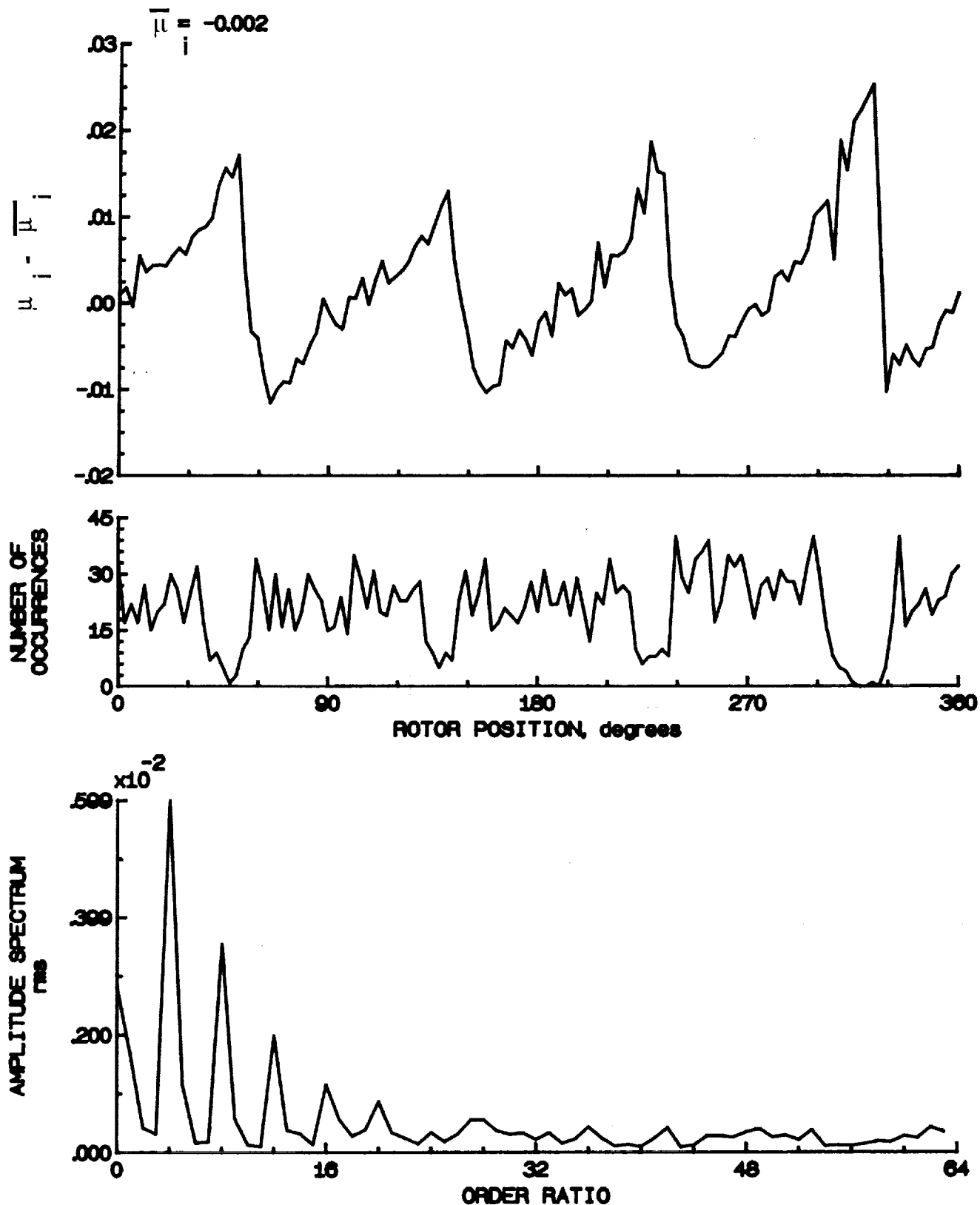


Figure 132.- Induced inflow velocity measured at 240 degrees and r/R of 0.20.

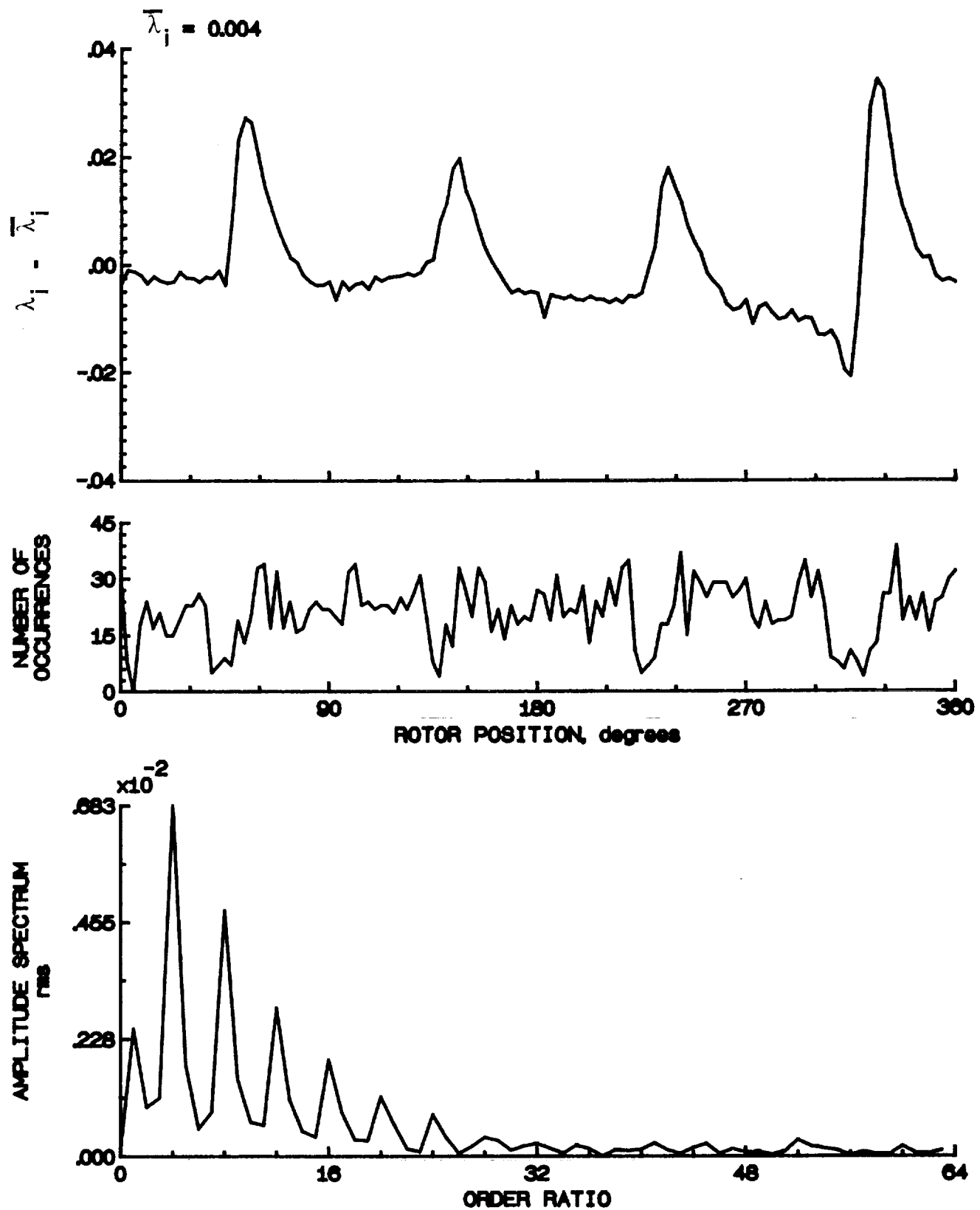


Figure 132.- Concluded.

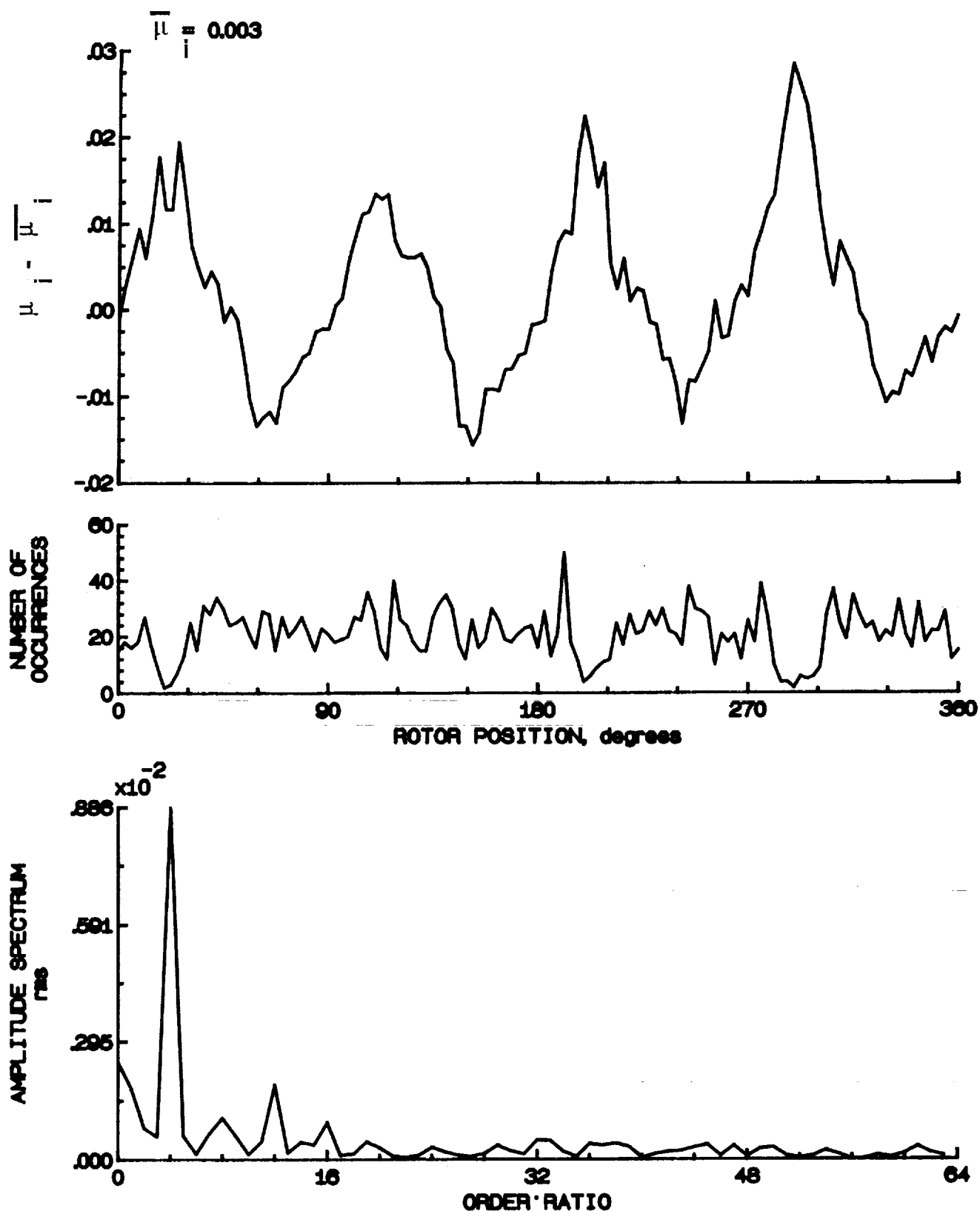


Figure 133.- Induced inflow velocity measured at 240 degrees and r/R of 0.40.

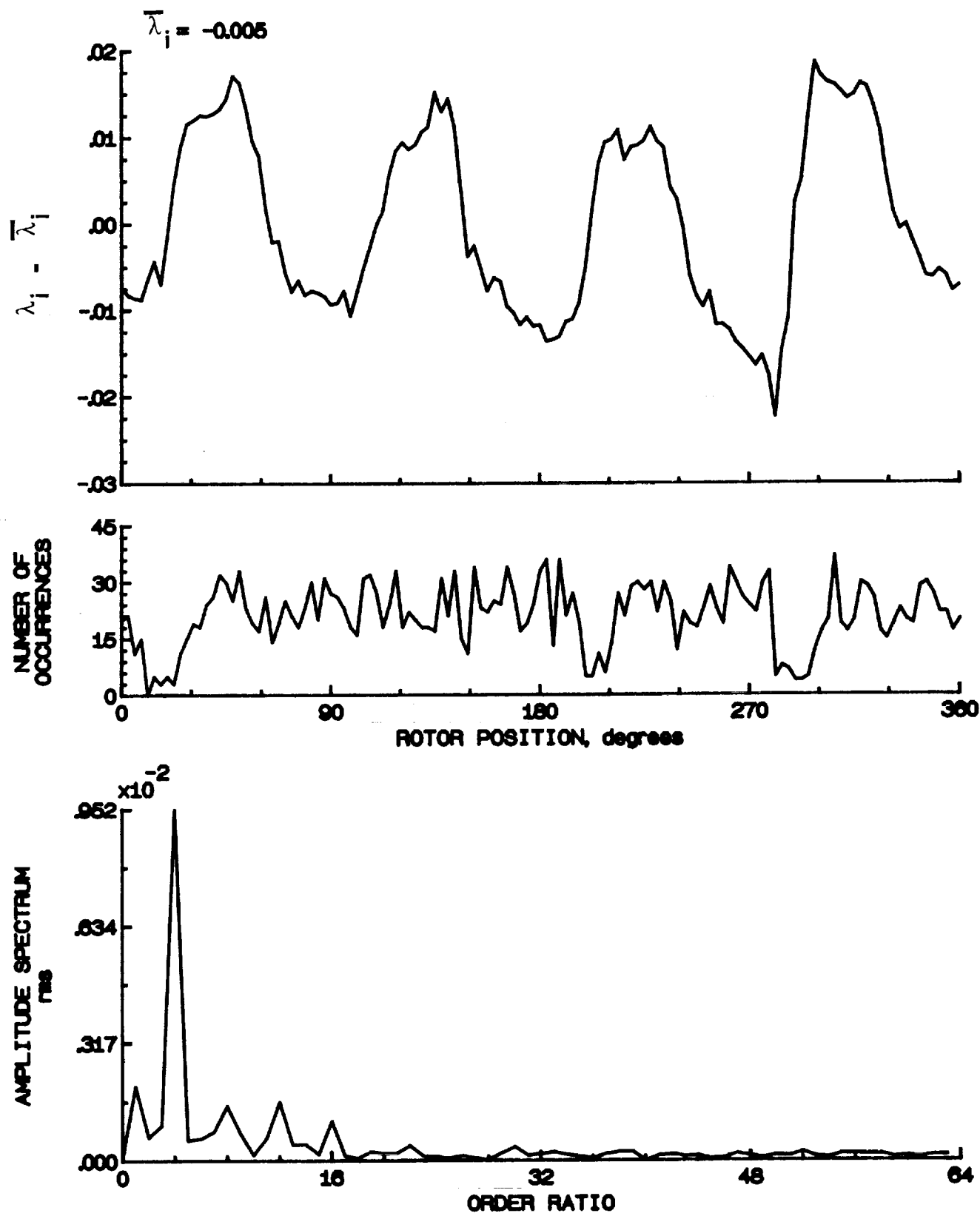


Figure 133.- Concluded.

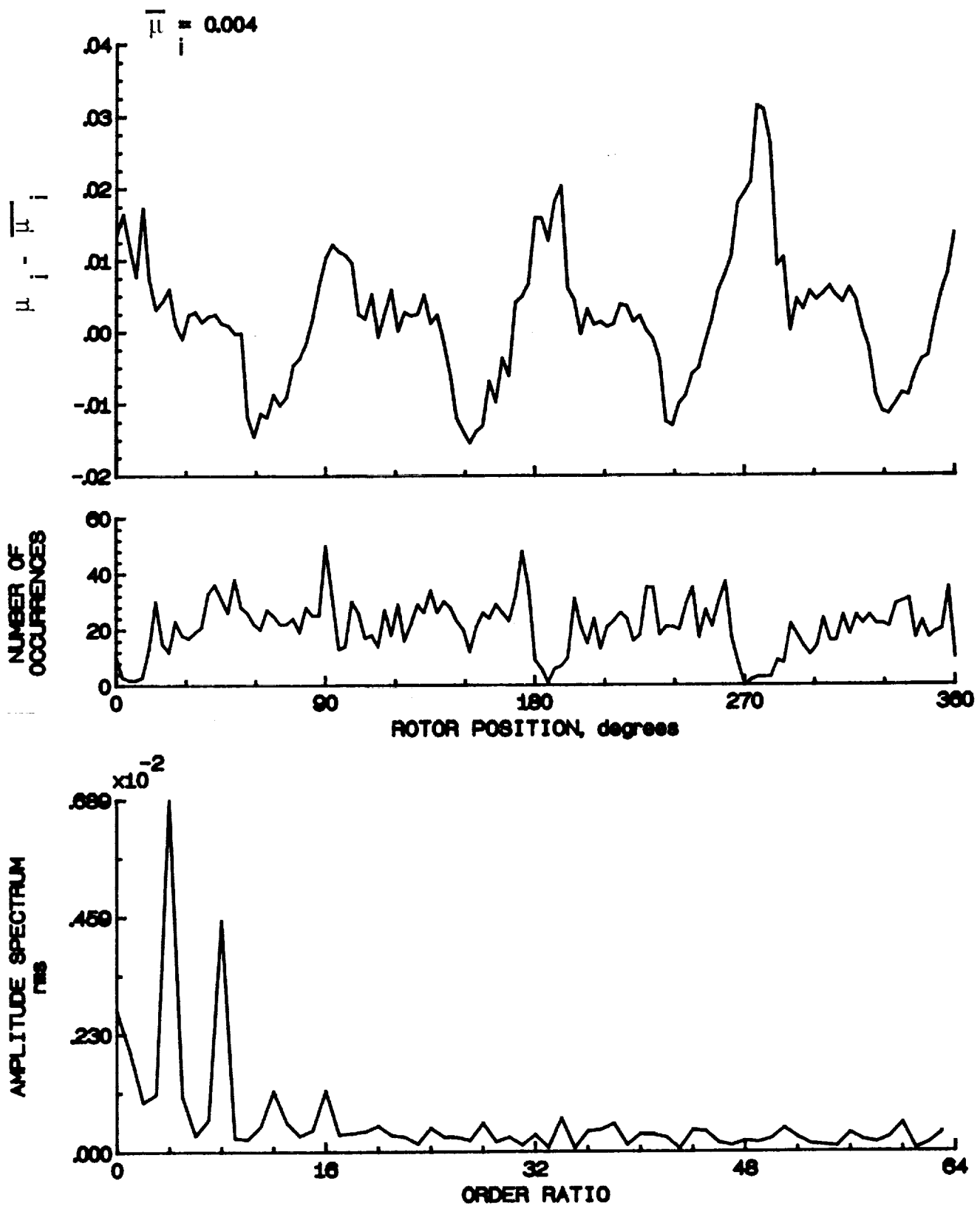


Figure 134.- Induced inflow velocity measured at 240 degrees and r/R of 0.50.

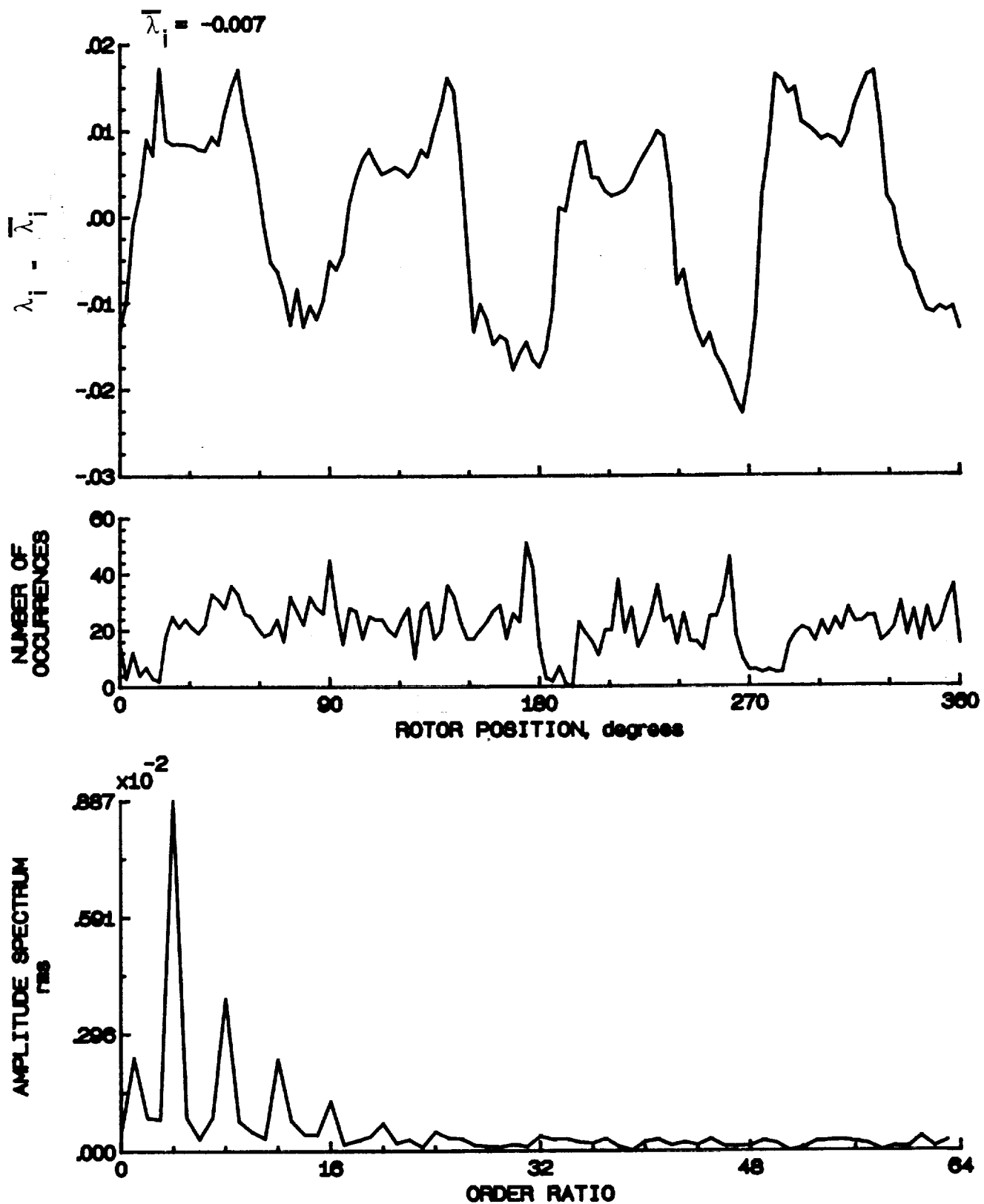


Figure 134.- Concluded.

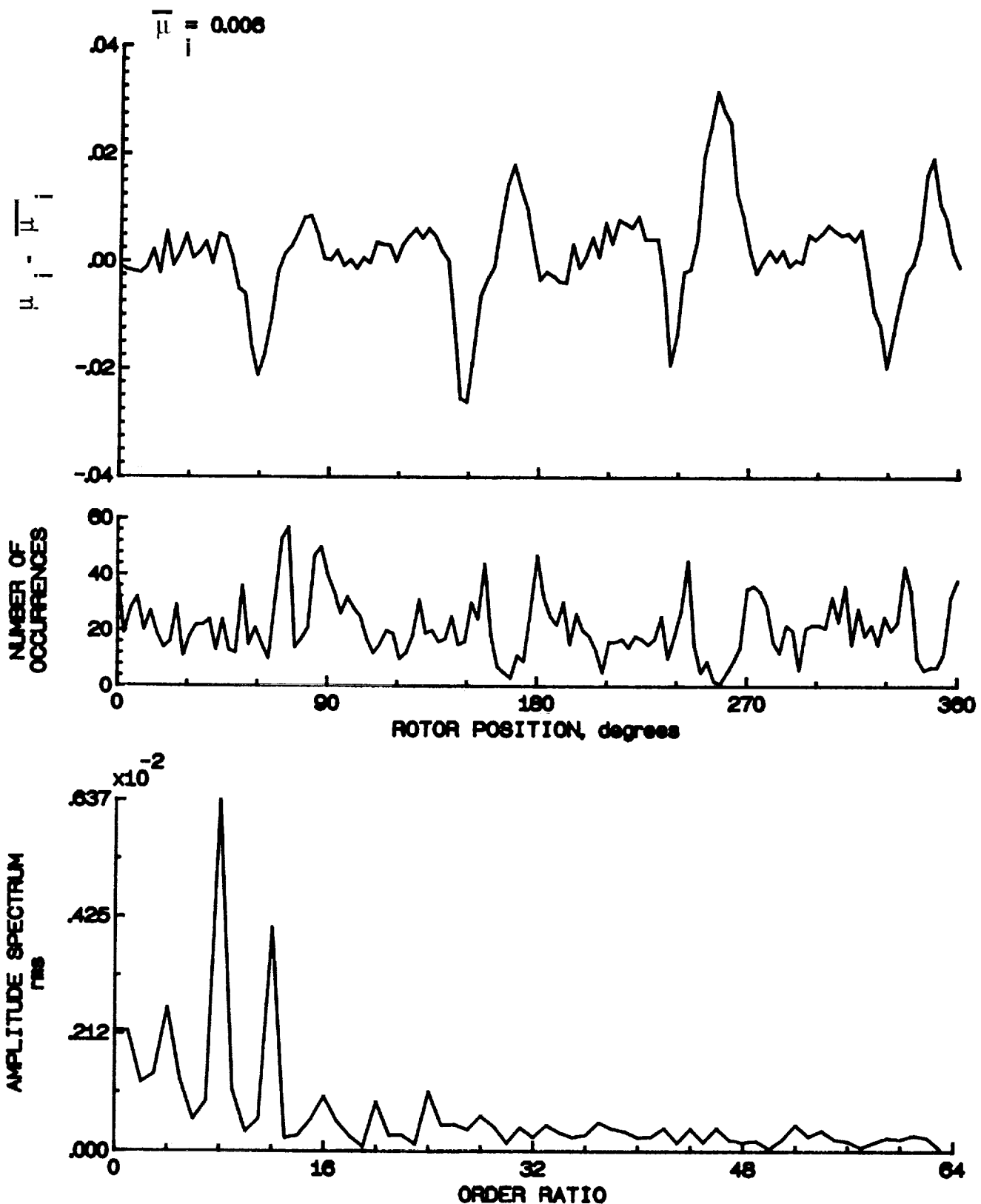


Figure 135.- Induced inflow velocity measured at 240 degrees and r/R of 0.00.

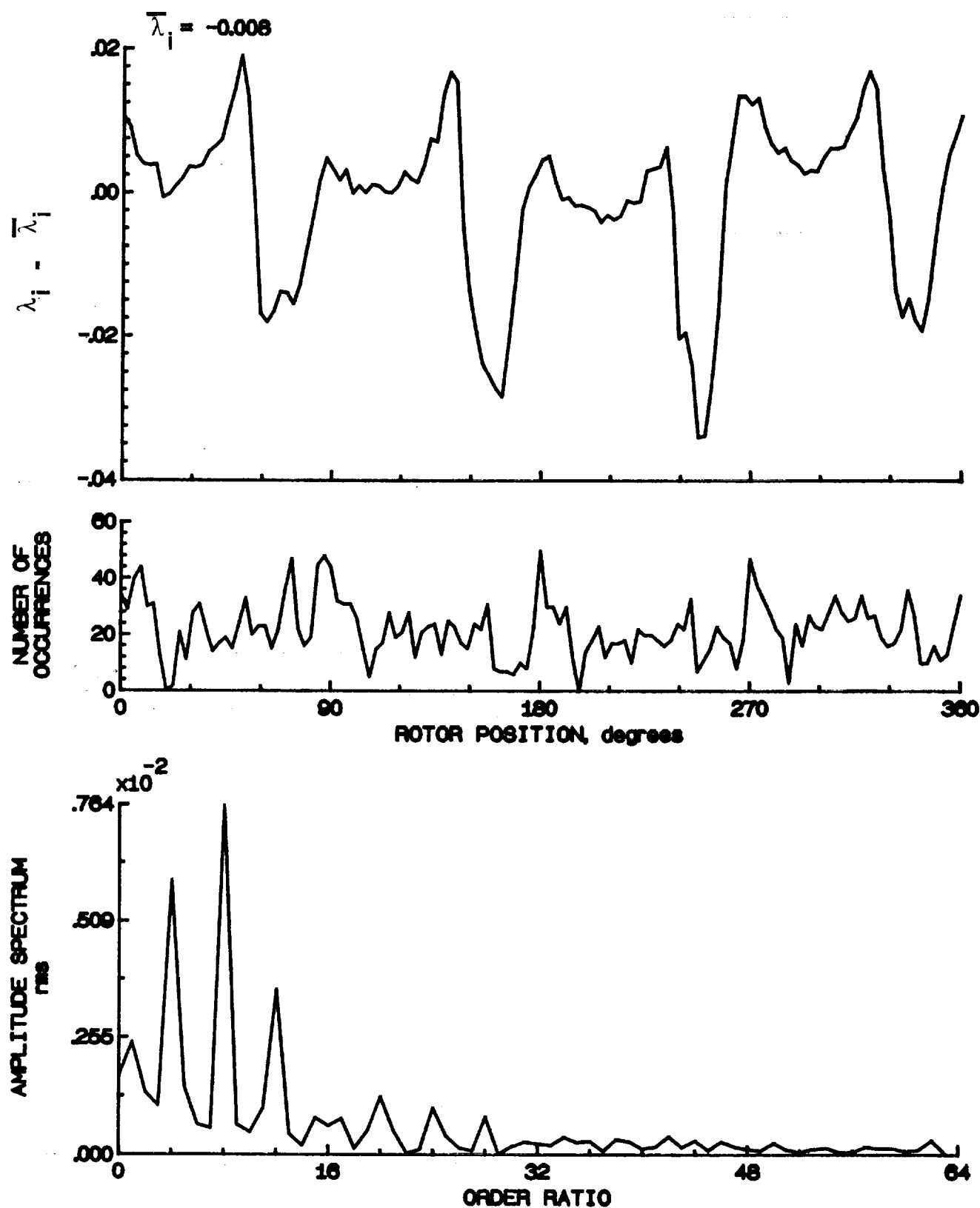


Figure 135.- Concluded.

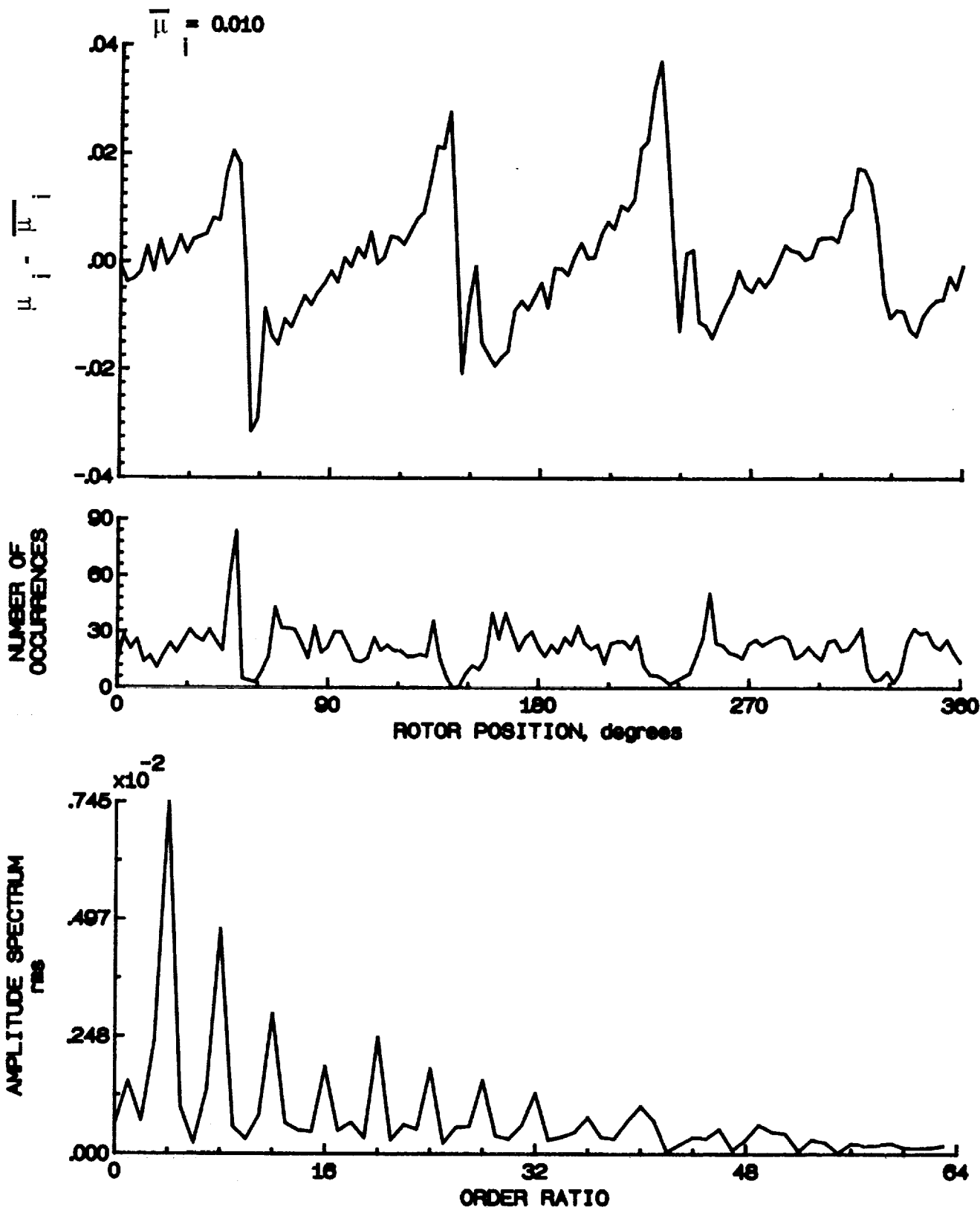


Figure 136.- Induced inflow velocity measured at 240 degrees and r/R of 0.70.

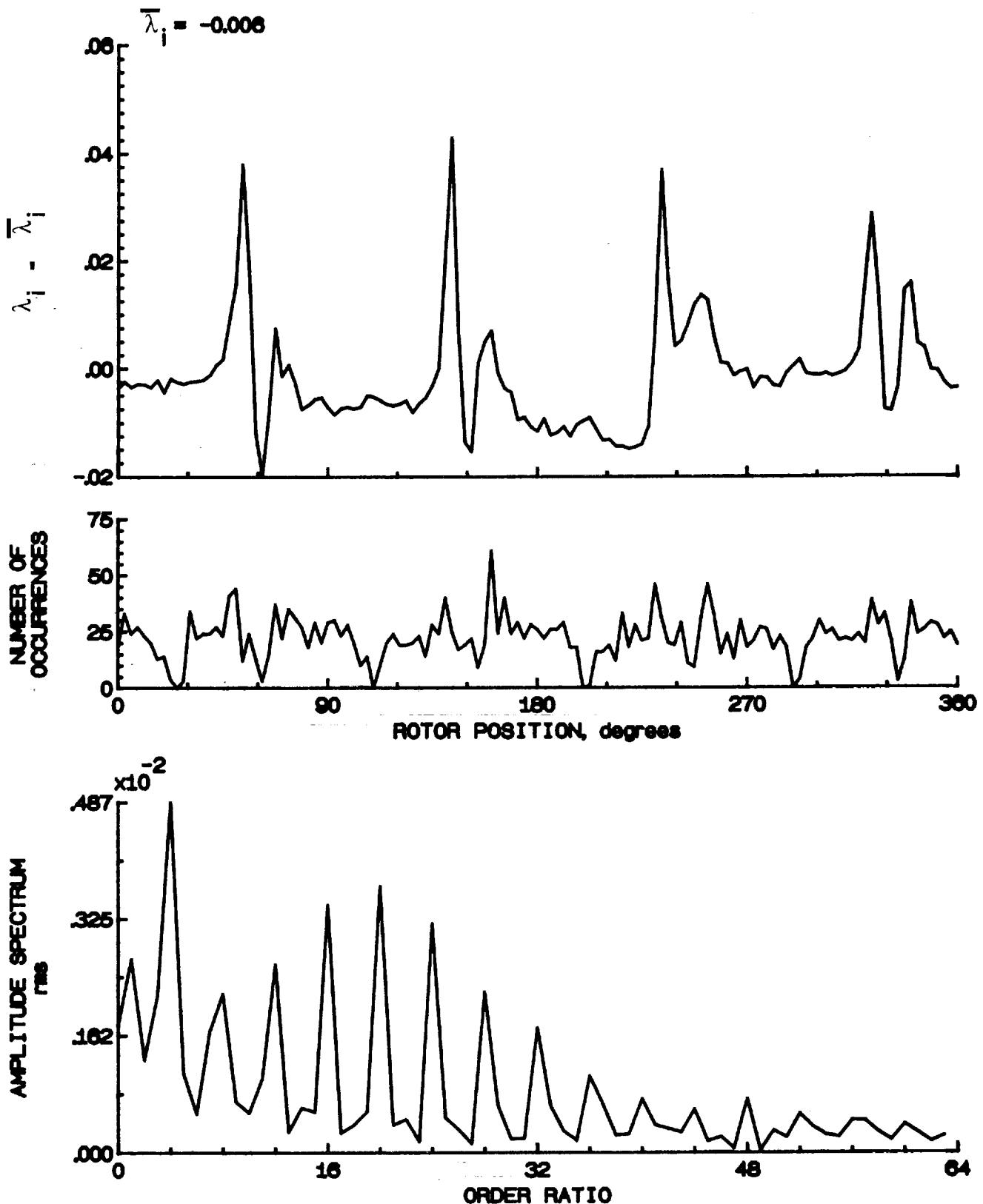


Figure 136.- Concluded.

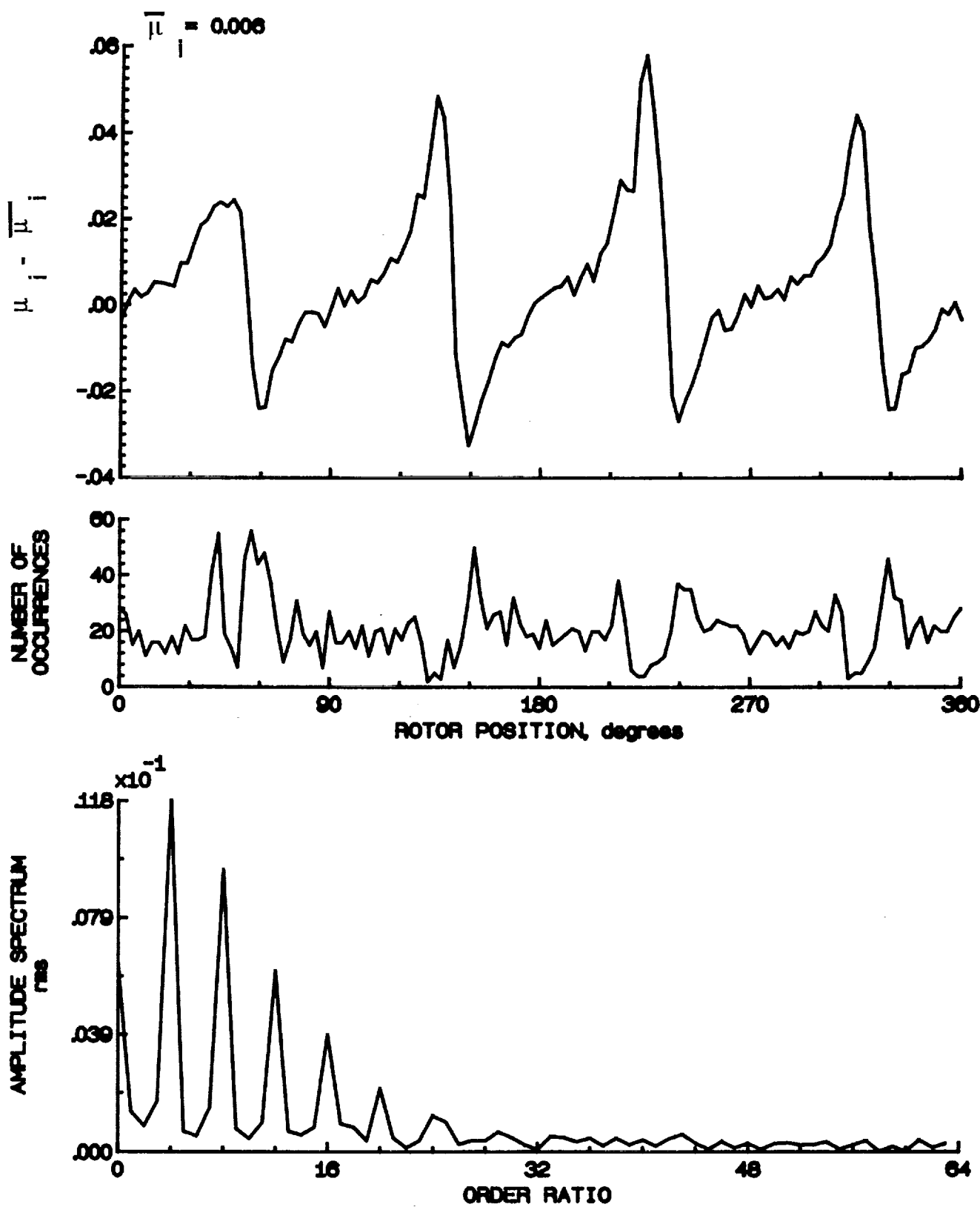


Figure 137.- Induced inflow velocity measured at 240 degrees and r/R of 0.74.

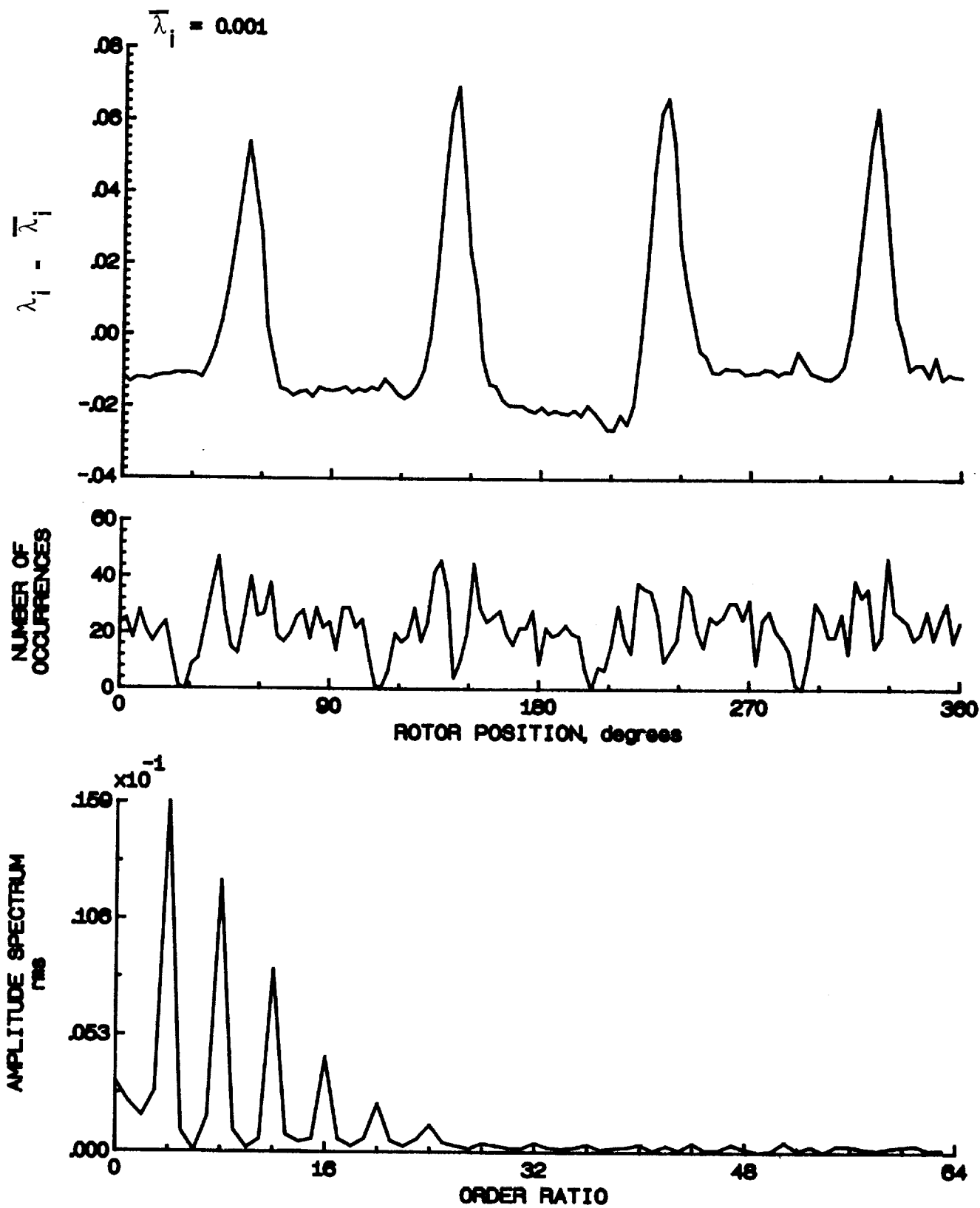


Figure 137.- Concluded.

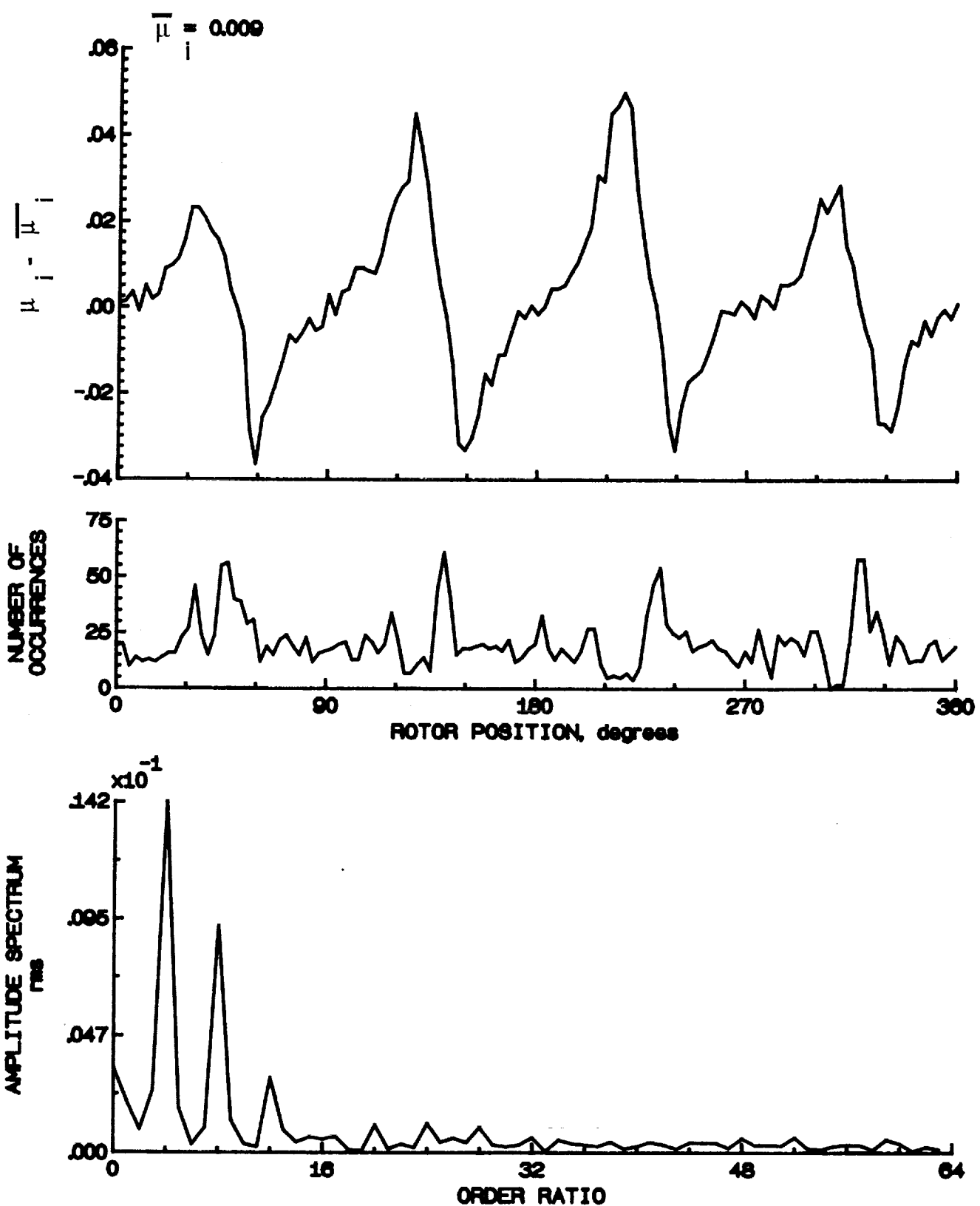
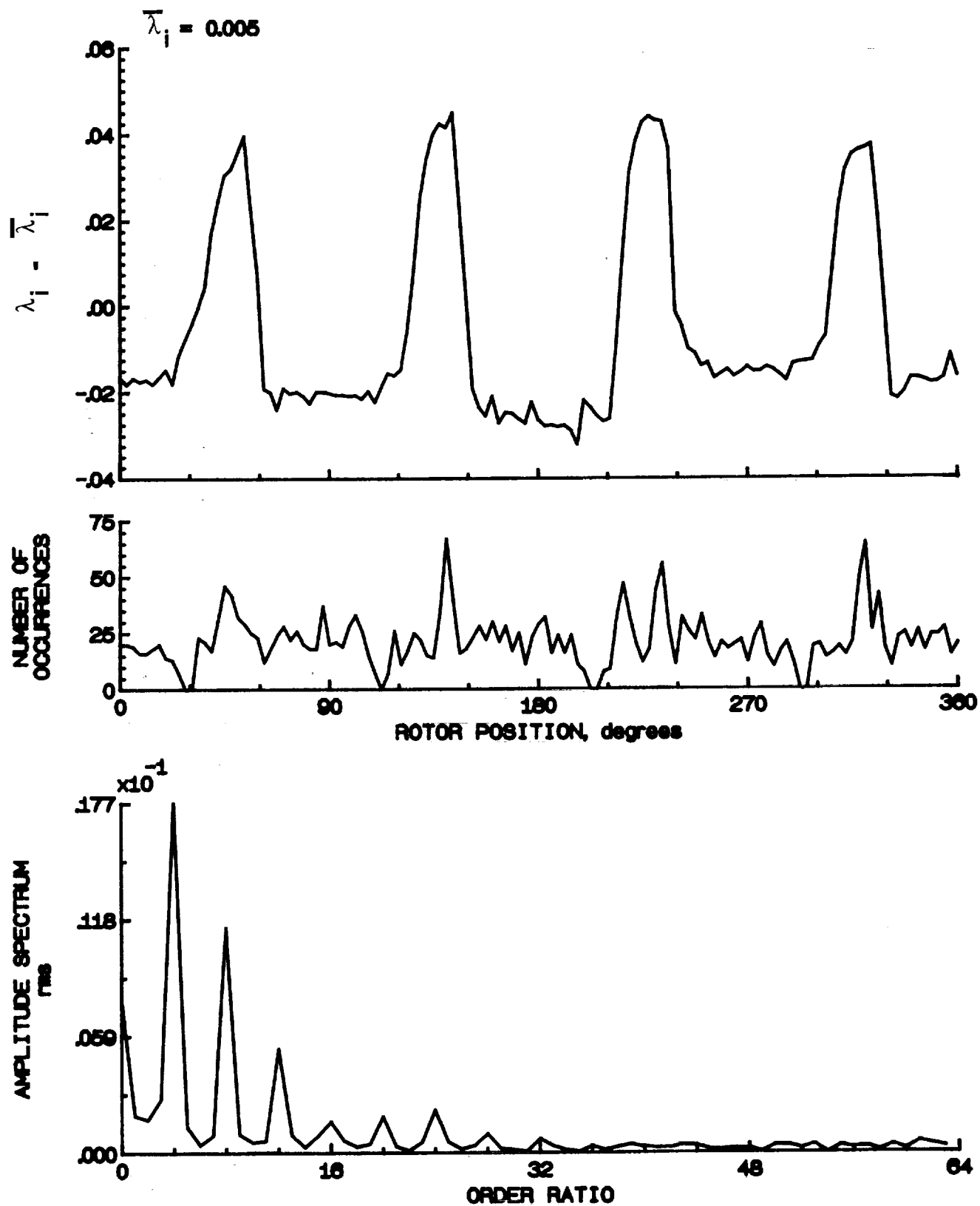


Figure 138.- Induced inflow velocity measured at 240 degrees and r/R of 0.78.



**Figure 138.- Concluded.**

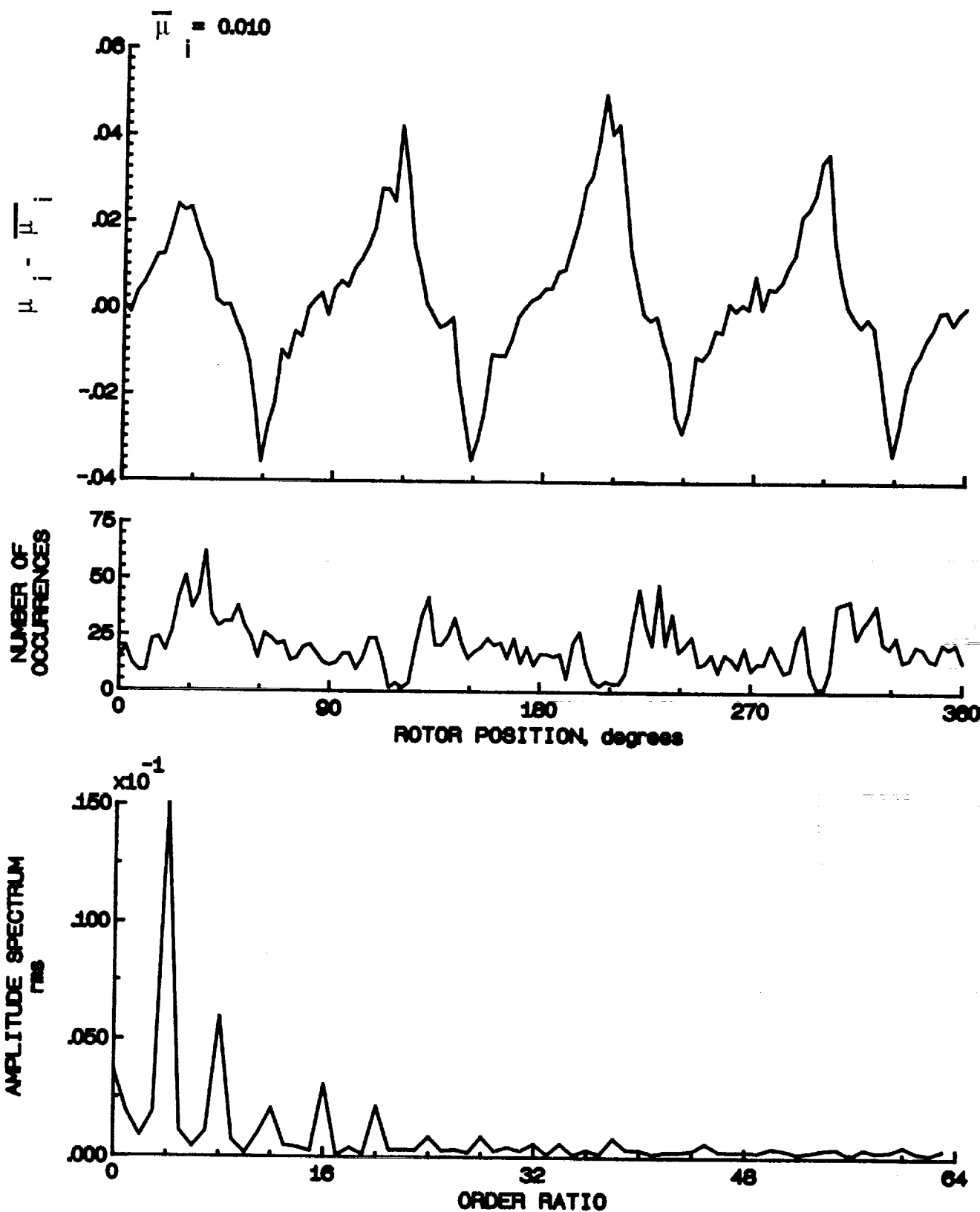


Figure 130.- Induced inflow velocity measured at 240 degrees and r/R of 0.82.

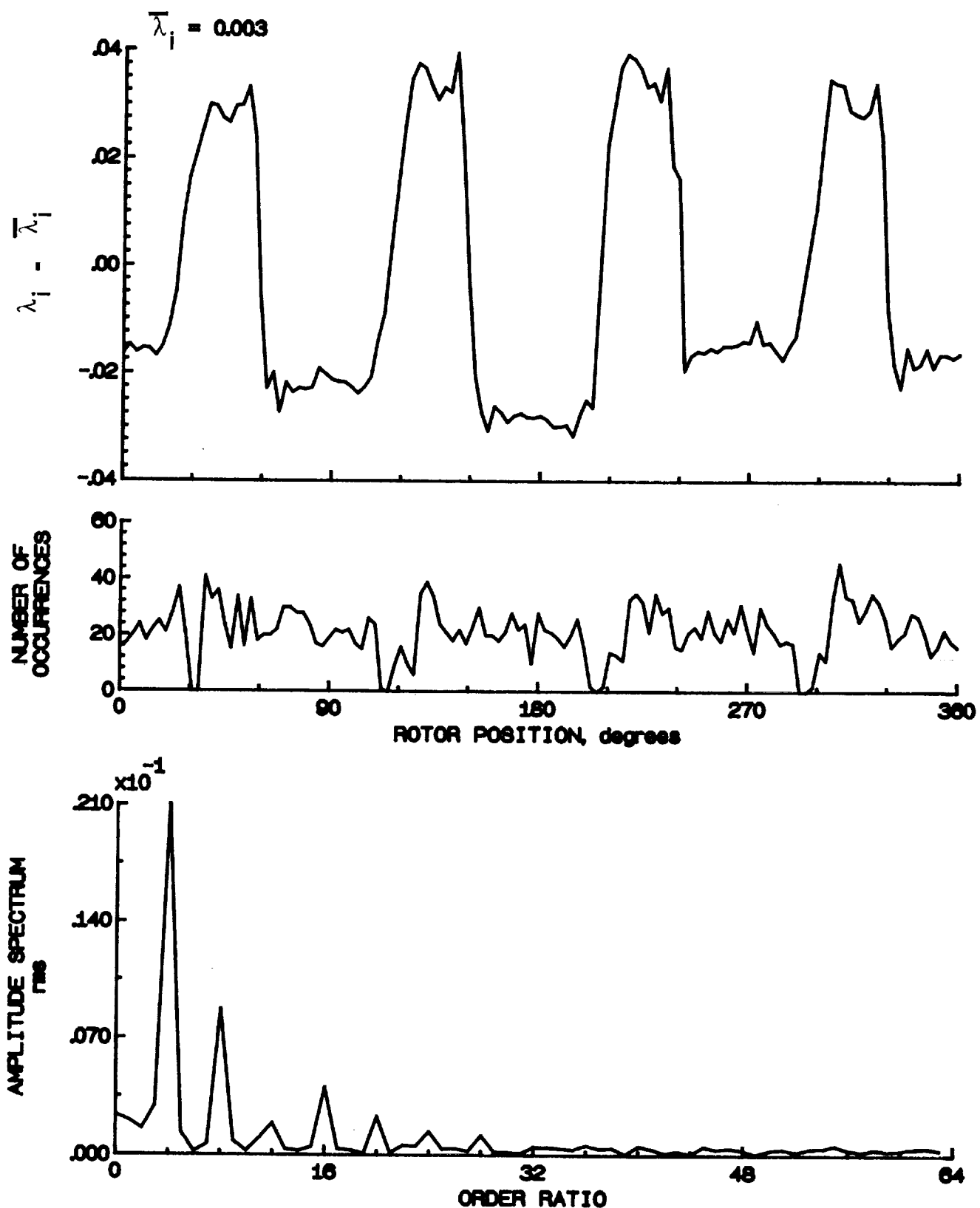


Figure 139.- Concluded.

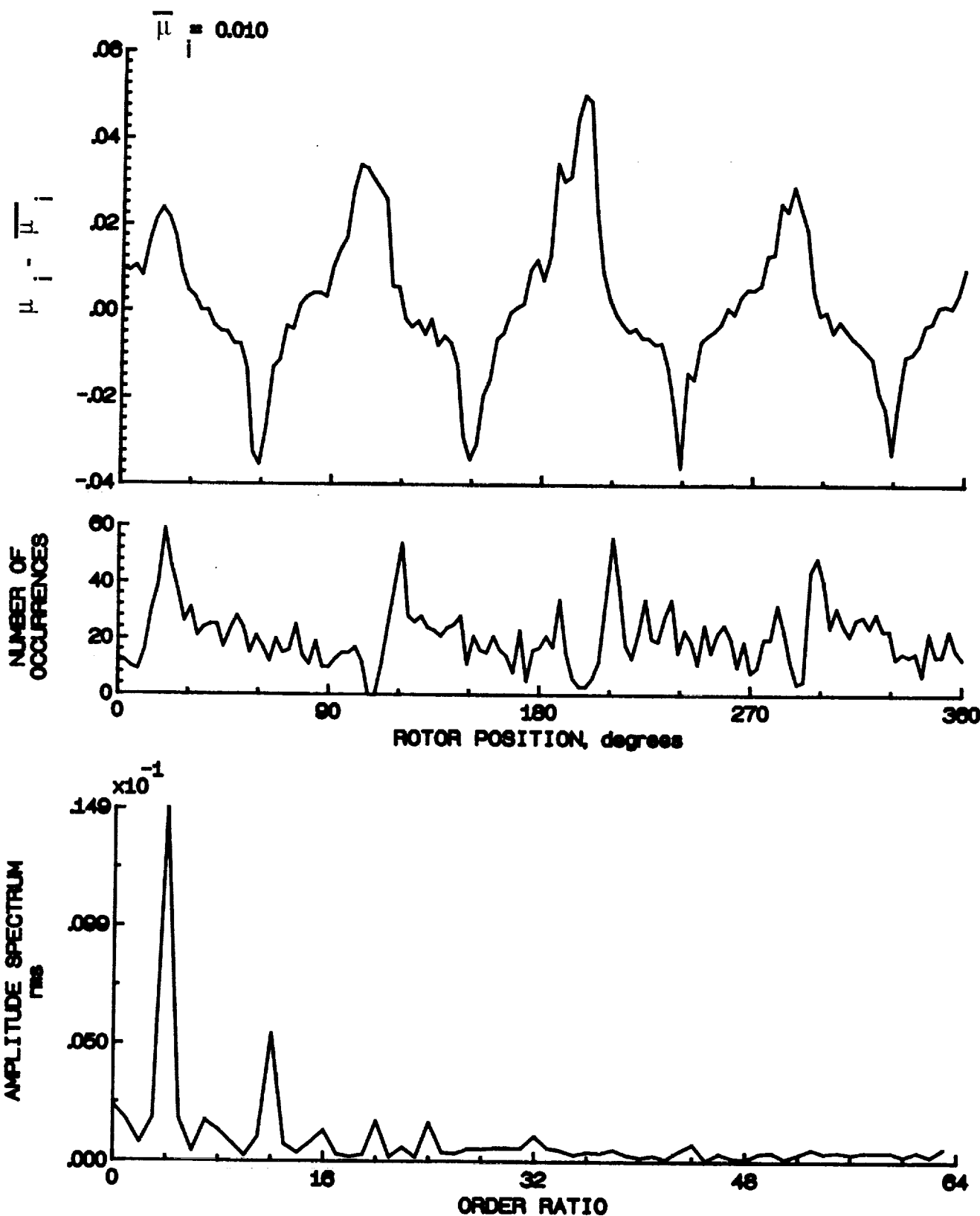


Figure 140.- Induced inflow velocity measured at 240 degrees and r/R of 0.86.

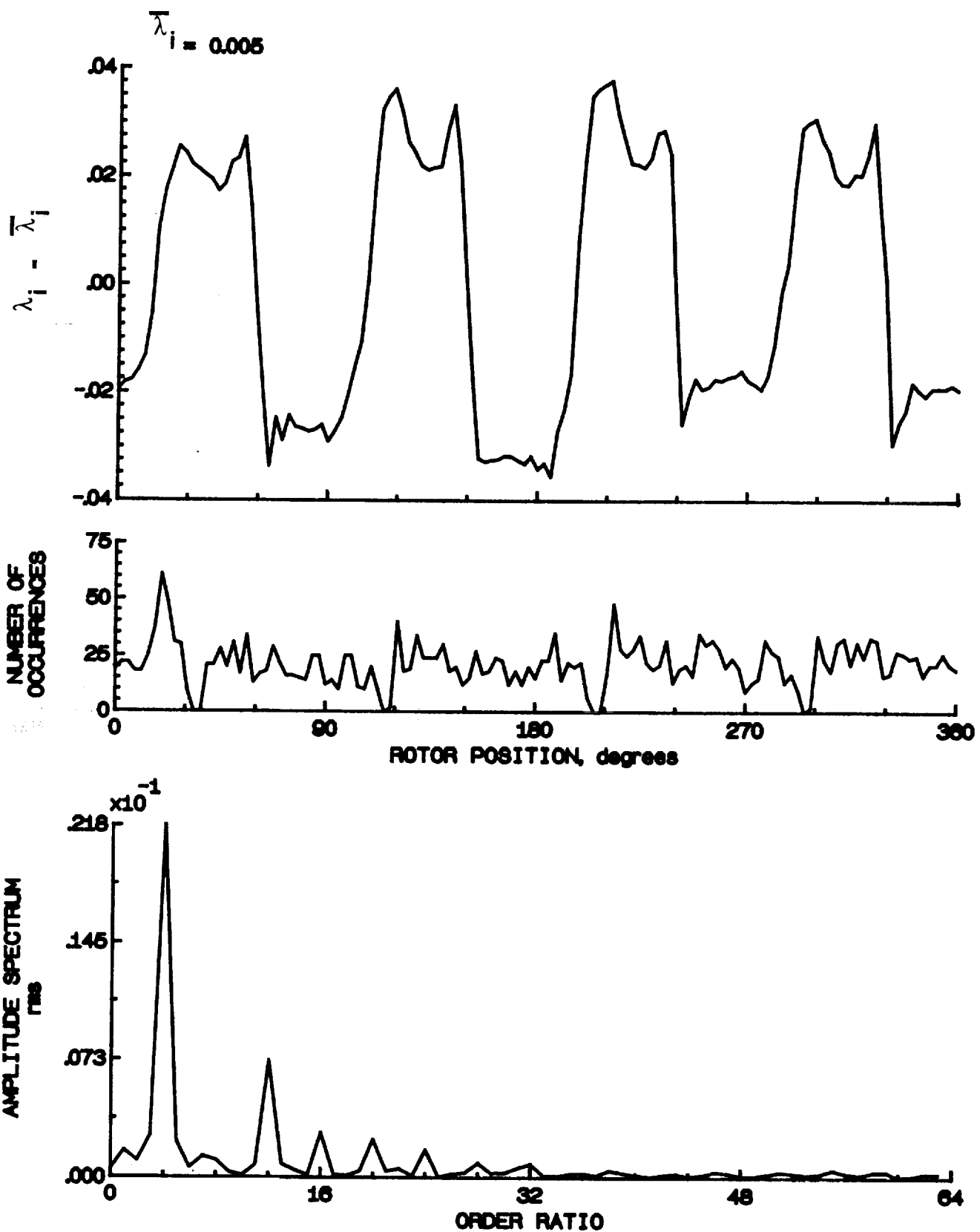


Figure 140.- Concluded.

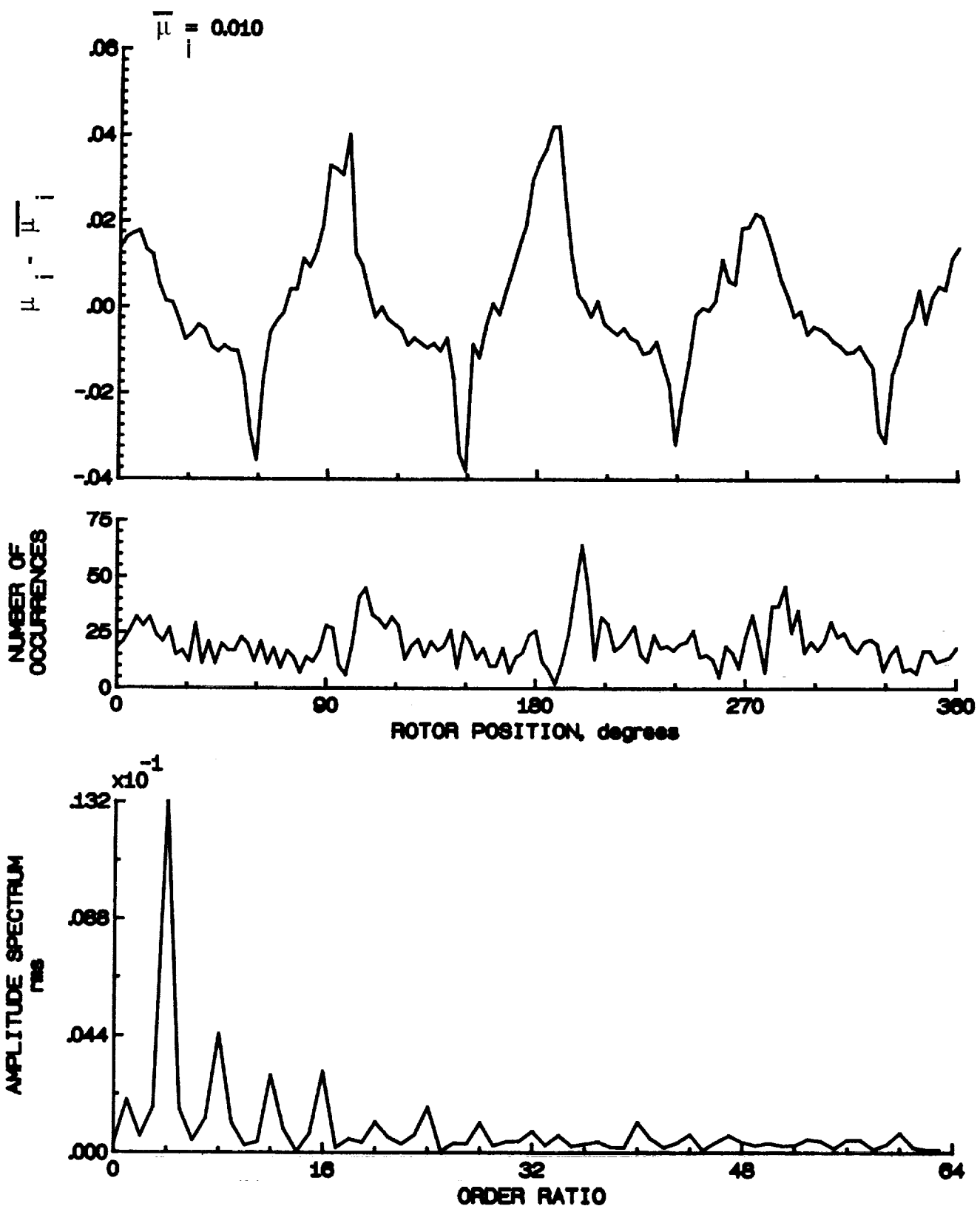


Figure 141.- Induced inflow velocity measured at 240 degrees and r/R of 0.90.

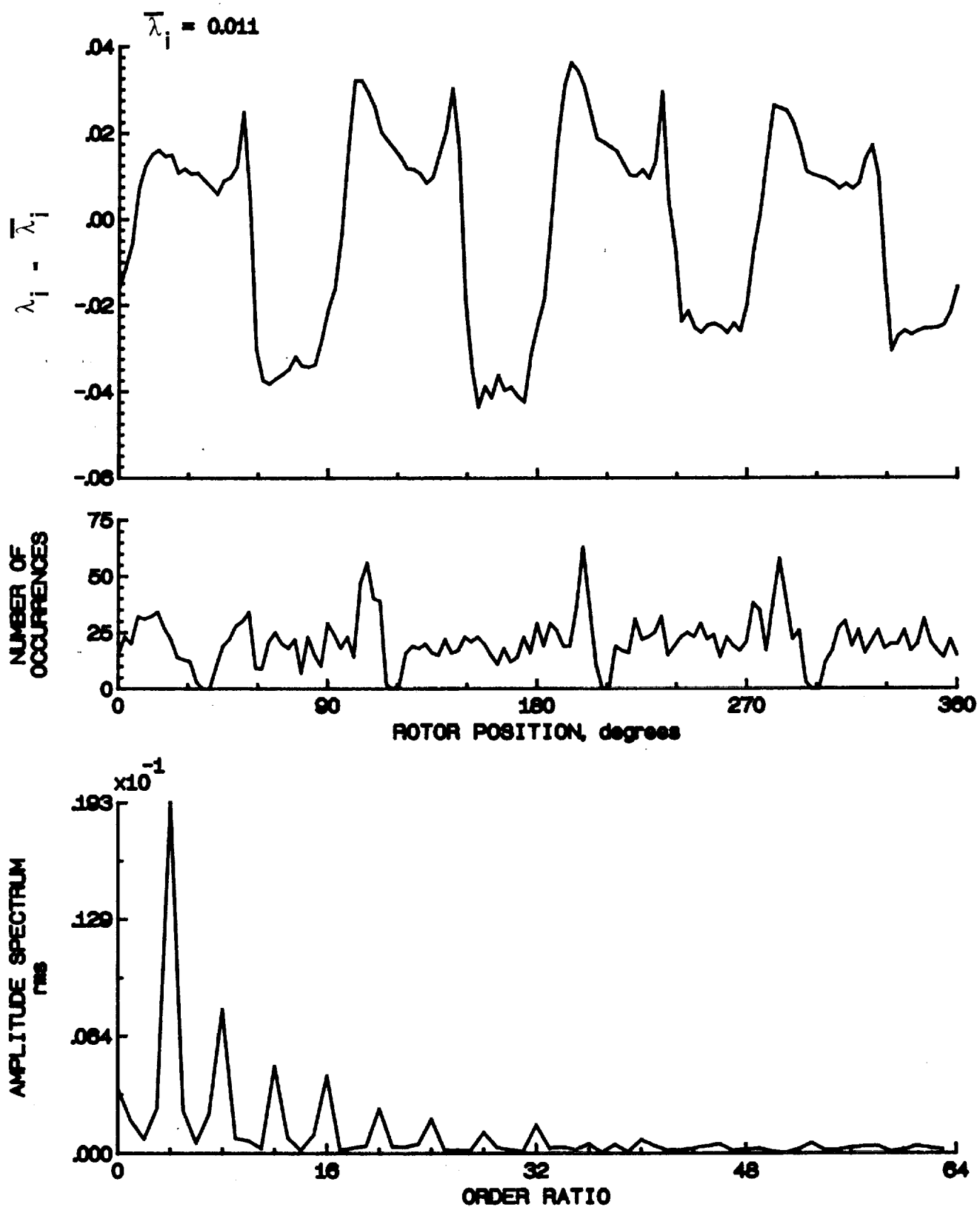


Figure 141.- Concluded.

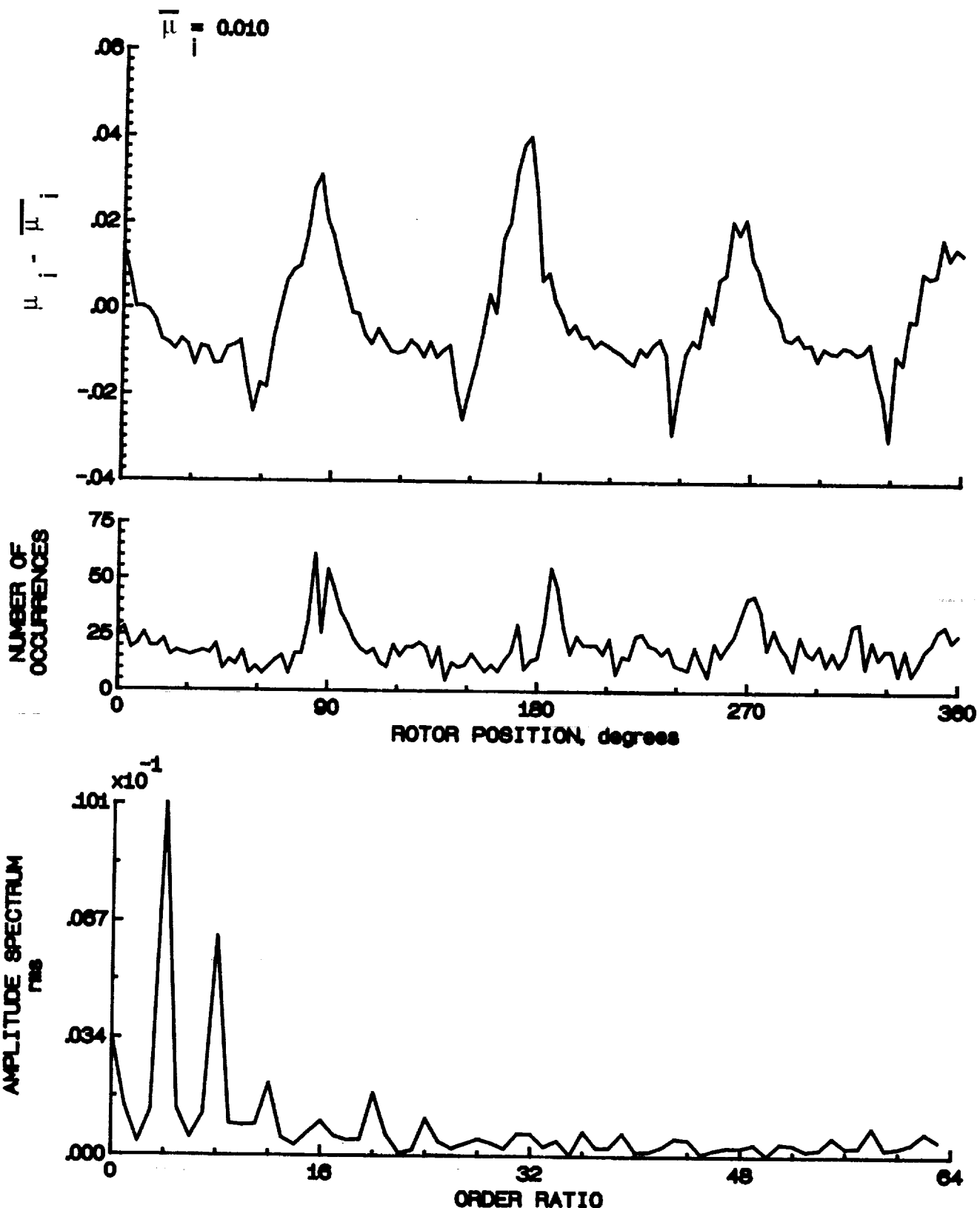


Figure 142.- Induced inflow velocity measured at 240 degrees and r/R of 0.94.

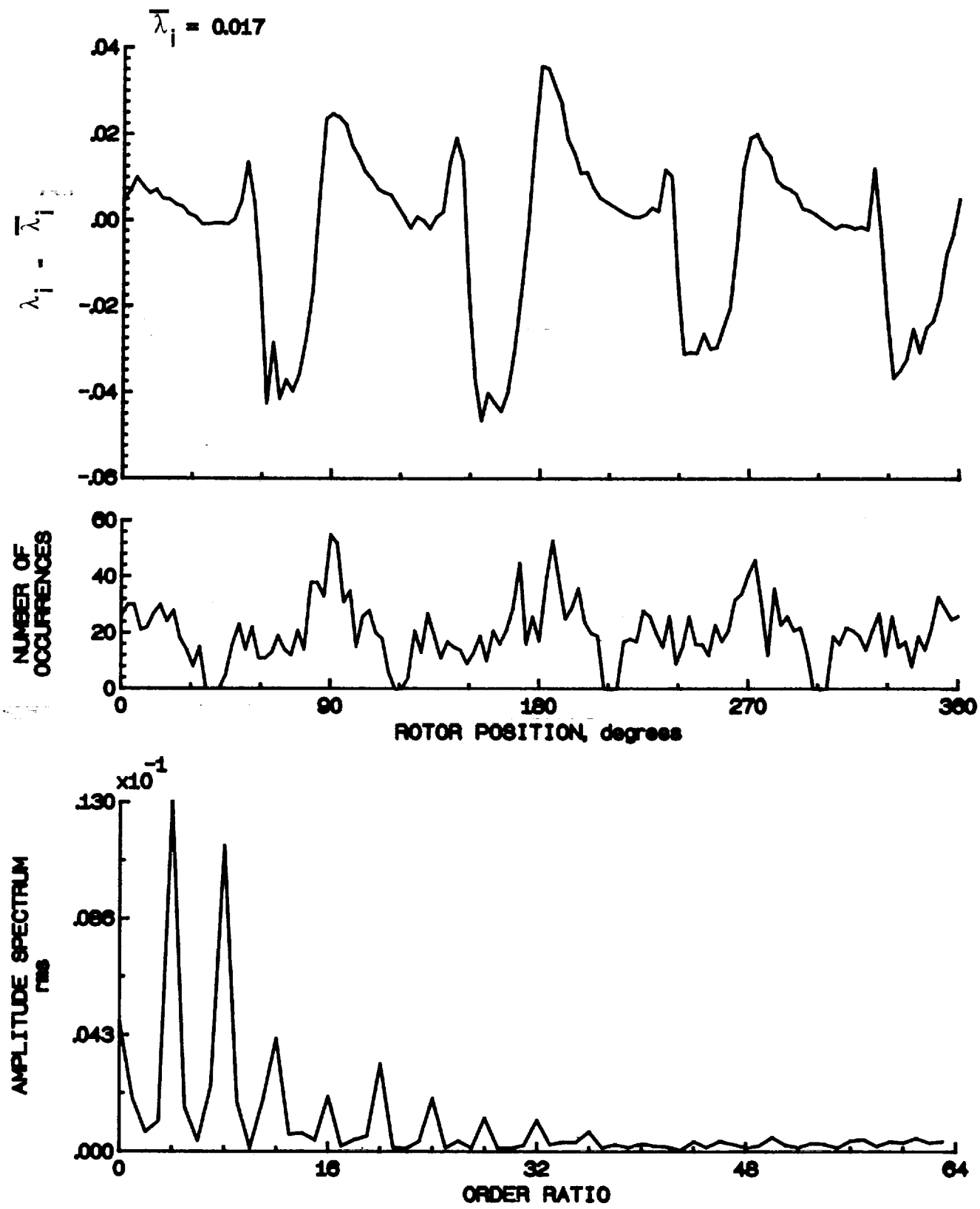


Figure 142.- Concluded.

c4

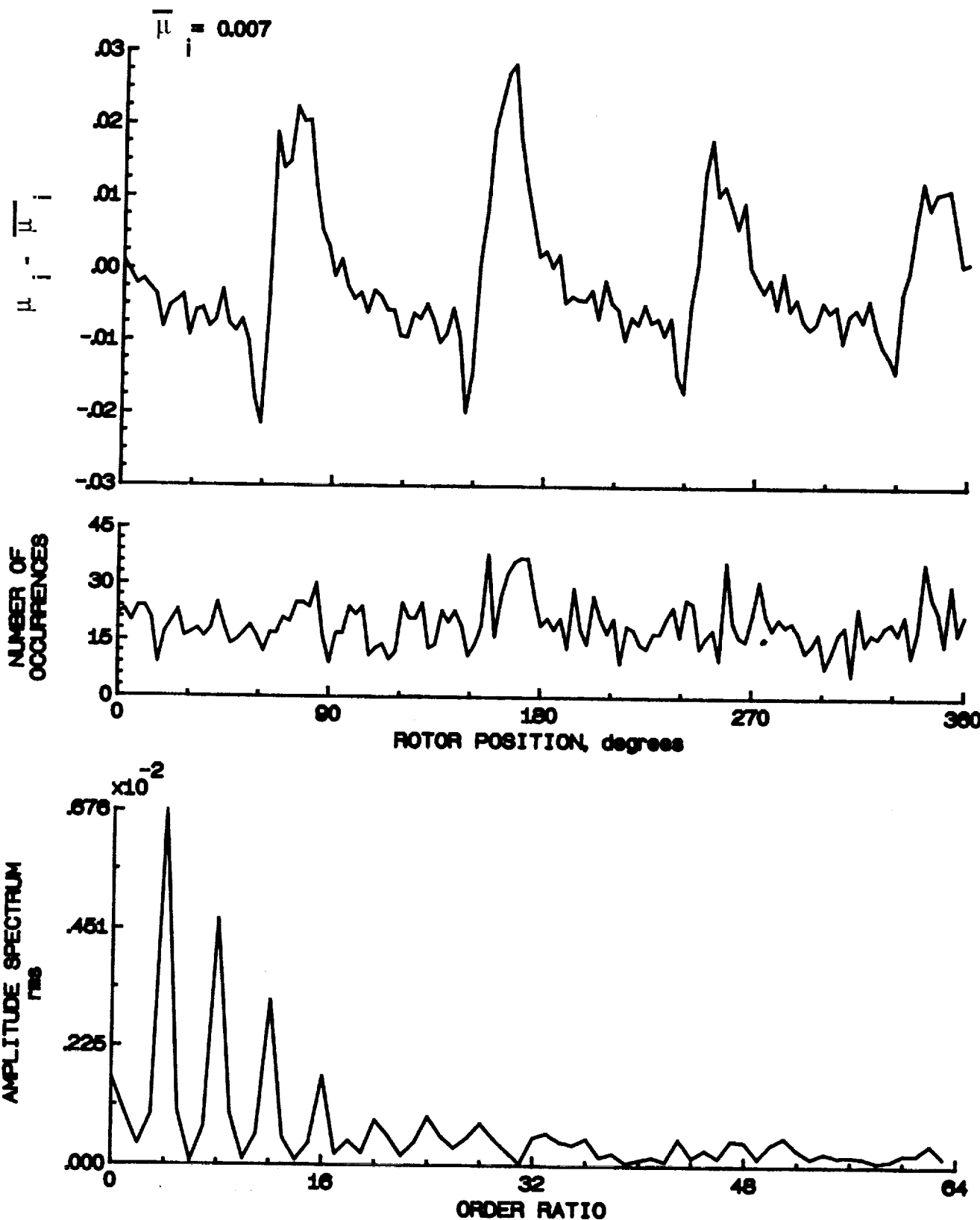


Figure 143.- Induced inflow velocity measured at 240 degrees and r/R of 0.93.

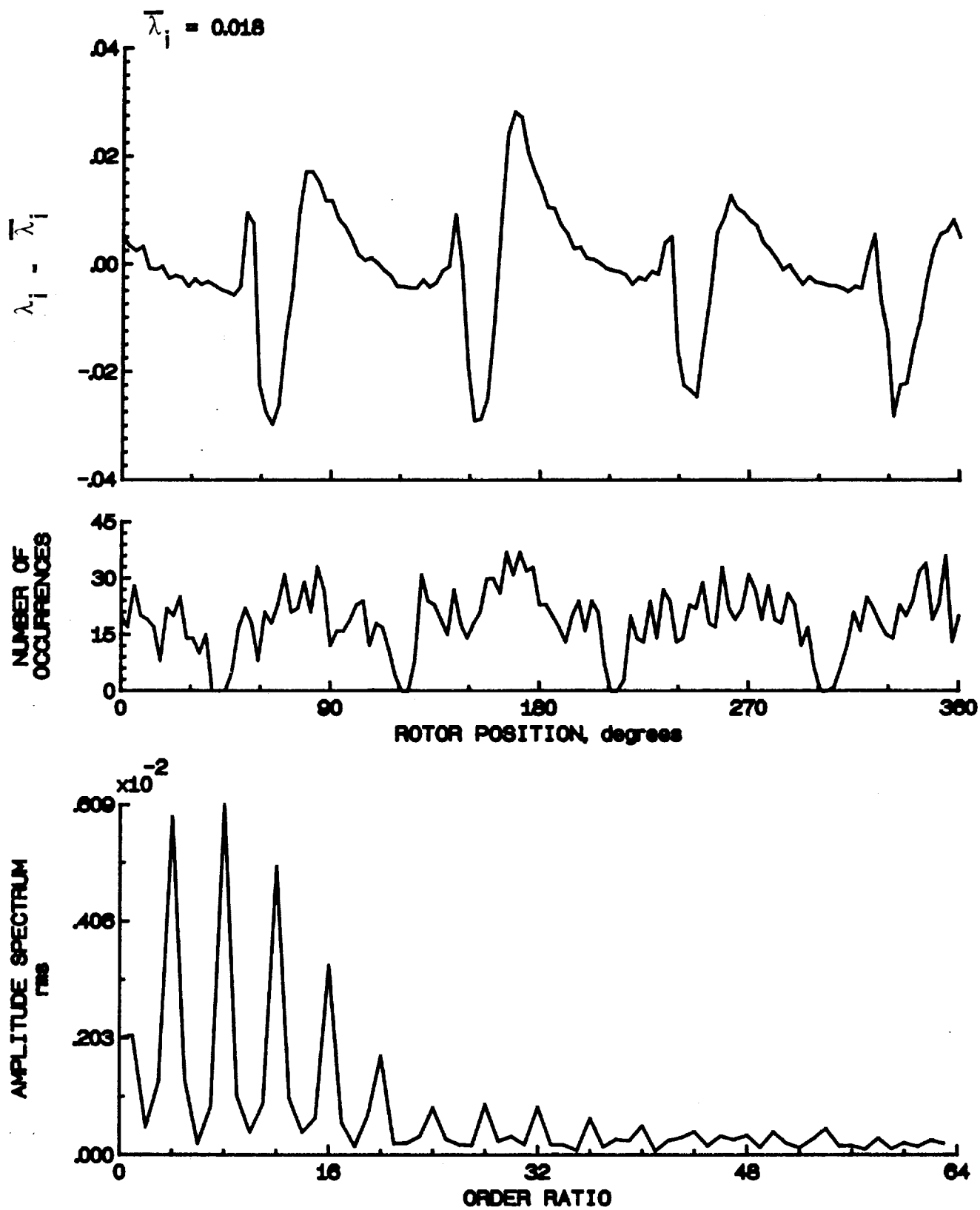


Figure 143.- Concluded.

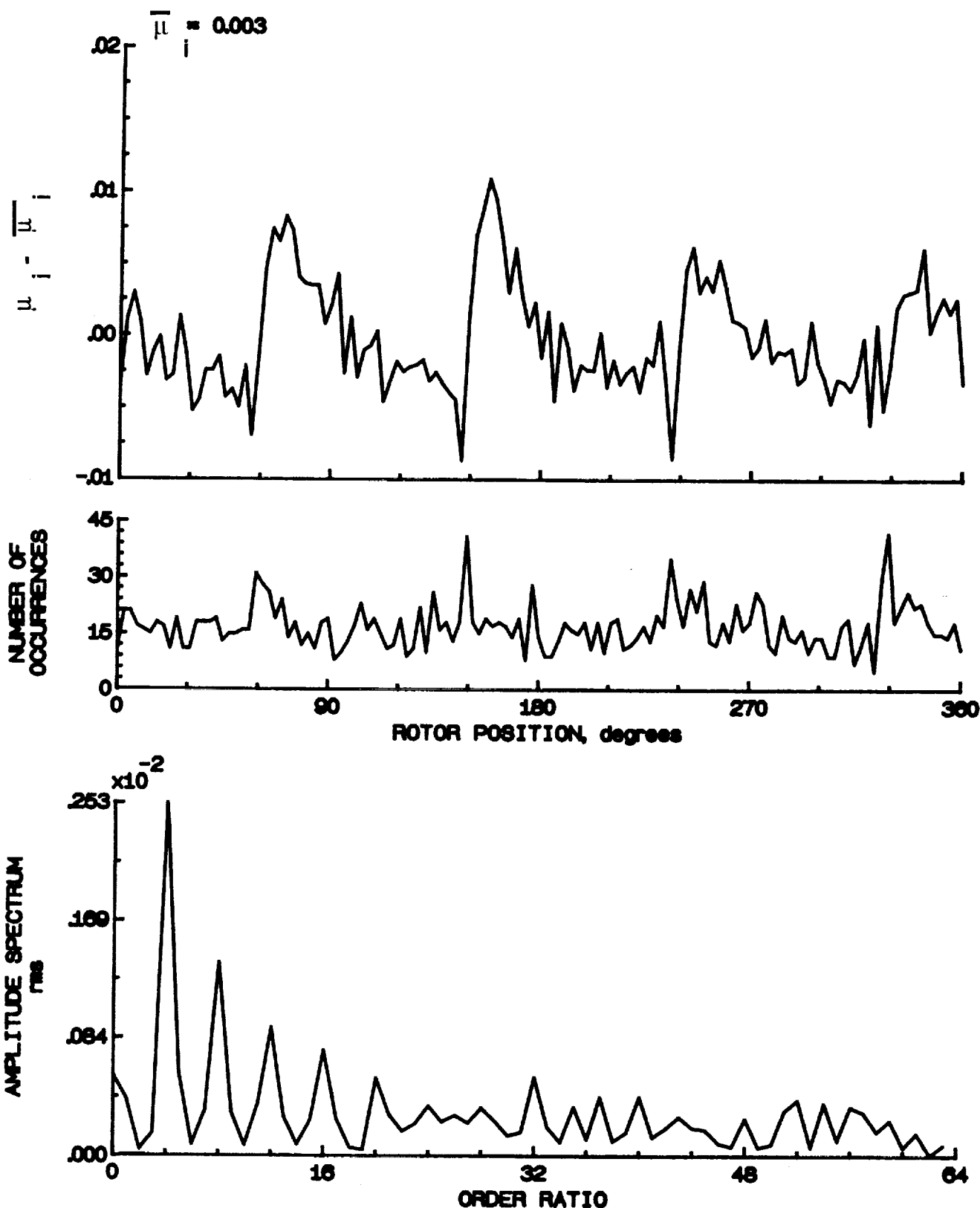


Figure 144.- Induced inflow velocity measured at 240 degrees and r/R of 1.02.

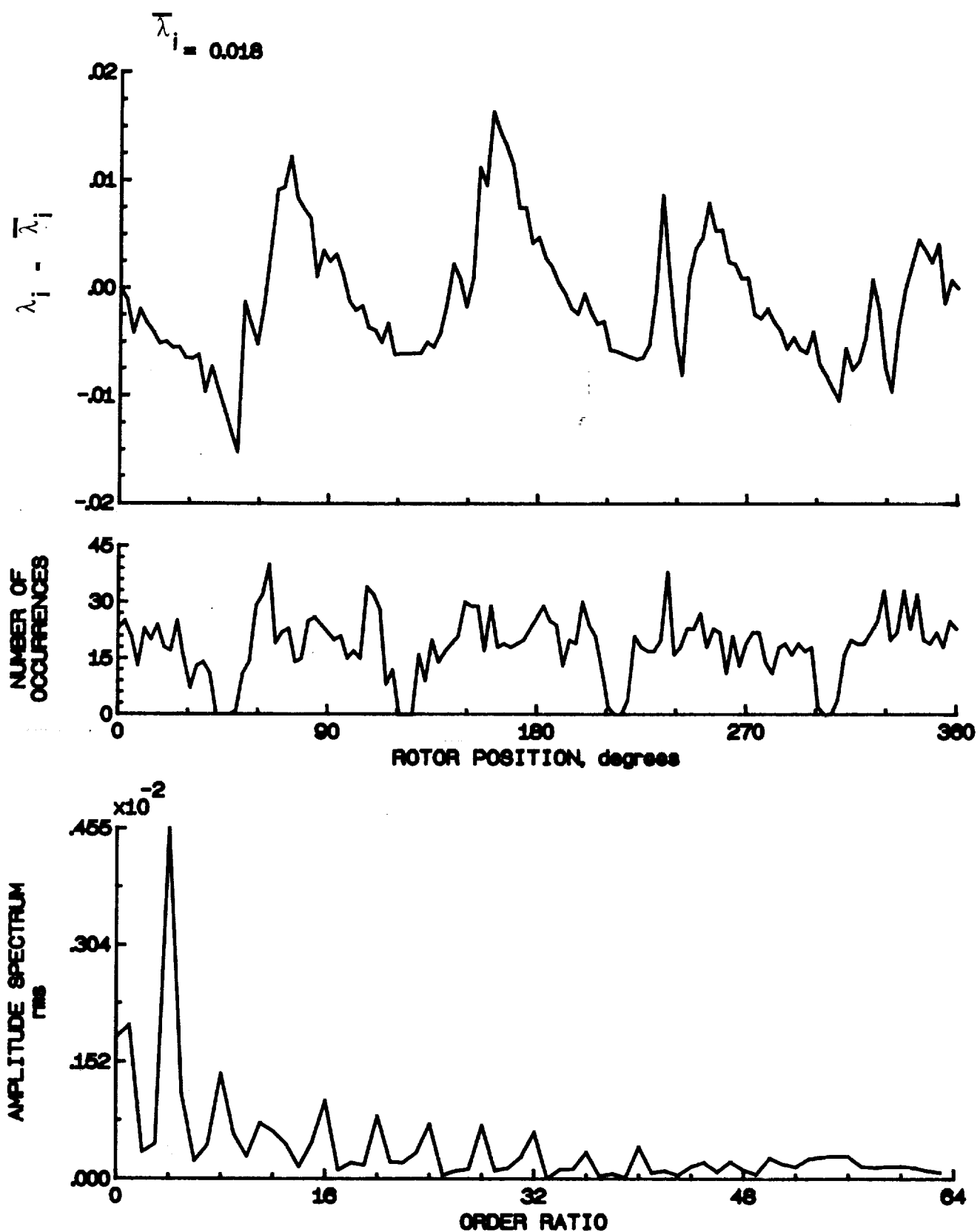


Figure 144.- Concluded.

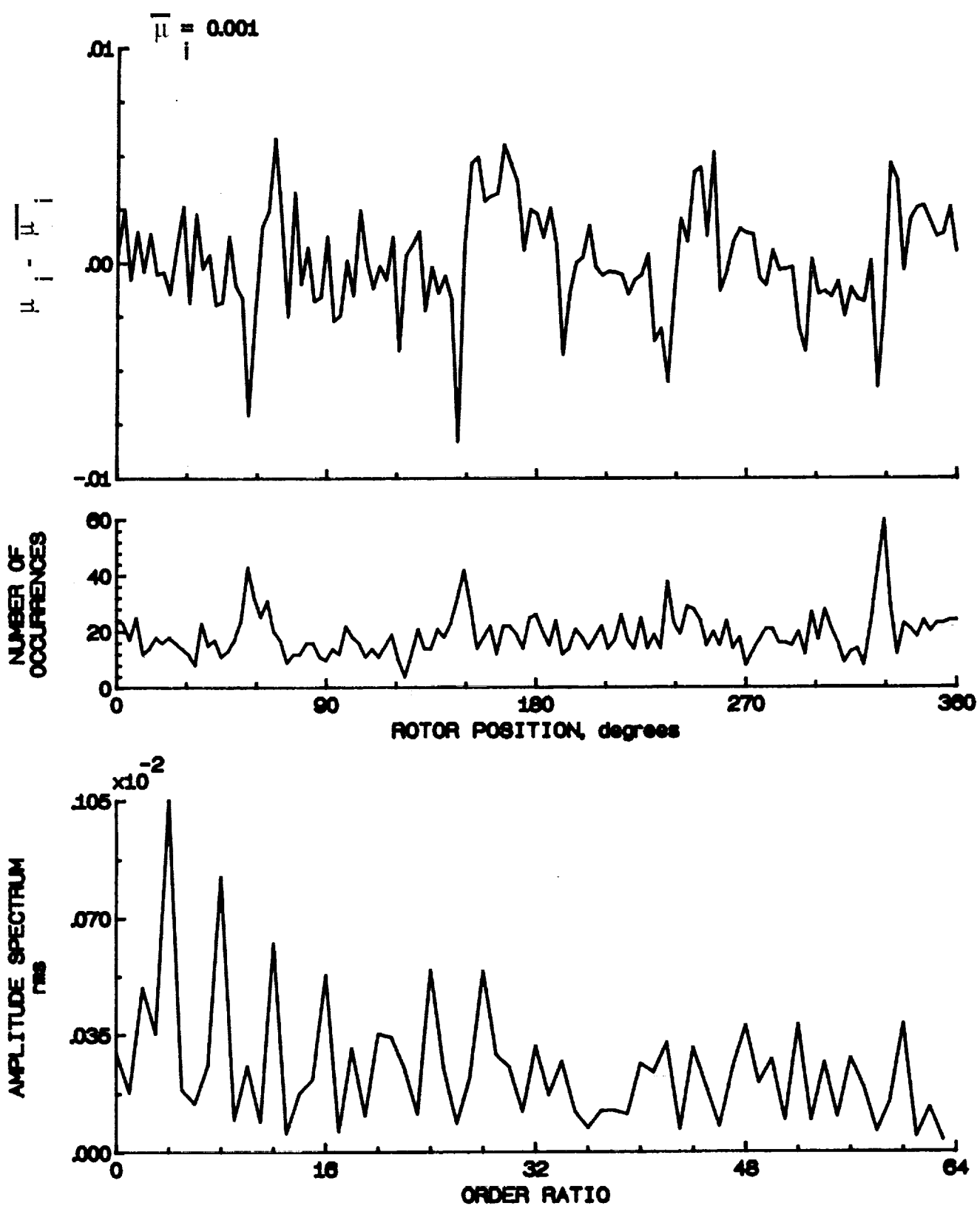


Figure 145.- Induced inflow velocity measured at 240 degrees and r/R of 1.04.

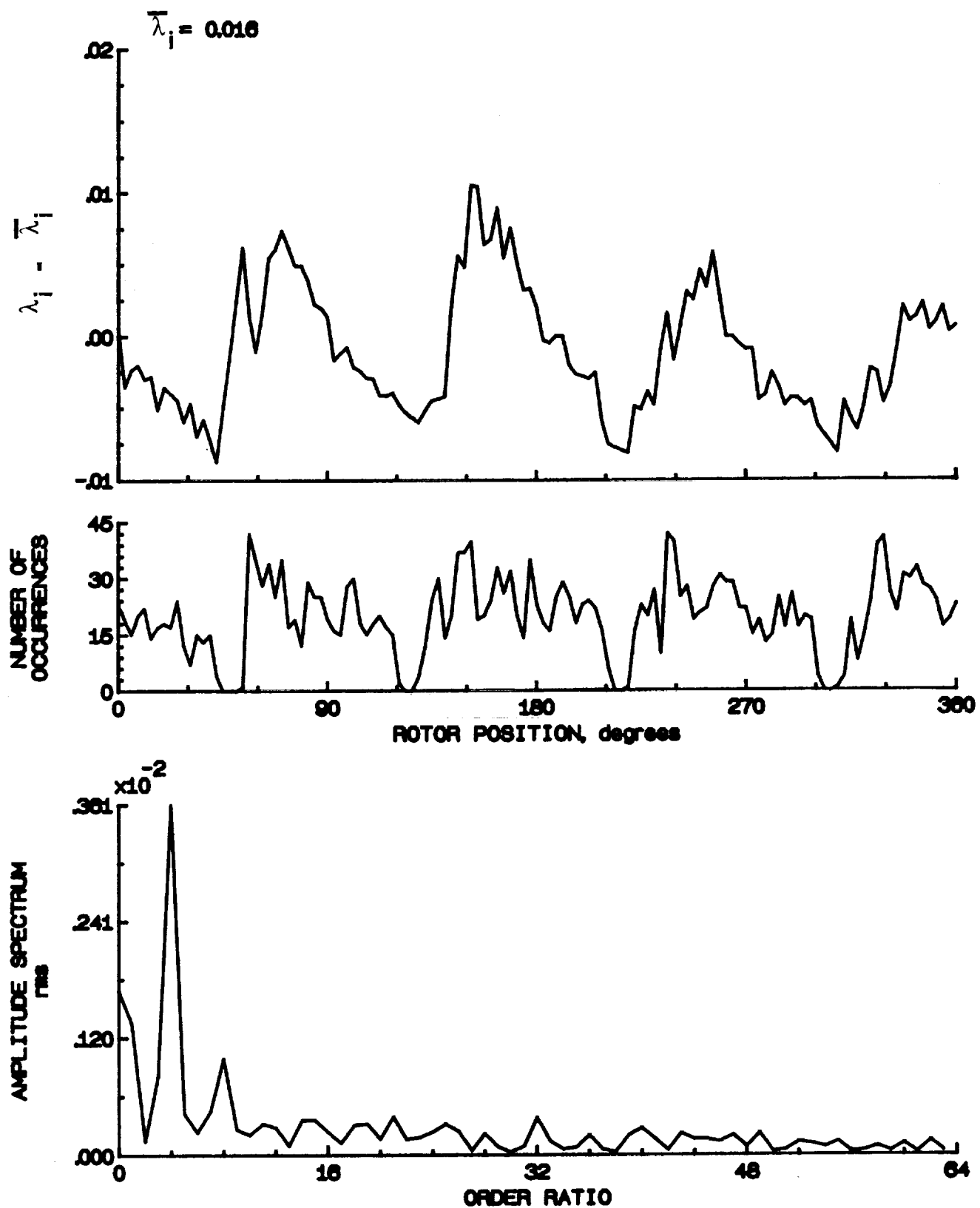


Figure 145.- Concluded.

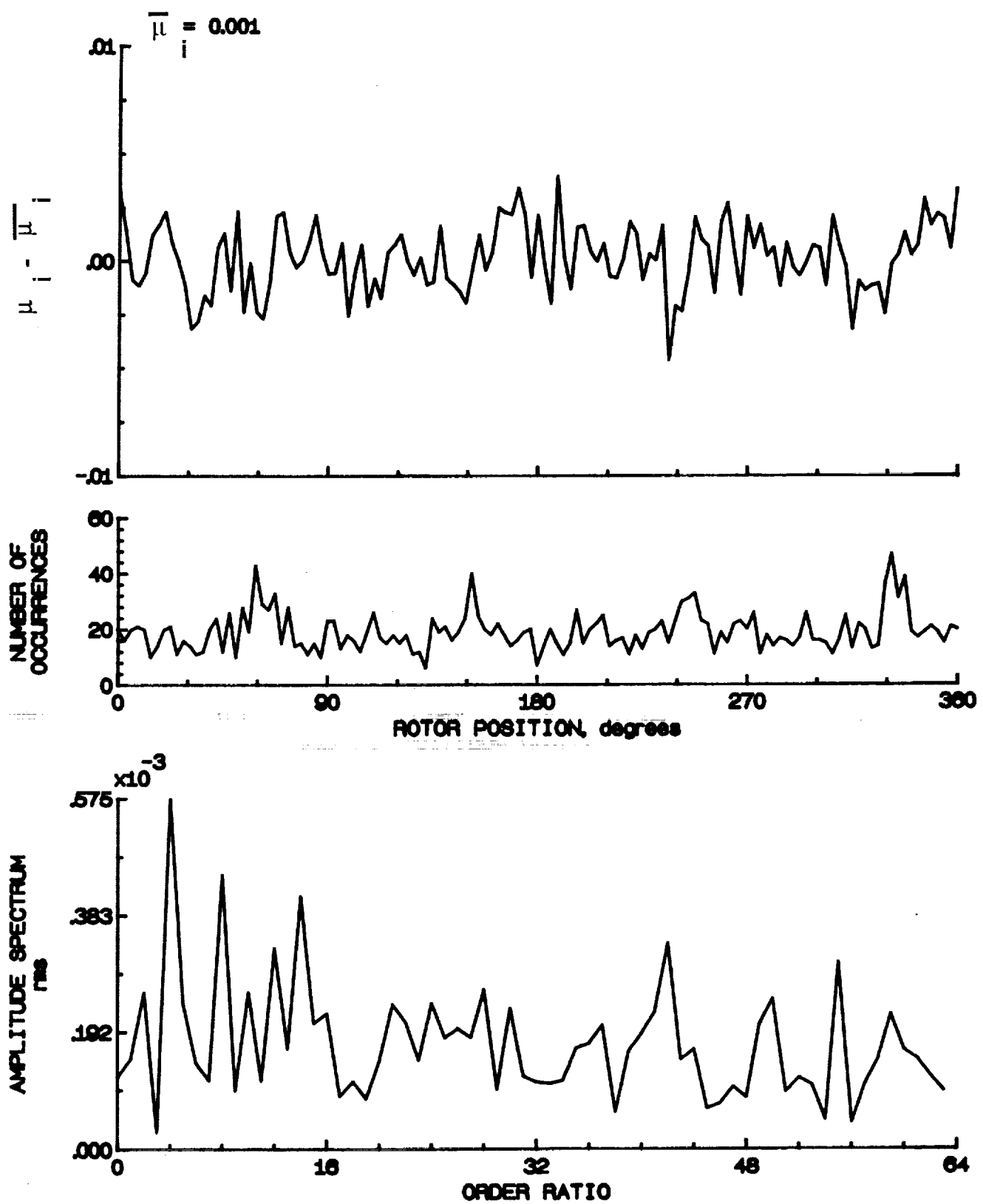


Figure 148.- Induced inflow velocity measured at 240 degrees and r/R of 1.10.

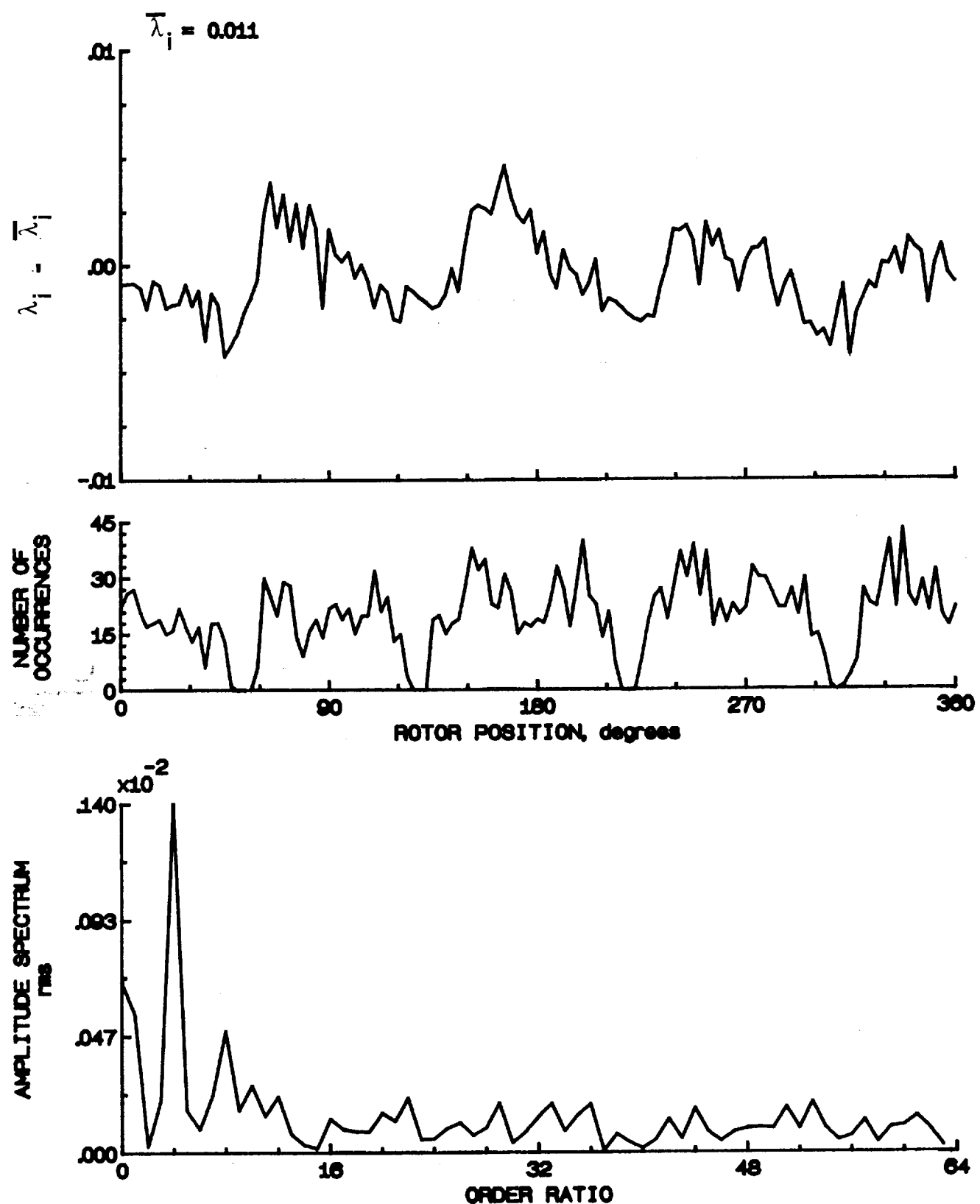


Figure 146.- Concluded.

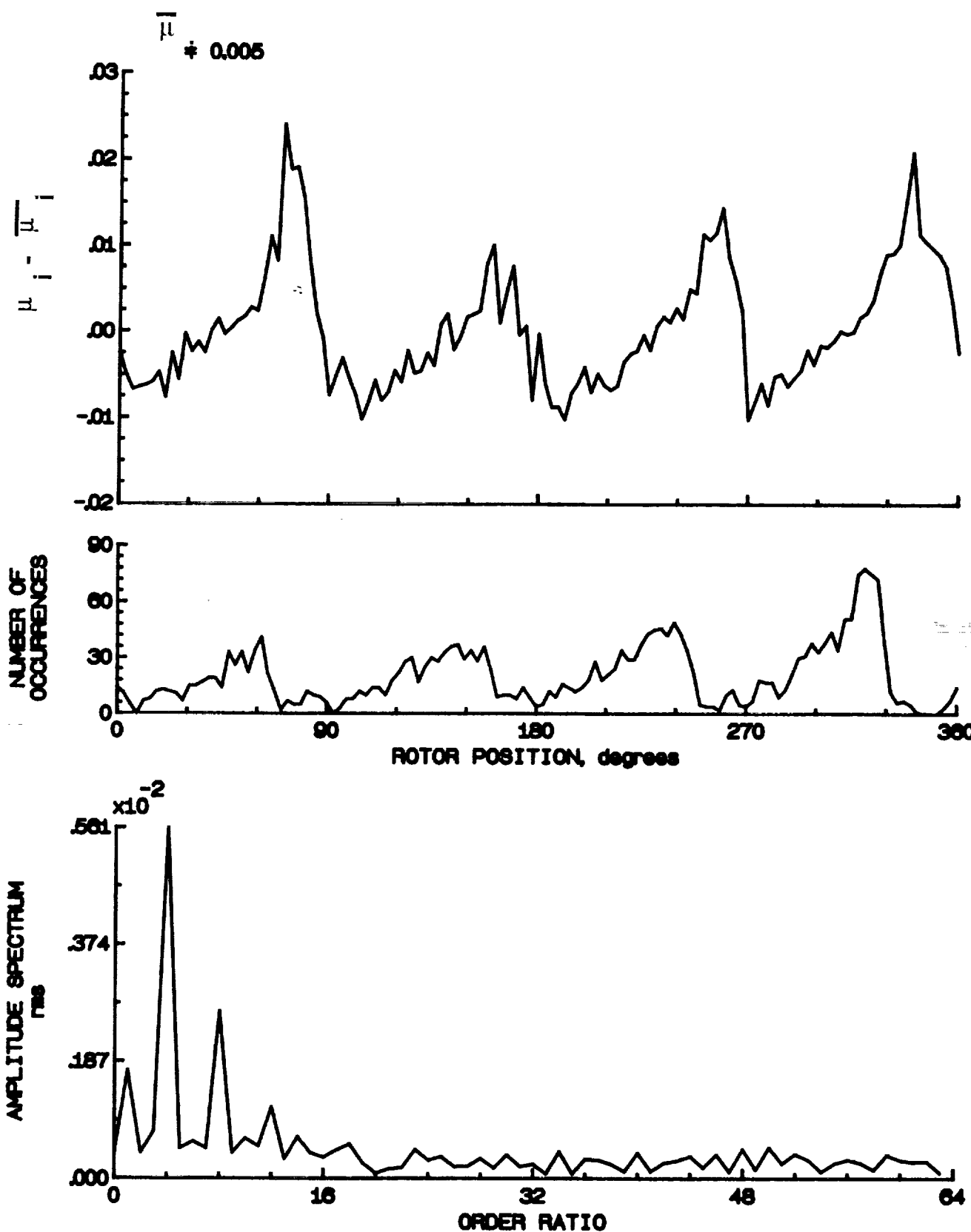


Figure 147.- Induced inflow velocity measured at 270 degrees and r/R of 0.20.

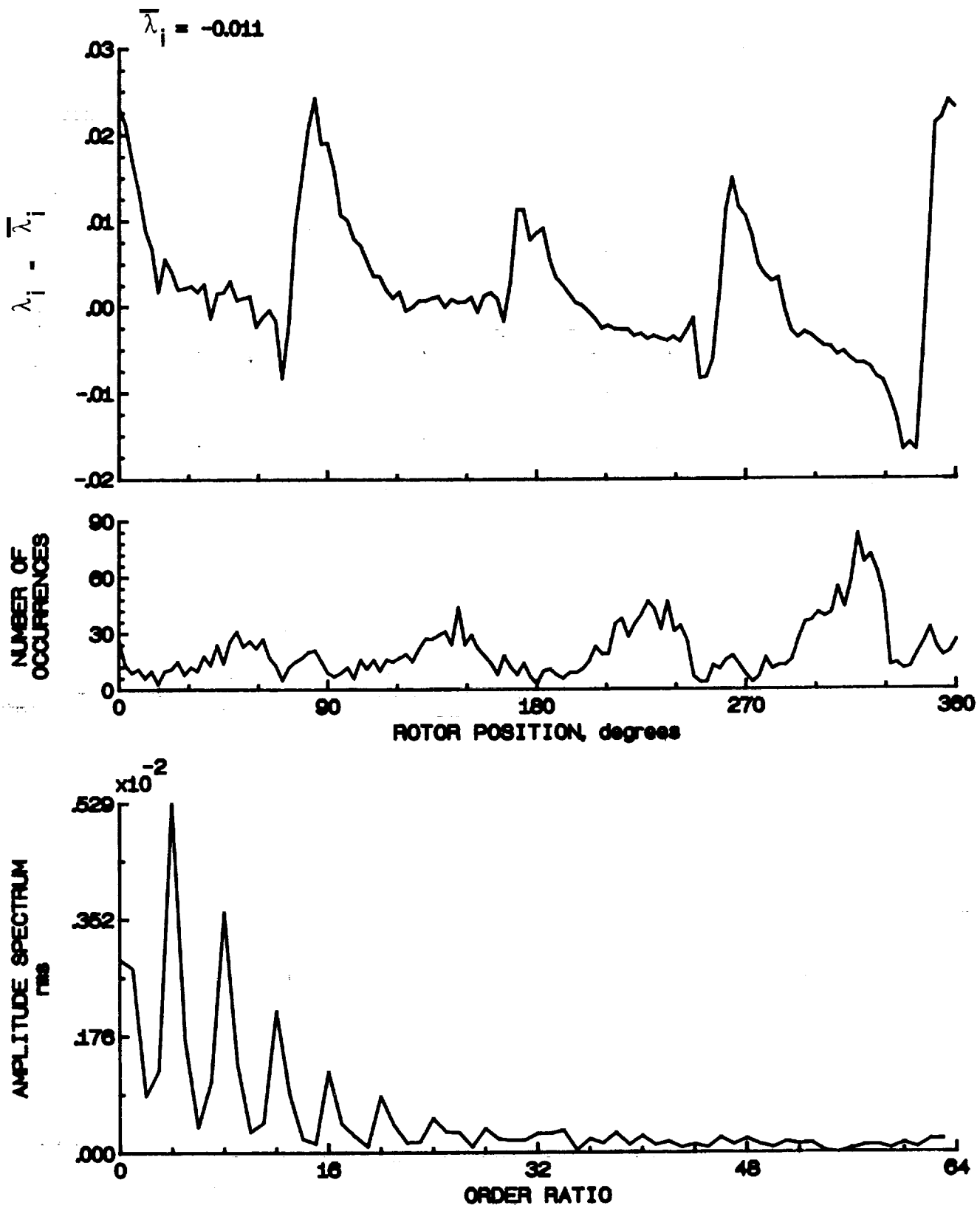


Figure 147.- Concluded.

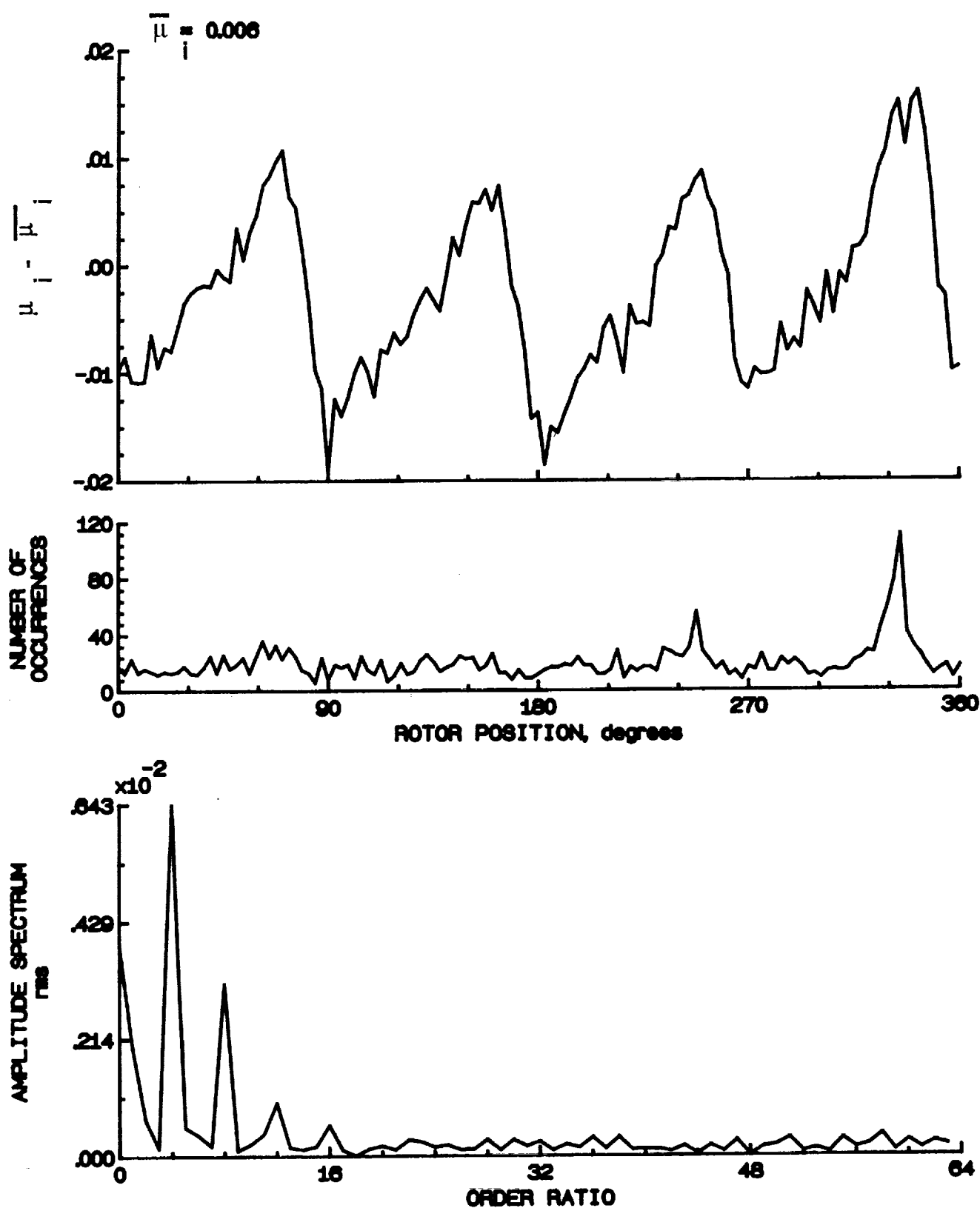


Figure 148.- Induced inflow velocity measured at 270 degrees and r/R of 0.40.

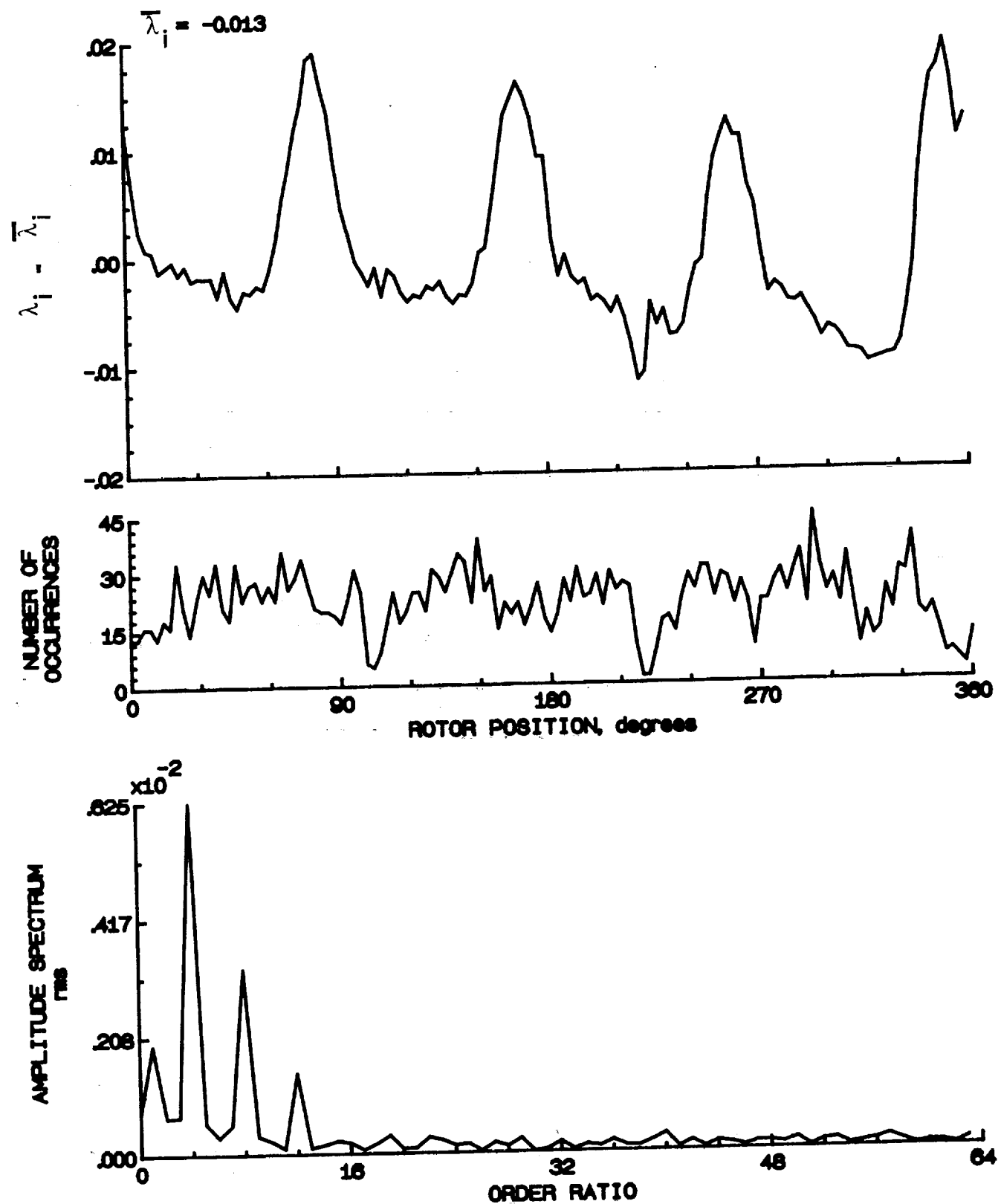


Figure 148.- Concluded.

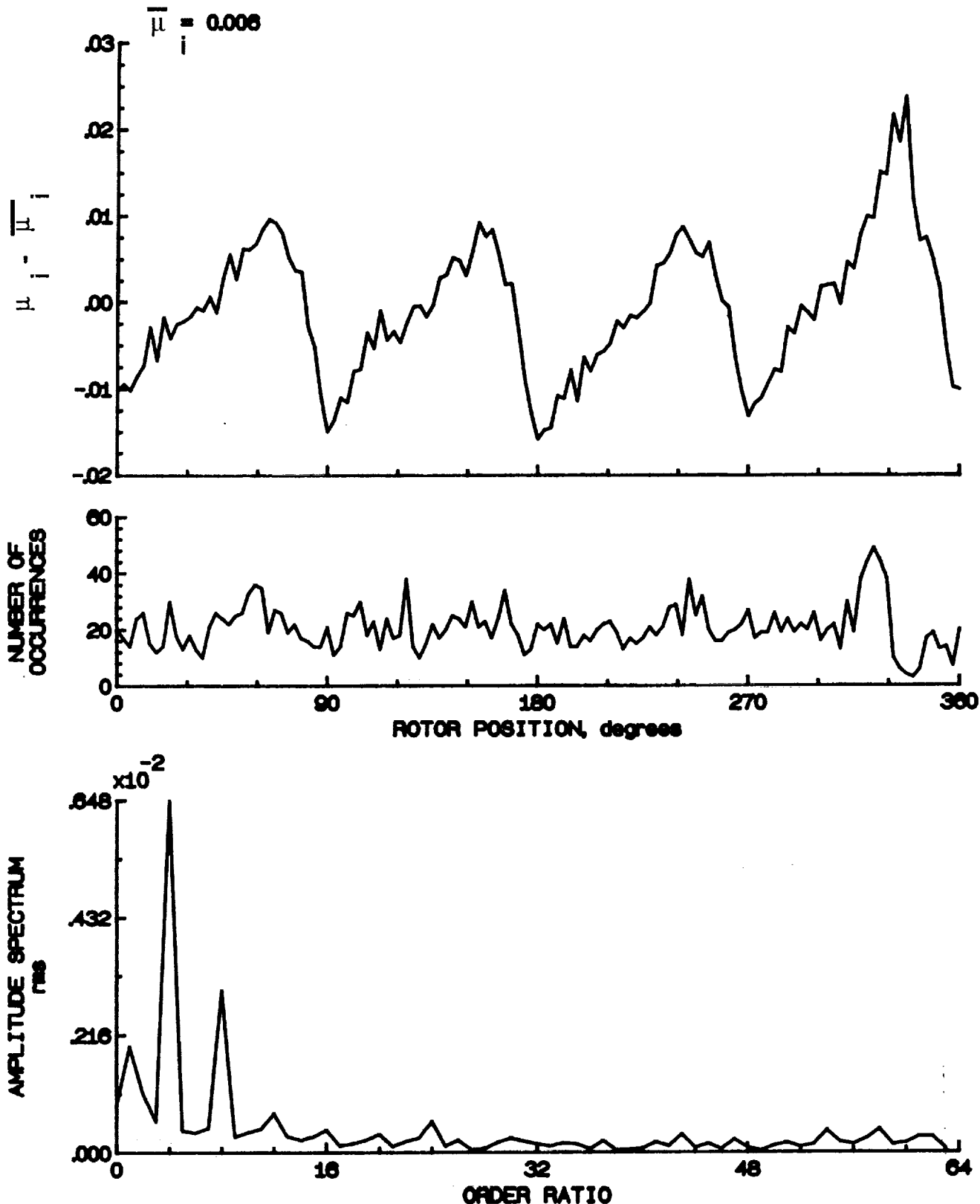


Figure 149.- Induced inflow velocity measured at 270 degrees and r/R of 0.50.

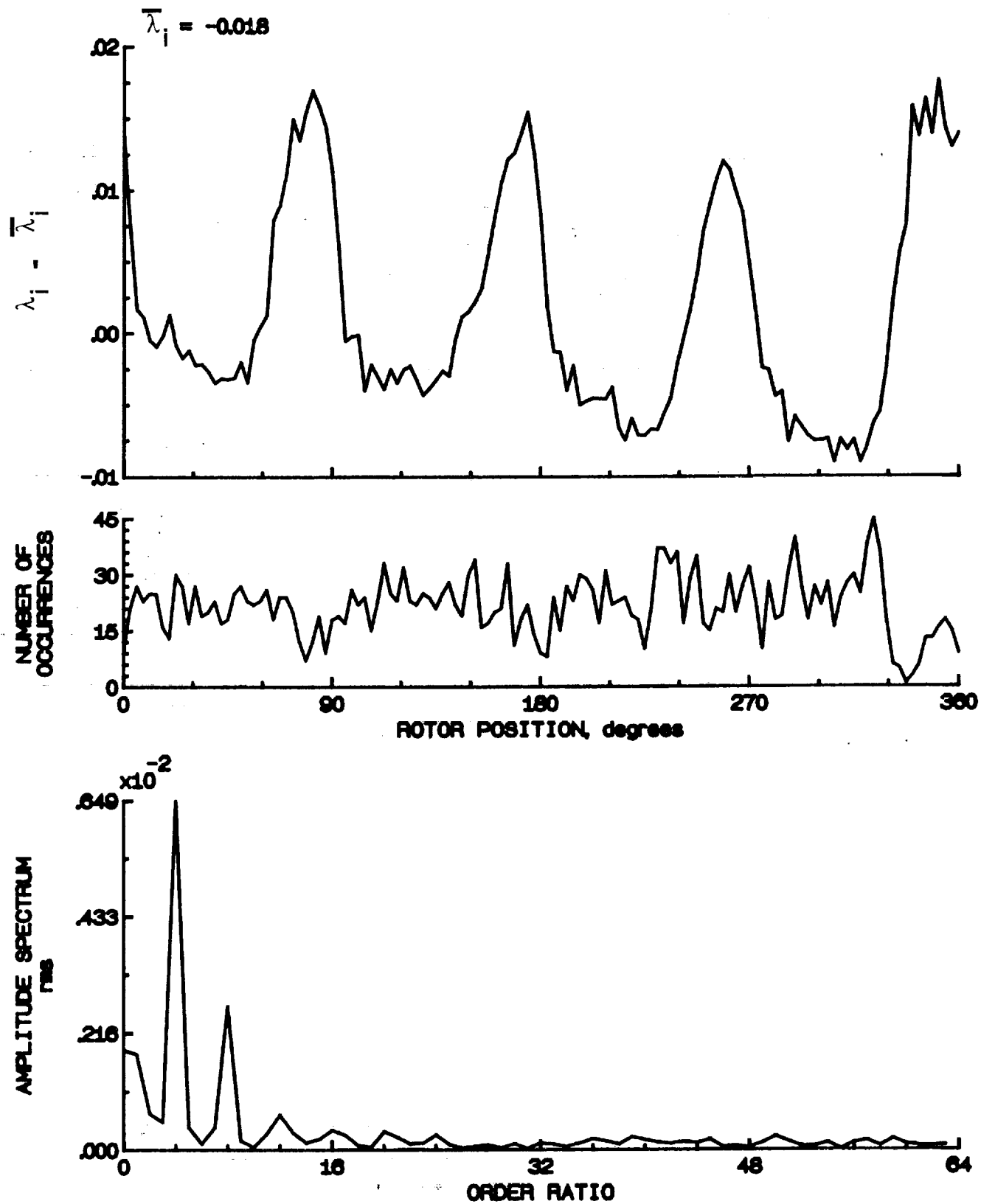


Figure 149.- Concluded.

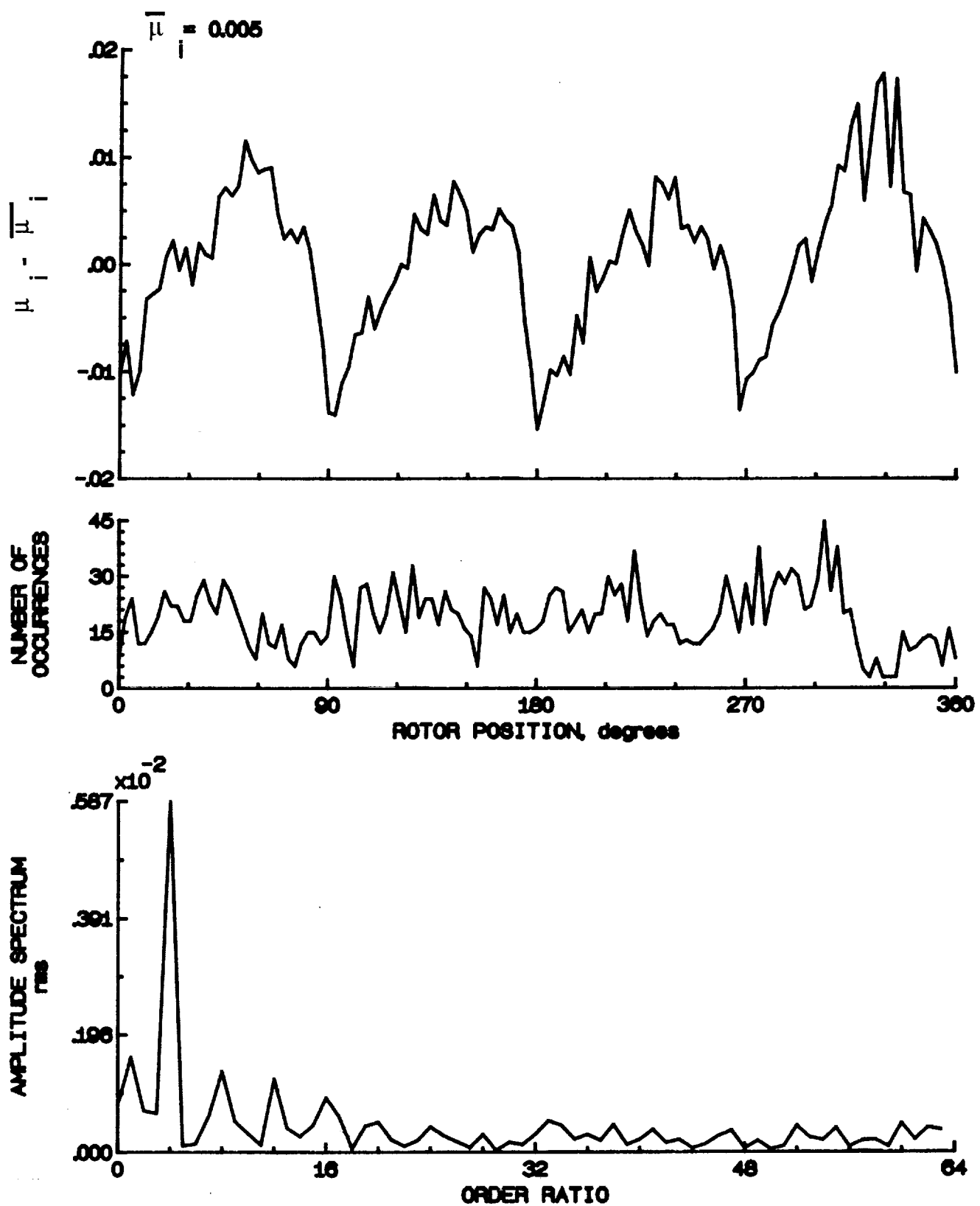


Figure 150.- Induced inflow velocity measured at 270 degrees and r/R of 0.60.

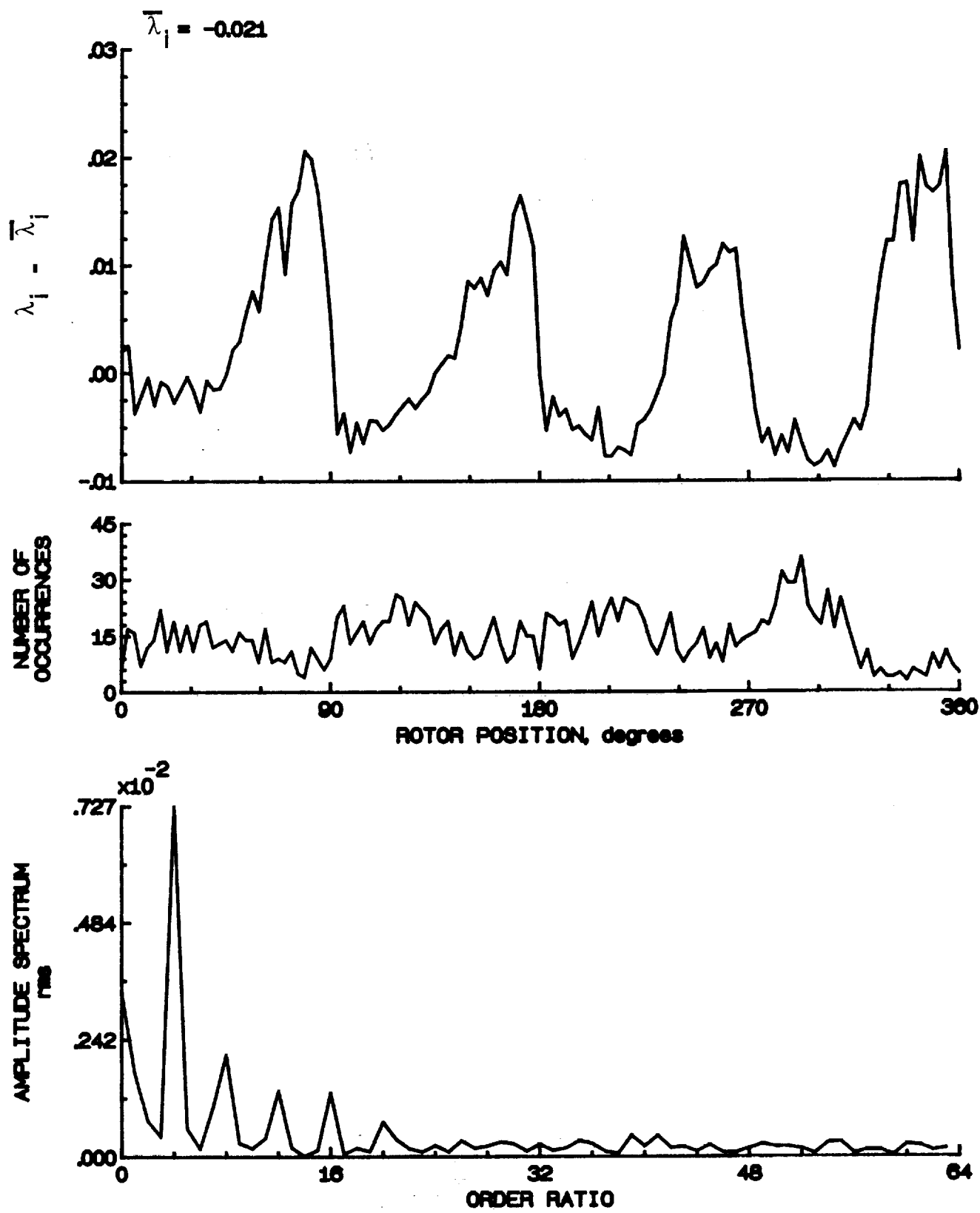


Figure 150.- Concluded.

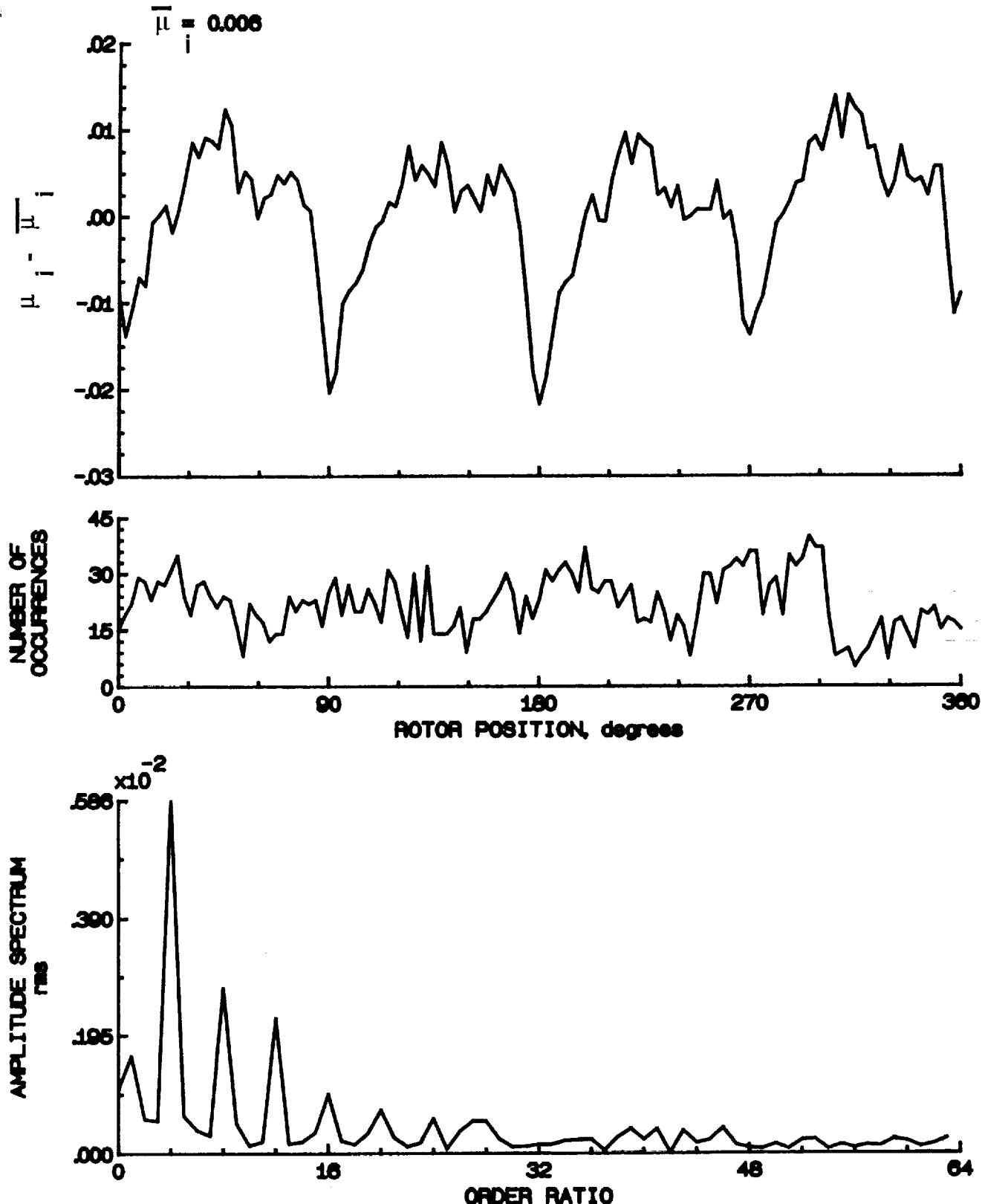


Figure 151.- Induced inflow velocity measured at 270 degrees and r/R of 0.70.

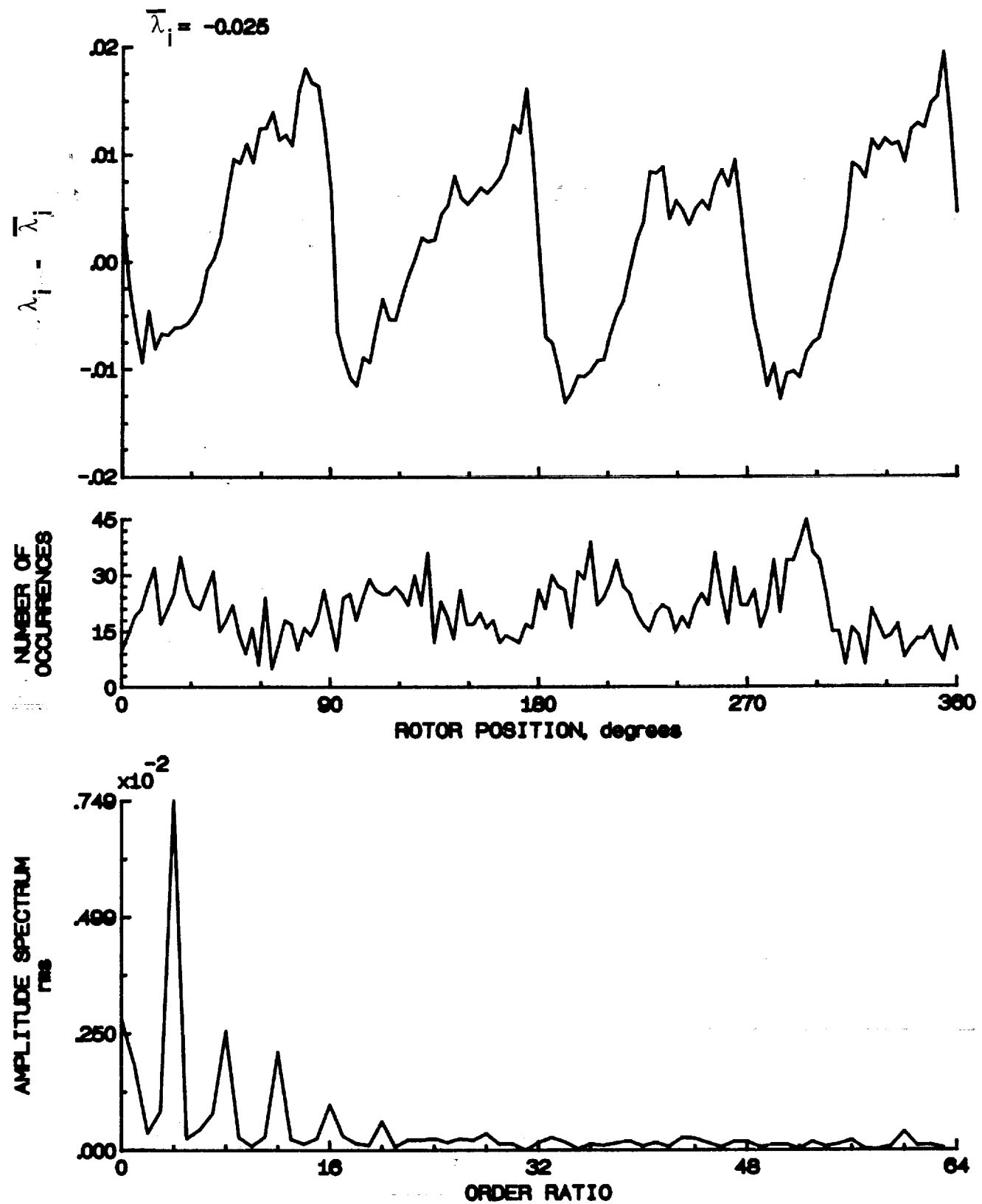


Figure 151.- Concluded.

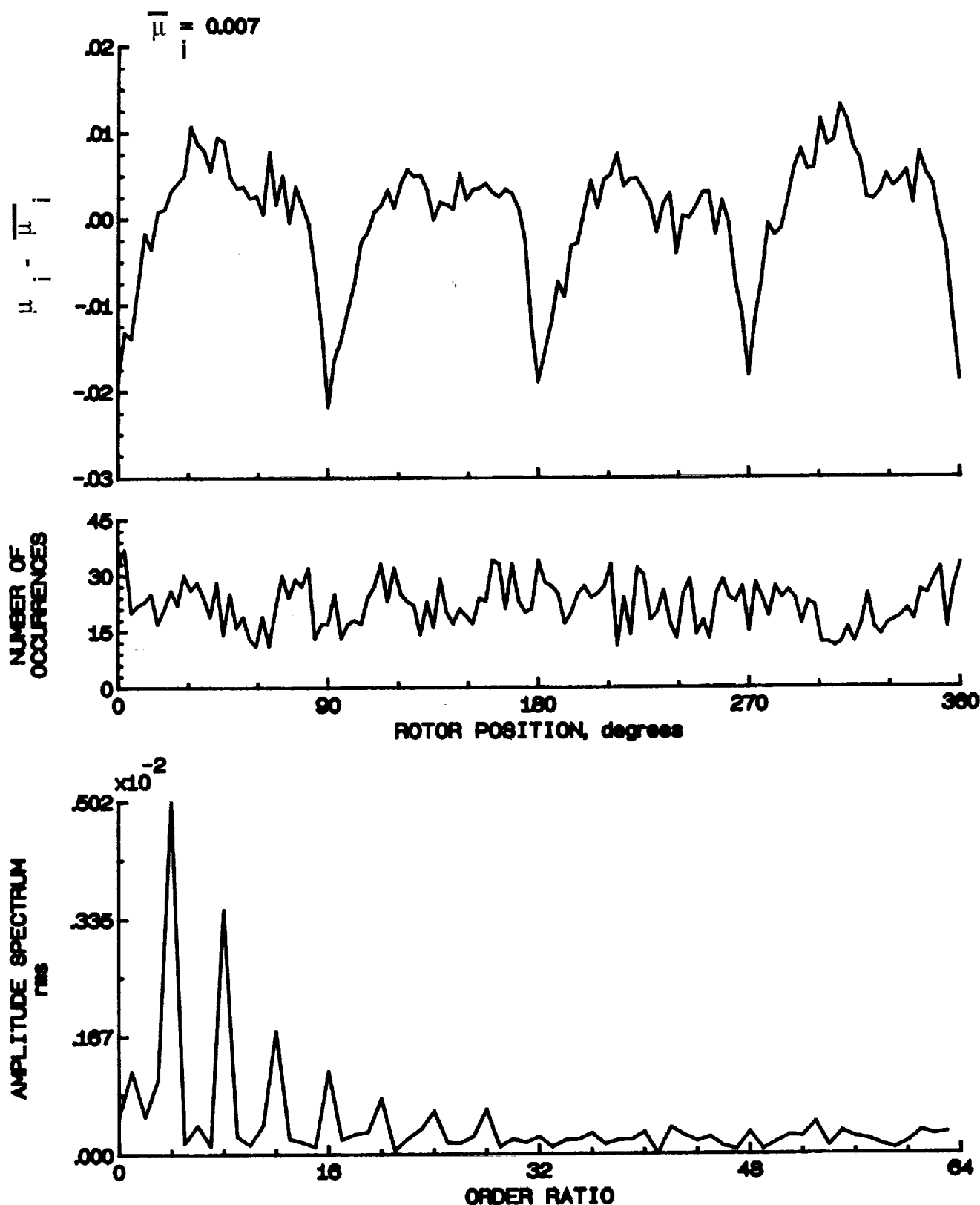


Figure 152.- Induced inflow velocity measured at 270 degrees and r/R of 0.74.

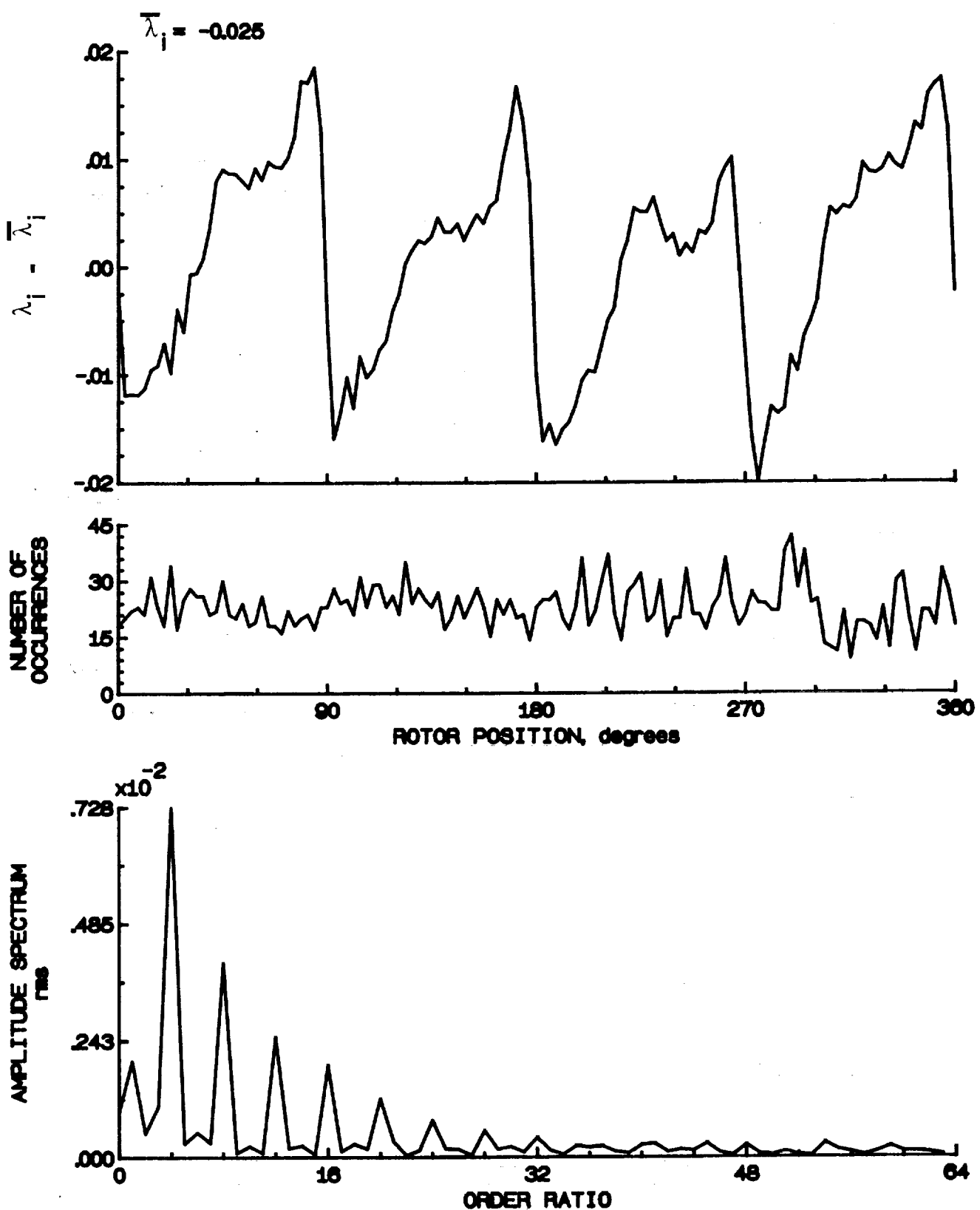


Figure 152.- Concluded.

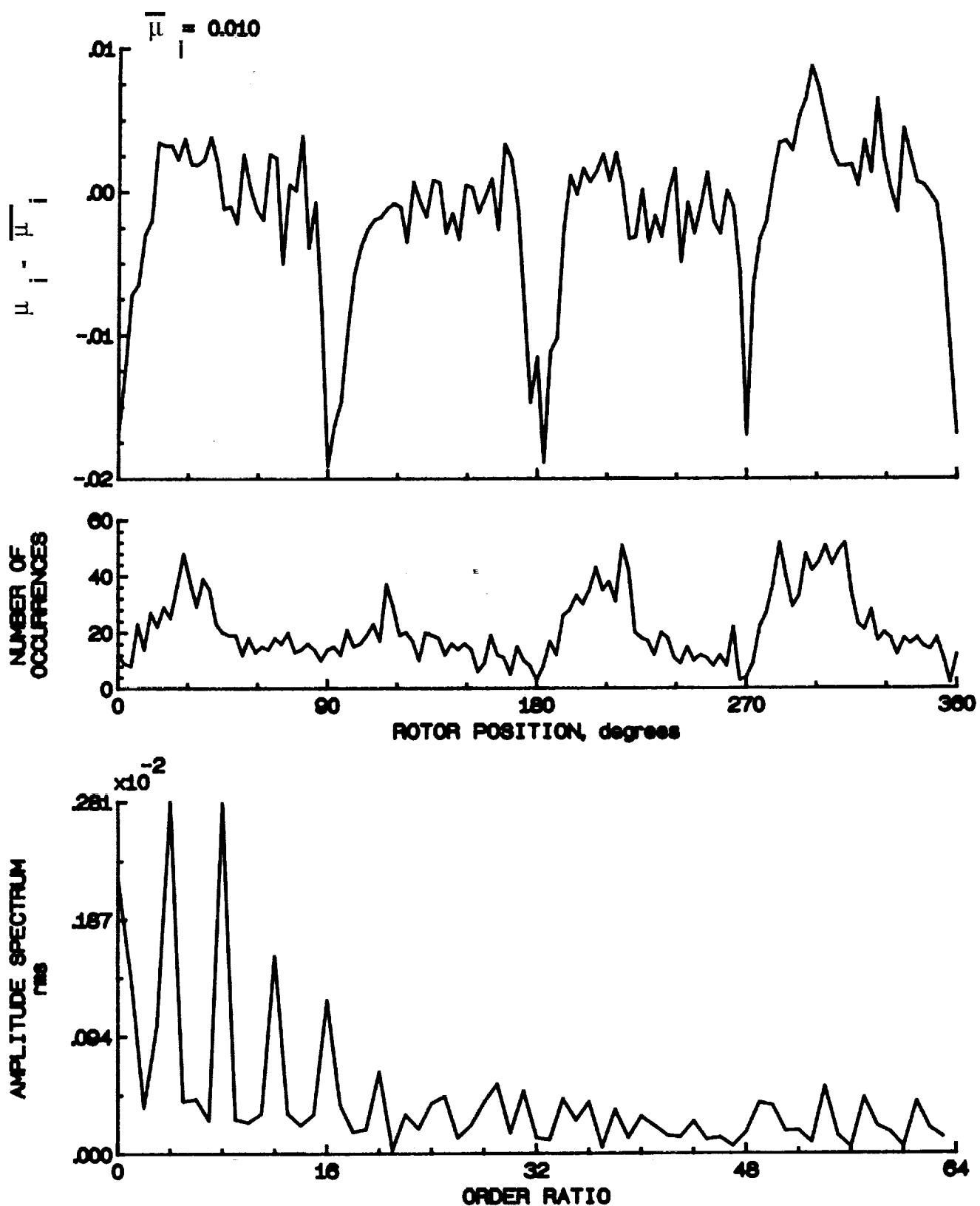


Figure 153.- Induced inflow velocity measured at 270 degrees and r/R of 0.78.

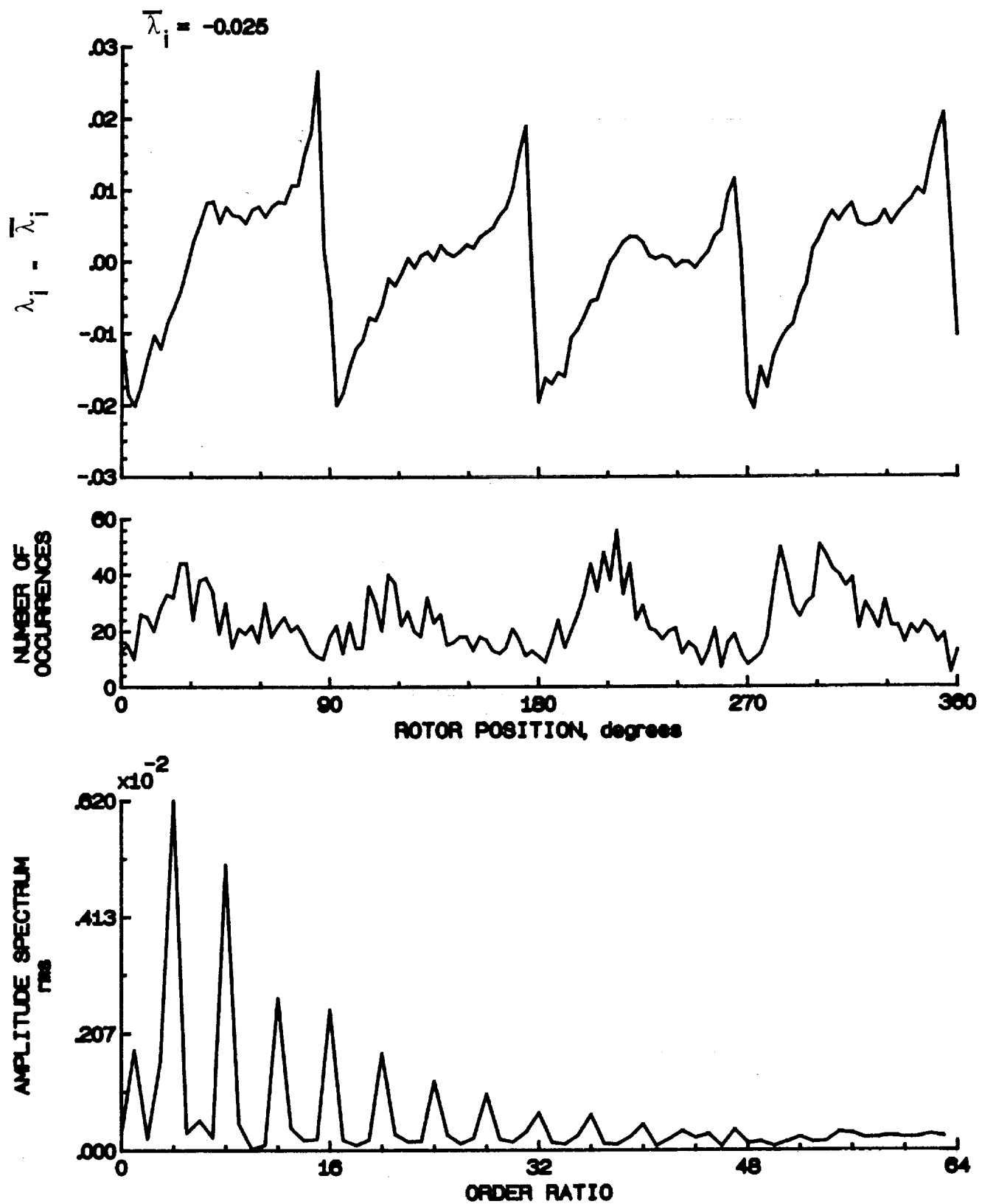


Figure 153.- Concluded.

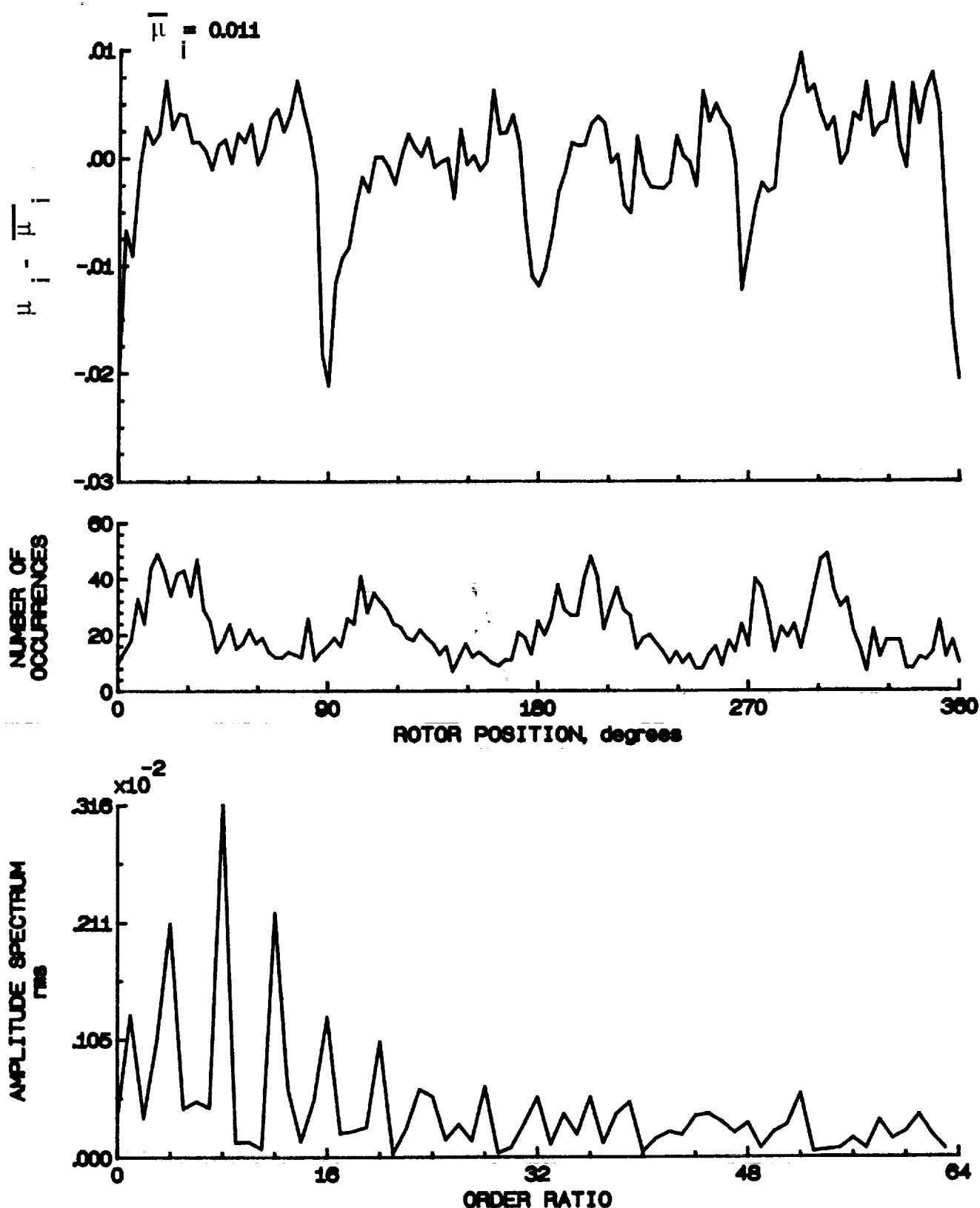


Figure 154.- Induced inflow velocity measured at 270 degrees and r/R of 0.82.

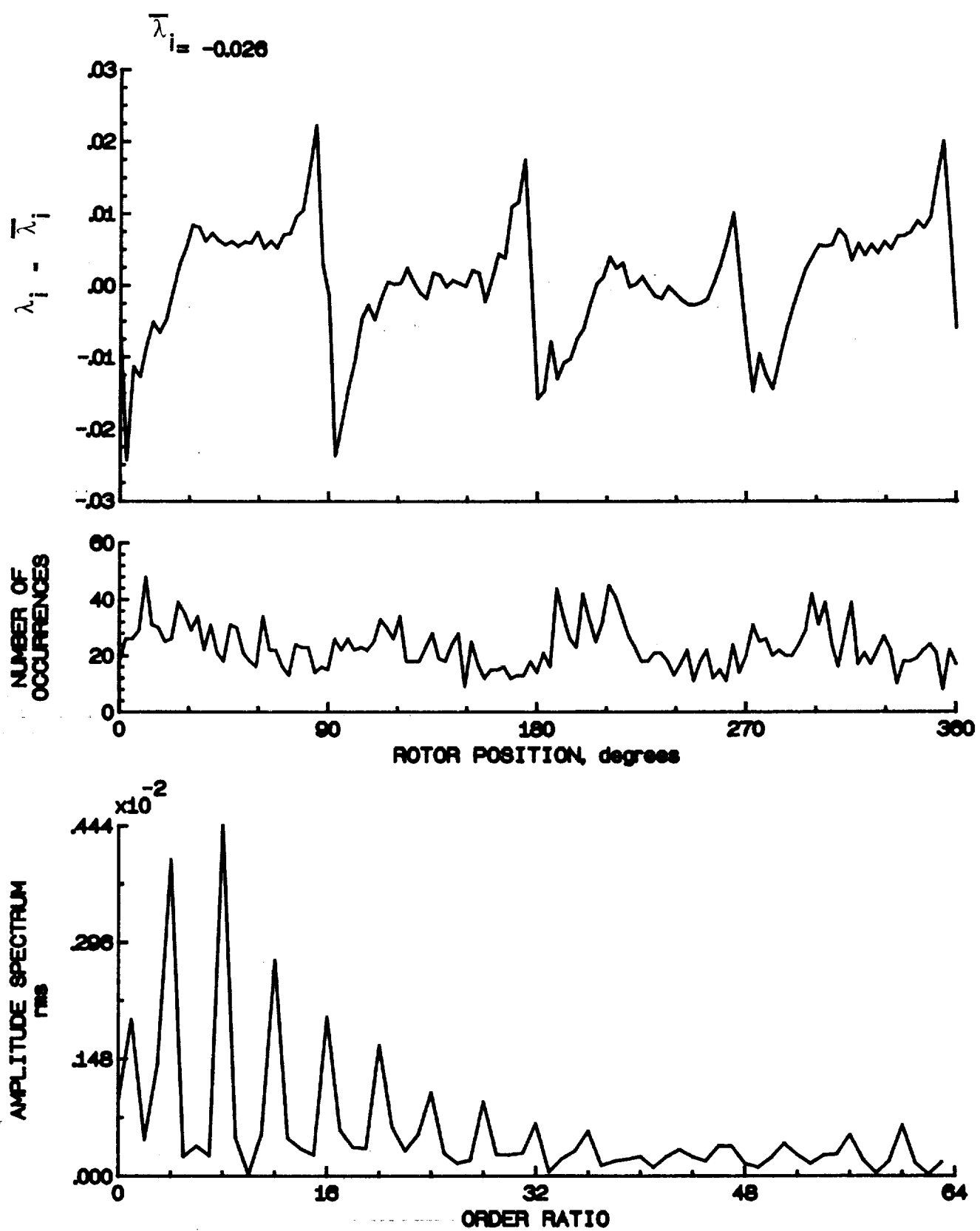


Figure 154.- Concluded.

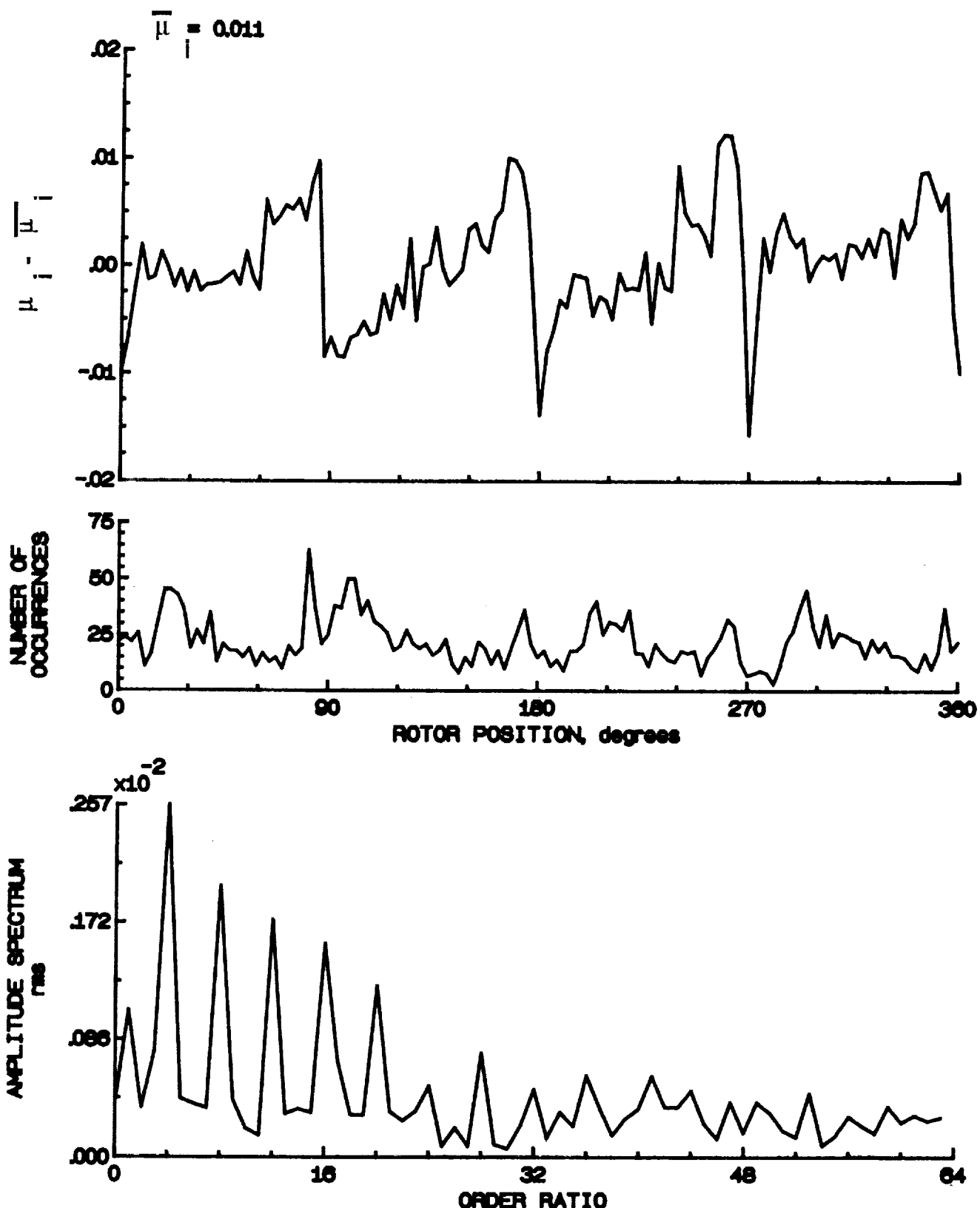


Figure 155.- Induced inflow velocity measured at 270 degrees and r/R of 0.80.

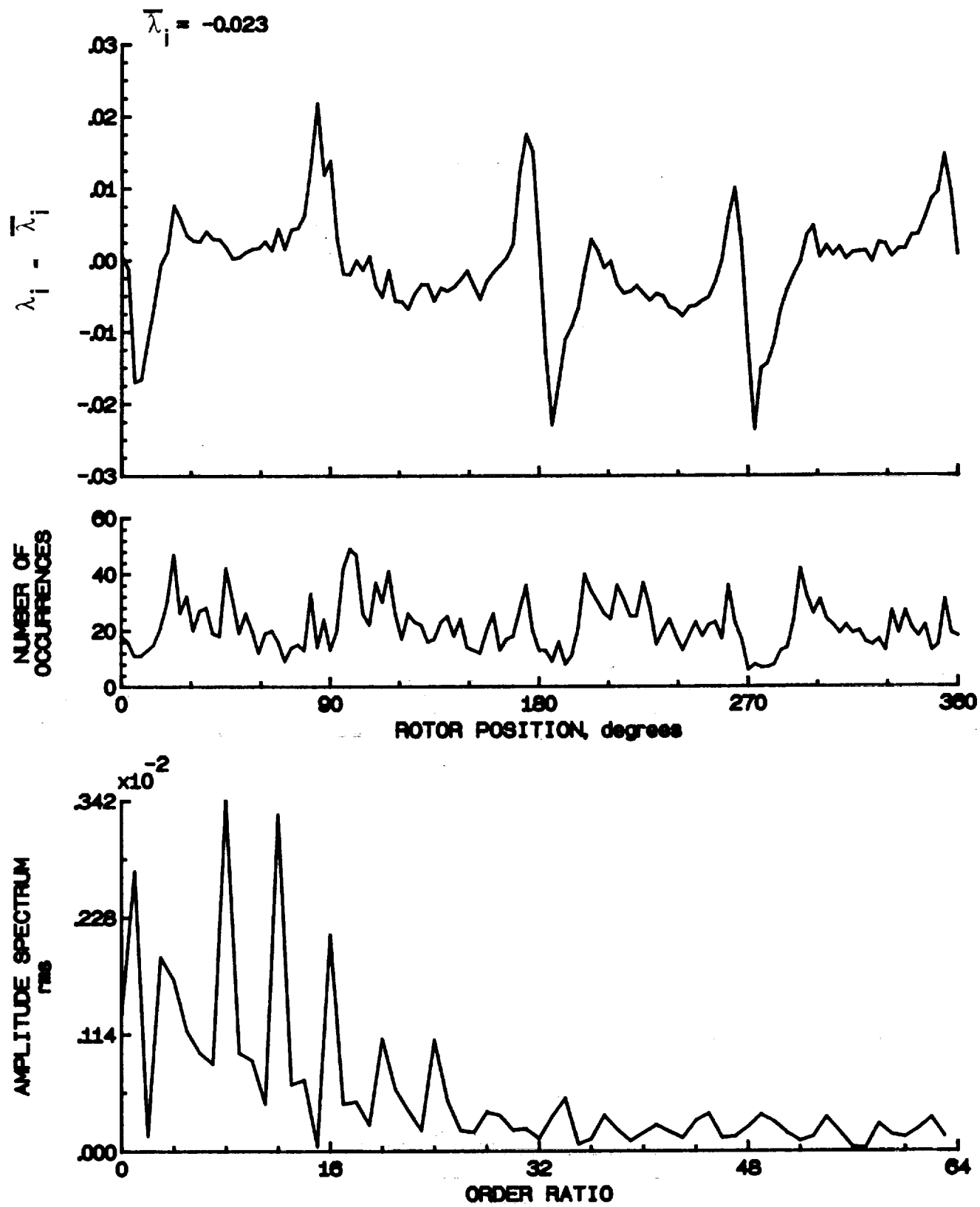


Figure 155.- Concluded.

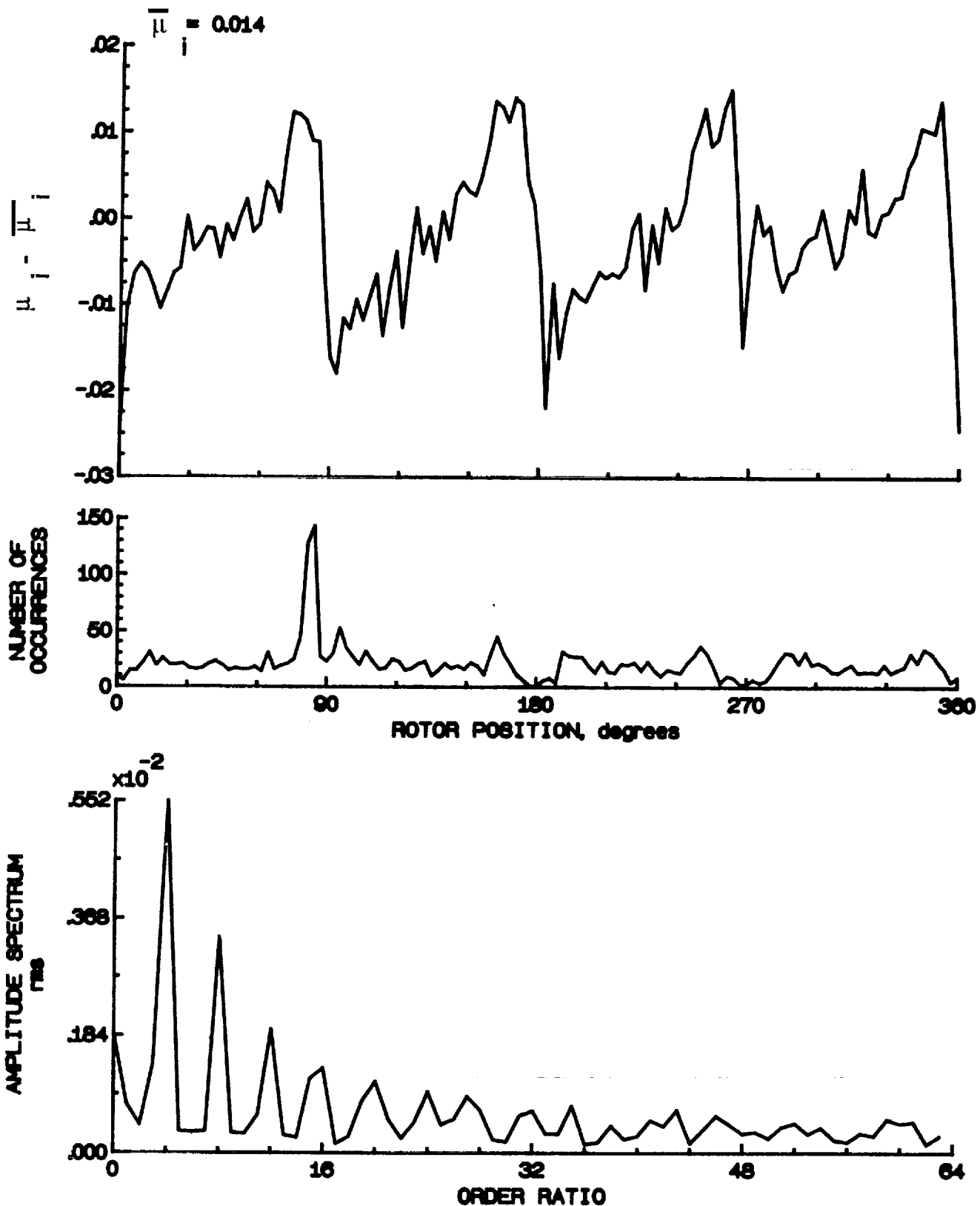


Figure 156.- Induced inflow velocity measured at 270 degrees and r/R of 0.90.

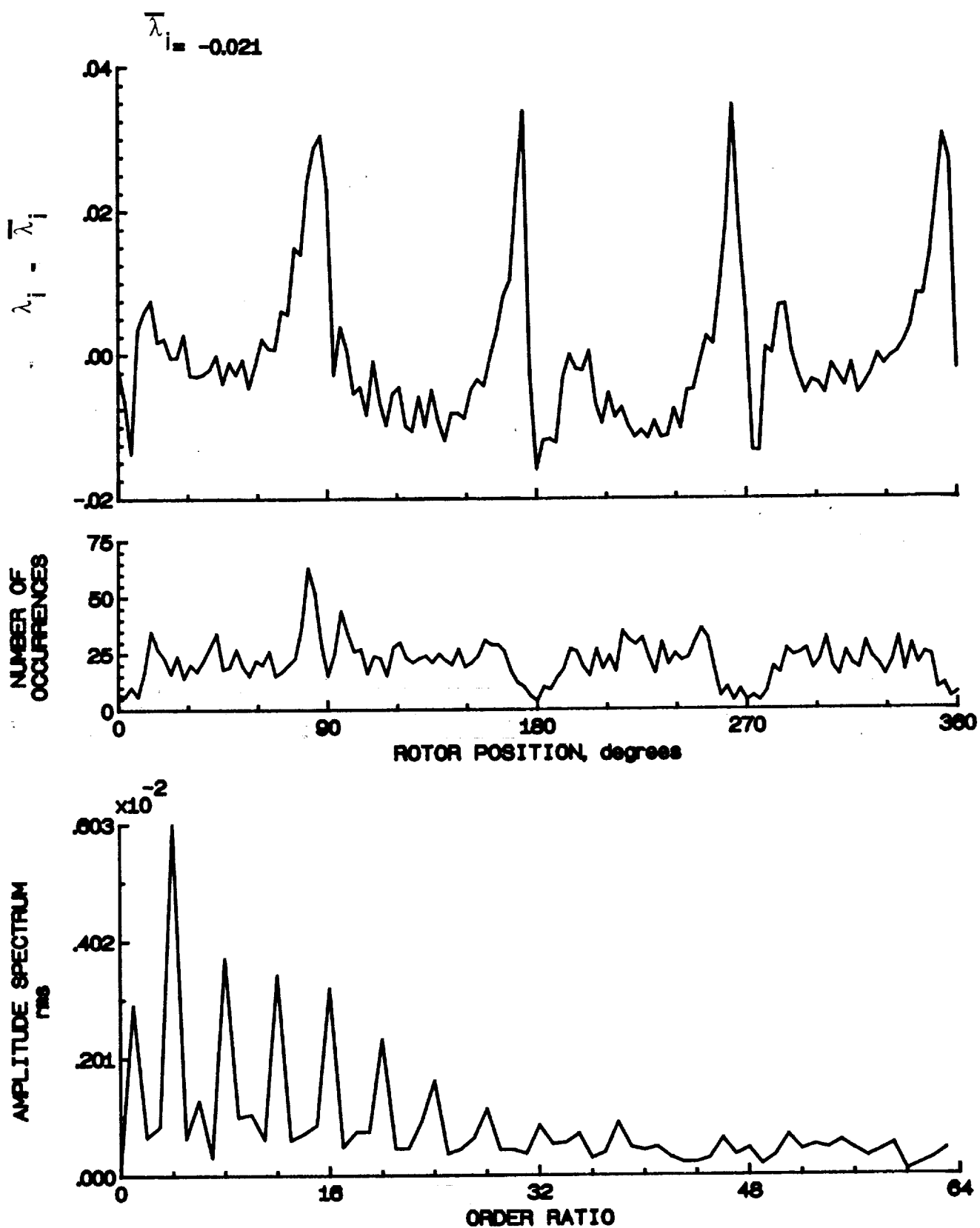


Figure 156.- Concluded.

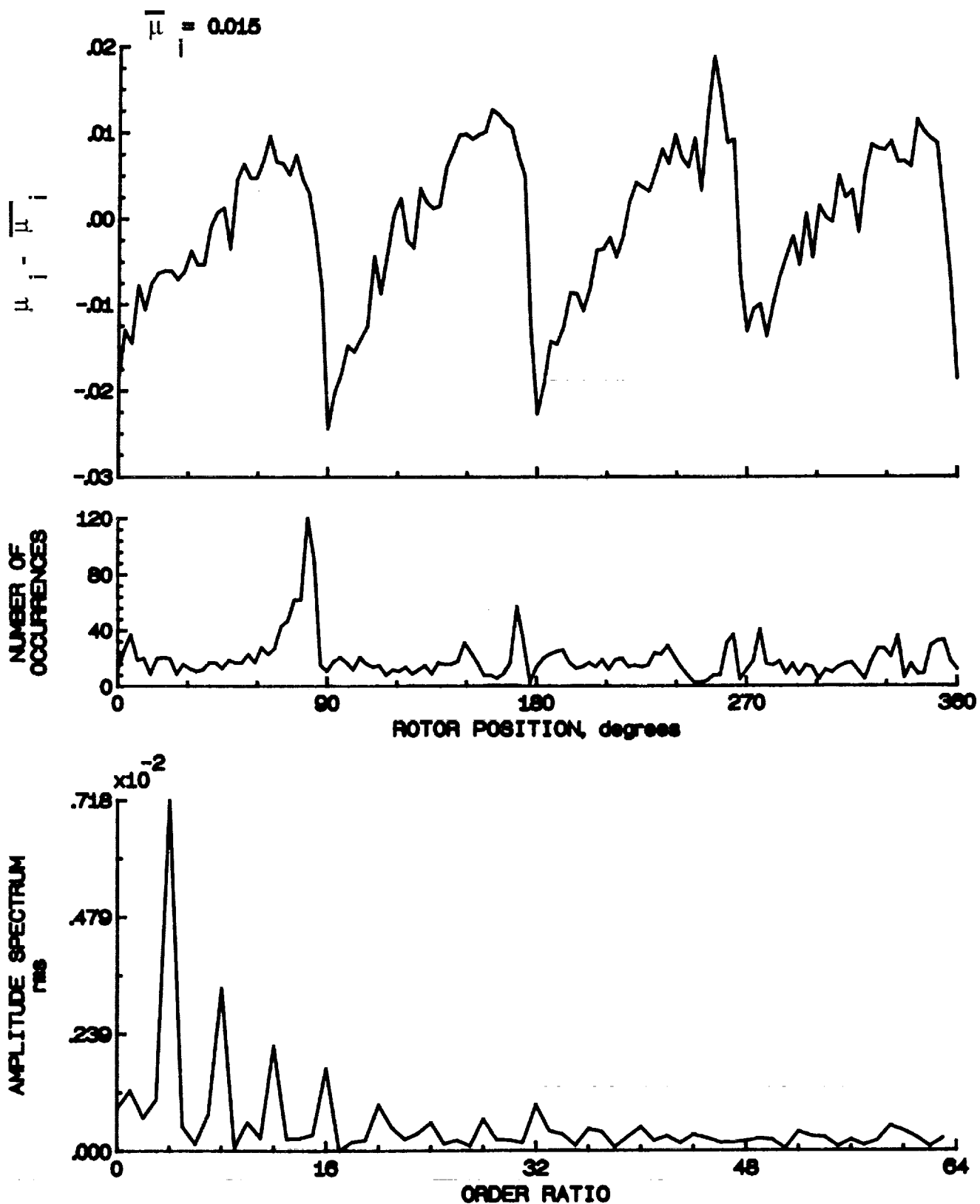


Figure 157.- Induced inflow velocity measured at 270 degrees and r/R of 0.94.

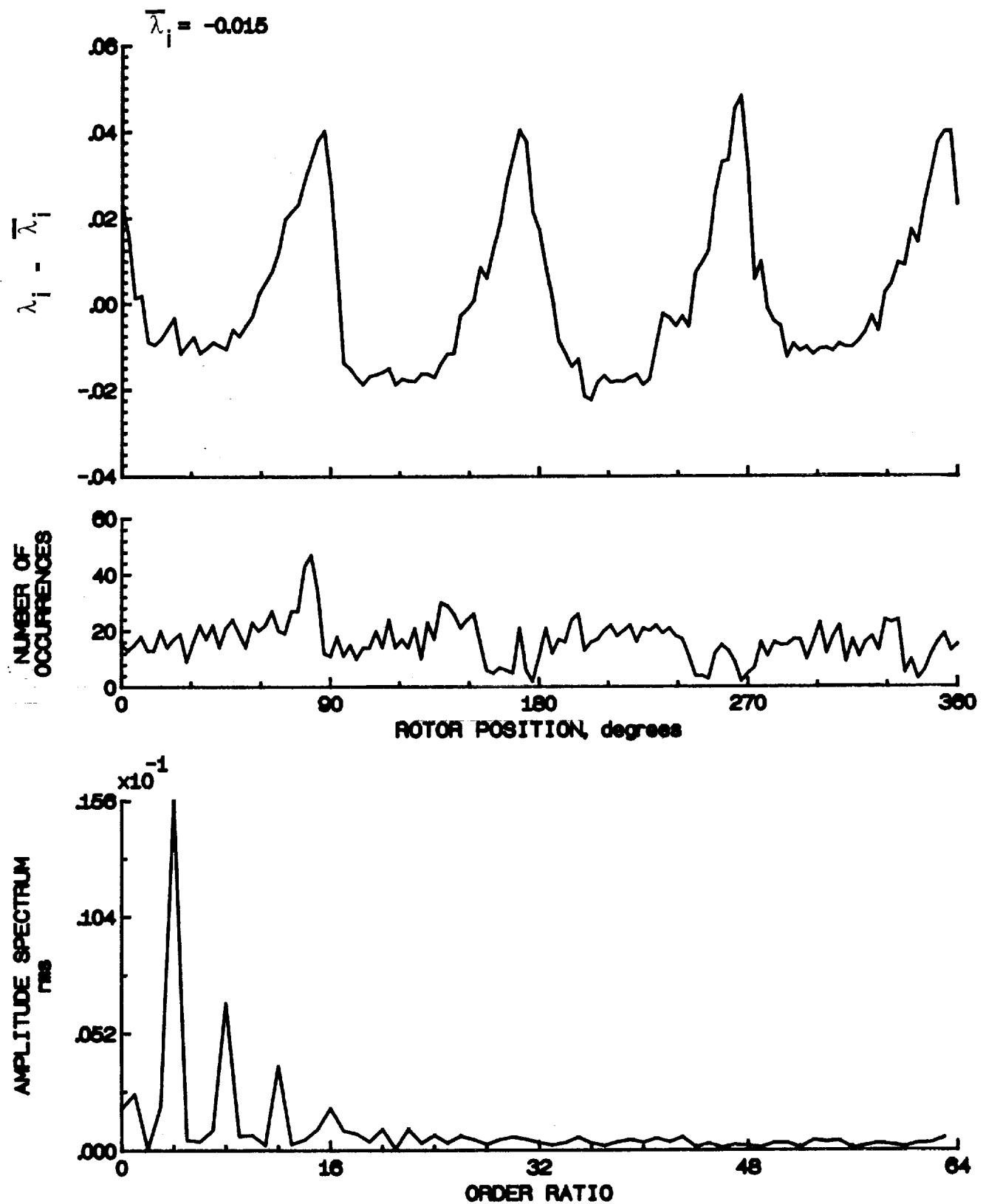


Figure 157.- Concluded.

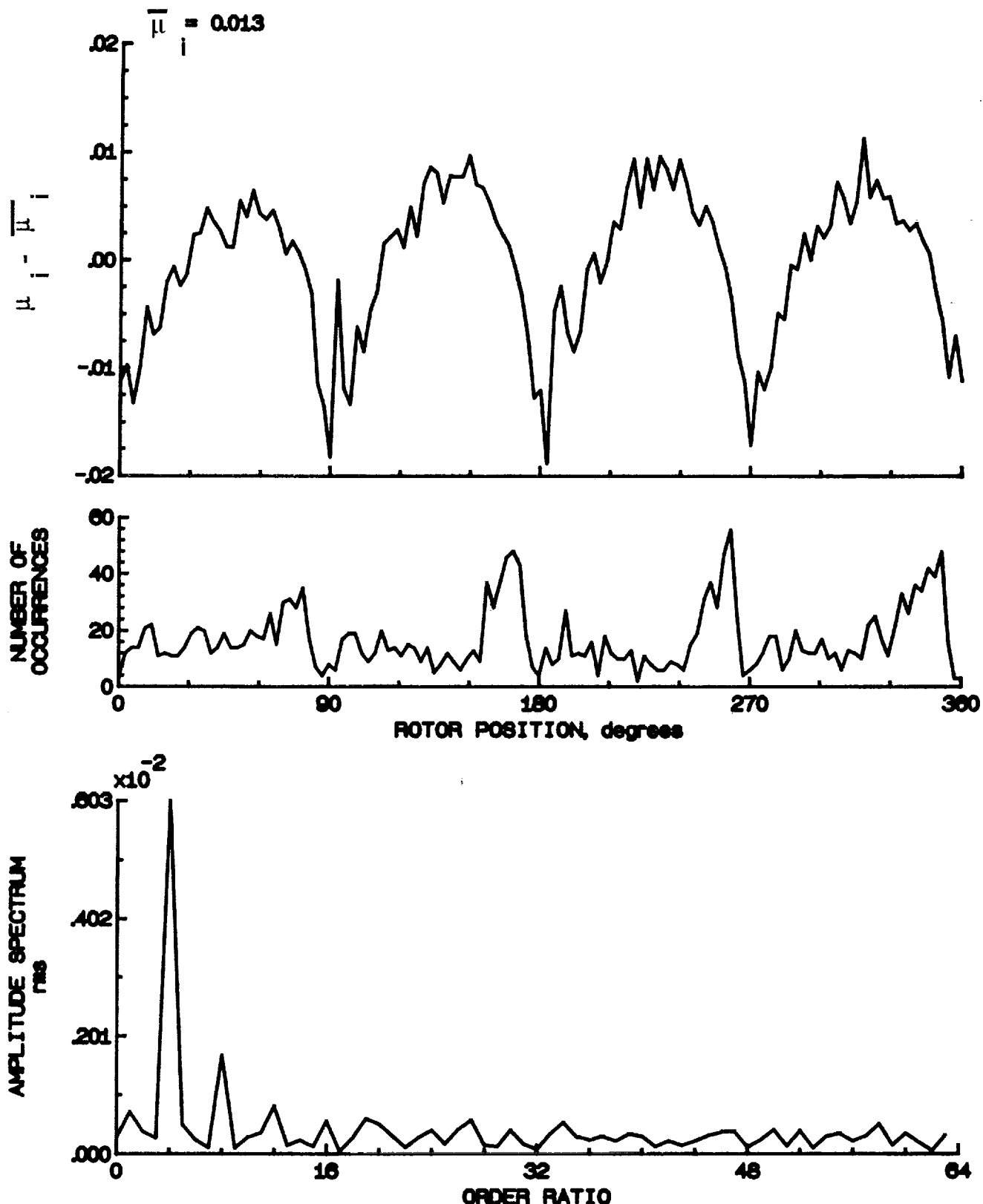


Figure 158.- Induced inflow velocity measured at 270 degrees and r/R of 0.98.

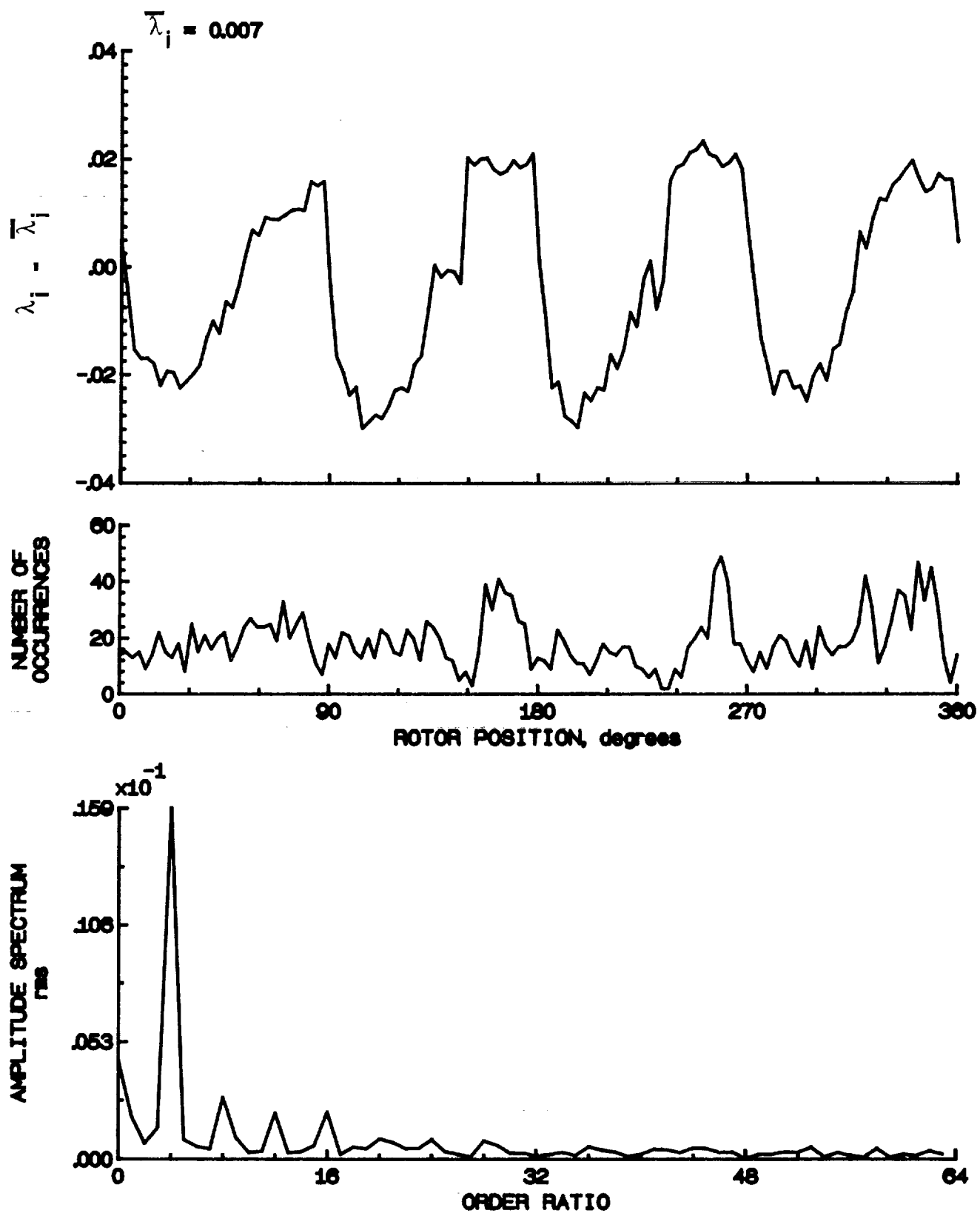


Figure 158.- Concluded.

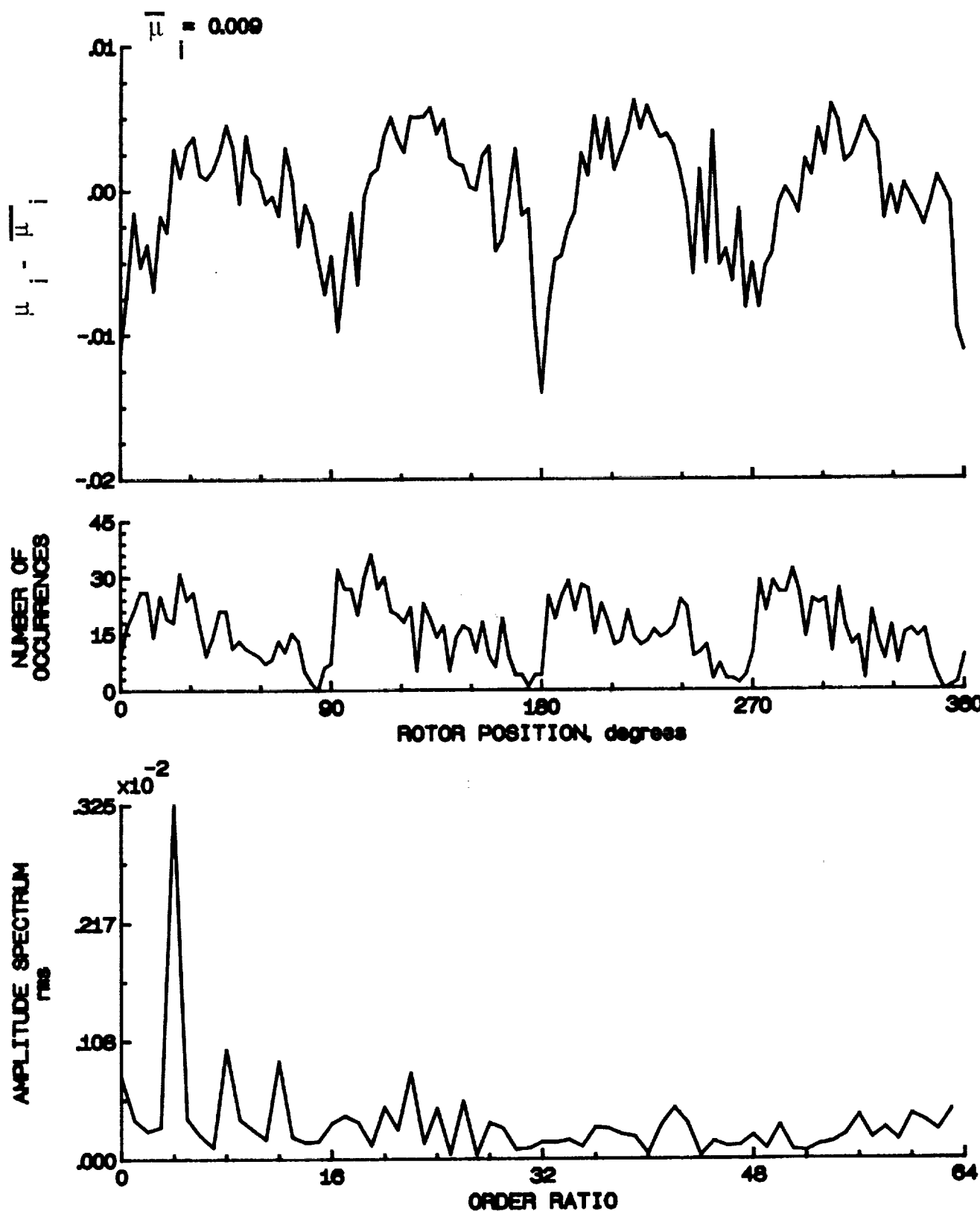


Figure 159.- Induced inflow velocity measured at 270 degrees and r/R of 1.02.

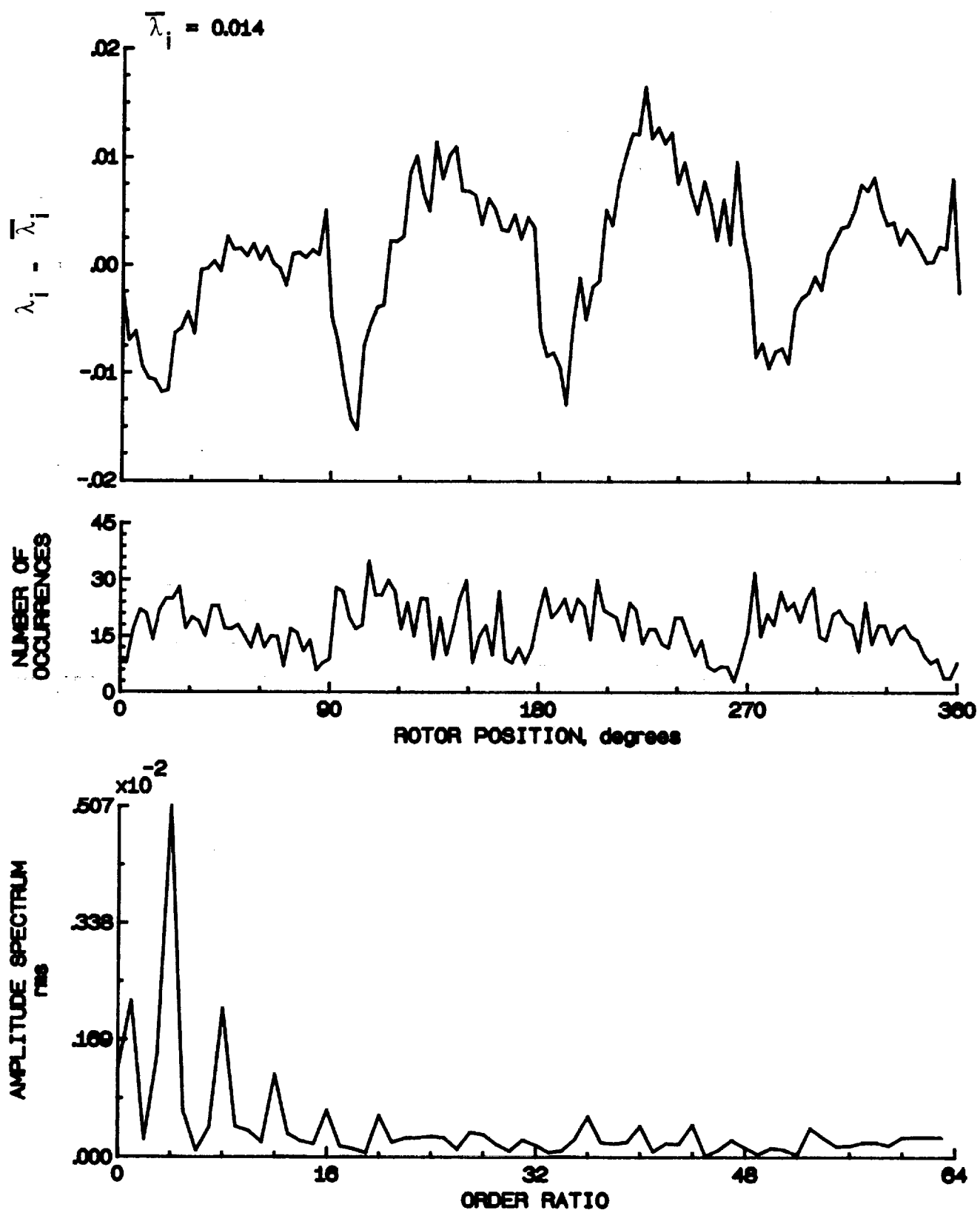


Figure 159.- Concluded.

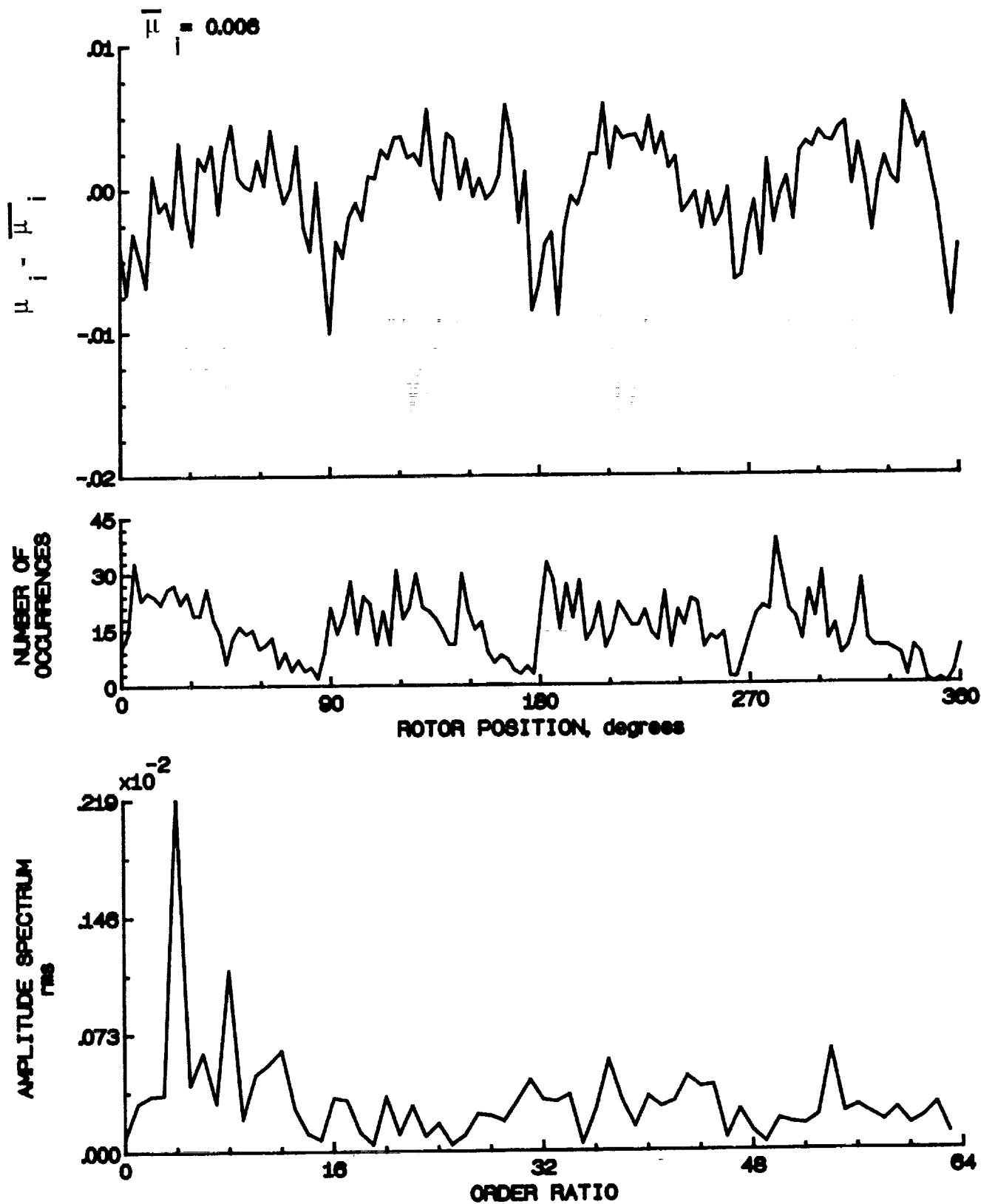


Figure 100.- Induced inflow velocity measured at 270 degrees and r/R of 1.04.

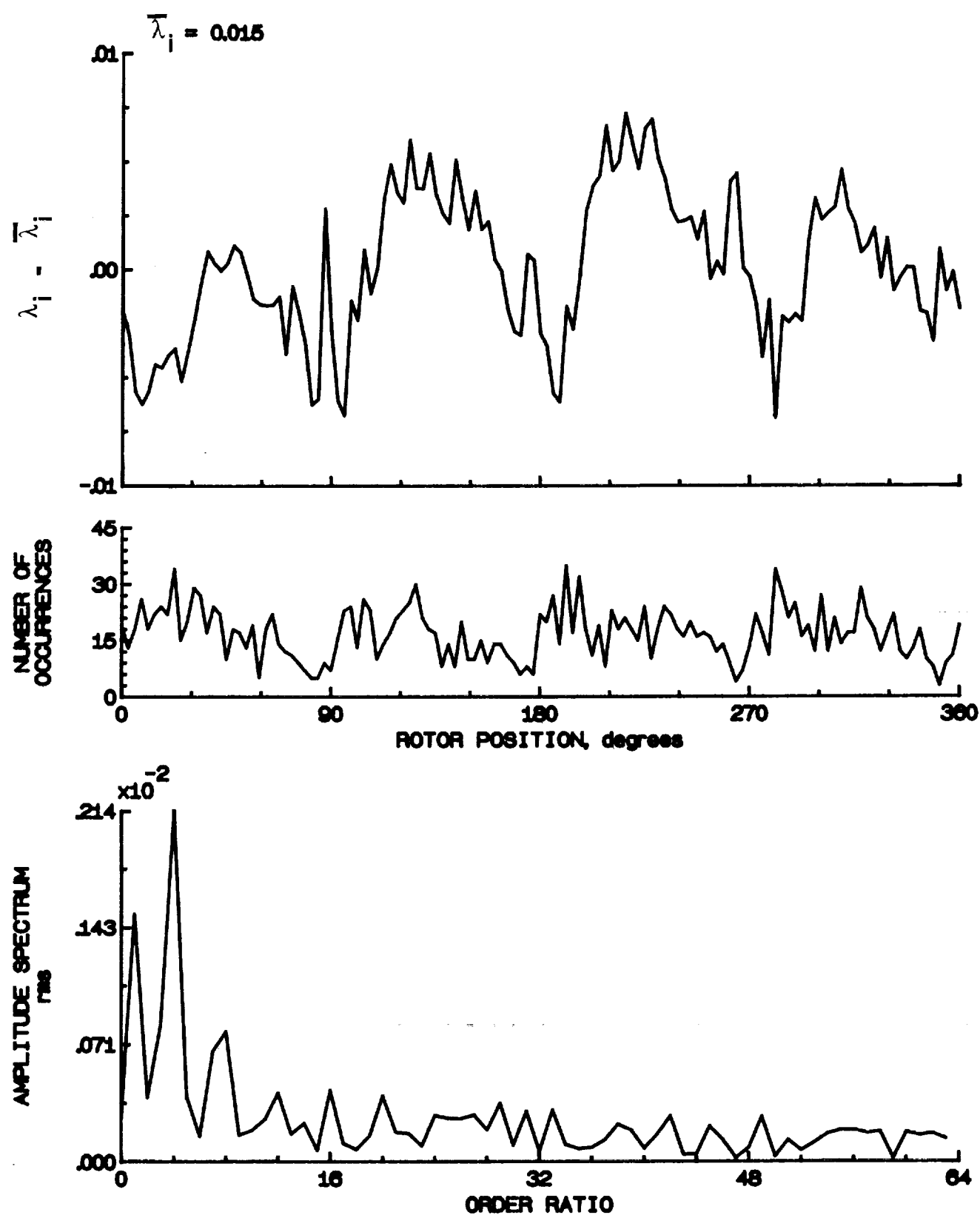


Figure 160.- Concluded.

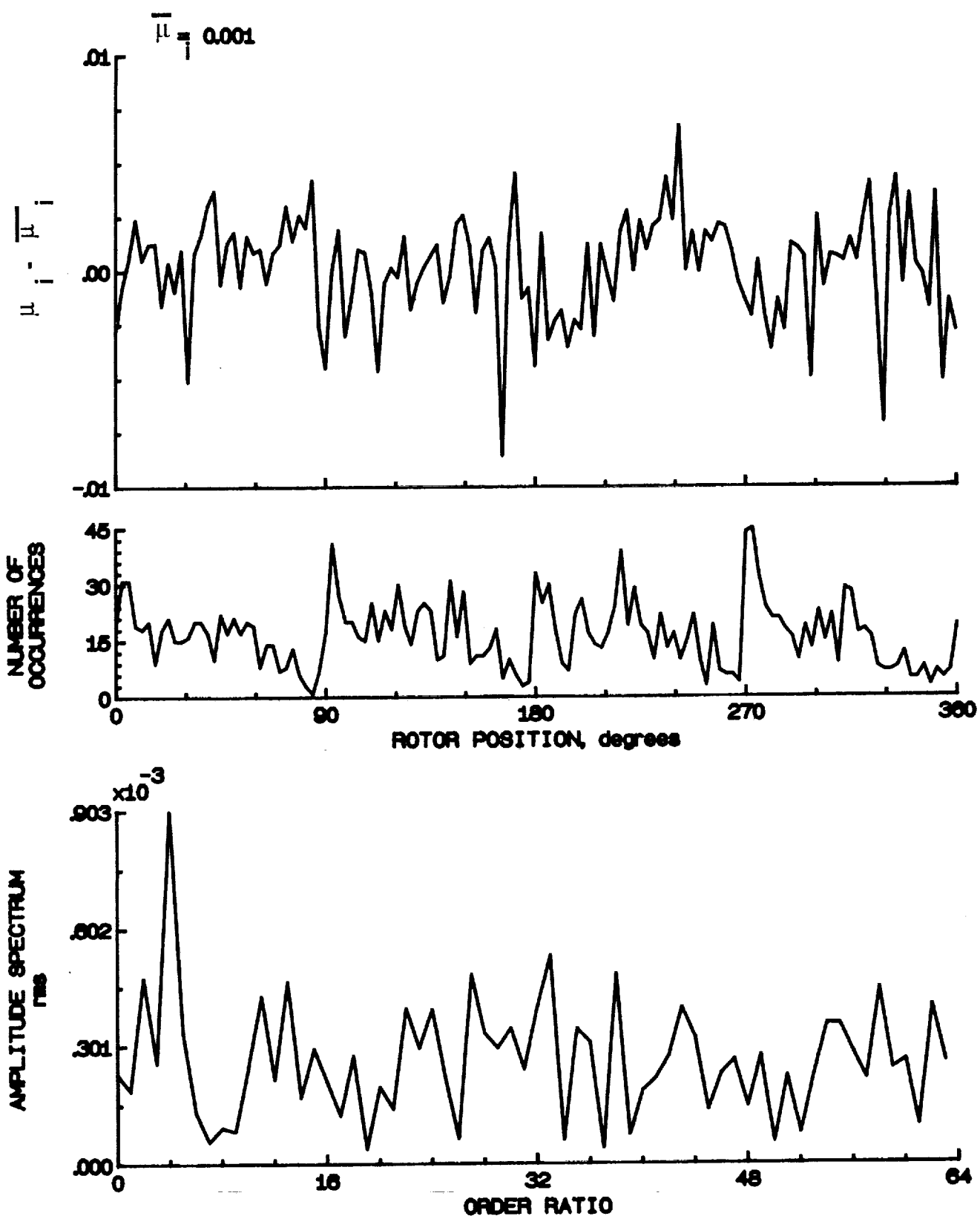


Figure 161.- Induced inflow velocity measured at 270 degrees and r/R of 1.10.

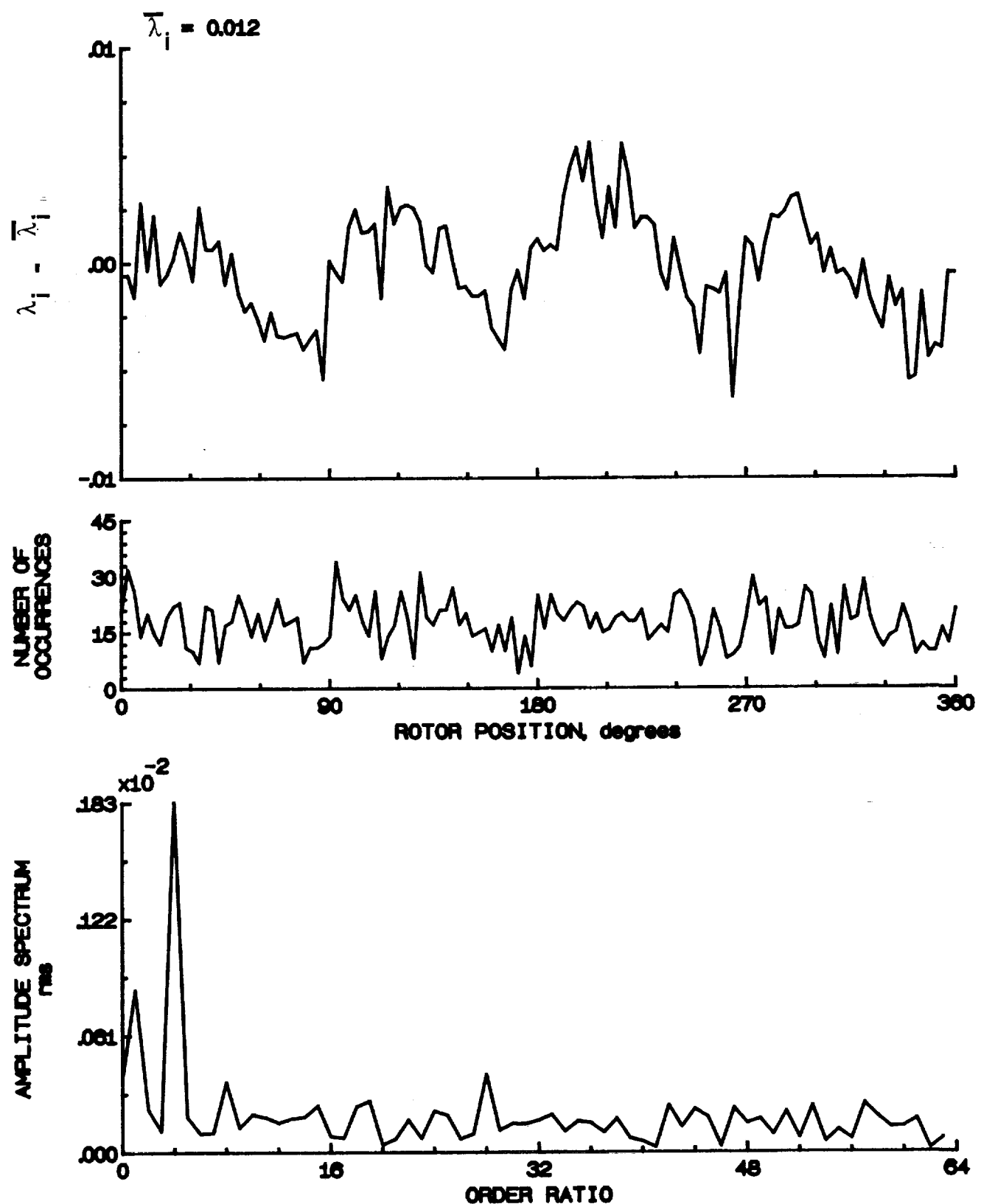


Figure 161- Concluded.

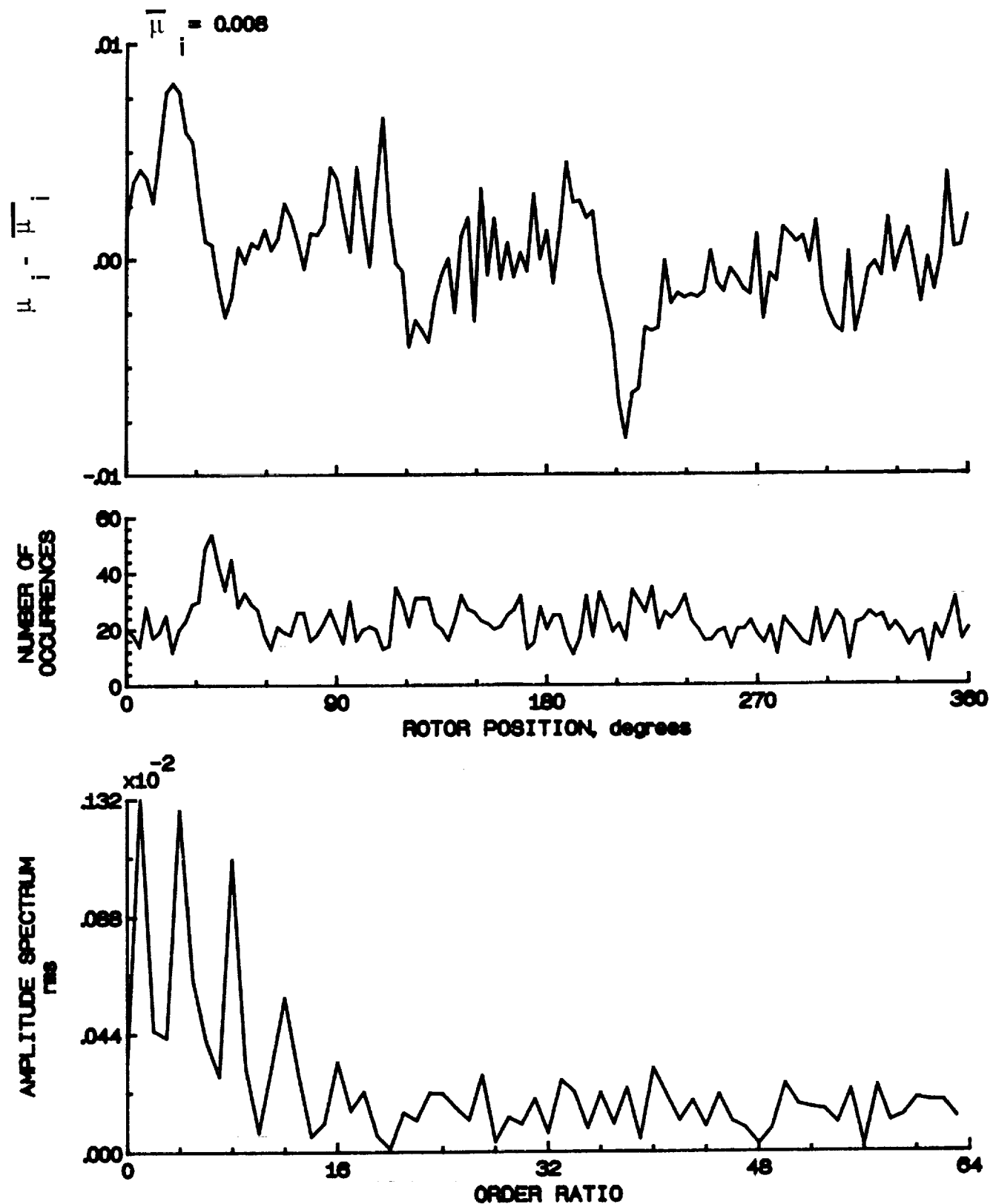


Figure 162.- Induced inflow velocity measured at 300 degrees and r/R of 0.40.

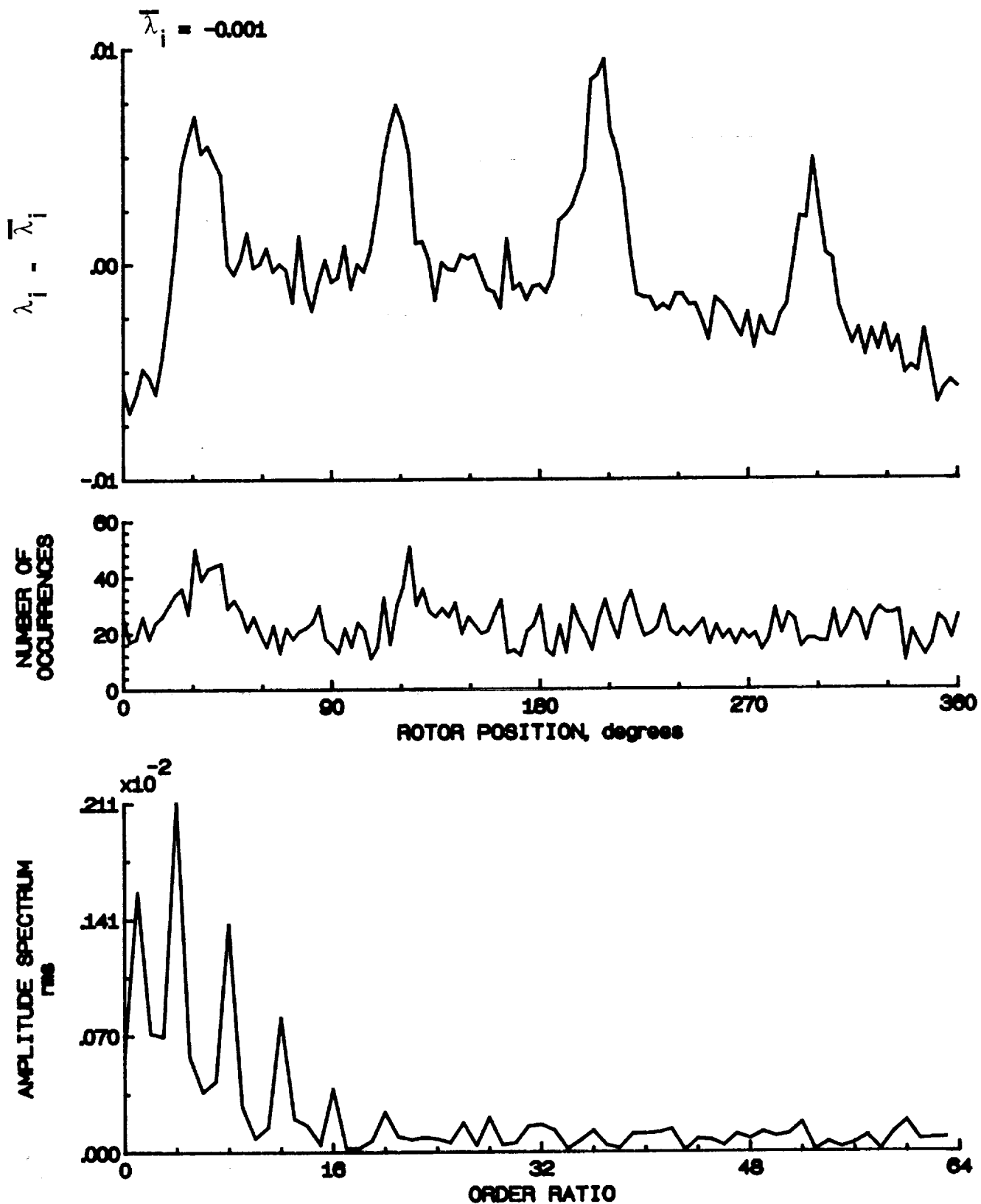


Figure 162.- Concluded.

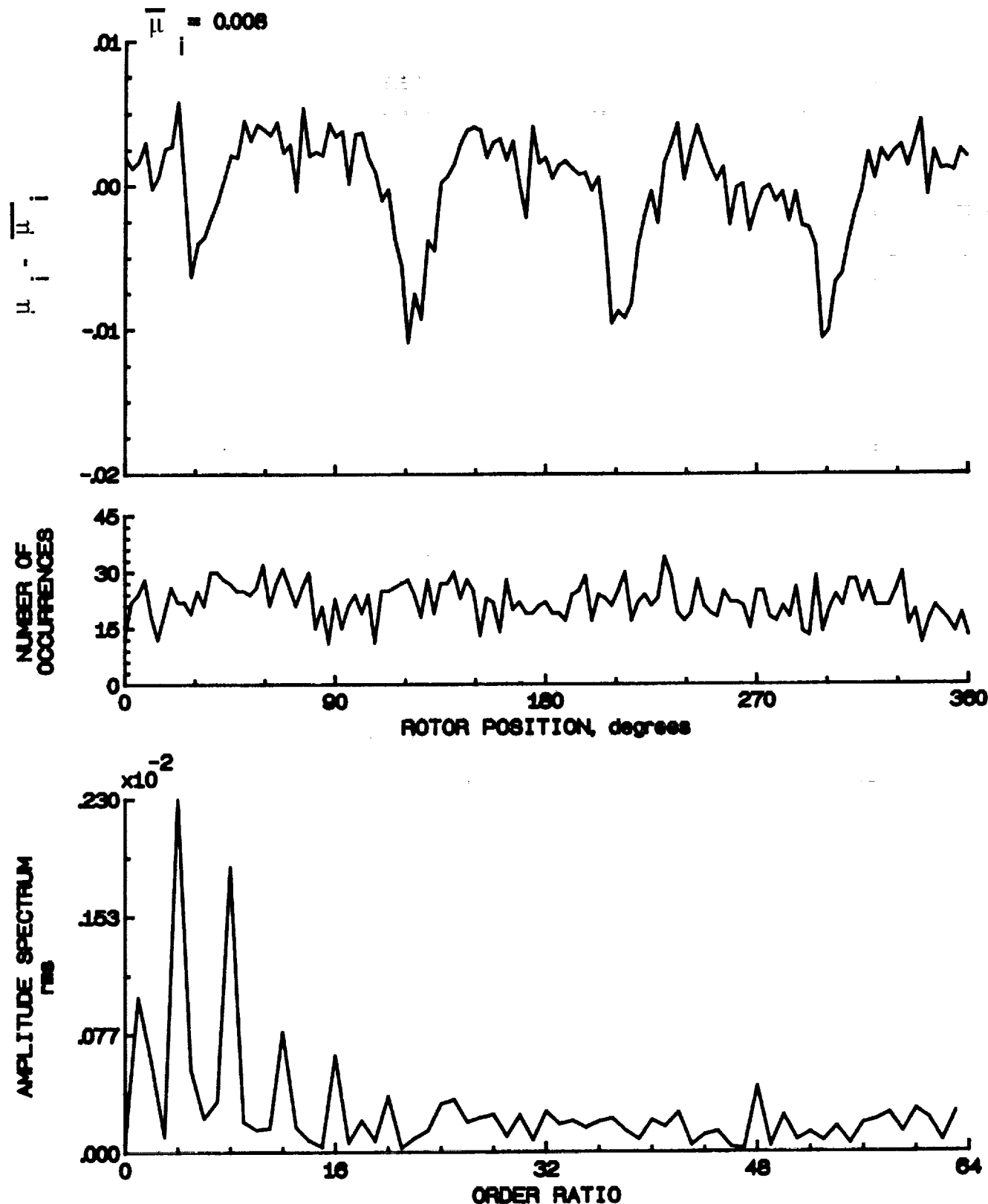


Figure 163.- Induced inflow velocity measured at 300 degrees and r/R of 0.50.

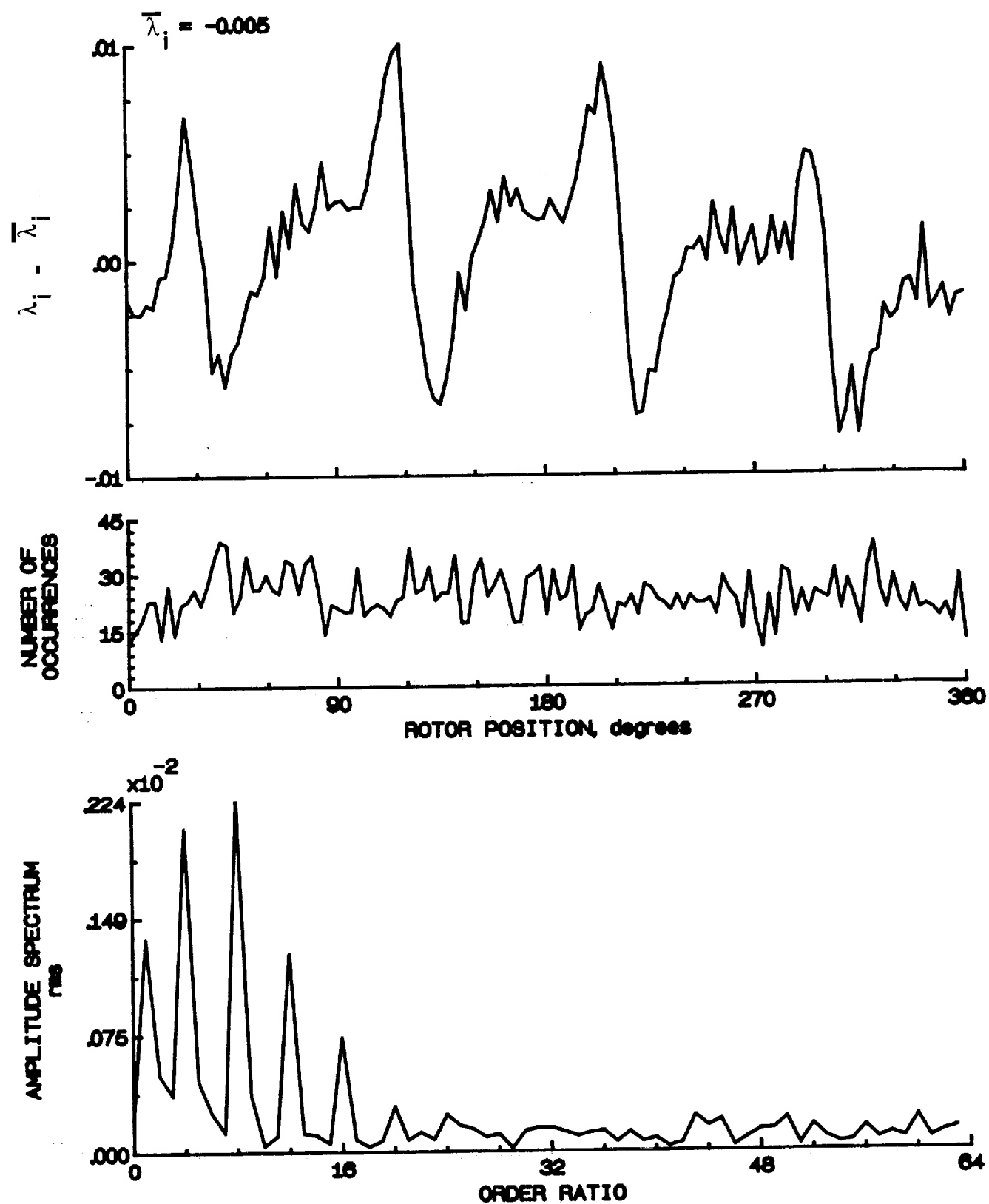


Figure 163.- Concluded.

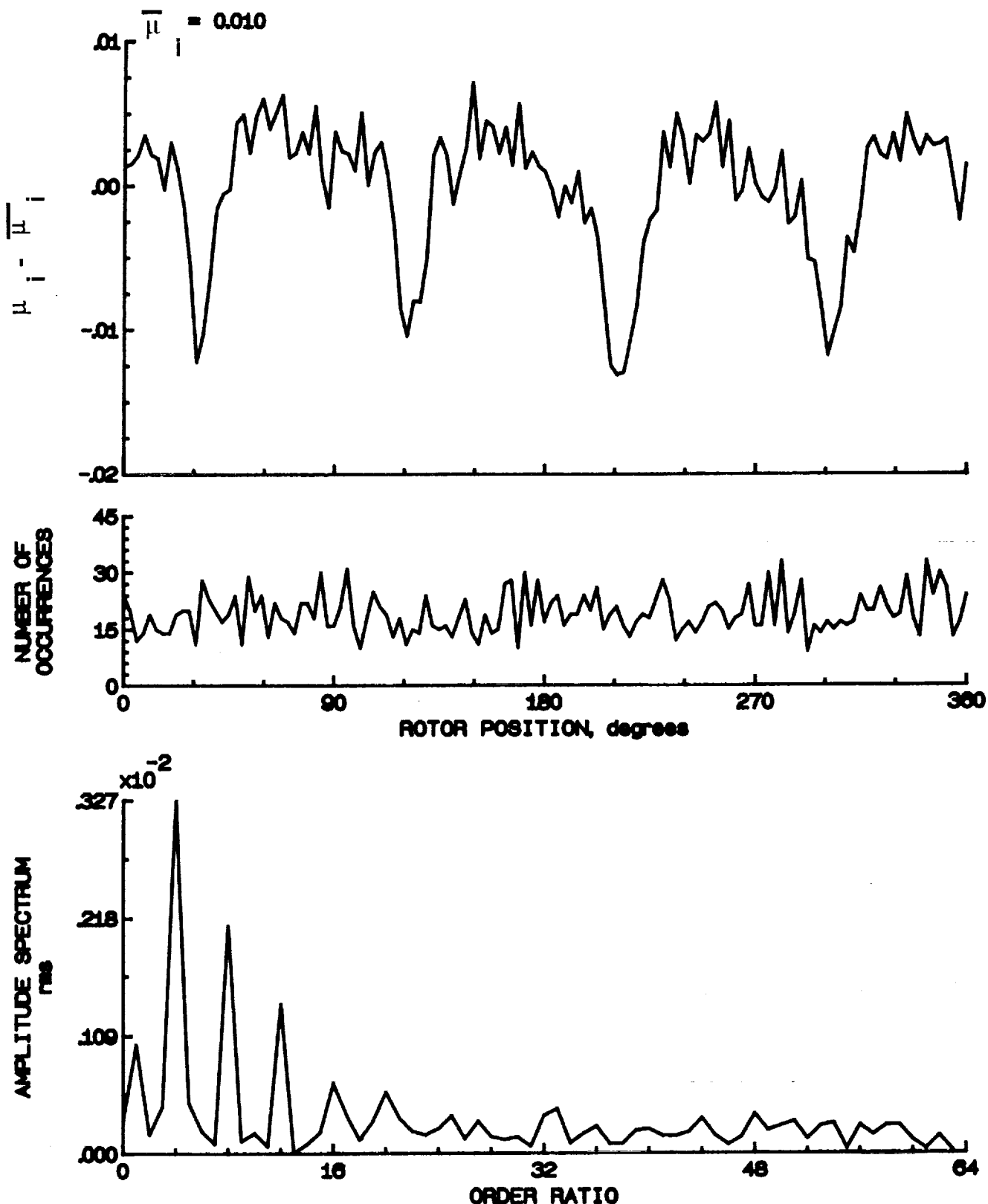


Figure 164.- Induced inflow velocity measured at 300 degrees and  $r/R$  of 0.00.

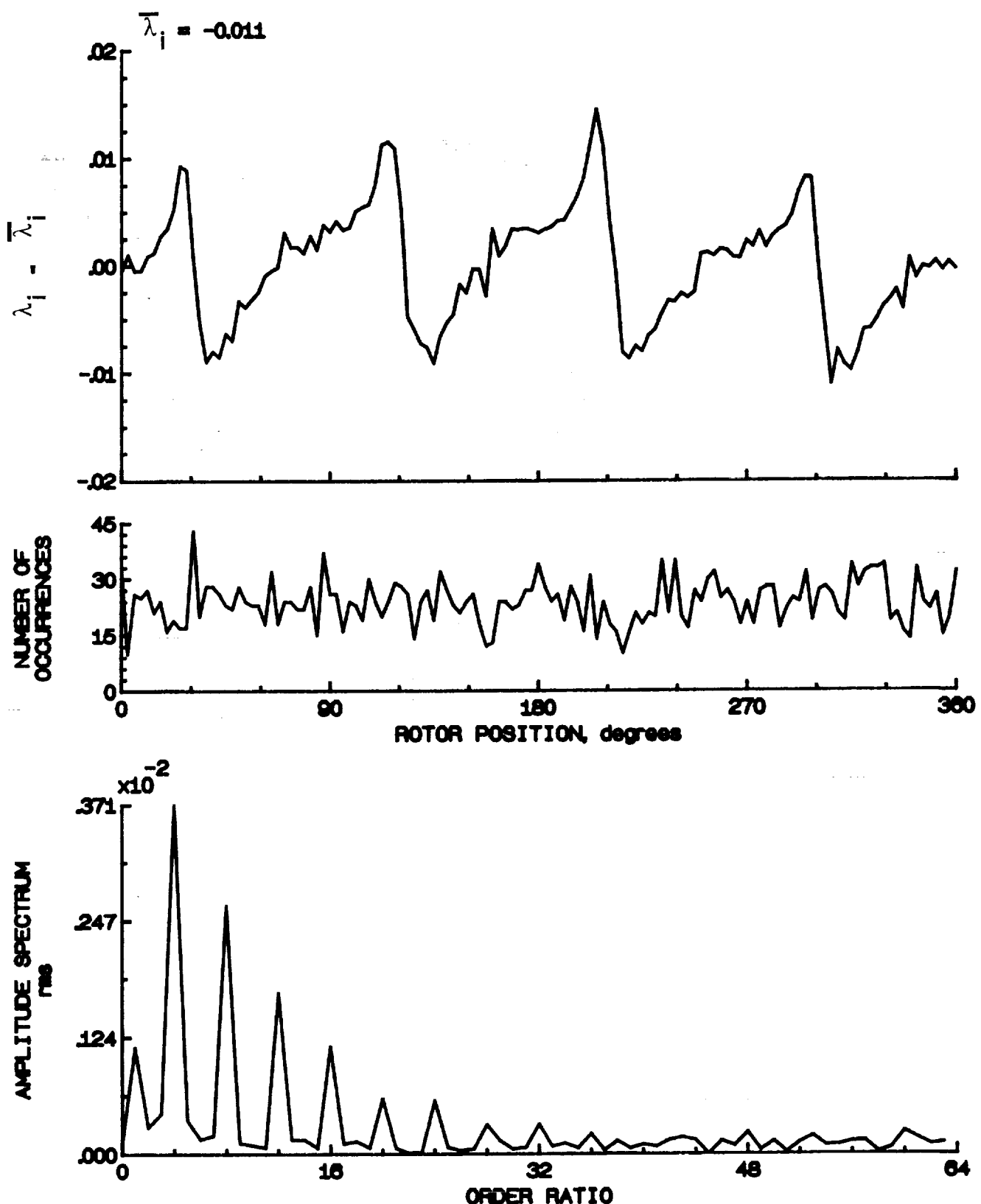


Figure 164.- Concluded.

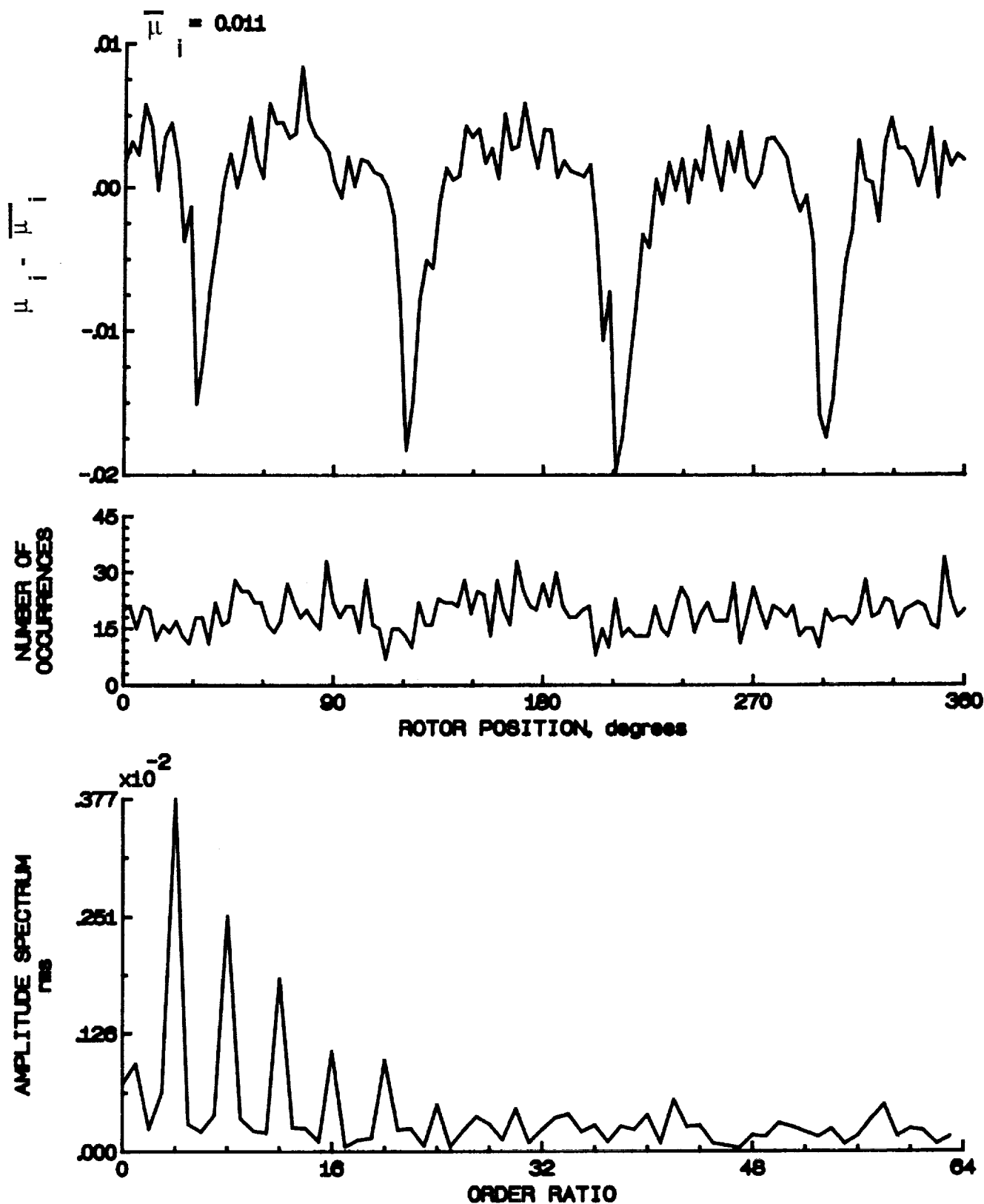


Figure 165.- Induced inflow velocity measured at 300 degrees and r/R of 0.70.

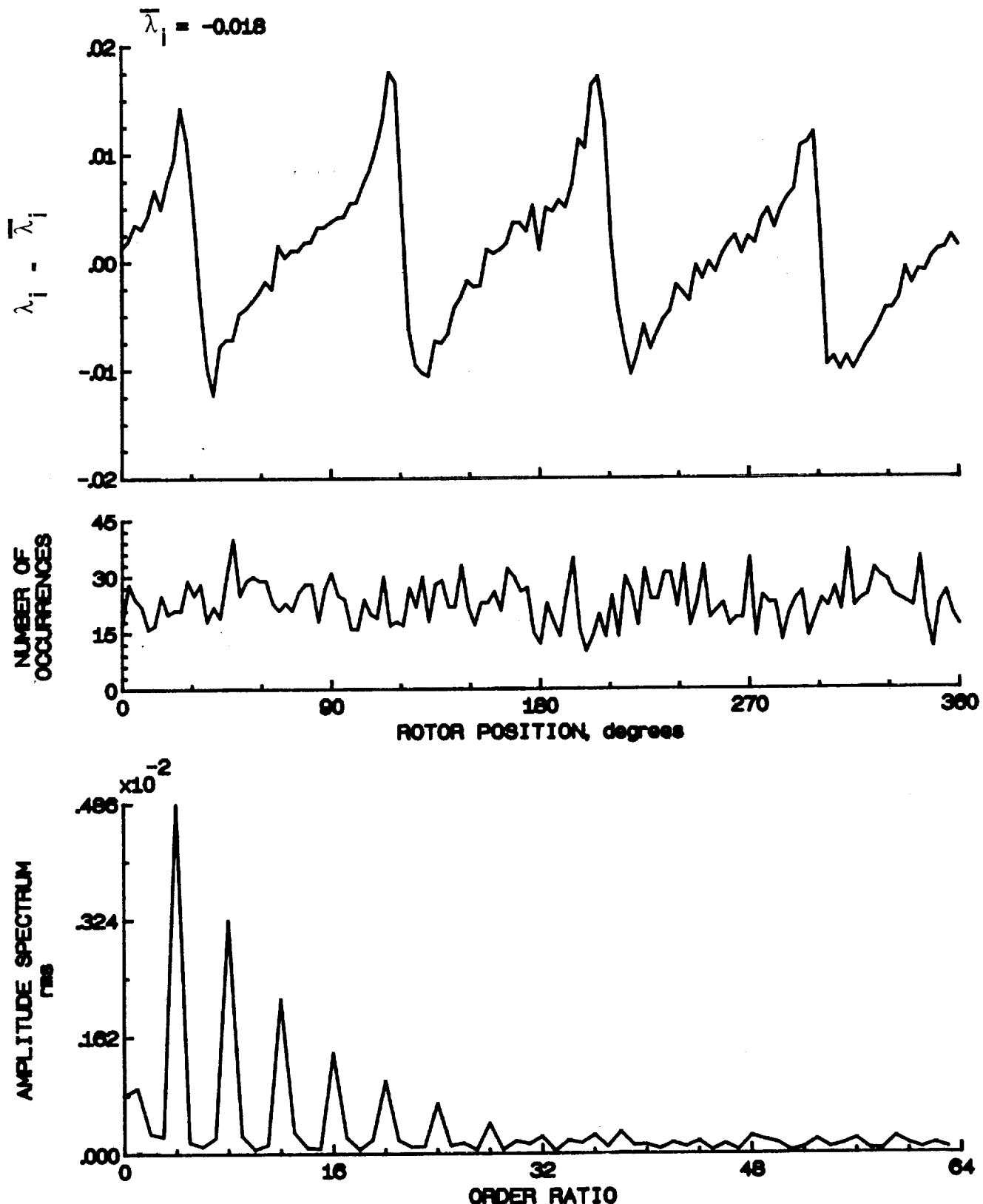


Figure 165.- Concluded.

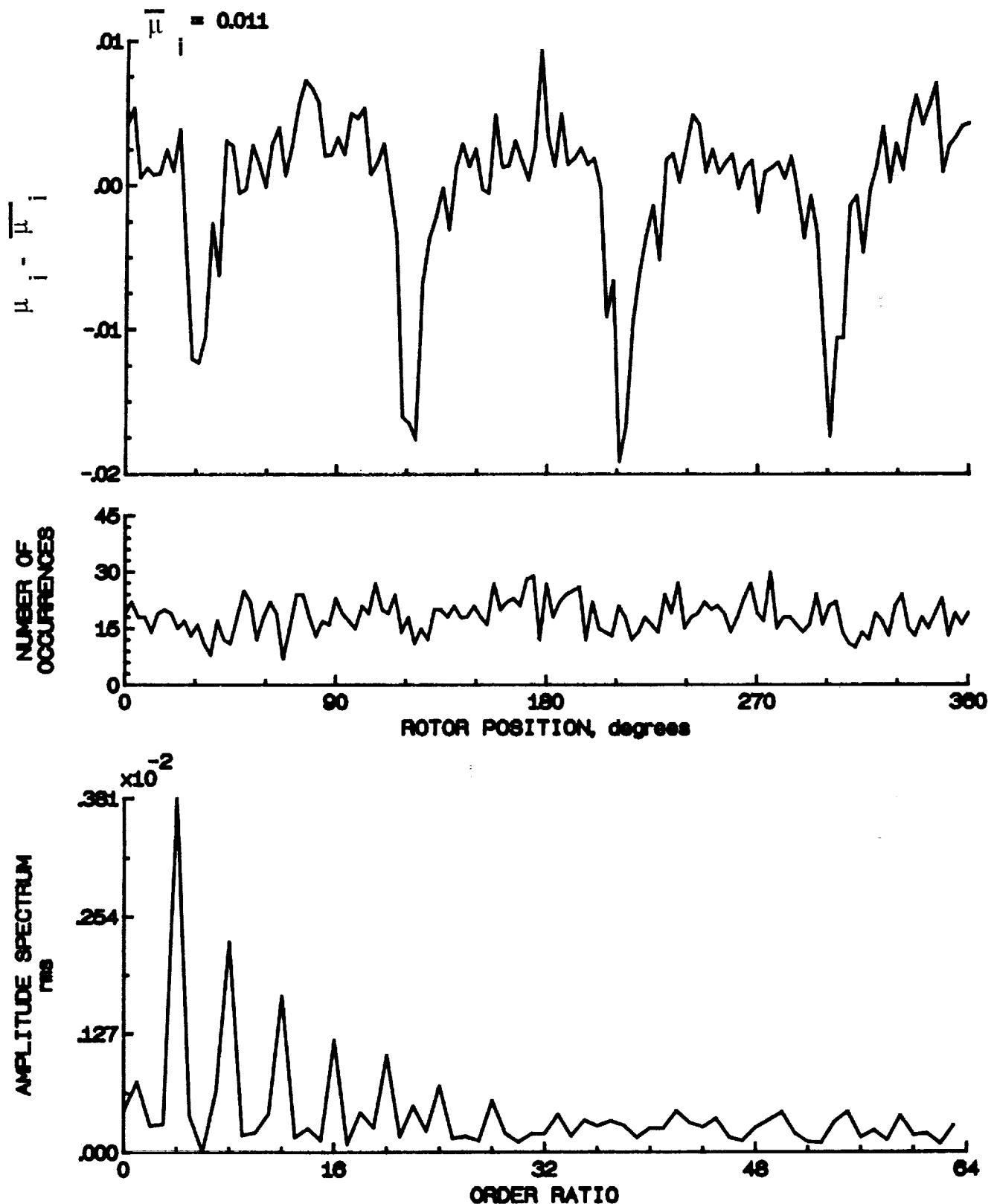


Figure 166.- Induced inflow velocity measured at 300 degrees and r/R of 0.74.

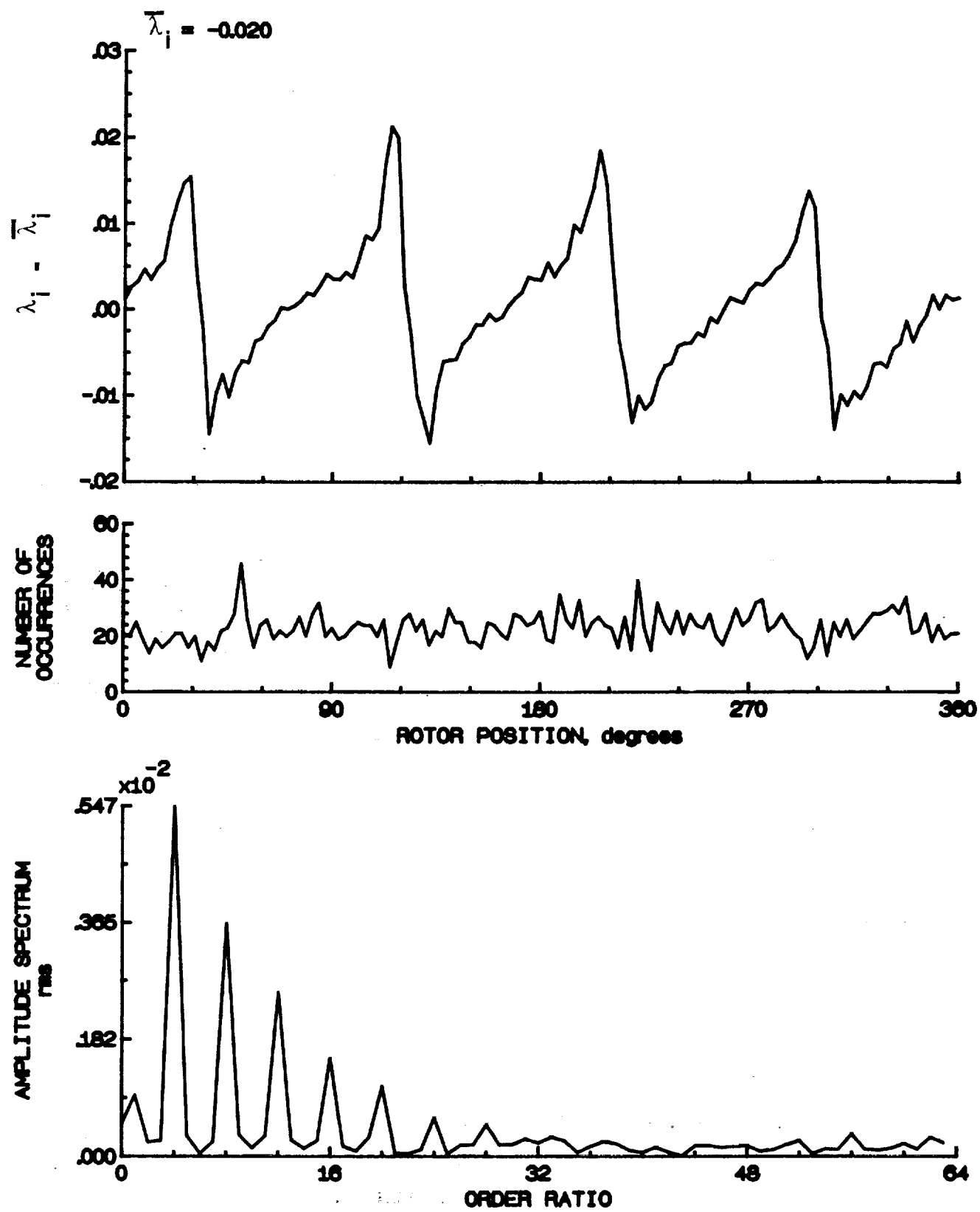


Figure 106.- Concluded.

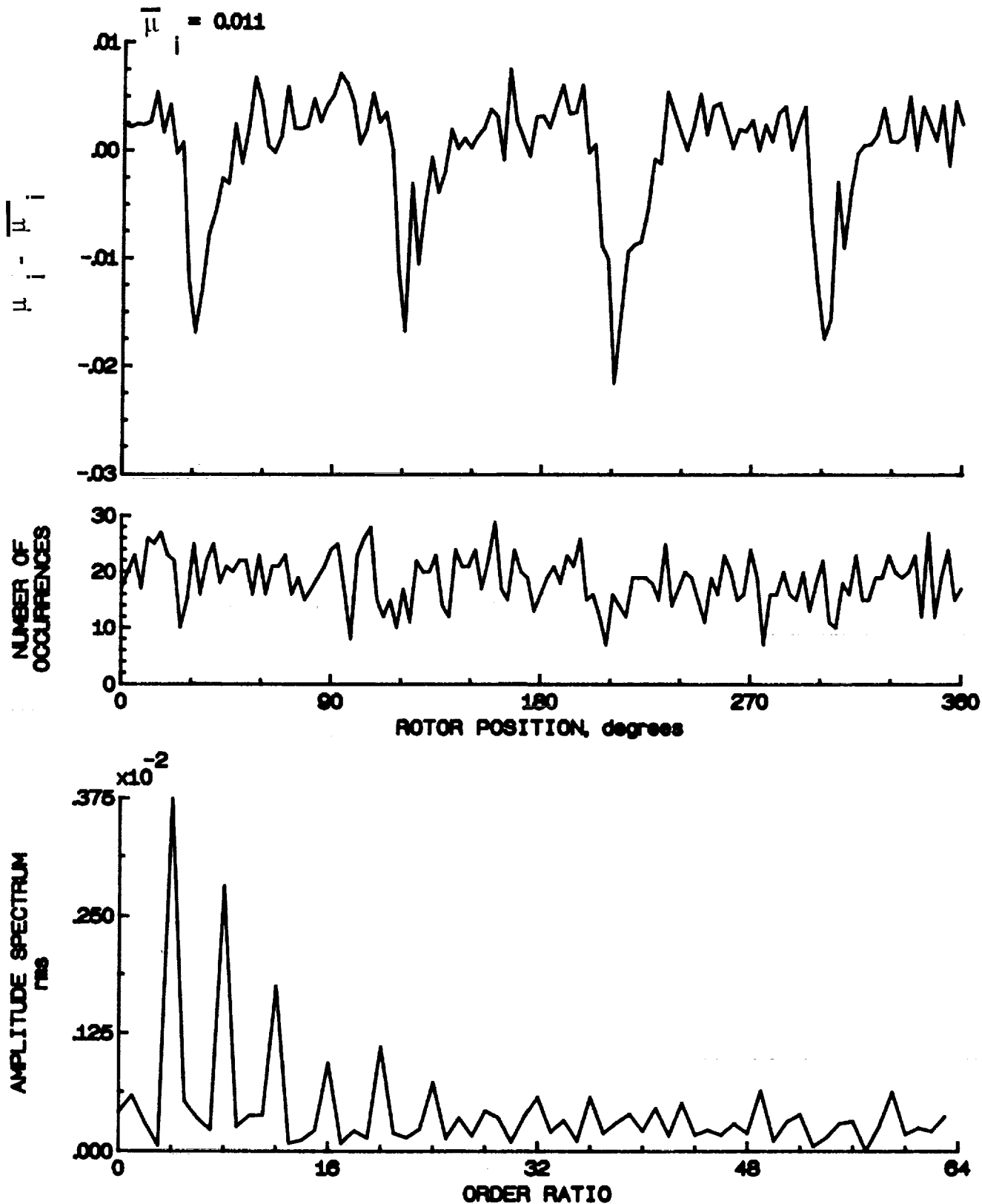


Figure 167.- Induced inflow velocity measured at 300 degrees and r/R of 0.78.

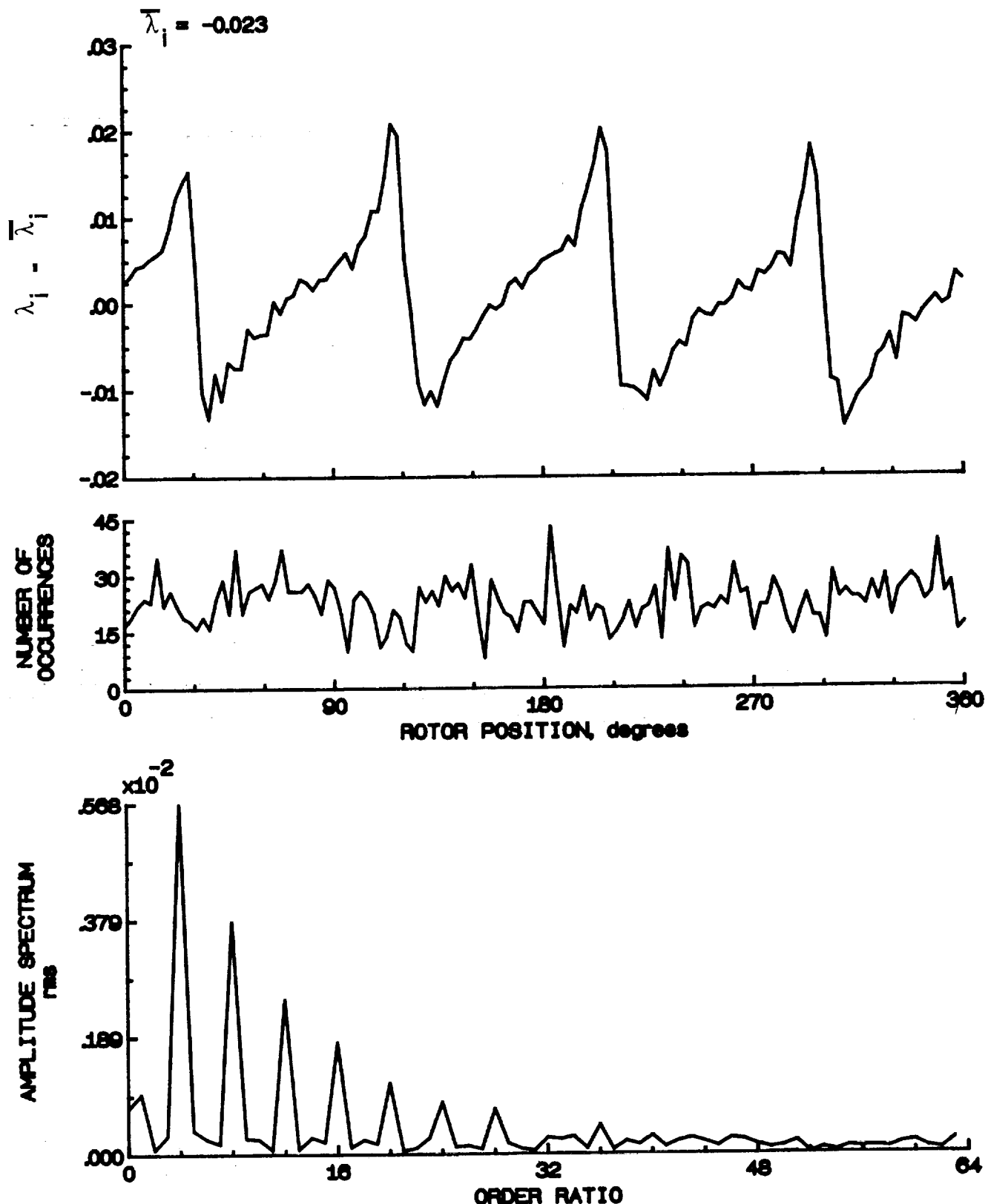


Figure 167.- Concluded.

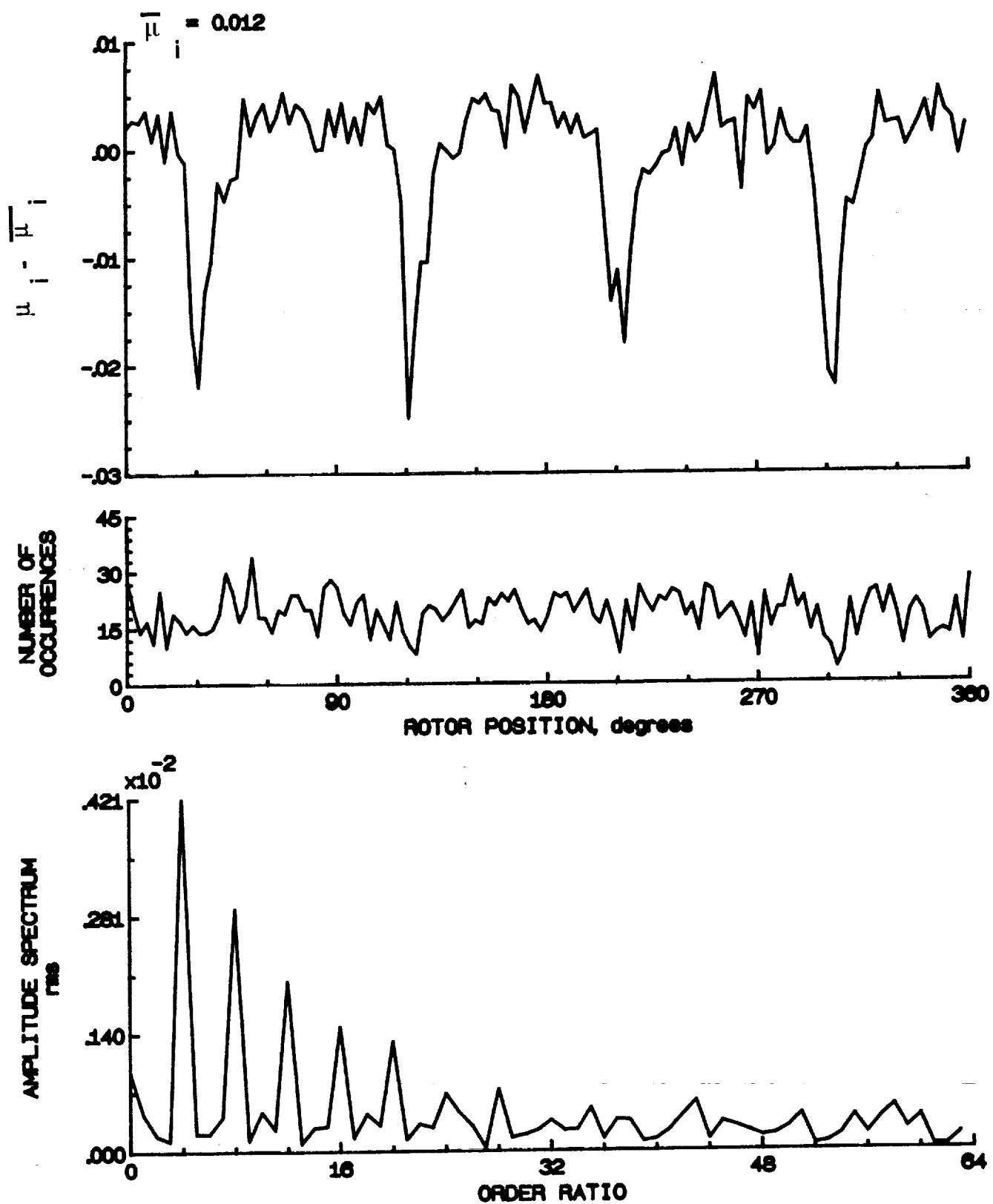


Figure 168.- Induced inflow velocity measured at 300 degrees and r/R of 0.82.

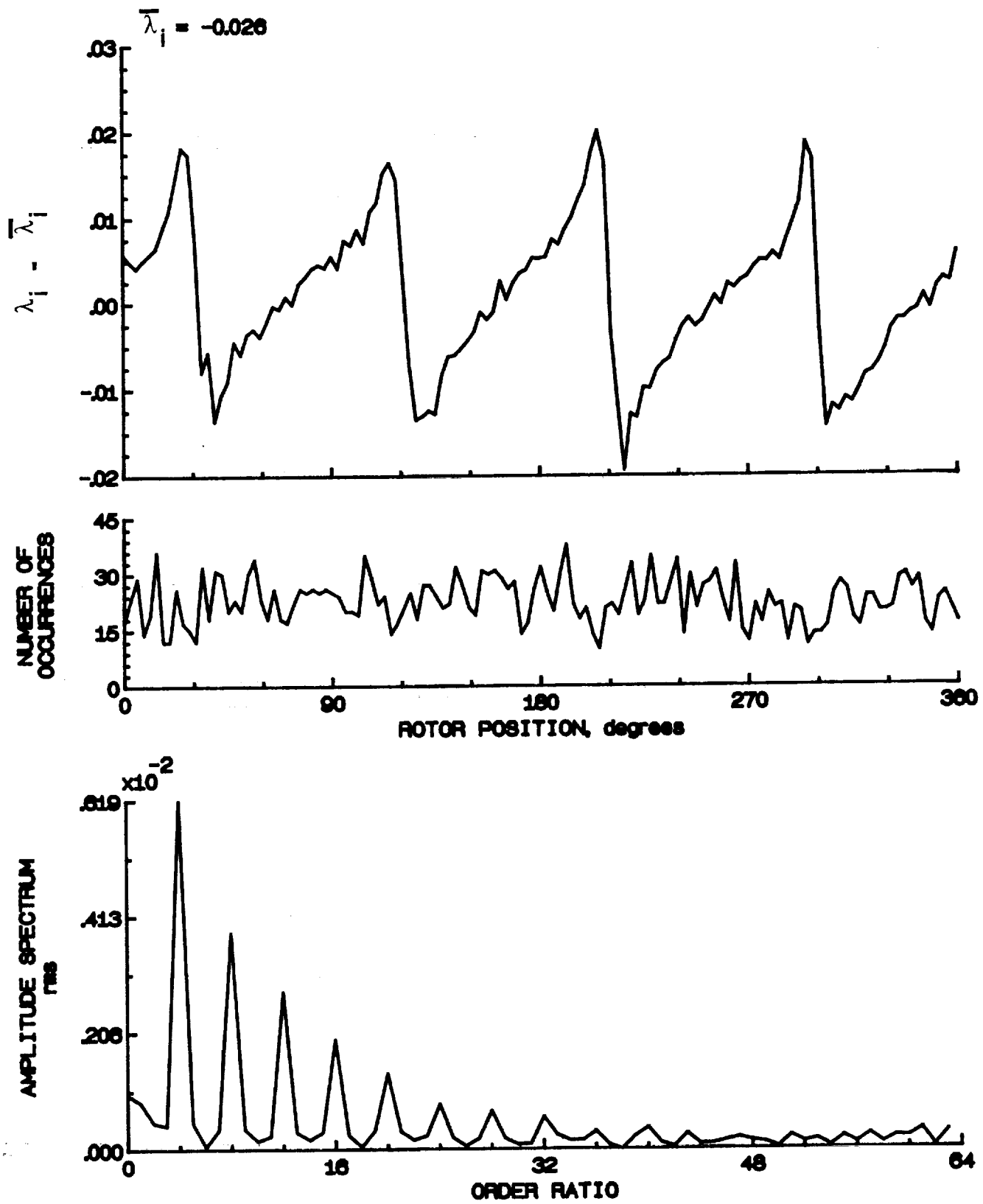


Figure 168.- Concluded.

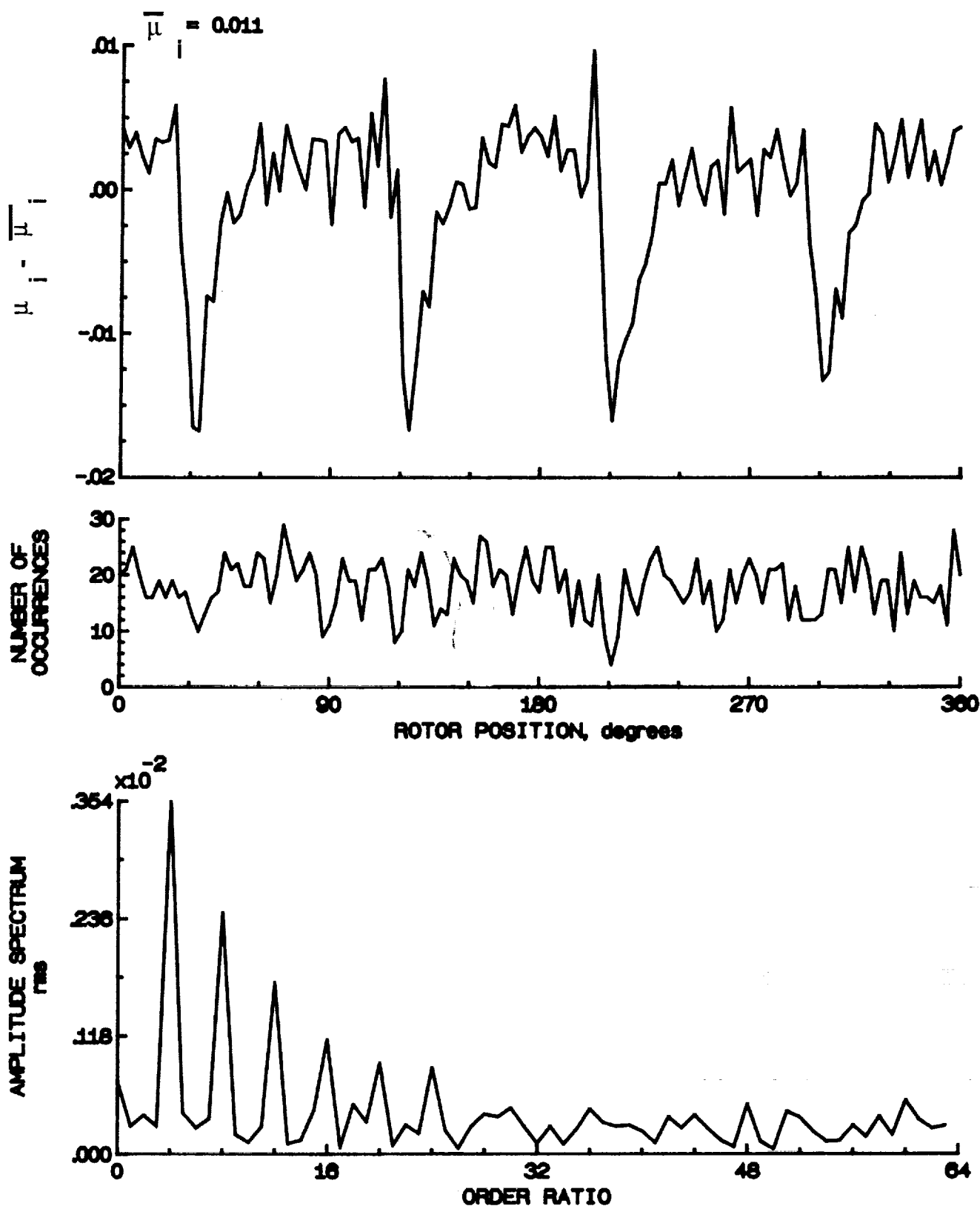


Figure 160.- Induced inflow velocity measured at 300 degrees and r/R of 0.86.

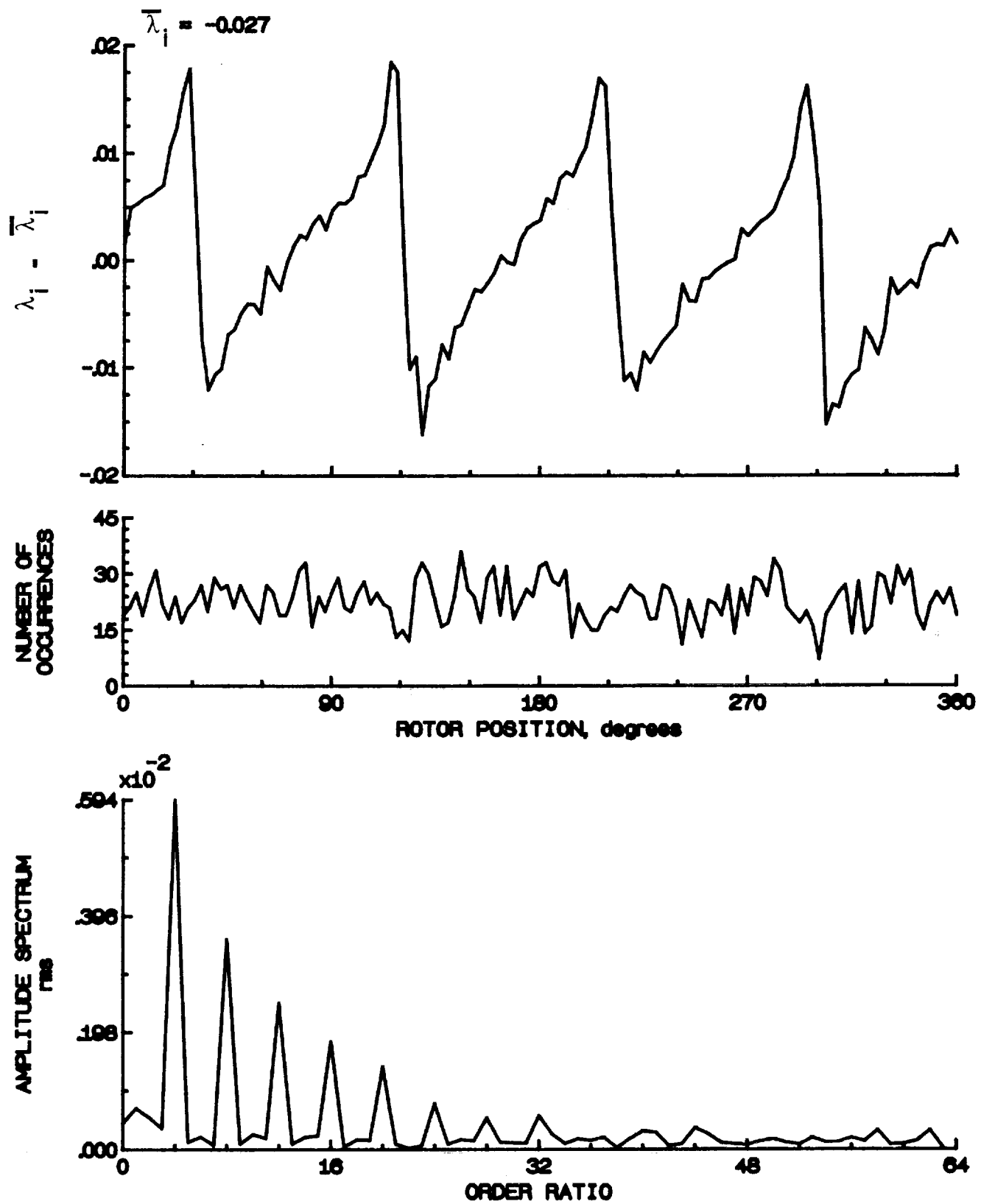


Figure 169.- Concluded.

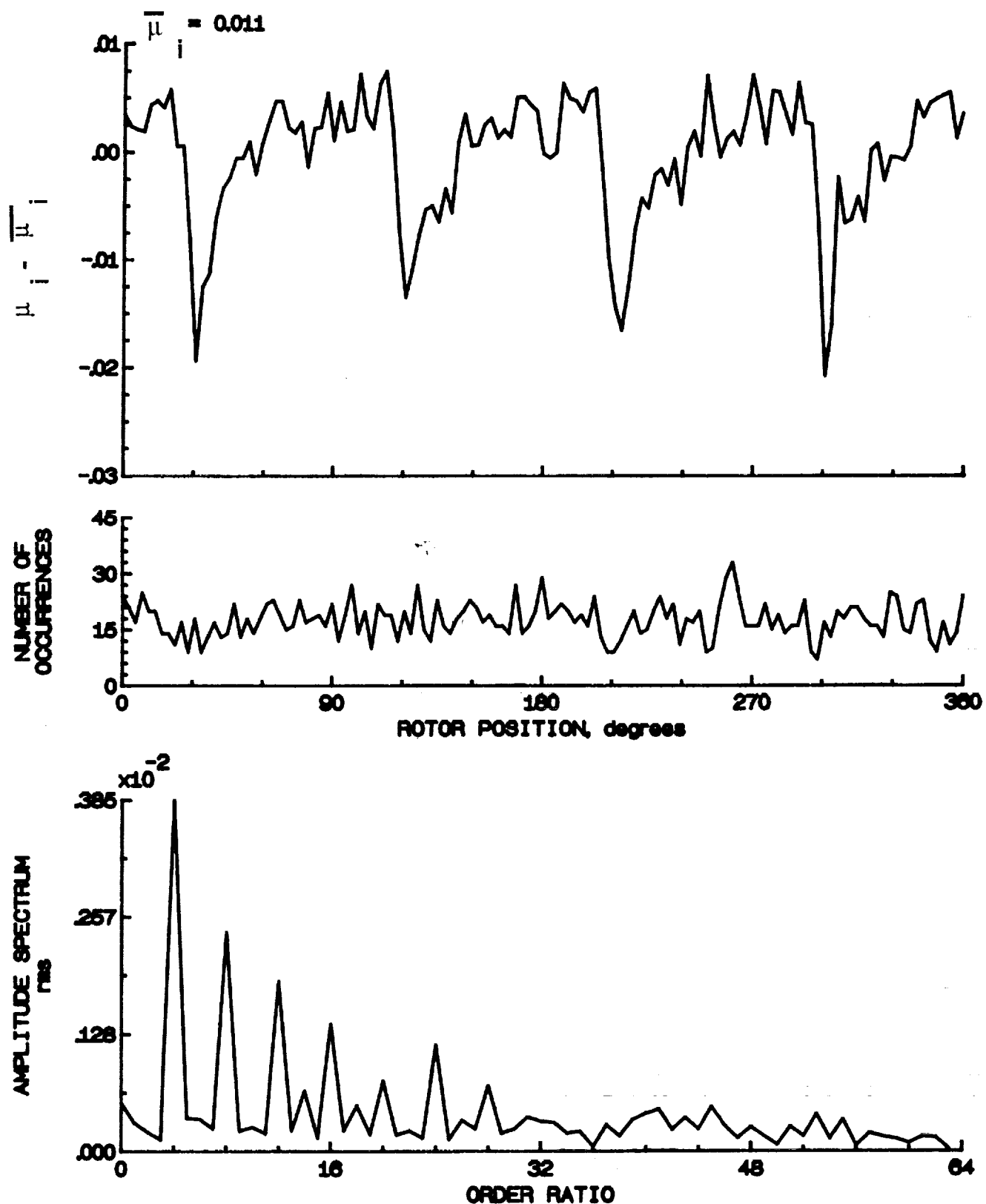


Figure 170.- Induced inflow velocity measured at 300 degrees and r/R of 0.90.

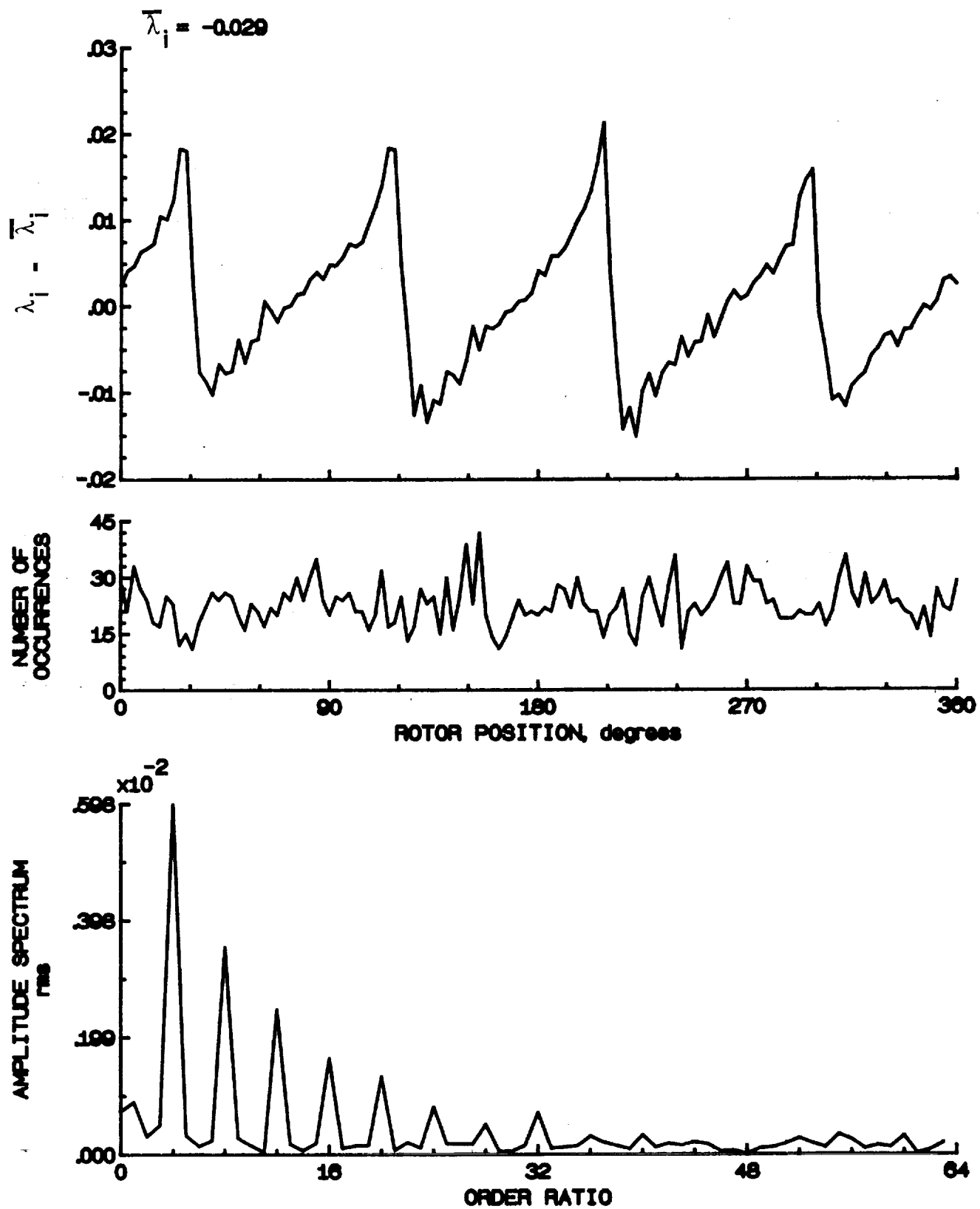


Figure 170.- Concluded.

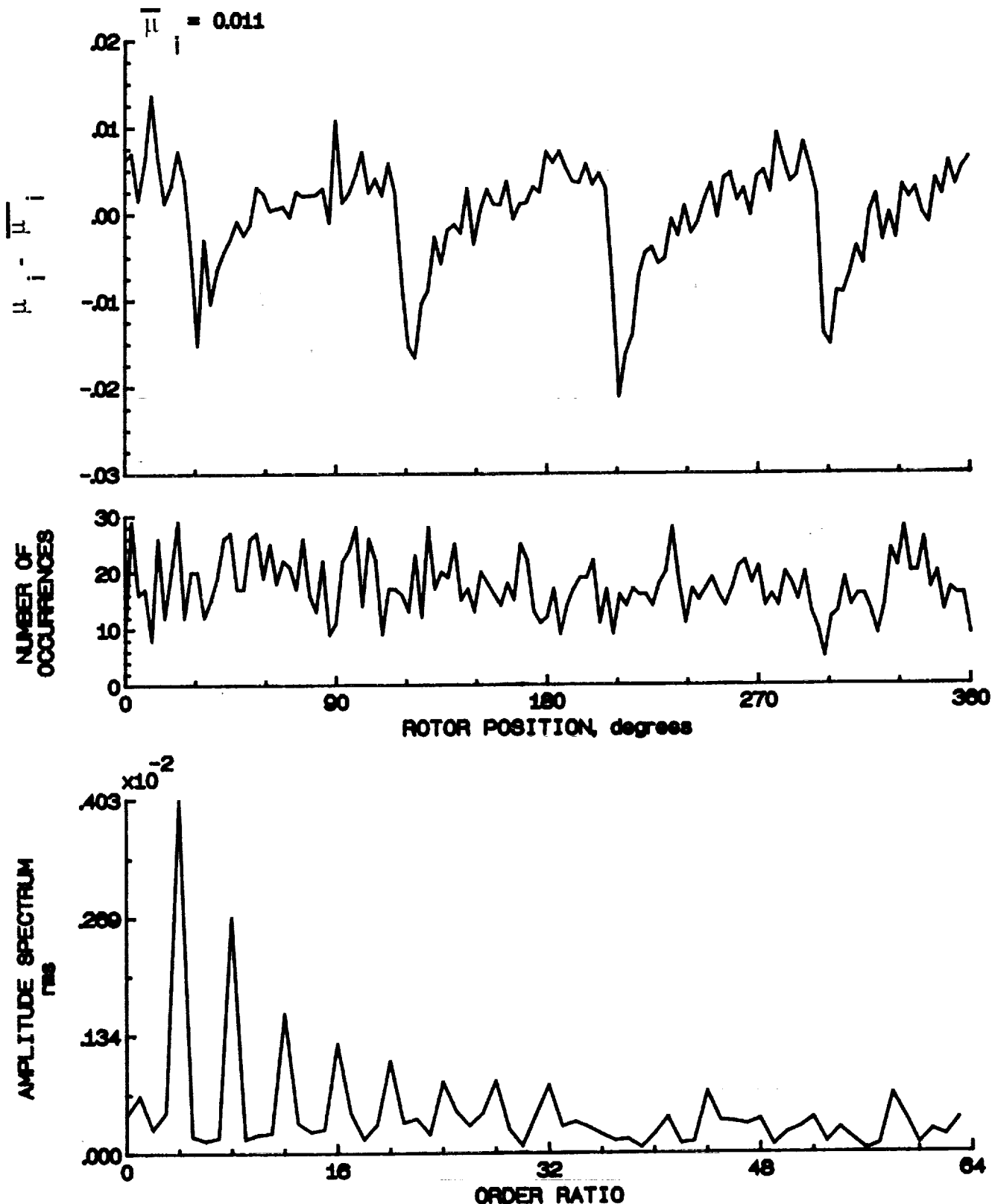


Figure 171.- Induced inflow velocity measured at 300 degrees and r/R of 0.94.

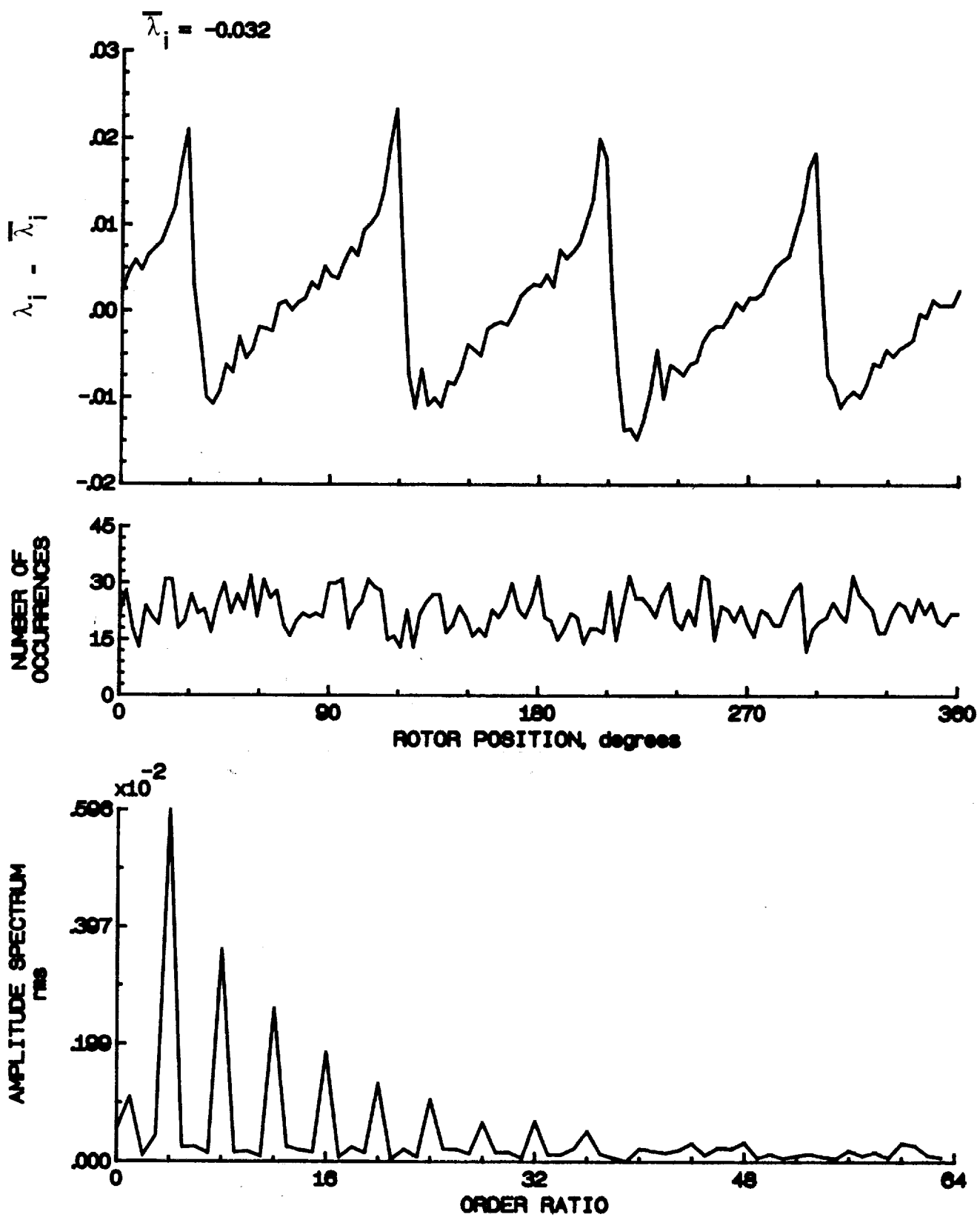


Figure 171.- Concluded.

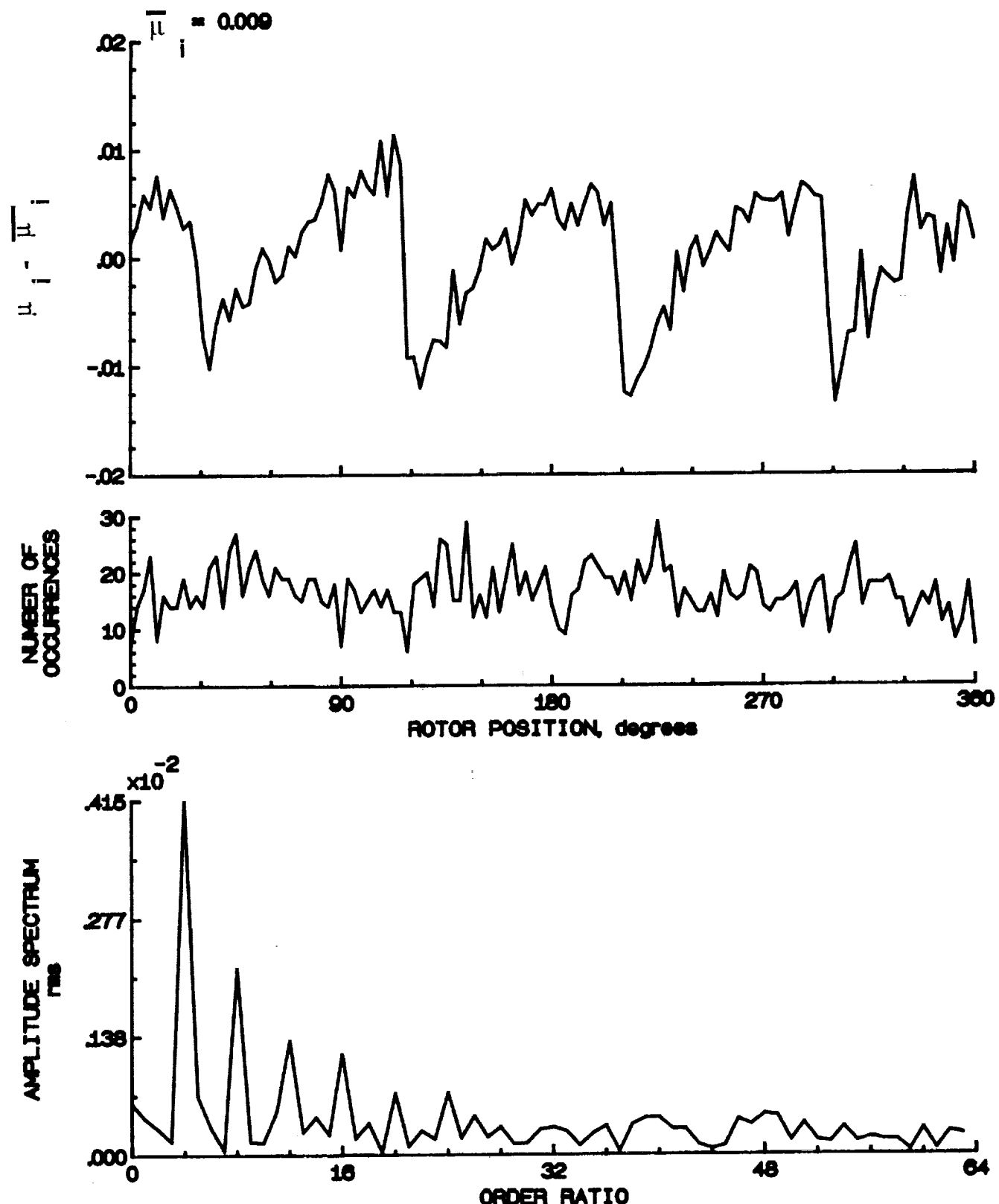


Figure 172.- Induced inflow velocity measured at 300 degrees and r/R of 0.98.

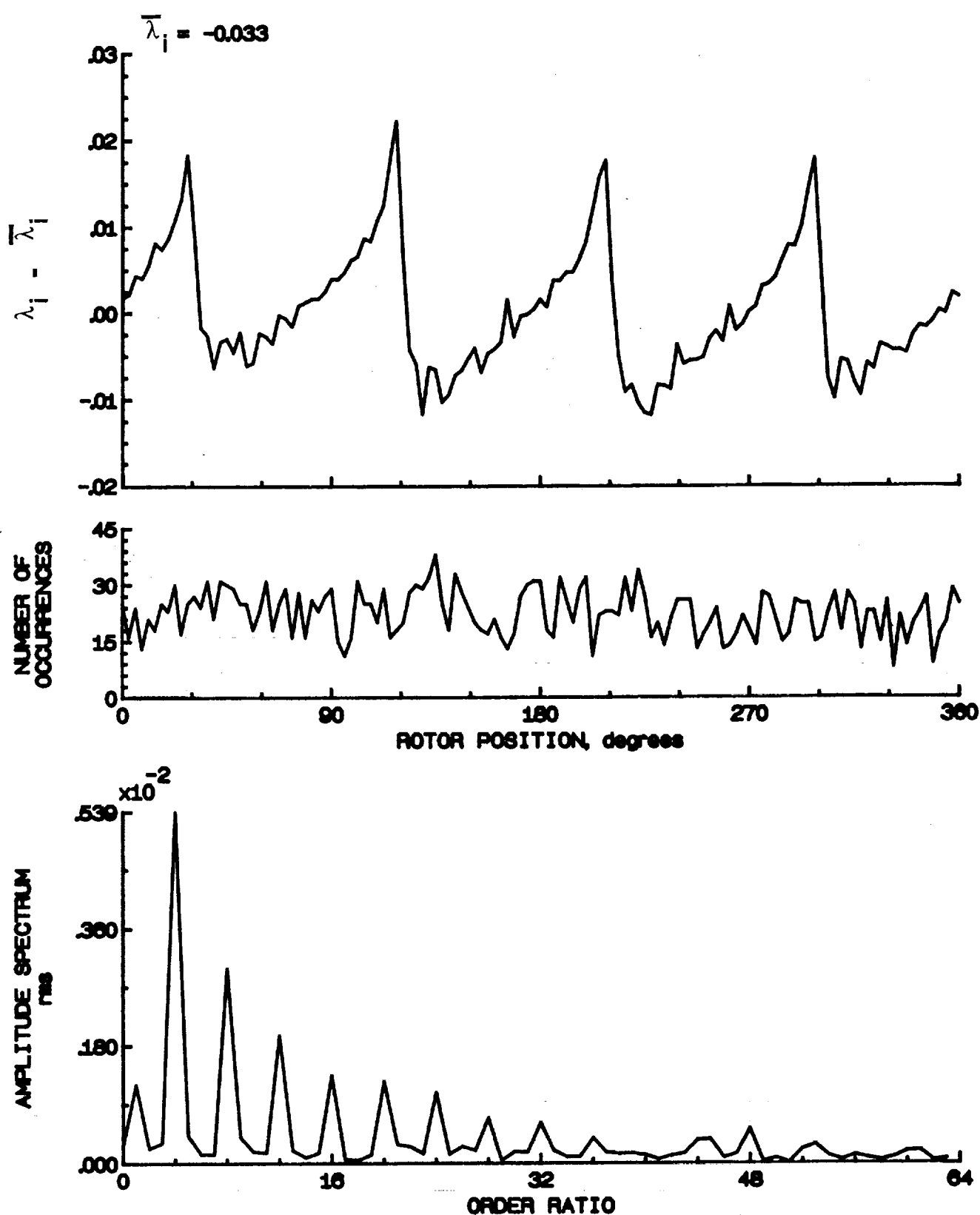


Figure 172.- Concluded.

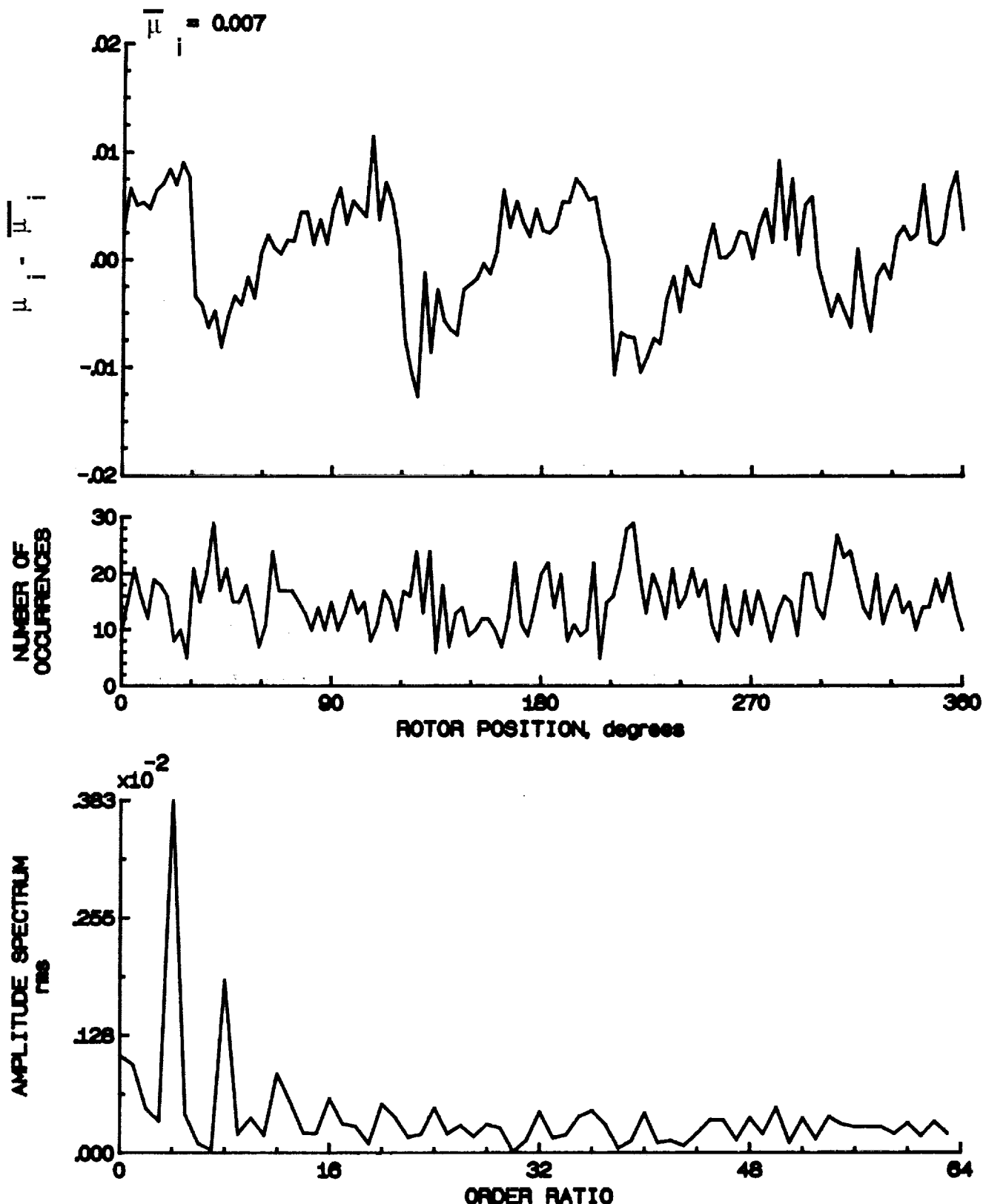


Figure 173.- Induced inflow velocity measured at 300 degrees and r/R of 1.02.

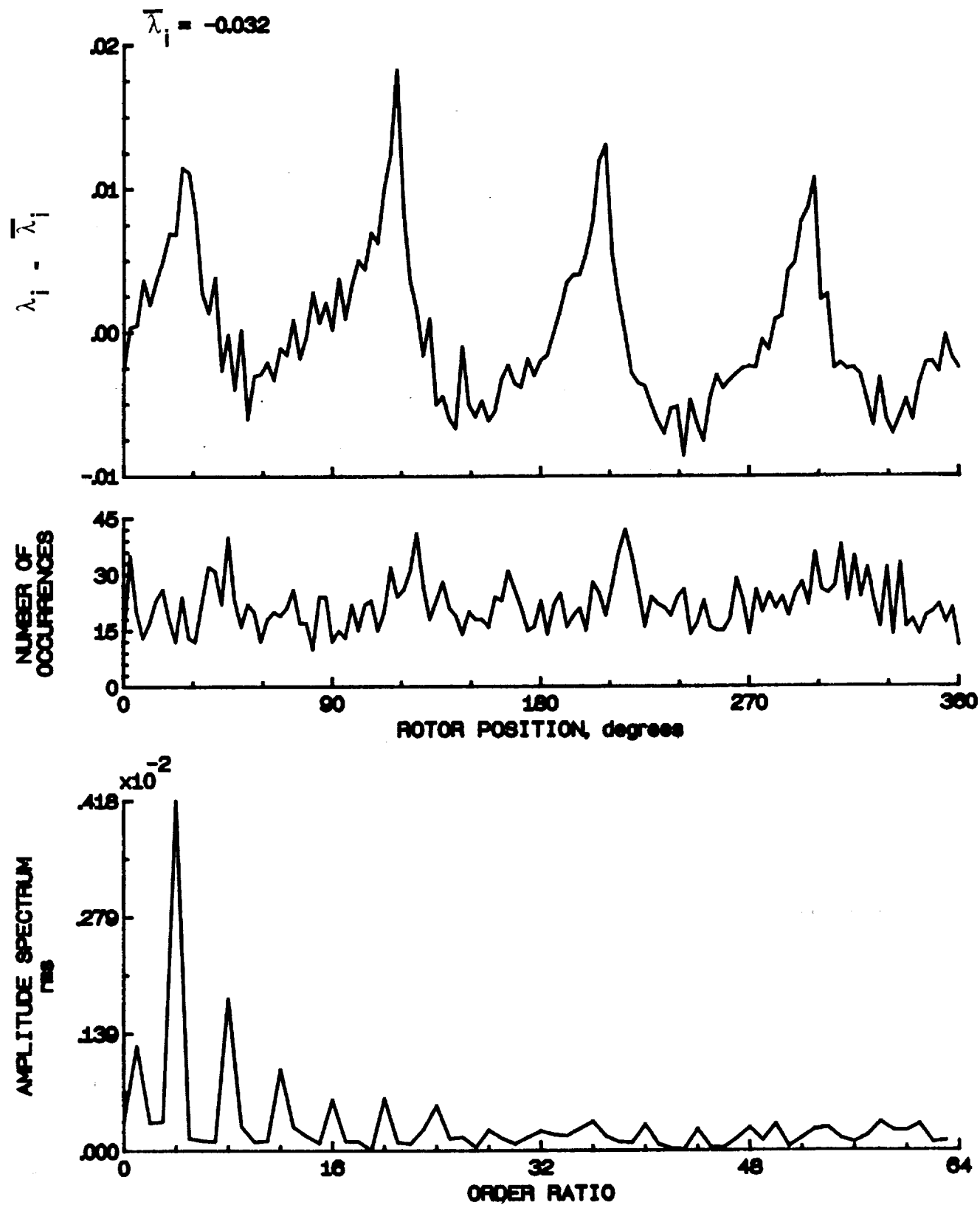


Figure 173.- Concluded.

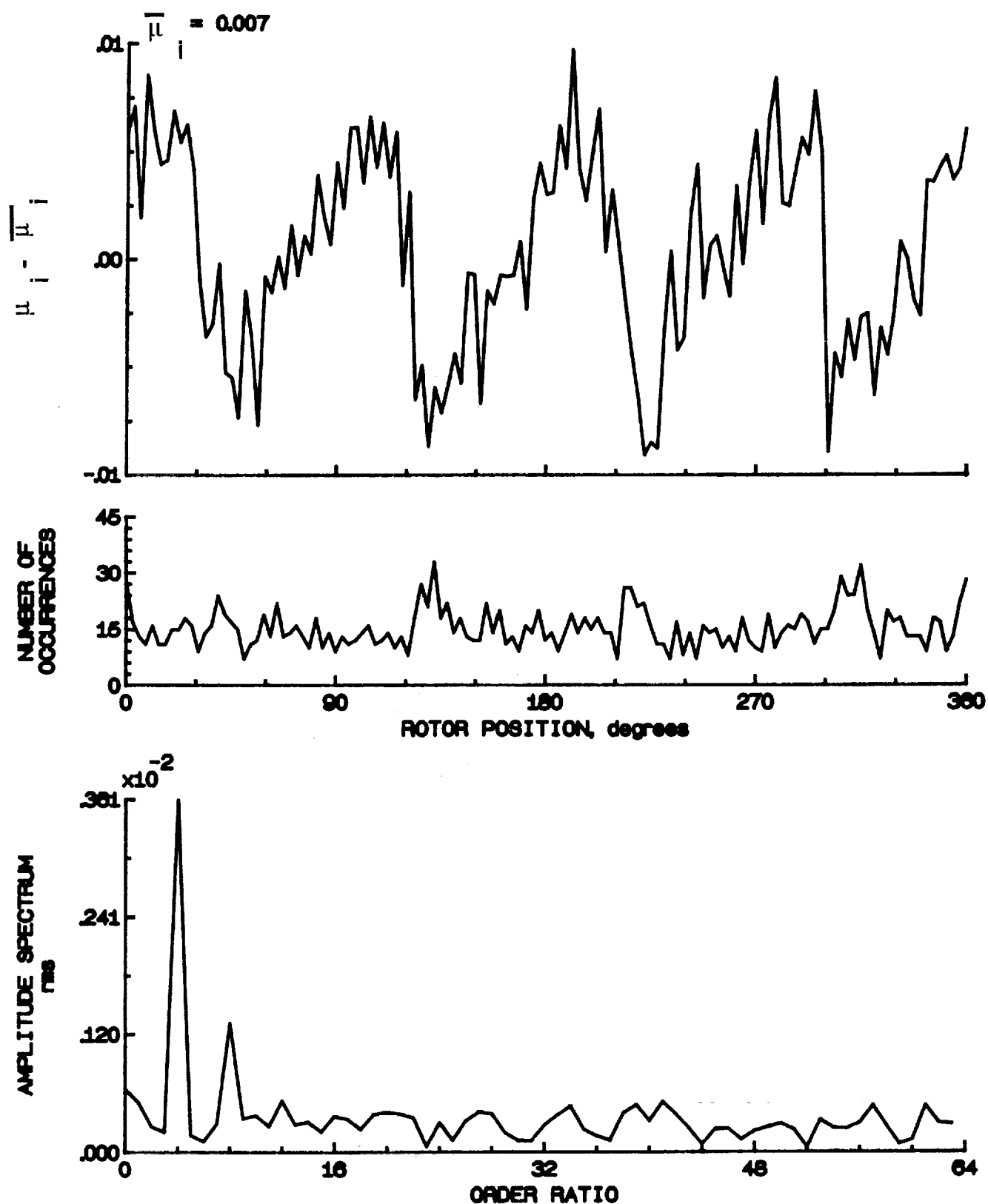


Figure 174.- Induced inflow velocity measured at 300 degrees and r/R of 1.04.

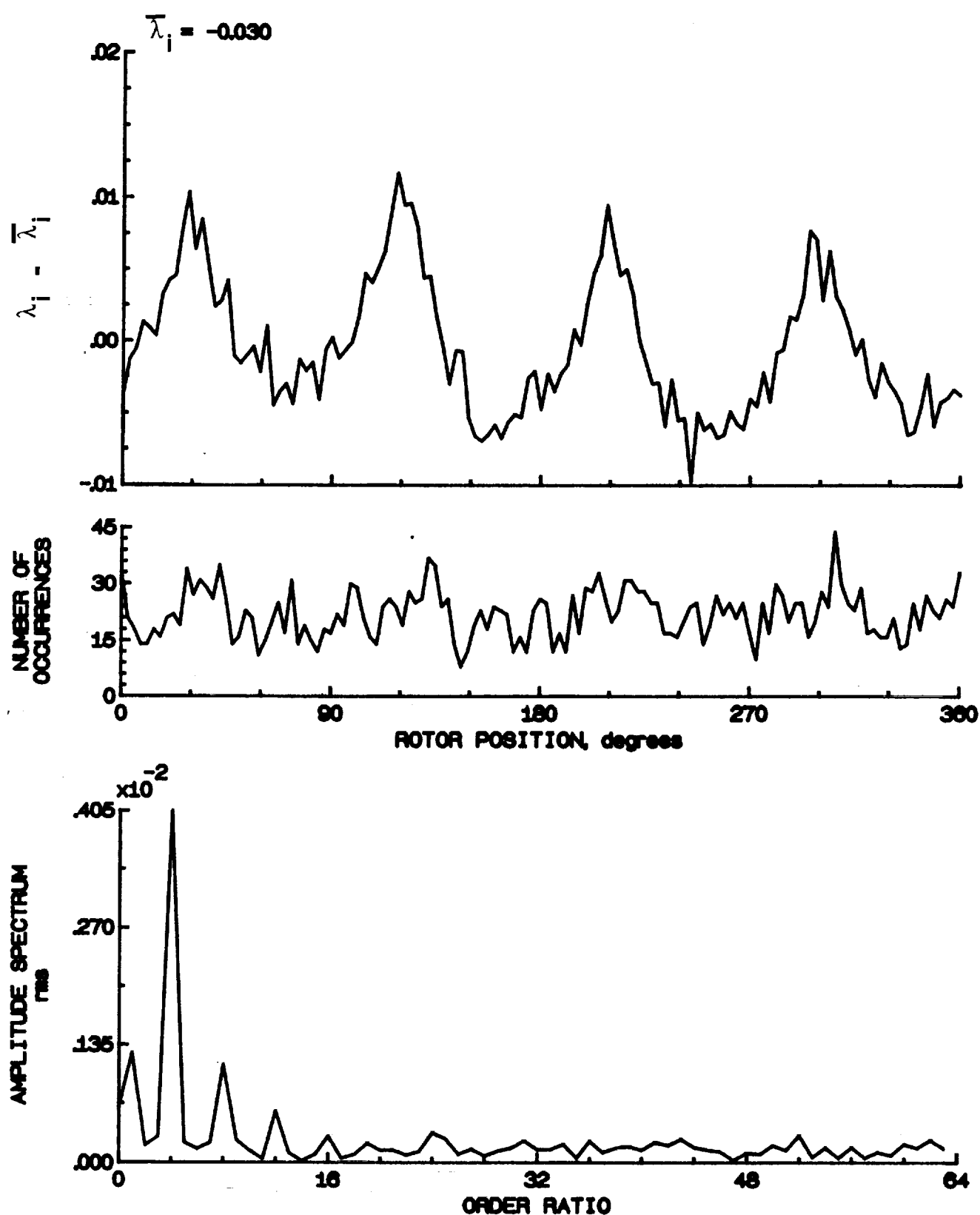


Figure 174.- Concluded.

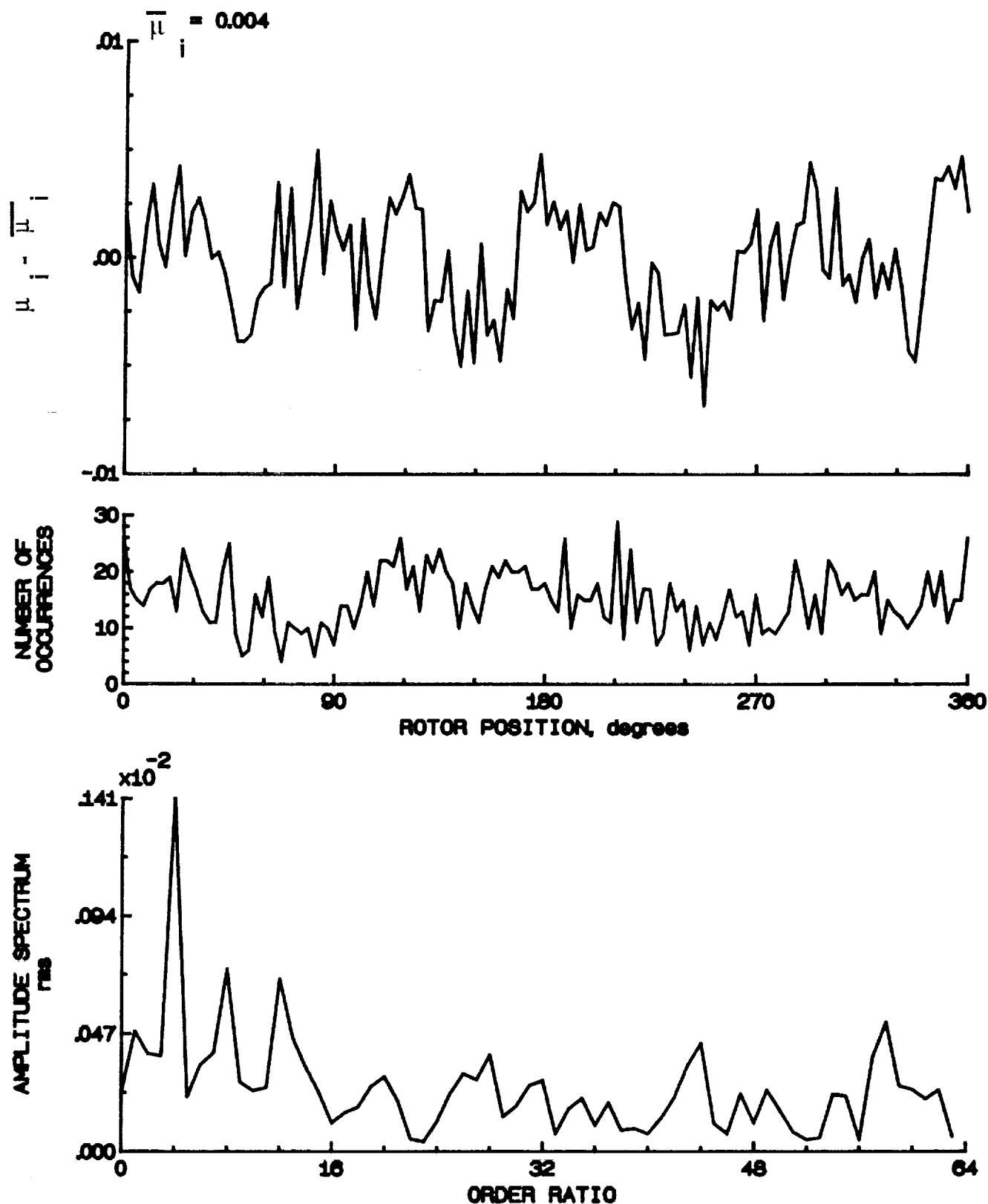


Figure 175.- Induced inflow velocity measured at 300 degrees and r/R of 1.10.

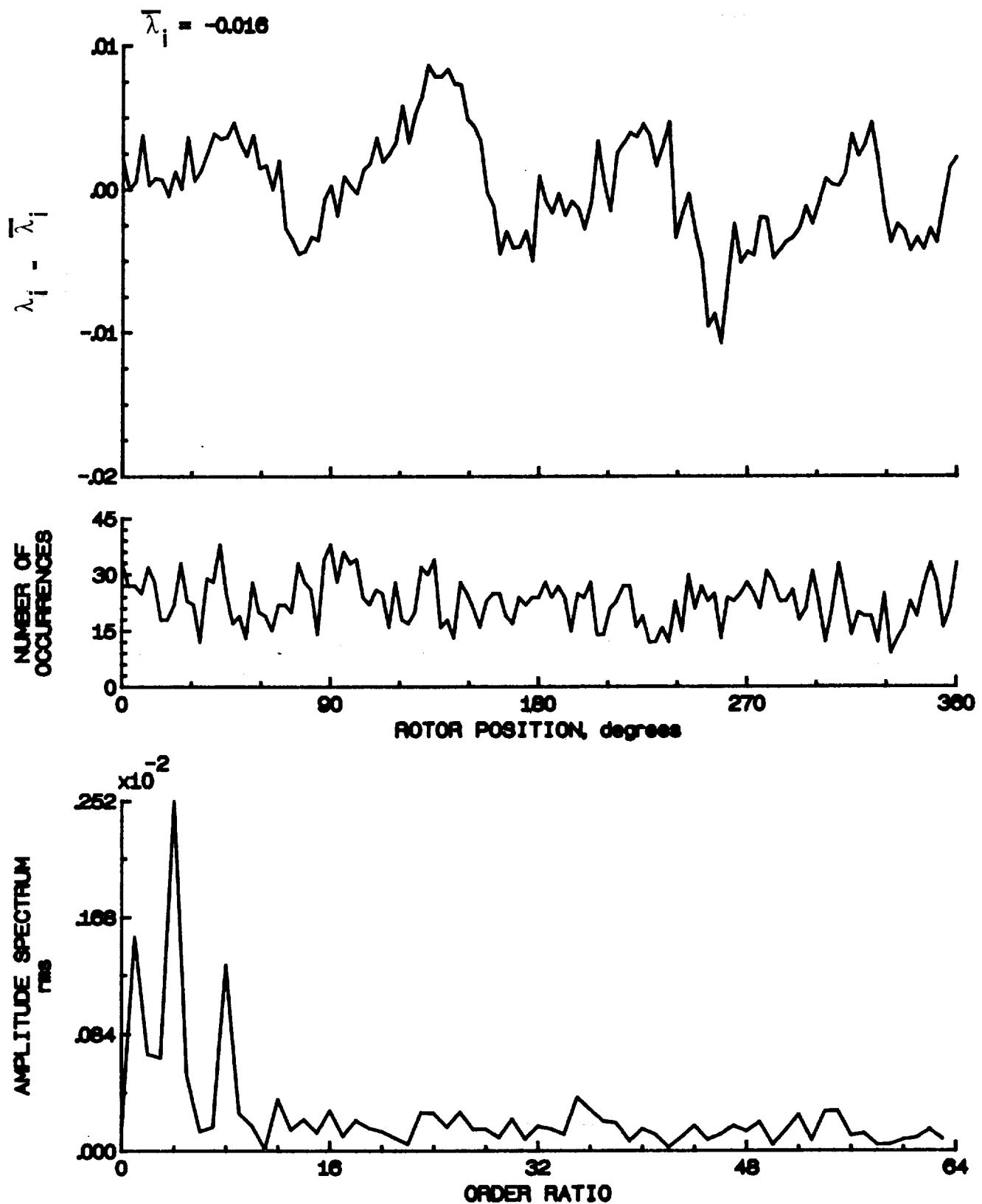


Figure 175.- Concluded.

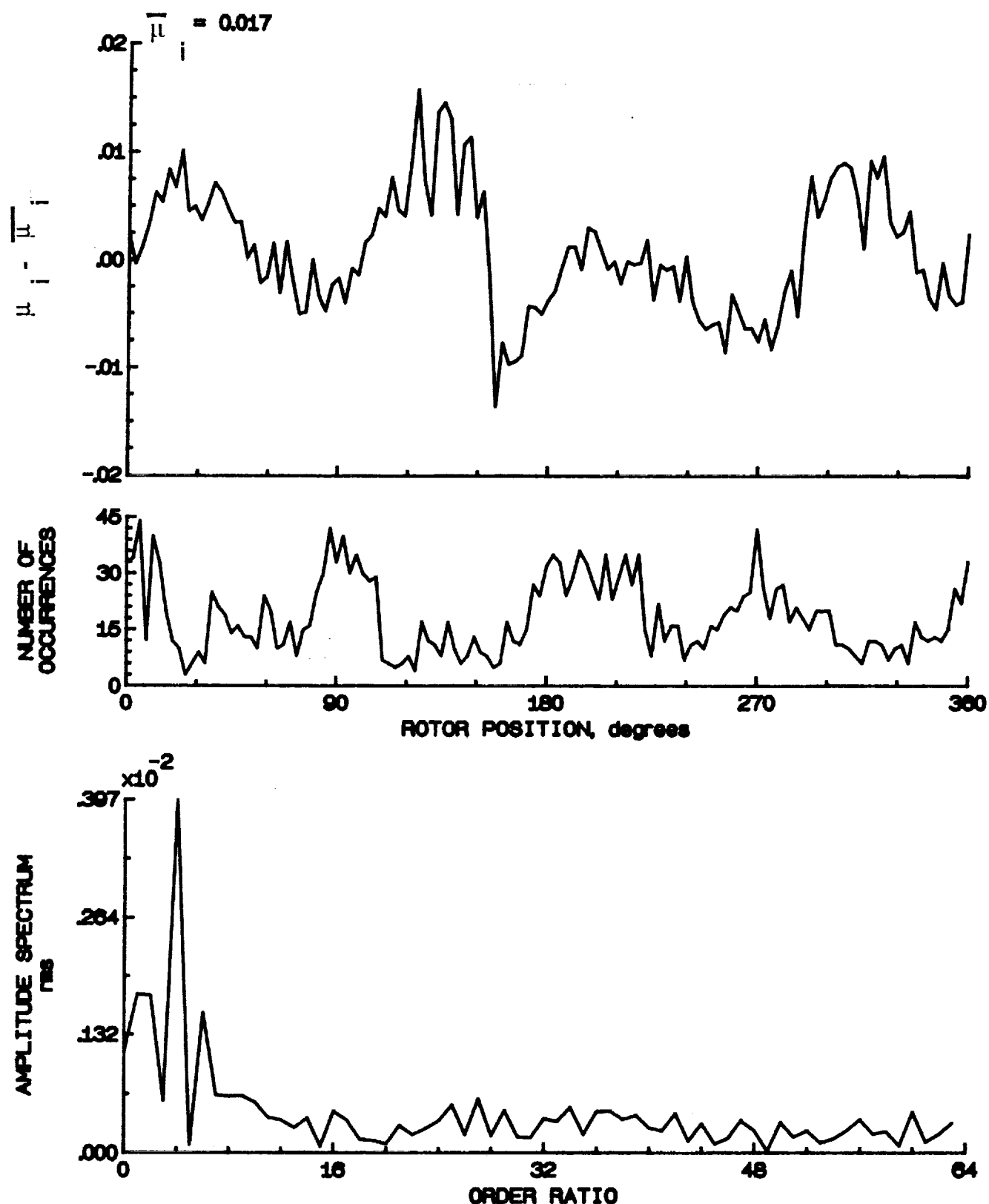


Figure 17a.- Induced inflow velocity measured at 330 degrees and r/R of 0.20.

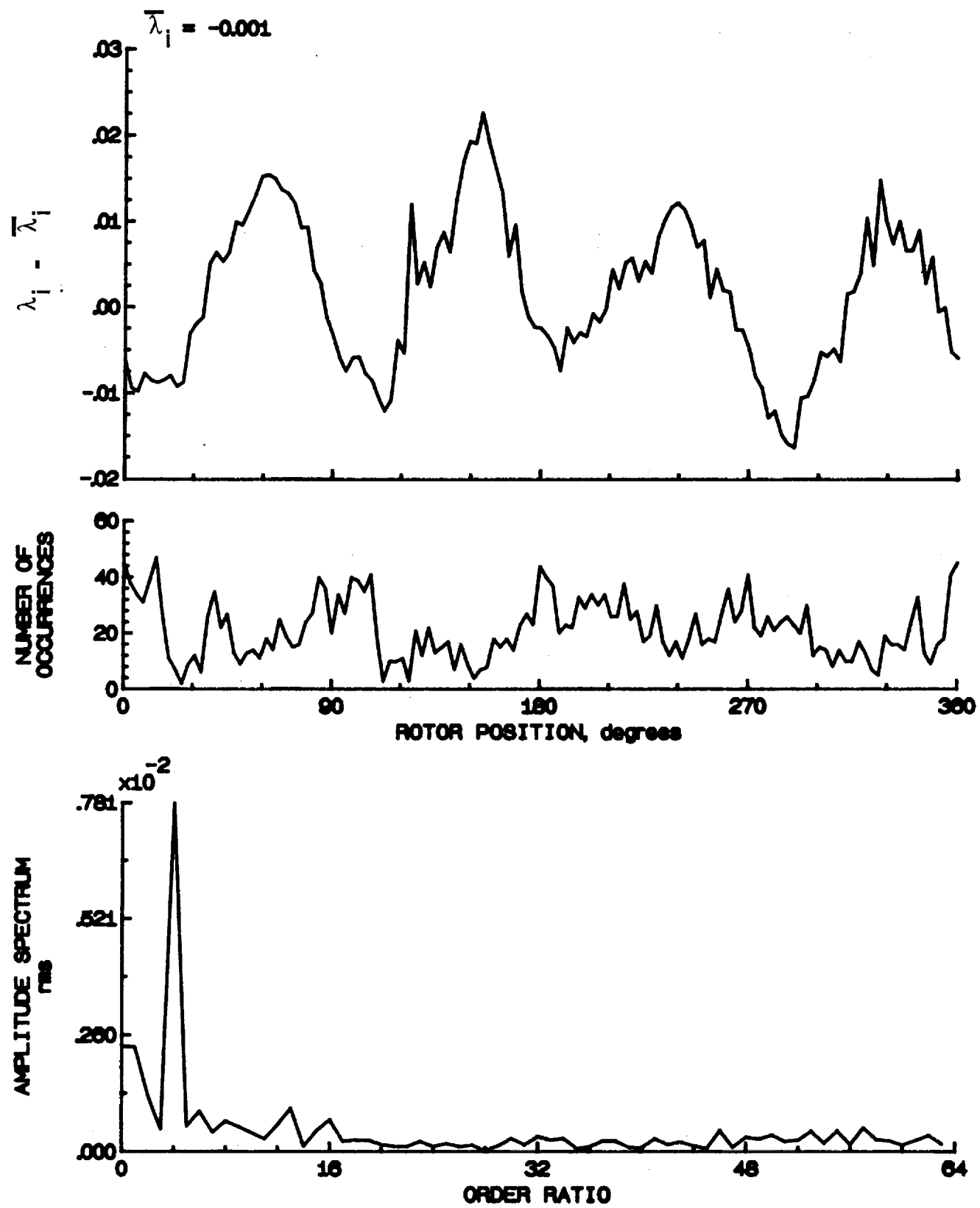


Figure 17a.- Concluded.

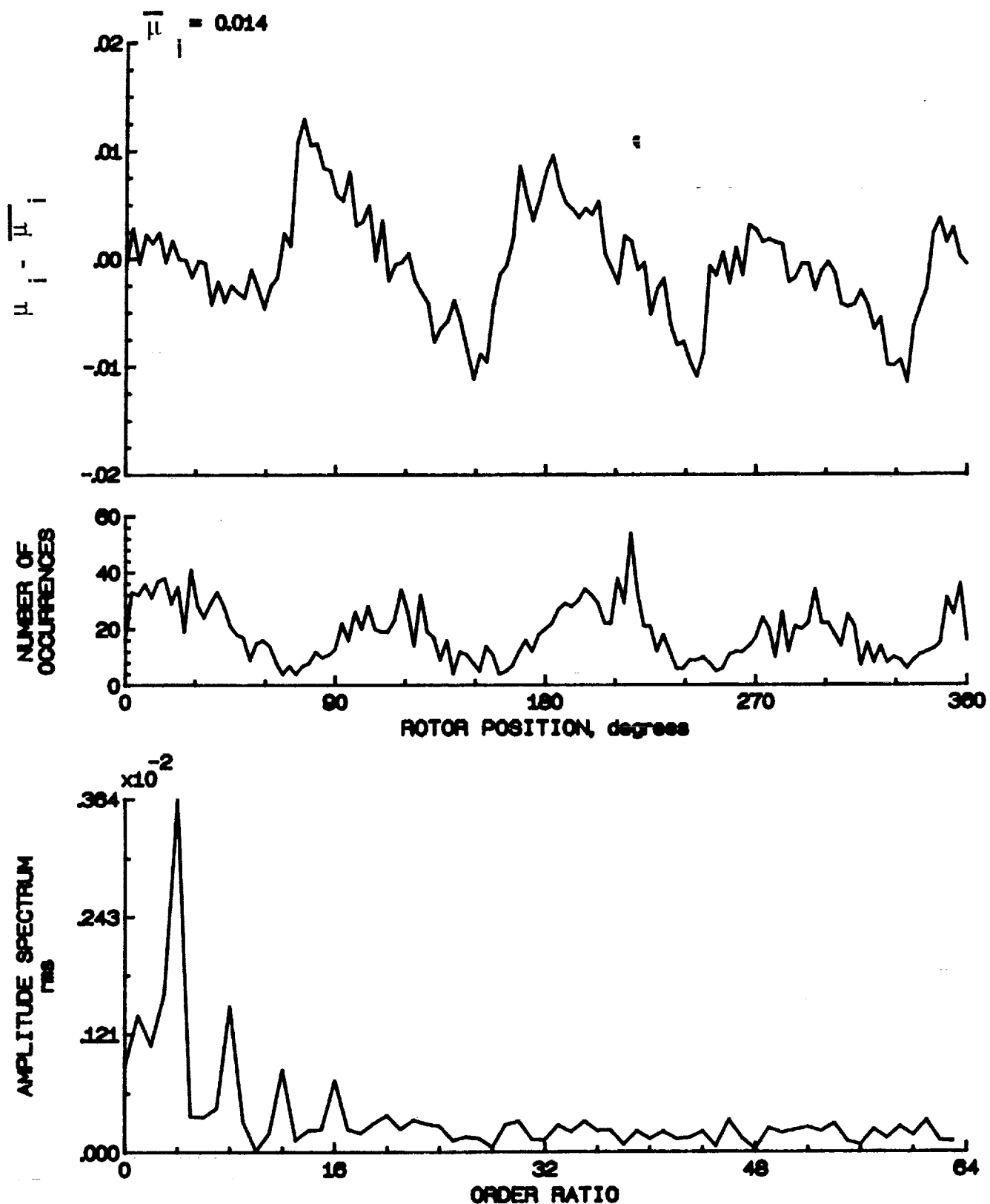


Figure 177.- Induced inflow velocity measured at 330 degrees and r/R of 0.40.

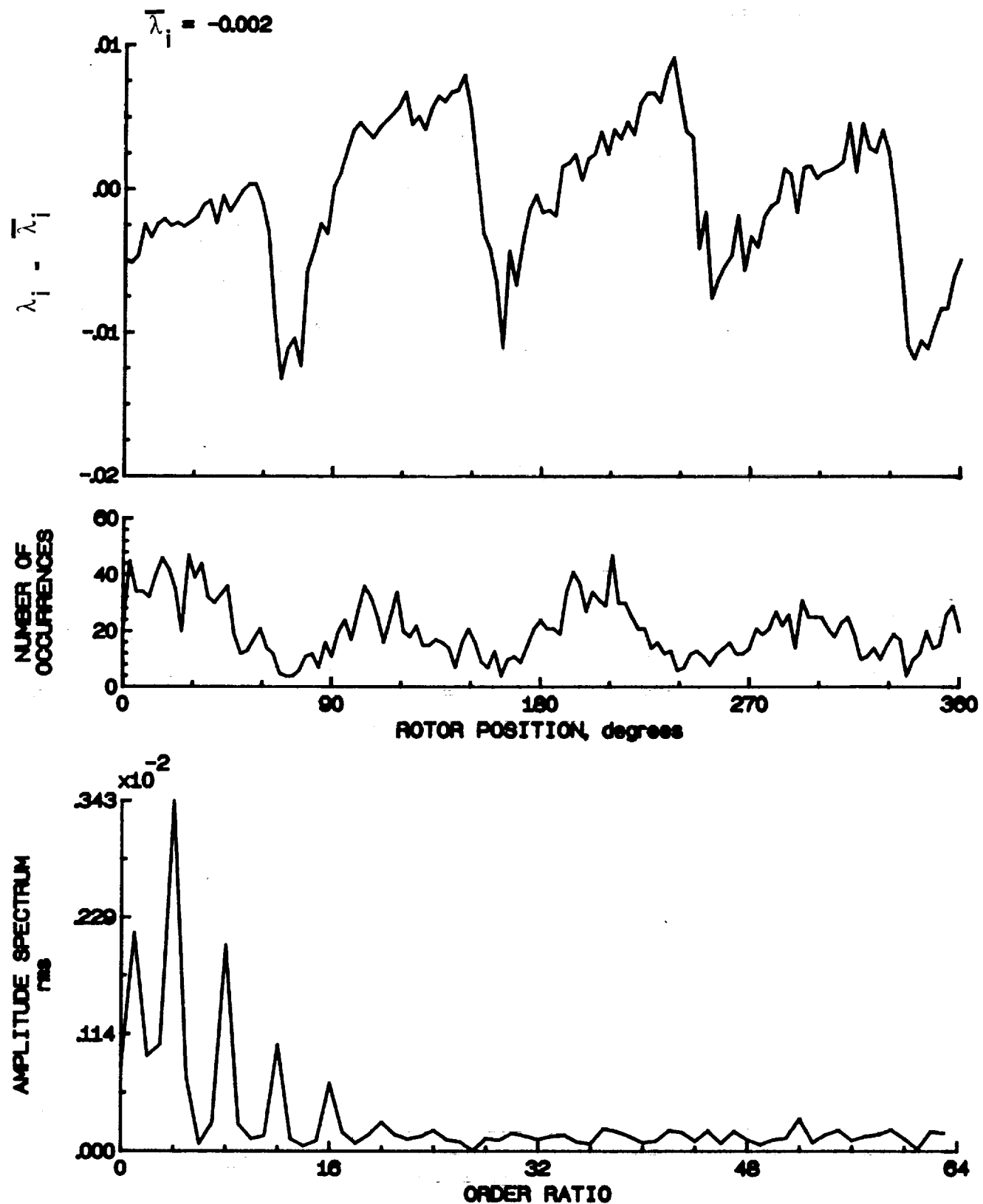


Figure 177.- Concluded.

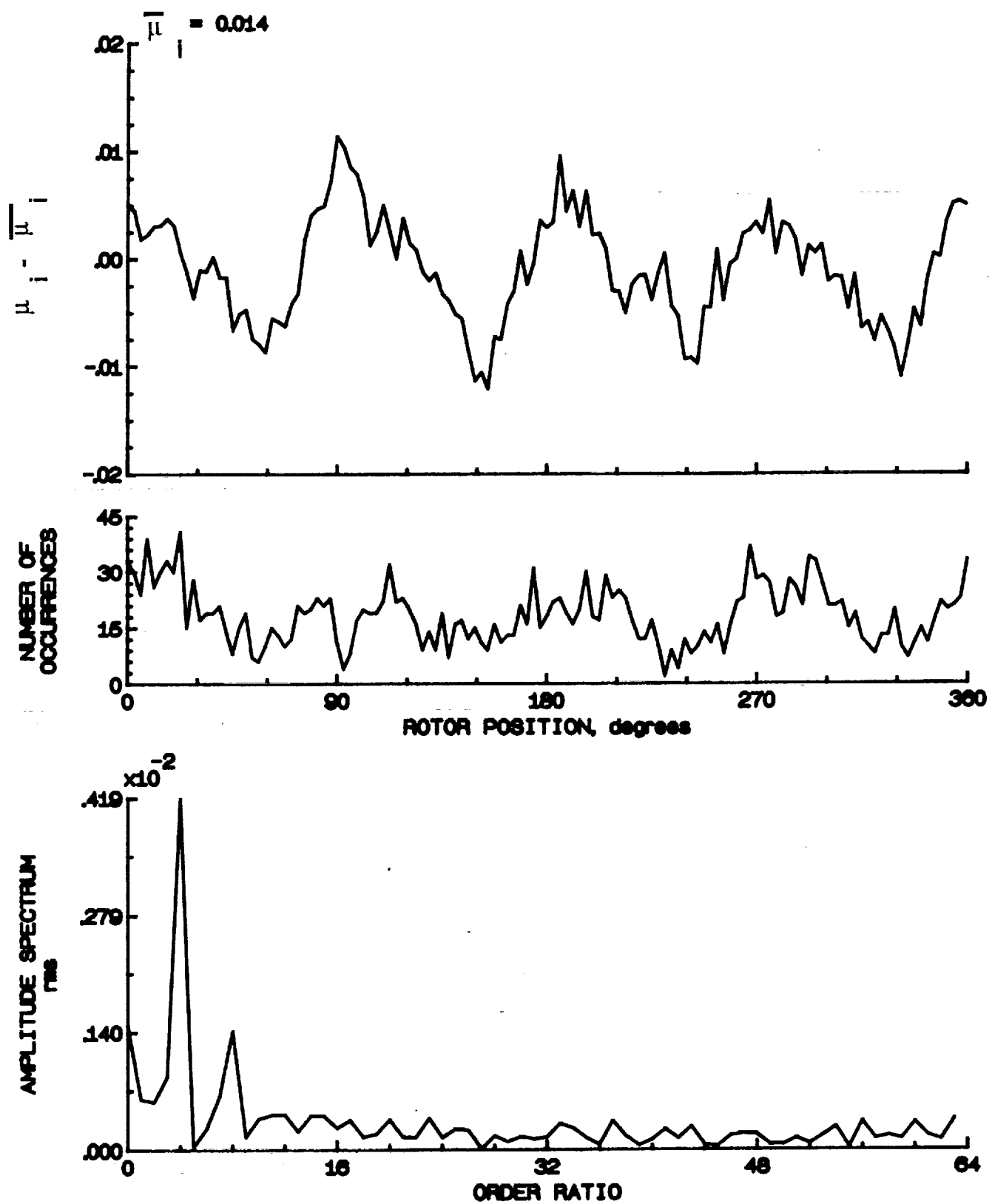


Figure 178.- Induced inflow velocity measured at 330 degrees and r/R of 0.50.

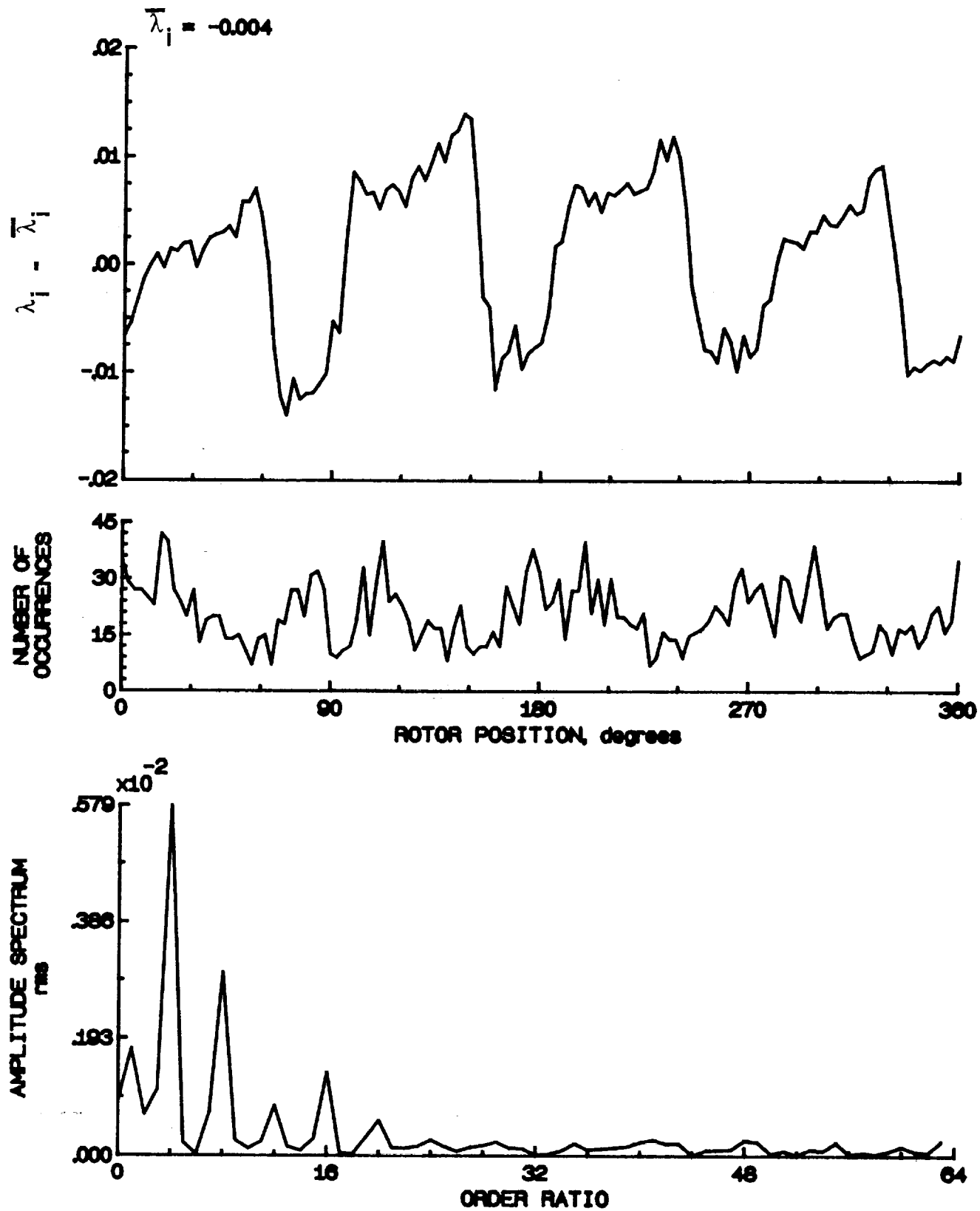


Figure 178.- Concluded.

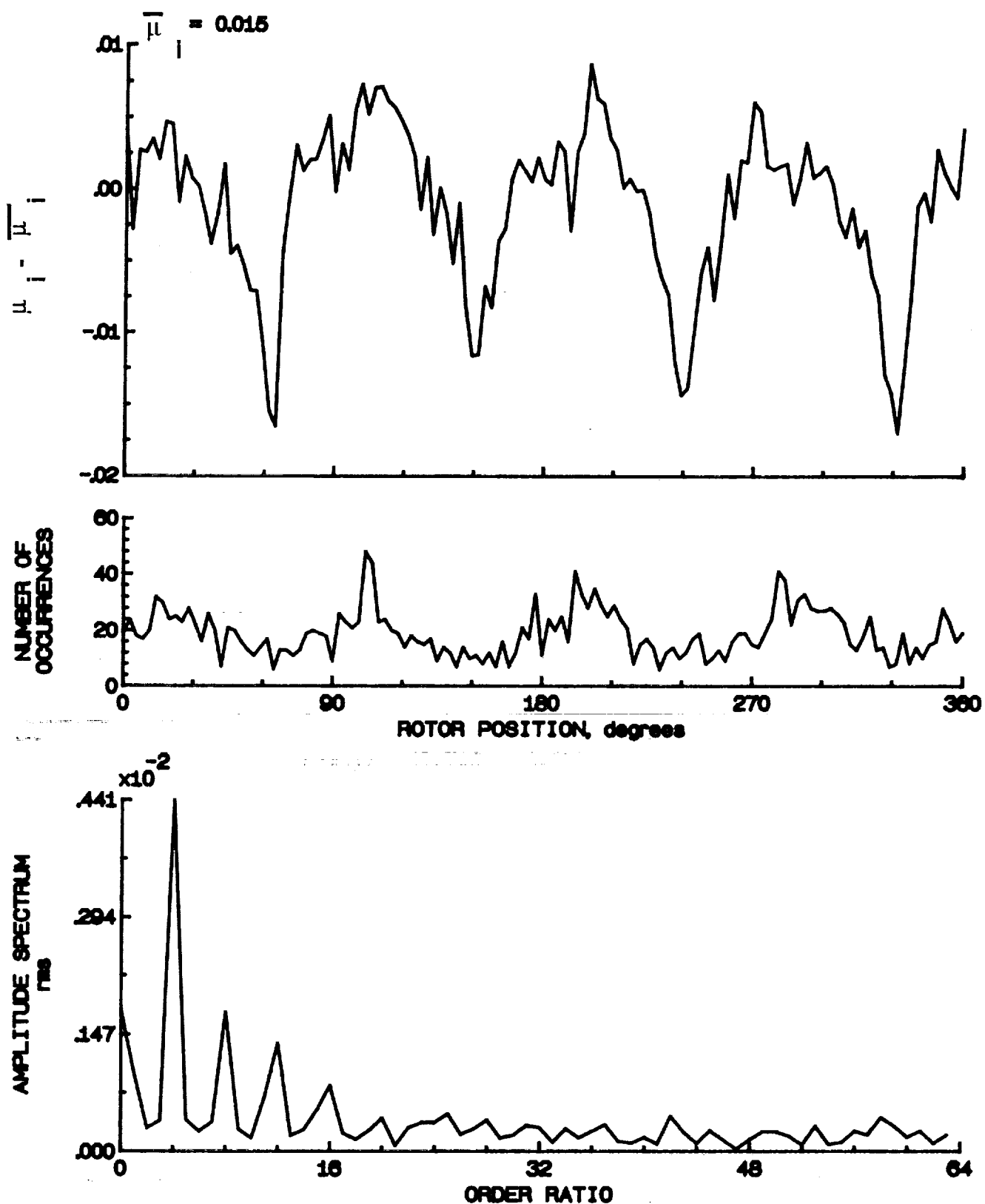


Figure 179.- Induced inflow velocity measured at 330 degrees and r/R of 0.60.

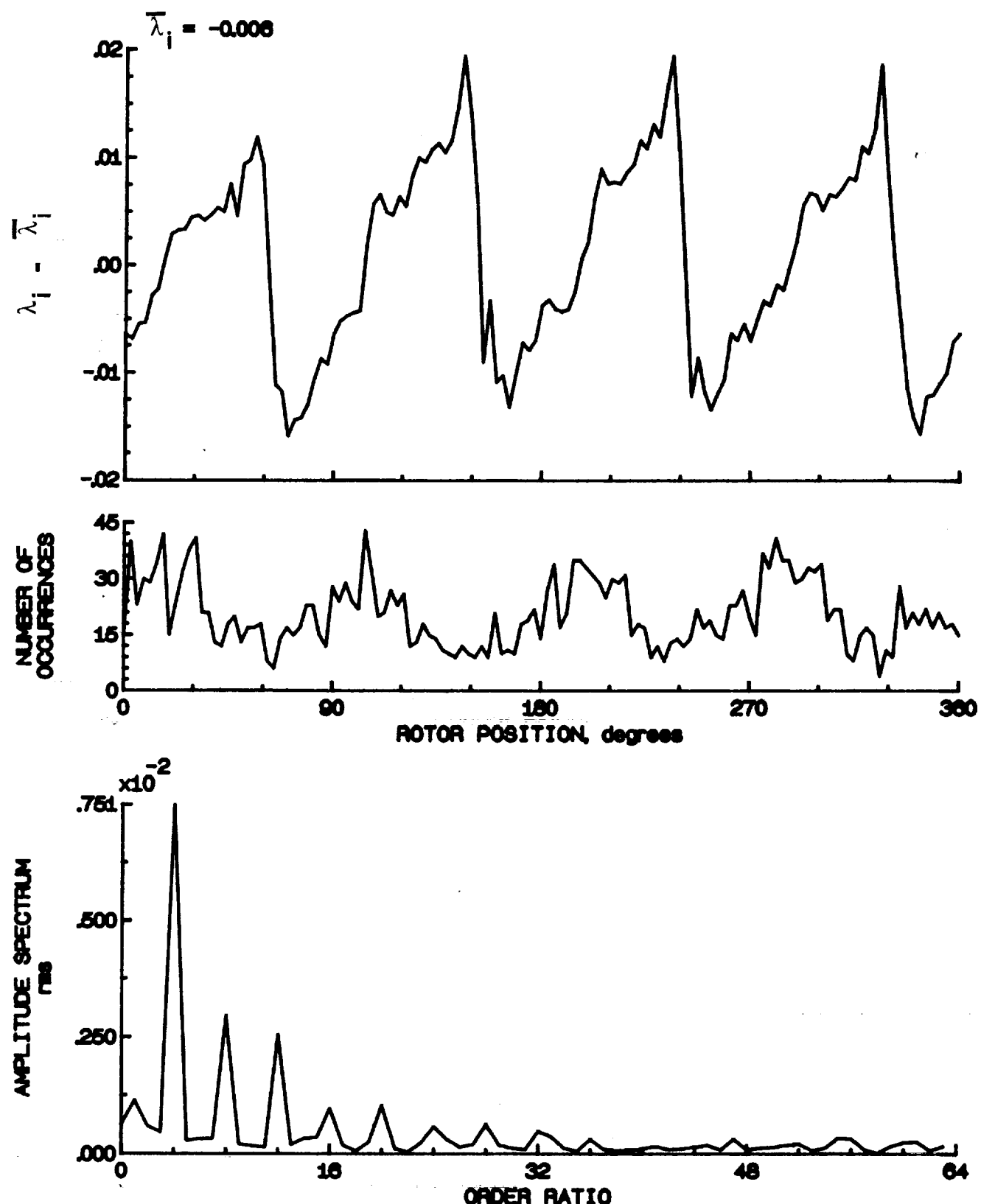


Figure 179.- Concluded.

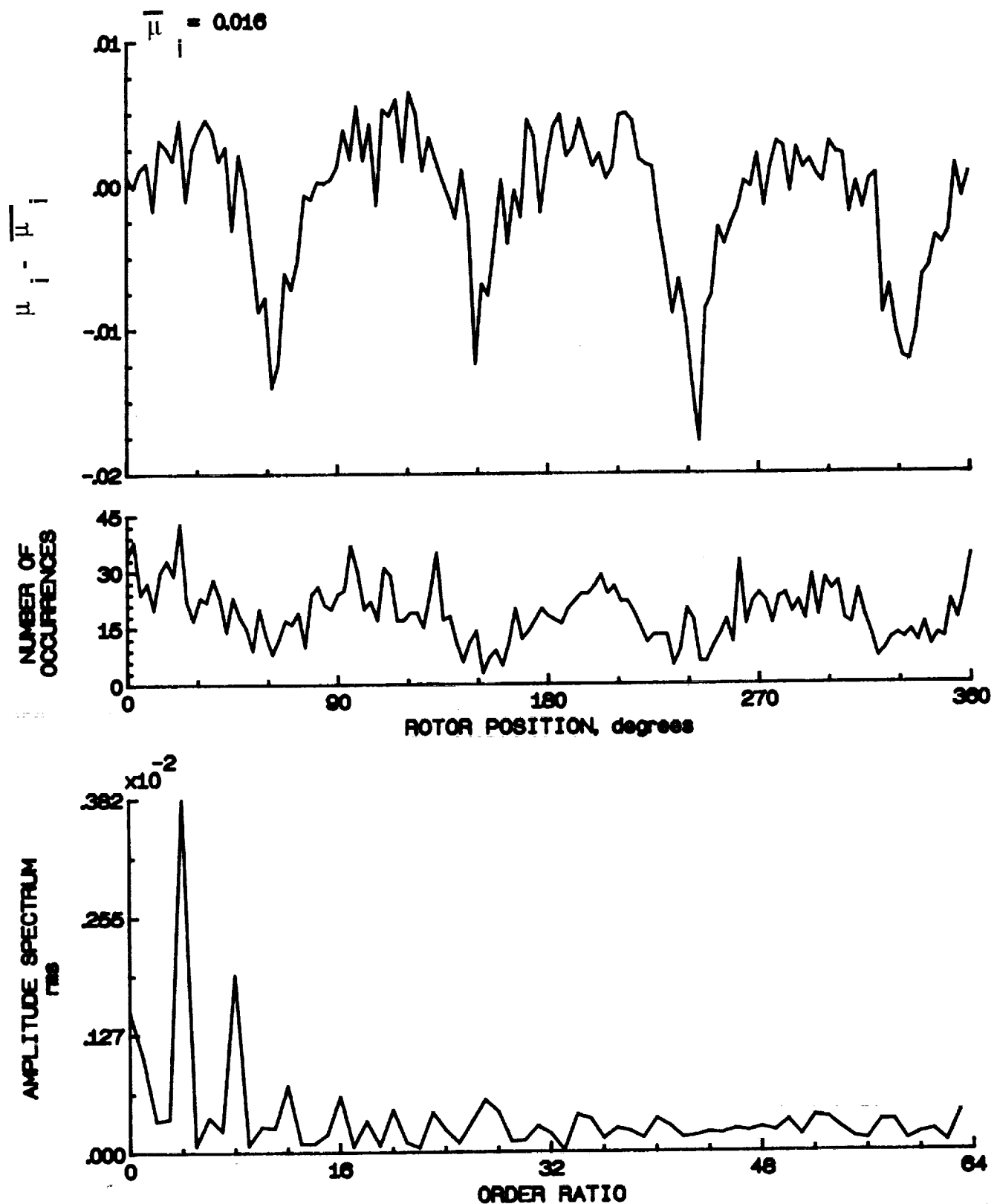
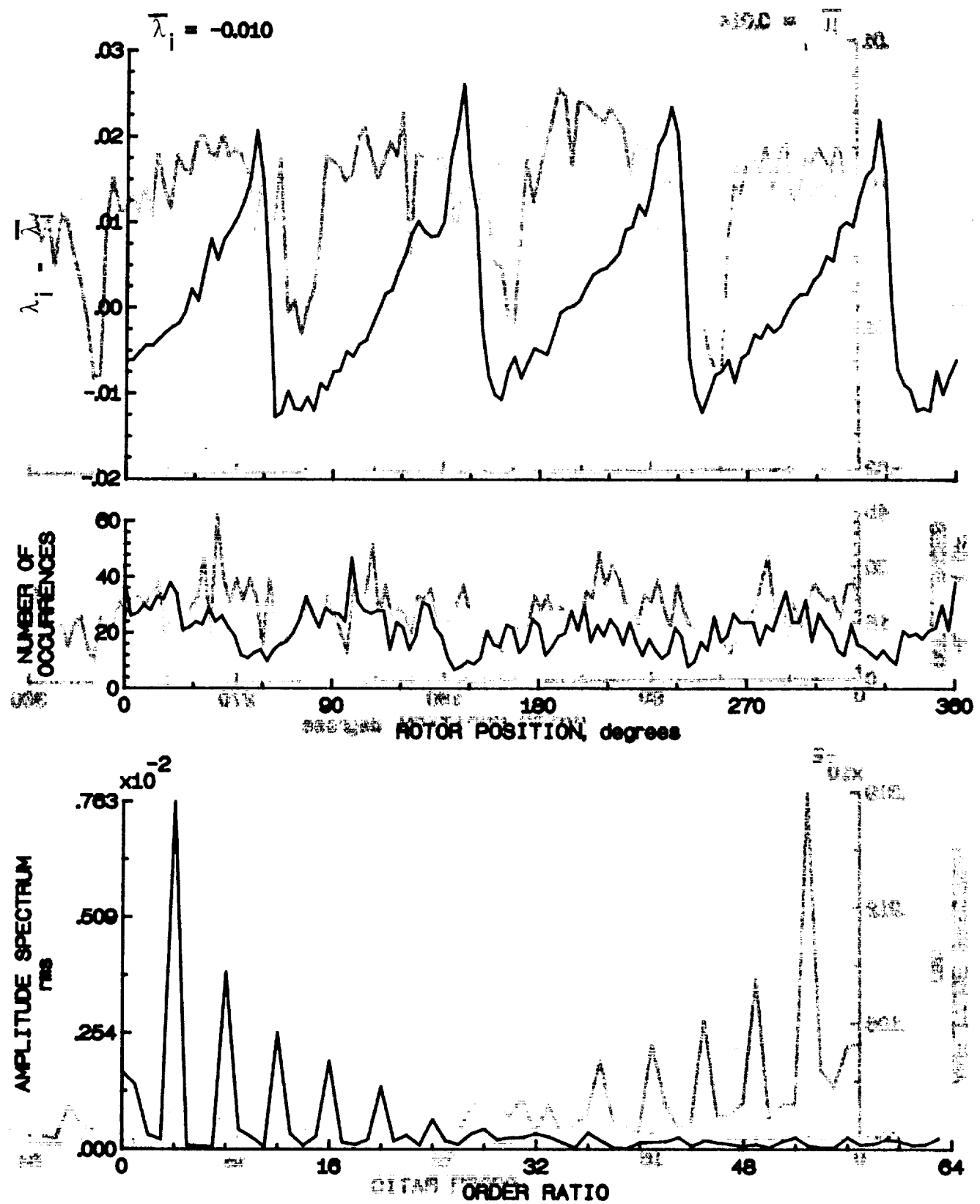


Figure 180.- Induced inflow velocity measured at 330 degrees and r/R of 0.70.



As before as in Figure 180.—Concluded.

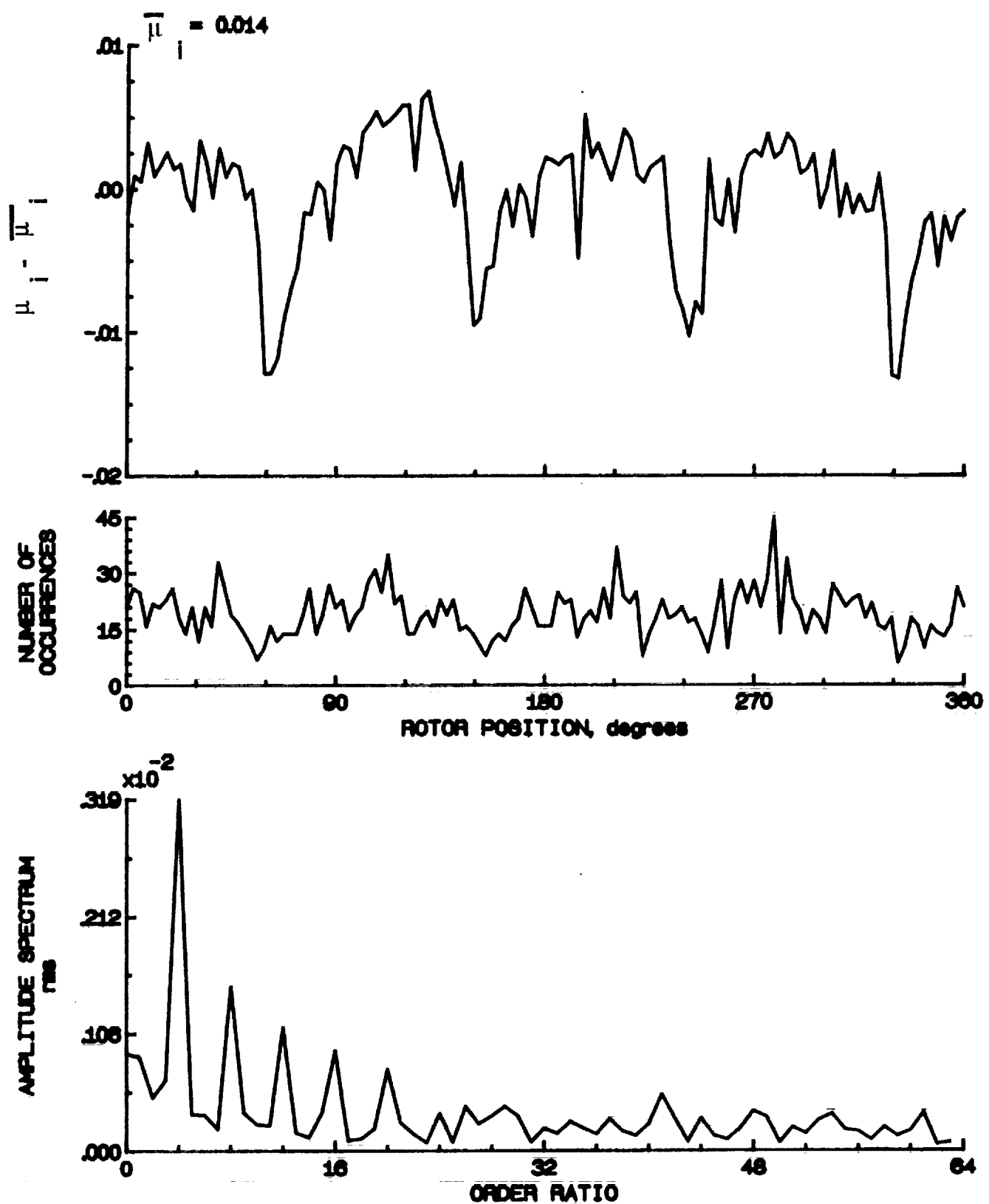


Figure 181.- Induced inflow velocity measured at 330 degrees and r/R of 0.74.

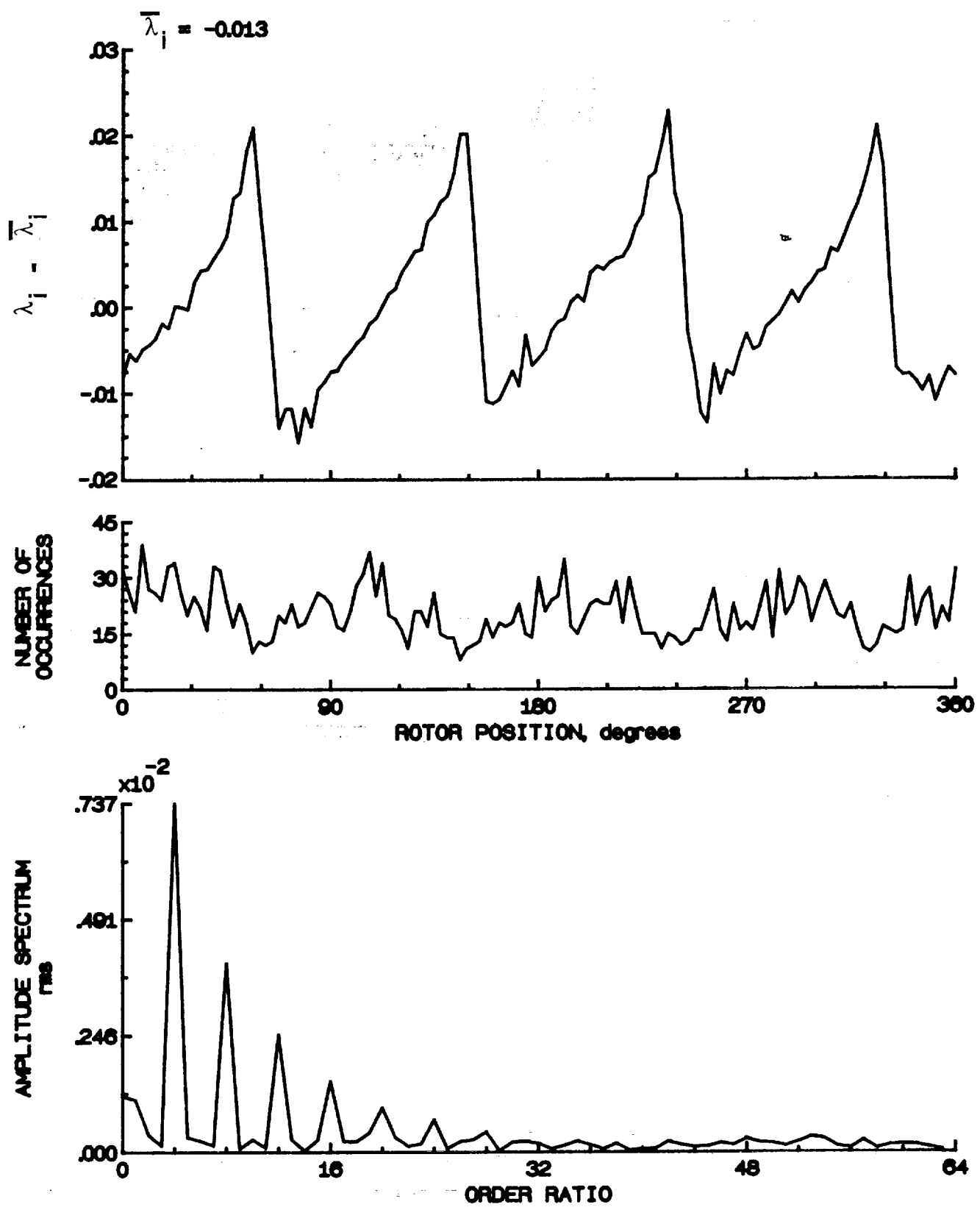


Figure 181.- Concluded.

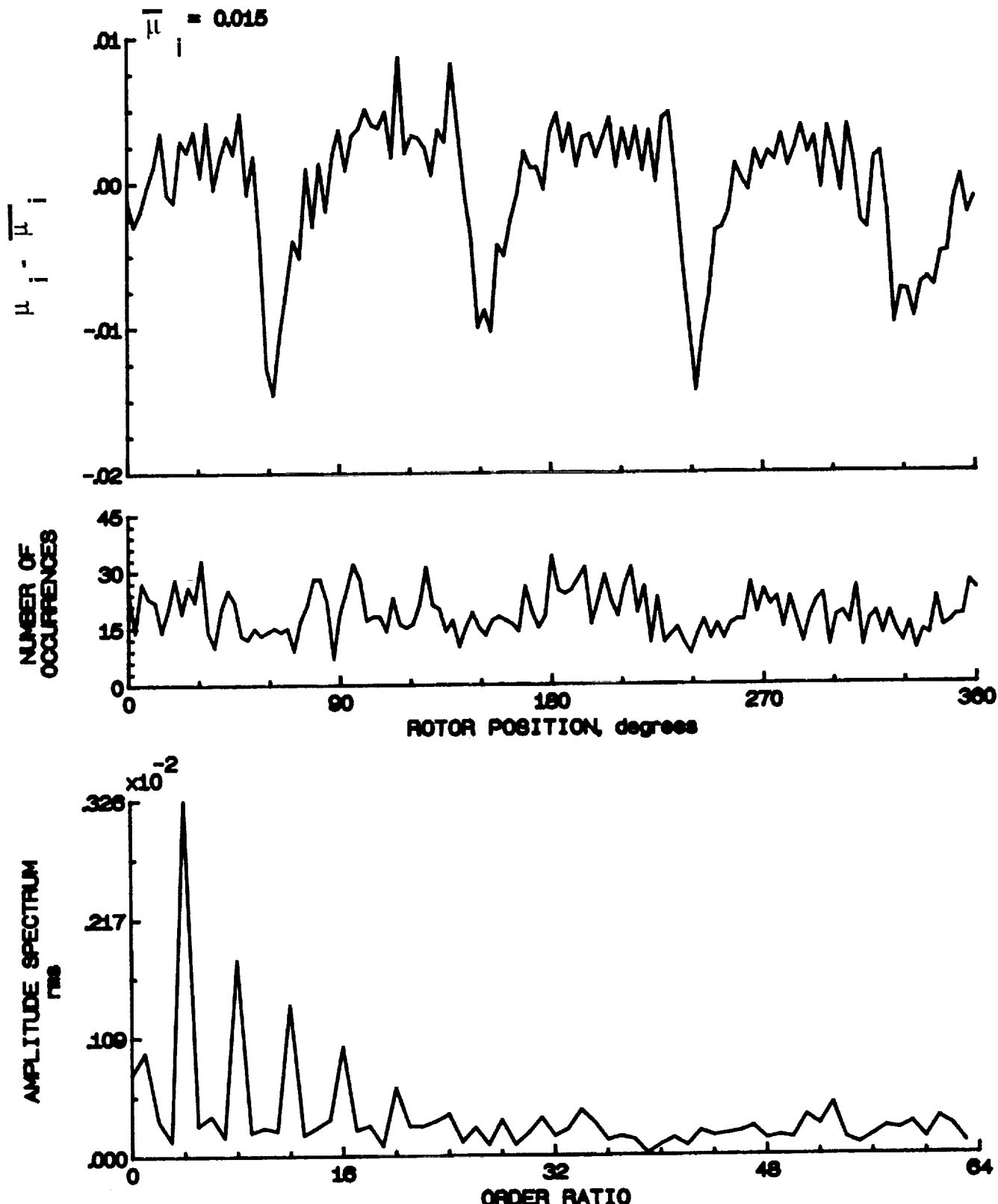


Figure 182.- Induced inflow velocity measured at 330 degrees and r/R of 0.78.

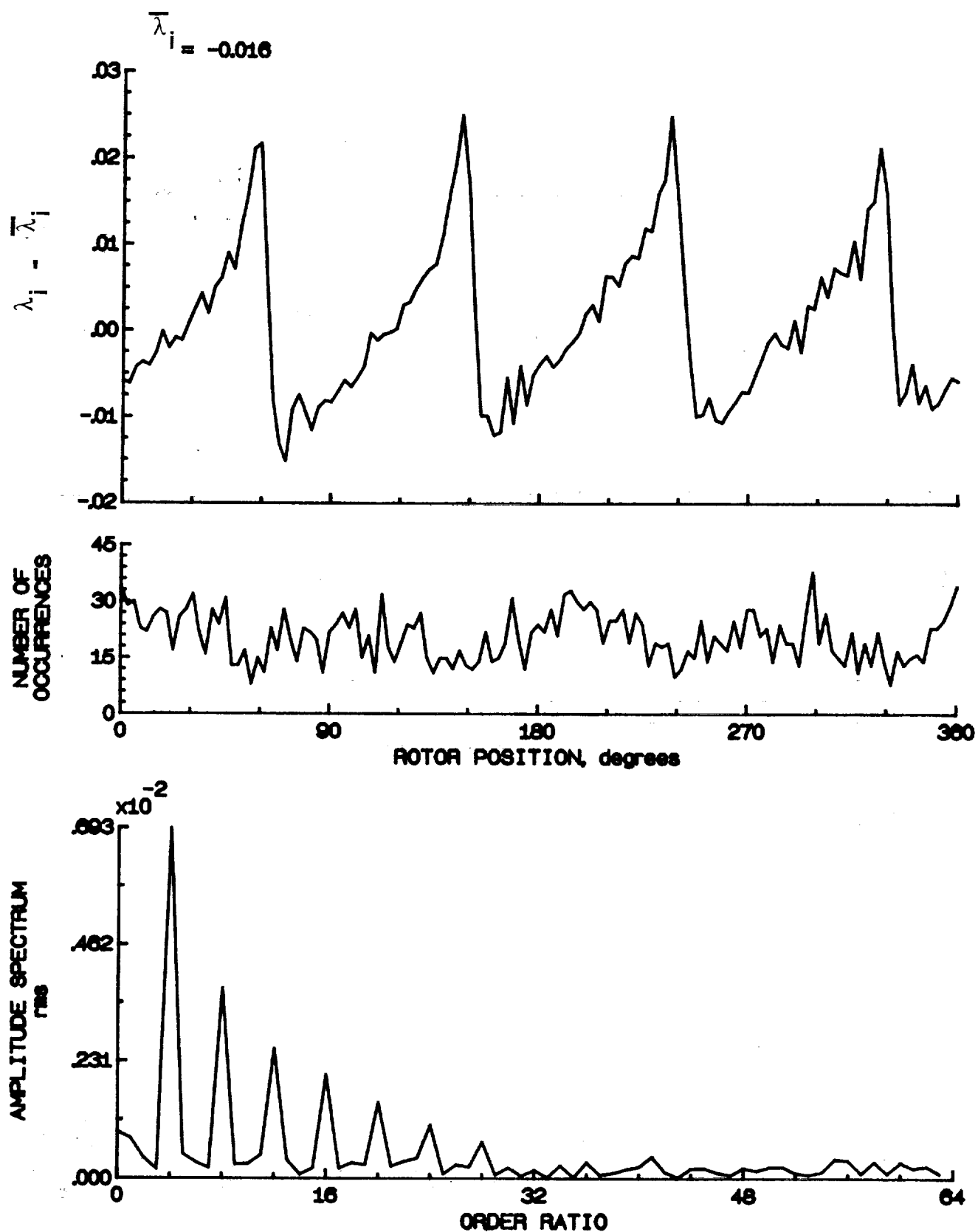


Figure 182.- Concluded.

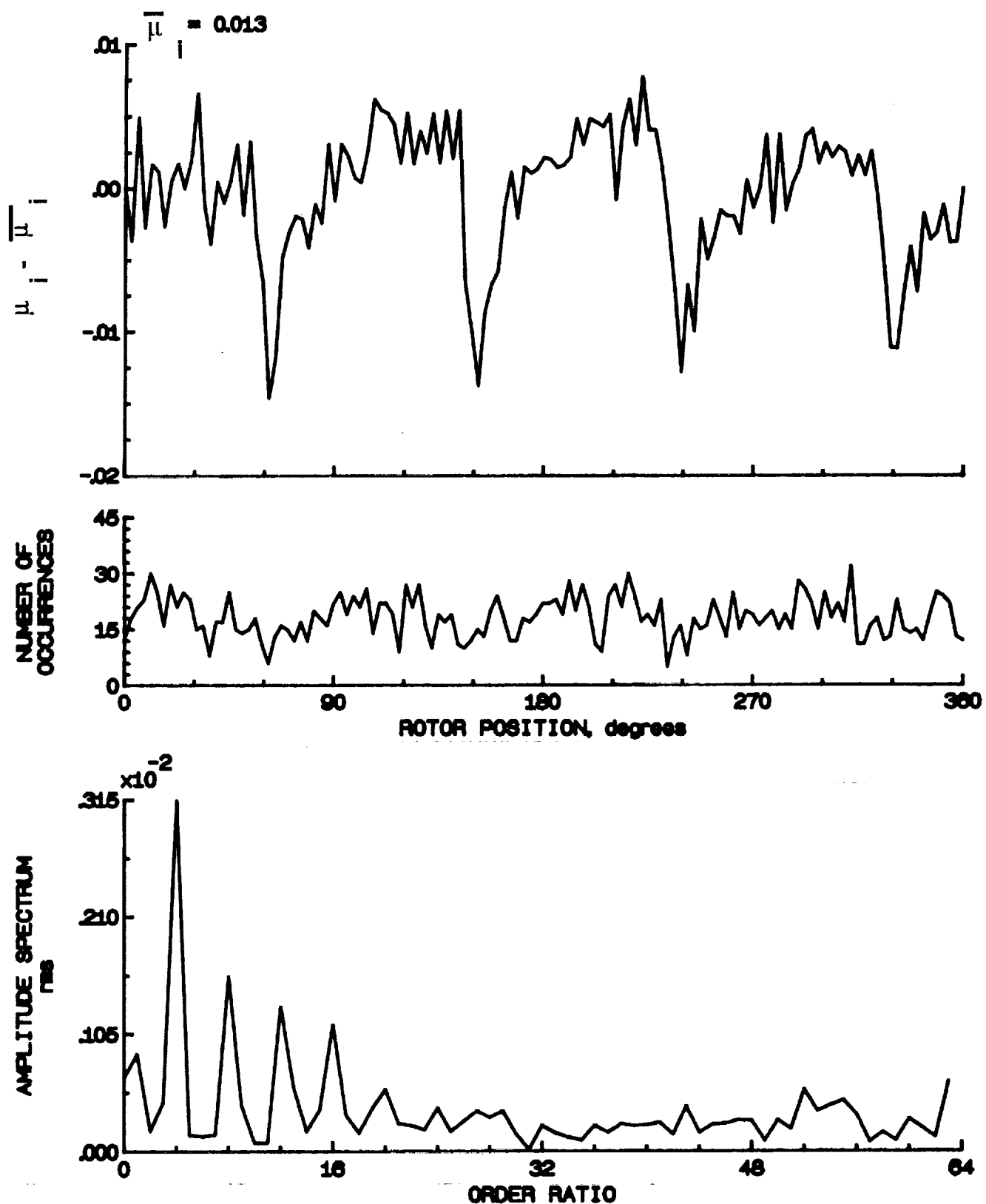


Figure 183.- Induced inflow velocity measured at 330 degrees and r/R of 0.62.

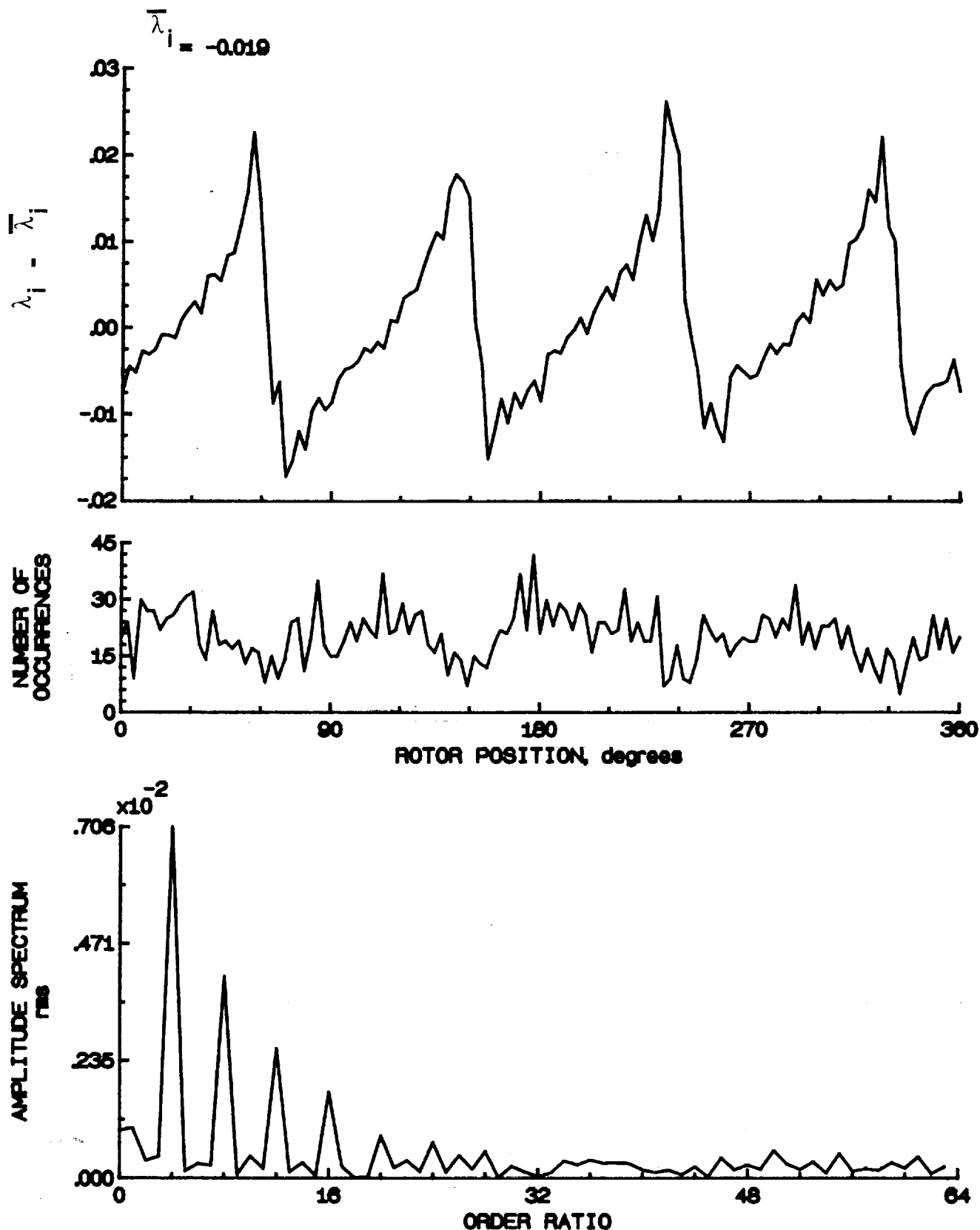


Figure 183.- Concluded.

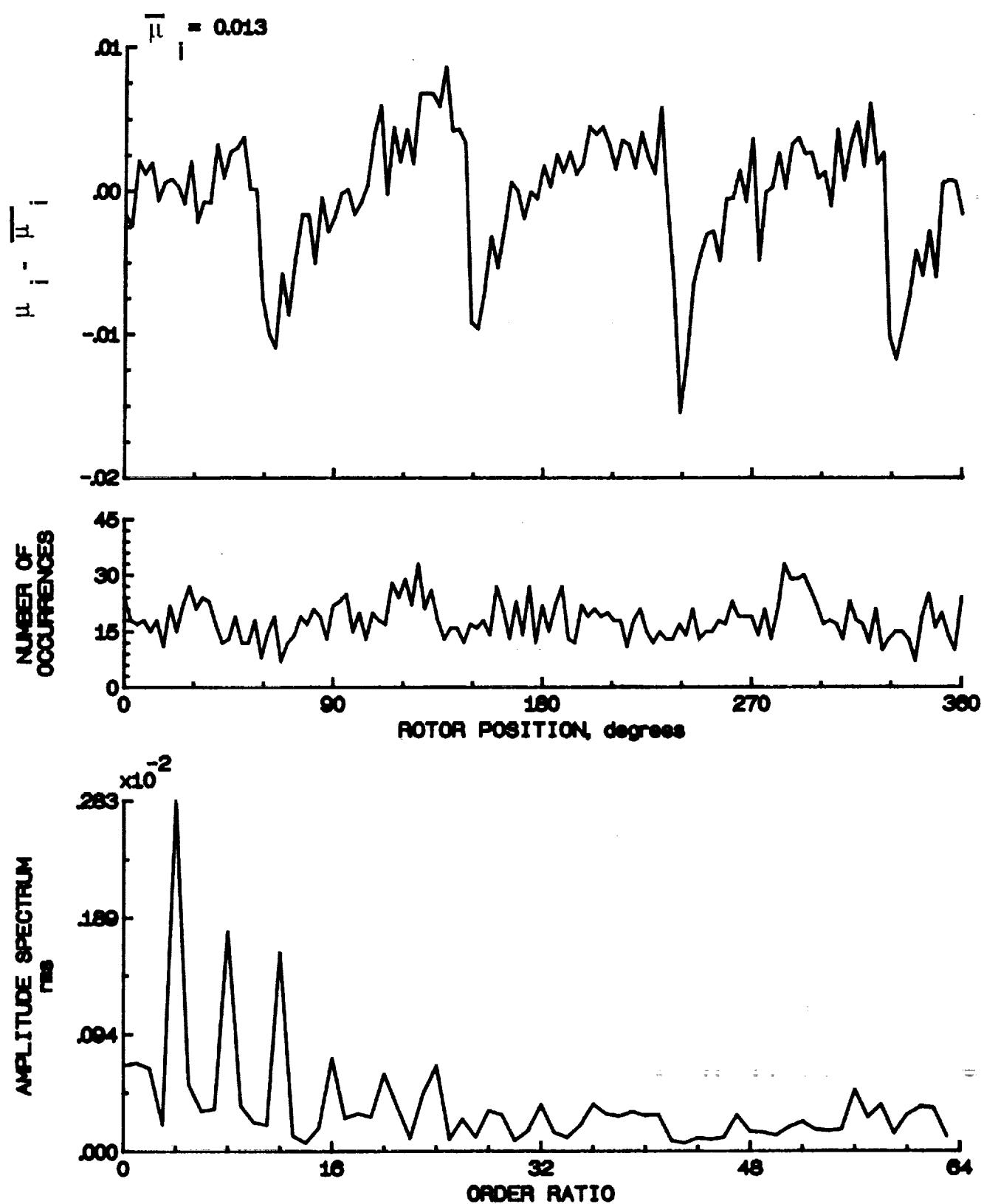


Figure 184.- Induced inflow velocity measured at 330 degrees and r/R of 0.86.

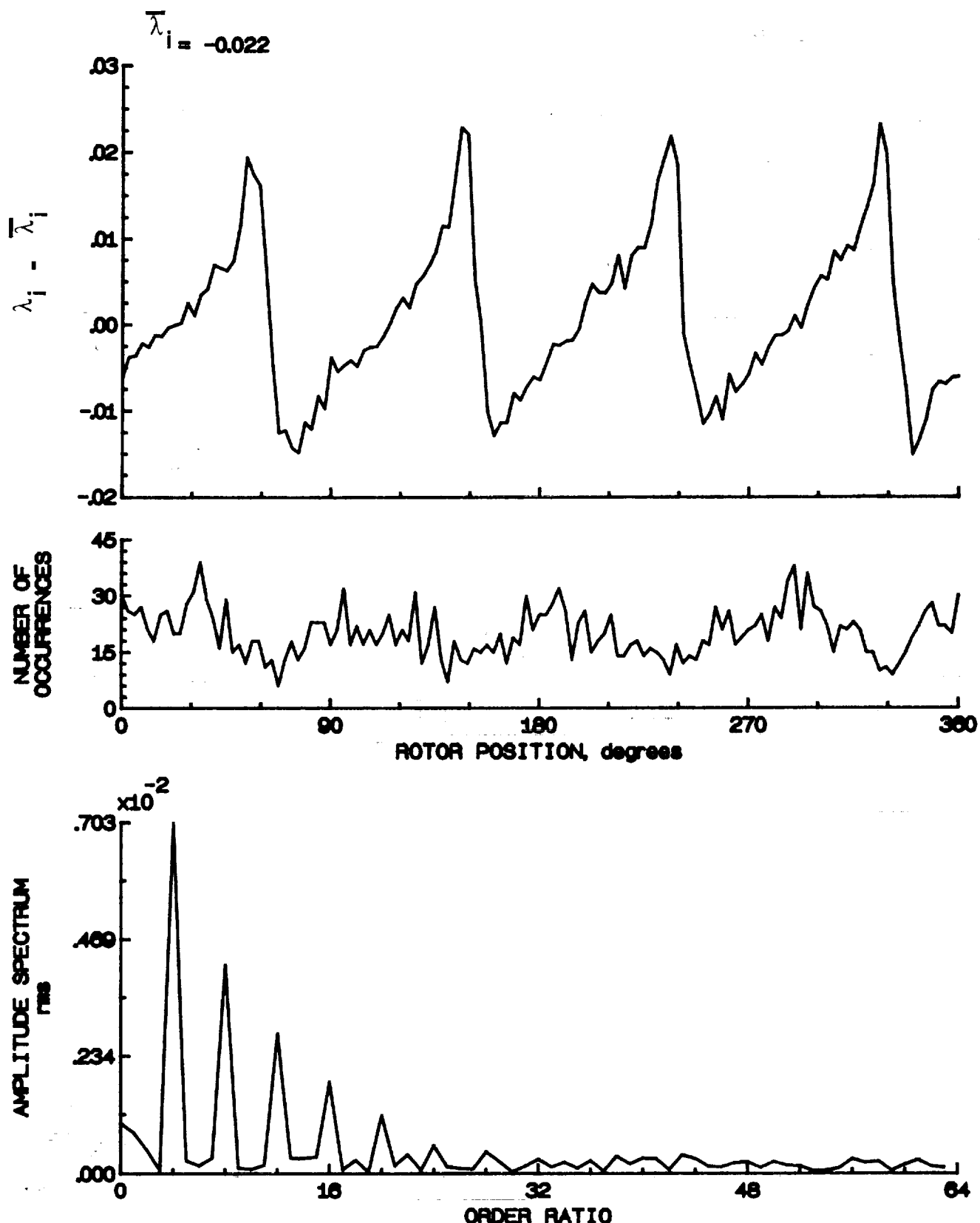


Figure 184.- Concluded.

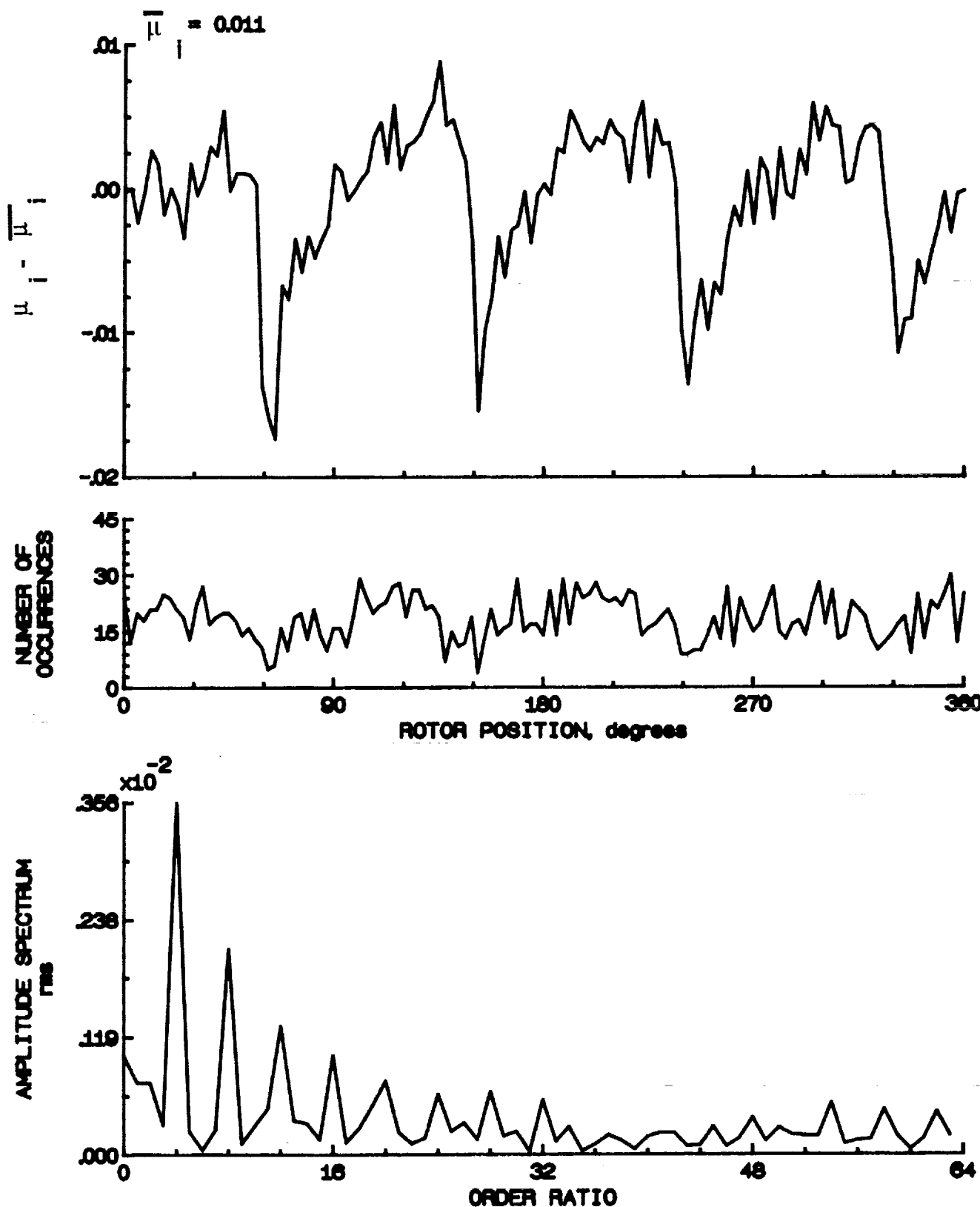


Figure 185.- Induced inflow velocity measured at 330 degrees and r/R of 0.90.

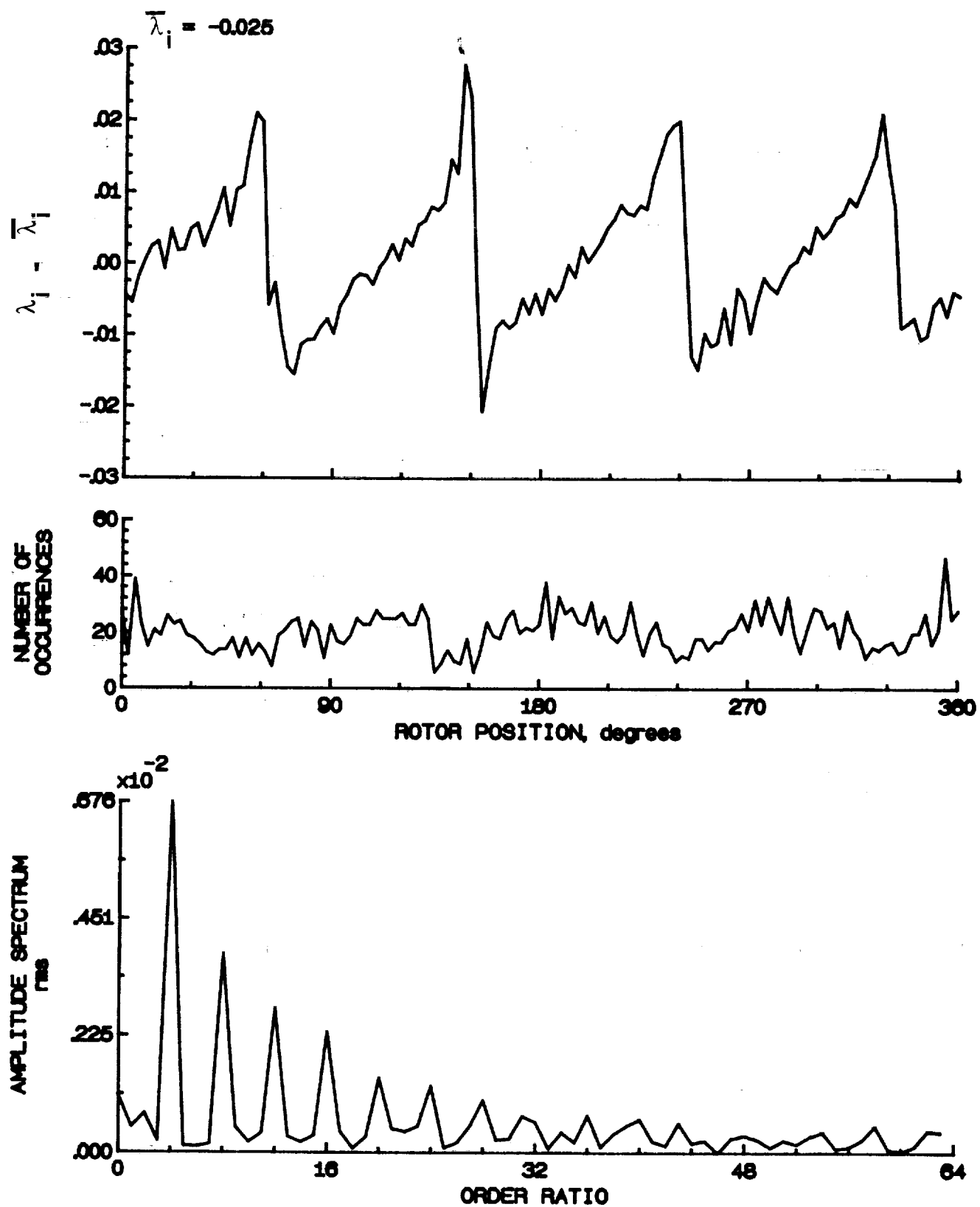


Figure 185.- Concluded.

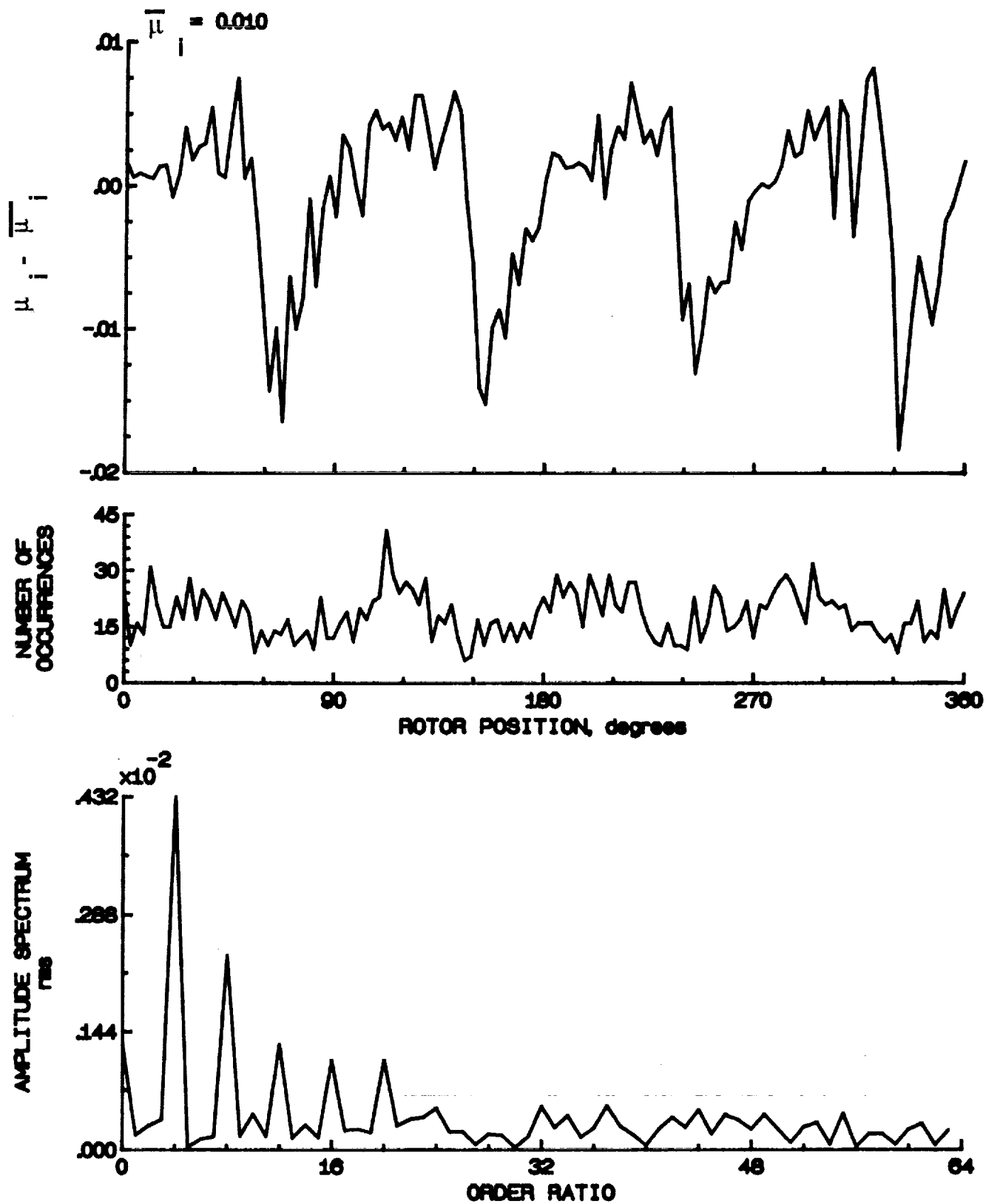


Figure 186.- Induced inflow velocity measured at 330 degrees and r/R of 0.94.

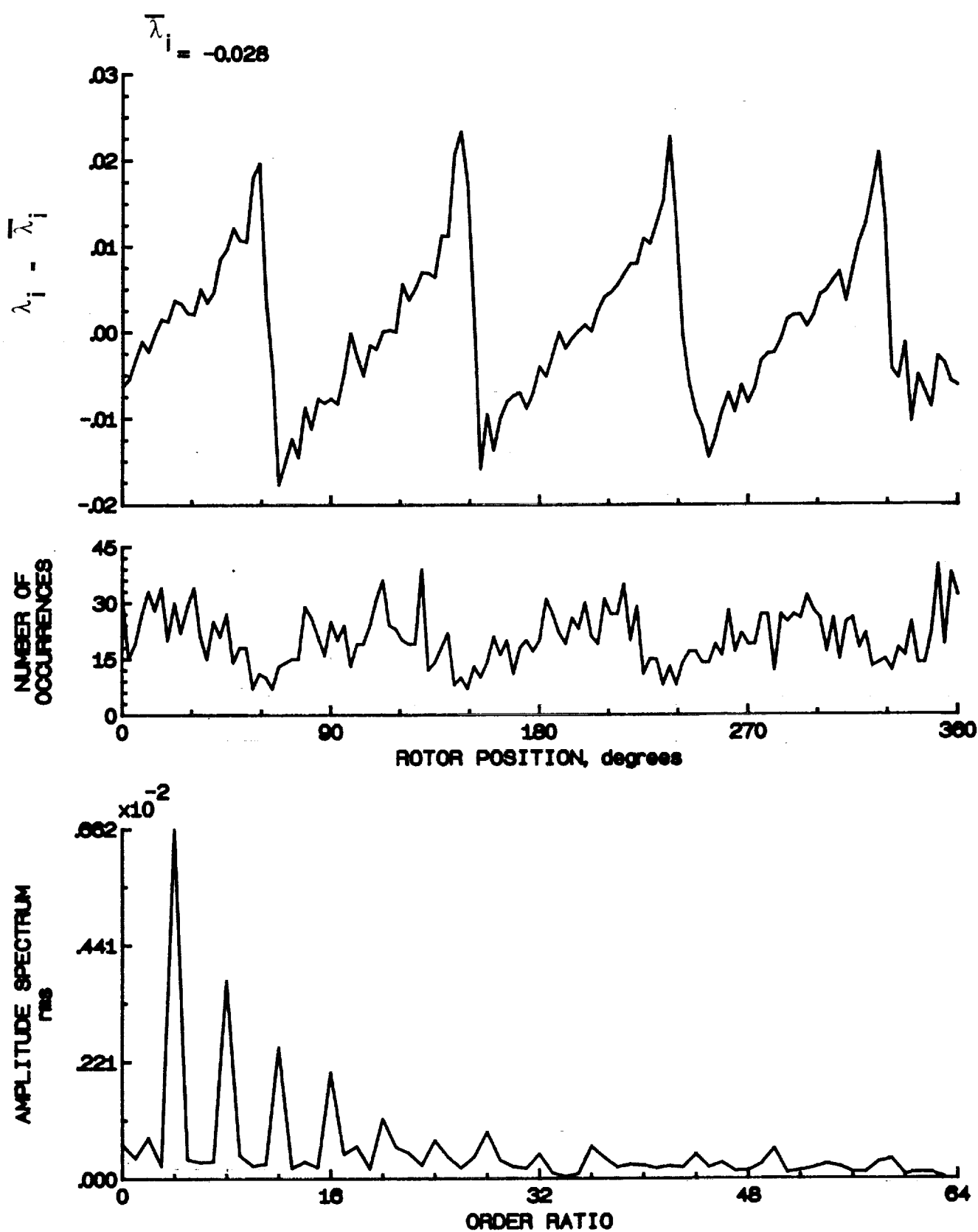


Figure 186.- Concluded.

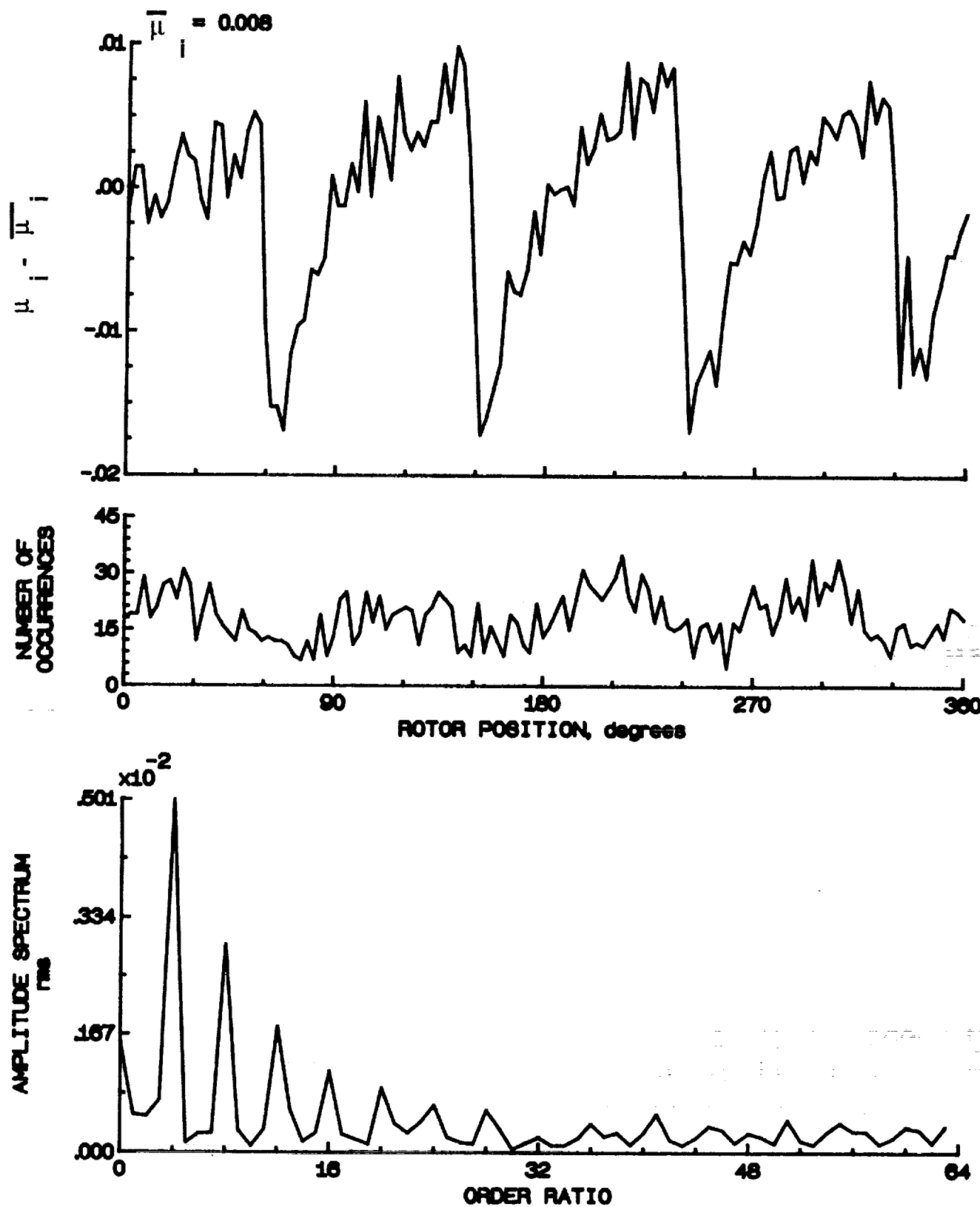


Figure 187.- Induced inflow velocity measured at 330 degrees and r/R of 0.98.

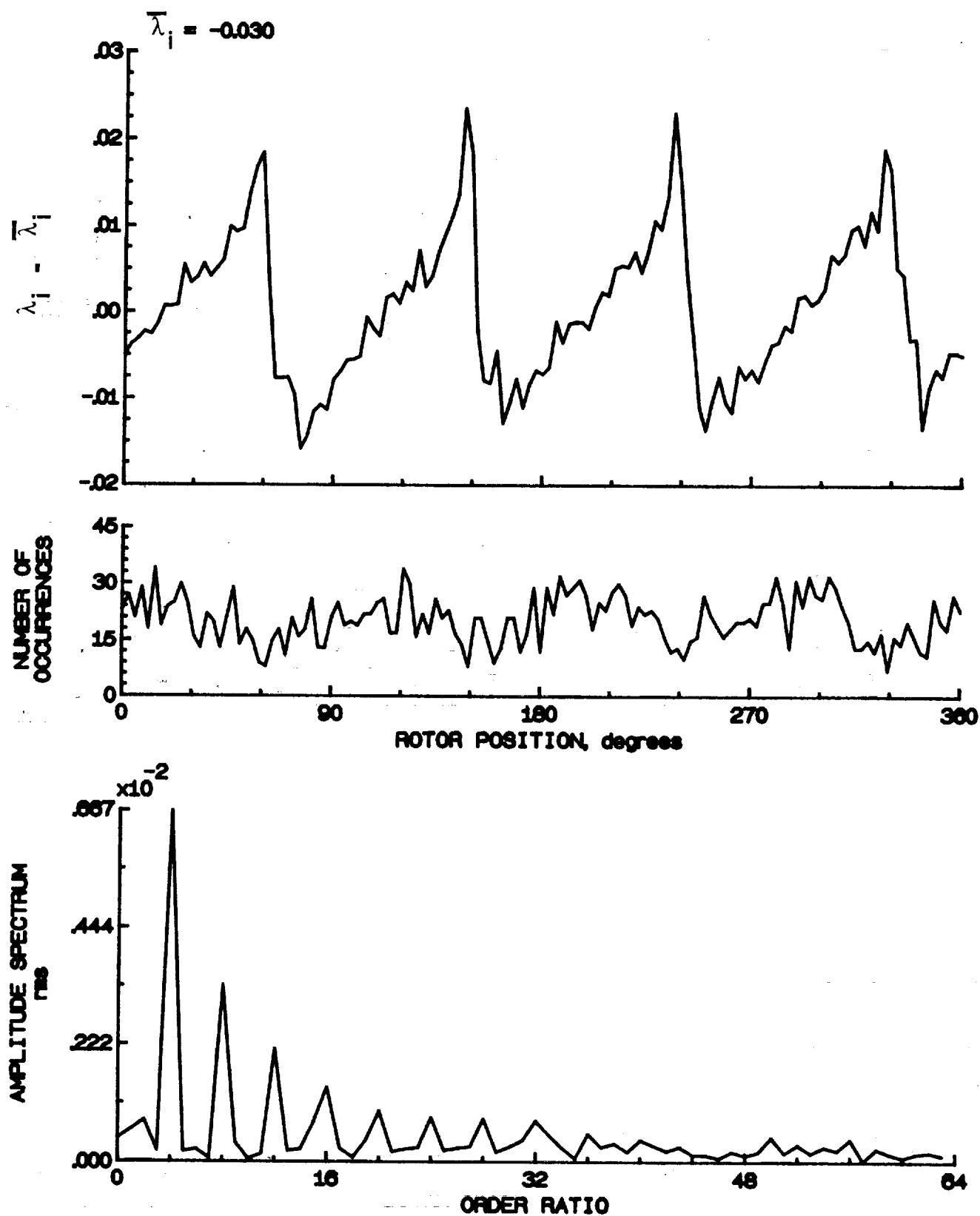


Figure 187.- Concluded.

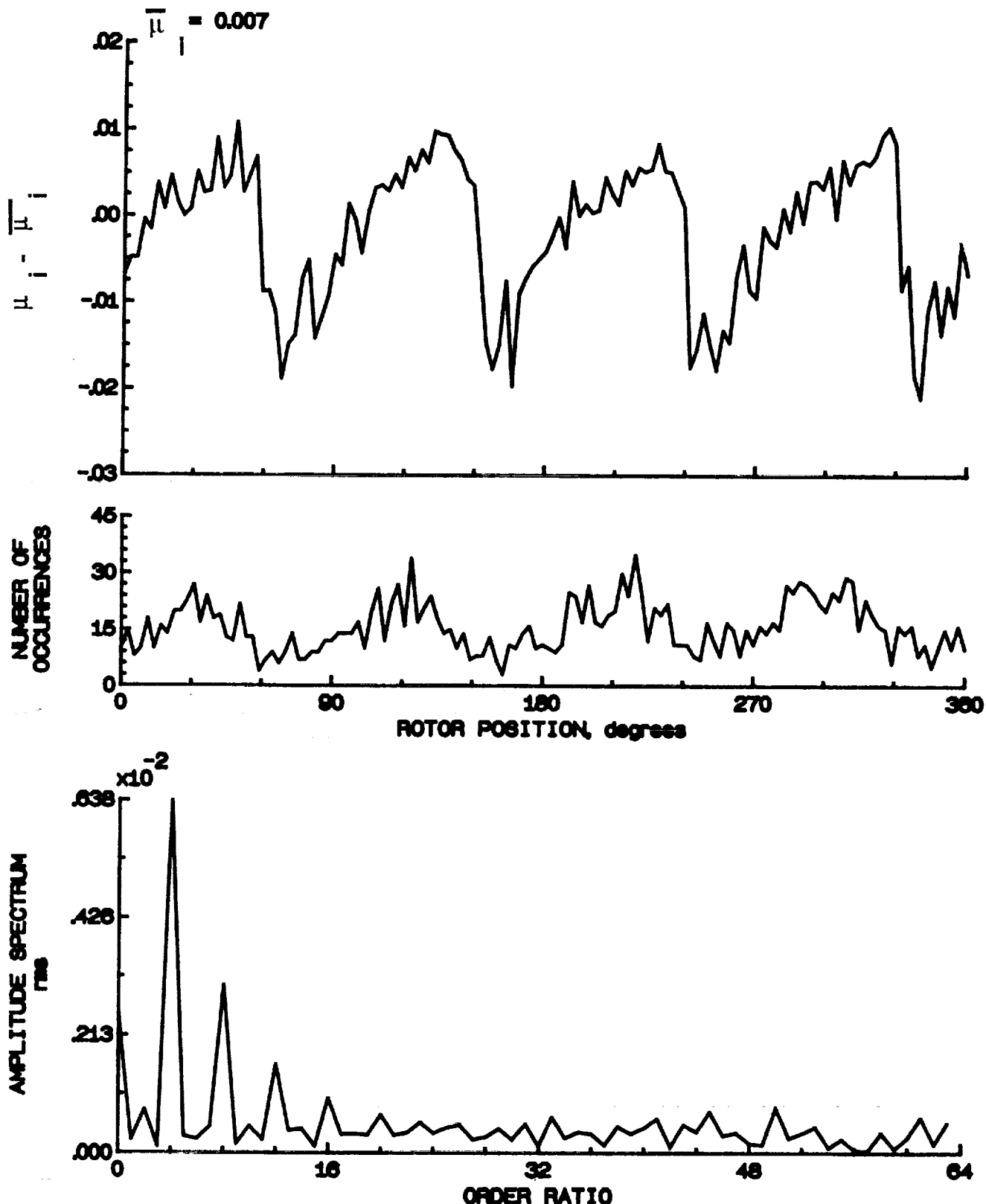


Figure 188.- Induced inflow velocity measured at 330 degrees and r/R of 1.02.

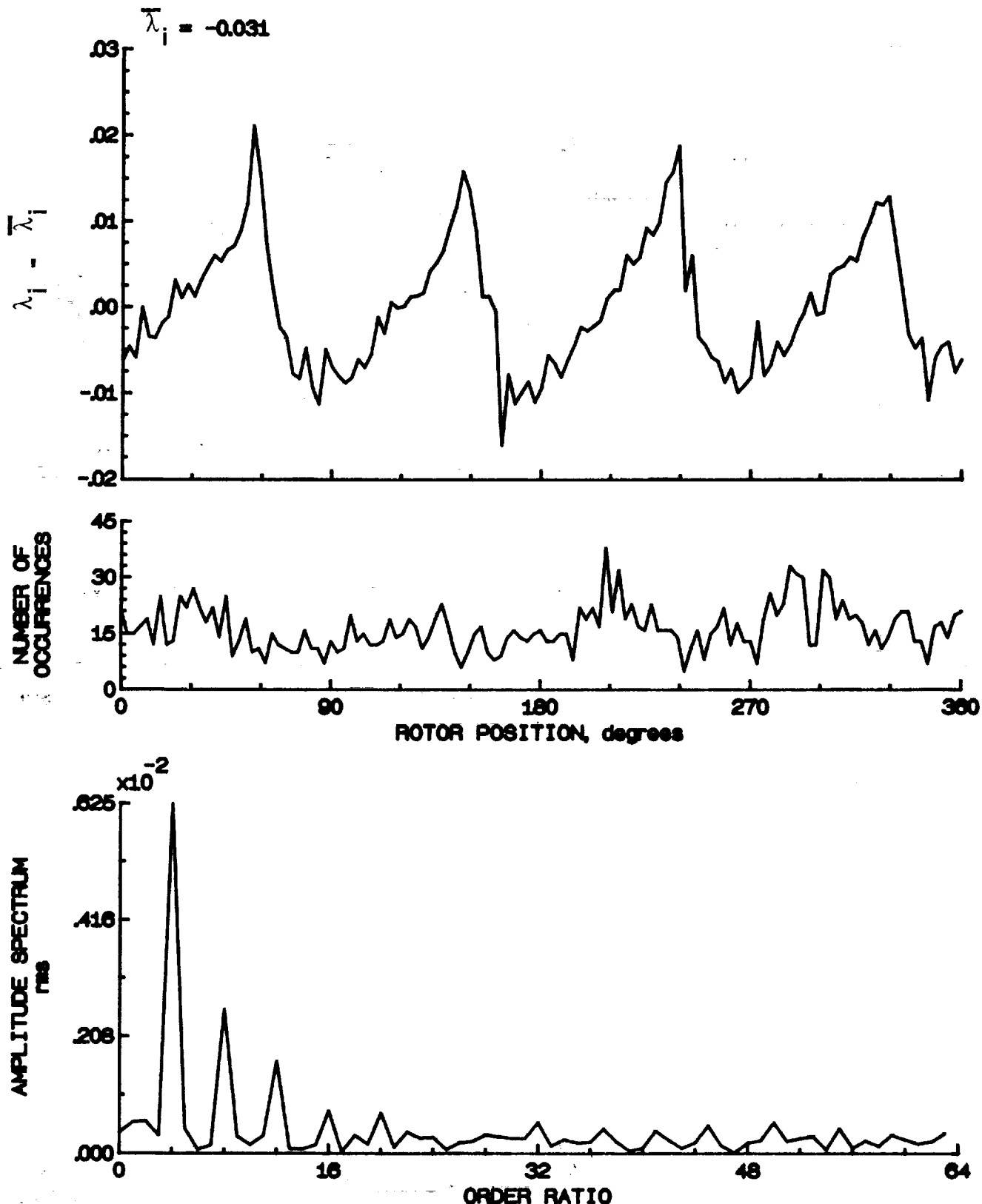


Figure 188.- Concluded.

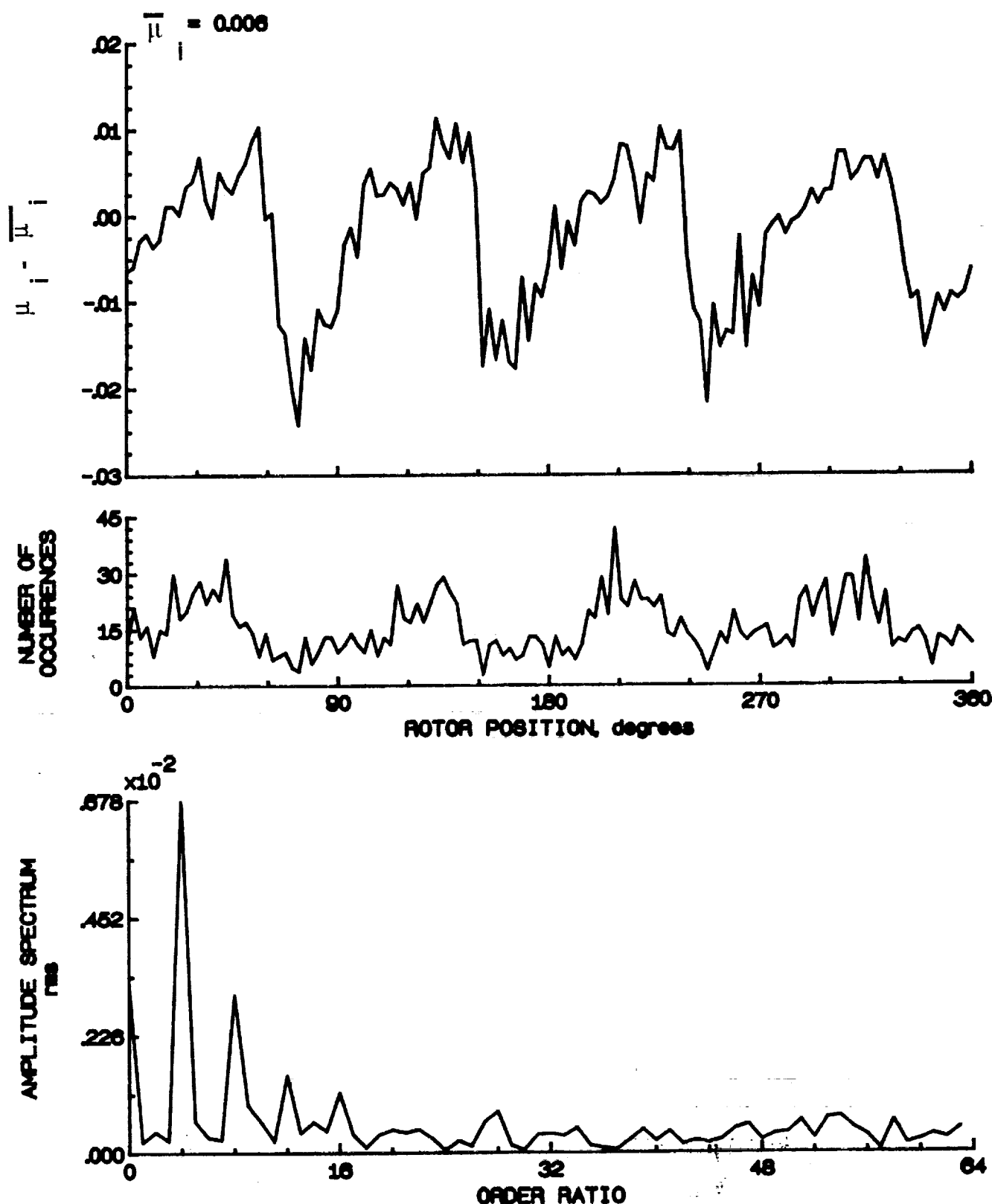


Figure 180.- Induced inflow velocity measured at 330 degrees and r/R of 1.04.

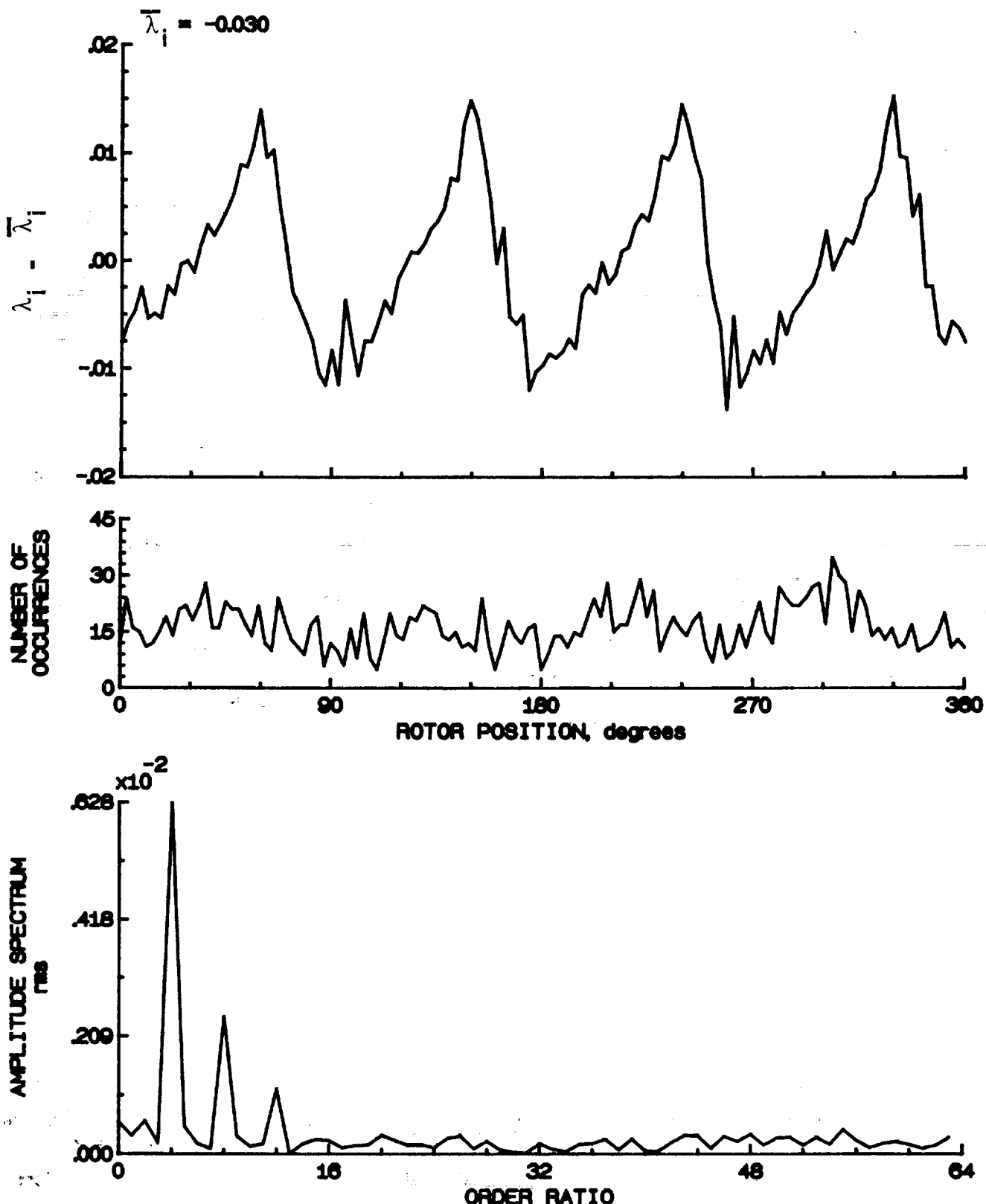


Figure 180.- Concluded.

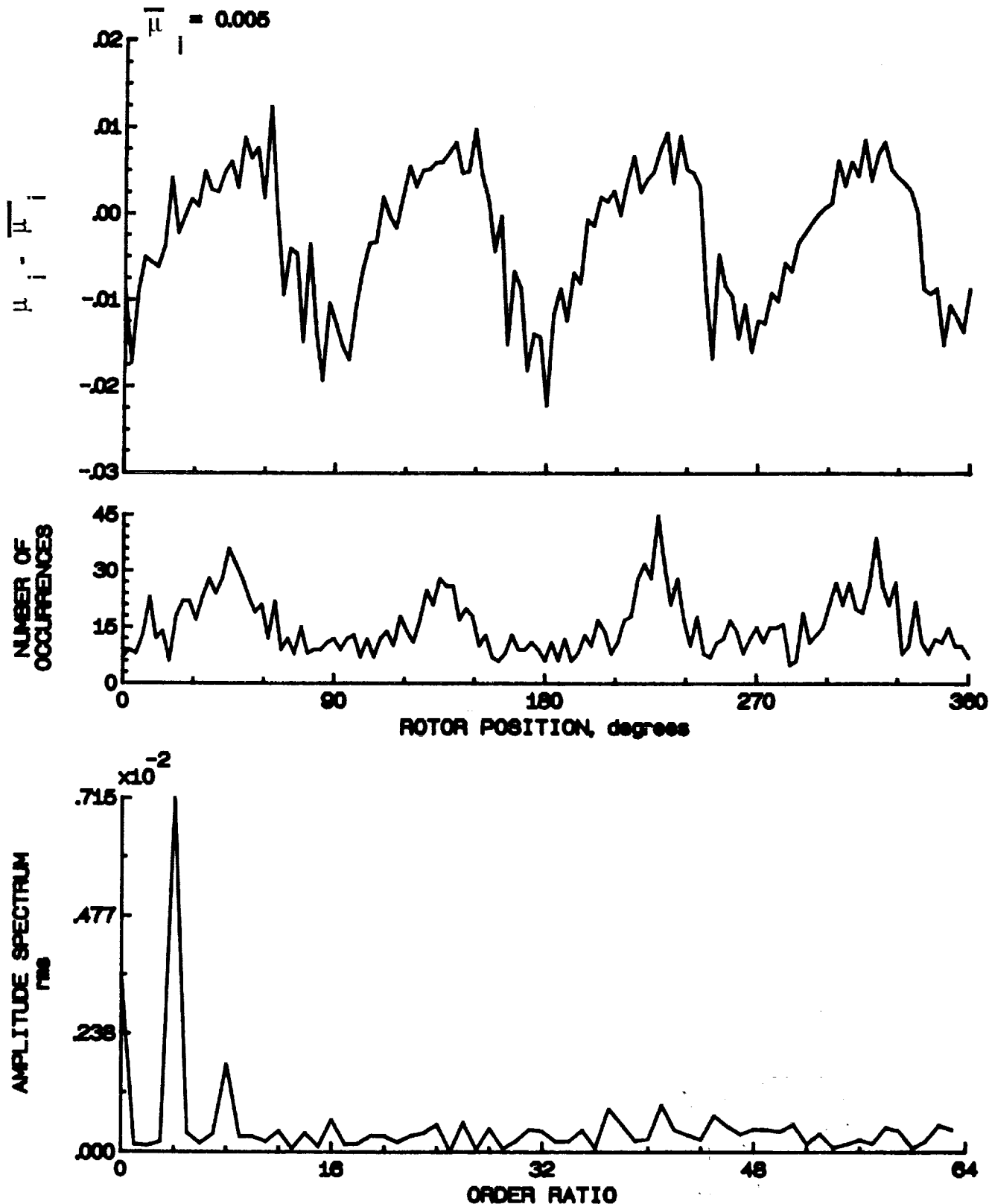


Figure 190.- Induced inflow velocity measured at 330 degrees and r/R of 1.10.

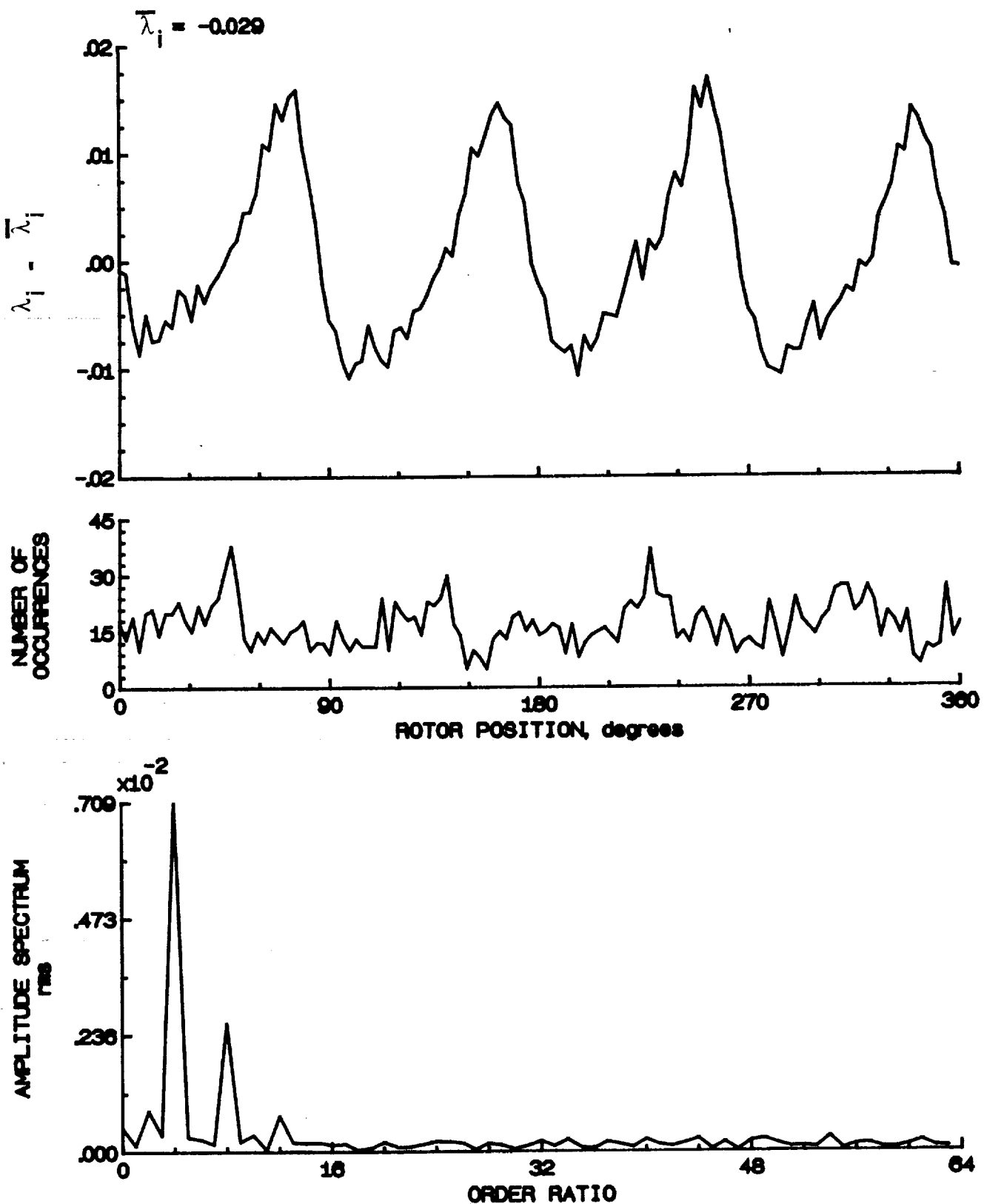


Figure 190.- Concluded.



## Report Documentation Page

1. Report No. NASA TM-102642 AVSCOM TM-90-B-007	2. Government Accession No.	3. Recipient's Catalog No.	
4. Title and Subtitle Inflow Measurements Made With a Laser Velocimeter on a Helicopter Model in Forward Flight--Volume VIII: Rectangular Planform Blades at an Advance Ratio of 0.23, 0.50 Chord Above the Tip Path Plane		5. Report Date May 1990	
7. Author(s) Susan L. Althoff Joe W. Elliott Danny R. Hoad Richard H. Sailey		6. Performing Organization Code	
9. Performing Organization Name and Address Aerostructures Directorate USAARTA-AVSCOM NASA Langley Research Center Hampton, VA 23665-5225		8. Performing Organization Report No.	
12. Sponsoring Agency Name and Address National Aeronautics and Space Administration, Washington, DC 20546-0001 and U.S. Army Aviation Systems Command, St. Louis, MO 63120-1798		10. Work Unit No. 505-61-51-10	
15. Supplementary Notes <p>Susan L. Althoff, Joe W. Elliott, and Danny R. Hoad: Aerostructures Directorate, USAARTA-AVSCOM, Hampton, Virginia. Richard H. Sailey: Lockheed Engineering &amp; Sciences Company, Hampton, Virginia.</p>		11. Contract or Grant No.	
16. Abstract <p>An experimental investigation was conducted in the 14- by 22-Foot Subsonic Tunnel at the NASA Langley Research Center to measure the inflow into a scale model helicopter rotor in forward flight (<math>\mu = 0.23</math>). The measurements were made with a two-component Laser Velocimeter (LV) 0.50 chord above the plane formed by the path of the rotor tips (tip-path-plane). A conditional sampling technique was employed to determine the position of the rotor at the time that each velocity measurement was made so that the azimuthal fluctuations in velocity could be determined. Measurements were made at a total of 178 separate locations in order to clearly define the inflow character. The mean and standard deviation of the induced inflow ratios and the azimuthally dependent induced inflow ratios are included on 5.25 flexible disk in the pocket on the inside of the rear cover of this report. These data are presented herein without analysis.</p>		13. Type of Report and Period Covered Technical Memorandum	
17. Key Words (Suggested by Author(s)) Rotor Inflow Laser Velocimeter		18. Distribution Statement Unclassified-Unlimited Subject Category 02	
19. Security Classif. (of this report) Unclassified	20. Security Classif. (of this page) Unclassified	21. No. of pages 388	22. Price A17